GUEST HOST CHEMISTRY

PART I: THE SYNTHESIS OF METAL SELECTIVE SENSORS

PART II: THE SYNTHESIS OF ANTIBIOTIC PRECURSORS AND INTERMEDIATES

by

Trevor Hagemann

A Dissertation Submitted in

Partial Fulfillment of the

Requirements For the Degree of

Doctor of Philosophy

in Chemistry

at

The University of Wisconsin – Milwaukee

May 2022

ABSTRACT

PART I: THE SYNTHESIS OF METAL SELECTIVE SENSORS
PART II: THE SYNTHESIS OF ANTIBIOTIC PRECURSORS AND INTERMEDIATES

by

Trevor Hagemann

The University of Wisconsin-Milwaukee, 2022
Under the Supervision of Professor Alan Schwabacher

Part 1: Metal Selective Sensors

The work herein describes the creation of a library of sensors for the detection of metal ions in aqueous systems. The solid support these dyes are attached to facilitates a continuous measurement of metal ion concentrations in aqueous systems. The sensors are based on an azo dye core structure wherein detection of metal ions is observed by the change in absorbance of the dye upon binding. These sensors are capable of detecting metal ions in the ppb range, specific dyes interacting with specific metal ions cause distinct spectral changes, providing substantial information. the aggregate response from multiple azo dyes affords a matrix of information that can be deconvoluted to determine individual metal ion identities and concentrations. Should this system be successively commercialized, metal ion detection in industry as well as households may be achievable.

Part 2: Antibiotics

The work herein describes the synthesis of precursors to potent antibiotics, including enduracididine. The enzymatic pathway for the biosynthesis of enduracididine is being probed by the synthesis of intermediate 4(s)-hydroxyarginine and mechanistic probe 3,4-dehydroarginine. 3,4-dehydroarginine has been synthesized and studied in the enzymatic pathway to elucidate the mechanism of biosynthesis for 4(s)-hydroxyketoarginine. Racemic 4-hydroxyarginine has been synthesized on gram scale quantities and enzymatically oxidized to 4(s)-hydroxyketoarginine.

In addition, a beta sheet initiator for the inhibition of Bam machinery in gram negative bacteria has been developed. This initiator is based on a bis-fused quinolone that mimics the alternating peptide hydrogen bonding network found in beta sheets. Dubbed the Janus quinolone, this beta sheet initiator should be modifiable to strongly interact with the Bam machinery and prevent proper folding. Should this create a pore in the outermembrane from unfolded Bam machinery, then once again the bacteria will be susceptible to antibiotics that it would otherwise be resistant to.

For my family, both new and old

Time is an illusion that helps things make sense

So we are always living in the present tense

It seems unforgiving when a good thing ends

But you and I will always be back then

- BMO

TABLE OF CONTENTS

LIST OF FIGURES

LIST OF TABLES

LIST OF ABBREVIATIONS

AAS - Atomic Absorption Spectroscopy

Abs - Absorbance

AcOH - Acetic Acid

BAM - Beta Barrel Assembly Machine

Boc - *tert*. Butoxycarbonyl

BSA - N,O-bistrimetylsilylacetamide

BSME – Bis-serine Methyl ester, **40**

DATP – diaminoterephthalate, **60**

DIPEA - diisopropylethylamine

DMAP - 4-Dimethylaminopyridine

DMF - dimethylformamide

DMSO - dimethyl sulfoxide

DMSS - dimethyl succinylsuccinate

EDTA - Ethylenediaminetetraacetic acid

ESI – Electro spray ionization

EtOH - ethanol

Fmoc - fluorenylmethyloxycarbonyl

NMP - N-Methyl-2-pyrrolidone

NMR - nuclear magnetic spectroscopy

PAR - 4-(2-Pyridylazo)resorcinol

Pd/c – Palladium on carbon

Ph – Phenyl

pH - $-\log[H^+]$, acidity

pK_a - $-\log(K_a)$

PLP - pyridoxal 5'-phosphate

Ppm – part per million

Ppb – part per billion

QAR - 4-(8-quinolylazo)resorcinol

HBTU - hexafluorophosphate benzotriazole tetramethyluronium

HGII - second-generation Hoveyda-Grubbs metathesis catalyst

ICP - inductively coupled plasma

IR - Infrared Spectroscopy

J - Coupling constant (NMR)

JQ – Janus Quinolone

K_d – Dissociation Constant

LCMS - Liquid Chromatography Mass Spectrometry

MeOH - methanol

MOPS - 3-(N-morpholino)propanesulfonic acid

MS - mass spectrometry

MsCl - Mesyl chloride

OAN – Ortho azo naphthol

QMA – Quinolone methyl anthranilate, **46**

Rf - retention factor

RT - room temperature

tBuOH – tert. Butanol

TFA - trifluoroacetic acid

THF – tetrahydrofuran

TLC - thin layer chromatography

TMS – trimethylsilyl

UV - Ultraviolet

LIST OF SCHEMES

Chapter I. Introduction

Guest Host Chemistry

The process of interacting with an unknown system to elicit change in order to generate a measurement is the basis of guest host chemistry[1]. These systems rely on inter-molecular interactions to facilitate association or dissociation. In its simplest form, guest-host chemistry can be described as follows [2], *figure 1*.

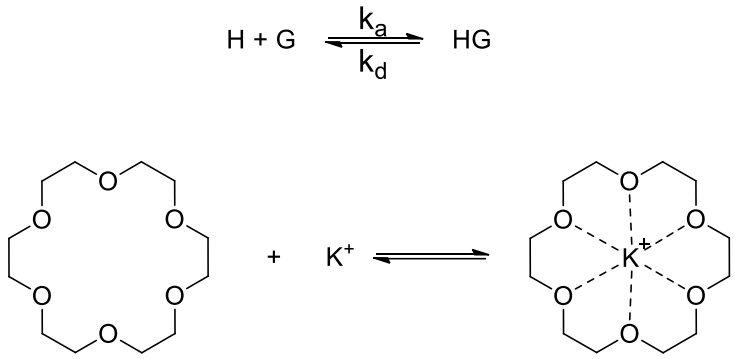

Figure 1: Guest Host Chemistry and 18-crown-6 with potassium

18-crown-6, *figure 1*, was found by Pedersen to be a host for potassium ions. Remarkably 18-crown-6 can solubilize potassium and other ions in very non-polar solvents like hexanes[3]. For his work on cyclic polyethers, Pedersen was awarded the Nobel prize in chemistry[4]. The strength of an association can be most readily understood by taking its inverse, or dissociation. Dissociation affords units of molarity that directly relates to the strength of the interaction. This k_d is a fundamental concept in chemistry that dictates how two species can interact and is seen in most facets of chemistry as a whole[5].

This process is not limited to crown ethers, metal ion chelators have long been known to chemistry[6] and medicine[7]. EDTA is arguably one of the most recognized chemicals in the field of chemistry as a whole and is a known metal ion chelator[8,9].

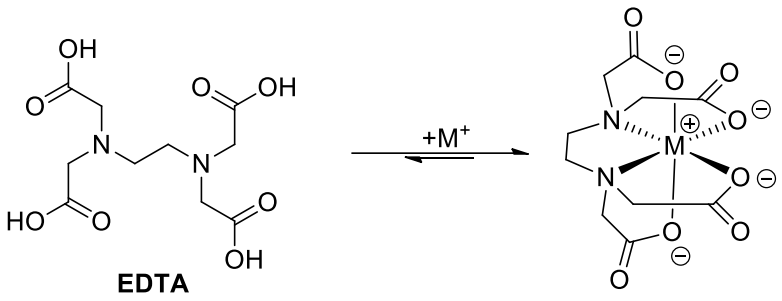

Figure 2: EDTA and Metal Ion Association

EDTA has been extensively studied and its affinity to almost every metal known has been observed. The structure of EDTA lends itself to the favorable interactions with metal ions in that it has enough flexibility and lone pairs of electrons to conform to most metal ion orbitals for first and second row transition metals[9,10]. This represents a much more complicated form of guest host chemistry, in that there are multiple interactions of EDTA toward metal ions that can be explained coulombically, sterically or in terms of solvation energies. One factor worth consideration is the preorganization of EDTA in that, upon one ligand binding to a metal ion, the other ligands will quickly associate due to proximity to the metal ion, aided by coulombic interactions and the net change in entropy from the loss of solvation. The remaining ligands associate quickly enough that the first association to metal ion can often be considered rate determining. All of these factors contribute to the heightened affinity of EDTA toward metal ions, specifically transition metals with 6 empty orbitals like those of the first and second row transition metal ions[10,11].

Guest host systems are a fundamental aspect of almost all biochemical processes[1,5]. These processes are significantly more complicated than association and dissociation, but in many cases can be

simplified as such[5]. Understanding these processes and how to perturb them has led to the development of modern medicine as we know it and so the development of methods for observing these processes is of vital importance to not just chemistry but to life itself[12]. Take for example the movement of zinc in the brain and the work done by Stephen Lippard[13].

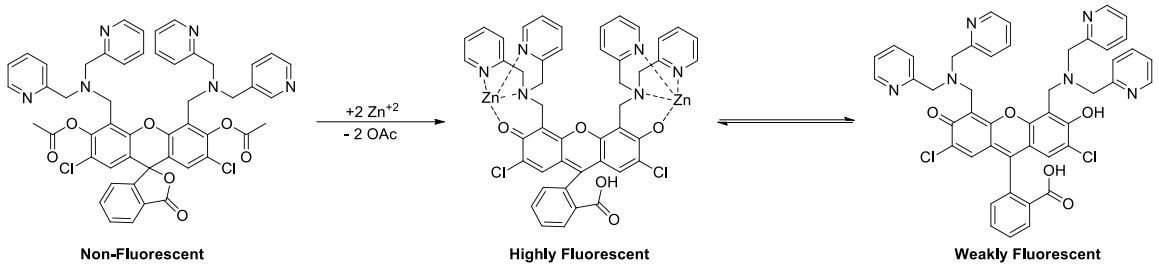

Figure 3: ZP1-TPP a Zinc Ion Chemosensor Developed by Lipard et. Al.

ZP1-TPP is a chemosensor that is selective for zinc metal ions and is incredibly fluorescent once the acetyl groups are removed, upon association with zinc, *figure 3*. This sensor is considered ratiometric, wherein the association with zinc has a fluorescence emission different from the unbound form, this allows for the direct quantification of zinc based on the ratio of bound to unbound sensor[14]. Furthermore, the high quantum yield for this chromophore allows for the detection of zinc ions in real time and in-vivo[14,15]. Being able to observe these processes in real time as well as being able to quantitate metal ion concentrations has illuminated processes that had limited understanding due to the previous inability to directly measure zinc ion concentrations[13].

Developing systems in which these processes can be observed or better understood has been the subject of intense research for as long as these systems were known[1]. Modern day advances have allowed for the development of sophisticated assays and specialized molecules that directly measure these events through secondary processes like FRET or BRET.

Chapter II. Metal Ion Chemosensors

Introduction

The quantification of metal ions in potable water has been of increasing concern over the last century as the harmful effects of metal ions in the body have come to light[16]. Metal ions are cofactors required for life however when metal ions that are incongruent to the biochemistry of living organisms are present, significant problems arise. Take for example lead, once known for its durability as water carrying pipes[17], its sweetening effects[18] as well as a chemical enhancer for generating higher octane rating in fuel[19]. Lead is a toxic metal[20] that accumulates in the body over time and causes significant problems with the kidneys, cardiovascular systems, reproductive systems and the nervous system[16,20,21]. It is known to cause developmental delays in children and permanent brain damage[19,22,23]. These factors have led the EPA to determine that no amount of lead in drinking water is permissible[20].

The EPA has outlined acceptable levels of metal ions in aqueous systems[16,24]. Currently multiple cities and townships are in far excess of those acceptable levels in the US[24]. This is the result of decaying infrastructure in addition to the difficulty in treating wastewater from industry to the levels dictated by the EPA. The cost of remedying this infrastructure has been deemed too substantial in many cases and as a result there has been limited interest in fixing these contaminated systems. Furthermore, testing these water systems is a long process that often produces answers long after the damage has already been done[17]. Metal ion remediation is used throughout the nation via processes that use polymers and sedimentation to remove metal ions[25,26], in many industries, this is done in house while sample testing and prepping is done via auxiliary labs[27].

Current methods for quantification of metal ions in aqueous solutions is heavily reliant on large and expensive analytical instruments like ICPMS and flame AAS. Currently, for metal ion qualification and quantitation, one would be required to obtain a sample and send it off for analysis in a lab equipped

to take those measurements[27]. This means that there exists a turn around time on these measurements that is often longer than the time it takes to treat waste water and pump it back into nature. Too often the result is non-compliance with the EPA such that manufacturers are constantly fined for excess levels of metal ions in waste water[24].

To circumvent the issues arround the treatment of wastewater, a system which utilizes a faster method of quantification needed to be developed. Measurements around UV-Vis absorbance are limited in rate by the speed of light and so a system that utilizes UV-Vis spectroscopy was envisioned. Because these measurements involve absorbance and fluorescence, a chemosensor based on these properties needed to be developed. When considering absorbance vs. fluorescence, the longevity of the sensor needed to be taken into account. UV light is typically used to excite fluorescent molecules, this light is short wave and very destructive over time when it comes to chromophores and can lead to photo bleaching[28]. Visible light is sufficiently low energy that it was believed a chemosensor that operated on the basis of absorbance in the visible range would generate a long lived sensor.

The most obvious choice of chromophore/chemosensor was based on azo dyes which have been long utilized in many industries[29], e.g. textiles, fabrics, food, plastics etc... Some azo dyes have been long known to chelate metal ions and in doing so cause a change in absorbance of the dye[30,31]. And so, if multiple azo dyes with different metal ion selectivities could be developed, there may be a chance at developing a sensor that continuously measures dissolved metal ions in waste water systems. The work described herein relates to the development of functionalized azo dyes that are capable of covalent attachment to a solid support that was developed cocurrently.

In this system, metal ions are detected via the change in absorbance of chemosensors as they chelate metal ions in a flowing solution. To achieve a continuous measurement that did not result in loss of sensing capabilities, the chemosensors had to be immobilized on a solid support. The solid support

chosen for this project is a hydrogel polymer similar to the structure of soft-contact lenses in that they swell with water and are optically transparant. The solid support itself is functionalized such that modified azo-dyes can be covalently attached to the solid support without washing out.

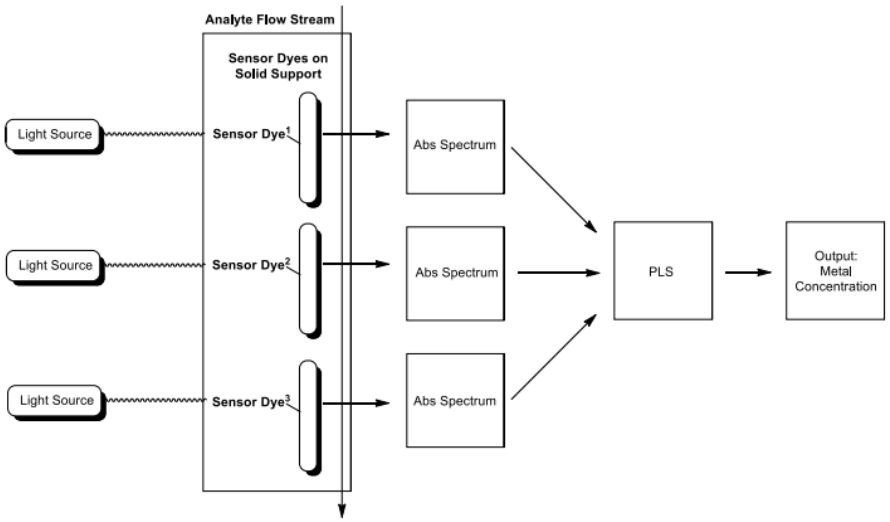

Scheme 1: Generalized schematic diagram of the sensor

The hydrogel polymer sits in a custom designed flow cell between a lightsource and a detector. Treated waste water then flows past the surface of the hydrogel polymer and changes the absorbance of the transparant polymer if metal ions are present. From a series of spectral deconvolutions and variables associated with accumulation over time, the identity and quantity of the metal ions can then be determined.

Azo Dyes

Azo dyes are used in many industries as the color function of products[29]. These dyes have different structures and functional groups that lend to the overall color of the dye. There has been a significant amount of research into azo dyes as they offer a rapid method of generating large libraries with

spectroscopically unique attributes. Minor changes to the structure of azo dyes can lend itself to dramatic changes in color[29].

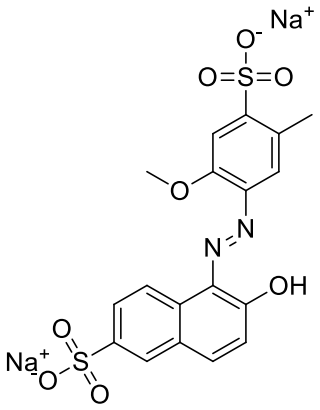

Figure 4: Allura Red AC or FDC #40 a Red Food Coloring Azo Dye

One commonly available azo dye is Allura Red AC, *figure 4*. This dye is special because it is used as food color additive also known as FDC #40[32]. This dye has been the subject of some controversy as it was found, in 2011, that many azo dyes are able to degrade into anilines, nitrosyl and nitro compounds over time and a set of researchers found a link between behavioral changes in children and these degrading azo dyes[32,33]. These pieces were not well understood at the time which resulted in most azo dyes being removed from food and textile industry products voluntarily. Since then, many of the azo dyes were found to be harmless even after degradation at the concentrations they are found in food and textiles, most notably FDC #40[34].

General Structure and properties

Azo dyes are generally made from aromatic amines and a phenol or aniline. Azo dyes are highly absorbing with extinction coefficients in the 10^5 to 10^6 range. Certain azo dyes are known to be metal ion chelators, the most notable of these being PAR (pyridyl azo resorcinol, **1a**).

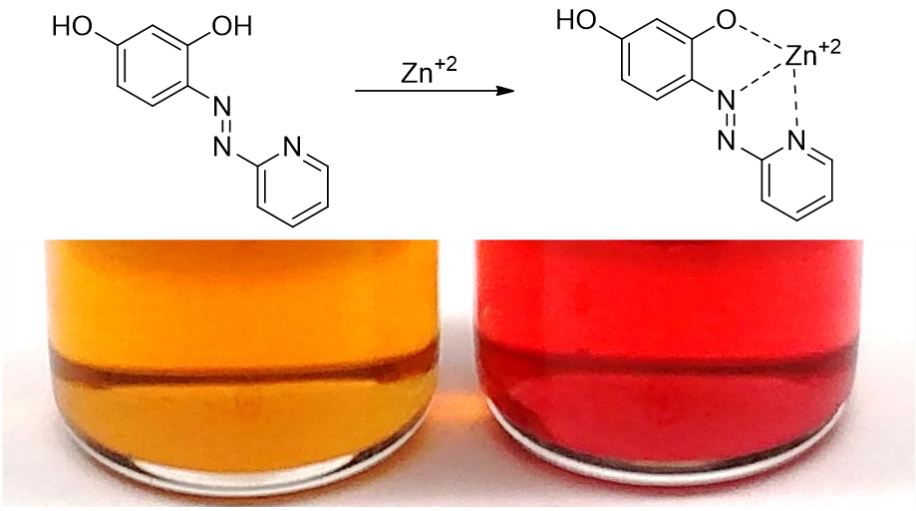

Figure 5: PAR Zinc Association and Color Change

2a, PAR, tends to have a response to divalent metal ions through changes in absorbance. The response can be measured via UV-Vis spectroscopy down to ppb levels of dissolved metal ions. The change in response has been found to be associated with the formation of a 2:1 complex of 2 **2a** to 1 divalent metal ion. **2a** is not selective for all divalent metal ions and only confers a change in absorbance from a select few metal ions, Ni, Cu, Zn etc.

An array of metal ion chemosensors was developed with the hope that their selectivity for metal ions would be different among themselves. Then from an aggregate response of multiple azo dye chemosensors it was postulated that metal ion quantity and quality could be ascertained from a mixture of metal ions.

General Synthesis of Azo Dyes

There are multiple methods for generating azo dyes[35–37]. The most generally accommodating procedure uses acid and nitrite to form a diazonium salt which then electrophilically attacks ortho to an aromatic amine or phenol, *scheme 2*.

Acidic Method - Diazonium

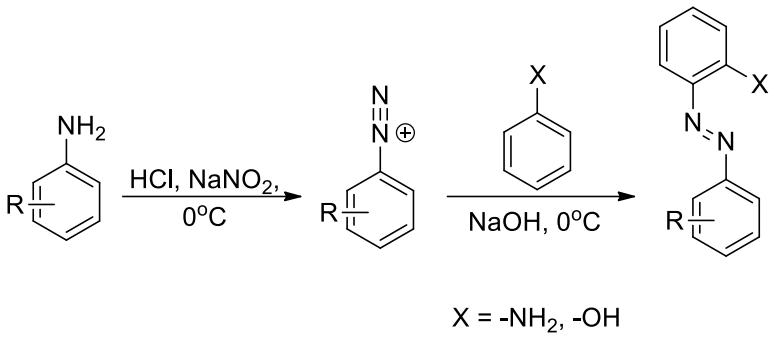

Scheme 2: Acidic method for generating Azo Dyes

This method works well for most electron-rich aromatic amines where the C -$^{+}N_2$ bond is best stabilized. This sequence is problematic from the stance that electron poor aromatic amines like 2-aminopyridine are unable to form azo dyes under these conditions.

Diazonium salts are known to undergo a variety of reactions like the Sandmeyer reaction[38,39] or in some circumstances they can be used in cross coupling reactions like Suzuki couplings[40]. Diazonium salts tend to be spontaneously explosive when isolated[41], and the reaction conditions to form diazonium salts also generates NO when the reaction is heated above ~5 °C. Safety precautions must be taken into consideration when generating and handling diazonium salts.

Electron poor aromatic amines will readily undergo ipso-substitution when a diazonium salt is formed. This is most clearly seen when looking at aromatic amines like 2-aminopyridine.

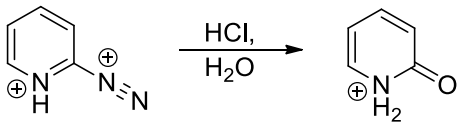

Figure 6: Electron Poor Diazonium Hydrolysis

Because this reaction is performed in acid, there is some fraction of the pyridine 2-diazonium that is protonated on hetero-nitrogen. This dramatically enhances the ipso-substitution of H_2O at the 2 position which then results in the formation of 2-pyridone. A common procedure to convert 2-aminipyridine into 2-alkoxypyridine take advantage of this phenomenon[42].

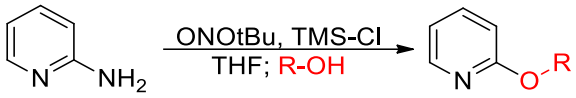

Figure 7: Synthesis of 2-pyridyl ethers

To surmount this, a method that uses base to form a diazonium like product is needed.

Electron poor aromatic amines are capable of making azo dyes, but they require much harsher and longer reaction times to form in any appreciable yield[35,43], *scheme 3*.

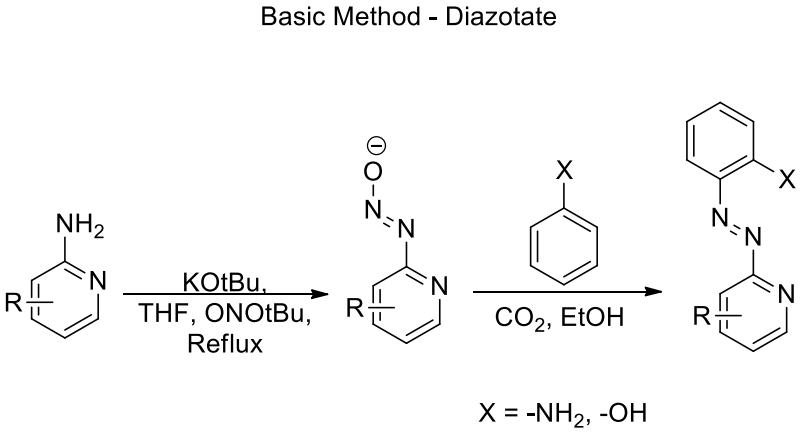

Scheme 3: Basic Method for generating Azo Dyes

This reaction works by deprotonation of 2-aminopyridine followed by substitution of the tert butyl nitrite to form a diazotate. The diazotate is then suspended in EtOH containing the phenol/aromatic amine and CO_2 is bubbled through the reaction mixture over multiple days as a coolant and buffer. This allows for the slow conversion of diazotate to diazonium under slightly basic conditions and facilitates

the coupling. This process is unfortunately incredibly slow and often poor yielding, on the order of 20 – 50 % and occasionally above 70% after multiple days.

While there are other methods of generating azo dyes, these two methods were applicable to all the azo dyes generated via this research.

Synthetic Targets – High and Low affinity Chemosensors

Both high and low affinity sensors have been synthesized. The largest difference between these groups are the number of ligands and their arrangement when bound to metal ions.

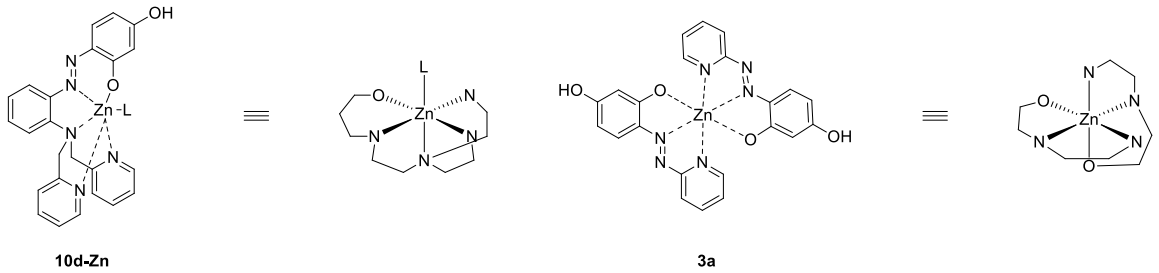

Figure 8: High Vs. Low Affinity Azo Dyes

The high affinity dyes have 4 – 5 ligands that can satisfy the orbitals of the metal ion and generally have a ligand on the metal as well e.g., H_2O. The low affinity dyes tend to form complexes without additional ligands from H_2O or elsewhere. The formation of the metal complex is associated with a change in absorbance either due to cis-trans tautomerization of the azo bond upon association of metal ion or from the direct interaction of the azo bond to the metal ion.

It was assumed that in order to develop a continuous flow system that can monitor metal ion concentration it would take a very selective and very high affinity chemosensor. The first target was the creation of a presumed chemosensor that would be selective for zinc in binding and give a large spectral change in absorbance, **10d**.

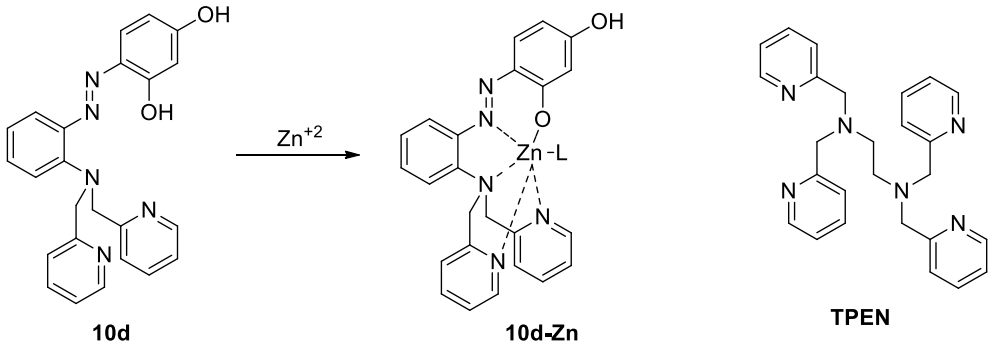

Figure 9: TPEN vs. High Affinity Azo Dye

10d utilizes dipicolylamine, **7a**, which is a known zinc ion chelator[14,15,44–46]. Dipicolylamine is used in extremely high affinity ligands[46] for zinc ions like TPEN[47]. Thus, its inclusion into the structure of the desired product was presumed to give the dye selectivity towards zinc. Retrosynthetic analysis indicates the reaction sequence could start from dipicolylamine which could then be converted into an o-nitroaniline. Reduction of this nitro-aniline and azo coupling conditions would then make the desired azo dye.

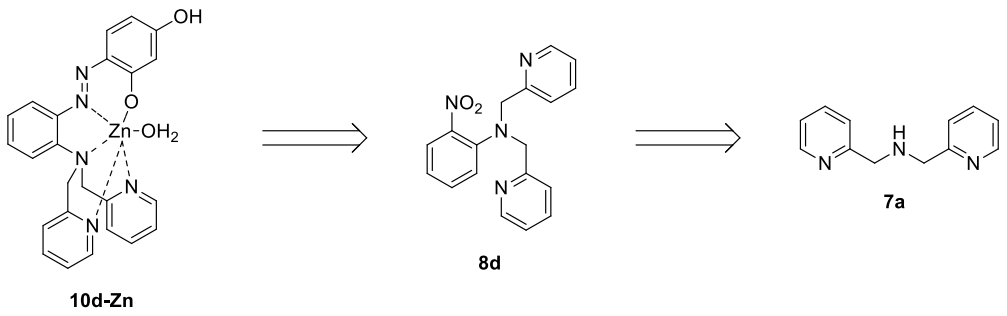

Figure 10: Retro Synthetic Analysis of High Affinity Sensors

A set of conditions was found to make this product starting with the synthesis of 2,2'-dipicolylamine, **7a**.

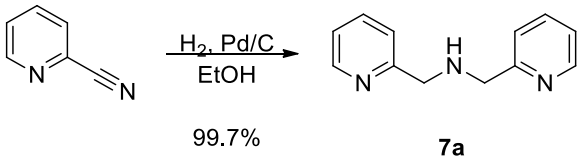

Scheme 4: The synthesis of 2,2'-dipicolylamine, 7a

2-cyanopyridine can be quantitatively converted into **7a**. This requires maintaining 1 atm of H_2 as the reaction progresses which can be accomplished by leaving a balloon of H_2 on the reaction mixture and replacing as needed. Ammonia is evolved as a side product of the reaction. It is believed that the imine that forms from the first equivalent of hydrogen is still tightly associated with the palladium such that another fully reduced 2-picolylamine can add into the imine and lose ammonia, *figure 11*.

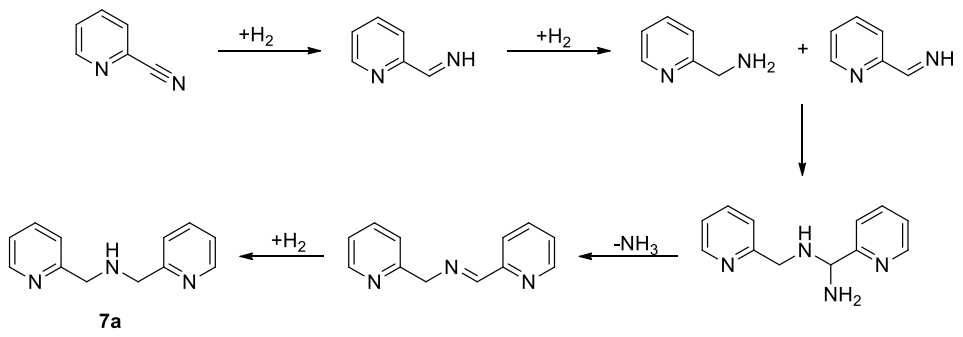

Figure 11: Proposed Mechanism of Dipicolylamine Formation

It is believed that the inclusion of a weak acid like acetic acid should aid in the transformation of picolylamine to the desired **7a** by encouraging the loss of ammonia as the reaction progresses. This does add the potential for overreaction and the formation of tripicolylamine, but one could conceivably find the right ratio of acetic acid to substrate to encourage only the formation of **7a**. As is, the reaction takes about a week at a constant pressure of 1 atm H_2 but affords the product in quantitative yields.

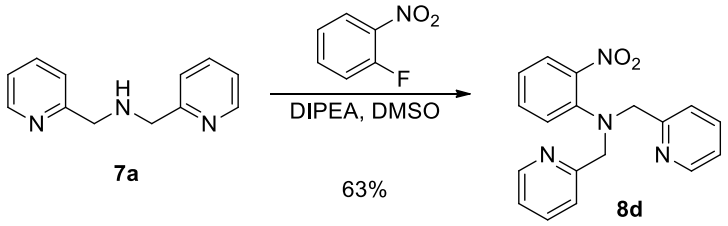

Scheme 5: The synthesis of o-nitroaniline 8d

The second step is incredibly slow, the substitution of **7a** in DMSO takes on the order of a week to get to 63% yield. This is due in part to dipicolylamine being a hindered 2° amine and the inability to heat these reactions without significant side product formation. Once a set of conditions had been made to substitute an amine with o-fluoronitrobenzene, a library of compounds was generated, *table 1*.

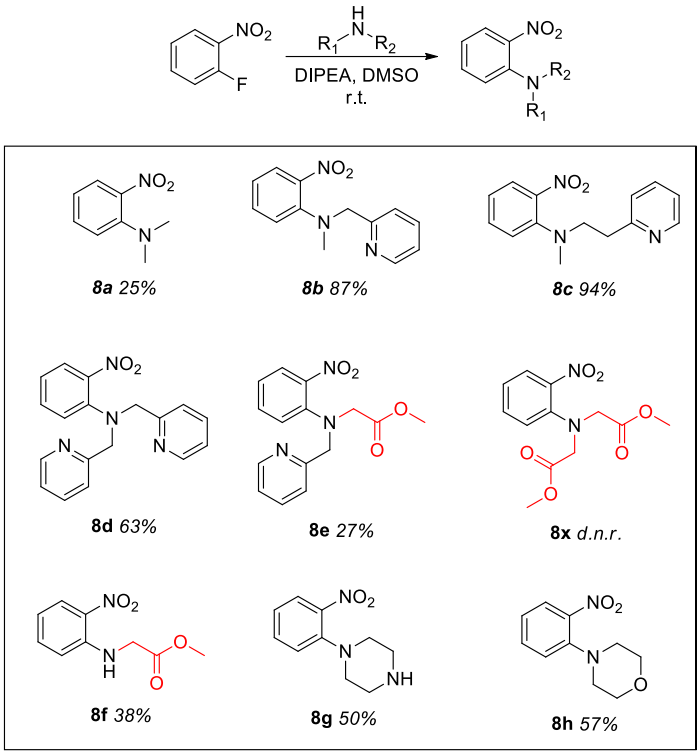

Table 1: Library Synthesis of o-Nitroanilines

Hindered 2° amines appear to react more poorly than unhindered 2° amines. The only amine that would not react under these conditions was iminodiacetate which is very hindered and effectively non-nucleophilic as a double amide. After substitution, hydrogenation over Pd/C afforded the substituted aniline. The procedure for reduction of **8** to **9** is run immediately prior to diazotization due to the oxidizable nature of o-diaminobenzenes. However, some reduced products, **9a**/**9b**, have been isolated to ensure efficacy of this method, *scheme 6*.

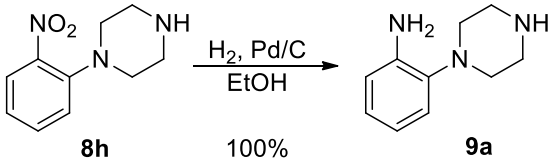

Scheme 6: Reduction of o-Nitroaniline 8h to 9a

These anilines, **9**, should be able to react via the acidic method to produce the azo coupled product, but some appeared to suffer from a significant complication, *figure 12*.

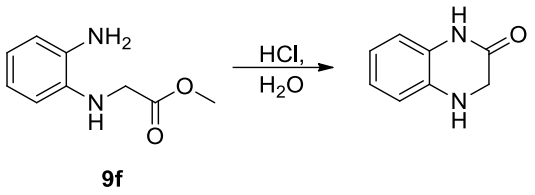

Figure 12: Claisen Condensation of o-glycineaniline

All of the **9** variants that had a glycine-like structure appeared to have undergone a Claisen condensation faster than diazonium could form. The same situation arose when the derivative was an acid, thus only derivatives that did not have a glycine-like residue were able to be coupled via acidic azo coupling. The acidic method of azo dye formation was used because these substituted anilines are very electron rich and were expected to readily form a diazonium salt and couple, *scheme 7*.

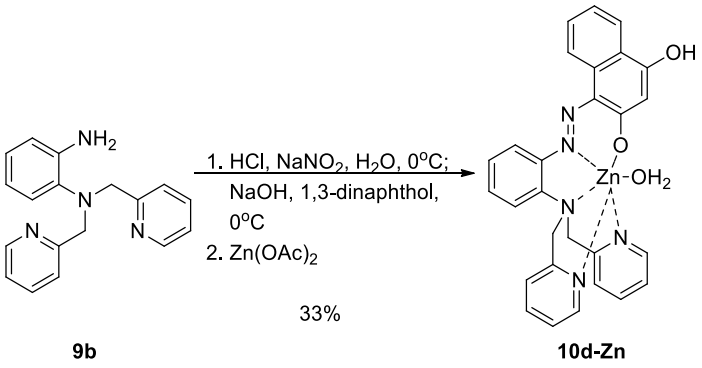

Scheme 7: Synthesis of High Affinity Sensor 10d-Zn

10d is not very crystalline in its unbound form. It was discovered that the addition of zinc acetate would precipitate **10d-Zn** selectively from the reaction mixture. Despite the low yield, which is likely a steric

problem, the method of precipitation with zinc affords a very clean product. Complexes have been observed via NMR with correct stoichiometry containing a single molecule of H_2O per azo dye when made via this method.

10d, 11 and **10d-Zn** were compared spectroscopically via ^1H NMR, *figure 13*.

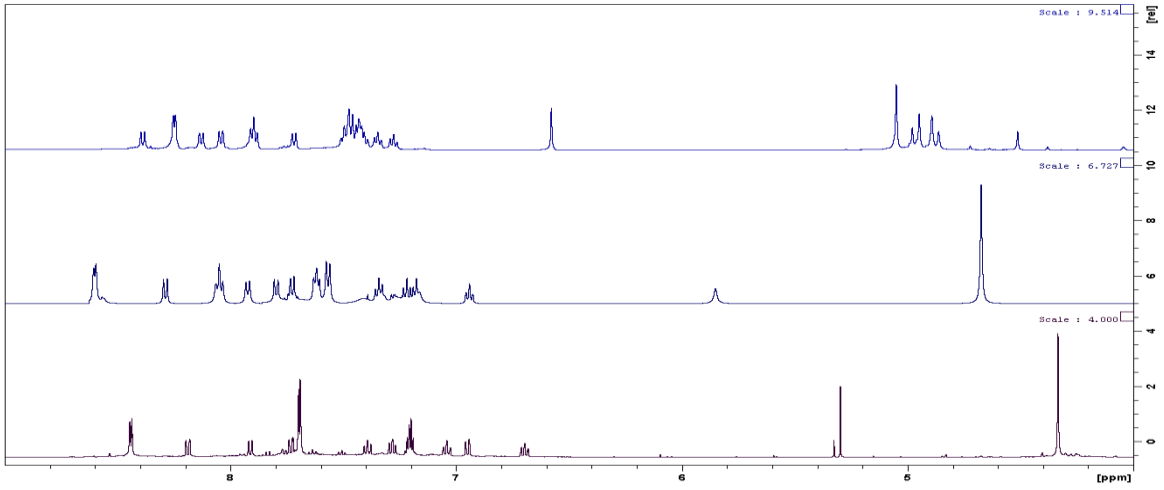

Figure 13: ^1H NMR of 10d (bottom), 10d-Zn (middle) and 11 (top)

The peaks associated with the pyridine portion of the molecule appear to shift from unbound to bound zinc complex. Notably, the pyridine 2-hydrogen was seen to shift downfield upon association with zinc. Further, the methylene peaks for the picolylamine portion of the molecule also shift down filed after association with zinc, curiously upon alkylation the methylene hydrogens split into broad doublets which is indicative of a restricted conformation, this is not seen in the non-alkylated spectrum.

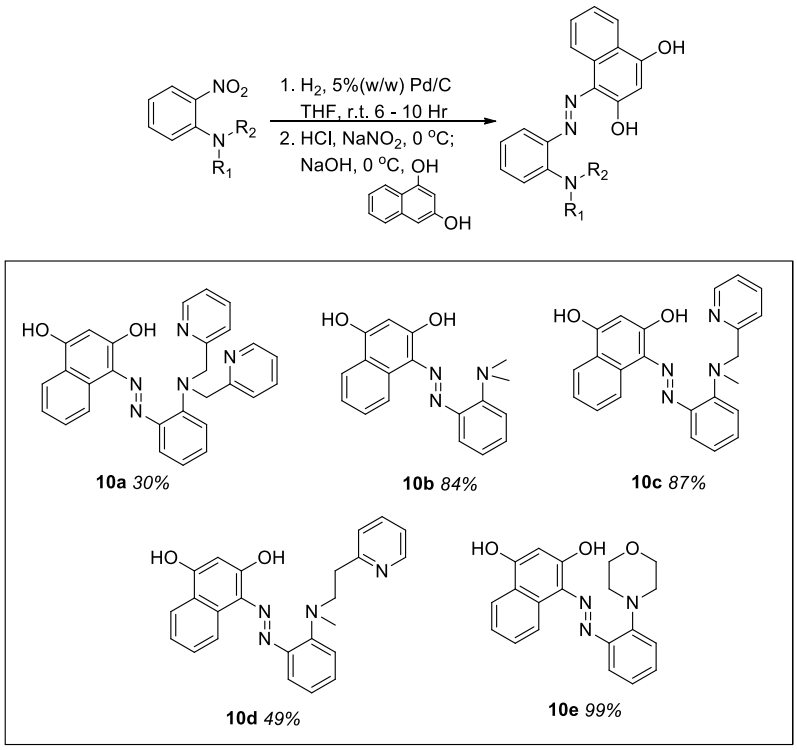

Figure 14: Library of High Affinity Azo Dyes

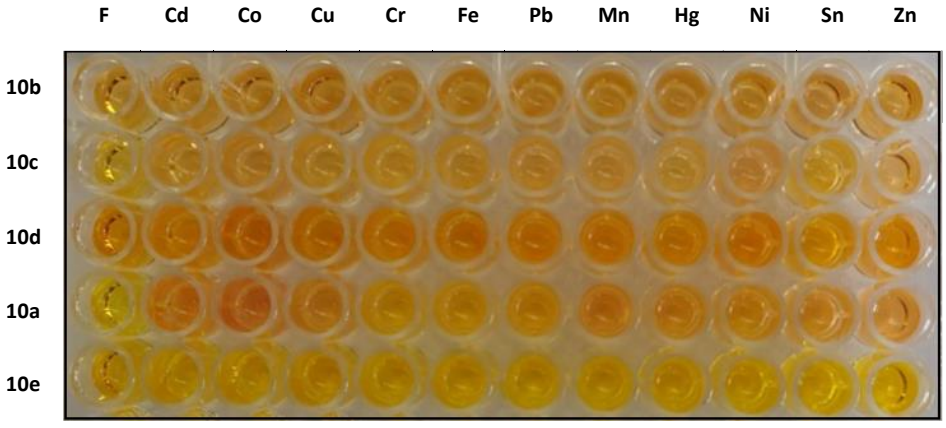

Figure 15: Metal Ion Response of High Affinity Azo Dyes

From the initial library of azo dyes that was attempted **10a-e** were compared for their metal ion selectivity.

More delicate analysis of UV-Vis spectra highlighted significant differences in selectivity for metal ions, *table 2*.

	Free	Al	Cd	Ca	Cr	Co	Cu	Fe	Pb
10a	454		**491**			**499**	**492**		**491**
10b	462	464	457	**479**	471	**477**	**493**		**446**
10c	457		460			**504**	**491**		466
10d	457		461			**491**	**489**		**466**
10e	454						**482**		463

	Free	Mg	Mn	Hg	Ni	K	Na	Sn	Zn
10a	454		**503**		**502**			**465**	**491**
10b	462		474		468	481		**447**	467
10c	457		463	458	**491**			473	**487**
10d	457			460	**479**			**478**	**484**
10e	454			462				**477**	

Table 2: Max Wavelength for each High Affinity Dye with respect to each metal ion (Joe Laboets)

There appears to be little difference between **10a** and **10c**, which makes sense given the two differ only by number of ligands. When compared, **10d,** which was thought to afford significantly different selectivity's, shares the same response as **10a** overall. Surprisingly, **10b** does not appear to yield a response to zinc and its metal ion response overall is weak compared to the others excluding **10e** which does not appear to have any metal ion selectivity. This array can distinguish between Cd, Ca, Co, Cu, Pb, Mn, Hg, Ni, Sn, Zn from one another when considering the aggregate response from this array.

10d-Zn had to be functionalized before it could be attached to the solid support, *scheme 8*.

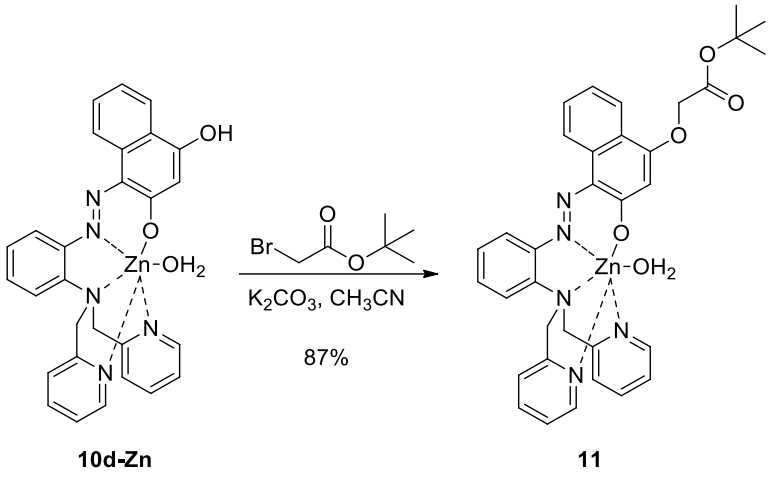

10d-Zn **11**

Scheme 8: Alkylation of High Affinity Dye

In this reaction, the zinc helps to prevent the other amines and phenol from reacting with tert butyl bromoacetate. The product of this reaction can then be saponified and undergo standard peptide coupling methods to become covalently attached to an amine terminated solid support. It was thought that alkylation of this distal phenol caused a change in the absorbance profile of the dye such that the difference in metal bound and unbound dye were more similar. As a result of these issues the sequence was modified to make the point of attachment further away from the conjugation of the azo dye itself.

Literature search afforded a procedure to take o-fluoronitrobenzene and place a sulfonamide meta to the nitro group[48], *scheme 9*.

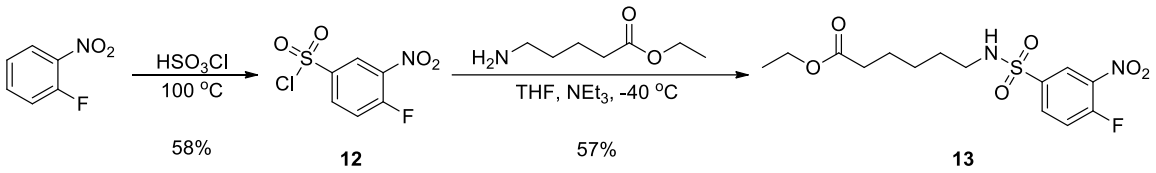

Scheme 9: The Synthesis of fluoronitrosulfonamide 13

The first step makes a sulfonyl chloride on the benzene ring, this is the most reactive portion of the molecule and thus addition of ethyl 6-aminohexanoate forms the desired sulfonamide **13**. The formation of the sulfonamide does two important things. Firstly, it adds a handle for attachment to amine terminated polymers far away from the chromophore core. Secondly the sulfonamide is sufficiently electron withdrawing that it increases the reactivity of fluorine substitution toward the level of 2,4-dinitrofluorobenzene. This synthesis, *scheme 10*, requires a column to separate sulfonamide-nitro-fluorobenzene from sulfonamide-nitro-aniline.

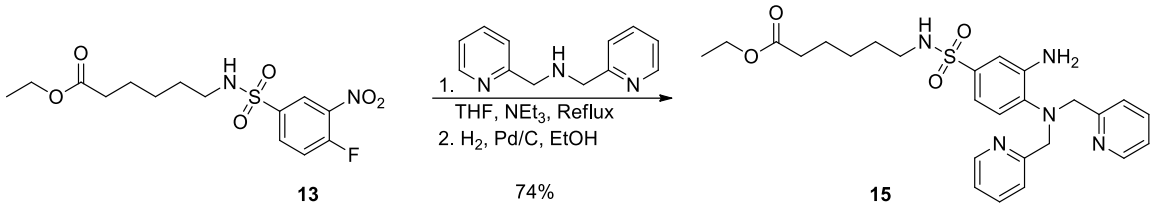

Scheme 10: Synthesis and reduction of o-nitroanilinesulfonamide

Substitution of **13** with dipicolylamine goes in higher yield and over a much shorter time span, hours compared to days. This illustrates the heightened reactivity of **13** compared to o-fluoronitrobenzene.

Reduction over palladium on carbon goes quantitatively over 6 – 10 hours. A small library of compound **14** variants was created from **13** to screen its reactivity, table 3.

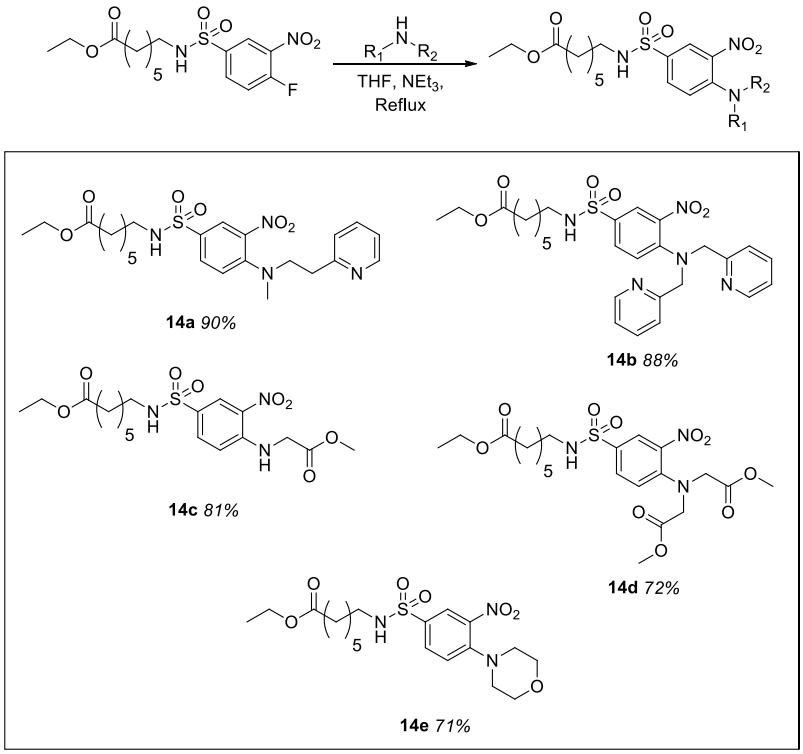

Table 3: Library Synthesis of o-nitroanilinesulfonamides

From this data the clearest indication of a more reactive species can be seen with the successful substitution of iminodiacetate which was found to not occur with the simple o-fluoronitrobenzene. Thus, this route constitutes a method to substitute less reactive ligands.

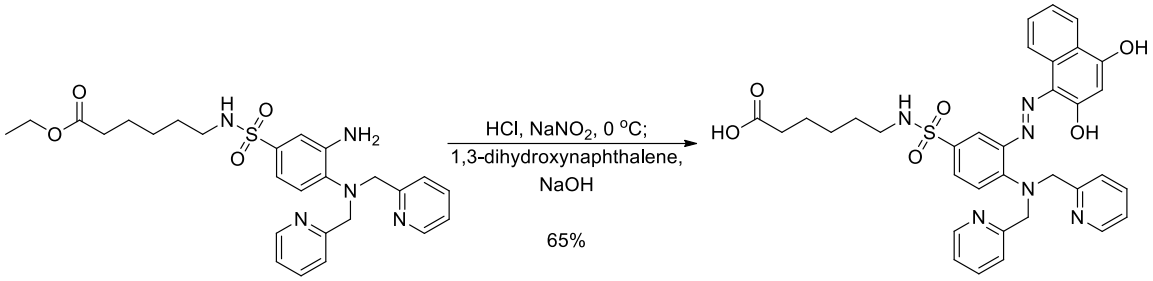

15 **16a**

Scheme 11: Synthesis of Functionalized High Affinity Dye

The azo coupling, *scheme 11*, also works well with a 65% yield of isolated metal free dye compared to the 33% of metallated dye from the original route. Across all steps starting with o-fluoronitrobenzene the yield is 16 - 19%. The azo coupling was performed for three naphthols to determine how the naphthol portion of the molecule affects selectivity as well as the native absorbance of the molecule, *figure 16*.

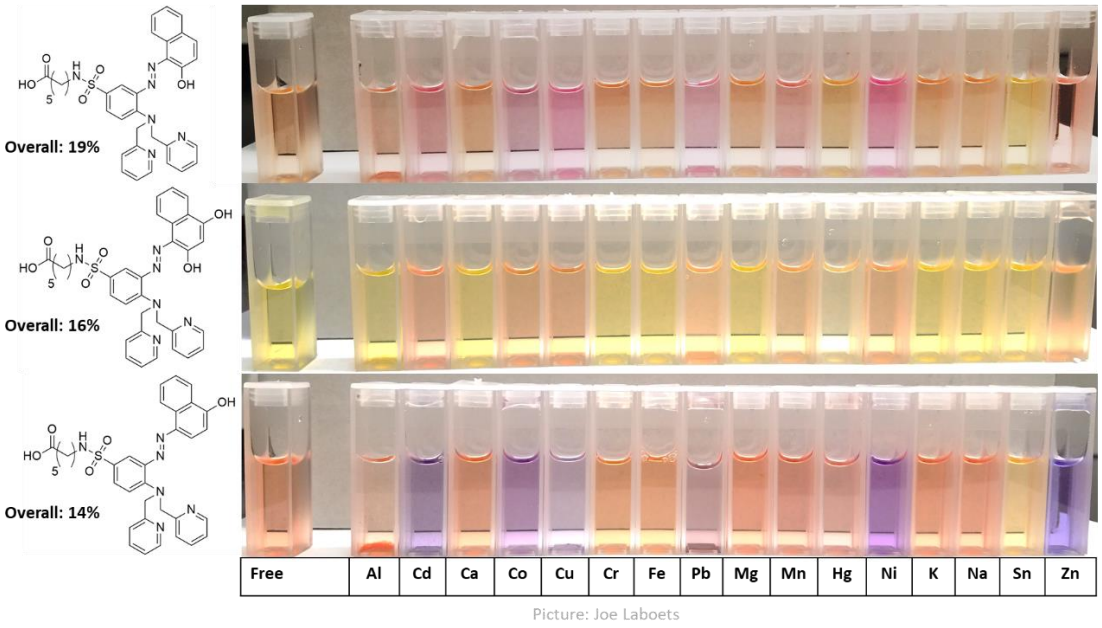

Figure 16: Metal ion response of the high affinity sulfonamide sensor array

These molecules differ in the position of their phenols and number of phenols. Note the most dramatic color change upon ligation of a metal ion is for the dye in which there is only a phenol para to the azo bond. This is a very highly conjugated molecule that likely tautomerizes upon ligation of metal ions to the N-H ketone tautomer therein dramatically changing the length of conjugation of the molecule and resulting in a dramatic (~100+ nm shift in absorbance). Aside from the difference in native absorbance, the metal ion selectivity appears to be identical, which makes sense given the nature of the ligand, however it may be possible to use the unique metal ion responses as a means of discriminating metal ions as opposed to a binary system of yes and no for data collection. Furthermore, one may notice the degradation of azo dye in the tin and mercury samples shown above, this is likely the result of reduction of the azo bond.

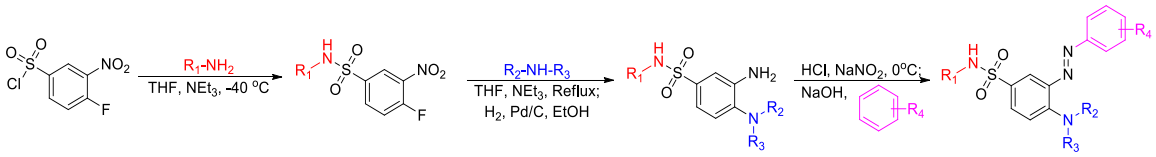

Scheme 12: Functionalized High Affinity Dye Sulfonamide Synthesis

This pathway, *scheme 12*, allows for variation at each step. First the sulfonamide formation should go with any aliphatic amine and introduces a handle far away from the chromophore of the molecule. Second is the ligand substitution which can work with almost any amine or other nucleophilic ligand. Lastly the phenolic portion of the molecule can be modified with any phenol/aromatic amine. The biggest draw-back of this sequence is the need for multiple columns to purify intermediates, specifically for the sulfonamide-nitro-fluorobenzene product which runs in similar Rf to its bis substituted side product. This sequence affords an azo dye that can be readily attached to a solid support with no change in spectra compared to the free dye.

The biggest issue with these sensors is that their affinity to metal ions is significantly higher than was assumed during the initial design of the molecule. The K_d for zinc binding to one of these dipicolylamine sensors was deemed to be too high for even a 15 cm pathlength cell to accurately determine and so its affinity was approximated using EDTA in competition.

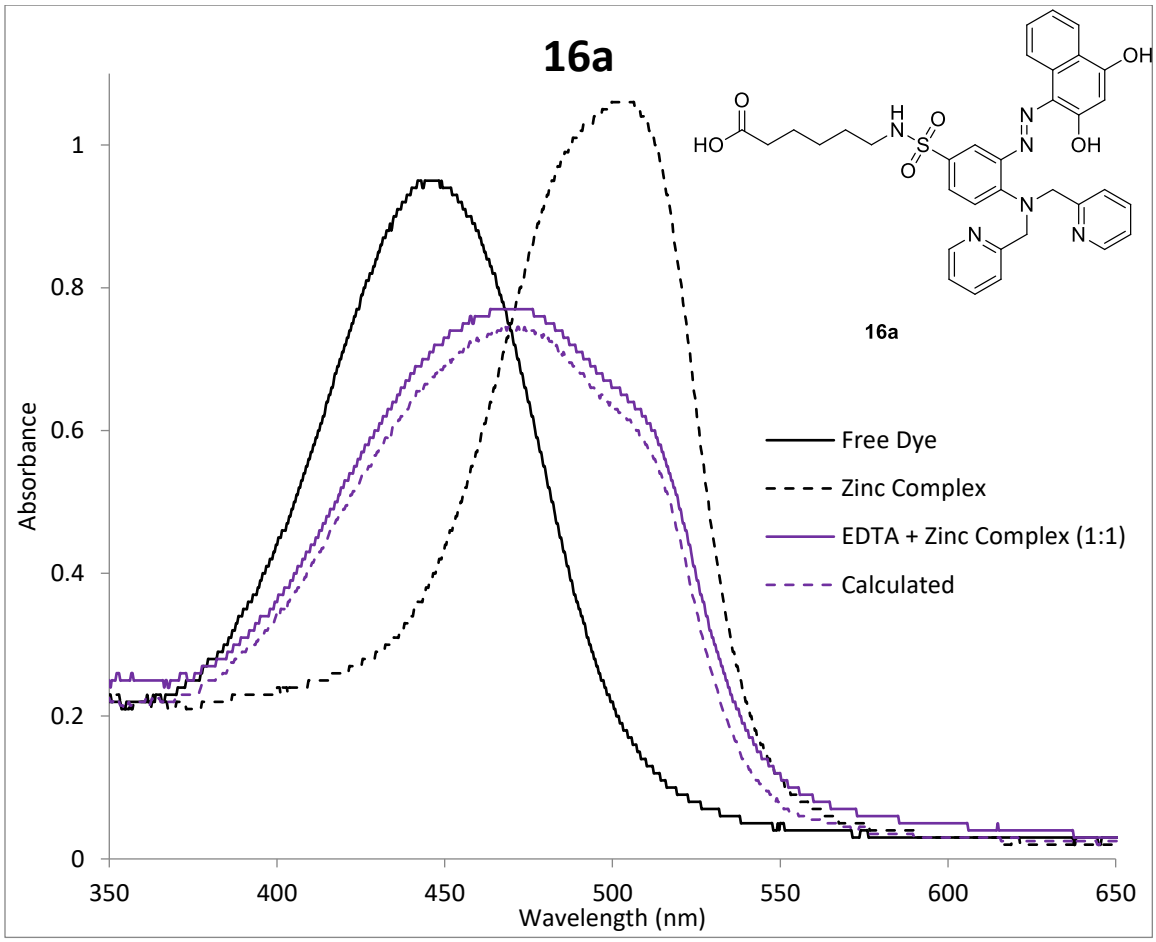

Figure 17: Zinc response of 16a

Shown, *figure 17*, are spectra corresponding to high affinity dye **16a** in various states. Note that the calculated spectra (the average of the free dye and zinc complex spectra) is almost identical to the 1:1 EDTA and azo dye zinc complex.

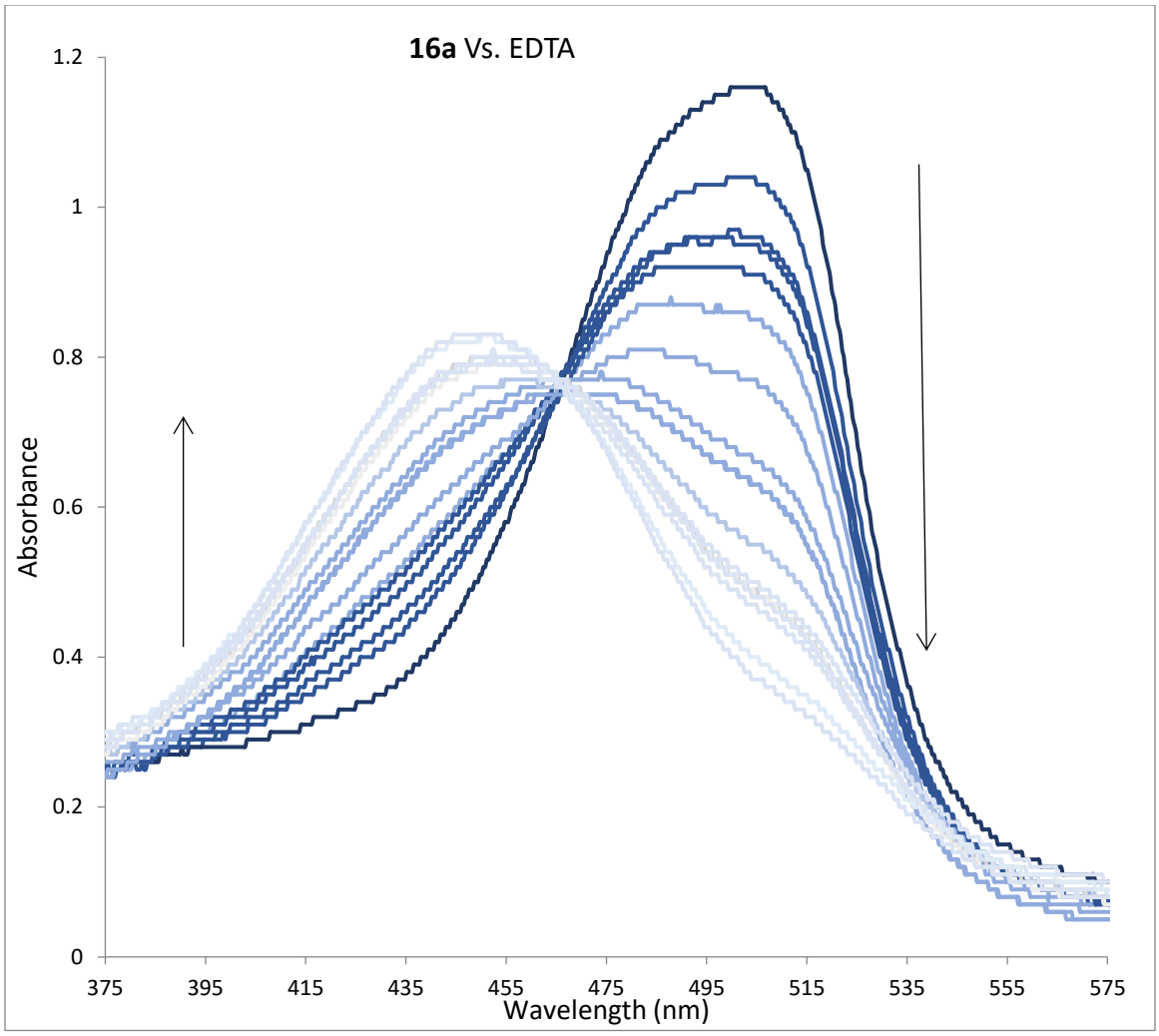

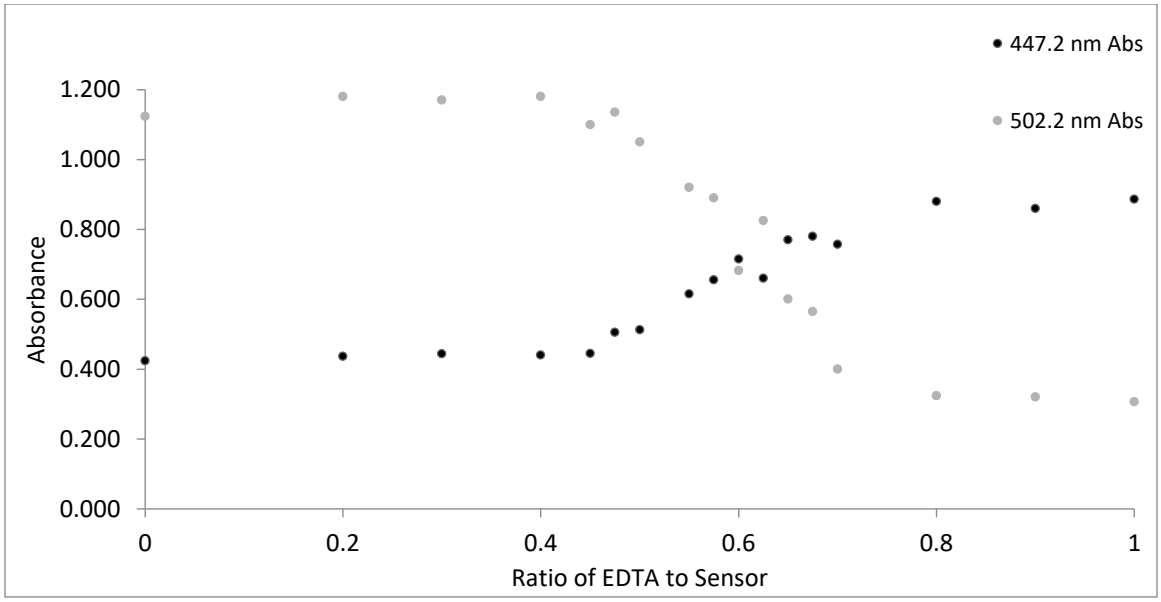

Figure 18: Competition titration of 16a with EDTA

The K_d for EDTA toward zinc is ~ 10^{-16} M, from the titration data it was found that this sensor is approximately within an order of magnitude weaker in affinity for zinc than EDTA. Thus K_d ~10^{-15} M for zinc or in the femtomolar range.

With an affinity this strong and for the purpose of this project, these high affinity sensors were deemed un-useable for reasons that were determined after the dye was placed onto the amine terminated solid support.

Because of the results for the high affinity dyes regarding approximate K_d, attention was shifted toward the synthesis of lower affinity (K_d ~10^7) dyes that would not require large amounts of EDTA to remove metal ions or large amounts of concentrated acid. And so, tri-dente azo dyes were generated that are similar in structure to PAR but differ in a variety of ways.

Because the acidic method of making azo dyes is quick, libraries of azo dyes can be made rapidly and tested against metal ions even as crude mixtures. The first library of low affinity azo dyes attempted used 8-aminoquinoline as the electron rich aniline and a variety of naphthols to couple to, *scheme 13*.

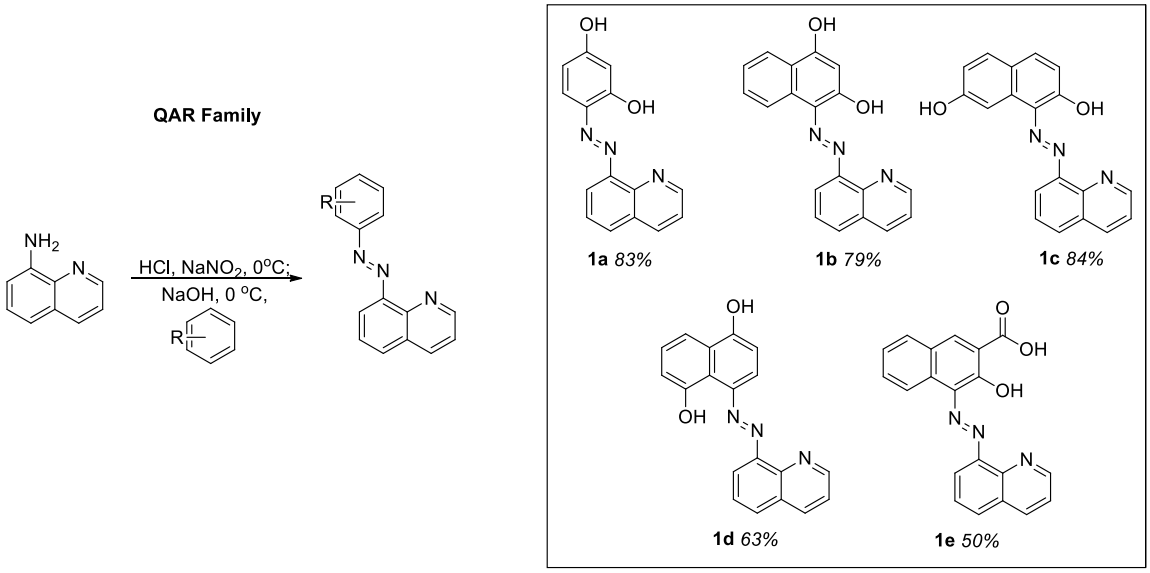

Scheme 13: Library Synthesis, the QAN Family

The yields vary from 50 - 84% when coupling 8-aminoquinolone to various naphthols. Each of these dyes are unique in their response to metal ions, but most of those changes are incredibly minor with respect

to absorbance. This could be a tautomeric effect where because the azo-bond itself is not switching between E and Z the only response being measured is the direct association of metal ion to azo dye.

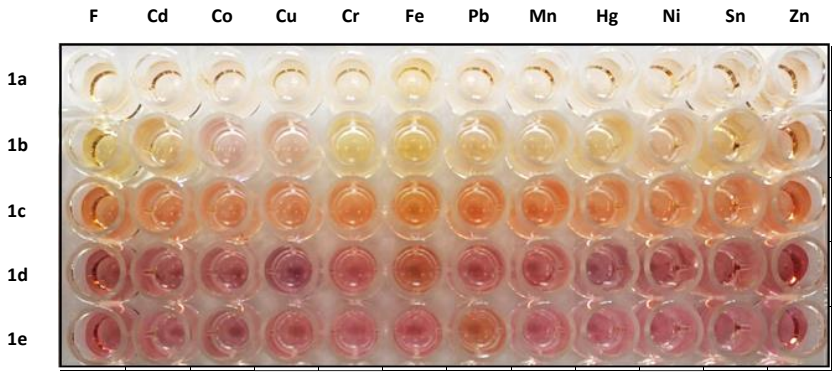

Figure 19: Metal Ion Response of QAN family to metal ions

These azo dyes have limited changes in absorbance upon binding of metals, *figure 19*, and this holds true for all the naphthol variants.

	Free	Al	Cd	Ca	Cr	Co	Cu	Fe	Pb
1a	413	**468**	453			**525**	**492**		453
1b	460				456	**568**	**526**		450
1c	482				473		485		
1d	532				**545**		547		534

	Free	Mg	Mn	Hg	Ni	K	Na	Sn	Zn
1a	413		**463**		**386/492**			**413**	**388/490**
1b	460		471	**480**	**550**			460	**529**
1c	482								
1d	532			544					

Table 4: Max Wavelength Response for the QAN Family to their Respective Metal Ions (Joe Laboets)

The metal ion responses, *table 4*, indicate minor changes in absorbance but appear to be sufficiently different in their absorbance profiles to work as an array, albeit less so than other dyes.

Despite their limited use as metal ion chemosensors, **1d** is incredibly solvatochromic. This was noticed when cleaning glassware that had the dye in it with different solvents and seeing a variety of colors.

When compared to the polarity of the solvent, the shift in absorbance can be seen more clearly.

	Dipole moment (D)	λ_{Max}	
Toluene	0.3	492 nm	DMSO
$CHCl_3$	1.2	476 nm	NMP
Et_2O	1.2	487 nm	DMF
CH_2Cl_2	1.6	502 nm	MeOH
tBuOH	1.7	504 nm	Acetone
iPrOH	1.7	520 nm	EtOH
EtOH	1.7	507 nm	iPrOH
MeOH	1.7	510 nm	H_2O
EtOAc	1.8	491 nm	Ether
Pyridine	2.4	591 nm	EtOAc
NEt_3	2.8	495 nm	Toluene
Acetone	2.9	508 nm	Dioxane
DMF	3.8	580 nm	THF
CH_3CN	3.9	563 nm	Dichloroethane
DMSO	4.0	513 nm	$CHCl_3$
			CH_2Cl_2

Table 5: Dipole of solvent compared to 1d max wavelength (Joe Laboets)

From this data, *table 5*, it appears that there is a correlation between the polarity of the solution and the shift in absorbance, however factors like hydrogen-bonding or basicity of the solvent could lead to other effects that change the absorbance of the sensor.

A family of 2-aminopyridine based sensors was then created based on standard methods for PAR synthesis, *scheme 14*.

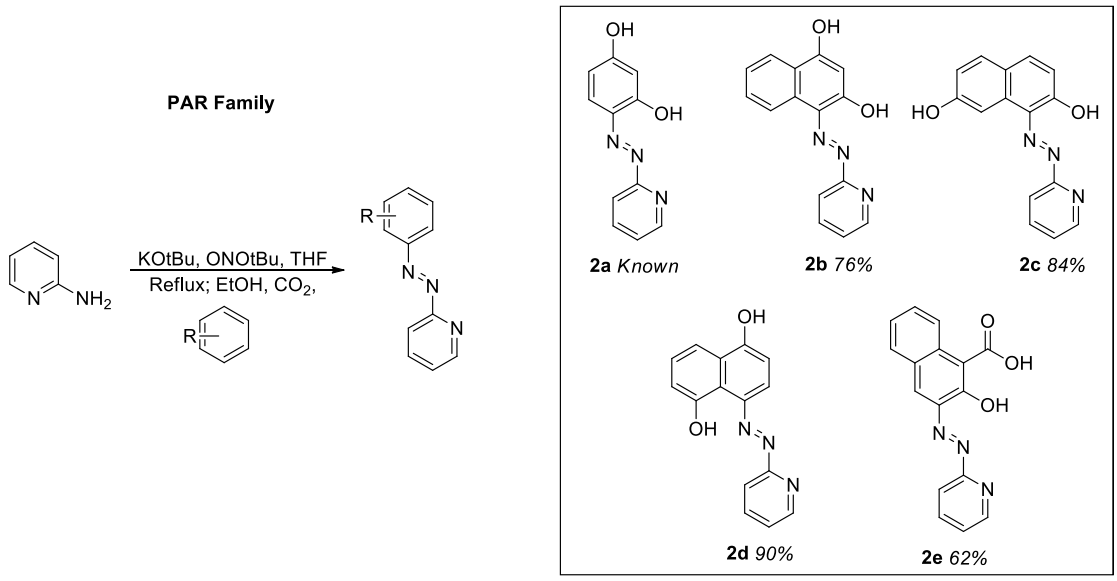

Scheme 14: Library Synthesis of PAN Family

The PAR family was found to have more utility as metal ion chemosensors than the QAR family. Metal ion selectivity among this family showed promise as each dye has its own unique set of metal ions in which they respond to.

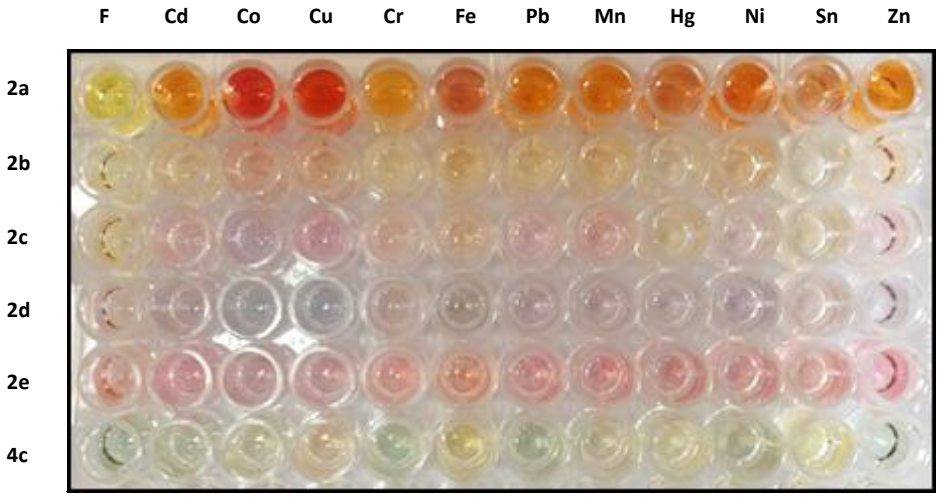

Figure 20: Metal Ion Response of PAN Family and their respective Metal Ions

The metal ion responses among these dyes, *figure 20*, are somewhat similar. Generally, every dye responds to copper, cobalt, nickel and zinc. The most noticeable differences appear for **2c** and **2d** wherein it appears these dyes respond to most of these metals in a unique manner. The last row **4d** is

also interesting as these colors only appear after multiple minutes, whereas the other responses are instantaneous.

	Free	Al	Cd	Ca	Cr	Co	Cu	Fe	Pb
2a	450		**497**			**509**	**509**	**491/530**	**521**
2b	424					**481**	**476**	419	
2c	460		**519/565**		454	**530**	**536**	464	**515**
2d	480	365	**568**			**636**	**602**	**600**	**585**

	Free	Mg	Mn	Hg	Ni	K	Na	Sn	Zn
2a	450			414	**495**			**393**	**491**
2b	424			**393**	**492**			**404**	**492**
2c	460			**447**	**525/564**			**443**	**513/550**
2d	480		**567**	573	**602**			482	**586**

Table 6: Max Wavelength of PAN Family and their respective metal ions (Joe Laboets)

Table 6 shows the overall metal ion response for the PAR family of azo dyes **2a-d**, there are many differences among them. Metal ion responses with weak changes in absorbance are underlined while the strong responses are shown in **bold**. While there is a response to tin and mercury for some azo dyes, generally the response is followed by the degradation of the azo dye via reductive processes. This array

of 4 dyes could be able to distinguish Al, Cd, Cr, Co, Cu, Fe, Pb, Hg, Ni, Sn and Zn from one another thanks to their unique change in absorbance.

Of these dyes, **2c** was extensively studied as it gave unique responses to many of the metal ions of interest and it was believed that the distal hydroxyl did not interfere with metal ion selectivity and modification of that hydroxyl for attachment to a solid support should not affect the absorbance change either.

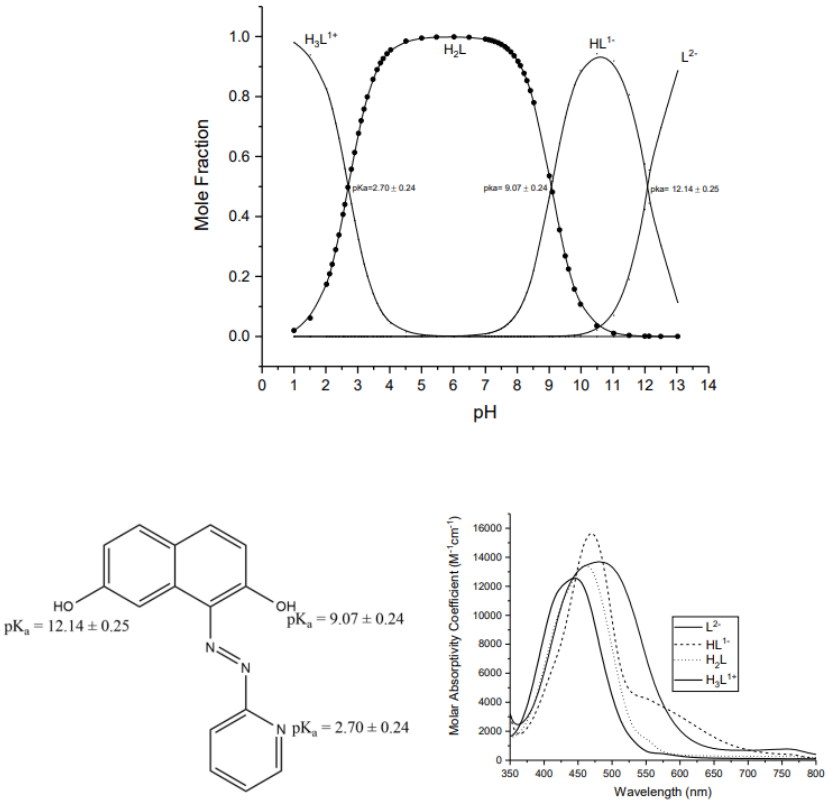

Figure 21: PAN-7OH, 2c, its relative pK_a's and pH dependent UV-Vis Spectra (Joe Laboets)

The pKa's of the molecule were determined experimentally, *figure 21*, in addition to the protonation states of **2c** in regard to its spectra. This process was repeated for many of the azo dyes described herein.

2c	K_d (M^{-1})	Ionic Radius (Å)
Cu	6.324E-07	0.73
Co	8.600E-07	0.75
Zn	9.528E-07	0.74
Ni	9.705E-07	0.69
Cd	8.119E-06	0.97
Pb	1.799E-05	1.2

Table 7: 2c K_d for multiple metal ions and their relative ionic radius (Joe Laboets)

Shown, *table 7*, are the relative affinities of **2c** toward various first row transition metals. It appears that this azo dye is most selective and has the highest affinity for copper which also happens to be one of the smallest of the divalent metal ions in the transition metal block. While **2c** has a response to lead and cadmium the affinity appears be less which is understood to be the result of the increasing ionic radius of the metal ions. Other considerations are the general shape of the orbitals for these divalent metal ions and the ability for the azo dye to satisfy those empty orbitals.

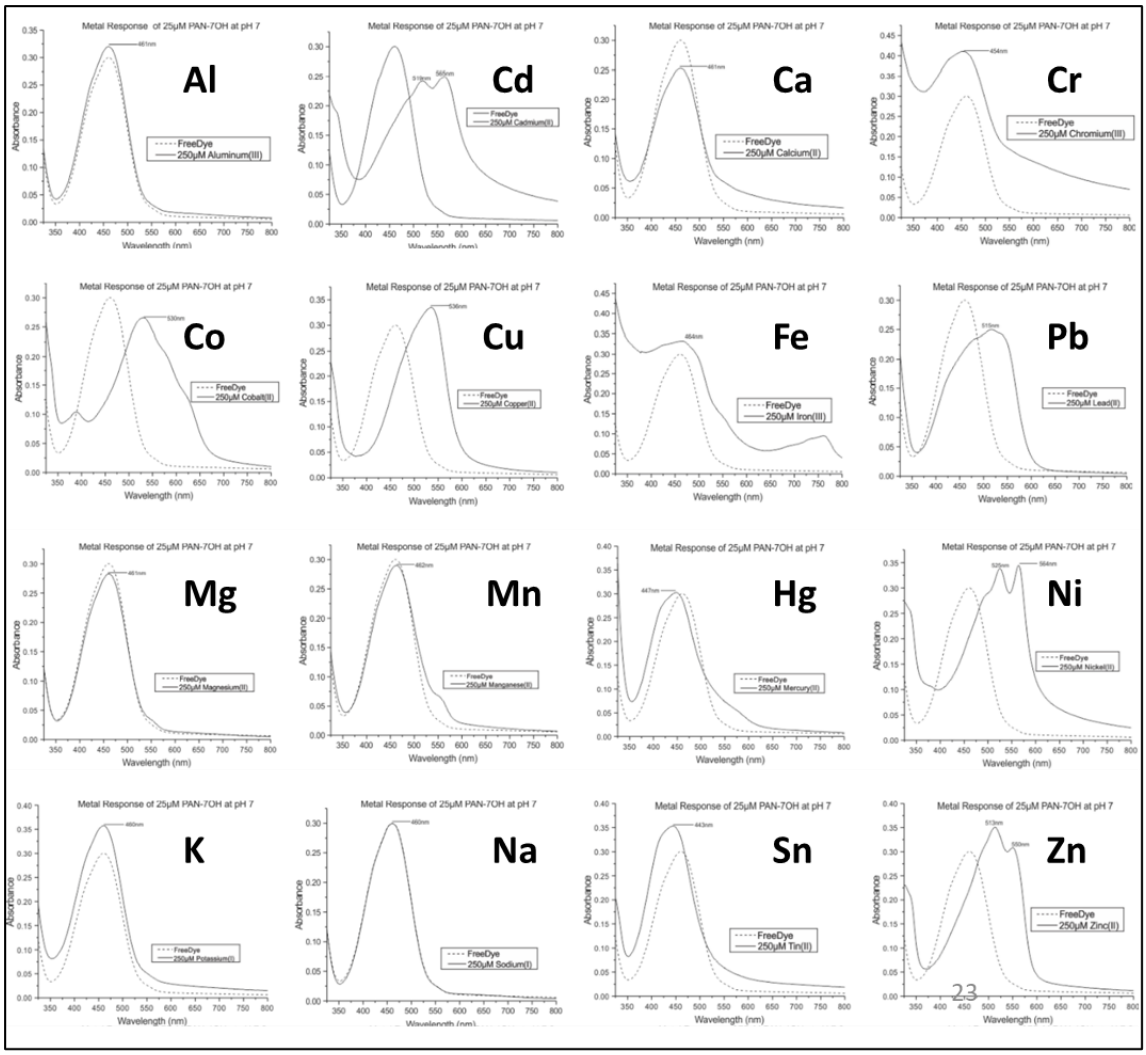

Figure 22: Spectral response for 2c compared to multiple metal ions, UV-Vis data (Joe Laboets)

The direct measurements of metal ion response of **2c** in MOPS buffer at pH 7 are shown, *figure 22*. These spectra are a better indication of the metal ion response, more detailed observations can be made from these, most notably that **2c** is able to distinguish among the metal ions it responds to based on the unique shape of its metal bound spectra. This type of analysis was performed on most of the dyes described herein.

2d was also found to be solvatochromic just like the QAR variant, both of these dyes are coupled to 1,5-dihydroxynaphthalene which is believed to afford the solvatochromic response, *figure 23*.

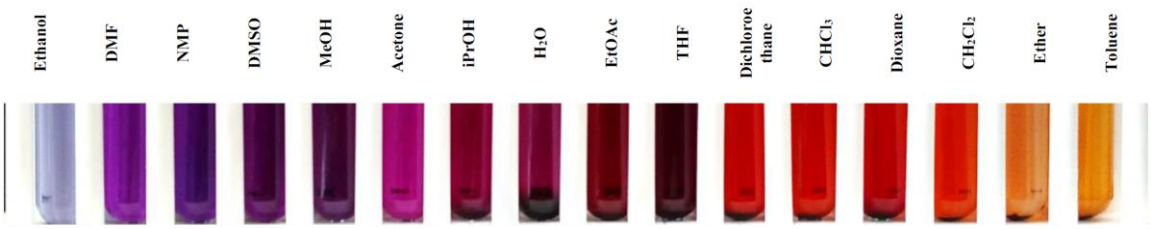

Figure 23: Solvatochromic behavior of PAN-1,5OH, 2d, in various solvents

The biggest difference between the QAR and PAR variant is the distribution of colors on the spectrum. The PAR version appears to have a smaller color range than the QAR variant. This is likely explained by tautomeric effects as well as hydrogen-bond stabilization in those tautomeric states, *figure 24*.

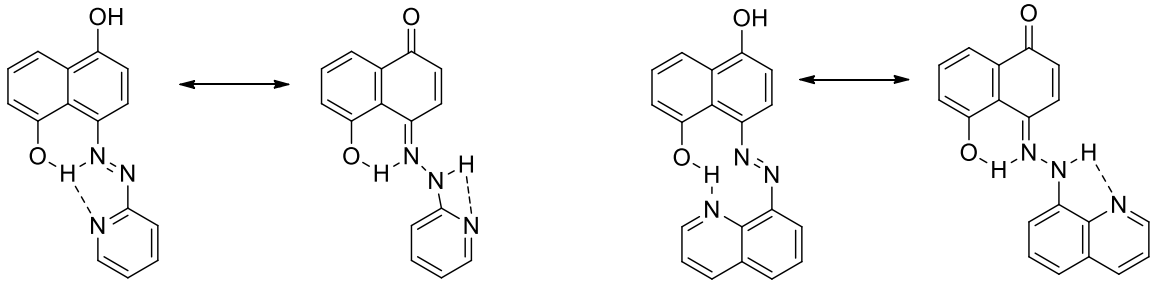

Figure 24: Proposed Tautomerization of 1d and 2d

The QAR variant is stabilized by the hydrogen bonding array in either state, but it's likely that as the polarity decreases the ketone is present in greater amounts, this state is stabilized by the 5-member hydrogen-bonding ring of the azo NH and the quinoline hetero nitrogen. This hydrogen bond in the PAR variant would be a 4-member ring and less stabilized, meaning the enol tautomer is likely present in greater amounts in less polar solvents than the QAR variant.

These two families, PAR and QAR, represent a library where the naphthol portion of the molecule is varied while the ligand is kept constant. A variety of isomers of aminoquinoline and various 2-aminopyridine derivatives were then coupled to resorcinol to see what the effect on metal ion

selectivity may be. These iso-quinolines and pyridines require the basic method to be synthesized. From a crude reaction screening the following results were noted.

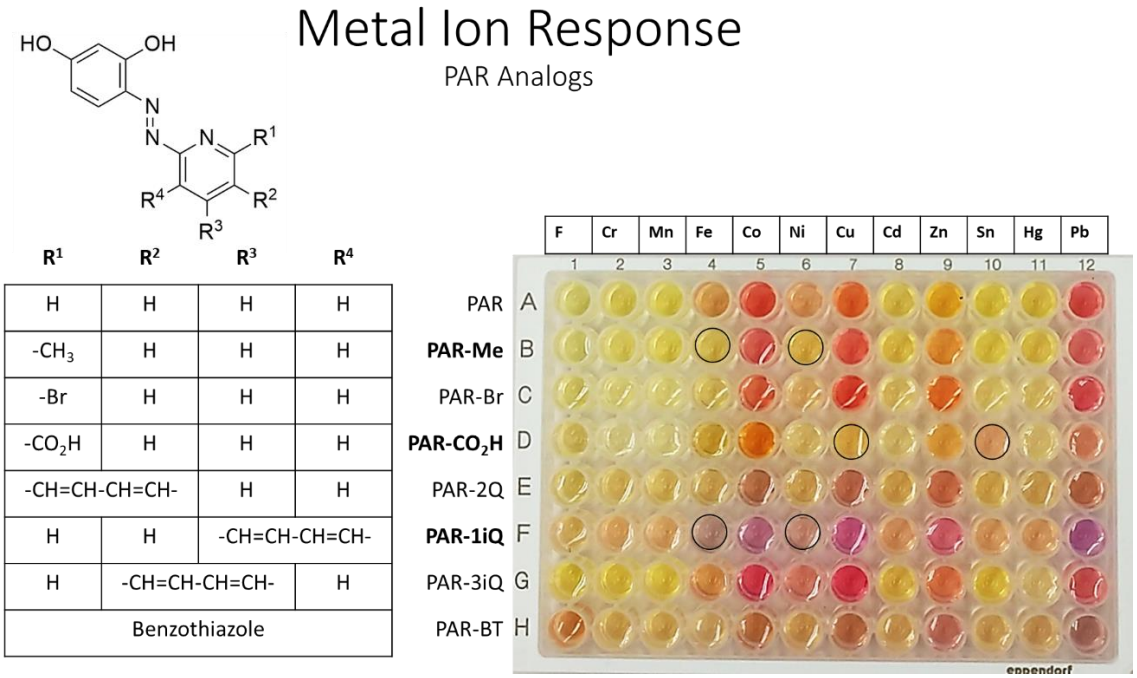

R^1	R^2	R^3	R^4
H	H	H	H
$-CH_3$	H	H	H
-Br	H	H	H
$-CO_2H$	H	H	H
-CH=CH-CH=CH-		H	H
H	H	-CH=CH-CH=CH-	
H	-CH=CH-CH=CH-		H
Benzothiazole			

Figure 25: Library of PAR analogs with varying pyridine-like substituents

These results, *figure 25*, indicate a means to achieve a difference in selectivity in azo dye through the variation of the ligand. In this case the highlighted dyes would constitute an array that could distinguish iron, cobalt, nickel, copper, tin and lead from a mixture of these metal ions in solution. But for the most part these azo dyes do not offer any truly significant selectivity's or metal ion responses when compared to the simple PAR family of azo dyes and the precursors to these chemosensors are significantly more costly.

The solid support utilized in the subsequent experiments is an amine terminated hydrogel polymer covalently attached to a glass surface, *scheme 15*.

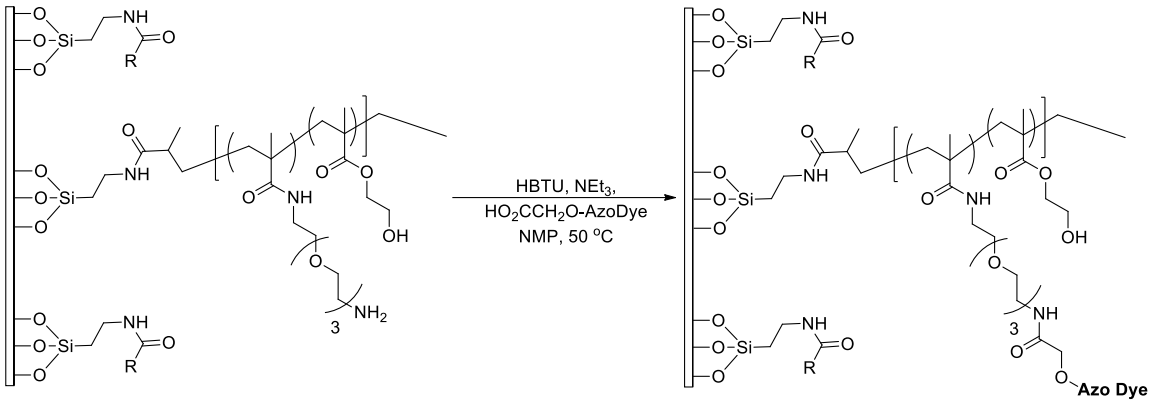

Scheme 15: Synthesis of final sensor

Because the polymer retains terminal amines, the most convenient method of dye attachment to the solid support that would result in a very stable bond is via peptide coupling methods. Methods were developed to install a functional handle on the low affinity dyes.

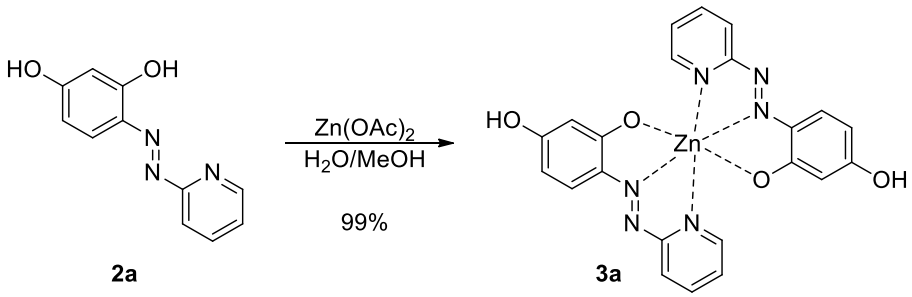

Scheme 16: Metallation of PAR, 2a

The first step of the sequence, *scheme 16*, involved the formation of a zinc complex with **2a**. This step serves multiple purposes. First it protects the binding side of the molecule from alkylation in the

subsequent steps, i.e. zinc acts as a protecting group. Second, it creates a pocket that specifically accommodates zinc ions. Thus when the dye is incorporated into the polymer, the binding pocket for metal ions is templated for zinc specifically. Now that the molecule is sufficiently protected, the distal phenol of **3a** may be alkylated.

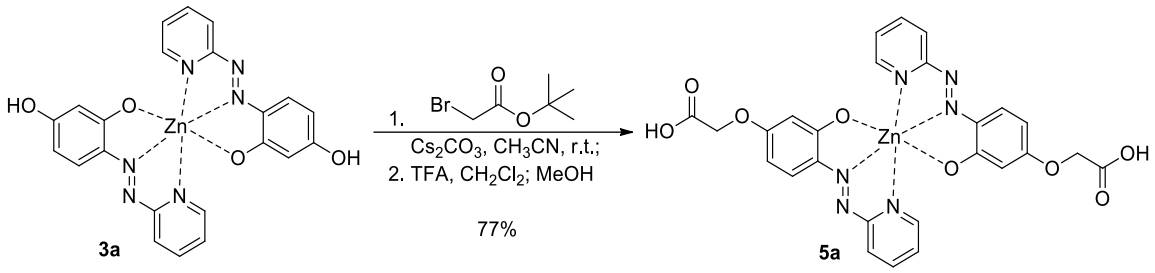

Scheme 17: Alkylation of 3a, PAR_2Zn complex

This reaction, *scheme 17*, works well and goes at room temperature overnight. Potassium carbonate also works well for this reaction, but higher yields were found when using cesium carbonate instead. **4a**, from the first step, is very organic soluble and easily extracted and isolated as the complex. Methods were also developed to remove zinc from the complex and allow for the isolation of **6**, *scheme 18*.

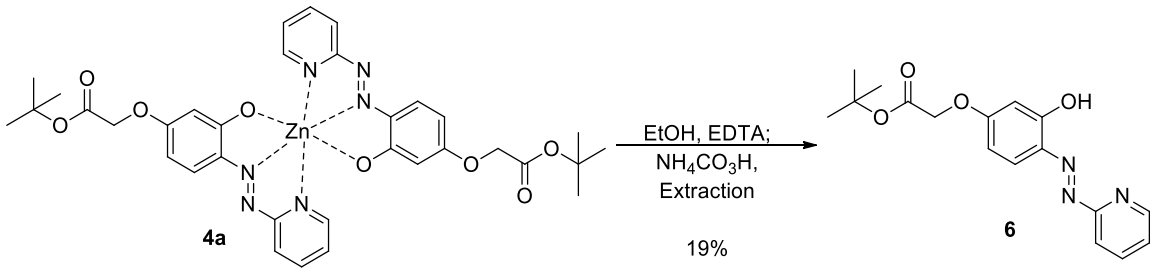

Scheme 18: Removal of Zinc from alkylated complex

6 was readily isolated from an ethanolic solution containing EDTA and ammonium bicarbonate. The extraction requires large volumes to overcome the emulsion formed from the ethanol/EDTA mixture. ^1H NMR was used to verify the method and no trace of complex remained. Subsequent experiments

showed that the acylation conditions for polymer loading are not entirely compatible with this product due to the un-alkylated phenol being a reactive species.

After deprotection of **4a** tert. Butyl groups to acids with TFA, the crude mixture is suspended in methanol multiple times to ensure the complex **5a** is reformed. Most acids are capable of degrading the complex and so it is important that after treatment with acid the complex is reformed. Once this complex is in hand, the dye complex may react with the polymer via peptide coupling conditions. Initial conditions for peptide coupling were as follow, *scheme 19*.

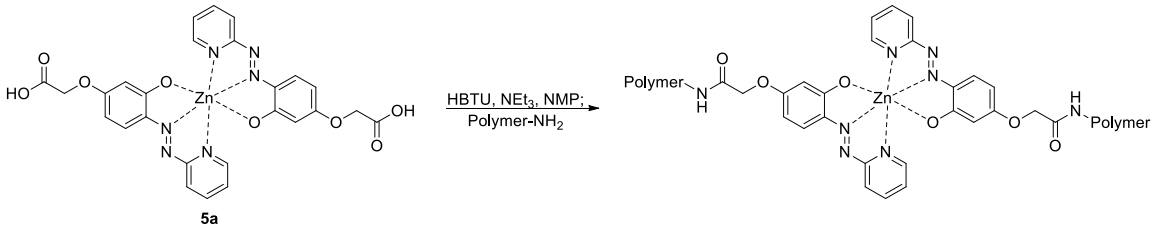

Scheme 19: Peptide coupling of deprotected alkylated azo dye to polymer

The reaction was initially run at room temperature out of fear of polymer degradation. However, it was noticed that the polymers loaded with dyes via this method did not adsorb much of the complex and less formed covalent bonds. To find the best coupling conditions, a series of reactions were set up at different concentrations for 24 hours and after rinsing the polymer with base, acid and compatible organic solvents their spectra were taken in MOPS buffer, pH ~7, *figure 26*.

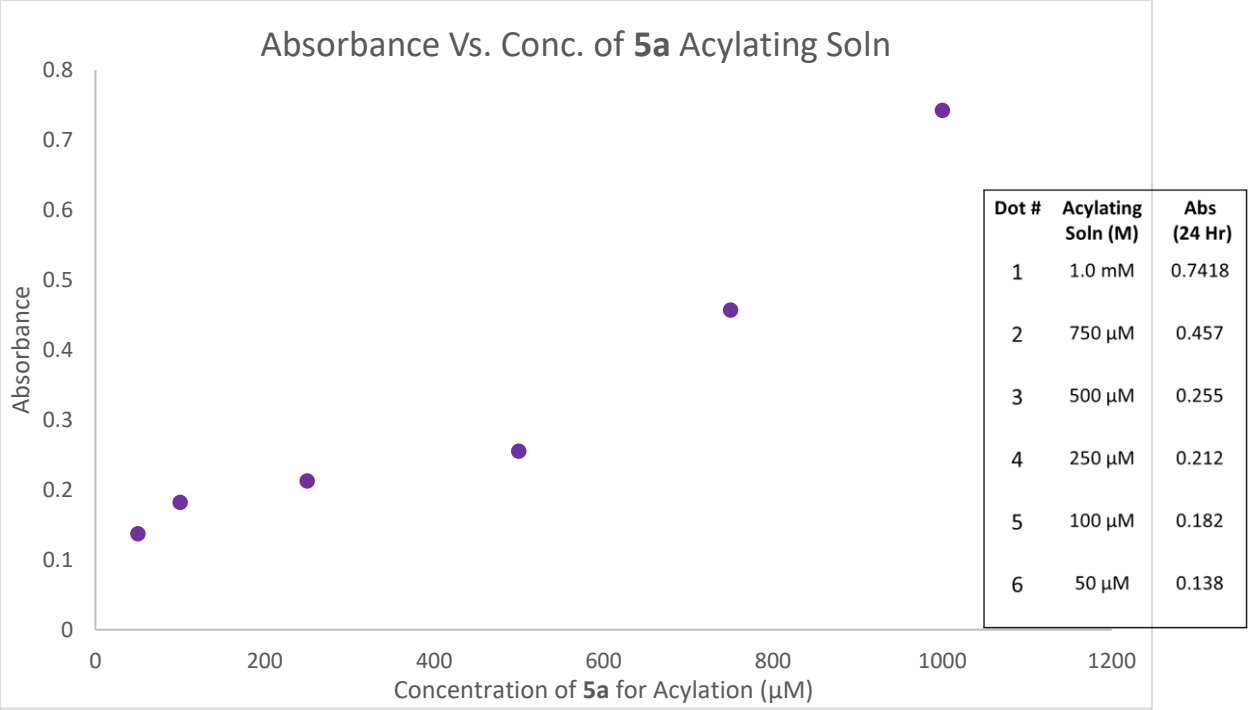

Figure 26: Absorbance Vs. Conc of Acylating solution over 24 hours

From this data, *figure 26*, it became apparent that these methods were too slow and did not sufficiently load the polymer dot with dye. It was hypothesized that the reason this acylation was taking longer than expected was due to the cross-linking effect of dye-complex to the surface of the polymer. This would, in effect, create a barrier that would limit the diffusion of dye into the polymer matrix. As a result of this it is believed that these polymer dots are acylated as a gradient with the outer-most part of the polymer being much higher in loading than the inner-most part of the polymer, *figure 27*.

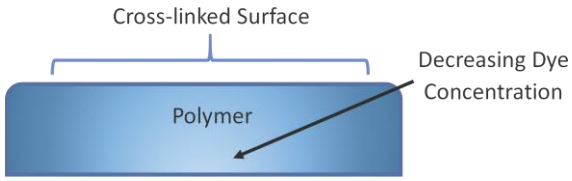

Figure 27: Crosslinking of polymer due to acylation of azo dye to polymer

Eventually a new set of conditions were found wherein the solution is shaken while being heated with an IR lamp over a few hours at ~50°C and the loading of dye significantly increased. The shaking of the polymer dots in solution greatly increased the rate of acylation compared to passive diffusion, as was expected, *scheme 20*.

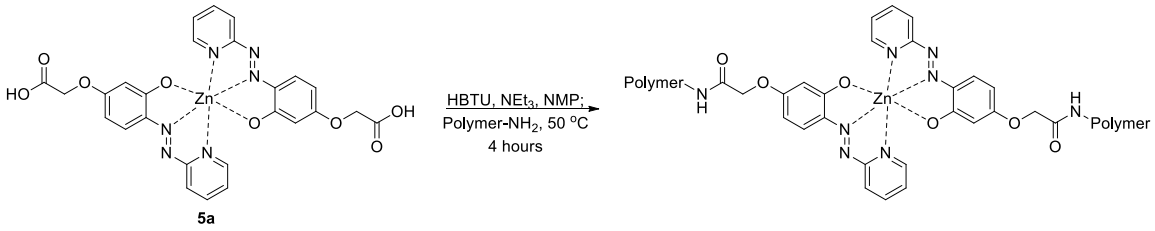

Scheme 20: Current method for attachment of azo dye to solid support

This method allowed for dye loading to an effective absorbance of ~ 1.5 – 2.0 depending on the concentration of acylating solution, for 1 – 2 Abs a 2 mmol dye solution was used and could be reused. The polymer dots require extensive rinses and washes to remove any residual acylating reagent, excess dye and any residual zinc from the complex. It was found that by shaking the polymer dots in these washing solutions all the residual contaminants were easily removed. The acylating solutions are also able to be reused if they are stored at -20 °C, under N_2 and kept anhydrous when not in use. The polymer dots are thoroughly washed and are then stored in 18 MΩ H_2O or in NMP until they are used.

Functional Polymer Results

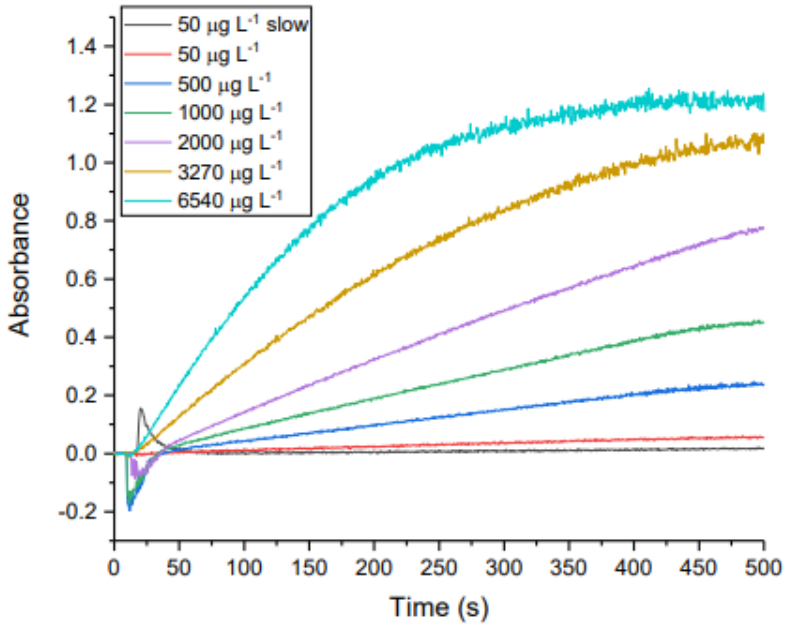

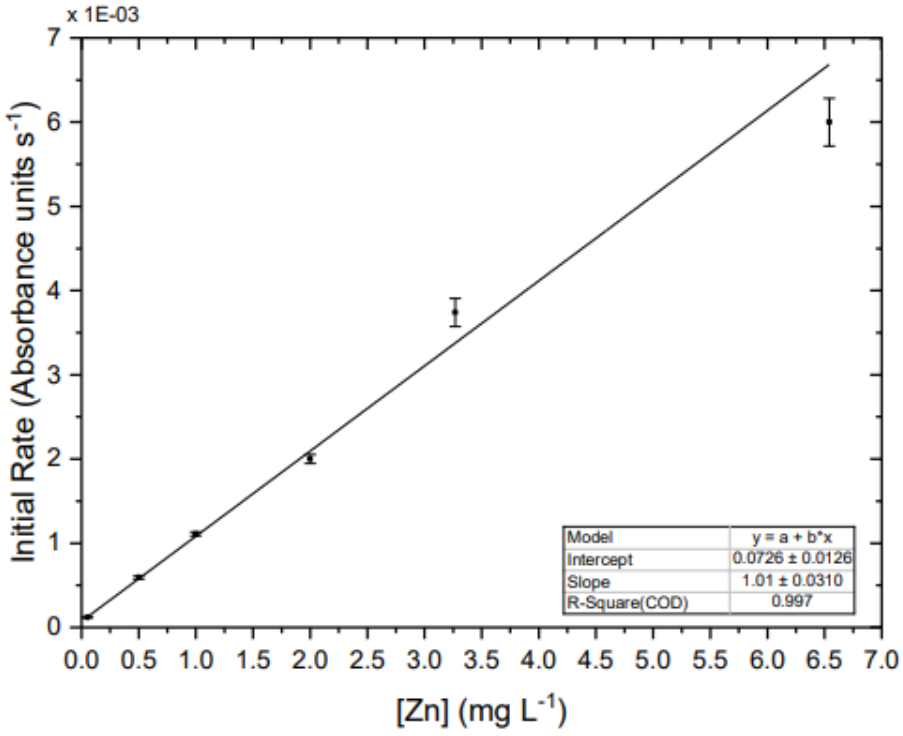

Figure 28: Concentration dependence of differential rate of change of absorbance compared to concentration of zinc ion.

The method behind metal ion quantification is based on the rate of change in the absorbance of the polymer dot in an analyte flow. It is entirely concentration dependent, *figure 28*, furthermore the

relationship appears to be linear which makes the correlation easier to compute. These rate of change spectra when graphed as initial rate vs concentration appear linear as well, meaning there is a significant correlation between measurements of different concentrations of metal ions in solution.

Thus, from initial rate measurements it is possible to determine metal ion concentration as a function of rate of change in absorbance.

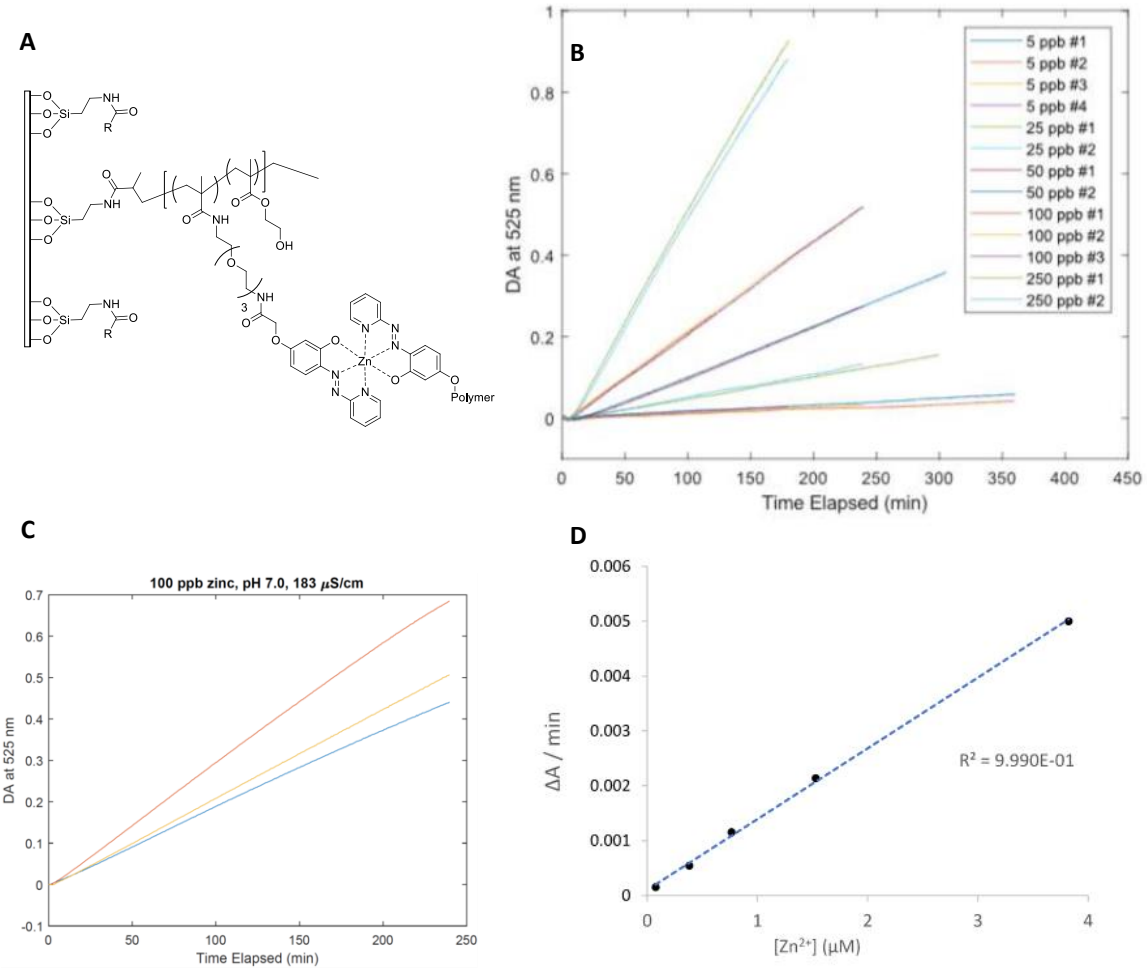

Figure 29: A, the structure of the sensor polymer, B differential absorbance as a function of time, C, Different slopes based on polymer charge, D, correlation of zinc concentration to the change in absorbance over time.

The spectra obtained from these experiments, *figure 29*, show a linearity that is associated with a concentration of zinc in solution and its accumulation over time. It is thought that the gradient of the dye-complex in the polymer is associated with this very stable and linear measurement over hours.

When analyte flow is kept sufficiently dilute, accurate measurements of metal ion concentrations can be obtained as low as individual ppb levels.

These measurements are very stable over time and very repeatable, the longer the measurement the more accurate the data obtained and thus a more reliable metal ion concentration and identity. In order to regenerate the free azo dye bound polymer and remove any residual metal, dilute HCl washes are used such that the flow of acid carries out the metal ions while protonating the azo-dyes and preventing them from binding, *figure 30*.

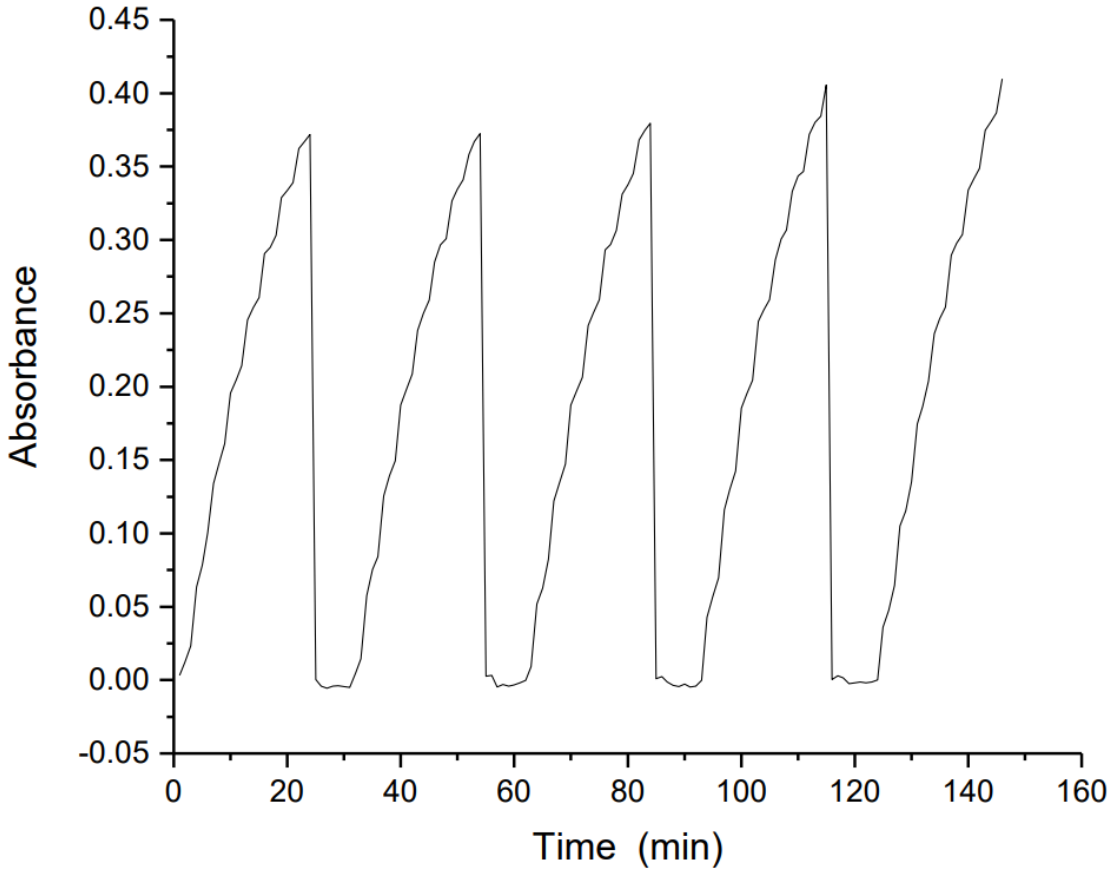

Figure 30: Regeneration of polymer dots via acid rinse and a period of buffering. (Joe Laboets)

This constitutes a method to continuously measure metal ions in solution and regenerate the polymer dye. Collaborator use has shown that there is no obvious degradation after a year of almost continuous use and thousands of repeated measurements. Furthermore, the dye bound to the polymer does not

appear to oxidize or degrade when compared to solution based azo dyes, even after treatment with raw wastewater.

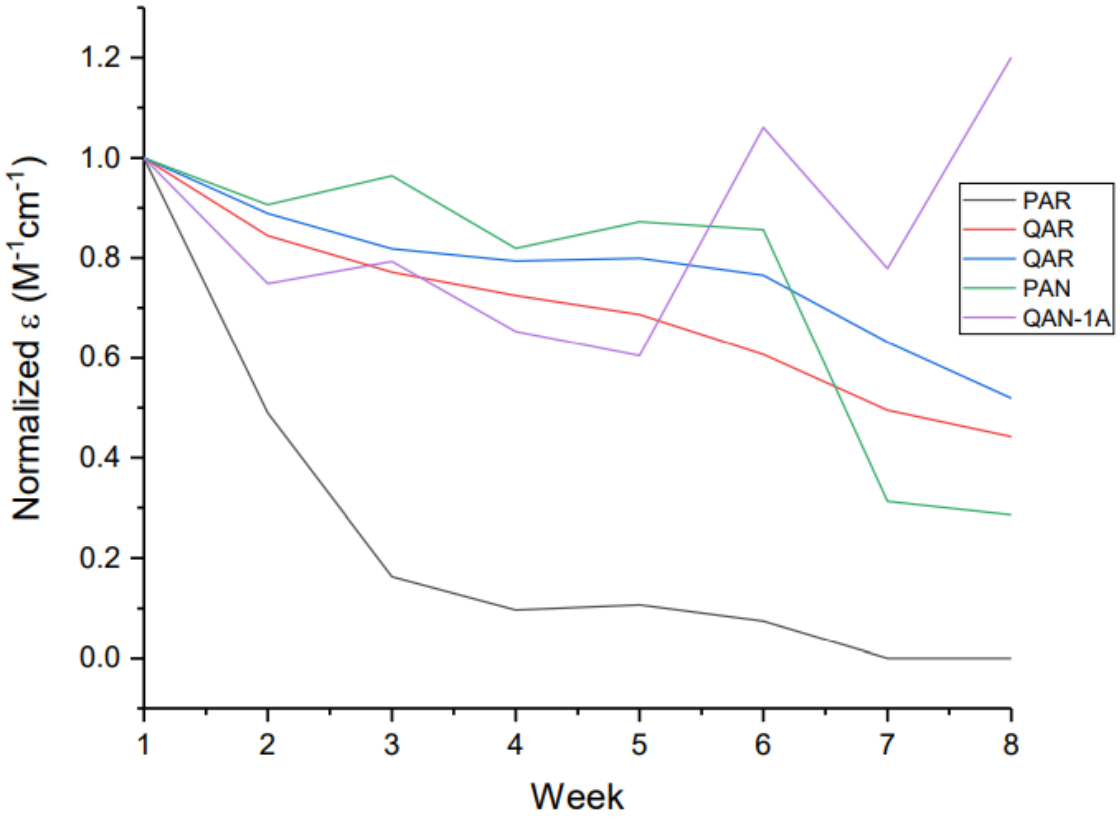

Figure 31: Degradation of solution based dyes over time (Joe Laboets)

When considering the solution-based sensors, *figure 31*, there is obvious degradation as quickly as a week after dissolving. These solutions were exposed to atmosphere and refilled with solvent as it escaped. The result is a general decrease in absorbance and increased complexity of the spectra meaning that the azo dye is degrading in solution. This phenomenon is not observed in the polymer bound azo dyes even after a year of continuous use.

Multiple azo dyes have been acylated to polymer dots to date that are capable of detecting metal ions in solution. The method for derivatizing the low-affinity dyes for acylation to the polymer dots has been applied to the library of compounds generated, each with unique properties. Some of the

most remarkable findings has been associated with the high affinity dyes that have limited utility in this project but may have utility in other areas of research.

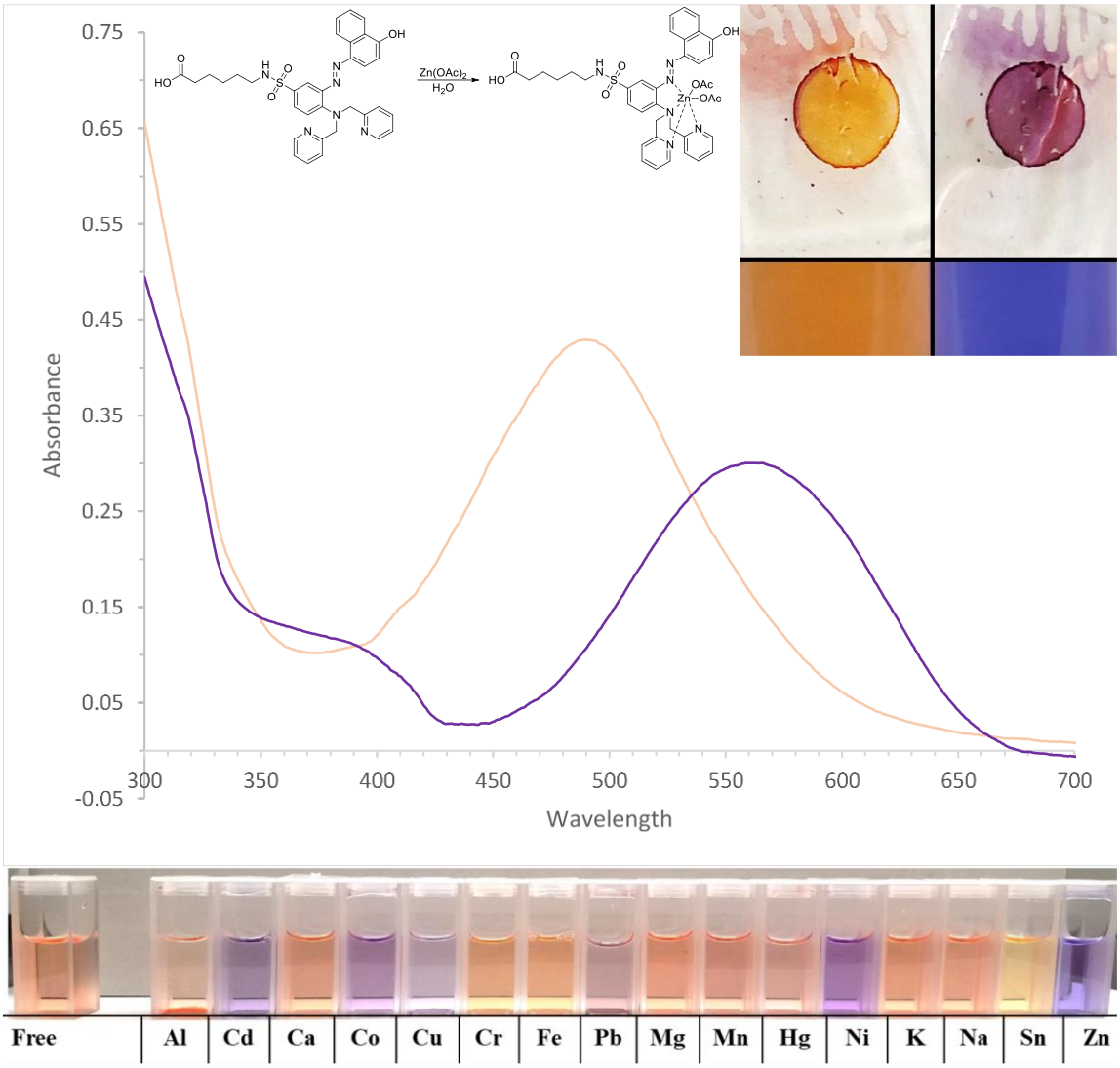

Figure 32: Comparison of High affinity dye in solution and on the polymer dot

For the High-affinity dyes it became apparent very quickly that the solution-based spectra and solid-support based spectra of these dyes are identical to one another, *figure 32*. That by having the functional handle far away from the chromophore portion of the molecule the solution-based spectra

would be representative of the solid support spectra which would make the determination of what sensors to use easier as these determinations could be based solely on their solution-based spectra.

The biggest issue with the high affinity dyes was the inability to wash out metal ions via flow of HCl which had become the standard method for the low affinity sensors. Even flow of 6M HCl was unable to remove the zinc from the polymer matrix fitted with **11** and **16c**, that upon flow of pH 7 buffer the spectra quickly shifted toward their metal bound state. It was believed that the incredibly high affinity of the azo dyes for zinc coupled with the gradient of dye through the matrix prevented the acid from abstracting the metal from the polymer matrix.

These experiments constitute a method for the creation of a hydrogel polymer with metal ion detection capabilities. When combined with a customized flow-cell specifically fitted for these hydrogel polymers and custom spectrometer one can detect the accumulation of metal ions in real time in a flow system. This has significant utility in monitoring treated wastewater to ensure EPA compliance or perhaps as a home use detector to ensure potable water is free of deadly metals like lead and mercury.

Subsequent studies into metal ion chemosensors will involve the development of a high affinity selective lead sensor that utilizes the high affinity dye scaffold. Beyond lead, dyes will be developed to detect a large array of metal ions with greater specificity and affinity based on the experimental results from these studies.

General Synthesis of Azo Dyes **1** and **2**:

Acidic Method – Diazonium **1x**

QAR Family – General Procedure:

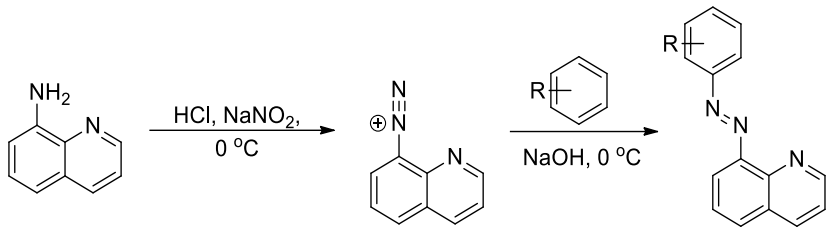

1 eq (1 mmol) of 8-aminoquinolone is dissolved into 5 ml of H_2O with 2 eq (2 mmol) of HCl and chilled to 0 °C. Once chilled, 1 eq (1 mmol) of $NaNO_2$ in 1 ml of H_2O is dropwise added to the reaction mixture, while maintaining 0 °C through the addition. Once delivered, the reaction mixture was tested for any excess oxidant via KI-starch paper. While still at 0°C, this solution was delivered dropwise and very slowly to a solution containing 4 eq (4 mmol) of NaOH and 1 eq (1 mmol) of phenol/naphthol chilled to 0°C. once fully delivered, the reaction mixture was allowed to warm to room temperature overnight. The solution is then acidified with acetic acid and the precipitate collected via vacuum filtration. The solid is washed with H_2O then ice cold MeOH. The solid is dried and then boiled in diethyl ether, filtered and dried under reduced pressure.

1a QAR - 4-(quinolin-8-yldiazenyl)benzene-1,3-diol

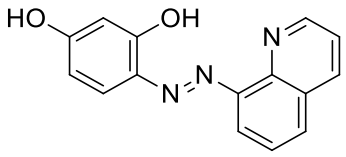

Yield: 83%, m.p. +320 °C,

1H NMR 500 MHz (CD_3OD): δ 8.86 (1H, dd, J = 1.8 , 4.2 Hz), 8.25 (1H, dd, J = 1.8, 8.4 Hz), 7.98 (1H, dd, J = 2.1, 6.6 Hz), 7.61 (1H, m), 7.56 (1H, m), 7.50 (1H, dd, J = 4.2, 8.4 Hz), 6.98 (1H, d, J = 9.6 Hz), 6.21 (1H, d, J = 9.6 Hz), 5.68 (1H, d, J = 2.1 Hz)

13C NMR 500 MHz (CD_3OD): δ 148.72, 135.56, 134.83, 128.8, 126.91, 123.90, 121.62, 121.32, 116.72, 110.60, 106.

1b QAN-4OH - 4-(quinolin-8-yldiazenyl)naphthalene-1,3-diol

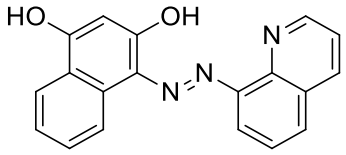

Yield: 80%, m.p. 275 - 277 °C,

H NMR 300 MHz (CD_3OD): δ 8.86 (1H, dd, J = 1.5, 4.2 Hz), 8.45 (1H, d, J = 8.1 Hz), 8.24 (1H, dd, J = 1.5, 8.1 Hz), 8.07 (2H, m), 7.60 (1H, t, J = 7.8 Hz), 7.51 (3H, m), 7.36 (1H, t, J = 7.2 Hz), 5.83 (1H, s)

1c QAN-7OH - 1-(quinolin-8-yldiazenyl)naphthalene-2,7-diol

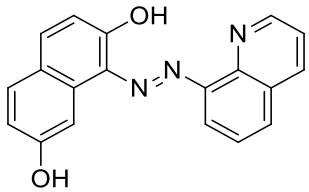

Yield: 84%, m.p. 224 - 225 °C,

1H NMR 300 MHz (CD_3OD): δ 8.95 (1H, d, J = 3.9 Hz), 8.37 (1H, dd, J = 2.7, 8.1 Hz), 8.34 (1H, t, J = 8.1 Hz), 7.71 (2H, m), 7.60 (1H, s), 7.57 (1H, t, J = 4.5 Hz), 7.28 (1H, d, J = 8.4 Hz), 6.74 (1H, dd, J = 2.4, 8.7 Hz), 6.27 (1H, d, J = 9.3 Hz)

1d QAN-1,5OH - 4-(quinolin-8-yldiazenyl)naphthalene-1,5-diol

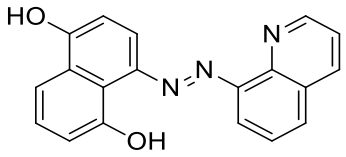

Yield: 40%, m.p. 193 – 195 °C,

1H NMR 500 MHz ($CDCl_3$): δ 12.10 (1H, s_{broad}), 10.99 (1H, s_{broad}), 8.84 (1H, d, J = 1.5 Hz), 8.21 (1H, d, J = 8.5 Hz), 7.97 (1H, d, J = 10.5 Hz), 7.81 (1H, d, J = 7.5 Hz), 7.59 (1H, t, J = 8 Hz), 7.53 (3H, m), 7.44 (1H, t, J = 8 Hz), 7.29 (1H, d, J = 7.5 Hz), 6.83 (1H, d, J = 10 Hz)

1e QAN-3A - 3-hydroxy-4-(quinolin-8-yldiazenyl)-2-naphthoic acid

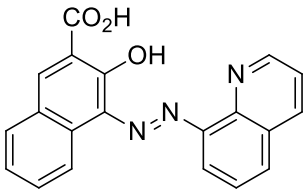

Yield: 45%, m.p. 124 - 125 °C,

1H NMR 300 MHz (CD_3OD): δ 8.71 (1H, dt, J = 1.2, 4.2 Hz), 8.17 (1H, td, J = 1.5, 8.4 Hz), 7.80 (1H, dd, J = 2.7, 6.3 Hz), 7.39 (5H, m), 7.28 (1H, td, J = 2.7, 6.9 Hz), 7.17 (1H, dd, J = 1.5, 9.6 Hz), 6.38 (1H, dd, J = 3.6, 9.6 Hz)

Basic Method – Diazotate **2x**

PAR Family – General Procedure

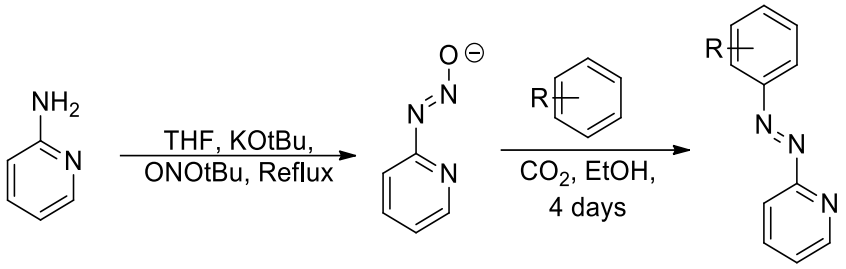

1 eq (1 mmol) of 2-aminopyridine and 1 eq (1 mmol) of potassium t.butoxide was dissolved in 1.5 ml of THF and stirred for 30 minutes before addition of 1 eq (1 mmol) of t.butyl nitrite. The reaction mixture was then heated to reflux for three hours and after TLC indicated the consumption of starting 2-aminopyridine the reaction was stopped. The mixture was cooled to room temperature and the precipitate collected via vacuum filtration. The solid was then washed with diethyl ether and while still wet with ether, dissolved in 10 ml of EtOH chilled to -20 ^{o}C. This solution was then added in portions to a solution of 1 eq (1 mmol) phenol/naphthol in 10 ml of EtOH while CO_2 was bubbled through the solution. CO_2 bubbling was continued for multiple days until the solution had gone dry.

The crude residue was then suspended in 10 ml of MeOH and acidified with AcOH while heating. This solution was diluted into 50 ml of H_2O and the precipitate collected via vacuum filtration. The crude solid was then boiled in 50 ml of diethyl ether, filtered and dried under reduced pressure for multiple days.

2a PAR - 4-(pyridin-2-yldiazenyl)benzene-1,3-diol

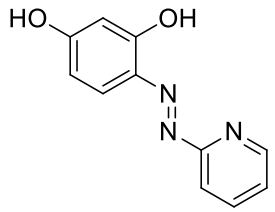

Yield: 40%, m.p. 192 - 202 °C,

1H NMR 500 MHz (DMSO – d6): δ 13.87 (1H, s_{broad}), 8.58 (1H, d, J = 3.9 Hz), 7.97 (1H, td, J = 1.7, 8.2 Hz), 7.80 (1H, d, J = 8.1 Hz), 7.59 (1H, d, J = 8.1 Hz), 7.41 (1H, t, J = 6.3 Hz), 6.53 (1H, dd, J = 2.2, 9.0 Hz), 6.24 (1H, s)

2b PAN-4OH - 4-(pyridin-2-yldiazenyl)naphthalene-1,3-diol

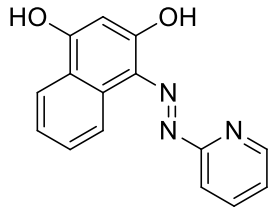

Yield: 79%, m.p. +340 °C,

1H NMR 500 MHz (CD3OD): δ 8.31 (1H, d, J = 8 Hz), 8.15 (1H, d, J = 3.5 Hz), 8.00 (1H, d, J = 8 Hz), 7.79 (1H, t, J = 7 Hz), 7.71 (1H, d, J = 8.5 Hz), 7.47 (1H, t, J = 7 Hz), 7.38 (1H, t, J = 7.5 Hz), 6.95 (1H, m), 5.74 (1H, s)

2c PAN-7OH - 1-(pyridin-2-yldiazenyl)naphthalene-2,7-diol

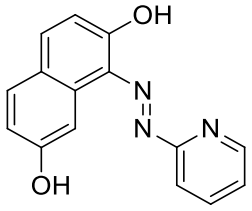

Yield: 84%, m.p. 228 - 230 °C,

1H NMR 300 MHz (CD_3OD): δ 8.35 (1H, d, J = 7.8 Hz), 7.94 (1H, td, J = 1.8, 6.3 Hz), 7.92 (1H, s), 7.77 (1H, d, J = 2.1 Hz), 7.69 (1H, d, J = 9.6 Hz), 7.42 (1H, d, J = 8.4 Hz), 7.22 (1H, td, J = 2.1, 6.3 Hz), 6.88 (1H, dd, J = 2.4, 8.4 Hz), 6.41 (1H, d, J = 9.6 Hz)

2d PAN-1,5OH - 4-(pyridin-2-yldiazenyl)naphthalene-1,5-diol

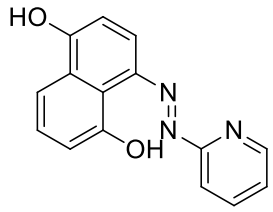

Yield: 90%, m.p. 241 – 245 °C,

1H NMR 300 MHz (CD_3OD): δ 8.86 (1H, dd, J = 1.5, 4.2 Hz), 8.45 (1H, d, J = 8.1 Hz), 8.24 (1H, dd, J = 1.5, 8.1 Hz), 8.07 (2H, m), 7.60 (1H, t, J = 7.8 Hz), 7.51 (3H, m), 7.36 (1H, t, J = 7.2 Hz), 5.83 (1H, s)

2e PAN-1a - 2-hydroxy-3-(pyridin-2-yldiazenyl)-1-naphthoic acid

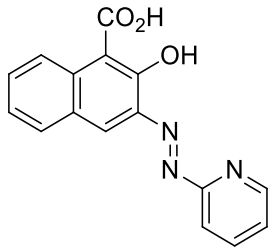

Yield: 62%, m.p. 228 - 230 °C,

1H NMR 300 MHz (CD_3OD): δ 9.23 (1H, d, J = 8.7 Hz), 7.85 (1H, d, J = 8.7 Hz), 7.80 (1H, s), 7.74 (1H, t, J = 7.2 Hz), 7.47 (1H, t, J = 7.2 Hz), 7.29 (1H, t, J = 7.5 Hz), 7.09 (1H, d, J = 9 Hz), 6.87 (1H, d, J = 8.7 Hz), 6.79 (1H, t, J = 6.3 Hz)

General Synthesis of Zinc Complexes **3**

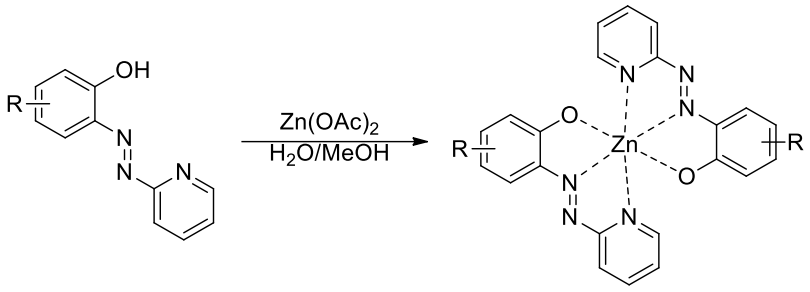

2 eq (2 mmol) of azo dye is suspended in 100 ml of a 50:50 mixture of MeOH and H_2O and heated to reflux, then 1.1 eq (1.1 mmol) of $Zn(OAc)_2$ is added to the solution and the solution is stirred overnight at room temperature. The resulting precipitate is collected via vacuum filtration and washed with H_2O until the filtrate run clear. The solid is then dried under reduced pressure for multiple days to afford the desired zinc complex.

3a PAR_2Zn - 4-(pyridin-2-yldiazenyl)benzene-1,3-diol Zn Salt

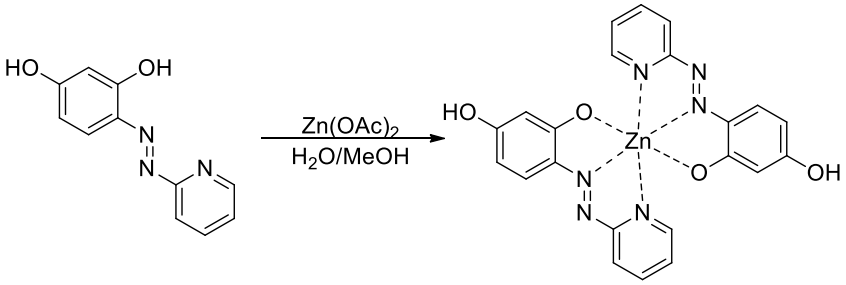

Yield: 99%, m.p. +340 °C,

1H NMR 500 MHz (DMSO-d6): δ 10.71 (1H, s_{broad}), 7.99 (1H, t, J = 7.6 Hz), 7.71 (2H, d, J = 8.8 Hz), 7.58 (1H, d, J = 4.4 Hz), 7.19 (1H, t, J = 6.2 Hz), 6.20 (1H, d, J = 9.3 Hz), 5.85 (1H, s)

13C NMR 500 MHz (DMSO-d6): δ 176.3, 169.6, 159.3, 146.0, 141.8, 132.1, 123.8, 122.3, 119.9, 111.6, 104.9

3b PAN-7OH_2Zn - 1-(pyridin-2-yldiazenyl)naphthalene-2,7-diol Zn Salt

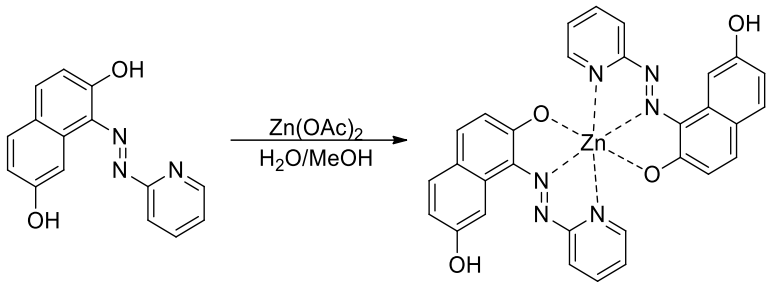

Yield: 95%, m.p. +340 °C,

1H NMR 500 MHz (CD_3OD): δ 8.37 (1H, d, J = 4.6 Hz), 7.94 (2H, m), 7.80 (1H, d, J = 2.4 Hz), 7.71 (1H, d, J = 9.6 Hz), 7.59 (1H, d, J = 8.8 Hz), 7.45 (1H, d, J = 8.4 Hz), 7.23 (1H, m), 6.44 (1H, d, J = 9.6 Hz)

13C NMR 500 MHz (DMSO-d6): δ 178.7, 161.0, 160.2, 145.6, 143.5, 142.1, 132.0, 129.5, 129.0, 123.3, 122.4, 121.8, 120.9, 114.5, 111.8

General Synthesis of Alkylated Zinc Complexes **4**

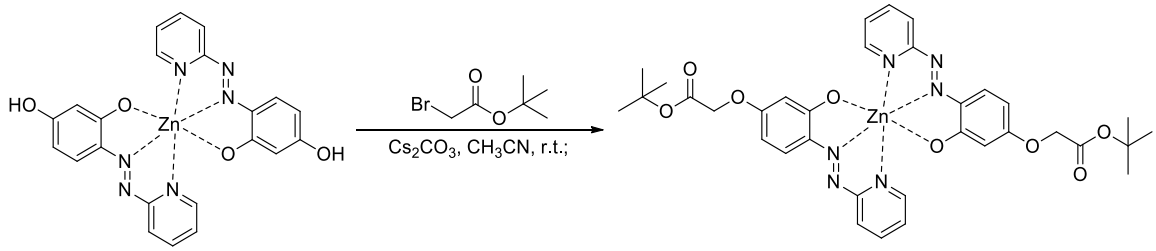

1 eq (1 mmol) of Azo-dye/zinc complex **3** is suspended in 15 ml of CH_3CN with 2.2 eq (2.2 mmol) of Cs_2CO_3. Then 2.2 eq (2.2 mmol) of t. butyl bromoacetate is added to the reaction mixture and the solution is stirred overnight at room temperature. After 18 hours the solution is filtered to remove excess salt. The organic is then concentrated under reduced pressure and the resulting oil boiled in 50 ml of hexanes and the resulting solid collected via filtration. The solid was then dried under reduced pressure.

4a PAR_2Zn-Alk - tert-butyl 2-(3-hydroxy-4-(pyridin-2-yldiazenyl)phenoxy)acetate Zn Salt

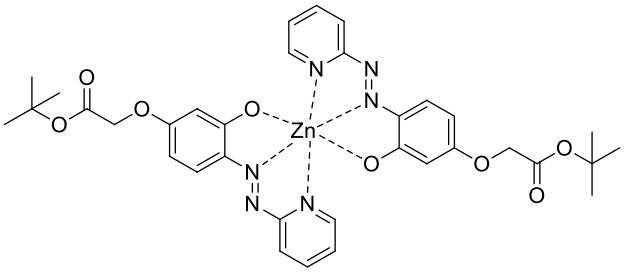

Yield: 94%, m.p. 133 - 137 °C,

1H NMR 500 MHz (DMSO-d6): δ 8.04 (2H, td, J = 1.5, 7.8 Hz), 7.80 (2H, d, J = 6.9 Hz), 7.75 (2H, d, J = 9.5 Hz), 7.64 (2H, dd, J = 1.0, 5.0 Hz), 7.25 (2H, t, J = 5.0 Hz), 6.29 (2H, dd, J = 2.6, 9.5 Hz), 5.92 (2H, d, J = 2.6 Hz), 4.67 (4H, s), 1.41 (18H, s)

13C NMR 500 MHz (DMSO-d6): δ 176.2, 168.4, 167.4, 159.0, 146.2, 142.2, 132.4, 124.5, 122.9, 119.4, 110.9, 103.7, 82.1, 65.4, 28.1

4b PAN-7OH$_2$Zn- Alk – Bis-tert-butyl 2-((7-hydroxy-8-(pyridin-2-yldiazenyl)naphthalen-2-yl)oxy)acetate Zn Salt

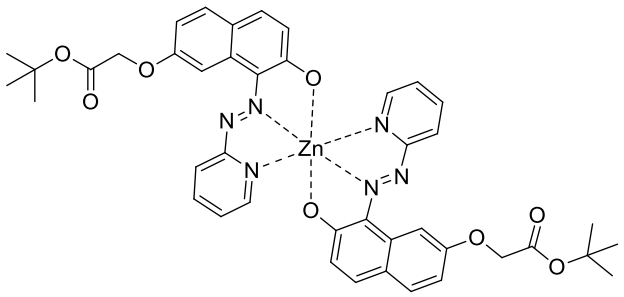

Yield: 42%, m.p. 220 – 221 °C

1H NMR 500 MHz (CDCl3): δ 9.57 (1H, d, J = 2.6 Hz), 7.78 (2H, d, J = 3.4 Hz), 7.66 (1H, d, J = 9.3 Hz), 7.60 (1H, d, J = 5 Hz), 7.52 (1H, d, J = 8.6 Hz), 7.00 (1H, dd, J = 2.6, 8.6 Hz), 6.91 (1H, q, J = 4.7 Hz), 6.74 (1H, d, J = 9.2 Hz), 4.74 (2H, s), 1.46 (9H, s)

1H NMR 500 MHz (DMSO-d6): δ 9.44 (1H, d, J = 2.3 Hz), 8.08 (1H, t, J = 8.5 Hz), 7.86 (2H, d, J = 8.9 Hz), 7.70 (1H, d, J = 8.6 Hz), 7.58 (1H, d, J = 4.3 Hz), 7.19 (1H, t, J = 6.3 Hz), 7.05 (1H, dd, J = 2.5, 8.5 Hz), 6.59 (1H, d, J = 9.2 Hz), 4.88 (2H, s), 1.40 (9H, s)

13C NMR 500 MHz (DMSO-d6): δ 178.6, 168.3, 160.6, 159.8, 145.5, 143.1, 142.1, 131.7, 129.0, 123.6, 123.2, 122.8, 122.1, 114.1, 109.1, 82.1, 65.5, 28.4

4c PAN-Alk – Bis-tert-butyl 2-((1-(pyridin-2-yldiazenyl)naphthalen-2-yl)oxy)acetate

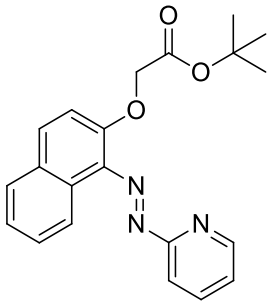

Yield: 25%, m.p. 76 - 79 °C,

1H NMR 500 MHz (DMSO-d6): δ 8.76 (1H, d, J = 4.9 Hz), 8.49 (1H, d, J = 8.7 Hz), 8.09 (2H, m), 7.99 (1H, d, J = 8.1 Hz), 7.77 (1H, d, J = 8.0 Hz), 7.6 (2H, m), 7.52 (2H, d, J = 9.1 Hz), 4.94 (2H, s), 1.40 (9H, s)

13C NMR 500 MHz (CDCl3): δ 168.1, 164.0, 149.7, 149.6, 139.3, 135.3, 133.1, 129.3, 129.2, 128.6, 127.0, 126.0, 125.3, 123.2, 116.3, 113.2, 82.0, 67.1, 28.2

5a PAR_2Zn A.A. – Bis-2-(3-hydroxy-4-(pyridin-2-yldiazenyl)phenoxy)acetic acid Zn Salt

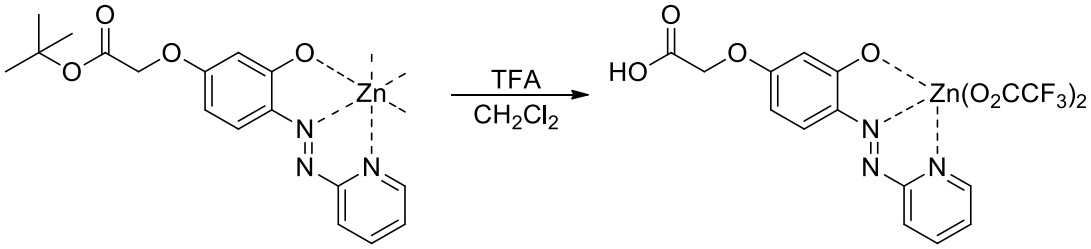

2.9245g (4.05 mmol) of **4a** was dissolved into 25 ml of CH_2Cl_2 and stirred while 4 ml of TFA was added to the reaction mixture. This solution was stirred for 1 hour before concentrating under reduced pressure and drying azeotropically with toluene. The solid was then resuspended in MeOH and concentrated under reduced pressure three times before drying under vacuum for multiple days. Yield. 3.201 g (100%) m.p. 133 – 135 °C

1H NMR 500 MHz (CDCl3): δ 8.55 (1H, s), 8.07 (1H, t, J = 7.6 Hz), 7.87 (1H, d, J = 8.1 Hz), 7.69 (1H, d, J = 9.2 Hz), 7.49 (1H, t, J = 4.6 Hz), 6.57 (1H, d, J = 8.9 Hz), 6.38 (1H, s), 4.81 (2H, s)

13C NMR 500 MHz (CDCl3): δ 169.8, 160.0, 159.2, 158.9, 158.6, 158.4, 148.8, 140.4, 133.3, 129.3, 128.6, 125.7, 124.8, 117.4, 115.0, 110.8, 103.1, 65.

5b $PAN\text{-}7OH_2Zn$ A.A. – Bis-2-((7-hydroxy-8-(pyridin-2-yldiazenyl)naphthalen-2-yl)oxy)acetic acid Zn Salt

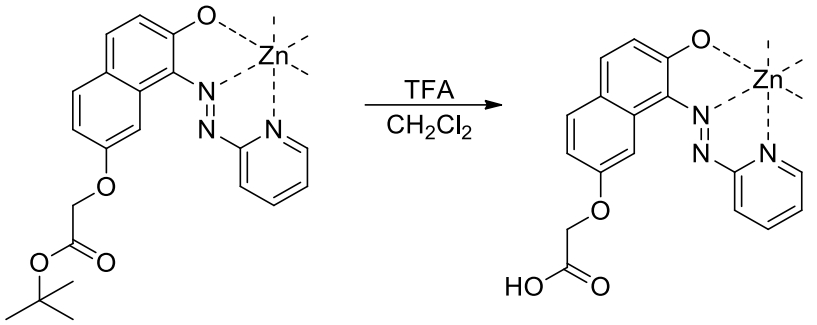

0.8463g (1.03 mmol) of **4b** was dissolved in 5 ml of CH_2Cl_2 before addition of 2.0 ml of TFA. The reaction mixture was stirred for 18 hours then concentrated via rotary evaporation. The solid was then resuspended in CH_3CN and azeotropically dried with toluene three times before drying under reduced pressure for multiple days. Yield 0.73g (100%), m.p. 235 – 236 °C

1H NMR 500 MHz (CDCl3): δ 15.79 (1H,s), 13.12 (1H, s_b), 8.42 (1H, d, J = 4.8 Hz), 7.97 (2H, m), 7.84 (1H, d, J = 9.6 Hz), 7.76 (1H, s), 7.63 (1H, d, J = 8.5 Hz), 7.26 (1H, t, J = 6.5 Hz), 7.07 (1H, d, J = 8.5 Hz), 6.52 (1H, d, J = 9.6 Hz), 4.84 (2H, s)

13C NMR 500 MHz (DMSO-d6): δ 181.2, 170.5, 159.6, 155.1, 149.1, 143.7, 139.7, 135.0, 131.6, 130.2, 124.4, 123.0, 121.4, 115.5, 110.1, 106.6, 65.2

6 tert-butyl 2-(3-hydroxy-4-(pyridin-2-yldiazenyl)phenoxy)acetate

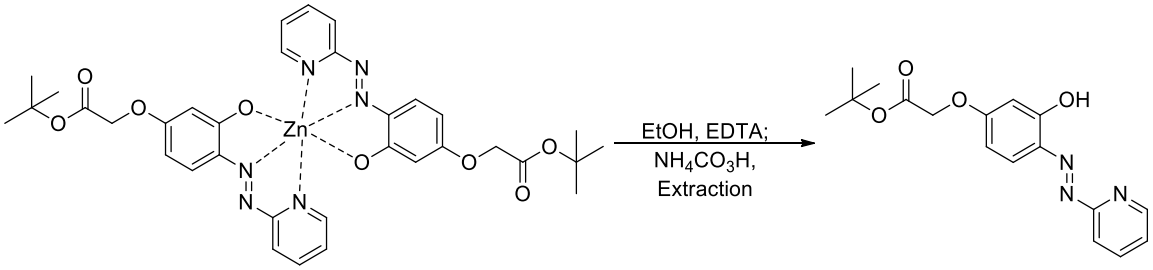

0.6802 g (1 mmol) of **4a** was suspended in 20 ml of EtOH and with stirring, 75 ml of sat. NH_4CO_3H in 0.1 M EDTA was added to the rapidly stirring solution. The solution was then extracted with 200 ml of CH_2Cl_2, dried over $MgSO_4$ and concentrated under reduced pressure. Yield: 0.119g (19%), m.p. 48 – 50 °C

1H NMR 500 MHz (DMSO-d6): δ 8.63 (1H, d, J = 4.3 Hz), 8.01 (1H, t, J = 7.8 Hz), 7.85 (1H, d, J = 8.2 Hz), 7.71 (1H, d, J = 9.2 Hz), 7.47 (1H, t, J = 6 Hz), 6.66 (1H, dd, J = 2.3, 8.9 Hz), 6.46 (1H, d, J = 2.4 Hz), 4.80 (2H, s), 1.45 (9H, s).

13C NMR 500 MHz (DMSO-d6): δ 167.5, 164.4, 161.7, 160.8, 149.6, 139.3, 133.9, 130.0, 124.8, 112.5, 110.7, 82.2, 65.7, 28.1

Synthesis of Ligands **7x**

7a 2,2'-Dipicolylamine

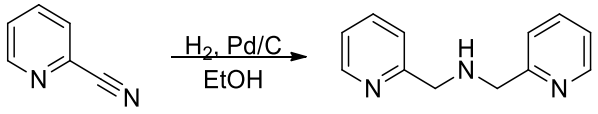

10.1015g (96.05 mmol) of 2-cyanopyridine and 0.4966g of 5% (w/w) Pd/C was suspended in 17 ml of anhydrous ethanol and rapidly stirred. 3L of H_2 was flushed through the system and an additional 1L left to incorporate at 1 atm. Every 24 hours another 3L of H_2 is flushed through the system and 1 L left to incorporate at 1 atm, after 72 hours TLC indicated the consumption of starting 2-cyanopyridine. The reaction mixture was then filtered through a vacuum-packed plug of celite and washed with 50 ml of hot EtOH. The filtrate was then concentrated under reduced pressure to a constant mass. Yield: 9.540g (99.7%) – transparent yellow oil.

1H NMR 300 MHz ($CDCl_3$): δ 8.56 (2H, d, J = 4.7 Hz), 7.62 (2H, t, J = 7.7 Hz), 7.36 (2H, d, J = 7.8 Hz), 7.14 (2H, t, J = 6.2 Hz), 3.97 (4H, s), 2.66 (1H, s_b)

13C NMR 500 MHz (CDCl3): δ 166.6, 159.6, 149.4, 136.4, 122.2, 121.9, 54.7

7b methyl 2-((pyridin-2-ylmethyl)amino)acetate

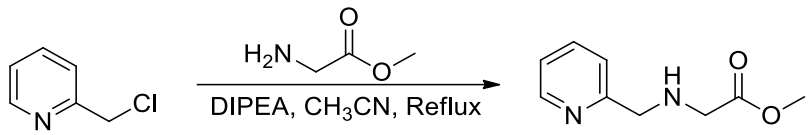

1.6641g (10.41 mmol) of picolylchloride HCl, 2.5273g (20.13 mmol) of glycine methyl ester HCl and 5.0460g (39.03 mmol) of diisopropylethylamine was combined in 20 ml of CH_3CN and heated to reflux. After 7 hours the reaction was complete by TLC and reflux was stopped. The reaction was concentrated under reduced pressure and the crude residue was resuspended in 50 ml of CH_2Cl_2 and washed with 150 ml of dilute $NaHCO_3$. The organics were then dried over $MgSO_4$ and concentrated under reduced pressure. Yield 1.5027g (83%), m.p. 158 – 160 ^oC.

1H NMR 500 MHz (DMSO-d6): δ 8.75 (1H, d, J = 4.9 Hz), 8.14 (1H, t, J = 7.7 Hz), 7.87 (1H, d, J = 8 Hz), 7.65 (1H, t, J = 6.4 Hz), 4.48 (2H, s), 4.10 (2H, s), 3.74 (3H, s).

General Synthesis of o-nitroanilines **8**

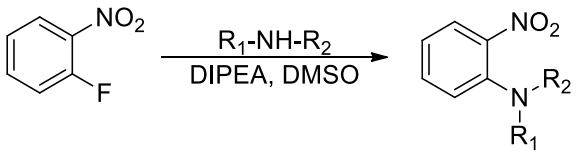

1 eq (1 mmol) of amine and 1 eq (1 mmol) of DIPEA and 1 eq (1 mmol) of o-fluoronitrobenzene are mixed in 5 ml of anhydrous DMSO for multiple days. After TLC shows consumption of starting materials, the solution is diluted into 50 ml of H_2O and extracted with CH_2Cl_2. The organic extracts are then washed with dilute NaOH then sat. NaCl, dried over $MgSO_4$ and concentrated under reduced pressure. When possible the nitro-anilines are crystallized from CH_2Cl_2/Hexanes.

8a N,N-dimethyl-2-nitroaniline

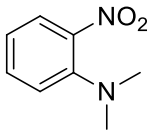

Yield: 25%, red oil

1H NMR 500 MHz (DMSO-d6): δ 7.75 (1H, dd, J = 1.5, 8.0 Hz), 7.49 (1H, td, J = 1.5, 7.0 Hz), 7.16 (1H, dd, J = 2.5, 7.5 Hz), 6.88 (1H, td, J = 1.0, 8.0 Hz), 2.79 (6H, s)

8b N-methyl-2-nitro-N-(pyridin-2-ylmethyl)aniline

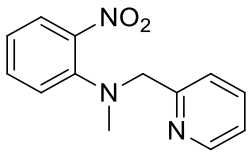

Yield: 87%, red-orange oil

1H NMR 500 MHz (DMSO-d6): δ 8.51 (1H, dd, J = 0.5, 5.0 Hz), 7.77 (1H, td, J = 1.5, 7.5 Hz), 7.75 (1H, dd, J = 2.0, 7.5 Hz), 7.45 (1H, td, J = 2.0, 7.5 Hz), 7.33 (1H, d, J = 7.5 Hz), 7.27 (1H, td, J = 0.5, 5.0 Hz), 7.22 (1H, dd, J = 1.0, 8.5 Hz), 6.93 (1H, td, J = 1.0, 8.5 Hz), 4.50 (2H, s), 2.78 (3H, s)

8c N-methyl-2-nitro-N-(2-(pyridin-2-yl)ethyl)aniline

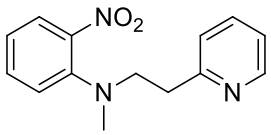

Yield: 94%, red-orange oil

1H NMR 500 MHz (DMSO-d6): δ 9.22 (1H, d, J = 4.5 Hz), 8.47 (1H, dd, J = 1.0, 8.0 Hz), 8.43 (1H, td, J = 1.5, 8.0 Hz), 8.23 (1H, td, J = 1.0, 8.0 Hz), 8.01 (2H, m), 7.95 (1H, td, J = 1.5, 7.0 Hz), 7.67 (1H, t = 7.5 Hz), 4.28 (2H, t, J =8.0 Hz), 3.75 (2H, t, J = 7.5 Hz), 3.55 (3H, s)

8d 2-nitro-N,N-bis(pyridin-2-ylmethyl)aniline

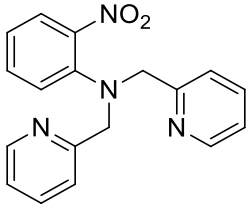

Yield: 63%, amber oil

1H NMR 300 MHz (CD_3Cl): δ 8.52 (2H, d, J = 4.2 Hz), 7.72 (1H, dd, J = 1.2, 8.1 Hz), 7.62 (2H, td, J = 1.8, 7.8 Hz), 7.45 (2H, d, J = 7.8 Hz), 7.36 (1H, td, J = 1.5, 6.9 Hz), 7.22 (1H, d, J = 8.1 Hz), 7.15 (2H, td, J = 6.9, 8.1 Hz), 7.01 (1H, t, J = 7.2 Hz), 4.48 (4H, s)

8e methyl 2-((2-nitrophenyl)(pyridin-2-ylmethyl)amino)acetate

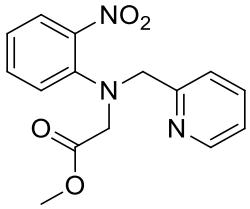

Yield: 27%, amber oil

1H NMR 300 MHz (CD_3Cl): δ 8.52 (1H, dd, J = 0.5, 4.0 Hz), 7.76 (1H, dd, J = 1.5, 8.0 Hz), 7.69 (1H, t, J = 8.0 Hz), 7.61 (1H, d, J = 8.0 Hz), 7.43 (1H, td, J = 1.5, 8.0 Hz), 7.38 (1H, d, J = 8.5 Hz), 7.19 (1H, t, J = 7.5 Hz), 7.05 (1H, td, J = 1.0, 8.0 Hz), 4.72 (2H, s), 3.95 (2H, s), 3.71 (3H, s)

8f methyl 2-((2-nitrophenyl)amino)acetate

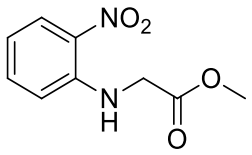

Yield: 38%, m.p. 70 - 71 °C,

1H NMR 500 MHz [DMSO-d6]: δ 8.37 (1H, s), 8.09 (1H, dd, J = 1.5, 8.5 Hz), 7.54 (1H, td, J = 1.0, 8.0 Hz), 6.92 (1H, d, J = 9.0 Hz), 6.75 (1H, td, J = 1.0, 7.0 Hz), 4.28 (2H, d, J = 6.0 Hz), 3.70 (3H, s)

8g 1-(2-nitrophenyl)piperazine

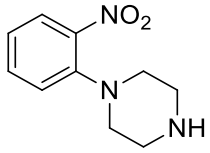

Yield: 50%, m.p. 123 - 125 °C Red – orange powder, very hygroscopic

1H NMR 500 MHz (DMSO-d6): δ 7.79 (1H, d, J = 8.5 Hz), 7.58 (1H, t, J = 7.0 Hz), 7.30 (1H, d, J = 8.5 Hz), 7.12 (1H, t, J = 8.0 Hz), 2.94 (4H, d, J = 5.0 Hz), 2.84 (4H, d, J = 5.0 Hz)

8h 4-(2-nitrophenyl)morpholine

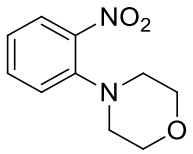

Yield: 57%, red-orange oil

1H NMR 500 MHz (DMSO-d6): δ 7.80 (1H, d, J = 8.0 Hz), 7.60 (1H, t, J = 7.5 Hz), 7.32 (1H, d, J = 7.0 Hz), 7.15 (1H, t, J = 7.5 Hz), 3.68 (4H, t, J = 4.5 Hz), 2.97 (4H, t, J = 4.5 Hz)

8i (S)-methyl 1-(2-nitrophenyl)pyrrolidine-2-carboxylate

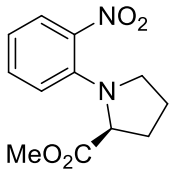

Yield: 99%, red-orange semi-solid

1H NMR 500 MHz ($CDCl_3$): δ 7.70 (1H, d, J = 7.5 Hz), 7.37 (1H, t, J = 7.5 Hz), 6.83 (1H, d, J = 9.0 Hz), 6.80 (1H, t, J = 7.5 Hz), 4.27 (1H, t, J = 7.5 Hz), 3.68 (3H, s), 3.54 (1H, q, J = 8.5 Hz), 3.18 (1H, t, J = 8.5 Hz), 2.45 (1H, m), 2.11 (2H, m), 1.95 (1H, m)

Reduction of Nitroanilines **9**

9a 2-(piperazin-1-yl)aniline

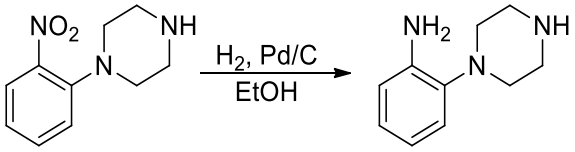

0.9646g (4.65 mmol) of **8g** and 0.3447g of 5% (w/w) Pd/C was stirred rapidly in 25 ml of EtOH while 4 L of H_2 was flushed through the system. 1L of H_2 was then allowed to slowly incorporate over 8 hours. Once complete by TLC, the reaction mixture was filtered through 1 cm of vacuum packed celite. The celite was then washed with 50 ml of boiling CH_2Cl_2 and the combined filtrates were concentrated under reduced pressure. Yield: 8.25g (100%), m.p. 159 – 161 ^oC

1H NMR 500 MHz (DMSO-d6): δ 6.86 (1H, d, J = 7.7 Hz), 6.79 (1H, t, J = 7.5 Hz), 6.67 (1H, d, J = 7.8 Hz), 6.53 (1H, t, J = 7.5 Hz), 4.76 (2H, s_b), 2.96 (4H, m), 2.79 (4H, m)

13C NMR 500 MHz (DMSO-d6): δ 142.8, 138.7, 124.5, 119.6, 117.0, 114.8, 50.7, 45.6

9b N1,N1-bis(pyridin-2-ylmethyl)benzene-1,2-diamine

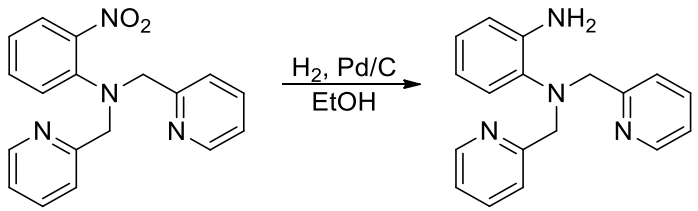

0.3232g (1 mmol) of **8d** and 0.1430g of 5% (w/w) Pd/C was suspended in 25 ml of anhydrous ethanol. With rapid stirring, 3 L of H_2 was flushed through the system with an additional 1L of H_2 left to incorporate at 1 atm. After 18 hours the starting material had been consumed by TLC and the reaction mixture was filtered through a 1 cm thick pad of vacuum packed celite. The celite was washed with 50 ml of hot EtOH and the filtrate concentrated. Yield: 0.2850g (98%) – red oil.

General Synthesis of OAN family **10**

Freshly reduced amine (1 eq, 2.0 mmol) is dissolved in 5 ml of 1M HCl and chilled to 0°C. Once chilled, $NaNO_2$ from a stock solution (2.2 eq, 4.4 mmol) is added to the mixture dropwise and slowly to maintain

sub 5 °C temperature throughout addition. This solution is stirred for 30 min at 0 °C before dropwise addition to a rapidly stirring solution of 1,3-dihydroxynaphthalene (1.25 eq, 2.5 mmol) in 10 ml of 1.0 M NaOH. The solution is then stirred for 24 hours during which the solution was allowed to reach room temperature. Then the solution is acidified to ~ pH 7 with AcOH, chilled and the precipitate collected via vacuum filtration. The resulting solid is then boiled in 50 ml of diethyl ether for 1 hour, filtered and washed with 50 ml of diethyl ether. The solid is then dried under reduced pressure for multiple days to afford the desired azo dye **9x**.

10d 4-((2-(bis(pyridin-2-ylmethyl)amino)phenyl)diazenyl)naphthalene-1,3-diol

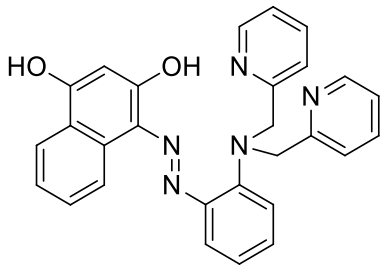

Yield: 30% m.p. 218 - 227 °C

1H NMR 500 MHz (DMSO-d6): δ 8.43 (2H, d, J = 1.4 Hz), 8.18 (1H, d, J = 7.8 Hz), 7.91 (1H, d, J = 7.4 Hz), 7.73 (1H, d, J = 8.1 Hz), 7.68 (3H, m), 7.38 (1H, t, J = 7.2 Hz), 7.26 (2H, m), 7.18 (3H, m), 7.03 (1H, t, J = 8.2 Hz), 6.94 (1H, d, J = 7.9 Hz), 6.69 (1H, t, J = 8.2 Hz), 5.30 (1H, s), 4.31 (4H, s), 4.13 (1H, s_b)

13C NMR 500 MHz (DMSO-d6): δ 179.1, 177.8, 158.5, 148.9, 140.1, 136.8, 136.3, 135.1, 132.6, 128.7, 126.0, 125.6, 124.8, 123.7, 123.2, 122.6, 121.7, 120.7, 113.2, 105.2, 59.3

10d-Zn 4-((2-(bis(pyridin-2-ylmethyl)amino)phenyl)diazenyl)naphthalene-1,3-diol Zinc Salt

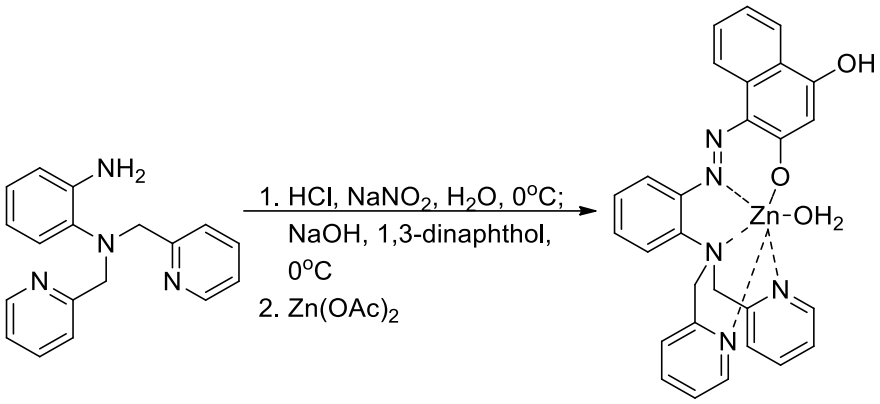

0.8581g (2.9 mmol) of **9b** was dissolved into 1 ml of 12 M HCl, diluted to 10 ml and chilled to 0 °C. Then 3 .0 ml of a 1.0 M $NaNO_2$ solution was added dropwise and slowly to the solution until KI-starch paper indicated excess oxidant. This solution was then dropwise delivered to a solution of 0.4633g (2.9 mmol) of 1,3-dihydroxynaphthalene in 25 ml of 1.0 M NaOH such that the temperature of solution was maintained at 0 °C. Once added the solution was stirred overnight and allowed to slowly warm to room temperature. After 24 hours the solution was diluted with 300 ml of H_2O, until the solution became homogenous. This solution was heated to reflux before addition of 30 ml of a 0.1 M $Zn(OAc)_2$ solution and the resulting solution was allowed to concentrate by ~ 100 ml. The solution was then chilled and the zinc complex was recovered via vacuum filtration and dried under reduced pressure for multiple days to afford a blue-pink-grey solid. Yield: 0.4788g (33%), m.p. 260 °C decomp

1H NMR 500 MHz (DMSO-d6): δ 8.63 (2H, d, J = 5.3 Hz), 8.30 (1H, d, J = 8 Hz), 8.07 (2H, t, J = 7.9 Hz), 7.93 (1H, d, J = 7.9 Hz), 7.83 (1H, d, J = 7.9 Hz), 7.74 (1H, d, J = 9.5 Hz), 7.64 (2H, t, J = 6.4 Hz), 7.60 (2H, d, J = 7.8 Hz), 7.36 (1H, t, J = 6.9 Hz), 7.24 (1H, t, J = 7.3 Hz), 7.19 (1H, t, J = 7.4 Hz), 6.97 (1H, t, J = 6.8 Hz), 5.84 (1H, s), 4.67 (4H, s)

13C NMR 500 MHz (DMSO-d6): δ 172.4, 155.8, 149.2, 148.1, 141.3, 138.7, 137.8, 130.4, 129.3, 128.8, 128.6, 126.1, 125.5, 124.7, 124.5, 123.9, 122.3, 121.3, 114.3, 108.2, 61.5

10a 4-((2-(dimethylamino)phenyl)diazenyl)naphthalene-1,3-diol

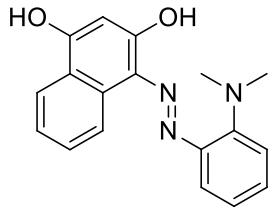

Yield: 84% m.p. 65 – 75 °C

1H NMR 500 MHz (DMSO-d6): δ 8.75 (1H, d, J = 8.0 Hz), 8.28 (1H, d, J = 8.0 Hz), 8.03 (1H, d, J = 8.0 Hz), 7.54 (1H, t, J = 7.0 Hz), 7.42 (2H, m), 7.29 (1H, t, J = 7.0 Hz), 7.17 (1H, t, J = 7.5 Hz), 5.67 (1H, s), 3.07 (6H, s)

10b 4-((2-(methyl(pyridin-2-ylmethyl)amino)phenyl)diazenyl)naphthalene-1,3-diol

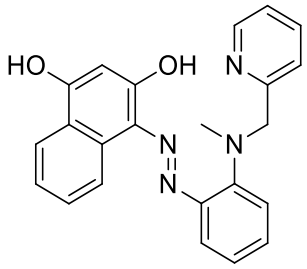

Yield: 86%, m.p. 198 – 202 °C

1H NMR 500 MHz (DMSO-d6): δ 8.47 (1H, d, J = 4.5 Hz), 8.19 (1H, d, J = 8.0 Hz), 7.90 (1H, d, J = 6.5 Hz), 7.83 (1H, d, J = 8.0 Hz), 7.77 (1H, t, J = 8.0 Hz), 7.75 (1H, d, J = 8.5 Hz), 7.38 (1H, t, J = 7.0 Hz), 7.28 (1H, d, J = 6.5 Hz), 7.24, (1H, t, J = 5.0 Hz), 7.15 (1H, d, J = 8.0 Hz), 7.09 (1H, t, J = 7.5 Hz), 6.84 (1H, t, J = 6.0 Hz), 5.26 (1H, s), 4.27 (2H, s), 2.62 (3H, s)

10b-Zn (E)-4-((2-(methyl(pyridin-2-ylmethyl)amino)phenyl)diazenyl)naphthalene-1,3-diol Zinc Salt

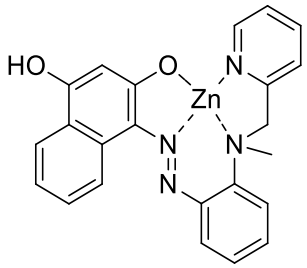

0.1557g (0.41 mmol) of **9b** was suspended in 20 ml of H_2O and heated to 60 °C. With rapid stirring, 4.5 ml of a 0.1M $Zn(OAc)_2$ solution was added to the reaction mixture dropwise and slowly. The reaction mixture was stirred for an additional 30 minutes before cooling and centrifugating. The solid was then resuspended in 20 ml of H_2O, centrifuged and dried under reduced pressure for multiple days. Yield: 0.1371g (75%) m.p. +310 °C

1H NMR 500 MHz (DMSO-d6): δ 8.78 (1H, d, J = 6.0 Hz), 8.30 (1H, d, J = 8.0 Hz), 8.08 (1H, t, J = 7.0 Hz), 7.85 (1H, d, J = 7.5 Hz), 7.68 (1H, t, J = 7.0 Hz), 7.56 (1H, d, J = 7.5 Hz), 7.47 (1H, d, J = 8.0 Hz), 7.32 (1H, t, J = 7.5 Hz), 7.23 (1H, t, J = 8.5 Hz), 7.12 (1H, t, J = 7.5 Hz), 6.89 (1H, t, J = 7.5 Hz), 5.16 (1H, s), 4.08 (2H, m), 2.57 (3H, s)

10c 4-((2-(methyl(2-(pyridin-2-yl)ethyl)amino)phenyl)diazenyl)naphthalene-1,3-diol

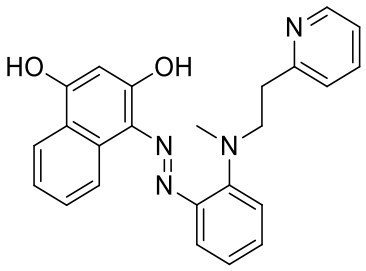

Yield: 49 %, m.p. 268 – 270 °C

1H NMR 500 MHz (DMSO-d6): δ 16.09 (1H, s), 8.41 (1H, d, J = 5.5 Hz), 8.17 (1H, d, J = 7.9 Hz), 7.89 (1H, d, J = 7.7 Hz), 7.74, (1H, d, J = 8.0 Hz), 7.62 (1H, t, J = 8.1 Hz), 7.37 (1H, t, J = 8.8 Hz), 7.30 (1H, d, J = 7.8 Hz), 7.25 (1H, t, J = 7.8 Hz), 7.14 (2H, m), 6.87 (1H, t, J = 8.9 Hz), 5.21 (1H, s), 3.21 (2H, m), 3.00 (2H, m), 2.75 (3H, s)

10e 4-((2-(piperazin-1-yl)phenyl)diazenyl)naphthalene-1,3-diol

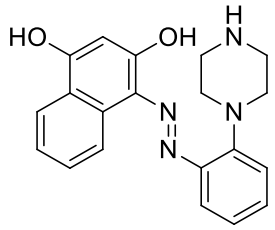

Yield: 93%, m.p. 302 °C decomp

1H NMR 500 MHz (DMSO-d6): δ 8.16 (1H, d, J = 8.0 Hz), 7.89 (1H, d, J = 7.5 Hz), 7.73 (1H, d, J = 8.0 Hz), 7.36 (1H, m), 7.25 (1H, m), 7.08 (2H, m), 6.86 (1H, m), 5.23 (1H, s), 2.96 (4H, s), 2.76 (4H, s)

10f 4-((2-morpholinophenyl)diazenyl)naphthalene-1,3-diol

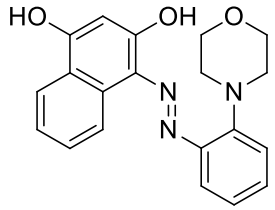

Yield: 99% m.p. +320 °C

1H NMR 300 MHz (CD_3OD): δ 8.37 (1H, d, J = 4.8 Hz), 8.04 (1H, d, J = 4.8Hz), 7.89 (1H, d, J = 5.1 Hz), 7.50 (1H, t, J = 4.5 Hz), 7.36 (1H, t, J = 4.5 Hz), 7.21 (2H, m), 7.02 (1H, t, J = 4.2 Hz), 5.85 (1H, s), 4.02 (4H, m), 2.96 (4H, m)

11 tert-butyl 2-((4-((2-(bis(pyridin-2-ylmethyl)amino)phenyl)diazenyl)-3-hydroxynaphthalen-1-yl)oxy)acetate zinc salt

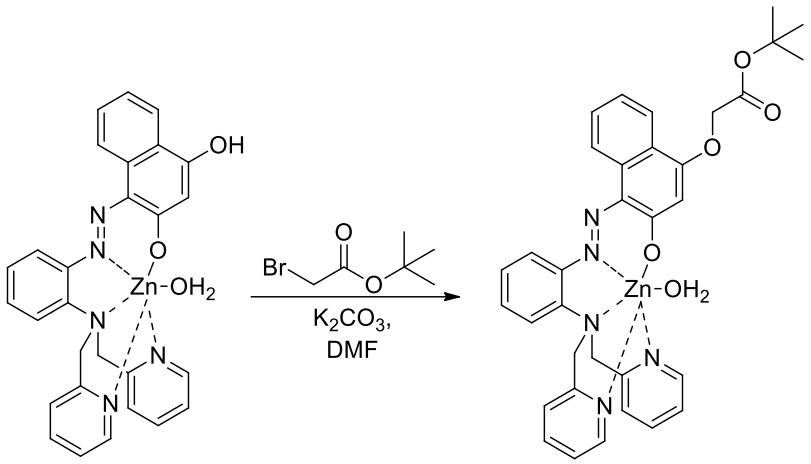

0.1057g (0.20 mmol) of **10d-Zn** was dissolved in 2 ml of DMF with 0.1347g (0.40 mmol) of Cs_2CO_3. With stirring, 0.30 ml (2.0 mmol) of t. butyl bromoacetate in 0.5 ml of DMF was added to the reaction mixture. After 24 hours the DMF was washed with 50 ml of hexanes and then concentrated via toluene azeotrope, the crude residue was then boiled in 50 ml of diethyl ether for an hour before cooling and filtering the reaction mixture. The solid was then dried under reduced pressure to afford a bright orange solid. Yield: 0.1103g (86%), m.p. 194 - 200 ^oC

1H NMR 500 MHz (DMSO-d6): δ 8.39 (1H, d, J = 8.5 Hz), 8.26 (2H, d, J = 5.0 Hz), 8.13 (1H, d, J = 8.4 Hz), 8.04 (1H, d, J = 8.3 Hz), 7.91 (2H, t, J = 7.6 Hz), 7.73 (1H, d, J = 8.3 Hz), 7.48 (6H, m), 7.35 (1H, t, J = 7.6 Hz), 7.28 (1H, t, J = 7.8 Hz), 6.56 (1H, s), 5.04 (2H, s), 4.98 (2H, d, J = 15.4 Hz), 4.83 (2H, d, J = 15.5 Hz), 1.52 (9H, s)

13C NMR 500 MHz (DMSO-d6): δ 169.3, 167.6, 160.7, 153.8, 146.9, 141.8, 140.3, 136.4, 129.4, 129.2, 127.5, 127.2, 125.2, 124.4, 123.7, 122.4, 121.7, 121.0, 116.0, 106.0, 82.3, 66.2, 62.5, 62.3, 28.2, 28.0

12 4-fluoro-3-nitrobenzene-1-sulfonyl chloride

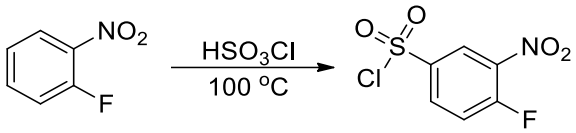

15.50 ml (0.233 mol) of chlorosulfonic acid was heated to 65 °C with rapid stirring. Then 14.1154g (0.100 mol) of o-fluoronitrobenzene was added to the reaction mixture and the solution was heated to 100 °C. After 20 hours the reaction was complete by TLC and the solution was cooled to 30 °C, poured over 100g of ice with 100 ml of CH_2Cl_2. The aqueous layer was then extracted with an additional 200 ml of CH_2Cl_2. The combined organic extracts were then washed with Sat. $NaHCO_3$ then Sat. NaCl, dried over $MgSO_4$ and concentrated under reduced pressure. Yield: 13.904g (58%)

1H NMR 500 MHz (CDCl3): δ 8.78 (1H, dd, J = 2.5, 6.5 Hz), 8.36 (1H, ddd, J = 1.5, 2.5, 9 Hz), 7.64 (1H, t, J = 9 Hz).

13C NMR 500 MHz (CDCl3): δ 160.0, 157.8, 140.5, 134.0, 126.1, 120.8

19F NMR 500 MHz (CDCl3): δ -104.3 (1F, m)

13 ethyl 6-(4-fluoro-3-nitrophenylsulfonamido)hexanoate

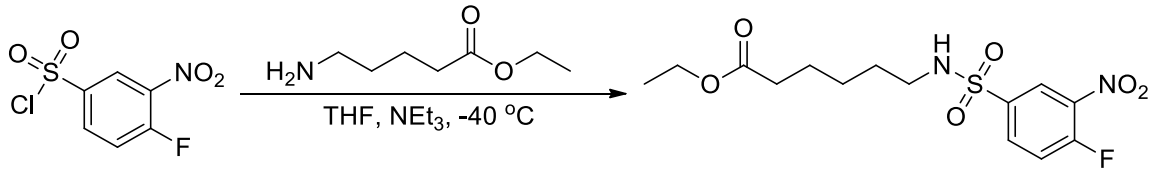

2.409g (10 mmol) of **11** was suspended in 15 ml of THF and cooled to -40 °C (CH_3CN/dry ice bath). Then 3.036g (30 mmol) of NEt_3 was added to the rapidly stirring solution. Once homogenous, a solution of 2.175g (11 mmol) of ethyl 6-aminohexanoate HCl in 5 ml of H_2O was added dropwise and slowly. The reaction was monitored by TLC and stopped after 1 hour at – 40 °C. The reaction was then warmed to

room temperature, diluted into 50 ml of H_2O and extracted into 100 ml of EtOAc. The organic layer was then washed with Sat. $NaHCO_3$, Sat NaCl, then dried over $MgSO_4$ and concentrated under reduced pressure. The product was isolated via flash chromatography, eluent 6% CH_3CN in CH_2Cl_2. Yield 2.0593g (57%), m.p: 32 – 34 ^oC

1H NMR 500 MHz (CDCl3): δ 8.57 (1H, dd, J = 2.3, 6.8 Hz), 8.15 (1H, m), 7.48 (1H, t, J = 9.4 Hz), 5.32 (1H, t, J = 6 Hz), 4.12 (2H, q, J = 7.2 Hz), 3.02 (2H, q, J = 6.8 Hz), 2.27 (2H, t, J = 7.3 Hz), 1.55 (4H, m), 1.34 (2H, m), 1.25 (3H, t, J = 7.2 Hz)

13C NMR 500 MHz (CDCl3): δ 173.7, 158.5, 156.3, 137.5, 134.1,125.6, 119.8, 60.4, 43.0, 33.9, 29.1, 25.8, 24.0, 14.1

19F NMR 500 MHz (CDCl3): δ -110.3 (1F, m)

General Synthesis of 4-sulfonamide-2-nitro-anilines **14**

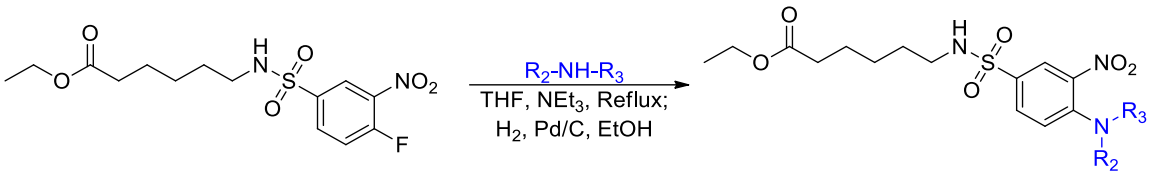

1 eq (1 mmol) **12** was dissolved into 1 ml of THF and stirred. To this was added, 1 eq (1 mmol) of ligand 1 eq (1 mmol) of NEt_3 in 3 ml of THF. Once combined the reaction was heated to reflux for 2 hours. The reaction mixture was diluted into H_2O and extracted with 50 ml of EtOAc. The organics were washed with sat $NaHCO_3$, sat NaCl then dried over $MgSO_4$ and concentrated under reduced pressure.

14a ethyl 6-(4-(methyl(2-(pyridin-2-yl)ethyl)amino)-3-nitrophenylsulfonamido)hexanoate

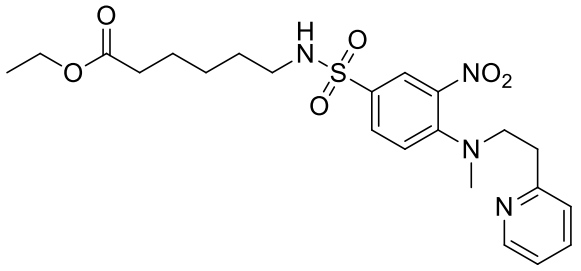

Yield: 90% red-orange oil

1H NMR 500 MHz (CDCl3): δ 8.52 (1H, d, J = 7.4 Hz), 8.19 (1H, d, J = 3.6 Hz), 7.75 (1H, dd, J = 3.6, 15.1 Hz), 7.62 (1H, td, J = 2.6, 12.8 Hz), 7.13 (3H, m), 4.76 (1H, t, J = 10 Hz), 4.12 (2H, q, J = 11.9 Hz), 3.78 (2H, t, J = 11.8 Hz), 3.12 (2H, t, J = 12.4 Hz), 2.96 (2H, q, J = 11.1 Hz), 2.90 (3H, s), 2.26 (2H, t, J = 12.1 Hz), 1.35 (1H, m), 1.24 (3H, t, J = 11.9 Hz)

14b ethyl 6-(4-(bis(pyridin-2-ylmethyl)amino)-3-nitrophenylsulfonamido)hexanoate

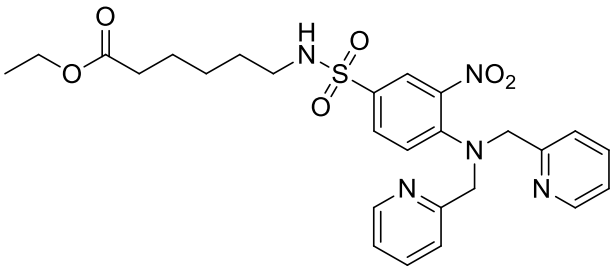

The crude residue was then subjected to flash chromatography [7.5% iPrOH in CH_2Cl_2]. Yield: Yield: 88%

– thick orange oil.

1H NMR 500 MHz (CDCl3): δ 8.53 (2H, d, J = 4.3 Hz), 8.23 (1H, s), 7.74 (1H, d, J = 9 Hz), 7.66 (2H, t, J = 7.8 Hz), 7.39 (2H, d, J = 7.8 Hz), 7.24 (1H, d, J = 9 Hz), 7.19 (2H, t, 6.1 Hz), 4.66 (1H, t, J = 6.2 Hz), 4.61 (4H, s), 4.14 (2H, q, J = 7.3 Hz), 3.74 (1H, d, J = 7.2 Hz), 3.00 (2H, q, J = 6.9 Hz), 2.28 (2H, t, J = 7.4 Hz), 1.59 (2H, t, J = 7.7 Hz), 1.52 (2H, t, J = 7.4 Hz), 1.34 (2H, m), 1.25 (4H, m).

13C NMR 500 MHz (CDCl3): δ 173.5, 156.2, 149.5, 147.4, 139.9, 136.9, 131.1, 130.5, 126.1, 122.7, 122.2, 121.6, 60.3, 58.6, 42.9, 33.9, 29.2, 25.9, 24.1, 18.4, 14.2

14c ethyl 6-(4-((2-methoxy-2-oxoethyl)amino)-3-nitrophenylsulfonamido)hexanoate

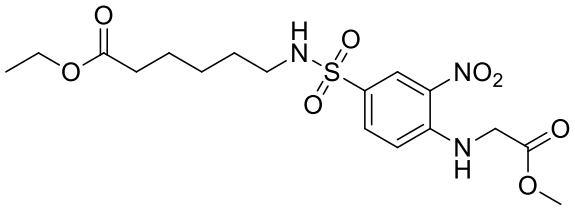

Yield: 81%

1H NMR 500 MHz (CDCl3): δ 8.74 (1H, s), 8.70 (1H, s), 7.89 (1H, d, J = 14.7 Hz), 6.81 (1H, d, J = 15 Hz), 4.61 (1H, t, J = 9.3 Hz), 4.17 (2H, d, J = 8.6 Hz), 4.12 (2H, q, J = 11.9 Hz), 3.86 (3H, s), 2.98 (2H, q, J = 11.0 Hz), 2.26 (2H, t, J = 12.1 Hz), 1.32 (2H, q, J = 11.6 Hz), 1.24 (3H, t, J = 11.8 Hz)

14d dimethyl 2,2'-((4-(N-(6-ethoxy-6-oxohexyl)sulfamoyl)-2-nitrophenyl)azanediyl)diacetate

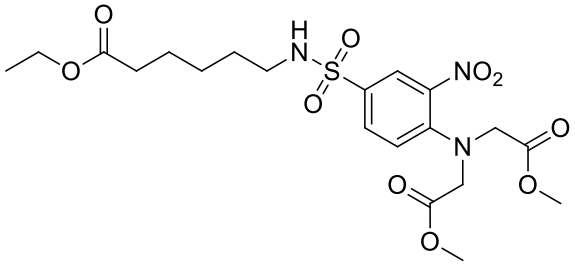

Yield: 72%, isolated via flash chromatography 10% EtOH in CH_2Cl_2 red-orange oil

1H NMR 500 MHz (CDCl3): δ 8.27 (1H, d, J = 3.3 Hz), 7.85 (1H, dd, J = 3.4, 14.7 Hz), 7.03 (1H, d, J = 14.9 Hz), 4.59 (1H, t, J = 10.0 Hz), 4.15 (6H, m), 3.80 (6H, s), 2.98 (2H, q, J = 10.9 Hz), 2.27 (2H, t, J = 12.0 Hz), 1.61 (6H, m), 1.37 (2H, q, J = 13.3 Hz), 1.25 (6H, m)

14e ethyl 6-(4-morpholino-3-nitrophenylsulfonamido)hexanoate

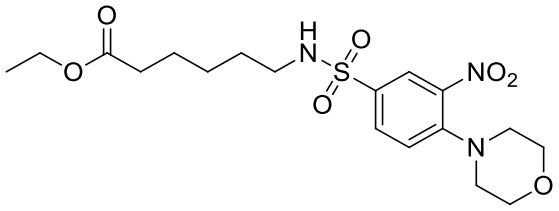

Yield: 71% red-orange oil

1H NMR 500 MHz (CDCl3): δ 8.27 (1H, d, J = 3.4 Hz), 7.91 (1H, dd, J = 3.6, 14.6 Hz), 7.16 (1H, d, J = 14.7 Hz), 4.63 (1H, t, J = 10.0 Hz), 4.13 (2H, q, J = 11.8 Hz), 3.85 (4H, m), 3.18 (4H, m), 2.99 (2H, q, J = 11.1 Hz), 2.26 (2H, t, J = 12.0 Hz), 1.35 (2H, q, J = 13.1 Hz), 1.25 (3H, t, J = 11.9 Hz)

15a ethyl 6-(3-amino-4-(bis(pyridin-2-ylmethyl)amino)phenylsulfonamido)hexanoate

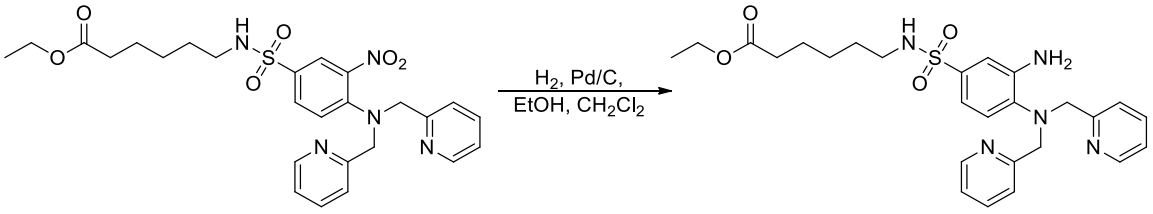

0.399g (0.74 mmol) o **14b** and 0.192g of 5% (w/w) Pd/C was suspended in 10 ml of 50:50 EtOH to CH_2Cl_2. With Rapid stirring, 2L of H_2 was flushed through the system with an additional 1L of H_2 left to incorporate at 1 atm overnight. After 18 hours reduction appeared complete by TLC and the reaction mixture was filtered through a 1 cm thick pad of vacuum packed celite. The celite was then washed with boiling CH_2Cl_2/EtOH. The filtrate was then concentrated under reduced pressure to afford an amber oil.

Yield: 0.379g (100%) – thick oil.

Synthesis of OAN-4OH-SA Family **16x**

16a 6-(4-(bis(pyridin-2-ylmethyl)amino)-3-((2,4-dihydroxynaphthalen-1-yl)diazenyl)phenylsulfonamido)hexanoic acid

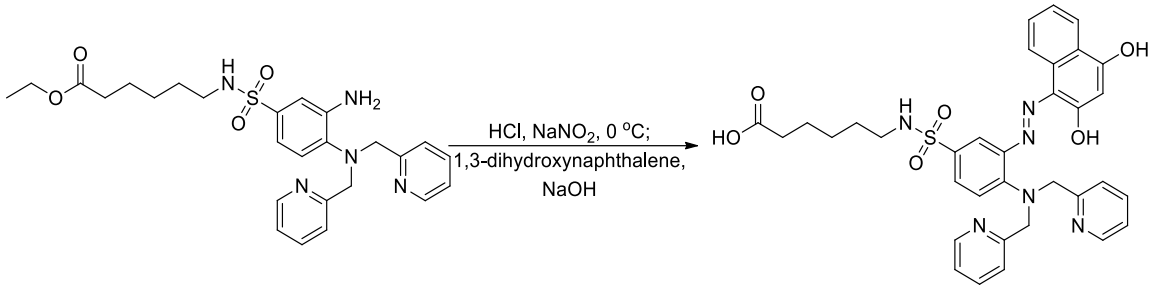

0.370g (0.70 mmol) of **15** was dissolved into 7 ml of 1M HCl and chilled to 0°C. Then 0.75 ml of 1.0 M $NaNO_2$ was added dropwise and slowly to the rapidly stirring solution. This solution was then added dropwise and slowly to a solution of 0.163g (1.0 mmol) of 1,3-dihydroxynaphthalene in 7 ml of 2M NaOH chilled to 0 °C such that sub 5 °C temperature is maintained throughout the addition. Once added the solution was allowed to stir at room temperature overnight. The precipitate was collected via vacuum filtration and dried under reduced pressure. Once dry the solid was triturated in 5 ml of ethanol and collected via vacuum filtration. Yield: 0.312g (65%), m.p. 138 – 140 °C

1H NMR 500 MHz (CD_3OD): δ 8.87 (2H, d, J = 5.5), 8.54 (3H, m), 8.23 (3H, m), 8.11 (1H, d, J = 8.7 Hz), 7.97 (4H, m) 7.85 (1H, m), 7.59 (1H, m), 7.44 (1H, t, J = 7.4 Hz), 6.45 (1H, s), 4.89 (4H, s), 3.59 (2H, d, J = 12.5 Hz), 3.33 (1H, s), 3.29 (2H, s), 2.88 (2H, m), 2.17 (2H, m), 1.29 (4H, m)

13C NMR 500 MHz (DMSO-d6): δ 174.8, 173.6, 154.3, 153.1, 149.0, 144.6, 143.7, 139.6, 139.3, 139.1, 139.0, 137.2, 134.8, 133.7, 133.6, 130.8, 130.1, 127.6, 126.6, 125.8, 125.6, 124.2, 123.2, 119.1, 113.1, 112.9, 105.4, 55.1, 52.6, 51.6, 42.8, 34.0, 33.5, 29.2, 26.0, 25.9, 24.4, 24.3

16b 5-(4-(bis(pyridin-2-ylmethyl)amino)-3-((2-hydroxynaphthalen-1-yl)diazenyl)phenylsulfonamido)pentanoic acid

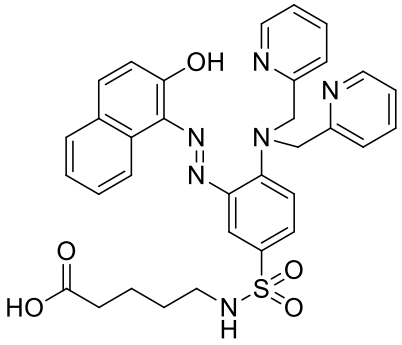

Yield 81%, m.p. 80 - 90 °C

ESI MS:

16c 5-(4-(bis(pyridin-2-ylmethyl)amino)-3-((4-hydroxynaphthalen-1-yl)diazenyl)phenylsulfonamido)pentanoic acid

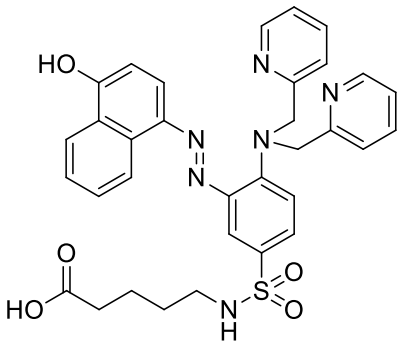

Yield 58%, m.p. 63 - 66°C

ESI MS:

General procedure for Solid Support attachment **17**

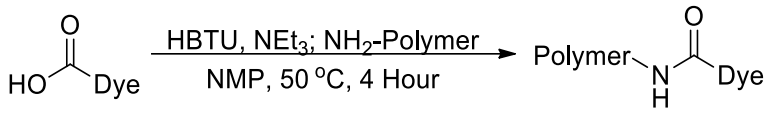

Stock solutions of dye complex with free carboxylic acids are prepared in addition to HBTU, and NET_3 solutions such that when mixed the final concentration of dye complex is ~ 2.00 mM as the activated dye complex. One polymer dot can be submerged in ~ 1.2 ml of acylating solution. With an IR lamp, the solutions are heated to ~ 50 °C on a slowly shaking vortexer. After 4 hours the polymer dot is removed from solution and washed with a 5% NEt_3 in NMP solution until all color had leached out of the polymer. The polymer was then slowly exchanged into ethanol then H_2O and finally acidic H_2O and thoroughly rinsed with 3M ethanolic HCl. The polymer dot is then rinsed with pH 7 MOPS buffer and stored in a vial with 10 ml of MOPS buffered H_2O. Only 18MΩ H_2O can be used as metal ions cannot be introduced to this process.

When the process is static and at room temperature for 24 hours instead, one can control the overall loading according to the following conditions.

Dot #	**Acylating Soln (M)**	**Abs**	**Dot #**	**Acylating Soln (M)**	**Abs**
1	1.0 mM	0.7418	4	250 µM	0.212
2	750 µM	0.457	5	100 µM	0.182
3	500 µM	0.255	6	50 µM	0.138

Chapter III. Oxidized Arginine Derivatives

Introduction

Enduracididine **28b** is an oxidized arginine found in several potent antibiotic structures like Mannopeptimycin, Teixobactin and Enduracidin[49–52], *figure 33*.

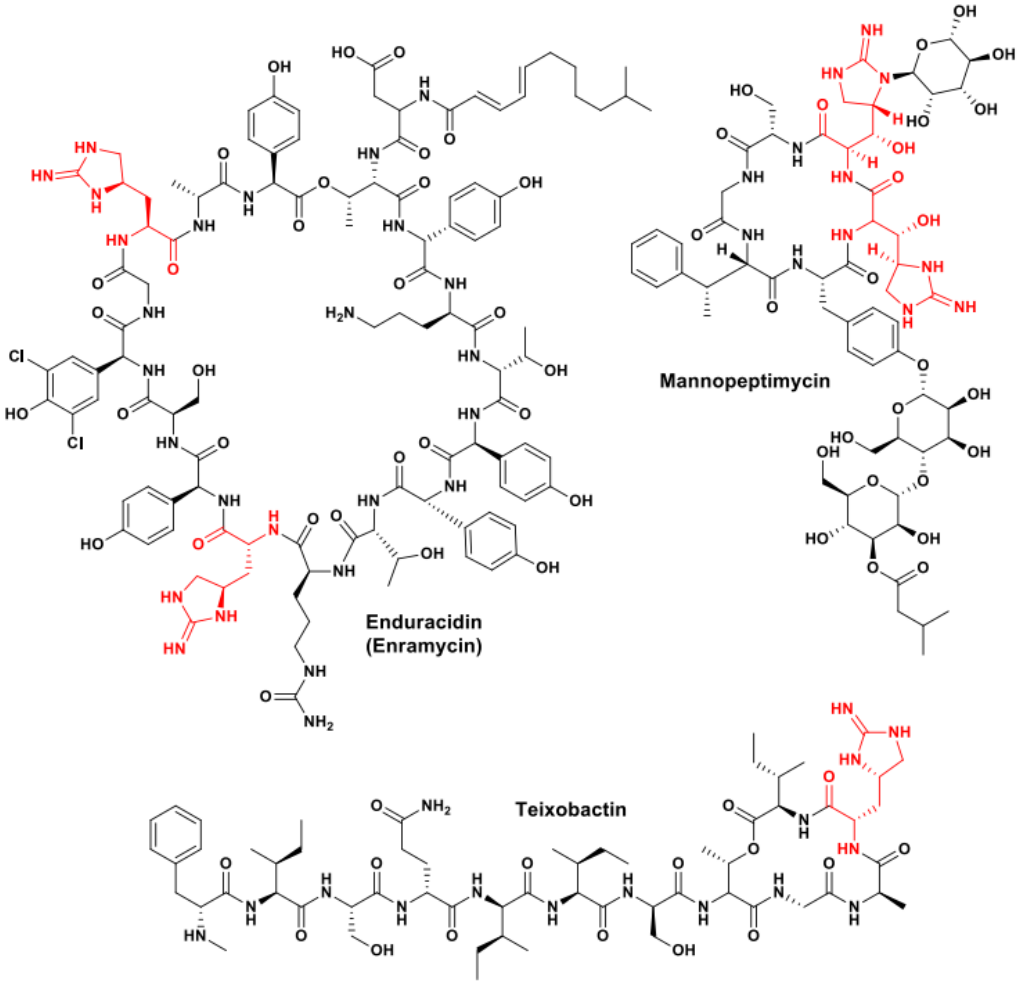

Figure 33: Structure of some potent antibiotics that retain the non-cannonical amino acid Enduracididine.

Presumably the conformational restriction of this arginine derivative, **28b**, is important to the selective interactions of derived molecules[53]. Biosynthesis in various organisms appears to follow distinct pathways[54–56]: via 4-hydroxyarginine **23e** in s. fungiscidicus, and via the related ketoacid **28** in s. hygroscopicus, scheme 21.

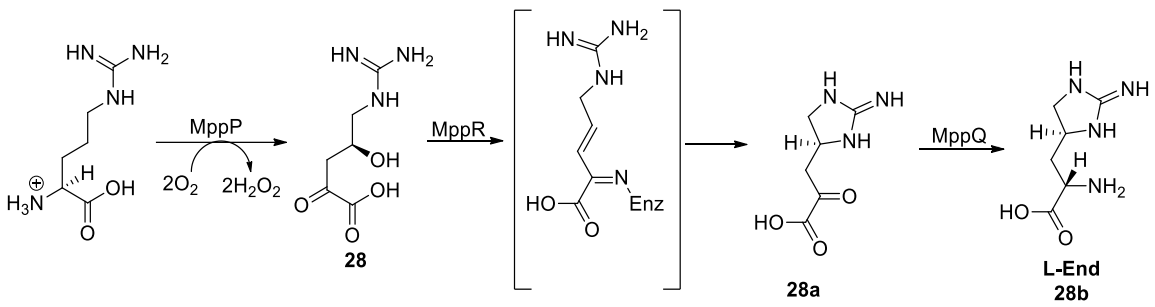

Scheme 21: The biosynthesis of enduracididine

It has recently been demonstrated that MppP is a PLP-dependent enzyme that uses molecular oxygen to convert arginine directly to ketoalcohol **28**, acting as the first example of a PLP-dependent hydroxylase[57,58]. This has been observed as the S enantiomer in the product complex crystal structure but this work is interested in stereochemical preferences, and whether related enzymes differ in intermediate stereochemical preferences. Closely related enzymes carry out distinct transformations so stereochemical variability seems possible as well.

Multiple investigations into this pathway have led to the discovery of intermediates in the biosynthesis of **28** from arginine.

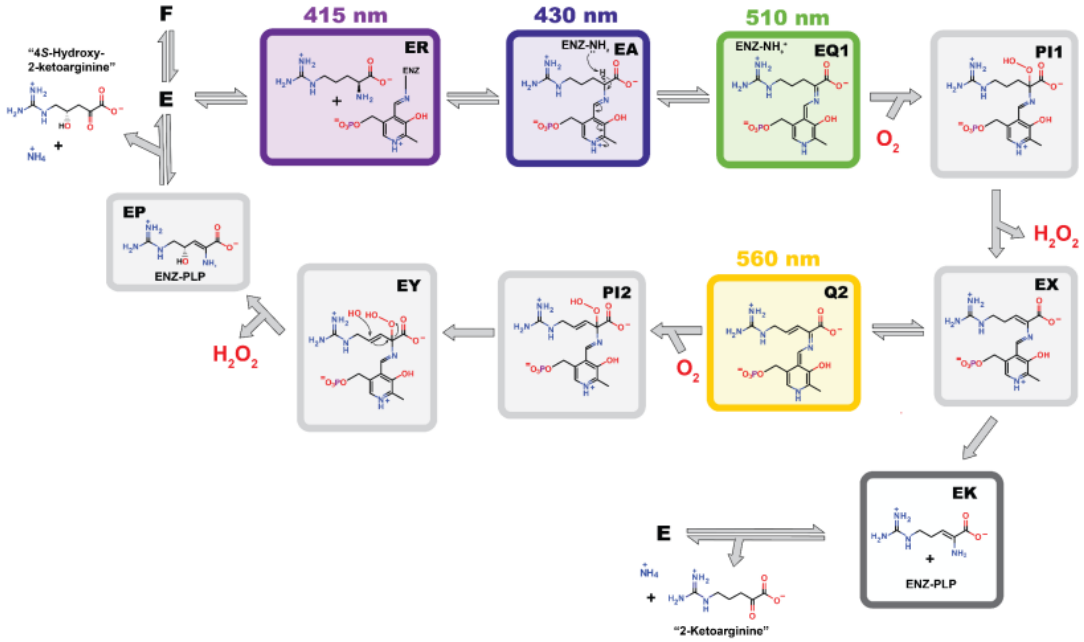

Figure 34: Proposed mechanism of MppP converting arginine to ketohydroxyarginine (Silvaggi)

From this pathway, *figure 34*, it is clear why both **28** and **35** would be attractive targets for synthesis. **28** is a product of this pathway, however MppP also leads to the formation of ketoarginine when fed arginine[56,57]. To make pure starting material for MppR, the subsequent enzymatic step, the synthesis of **28** was investigated. Furthermore, **35** appears as an intermediate in the conversion of L-arginine to 4(s)-hydroxyketoarginine. And so, it was believed that by feeding the enzyme pure **35** that the state Q2, a highly fluorescent state, could be observed for the sequence that leads to product. Thus both **28** and **35** constitute intermediates that could help solve the mechanism of transformation for the MppP(R,Q) enzyme(s) family.

γ-Hydroxyarginine

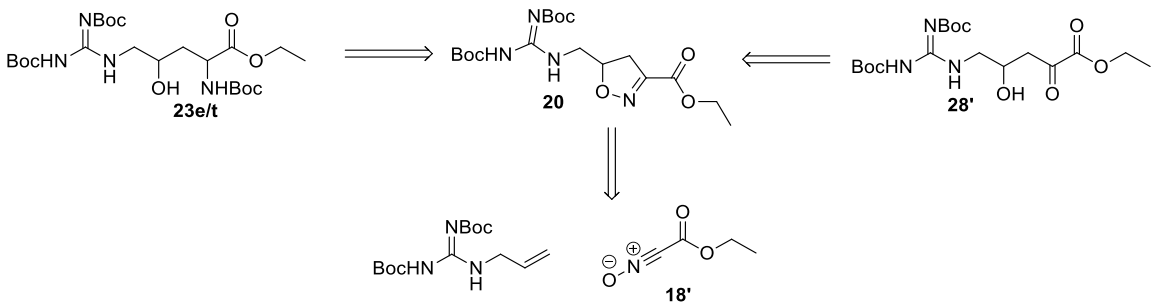

Figure 35: Retrosynthetic analysis for the synthesis of 4-hydroxyarginine

MppR transforms **28** to a cyclic ketoacid **28a**, which is thought to be transaminated by MppQ to form enduracididine[55], **28b**. An efficient preparation of **28'** would be of value in the kinetic and crystallographic investigations of these pathways, as is preparation of **23e** for study of the pathways involving this intermediate. While synthesis of **23e** is known and[59] prepared **28** from **23e** by treatment with L-AAO, it was considered whether a more direct synthesis of either or both compounds was possible, *figure 35*, that might provide access to other stereoisomers. Consequently, an efficient route to a stereochemical mixture was sought, assuming that diastereomers could be separated and enantiomers distinguished enzymatically.

Hydrogenolysis of isoxazolines with concomitant hydrolysis of the initially formed imine is a well-established method for the formation of β-hydroxyketones. Hydrogenolysis followed by imine hydrogenation, leading to aminoalcohols, is also known. Both target compounds **23e** and **28** are in principle available from the same penultimate intermediate **20**. While ketoacid **28** is the most desired target compound, this work focused on the hydroxyarginine **23e** as a potential route to separated enantiomers of **28**.

The synthesis of hydroxy arginine starts with the formation of eythl nitroacetate from ethyl acetoacetate, scheme 22.

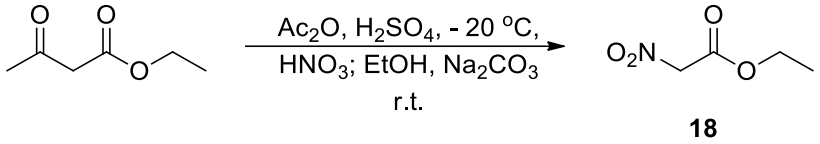

Scheme 22: Synthesis of ethyl nitroacetate

18 is easily obtained via vacuum distillation, b.p. 64°C at 4 torr. This reaction, will not work if an excess of carbonate is added, the carbonate is needed to neutralize the sulfuric acid only and will deprotonate the ethyl nitroacetate when added in excess.

To prepare **19**, the requisite nitrile oxide has been reported to form directly from **18** by dehydration in aqueous solution, scheme 23.

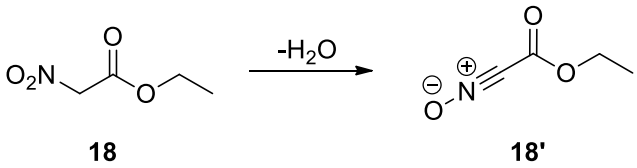

Scheme 23: dehydration of ethylnitroacetate to nitrile oxide

This unusual reaction has a long induction period that Blackmond demonstrated corresponds to the appearance of nitrite[60,61]; addition of nitrite reduces reaction times from days to hours. Presumably C-

nitrosation of **18** precedes elimination of nitrite to form nitrile oxide. We have found that aqueous reaction of allylammonium chloride with ethyl nitroacetate leads to isoxazoline **19** quite slowly, and that catalytic nitrite provides the expected dramatic acceleration. Installation of the guanidine function was uneventful, using the di-boc pyrazolylcarboxamidine reagent, scheme 24.

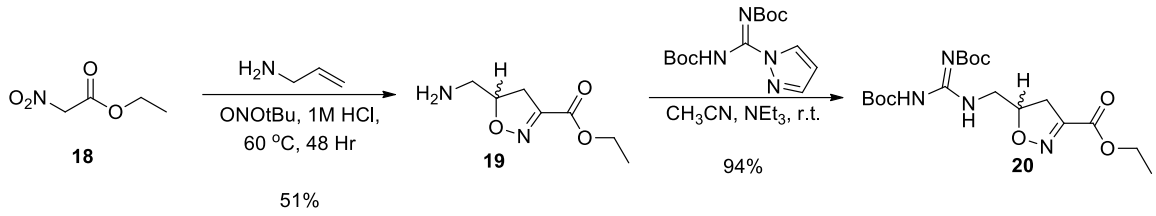

Scheme 24: Synthesis of quanidinylated isoxazoline

Hydrogenolysis of **20** was capricious, scheme 25. Despite the literature precedent for hydrogenolysis of isoxazolines into the corresponding β-hydroxyketone or hydroxyamine[62–68], the fully protected precursor **20** was unable to be consistently reduced under standard ambient pressure conditions using various catalysts and media. Sometimes complete reduction would take place, and sometimes under apparently the same conditions no product would result. When reaction did take place, products varied, indicating subsequent transformation. Consistent results were found with hydrogenolysis in ethanol under 60 psi of H2 with 20% Pd(OH)2/C in the presence of di-tert-butyldicarbonate (Boc2O). Reduction was consistent, and subsequent lactonization and other side reactions were avoided. With this catalyst and in situ amine acylation by Boc anhydride, atmospheric pressure hydrogenation also worked well even with Pd-C catalyst, but this has not been tested as many times as Parr shaker reaction.

Protected hydroxyarginine **21** was readily purified by flash chromatography. In contrast to closely related derivatives differentially protected, diastereomeric separation was also chromatographically

straightforward, allowing isolation of rac. Erythro and rac. Threo γ-hydroxyarginine, **21e** and **21t** respectively.

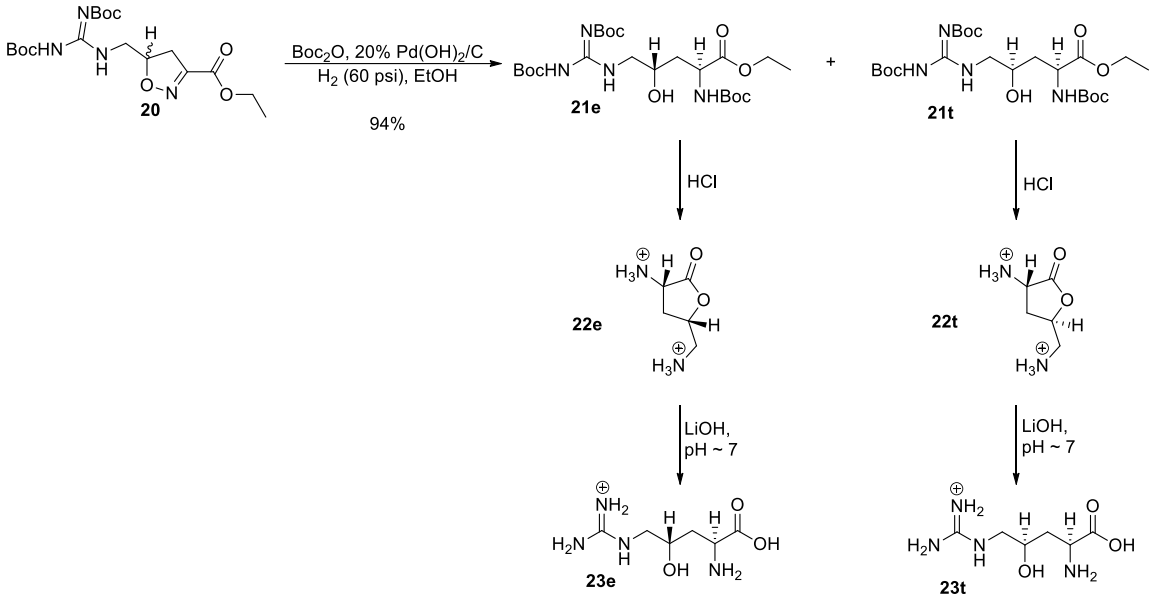

Scheme 25: reduction and separation of diastereomeric pairs

Acidic deprotection, scheme 25, also led to lactonization: workup involving saponification gave pure hydroxyarginine diastereomers **23e** and **23t** as pure crystalline racemates. This constitutes a succinct 4-step route to rac **23e** and **23t** in 37% and 42% yields respectively from ethyl nitroacetate, suitable for multigram preparation.

Lactonization allowed for direct comparison between an authentic standard of **22e** and a sample that was made via stereoselctive synthesis[69], *figure 36* (top).

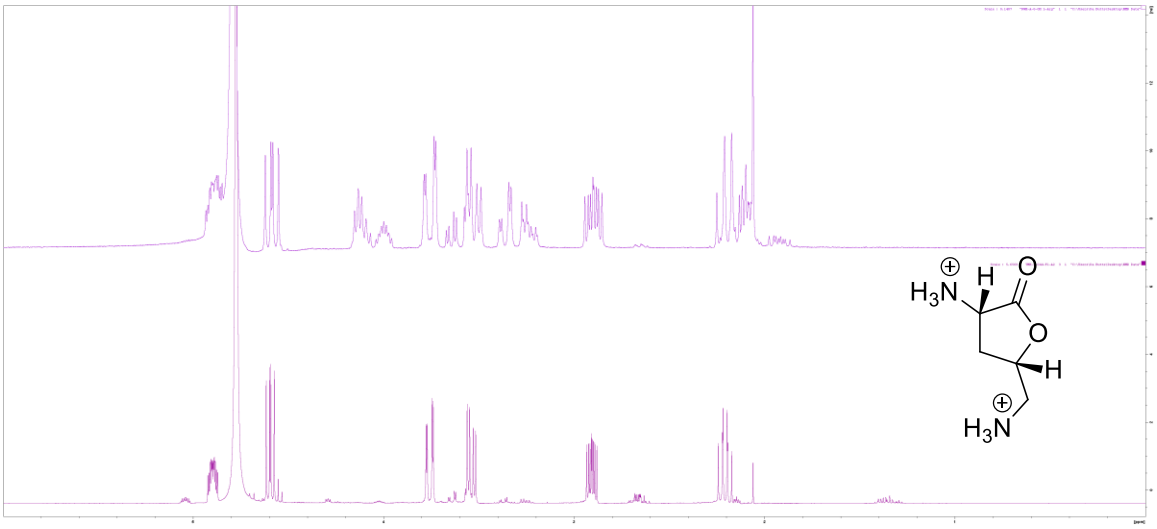

Figure 36: ^{1}H NMR comparison of authentic hydroxyarginine (top) that was synthesized enantioselectively to this work (bottom)

From this spectra, one can ascertain that the product made via this route (lower) is identical to the sample made via stereoselective route[69]. That said, the reaction mixture still produces a racemic mixture of erythro hydroxy arginine, **23e**.

The lactone is readily converted into its open chain amino acid form by saponification with LiOH and subsequent neutralization with dilute HCl.

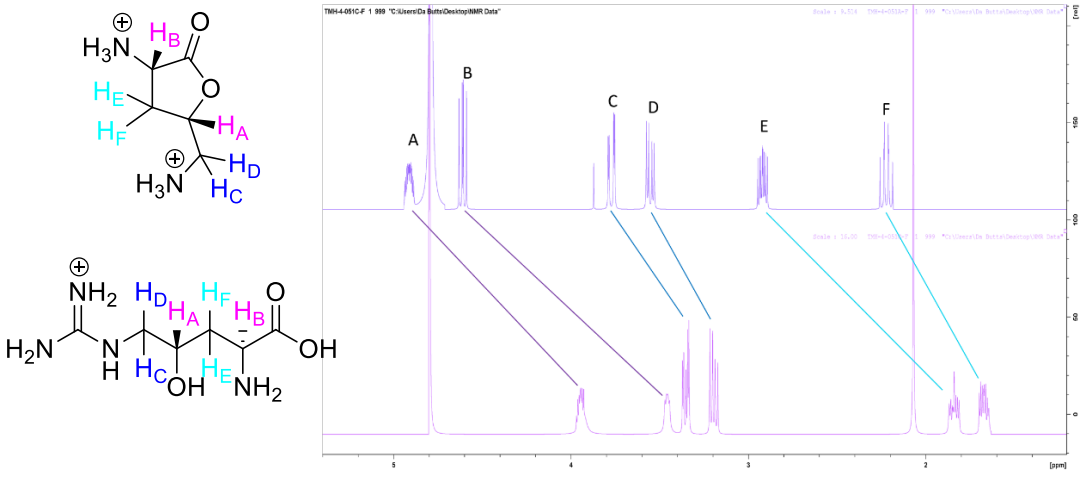

Figure 37: The difference between lactone and open amino acid by ^{1}H NMR

In addition to hydroxy arginine, a series of reactions were developed to make a diboc-guanidinylating reagent, scheme 26. These reactions are standard methods for making the reagent. **24** is made via 1,3-propane-di-al condensation with aminoguanidine bicarbonate[70]. Subsequent boc protection to **25** occurs via standard boc protection methods[71]. The diboc variant, **26**, takes hydride and refluxing THF to form, but works in high crystalline yield[72]. The triboc variant, **27**, was made[73] with the hope that one of the boc groups could be selectively cleaved, but these investigations did not pan out.

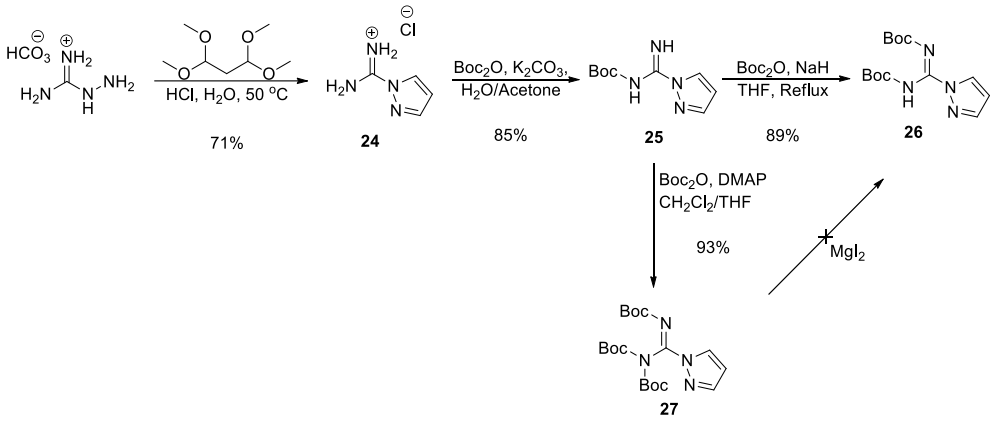

Scheme 26: Synthesis of diboc-quanidinylating reagent

The synthesis of **26** goes in good yield across all three steps, 54% overall. And the in house preparation of the reagent is desirable as **26** has been shown to degrade over time if not handled and stored properly.

With **26**, the overall scheme to make **23e/t** and the keto acid **28** from ethyl acetoacetate and the house made guanidinylating reagent becomes, scheme 27.

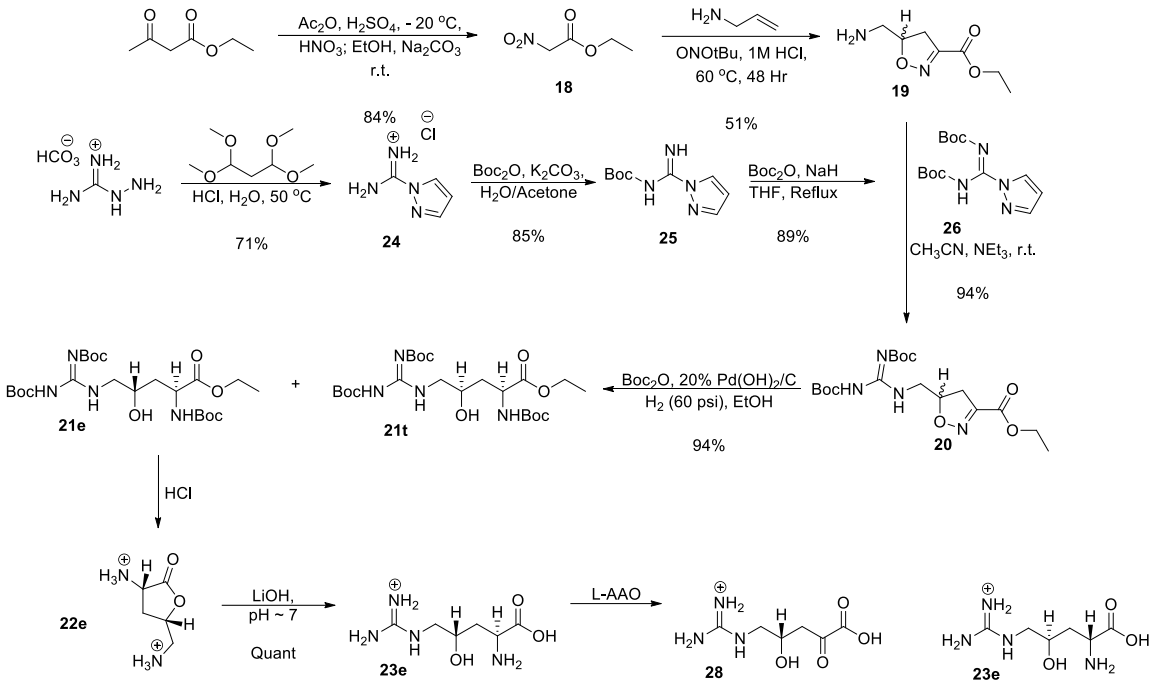

Scheme 27: Overall pathway to ketohydroxyarginine from ethyl acetoacetate

The final conversion of rac. erythro hydroxy arginine **23e** to keto **28** has been carried out enzymatically and isolation of pure 4-(s)-ketohydroxyarginine has been accomplished and as a consequence enantiomeric enrichment of **23e** was also achieved.

Further investigations into this pathway should be focused on the isolation of diastereomers via crystallization at either the protected **21** stage or the deprotected form **23**. Other possible experiments would be the isolation of enantiomers at the isooxazoline, **20**, stage where modification with another chiral center would allow for separation of formed diastereomers. Deprotection would result in enantiomerically enriched **20**. Reduction with Pd/C would form another stereocenter, however these products would be diastereomers and thus easily isolated via flash chromatography. This process would facilitate the isolation of enantiomerically enriched **23**.

The synthesis of dehydroargnine **35** is an already established procedure. The work herein focused on improving the sequence and increasing overall yield, scheme 28.

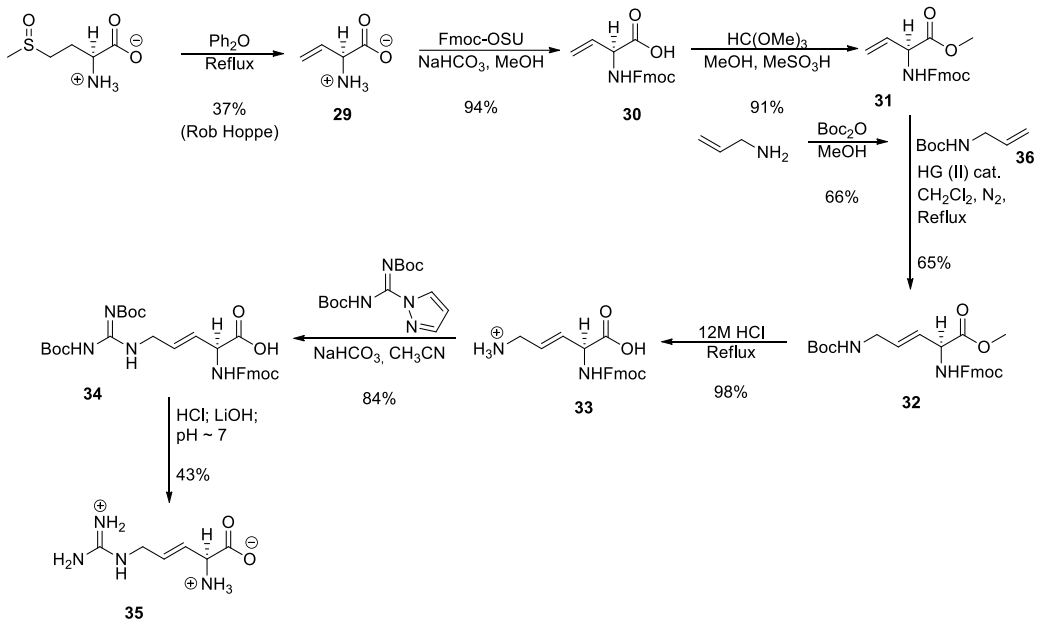

Scheme 28: The synthesis of 3,4-dehydroarginine

L-vinyl glycine is made via thermolysis of methionine sulfoxide in refluxing diphenyl ether such that the product carries over with refluxing diphenyl ether. This method, while low yielding, makes **29** in high purity from a relatively inexpensive starting material. Once **29** is in hand the subsequent reactions involve Fmoc protection and esterification of **29**.

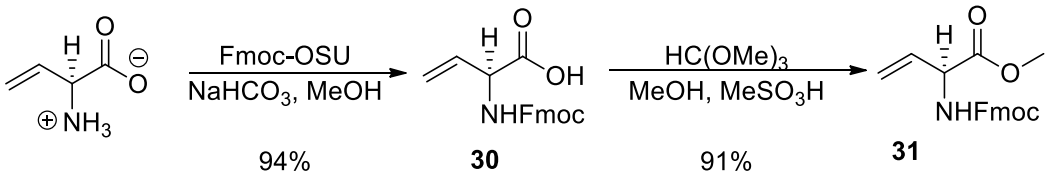

Scheme 29: Fmoc protection and esterification of L-vinylglycine

This is a well precedented set of reactions, scheme 29. The biggest concern when running these is the propensity of L-vinyl glycine to tautomerize to the alpha-beta unsaturated product under basic conditions. This would ultimately epimerize **29** until racemic when not controlled for. Thus, the subsequent steps involve sacrifice of starting material when using base to ensure no epimerization or tautomerization occurs.

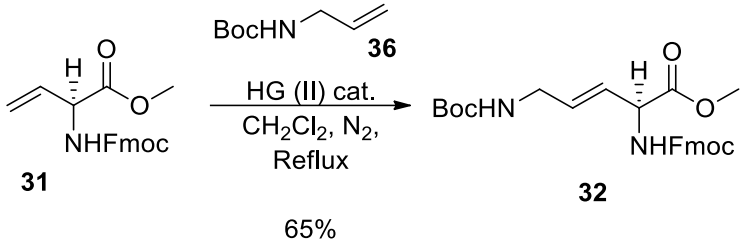

Scheme 30: Cross-Metathesis reaction

This is a metathesis reaction, scheme 30, wherein alkenes will be stitched together via metallo-cyclobutane mediated cross-metathesis. This reaction was initially low yielding (sub 30%) which was thought to be the result of a terminal catalyst that could not turn over anymore. It was found that yield could be increased up to 65% via slow addition of **36** over 24 hours. This is the most expensive and time-consuming step of the sequence; the product must be purified via flash chromatography to ensure total removal of catalyst. With **32** in hand, deprotecting and subsequent guanidinylation was optimized.

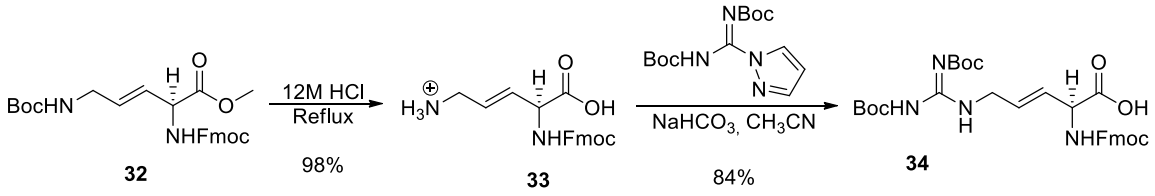

Scheme 31: installation of protected guanidinyl group

The boc removal goes smoothly at room temperature, but hydrolysis of the methyl ester required reflux temperatures, scheme 31. This product is then guanidinylated with **26** using a deficiency of bicarbonate in acetonitrile. While this reaction works in other solvents, acetonitrile appeared to be the fastest and most convenient.

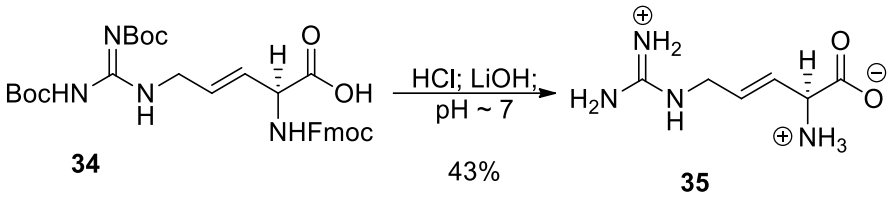

Scheme 32: Deprotection to 3,4-dehydroarginine

The deprotection of **34** was another tumultuous reaction, scheme 32. The removal of the boc groups occurs rapidly in even dilute HCl the Fmoc deprotection is much slower and has a competing reaction with epimerization, thus a deficiency of lithium hydroxide is used to ensure no epimerization occurs at the cost of yield. Lithium chloride is easily removed as it is a very organic soluble salt.

35 was made in 6 steps from L-vinyl glycine in 20% overall yield. Enzymatic studies have shown that the Q2 state, hypothesized by kinetic and UV-Vis data, exists and turns over to form **28**. This was determined by fluorescence studies of MppP under anaerobic conditions, *figure 38*.

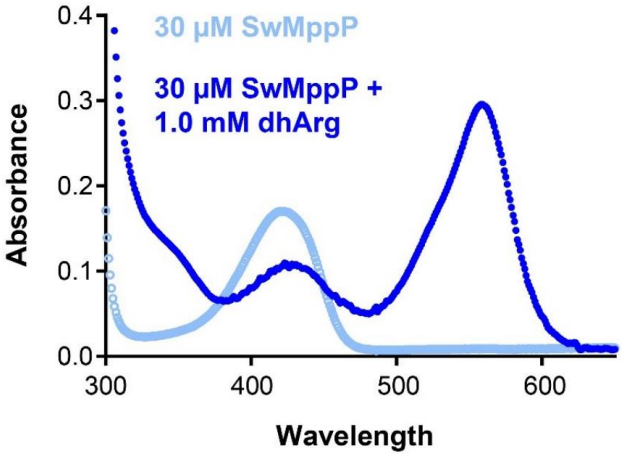

Figure 38: Observation of Q2 state forming under anaerobic conditions (Silvaggi)

These spectra were obtained anaerobically by feeding MppP **35** and appeared to increase at 535 nm over time. Once exposed to O_2 this state quickly diminished, meaning the enzyme will form Q2 anaerobically and requires molecular oxygen to turn over, thereby demonstrating the oxidative nature of this PLP dependent enzyme. More studies involving MppP are underway to nail down the mechanism of transformation and truly understand the thermodynamics and kinetics of the enzymatic pathway.

Synthesis of ethyl nitroacetate **18**

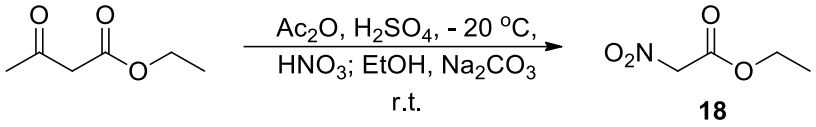

84%

To a large two neck flask was added 250ml (2.65 mol) of acetic anhydride and 0.60 ml (0.011 mol) sulfuric acid. The flask was submerged in a $CO_{2(s)}$/Sat. $NaCl_{(aq)}$ bath and the solution chilled to – 20 °C before slow addition of 50.00 ml (0.392 mol) of ethyl acetoacetate while maintaining sub 0 °C temperatures. Once added, 27.00 ml (0.432 mol) of 70% (w/w) nitric acid was added to the mixture with vigorous stirring at a rate that maintained sub – 10 °C temperatures throughout the addition (~ 1 drop / 4 seconds). Once the nitric acid addition was completed the solution was allowed to warm to room temperature over 90 minutes, with rapid stirring. Once at room temperature the solution was diluted into 500 ml of chilled ethanol and stirred for 24 hours. After 24 hours 6.779g (0.064 mol) of sodium carbonate that was thoroughly powderized was added to the stirring ethanol and the mixture was stirred for 30 minutes before filtering and concentrating via roto-evaporation. The crude oil obtained was then dissolved into 150 ml of EtOAc and washed three times with 200 ml of H_2O then 100 ml of Sat. NaCl, the aqueous washes were then back extracted with 100 ml of EtOAc. The organic extracts were combined, dried over $MgSO_4$.Yield: 43.058g (84%), transparent yellow oil.

1H-NMR 500 MHz (CDCl3): δ 1.36 (1H, t, J=7.16 Hz), 4.35 (1H, q, J=7.15 Hz), 5.21 (1H, s).

Synthesis of ethyl 5-(aminomethyl)-4,5-dihydroisoxazole-3-carboxylate **19**

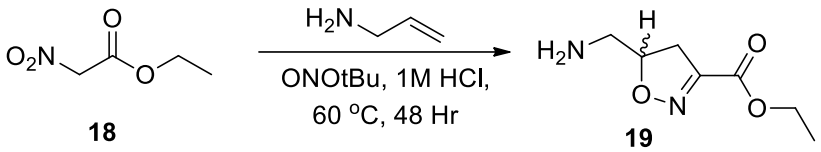

51%

To a large two neck flask was added 165 ml of 1.0M HCl, 12.9 ml (0.175 mol) of allylamine, 27.974g (0.189 mol) of ethyl nitroacetate and 0.60 ml (2% by mol) of tert. Butyl nitrite. Once combined the reaction was heated to 62 °C for 48 hours in an oil bath. The reaction mixture was then concentrated via roto-evaporation until only a white solid and an amber oil remained. The product was precipitated via trituration in 85 ml of CH_3CN. Yield: 18.0588g (51%), m.p. 202 – 203 °C

1H-NMR 500 MHz (D2O) 5.22 (1H, dddd, J=3.20, 6.45, 14.35, 16.90 Hz), 4.36 (2H, q, J=7.15 Hz), 3.54 (1H, dd, J=11.15, 18.20 Hz), 3.31 (1H, dd, J=3.15, 13.70 Hz), 3.23 (1H, dd, J=9.35, 13.70 Hz), 3.14 (1H, dd, J=6.80, 18.20 Hz), 1.33 (3H, t, J=7.15 Hz).

13C-NMR 500 MHz (D_2O): δ 171.9, 156.4, 78.0, 49.3, 43.7, 29.6.

ESI LCMS $[M+H]^+$ = 173.25 m/z.

Synthesis of ethyl 5-((2,3-bis(tert-butoxycarbonyl)guanidino)methyl)-4,5-dihydroisoxazole-3-carboxylate **20**

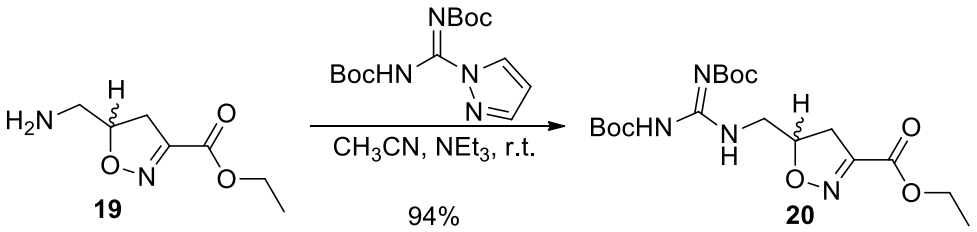

1.509g (7.23 mmol) of isoxazoline HCl was added to a flask containing 2.245g (7.23 mmol) of diboc-guanidinyl-pyrazole. To this was added 150 ml of CH_3CN followed by 1.02 ml (7.3 mmol) of triethylamine. This was stirred for 24 hours before TLC indicated the consumption of starting amine at which point the reaction mixture was concentrated then resuspended into 30 ml of CH_2Cl_2 and washed with 90 ml of H_2O. The organic layer was then concentrated after drying over $MgSO_4$ then crystallized directly from boiling hexanes. Yield: 2.718g (92%), m.p. 88 – 89 °C

1H-NMR 500MHz (CDCl3) 8.65 (1H, t, J=5.28 Hz), 5.01 (1H, dtd, J= 3.55, 7.30, 14.70 Hz), 4.35 (2H, q, J=7.12 Hz), 3.82 (1H, dtd, J=2.35, 9.83, 14.28 Hz), 3.59 (1H, m, J=5.93, 6.95 Hz), 3.29 (1H, dd, J=11.10, 17.90 Hz), 2.97 (1H, dd, J=7.75, 17.90 Hz), 1.49 (9H, s), 1.49 (9H, s), 1.37 (3H, t, J=7.13 Hz).

13C-NMR 500 MHz (CDCl3): δ 163.3, 160.4, 156.7, 152.9, 151.7, 83.4, 81.7, 79.5, 62.1, 43.4, 36.5, 28.2, 28.0, 14.1.

ESI LCMS $[M+H]^+$ = 415.50 m/z, $[M-H]^-$ = 413.20 m/z.

Synthesis of rac. ethyl 5-(2,3-bis(tert-butoxycarbonyl)guanidino)-2-((tert-butoxycarbonyl)amino)-4-hydroxypentanoate **21e/21t**

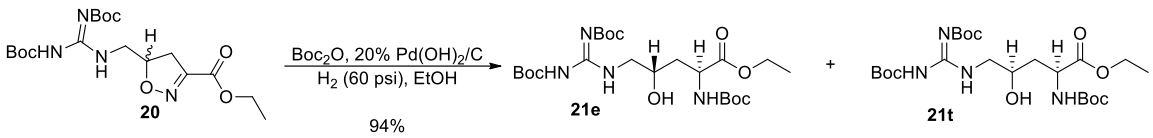

0.5114g (1.23 mmol) of diboc-guanidinylated isoxazoline, 0.283g (1.33 mmol) of Boc_2O and 0.050g of 20% $Pd(OH)_2/C$ was suspended in 5 ml of anhydrous ethanol in a parr shaker bottle with 2 glass beads. The mixture was then pressurized to 55 psi of H_2 after extensive flushing and shaken on a parr shaker for 48 hours at 55 psi H_2. After 48 hours the reaction mixture was filtered through 1cm of vacuum packed celite, which was subsequently washed with 50ml of boiling ethanol. The ethanol filtrate was then concentrated to afford 0.596g (94%) of a diastereomeric mixture **21e/t**.

Separation of Diastereomeric pairs was achieved by running a silica flash column with 10% CH_3CN/90% CH_2Cl_2. The first product to elute is the racemic erythro pair the last to elute is the racemic threo pair. The Erythro product was recrystallized from CH_2Cl_2 and hexanes through vapor diffusion and confirmed by LCMS, ^1H, ^{13}C NMR, HSQC and COSY to be the desired **21e** m.p. 128 – 130 ^oC.

1H NMR 500 MHz (CDCl3): δ 11.46 (1H, s), 8.71 (1H, s), 5.58 (1H, d, J=8.00 Hz), 5.00 (1H, s), 4.49 (2H, q, J=5.15 Hz), 4.21 (1H, m, J=3.17 Hz), 3.80 (1H, d, J=9.05 Hz), 3.66 (1H, m, J=3.52 Hz), 3.32 (1H, m, J=4.28 Hz), 1.92 (1H, s), 1.50 (9H, s), 1.49 (9H, s), 1.45 (9H, s), 1.28 (3H, t, J=7.13 Hz),.

13C-NMR 500 MHz (CDCl3): δ 172.5, 163.1, 156.9, 156.5, 152.9, 83.2, 80.2, 79.4, 67.3, 61.6, 50.9, 46.6, 38.3, 14.1.

ESI LCMS $[M+H]^+$ = 519.60 m/z, $[M-H]^-$ = 517.30 m/z.

21t was crystallized in the same manner as **21e** m.p. 120 – 122 ^oC.

1H-NMR 500 MHz (CDCl3): δ 11.43 (1H, s), 8.68 (1H, t, J=5.25 Hz), 5.51 (1H, d, J=5.80 Hz), 5.27 (1H, s), 4.33 (1H, d, J=5.50 Hz), 4.21 (2H, q, J=3.70 Hz), 3.92 (1H, d, J=3.70 Hz), 3.58 (1H, q, J=6.18 Hz), 3.41 (1H, m, J=3.82 Hz), 1.91 (1H, m, J=4.58 Hz), 1.50 (9H, s), 1.47 (9H, s), 1.28 (3H, t, J=7.13 Hz),.

13C-NMR 500 MHz (CDCl3): δ 172.6, 162.7, 157.5, 152.9, 83.6, 79.6, 69.1, 61.5, 51.6, 47.5, 37.3, 14.1.

ESI LCMS $[M+H]^+$ = 415.50 m/z, $[M-H]^-$ = 413.20 m/z.

Synthesis of rac. amino(((2S,4S)-4-amino-4-carboxy-2-hydroxybutyl)amino)methaniminium chloride **22e/23e**

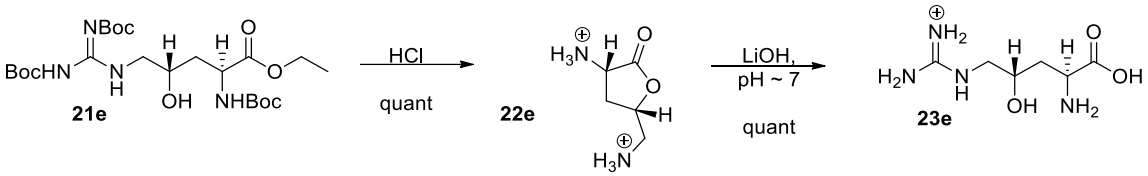

To a small round bottom flask was added 0.2733g (0.52 mmol) of **21e** followed by 1.5 ml of 12M HCl and stirred for 1 hour before concentrating and drying under vacuum to achieve constant mass.

Yield: 0.1509g (110%) m.p. 110-113 °C. **22e**

1H NMR 500 MHz (D_2O): δ 4.88 (1H, dddd, *J*=3.1, 6.3, 9.1, 12 Hz), 4.60, (1H, dd, *J*=8.8, 12.0 Hz), 3.76 (1H, dd, *J*=3.0, 15.7 Hz), 3.54 (1H, dd, *J*= 6.6, 15.7 Hz), 2.91 (1H, ddd, *J*=5.4, 8.9, 12.6 Hz), 2.21 (1H, td, *J*=10.6, 12.5 Hz).

13C-NMR 500 MHz (D_2O): δ 171.9, 156.4, 78.0, 49.3, 43.7, 29.6.

ESI LCMS $[M+H]^+$ = 173.20 m/z.

0.0565g (0.25 mmol) of **22e** was then subjected to 2 ml of 1.0M LiOH and stirred for 2 hours before being acidified to pH 7 using dilute HCl then concentrating. Once constant mass was achieved the solid was dissolved in a minimal amount of warm methanol then precipitated from THF and collected via centrifugation, decanting and drying. Yield: 0.052g (92%), m.p. 144 – 147 °C. **23e**

1H-NMR 500 MHz (D2O): δ 3.94 (1H, d, J=4.12 Hz), 3.40 (1H, dd, J=4.73, 8.39 Hz), 3.34 (1H, dd, J=3.43, 14.57 Hz), 3.18 (1H, dd, J=7.55, 14.42 Hz), 1.81 (1H, ddd, J=4.81, 9.38, 14.19 Hz), 1.63 (1H, ddd, J=3.93, 8.66, 13.92 Hz).

13C-NMR 500MHz (D_2O): δ 182.0, 156.5, 66.4, 52.1, 46.3, 37.7.

ESI LCMS $[M+H]^+$ = 191 m/z, $[M-H]^-$ = 189 m/z.

Synthesis of rac. amino(((2R,4S)-4-amino-4-carboxy-2-hydroxybutyl)amino)methaniminium chloride **22t/23t**

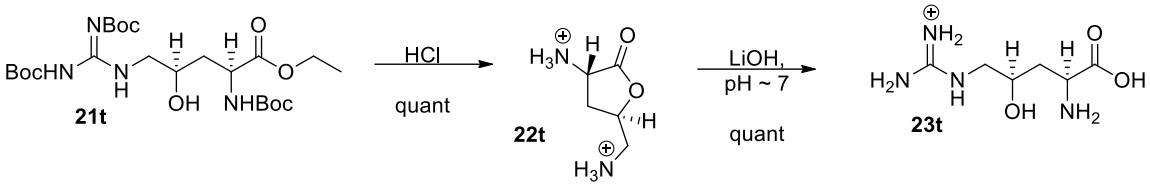

To a small roundbottom flask was added 0.2740g (0.53 mmol) of threo triboc ethyl 4-hydroxyarginine followed by 1.5 ml of 12M HCl and stirred for 1 hour before concentrating and drying under vacuum to achieve constant mass. Yield: 0.1403g (107%) m.p. 95-98°C. **22t**

1H-NMR 500 MHz (D2O): δ 4.99 (1H, m, J=3.66, 3.66 Hz), 4.49 (1H, t, J=10.02 Hz), 3.59 (1H, dd, J=3.70, 15.35 Hz), 3.50 (1H, dd, J=7.40, 15.35 Hz), 2.18 (1H, dd, J=2.52, 6.03 Hz), 1.92 (1H, m, J=3.20, 10.99 Hz).

13C-NMR 500 MHz (D_2O): δ 172.3, 156.3, 78.0, 47.6, 44.3, 33.3.

ESI LCMS $[M+H]^+$ = 173.25.

0.0415g (0.20 mmol) of **22t** was then subjected to 2 ml of 1.0M LiOH and stirred for 2 hours before being acidified to pH 7 using dilute HCl then concentrating. Once constant mass was achieved the solid was dissolved in a minimal amount of warm methanol then precipitated from THF and collected via centrifugation, decating and drying. Yield: 0.046g (100%) m.p. 121 – 125 °C. **23t**

1H-NMR 500 MHz (D2O): δ 3.92 (1H, d, J=7.20 Hz), 3.34 (1H, d, J=0.90 Hz), 3.30 (1H, d, J=2.65 Hz), 3.16 (1H, dd, J=7.40, 14.25 Hz), 1.80 (1H, m, J=6.45, 19.46 Hz), 1.63 (1H, m, J=6.90 Hz),.

13C-NMR 500 MHz (D_2O): δ 181.9, 156.9, 68.8, 54.5, 47.4, 39.5.

ESI LCMS $[M+H]^+$ = 191 m/z, $[M-H]^-$ = 189 m/z.

Synthesis of amino(1H-pyrazol-1-yl)methaniminium chloride **24**[70]

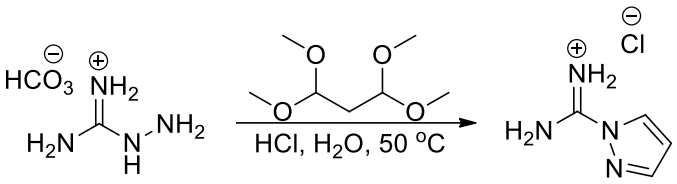

71% **24**

Aminoguanidine Bicarbonate (53.37g, 0.400 mol) was dissolved in 100 ml of H_2O and 68 ml of 12M HCl then heated to 50 °C. Then tetramethoxypropane (69 ml, 0.416 mol) was added dropwise over the course of three hours. Once addition was complete the reaction mixture was stirred for a 30 minutes before cooling to room temperature. The reaction mixture was then concentrated until about 100 ml of H_2O had been removed and a precipitate was observed. While warm, the crude solid was diluted with 500 ml of acetone and chilled until a significant amount of crystals formed. The crystals **24** were then collected via vacuum filtration, washed with 200 ml of cold acetone and dried under reduced pressure overnight. Yield: 41.87g (71%), M.p. 165°C - 166°C

1H-NMR 500 MHz (D_2O): δ 6.66 (1H, d, J=2.2 Hz), 7.91 (1H, d, J=4.6 Hz), 8.27 (1H, d, J=1.2 Hz)

13C-NMR 500 MHz (D_2O): δ 153.2, 147.2, 131.3, 112.6

Synthesis of tert-butyl (imino(1H-pyrazol-1-yl)methyl)carbamate **25**[71]

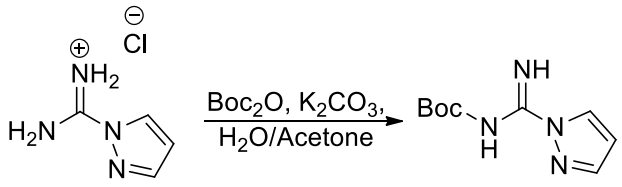

24 85% **25**

24 (7.7402g, 52.8 mmol) was dissolved in 10 ml of H_2O and added to a solution of Boc anhydride (12.986g, 59.5 mmol, 1.1 e.q) in 50 ml of acetone. While stirring rapidly, a solution of potassium carbonate (4.427g, 32 mmol) in 10 ml of H_2O was added to the acetone/water solution slowly over 10 minutes. The reaction mixture was then allowed to stir for 2 hours before removing the acetone via rotary evaporation and collecting the precipitate. The precipitate was then washed with 50 ml of H_2O followed by 100 ml of hexanes. The product was then crystallized from 75 ml CH_2Cl_2 and 75 ml Hexanes concentrated by 50 ml to afford white fluffy crystals **25**. Yield: 9.435g (85%), M.p. 94°C - 95°C

1H-NMR 500 MHz ($CDCl_3$): δ 1.55(9H, s), 6.40 (1H, d, J=4.3 Hz), 7.59 (1H, s), 7.68 (1H, d, J=1.2 Hz), 8.46 (1H, d, J=2.7 Hz), 9.06 (1H, s)

13C-NMR 500 MHz ($CDCl_3$): δ 163.4, 155.1, 146.7, 143.4, 108.9, 80.1, 27.4

Synthesis of tert-butyl (((tert-butoxycarbonyl)imino)(1H-pyrazol-1-yl)methyl)carbamate **26**[72]

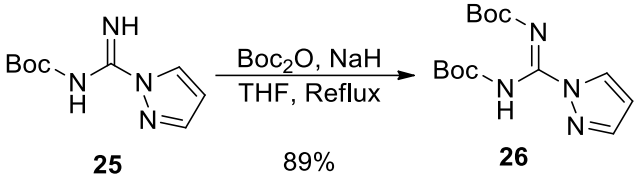

25 89% **26**

NaH (0.568g, 14.2 mmol) was stirred in 50 ml of THF at 0 °C. to this, **25** (2.7110g, 12.9 mmol), was added dropwise and slowly to maintain sub 5°C. Once added, 3.252g (14.9 mmol) of Boc anhydride was added to the solution and the reaction was heated to reflux. After 20 hours the reaction was cooled to room temperature and 5 ml (85 mmol) of AcOH was added and stirred for 30 minutes. The reaction mixture was concentrated under reduced pressure and the crude residue was dissolved in 100 ml of EtOAc. The organics were washed with 100 ml x3 of Sat. $NaHCO_3$ then 100 ml of sat. NaCl. The organics were dried

over $MgSO_4$ and concentrated under reduced pressure. The product was crystallized from the resulting yellow oil with 30ml hexanes to afford white crystals **26**. Yield: 3.108g (78%), M.p. 88°C - 89°C

1H-NMR 500 MHz ($CDCl_3$): δ 1.50 (9H, s), 1.56 (9H, s), 6.42 (1H, dd, J=2.8, 1.6 Hz), 7.63 (1H, d, J=1.6 Hz), 8.31 (1H, d, J=2.8 Hz), 8.94 (1H, s)

13C NMR 500 MHz ($CDCl_3$): δ

Synthesis of tert-butyl tert-butoxycarbonyl(((tert-butoxycarbonyl)imino)(1H-pyrazol-1-yl)methyl)carbamate **27**[73]

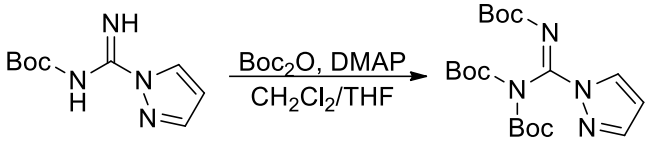

25 93% **27**

25 (7.405g, 30.15 mmol) and DMAP (0.3470g, 2.84 mmol, 10% by mol) was dissolved in 60 ml of CH_2Cl_2 and stirred rapidly while a solution of Boc_2O (13.336g, 61.10 mmol, 2.05 e.q) in 40 ml of THF was added dropwise over multiple hours. The reaction mixture was then allowed to stir overnight before concentrating via rotary evaporation. The crude product was then stirred in a solution of AcOH (0.50g, 8.3 mmol) in 60 ml of H_2O before filtering and drying under reduced pressure. This afforded 12.787g of

crude product which was then recrystallized from 75 ml CH_2Cl_2 and 75 ml of Hexanes, concentrated by 50 ml to afford **3**. Yield: 11.502g (93%), M.p. 160°C - 161°C

1H-NMR 500 MHz ($CDCl_3$): δ 1.39 (18H, s), 1.54 (9H, s), 6.45 (1H, dd, J=2.8, 1.6 Hz), 7.69 (1H, d, J=0.8 Hz), 8.20 (1H, d, J=2.4 Hz)

13C-NMR 500 MHz ($CDCl_3$): δ 156.3, 147.4, 143.6, 128.9, 109.9, 84.4, 83.0, 27.9, 27.6

Synthesis of (S)-2-((((9H-fluoren-9-yl)methoxy)carbonyl)amino)but-3-enoic acid **30**

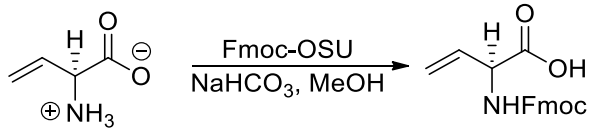

29 **30**

1.1931g (11.8 mmol) of **29**, 3.8264g (11.3 mmol) of Fmoc-OSU and 1.9631g (23.3 mmol) of $NaHCO_3$ was stirred in 40 ml of anhydrous MeOH for 20 hours. The reaction mixture was concentrated via rotary evaporation and then resuspended in 50 ml of 0.6M HCl. The product was extracted with 150 ml of CH_2Cl_2 and the organic extracts were washed with 100 ml of 1M HCl then 100 ml of sat. NaCl before drying over $MgSO_4$ and concentrating. The product was then crystallized from 200 ml of 50:50 CH_2Cl_2 and Hexanes. Yield: 3.438g (94%) m.p. 154 – 156 °C

1H NMR 500 MHz (DMSO-d6) δ 12.82 (1H, s), 7.93 (1H, d, J = 8.2 Hz), 7.90 (2H , d, J = 7.6 Hz), 7.74 (2H , dd, J = 7.3, 4.3 Hz), 7.42 (2H , t, J = 7.4 H), 7.33 (2H , t, J = 7.3 Hz), 5.93 (1H, ddd, J = 10.6, 6.3, 17.1 Hz),

5.34 (1H, d, J = 17.3 Hz), 5.22 (1H, d, J = 10.4 Hz), 4.62 (1H, t, J = 7.2 Hz), 4.29 (2H, d, J = 7.2 Hz), 4.23 (1H, t, J = 7.3 Hz).

13C NMR 500 MHz (DMSO-d6) δ 171.7, 155.8, 143.8, 143.7, 140.7, 132.9, 127.6, 127.0, 125.3, 120.1, 117.4, 65.8, 56.4, 46.6.

Synthesis of (S)-methyl 2-((((9H-fluoren-9-yl)methoxy)carbonyl)amino)but-3-enoate **31**

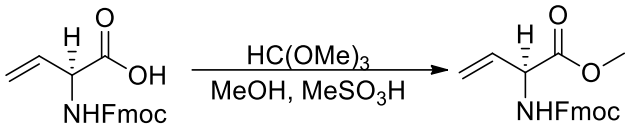

30 91% **31**

0.8495g (2.63 mmol) of **30** and 0.32ml (2.92 mmol) of trimethylorthoformate was combined in 20 ml of MeOH and stirred before addition of 50µL of $MeSO_3H$. The solution was stirred for four hours before concentrating to dryness. The crude residue was then suspended in 50 ml of diethyl ether and the solution washed with 100 ml of sat. $NaHCO_3$ then 100 ml of Sat. NaCl. The organics were combined, dried over $MgSO_4$ and concentrated. The solid was then crystallized from 10 ml CH_2Cl_2 and 35 ml of hexanes, conc. by 5 ml. Yield: 0.8103g (91%) m.p. 103 – 104 °C

H NMR 500 MHz (DMSO-d6) δ 8.08 (1H, d, J = 7.8 Hz), 7.91 (2H, d, J = 7.5 Hz), 7.74 (2H, dd, J = 6.9, 5.6 Hz), 7.43 (2H, t, J = 7.4 Hz), 7.34 (2H, t, J = 7.4 Hz), 5.92 (1H, ddd, J = 10.6, 6.7, 17.2 Hz), 5.36 (1H, d, J = 17.2 Hz), 5.26 (1H, d, J = 10.4 Hz), 4.71 (1H, t, J = 7.1 Hz), 4.32 (2H, td, J = 6.8, 2.5 Hz), 4.24 (1H, t, J = 6.9 Hz), 3.66 (3H, s).

13C NMR 500 MHz (DMSO-d6) δ 170.9, 155.8, 143.7, 140.7, 132.2, 127.6, 127.0, 125.2, 120.1, 118.2, 65.8, 56.4, 52.1, 46.5.

Synthesis of (S,E)-methyl 2-((((9H-fluoren-9-yl)methoxy)carbonyl)amino)-5-((tert-butoxycarbonyl)amino)pent-3-enoate **32**

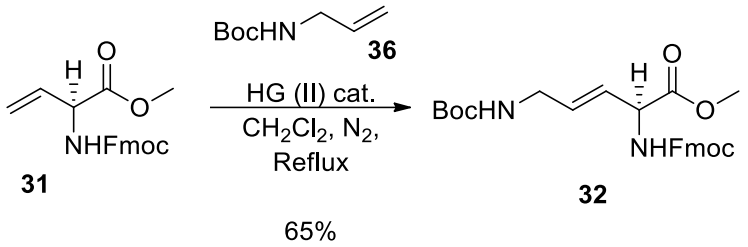

0.3322g (0.99 mmol) of **31** and 0.3760g (2.39 mmol) of **36** was combined in 20 ml of CH_2Cl_2 under a N_2 stream. To this was added 0.0539g (0.094 mmol) of HG (II) catalyst in 2 ml of CH_2Cl_2. The reaction mixture was heated to reflux and after 6 hours an additional 0.1694g (1.05 mmol) of **36** was added and the reaction was left to reflux for an additional 24 hours. Once complete the reaction mixture was concentrated and then subjected to flash chromatography, eluent: 50:50 diethyl ether and hexanes.

Yield: 0.298g (65%) m.p. 94 – 95 °C

1H NMR 500 MHz (DMSO-d6) δ 8.06 (1H, d, J = 7.8 Hz), 7.89 (2H, d, J = 7.6 Hz), 7.73 (2H, dd, J = 7.1, 4.4 Hz), 7.42 (2H, t, J = 7.4 Hz), 7.33 (2H, t, J = 7.4 Hz), 5.72 (1H, td, J = 5.0, 15.4 Hz), 5.61 (1H, dd, J = 6.6, 15.6 Hz), 4.67 (1H, t, J = 7.1 Hz), 4.28 (2H, d, J = 111 6.0 Hz), 4.22 (1H, t, J = 7.0 Hz), 3.63 (3H, s), 1.37 (9H, s).

13C NMR 500 MHz (DMSO-d6) δ 171.6, 156.2, 155.9, 144.2, 144.2, 141.1, 137.1, 131.9, 128.1, 127.5, 125.7, 120.5, 78.1, 66.3, 52.6, 47.0, 28.7, 25.9

Synthesis of (S,E)-4-((((9H-fluoren-9-yl)methoxy)carbonyl)amino)-4-carboxybut-2-en-1-aminium chloride **33**

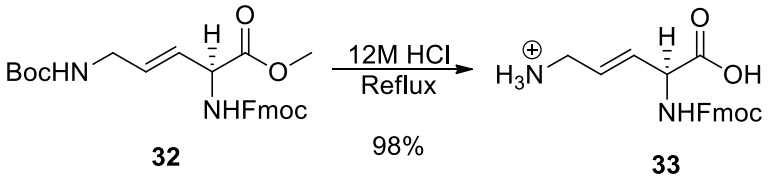

0.1400g (0.30 mmol) of **32** was heated to reflux in 3 ml of 12M HCl for 1 hour before cooling. The mixture was then concentrated via rotary evaporation using large volumes of toluene to azeotropically dry the solid. Yield: 0.1143g (98%), m.p. 190-192

1H NMR 500 MHz (DMSO-d6) δ 8.06 (3H, s_b), 8.02 (1H, d, J = 8.5 Hz), 7.91 (2H, d, J = 7.5 Hz), 7.75 (2H, dd, J = 7.2, 4.7 Hz), 7.43 (2H, t, J = 7.4 Hz), 7.34 (2H, t, J = 7.5 Hz), 5.97 (1H, dd, J = 6.2, 15.7 Hz), 5.81 (1H, td, J = 6.5, 15.2 Hz), 4.69 (1H, t, J = 7.1 Hz), 4.30 (2H, m), 4.24 (1H, m), 3.47 (3H, s_b).

13C NMR 500 MHz (DMSO-d6) δ 171.4, 155.8, 143.8, 140.7, 130.4, 128.0, 127.6, 127.1, 125.3, 125.0, 120.1, 65.8, 55.2, 46.6

Synthesis of (S,3E)-2-((((9H-fluoren-9-yl)methoxy)carbonyl)amino)-5-(2,3-bis(tert-butoxycarbonyl)guanidino)pent-3-enoic acid **34**

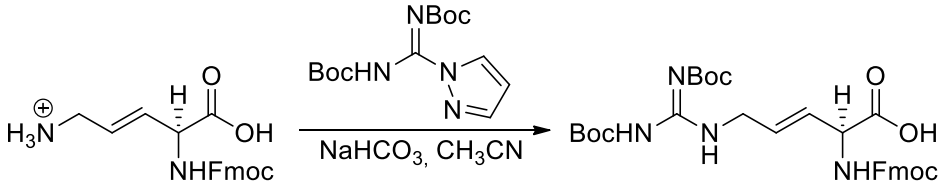

33 84% **34**

1H NMR 500 MHz (D_2O) δ 7.75 (2H, d, J = 7.2 Hz), 7.61 (2H, t, J = 6.1 Hz), 7.39 (2H, t, J = 6.5 Hz), 7.31 (2H, t, J = 7.4 Hz), 5.80 (1H, m), 5.66 (1H, d, J = 8.0 Hz), 4.97 (1H, t, J = 5.3 Hz), 4.46 (2H, d, J = 7.2 Hz), 4.40 (1H, t, J = 7.4 Hz), 4.23 (2H, t, J = 6.9 Hz), 4.07 (1H, s), 1.49 (18H, s).

Synthesis of (S,E)-5-((amino(iminio)methyl)amino)-2-ammoniopent-3-enoate chloride **35**

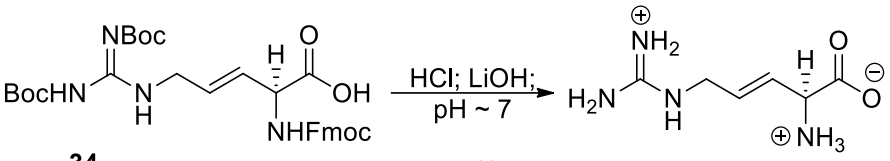

34 43% **35**

1H NMR 500 MHz (CD_3OD) δ 5.98 (1H, dtd, J = 0.9, 4.7, 15.7 Hz), 5.75 (1H, tdd, J = 1.8, 8.1, 15.8 Hz), 4.41 (1H, d, J = 7.9 Hz), 3.87 (2H, d, J = 4.9 Hz).

Synthesis of tert-butyl allylcarbamate **36**

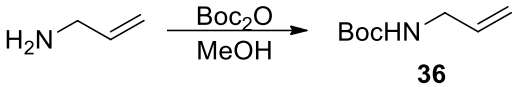

36

66%

10.287g (47.1 mmolO of Boc_2O was dissolved in 40 ml of chilled MeOH, then 4.0 ml (53.4 mmol) of allylamine was added dropwise to the reaction mixture. The solution was stirred for 2 hours before concentrating and subliming. Yield: 5.308g (66%), m.p. 30 – 31 °C

1H NMR 500 MHz (DMSO-d6) δ 6.97 (1H, s), 5.76 (1H, dtd, J = 10.5, 5.3, 17.0 Hz), 5.08 (1H, qd, J = 1.7, 17.2 Hz), 5.01 (1H, qd, J = 1.7, 10.5 Hz), 3.54 (2H, t, J = 5.2 Hz), 1.38 (9H, s).

13C NMR 500 MHz (DMSO-d6) δ 155.4, 135.9, 114.5, 77.5, 42.2, 28.2.

Chapter IV. The Janus Quinolone – a β-Sheet Initiator

Introduction

The beta barrel assembly machine, BAMa, is a transmembrane protein responsible for the folding of beta barrel proteins[74–77], including itself[78]. BAMa is also capable of spontaneous self-assembly. BAMa is in of itself a regulated pore[79,80] that transports molecules in or out of the cell, antibiotics included. The surface of the outer membrane of gram-negative bacteria is composed almost entirely of LPS and BAMa[80] meaning that the only way into the bacteria is via the BAMa complex[81–83].

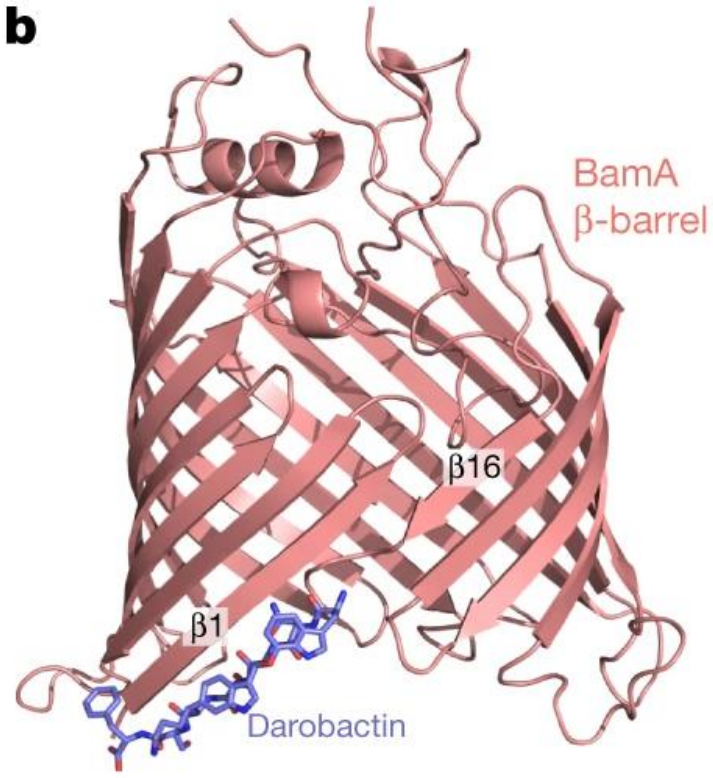

Figure 39: The crystal structure of BAMa with antibiotic Darobactin bound to the B1 lateral gate[84]

Recently, a new compound, darobactin[84], was discovered to be a potent antibiotic toward gram negative bacteria. This prompted an investigation into its mode of action, wherein it was discovered that the antibiotic binds to the beta1 strand responsible for closing the barrel.

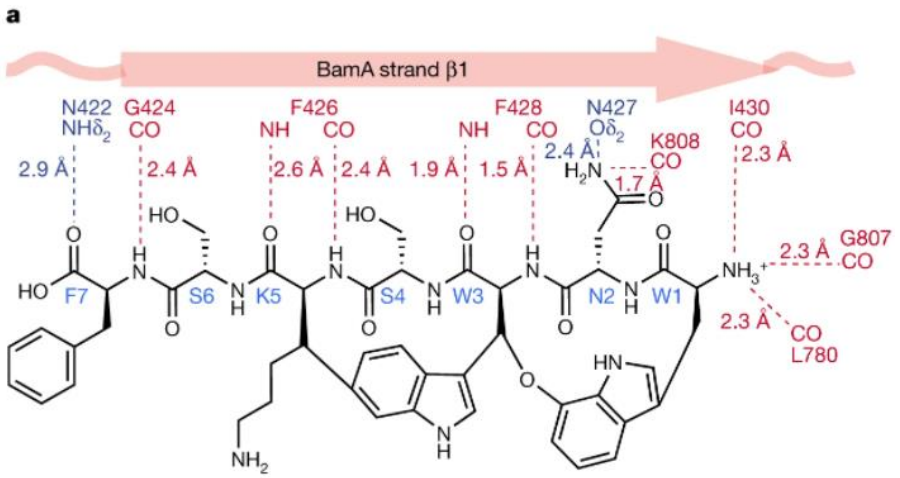

Figure 40: Specific Associations of Darobactin to β1 strand of BAMa[84]

BAMa utilizes its B1 and B16 strands as the catalytic site for beta barrel folding[81], the peptide is fed into the beta barrel where it associates with B1 and B16 and folds over onto itself until the mostly folded beta barrel can close and dissociate. During this folding process, it is hypothesized that the pore becomes unregulated[85] until the B1 and B16 strands anneal. Thus, if one were to lock BAMa into its open form and prevent the annealing of B1 and B16, then the bacteria might become susceptible to standard antibiotics like vancomycin or other potent antibiotics.

This work focuses on the development of a beta sheet mimic that can associate with the edge of the B1 strand of BAMa and inhibit its activity.

The development of a beta sheet mimetic in this work was inspired by and pays homage to James Nowick who pioneered the development of synthetic beta sheet mimetics[86,87] as well as Kemp[88]. Nowick sought to mimic the nature of beta sheet like peptides via synthetic peptide synthesis[89–92]. The work herein describes the synthesis of a family of bis-fused quinolines that mimic the hydrogen bonding pattern of a tripeptide in a beta sequence. Like Nowick's beta-sheet initiator, the target of this research is a flat molecule with alternating peptide like functional groups.

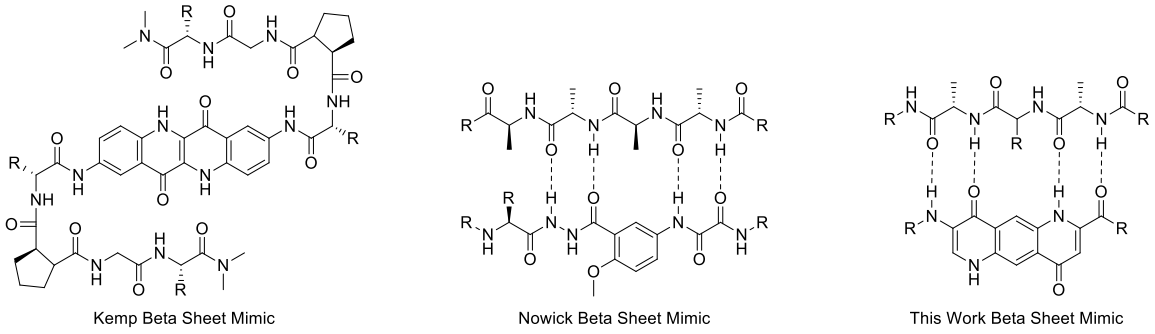

Figure 41: Kemp Beta Sheet initiator (left), Nowick's Beta Sheet Inhibitor (middle) and this work (right)

Nowick's beta sheet initiator used a hydrazine moiety that hydrogen bonds with a conveniently located methoxy group that confers rigidity in the molecule. This rigidity is necessary for function as a beta sheet initiator. The oxalyl group on the amide side of the benzene ring also aids in the flatness and rigidity of Nowick's initiator[89–91,93].

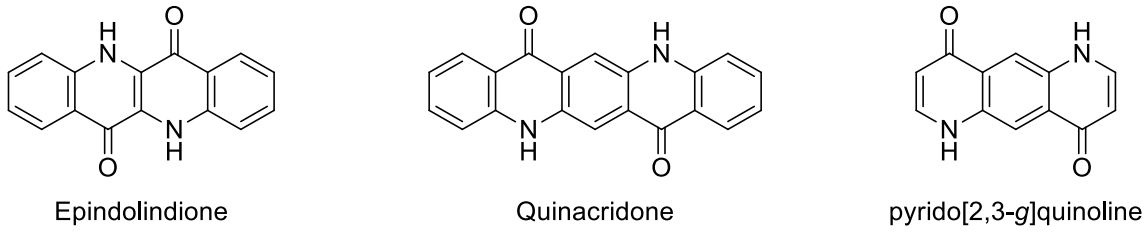

Figure 42: The structures of currently known bis-fused quinolones

Bis-fused quinolones have been made before[94–97], but not much research has been done to investigate their potential as drug candidates. These compounds are known to be very insoluble[88,95,96] and require very harsh conditions just to dissolve like pure H_2SO_4 or saturated hydroxide[98]. This work sought to overcome these potential difficulties and create a Bis-fused quinolone that could be incorporated into peptide coupling reactions for drug evaluation and hopefully inhibition of BAMa.

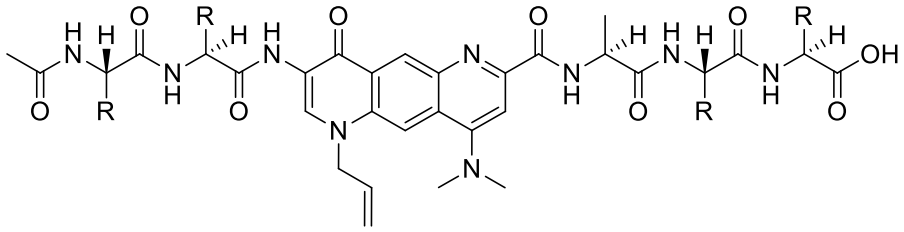

Figure 43: The functionalized Janus Quinolone

The most desirable intermediate on the way to this fully functional beta sheet initiator is **53**. Furthermore, the functionalities of **53** make it an ideal candidate for derivatization. Thus, this work sought to develop methods to make **53** and at scale.

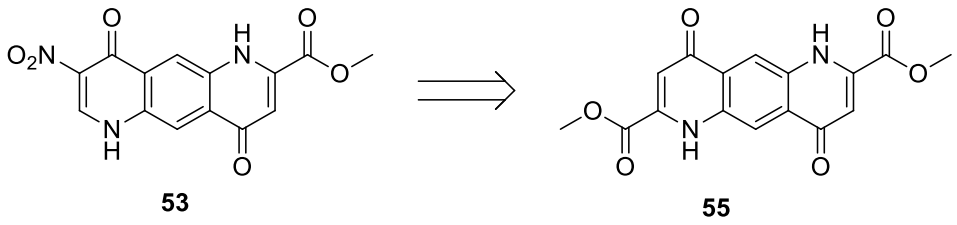

53 **55**

Figure 44: Retrosynthetic analysis for the synthesis of 55

53 was thought to be attainable via decarboxylation and nitration of **55**. Furthermore, **55** appeared to be a simple enough structure that it could be readily attained. Unfortunately this was not the case.

Symmetric Route

The first attempt at making the symmetric Janus quinolone, **55'**, involved a two-step procedure starting from p-diaminobenzene[99].

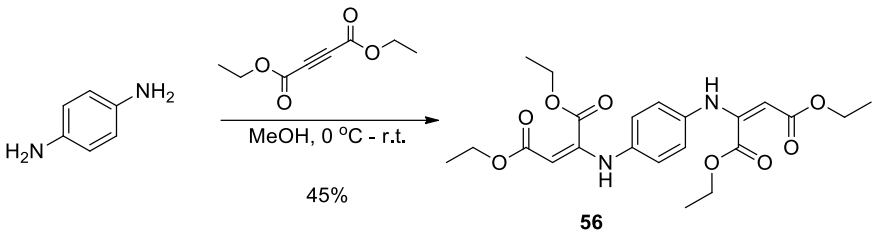

Scheme 33: Synthesis of Biseneamine 56

This reaction leads to **56** in 45% yield, lower than yields achieved by others, but for the purpose of a scout reaction this was considered good enough. From here **56** undergoes thermal cyclization at reflux in dowtherm, a mixture of Ph_2O and Ph_2.

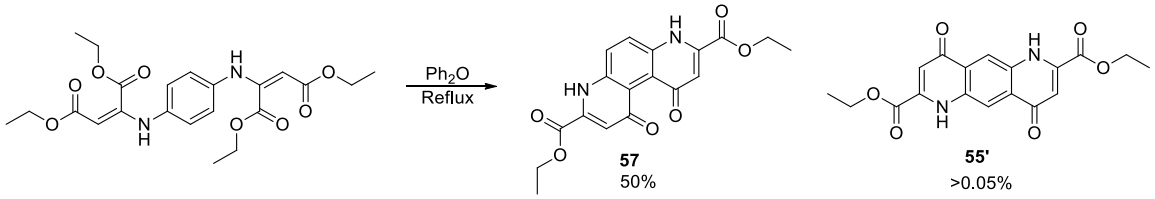

Scheme 34: Synthesis of kinked janus quinolone 57

Unfortunately, the major product of this pathway is a "kinked" variant of the target symmetric Janus quinolone. While the desired **55'** is the thermodynamically favored product, the kinetically favored product, **57**, wins out. Less than 0.05% of the product appears to be the desired product, this is close to the limit of detection of the NMR and so it is hard to say whether there really is any of the desired product. Regardless, this method is non-viable for the purposes of making a beta-sheet initiator.

From a retrosynthetic perspective, it appeared as though **55** could be made by starting with **60**, diaminoterephthalate. This method was desirable because the amine and ketone of the desired janus quinolone are preformed and unable to form **57**.

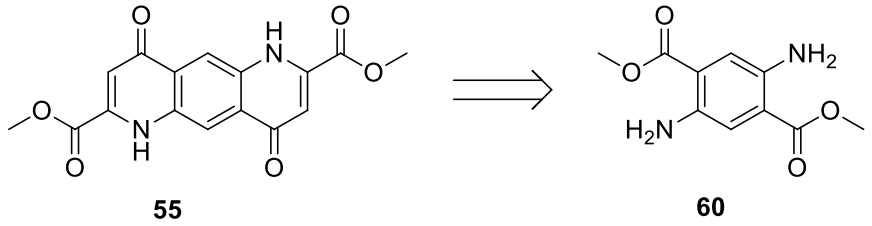

Figure 45: Retrosynthetic analysis for the synthesis of 55 from 60

The synthesis of dimethyl 2,5-bis((tert-butoxycarbonyl)amino)terephthalate **60** is an already well-established procedure[100].

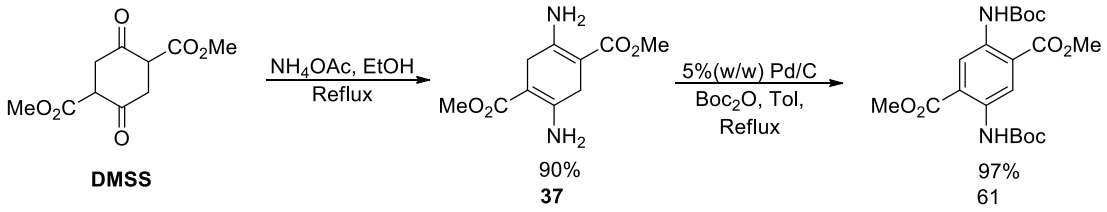

Scheme 35: the Synthesis of diboc-diaminoterephthalate

From DMSS, **61** was deprotected using standard deprotection methods to **60**. The thought was that methyl pyruvate should be able to either make an imine with the arylamines twice under slightly acidic conditions or make the double Claisen product under basic conditions. From there it was thought that base should cyclize the double imine product and heat or acid should be able to cyclize the double Claisen product.

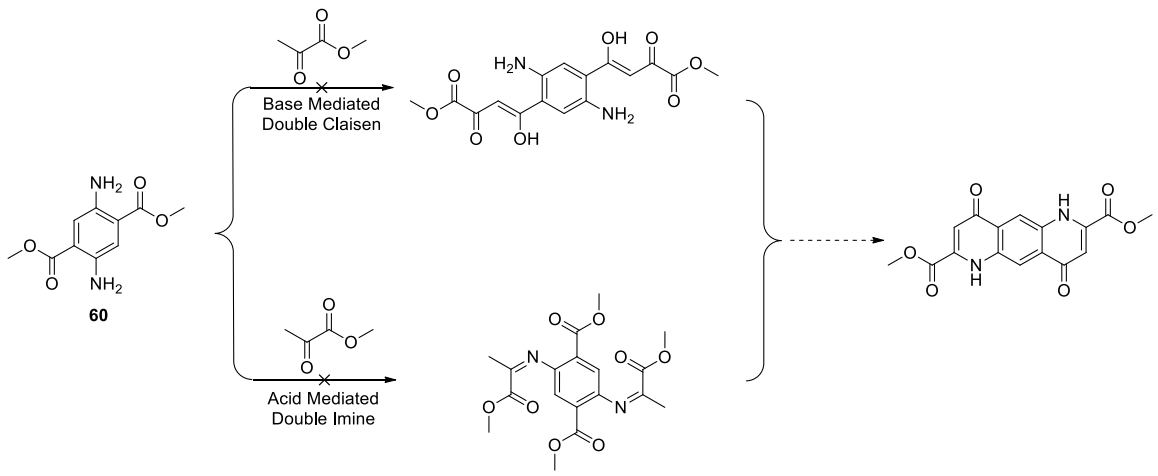

Scheme 36: The synthesis of 55 via pyruvate and 60

Multiple experiments were run to determine whether either of these approaches were possible. Most of these experiments failed for a variety of reasons. The double imine formation appeared to make a variety of products, all of which failed to survive column conditions. Thus, the route was considered too hydrolytically unstable to pursue and the Claisen route was investigated. The difficulty in the Claisen condensation was getting the reaction to proceed. It was assumed that the formation of multi-anionic intermediates in addition to the general unreactive nature of the starting **60** made this route significantly more difficult. An alternate route was envisioned when it appeared the **60** route would not work out.

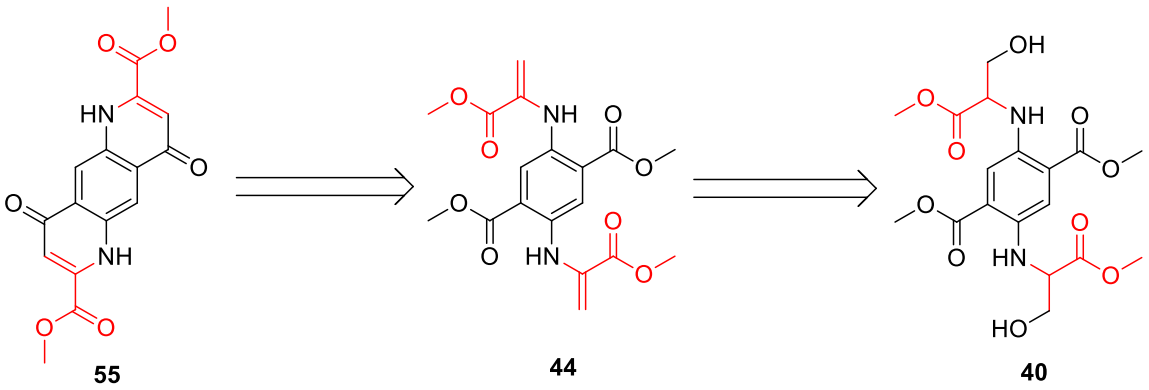

Figure 46: Retrosynthetic analysis for the synthesis of 55 from bis-serineterephthalate 40

The Janus quinolone could be made by installing the imine as a precursor. The bis-serine methyl ester **40** product of these arrows show that upon dehydration of the alpha-beta carbon of serine to **44** the creation of the desired quinolone, **55**, might be achieved. To test this route a series of experiments were performed.

It was found that under similar conditions to the synthesis of **60**, **40** could be made in high crystalline yield. There are some significant differences from the original synthesis however.

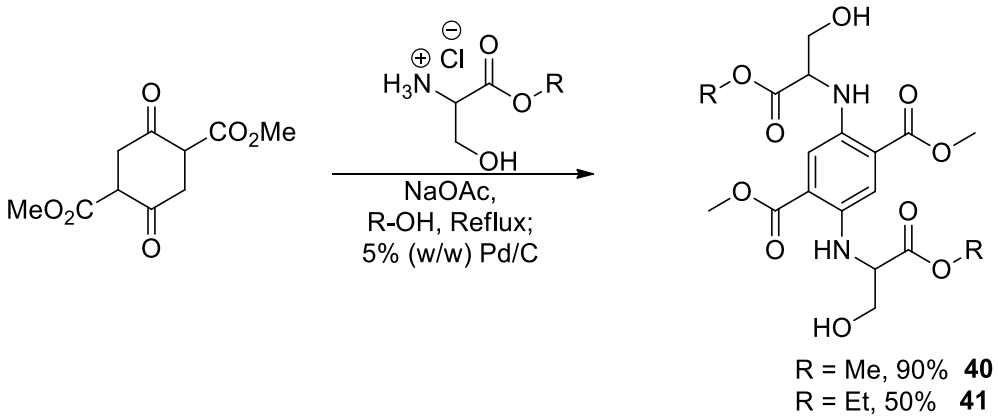

Scheme 37: The synthesis of Bis-Serineterephthalate methylester 40

The reaction is run such that **37'**, formerly isolated, is made after three hours with serine in 10% excess over DMSS in stoichiometry.

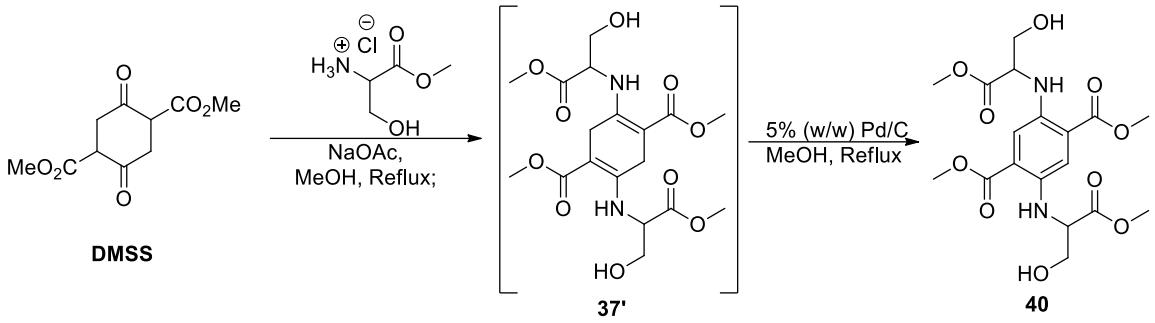

Figure 47: Stepwise transformation of DMSS to 37' to 40

While still hot, palladium on carbon is added to the mixture and reflux continued for 30 hours after which TLC indicated consumption of **37'**. It was found that serine methyl ester in methanol afforded more product in higher yield than the corresponding ethyl ester product. The yields as posted are crystalline product recovered. The lower yield with ethyl over methyl might be due to many factors such as crystallinity, serine degradation, solvent effects, etc… As a result, the methyl ester in methanol is the current method of synthesis.

This method is also very scale-able with respect to overall yield. Small scale tends to afford a higher yield than large scale, but the yields tend to stay above 80% crystalline yield. The largest scale performed to date has been ~25g with an 87% yield overall. Furthermore, palladium used in these reactions can be recycled for future reactions.

An alternative was briefly investigated, wherein alanine methyl ester HCl was used in place of serine.

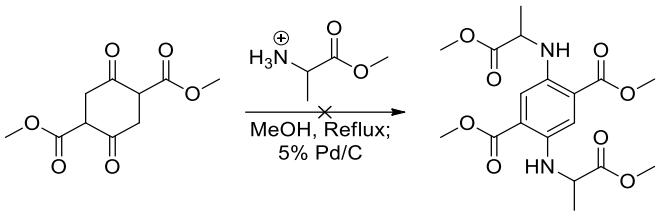

Scheme 38: Failed terephthalate synthesis with alanine

This utilized the exact methods for serine but suffered in conversion rate, with serine the reaction to fully aromatized **40** takes roughly a day and a half while alanine had barely progressed after multiple days. This led to the belief that the reason serine aromatizes so quickly and well is due to the ligating effect of serine to palladium. Specifically, the serine's hydroxyl aids in the disassociation of palladium from the aromatic ring, thereby increasing turnover. Thus, it makes sense that the conversion of **37'** to **40** would occur rapidly in a lower boiling solvent like methanol compared to the original method to synthesize **60**.

Once a scale-able method had been created for **40**, methods for its dehydration and cyclization were investigated. Many methods of dehydration were performed, with scale in mind BSA was investigated as a method for dehydrating the alpha-beta carbons of serine.

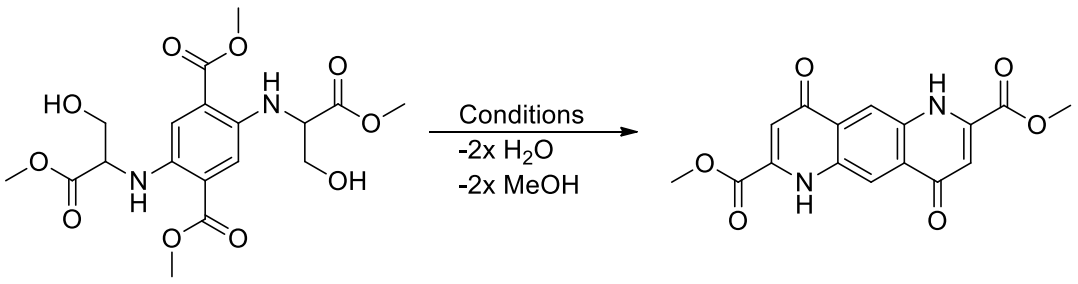

40 **55**

Base	Reagent(s)	Temp	Solvent	Result
--	--	260 °C	Ph_2O	
--	CDI	111 °C	Tol	
--	CDI ($MeSO_3H$)	260 °C	Ph_2O	**60**
NEt_3	$POCl_3$	111 °C	Tol	**60**
--	BSA	111 °C	Tol	
--	BSA	260 °C	Ph_2O	
NEt_3	BSA	260 °C	Ph_2O	
LiOtBu	BSA	260 °C	Ph_2O	
NaH	BSA	111 °C	Tol	**55**
NaH	BSA	65 °C	THF	**55**
NaH	BSA	111 °C	Tol/DMSO	**55**
NaH	BSA	25 °C	THF/DMSO	**55**

Table 8: Initial conditions to dehydrate and cyclize 40 into 55

These experiments illustrated how it was possible to dehydrate the alpha-beta carbons of both serine's on **40** as shown by the isolation of **60** from the $POCl_3/NEt_3$ conditions. Remarkably, the CDI in Ph_2O at reflux with catalytic $MeSO_3H$ was able to eliminate but was unable to cyclize. This meant that the

hydrogen bond of the aromatic amine on **40** is extraordinarily strong. This is further supported by the NMR of this product showing the N-H hydrogen bond as well as the serine's O-H proton split as a triplet. This means that **40** is very flat and held somewhat rigidly by its intramolecular hydrogen bonding.

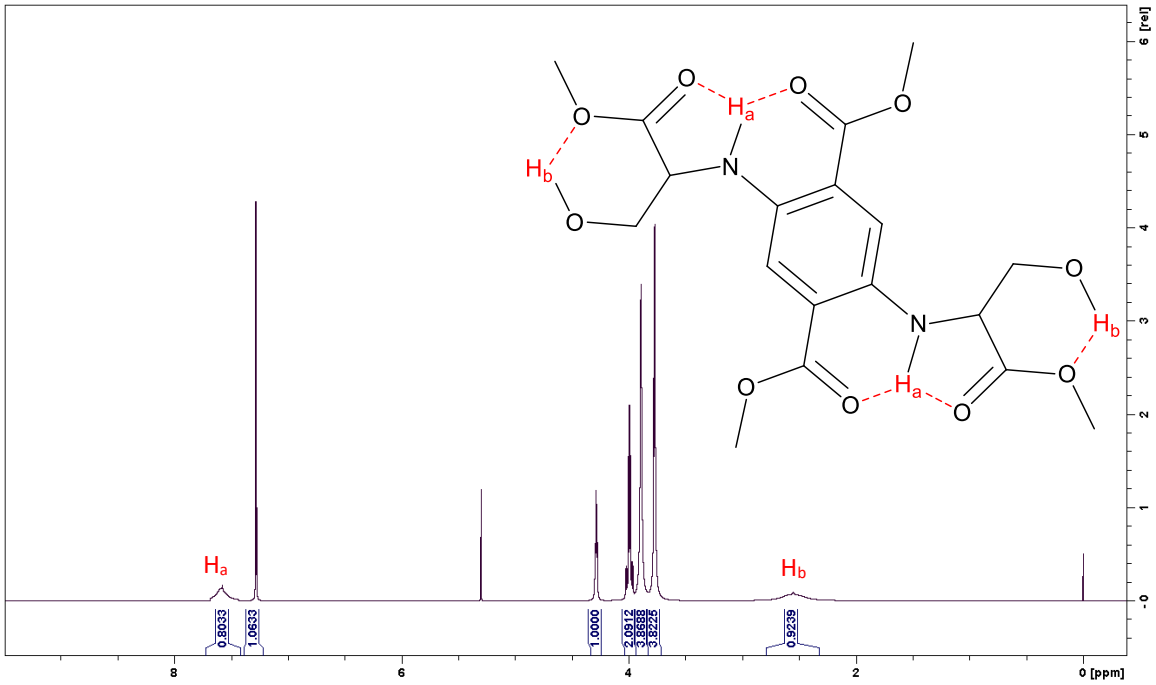

Figure 48: NMR of 40 with hydrogen bonds highlighted

Most of the initial reactions sought to use BSA as a reagent for scale up and ease of use, however acetamide became a problem at diphenyl ether reflux temperatures. Small amounts of product were found in the reactions that utilized sodium hydride as a base. It was determined that if a carbamate could be made between the aromatic amine and the serine alcohol, one could easily dehydrate and cyclize to the Janus quinolone with one equivalent of base. And so, a reaction was set up with **40** and CDI, with the hope that a carbamate could be formed.

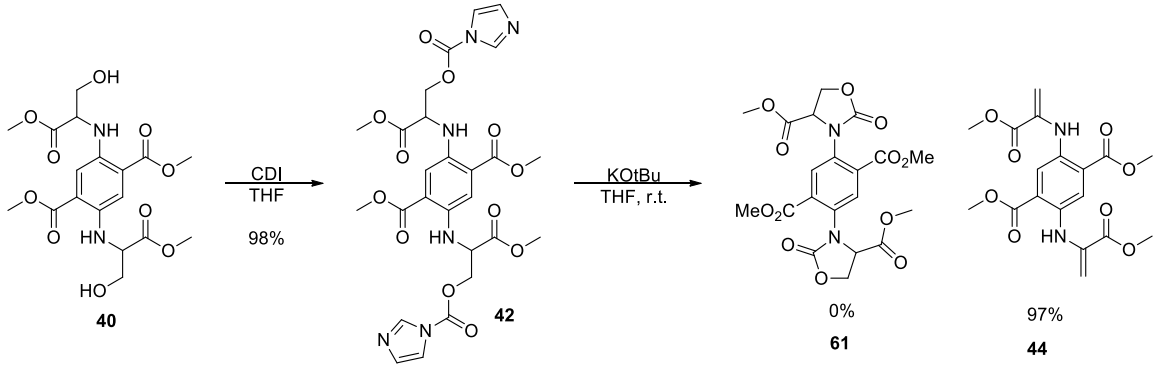

Scheme 39: the stepwise dehydration of 40

First the **40** was converted into **42** by simply mixing an excess of CDI over **40** in THF at room temperature. The reaction is extraordinarily fast, usually complete by the first TLC (~5 minutes). **42** was stirred in THF with an excess of potassium tert. butoxide at room temperature and after a few minutes showed a significant amount of precipitation. The precipitate was collected and an NMR was taken showing complete conversion of the imidazolide into the bis-dehydroalanine product, **44**. The reaction was repeated and after workup a 97% yield was afforded. The isolation of **44** solidified the means by which **60** was isolated from the early dehydration/cyclization attempts.

From this experiment, two methods of dehydration of **40** to **44** (**45**) were developed.

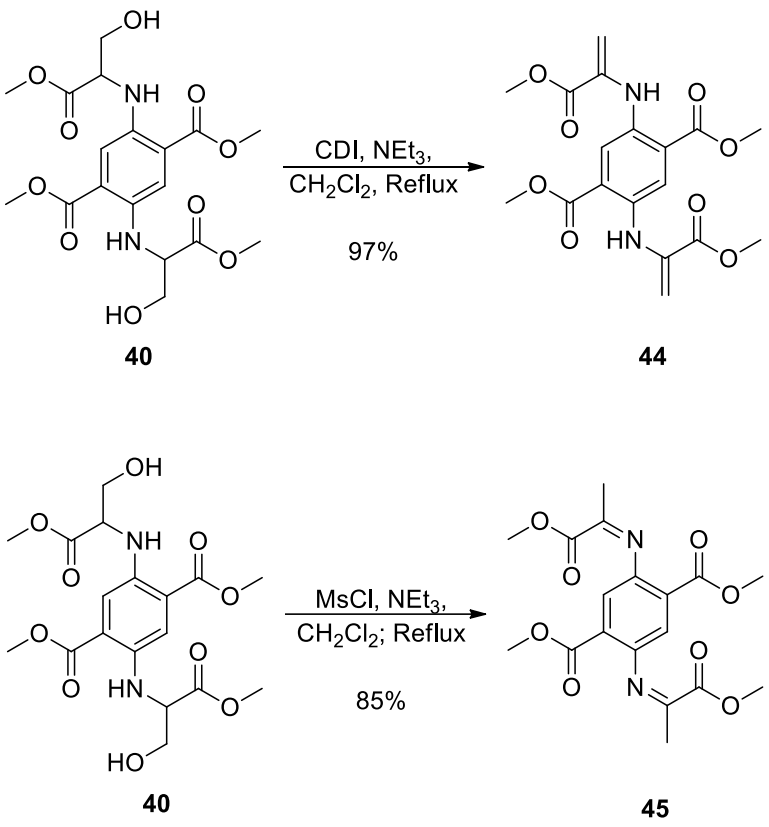

Scheme 40: The dehydration of 40 via MsCl and CDI and their products

Each method has its value, and while both are high yielding the CDI method appears more favorable simply due to the overall yield. Additionally, the MsCl method appears to first make **44** and overtime converts into **45** after crystallization. This means that it is easy for small amounts of methane sulfonic acid to slip past the workup and convert the solid into imine.

Despite its appearance, **44** IS incredibly stable and was able to be stored on a bench top for multiple months before degradation of the product was observed. Its stability is likely due to the intramolecular hydrogen bonding of the molecule that increases its crystallinity.

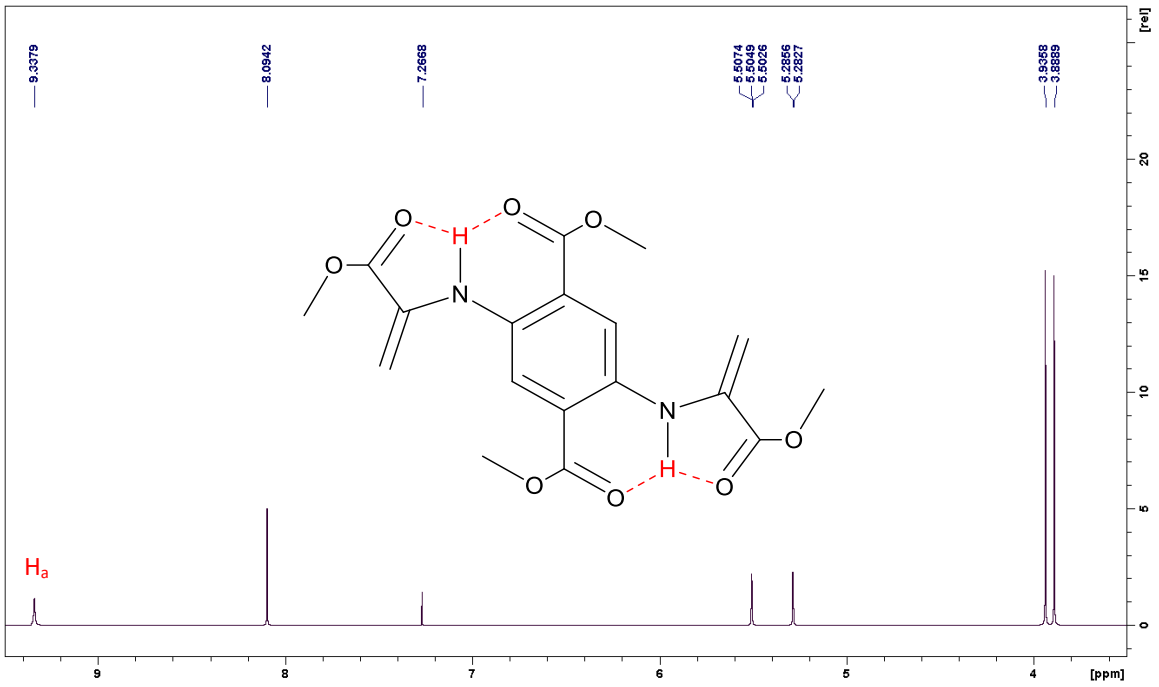

Figure 49: ^{1}H NMR of 44 illustrating the strong intramolecular hydrogen bonding interactions

After benchtop degradation was observed, the product was kept under active vacuum and only removed from vacuum as needed but no further precautions were required when handling this product. Crystallization of this product from neat CH_2Cl_2 affords very clean **44** without further purification necessary.

Few experiments were performed to investigate the conversion of **44** into Janus quinolone, **55**. It was assumed, based on previous experiments, that one could make **55** with a strong base like sodium hydride or sodium dimsyl. The subsequent cyclization reaction was carried out at 60 °C and 120 °C in DMSO with sodium dimsyl, the latter being the current method for synthesis

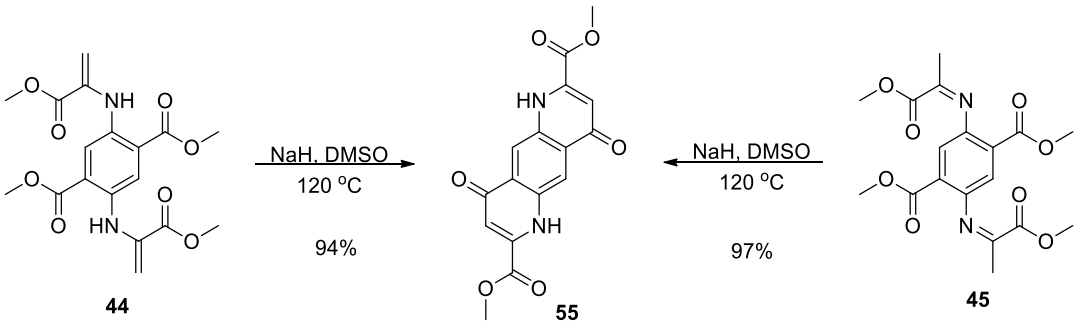

Scheme 41: the synthesis of 2,6-dicarboxybisquinolone 55 from imine and eneamine

Despite the propensity for the **44** to tautomerize over time when made from MsCl, the reaction to form **55** goes in remarkably high yield from either tautomer. There is concern in this scheme, that sodium dimsyl is not stable at high temperatures and 120 °C is very close to its auto-detonation temperature[101]. Thus, this does not constitute a method to form **55** at scale. However, the reaction has been performed up to 5g of starting **44** with no serious issues involving detonation. Further investigations into the synthesis of this Janus quinolone and others has led to the possibility of an alternate synthesis with methoxide in methanol at reflux and dimethyl carbonate.

When combined the overall yield of **55** from DMSS is between 72 - 85% depending on the method used. The product is a yellow solid that is almost entirely insoluble in every solvent apart from basic H_2O (pH + 10) and strong acids (TFA, H_2SO_4). Thus, the most succinct route to **55** is;

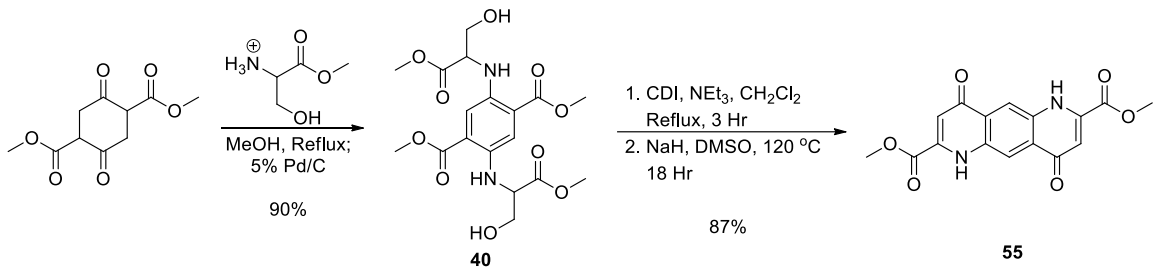

Scheme 42: the total synthesis of 55 starting from DMSS

Once **55** was isolated, the focus of this work shifted toward finding a method of breaking symmetry. The first set of experiments involved nitration of **55**. Unfortunately, due to the inability to solubilize the starting material it became apparent that breaking symmetry at the Janus quinolone stage was not a simple problem to solve. Multiple nitration experiments were performed with the only success resulting in nitration of the central aromatic ring on **55**.

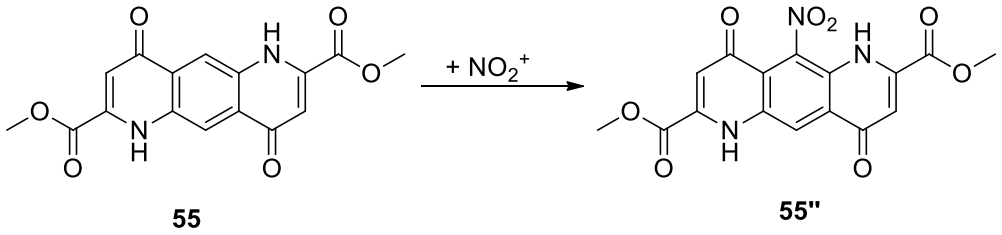

Scheme 43: Failed nitration of 55

These findings meant that breaking symmetry would have to happen before the creation of the bis-fused quinolone, the Janus quinolone.

Due to the difficulty in selectively nitrating the **55** it was decided that breaking symmetry earlier on might be advantageous, if only for authentic product to compare. There were two places to break symmetry either at the **40** step or at the DMSS step. Both of these routes were investigated.

Anthranilic acids are known to readily form nitro-enamines with reagents like methazoic acid under acidic conditions[102]. This nitro-enamine is also known to readily cyclize under dehydrating conditions with reagents like acetic anhydride, carbonyl diimidazole, diethoxy chlorophosphate etc[102–105]. If these conditions were applied to an anthranilic-like precursor, **51**, the desired asymmetric Janus quinolone, **53**, could be realized.

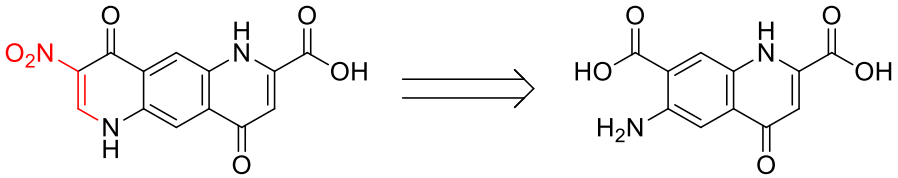

53 **51**

Figure 50: Retrosynthetic analysis for the synthesis of 53 via 51

This precursor to the target Janus quinolone would appear to be a half cyclized and half hydrolyzed product of **44**. It seemed plausible for there to be a method to take **40** and convert it into quinolone methyl anthranilate, **46.**

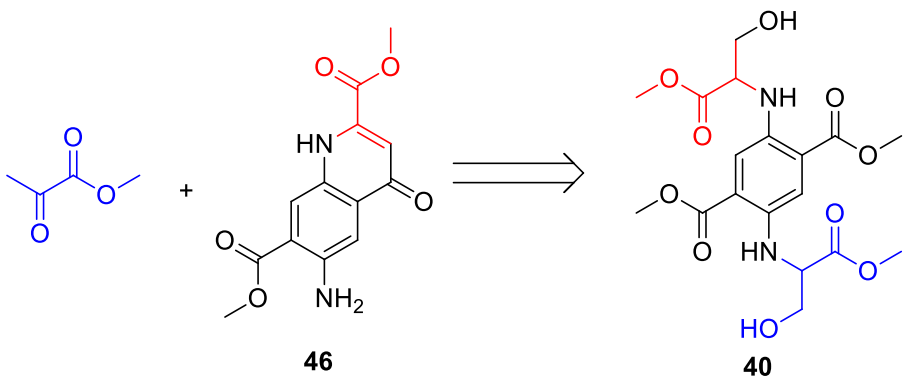

Figure 51: Retrosynthetic analysis for the synthesis of 46 from 40

To investigate the possibility of this route, an authentic product was first synthesized starting with DMSS utilizing a mixed pot method.

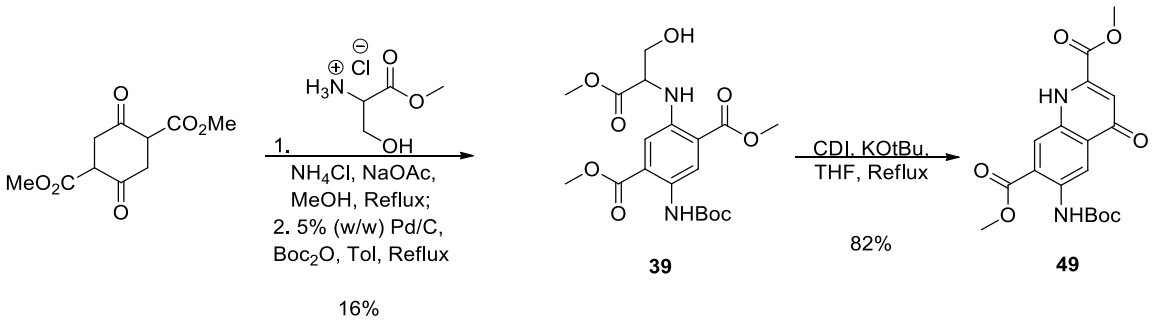

Scheme 44: Pathway 1 to bocQMA, 49, via Mixed pot method

The first pass at this reaction sequence afforded the boc protected quinolone methyl anthranilate **49** in low yield overall after column. **49** can be readily isolated from the complex mixture via flash chromatography with wet ether. The reaction was also performed with MsCl under the conditions used to convert **40** into **44** and afforded 65% of the desired product overall. With the authentic standard in hand a series of reactions were performed to see what it took to convert **40** into the desired **46**.

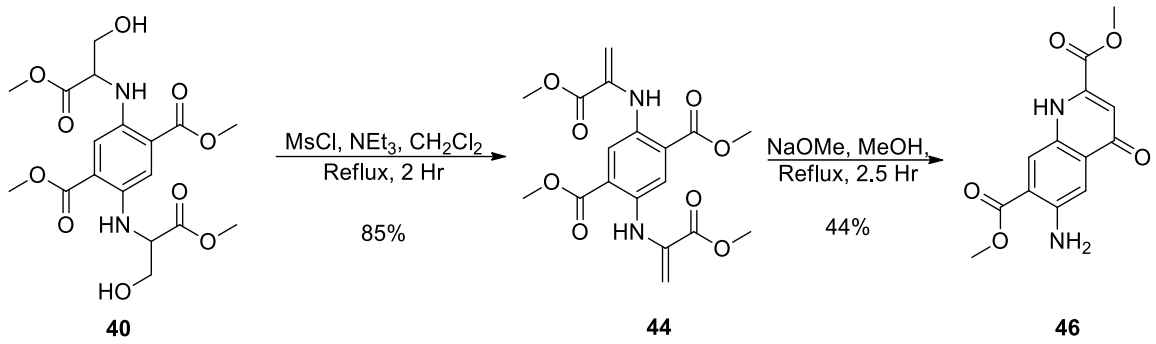

Scheme 45: Pathway 2 to QMA, 46, via two pot method

Cyclization conditions were investigated to see what base it took to form **46** and sodium methoxide in methanol appeared to be the best candidate. **46** as a product is insoluble in most solvents, as many quinolones also behave, and the hope was that by using a weaker base than sodium dimsyl and a less polar solvent than DMSO one might be able to make **46** selectively.

It appears that methanol is sufficiently lower boiling than DMSO and methoxide is sufficiently less basic than sodium dimsyl to produce primarily the mono cyclized product from **44**. While **55** is produced as a side product, conditions could in theory be made to optimize the mono cyclized product **46**. Once cyclized on one side **62** is readily hydrolyzed to **46** and methyl pyruvate under mild aqueous acidic conditions.

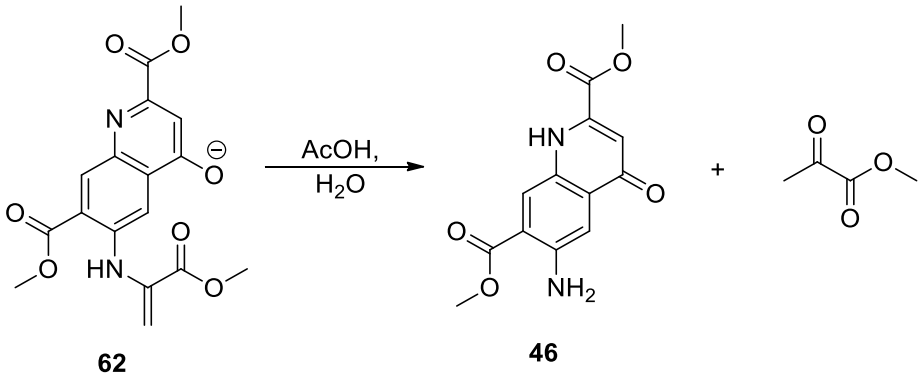

Figure 52: intermediate 62 hydrolysis to 46 and methyl pyruvate under aqueous acidic conditions

The reaction conditions appear to afford the correct product when compared to the standard, however isolation remained a mess with a significant amount of **55** contaminating **46** Additionally, for the purpose of scaling up, MsCl was not a desirable reagent to work with. And so, an alternate synthesis was envisioned wherein a one pot procedure to make **46** from **40** might be possible using relatively safe reagents. After multiple attempts a set of conditions were found.

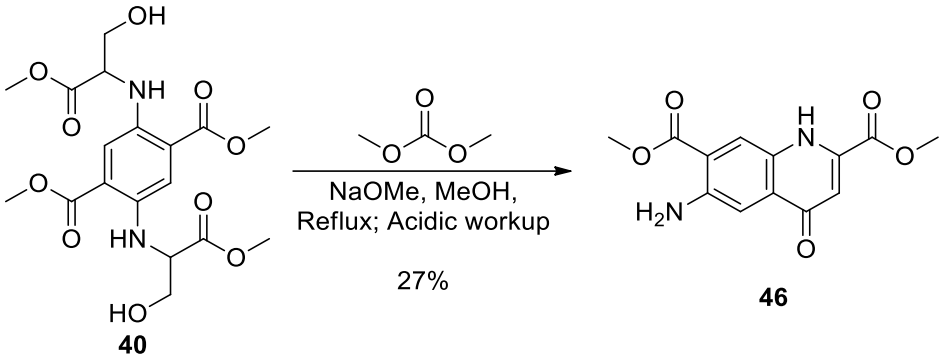

40 **46**

Scheme 46: Pathway 3 to QMA, 46, via one pot method

40	NaOMe	DMC:MeOH	Time	Yield	m.p.
0.025 M	0.5 M	20 ml : 20 ml	5 Hr	25% (pure)	278 – 280 °C
0.04 M	0.95 M	15 ml : 10 ml	1.5 Hr	27%	+300 °C
0.04 M	0.27 M	15 ml : 10 ml	6 Hr	20%	270 – 271 °C
0.10M	0.54 M	5 ml : 5 ml	6 Hr	20%	276 – 280 °C

Table 9: Conditions for the one pot synthesis of 46

These conditions are still very much under development, however based on some scouting it appears that it is likely possible to make **46** in higher yield under conditions similar to these. It should be possible

to increase the yield of **46** over **55** in this scheme by using a less polar solvent like THF. Unfortunately, the current method of isolation requires the use of acetic acid in the extraction on the order of solvent quantities to obtain any amount of product.

While these investigations were underway, alternative routes were established.

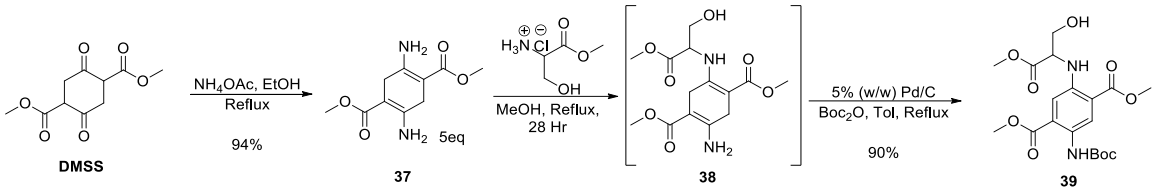

Scheme 47: Pathway 4a to bocASTP from DMSS via crystallization methods

This scheme was developed to see if it was possible to make the amine-serine-terephthalate, **39**, such that serine methyl ester would be conserved. **39** had been made previously through similar conditions, this set of conditions takes advantage of the difference in solubility of **37** and **39** to make **39** on a large scale. First, **37** is made from ammonium acetate in ethanol at reflux at a concentration in which the product crystallizes. Similar conditions are then used to transaminate serine with one of the amines.

It was found that 4 - 5 equivalents of **37** to one serine made exclusively **38** and none of **37'**. And so, by running the reaction at the crystallization concentration for **37** it was possible to keep 98% (by NMR) of the **39** generated in the methanol fraction of the crystallizing solution. That filtrate was then subjected to aromatization conditions used for **60** where the Boc_2O amount is determined by NMR of the crude **37** solution. A slight excess of boc anhydride is used with the excess being thermally decomposed by the refluxing toluene. From there the remaining **60** that was aromatized is separated via crystallization as **39** does not crystallize from neat CH_2Cl_2 while **60** does. This procedure was scaled up to 25g (product yield) which is about the limit for research lab settings and works in good yield, 80%.

This scheme was developed because a new lot of **49** needed to be made for high resolution data acquisition and the intermediates from **39** to **49** via CDI was needed. The following scheme was then developed.

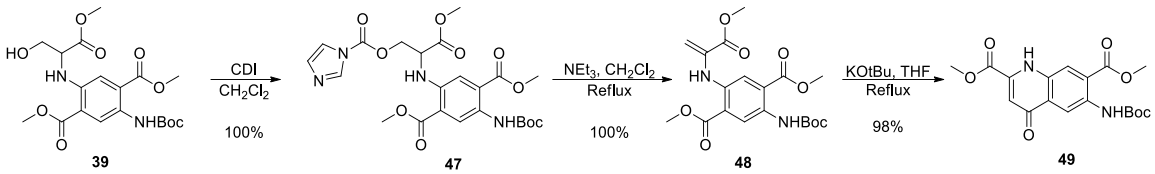

Scheme 48: Pathway 4b to bocQMA, 49, from 39

When run with purified **39**, columned and vapor diffused crystallized, it was possible to make **49** from **39** in 98% yield. Meaning that with the 90% yield based on serine to **39**, this scheme would afford a succinct multistep procedure to **49** from DMSS in 79% yield. While each step is remarkably high yielding, it is assumed that this sequence can be shortened even further. In retrospect there are multiple pathways to quinolone methyl anthranilate, **46**.

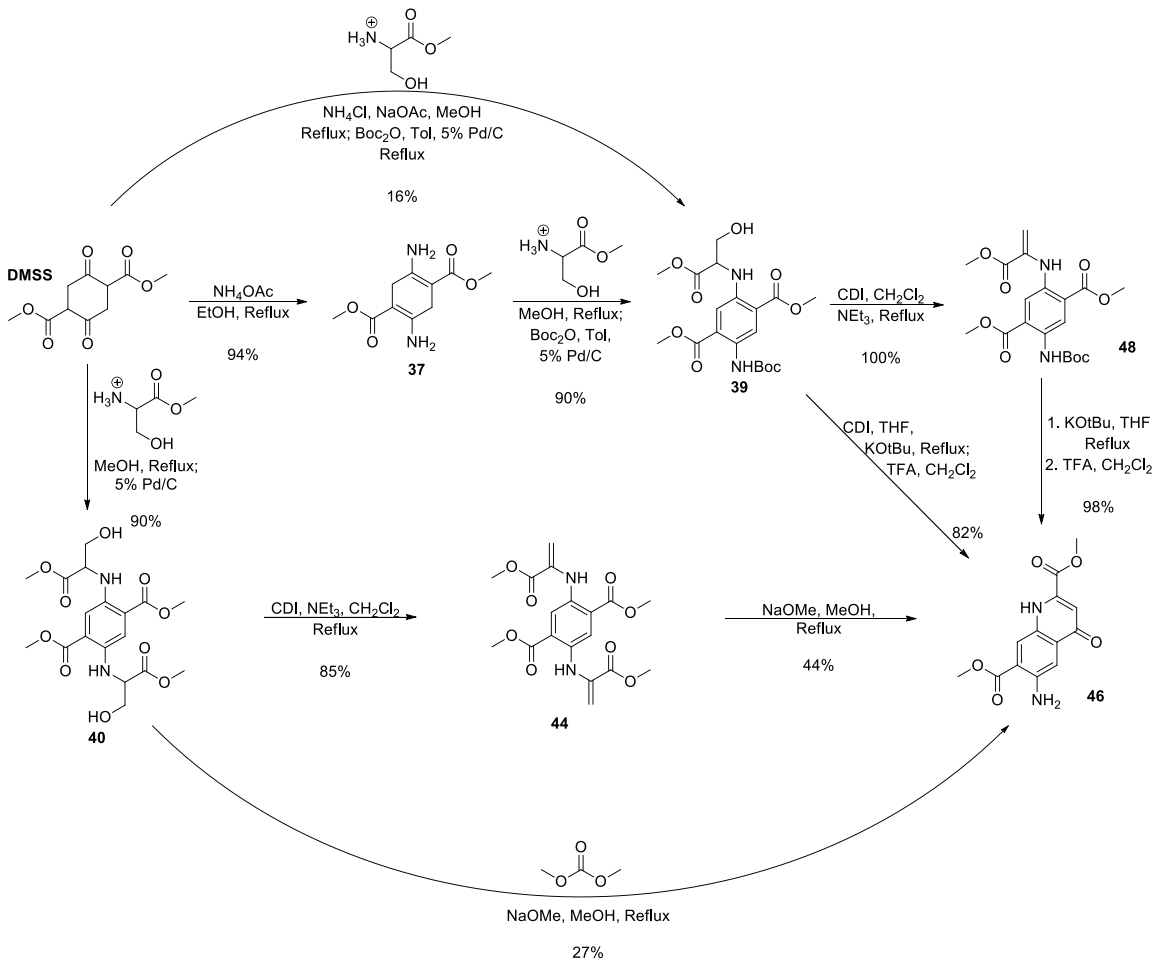

Scheme 49: All four pathways to 46

Now that a means to produce **46** from DMSS in good scale-able yield without the need for column had been developed, the final sequence to the asymmetric Janus quinolone, **53**, could be realized.

3-nitro-4-quinolones can be made from anthranilic acid via two step procedure involving the formation of a nitro eneamine and a cyclization under dehydrating conditions[102].

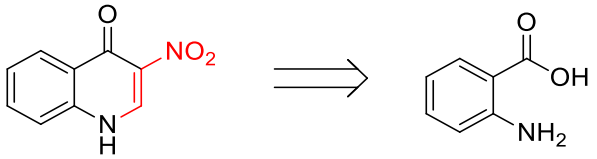

59

Figure 53: Retrosynthetic analysis for the synthesis of 3-nitro-4-quinolone, 59, from anthranilic acid

This process was investigated for its efficacy and modified for **51** and **53** in mind. The first step in this process was the creation of nitro eneamine reagents like methazoic acid and dimethylaminonitroethylene.

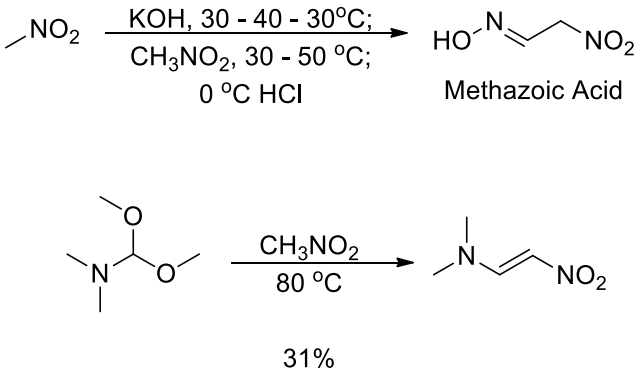

Scheme 50: The synthesis of dimethylaminonitroethylene and methazoic acid

The former, methazoic acid, is a standard reagent in nitro eneamine synthesis and forms under very controlled conditions. The heating and cooling process must be carried out carefully as this reaction can

very quickly exotherm and detonate. Additionally, the methazoic acid is a contact explosive when isolated pure and also reacts violently with atmospheric oxygen[106]. As a result, a secondary reagent was prepared that was shelf stable, non-explosive and an easy to handle solid. Dimethylaminonitroethylene reacts under acidic conditions with anilines and effectively does the same chemistry as methazoic acid[107]. Methods to prepare **58** were developed with both methazoic acid and dimethylaminonitroethylene in addition to **58'.**

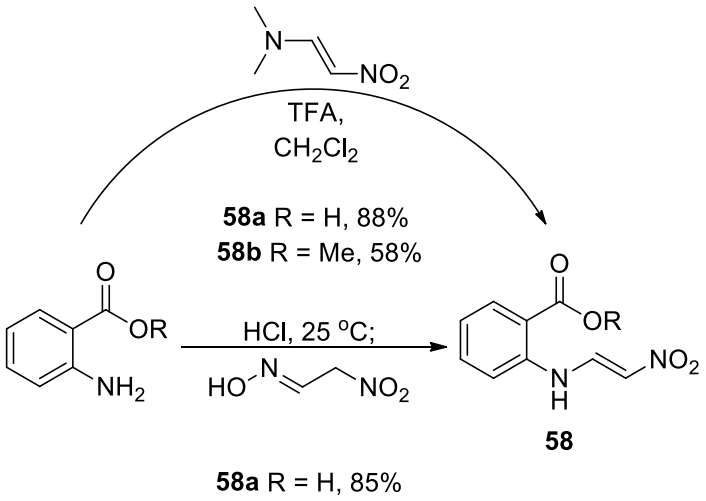

Scheme 51: Pathways to nitroeneamines 58a/b

The **58** forms readily under these conditions with yields in the range of 85 – 97%. The key to ensuring a pure product for this reaction is by first filtering the anthranilic acid/HCl solution to remove insoluble starting material. Furthermore, attempts at further purification has led to the degradation of product when using alcoholic solvents. The product of this reaction crystalizes out of solution anyway, so further purification is hardly needed. The dimethylaminonitroethylene variants, while lower yielding, were carried out under non aqueous conditions in case the aqueous acid route didn't work for **51** or **53**. The methyl ester variant **58'** was created in the hopes of shortening the sequence further. Once in hand, these nitro eneamines were cyclized.

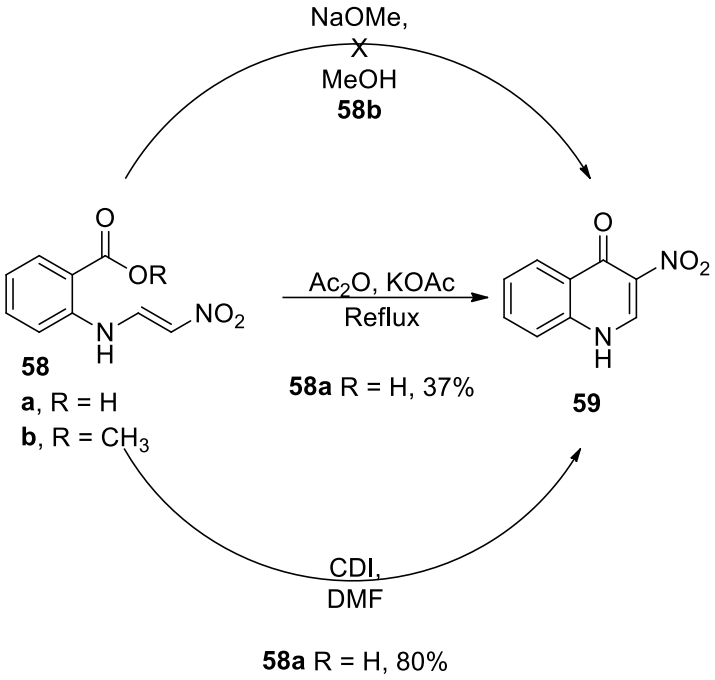

Scheme 52: Pathways to 59 from 58a/b

Acetic anhydride as a solvent with potassium acetate affords the **59** in 37% yield. This method is very simple to perform and obtain very clean product, but the low yield is very unattractive when considering the lengths it takes to make **51** and its related variants. Eventually, a procedure was found that uses CDI in DMF to cyclize **58** into **59** in much higher, 80%, yield[103]. The ester variant, **58b** has not been cyclized under basic conditions but undoubtably there exist conditions to cyclize **58b** under basic conditions.

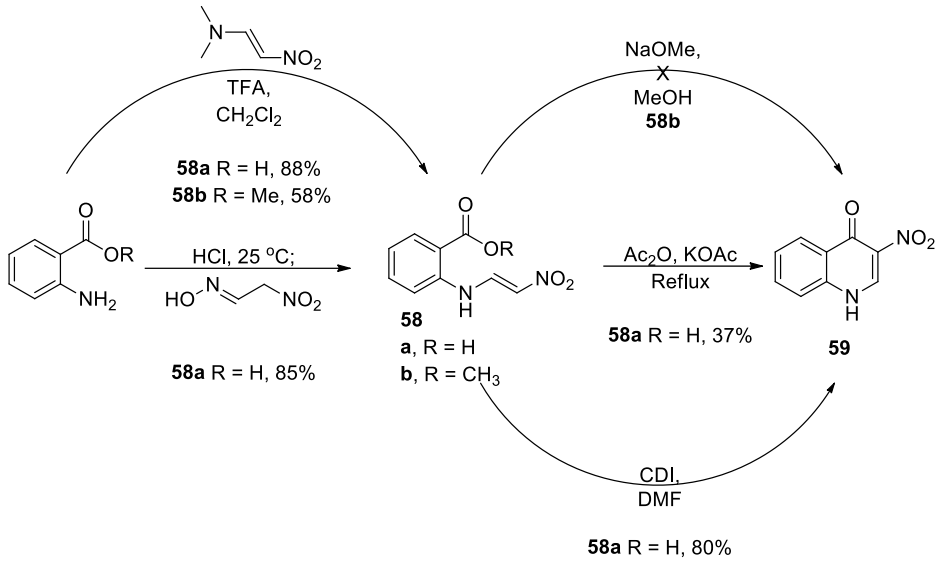

Scheme 53: Model syntheses to make 3-nitro-4-quinolone, 59

Because most of the syntheses toward the desired product have esters and are very insoluble in most solvents, the method to make **58** via HCl_{aq} was not ideal as aqueous acid isn't sufficiently solubilizing to allow for any significant proportion of **51** to dissolve.

Each of these routes showed promise and as a result the sequences were applied to **46**, **49**, **50** and **51**.

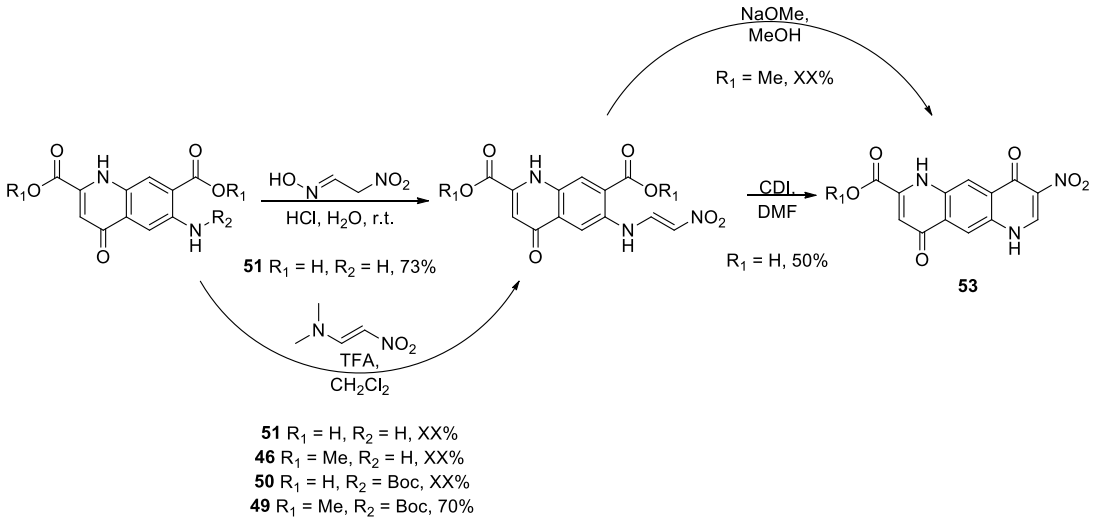

Scheme 54: The synthesis of Asymmetric Janus Quinolone, 53, and the applied model pathways

The biggest hurdle regarding this sequence is the insolubility of **51** in most solvents, 1 mmol scale reactions take on the order of +10 ml of conc. HCl to dissolve. Because of this the standard method was abandoned as it was difficult to control the reaction due to the large dilution factor. The non-aqueous methods were then employed on a variety of quinolone anthranilates, **46**, **49**, **50**, and **51** to make both the methyl ester and free acid variants of the nitro eneamine **52**. The non-aqueous route is very simple and affords the opportunity to crystallize the product from organic solvents that otherwise wouldn't be accessible.

The reaction with CDI in DMF allows for variation of the ester and allows for boc protection of the quinolone nitrogen on the nitro bearing ring.

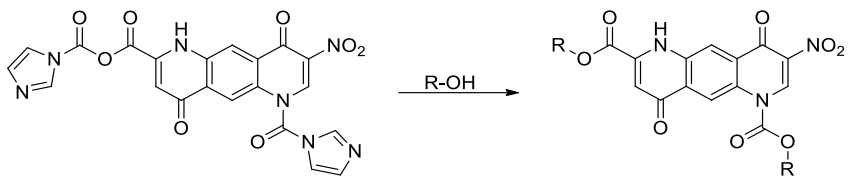

Figure 54: Consequence of cyclizing 52a via CDI/DMF

This however does not make the product noticeably more soluble in any solvents, multiple esters have been made all of which suffer the same relative insolubility. This product suffers from the same ailments **55** faces in terms of solubility. Alternative modifications have been investigated to help solubilize **53**. The asymmetric Janus quinolone can be made from DMSS in 33% overall yield. The possible routes to asymmetric Janus quinolone:

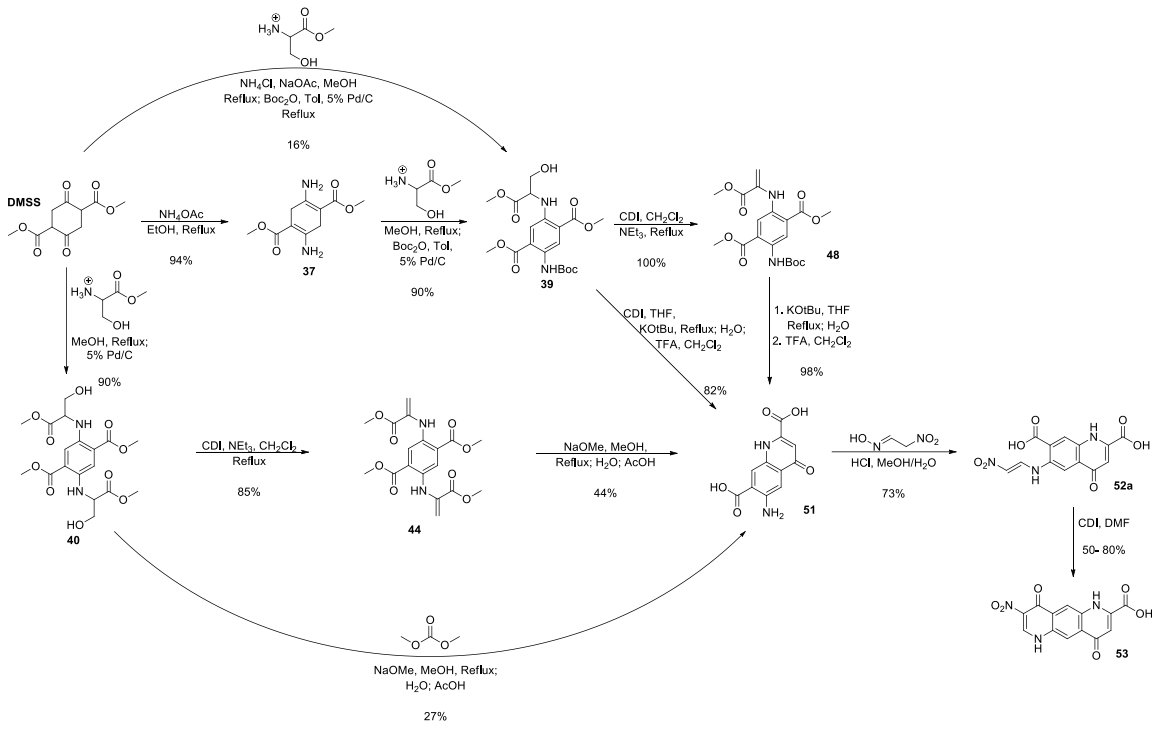

Scheme 55: Current pathways to 53 from DMSS

From here, conditions needed to be found to reduce the nitro group on the **53**. Because the product shared similar solubilities to the symmetric variant, reduction needed to happen one of three ways, under strongly basic conditions, strongly acidic conditions, or conditions where the reaction occurs at the interface of the solid. Multiple conditions were tested:

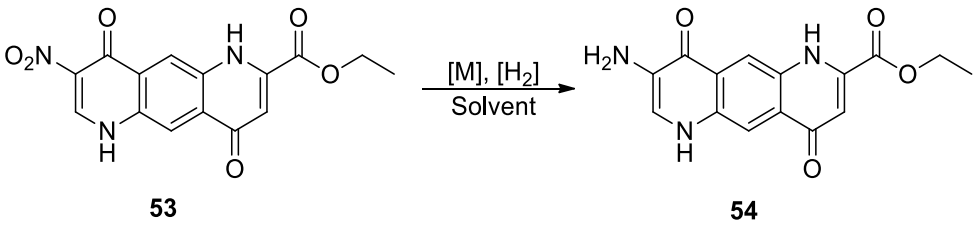

Scheme 56: The reduction of 53

	Source of H	Solvent	Fluorescence
$SnCl_2$	12 M HCl	H_2O	None
Zn^o	12 M HCl	H_2O	detected
Fe^o	12 M HCl	H_2O	detected
Pd/C	None, H_2	EtOH	detected

Table 10: Consequence of Reducing 53 via multiple methods

While there are other conditions that would likely reduce the nitro group, i.e, raney nickel, hydrazine etc., the most attractive of these is palladium on carbon as it requires only solvent and hydrogen. Unfortunately, the insolubility of **54** in addition to **53** makes this pathway unlikely. Zinc metal affords an interesting possibility as $Zn(OH)_2$ is very insoluble in basic H_2O and would make isolation of the product easier so long as the entirety of the starting material had been consumed.

Multiple fluorescence spectra have been obtained for **54** and intermediates on the pathway.

46 is among the most fluorescent intermediates in this pathway, even in its boc protected form it is incredibly fluorescent. This leads to the notion that **46** itself could be considered as an alternative beta sheet initiator.

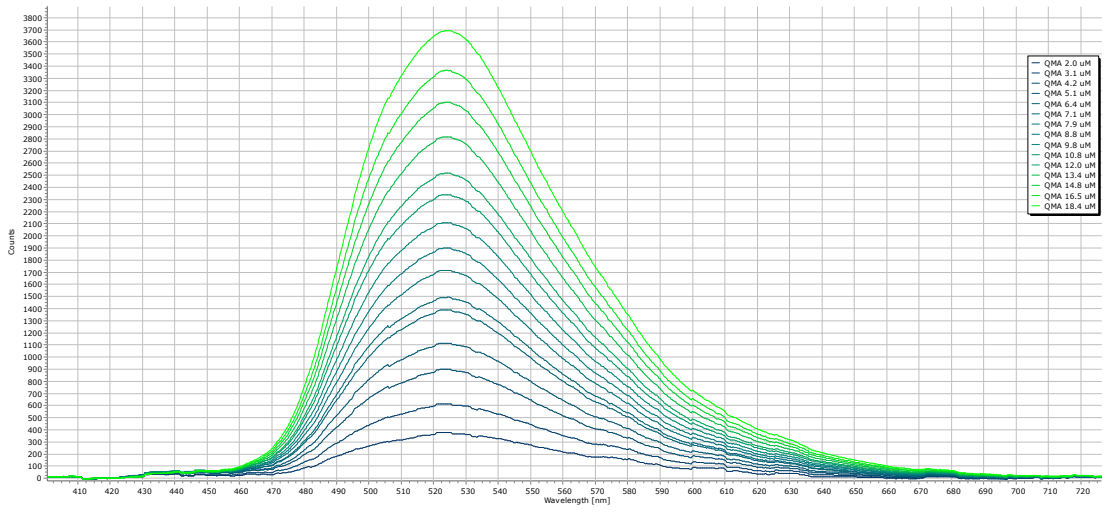

Shown, from 18 to 2.0 uM QMA in MOPS

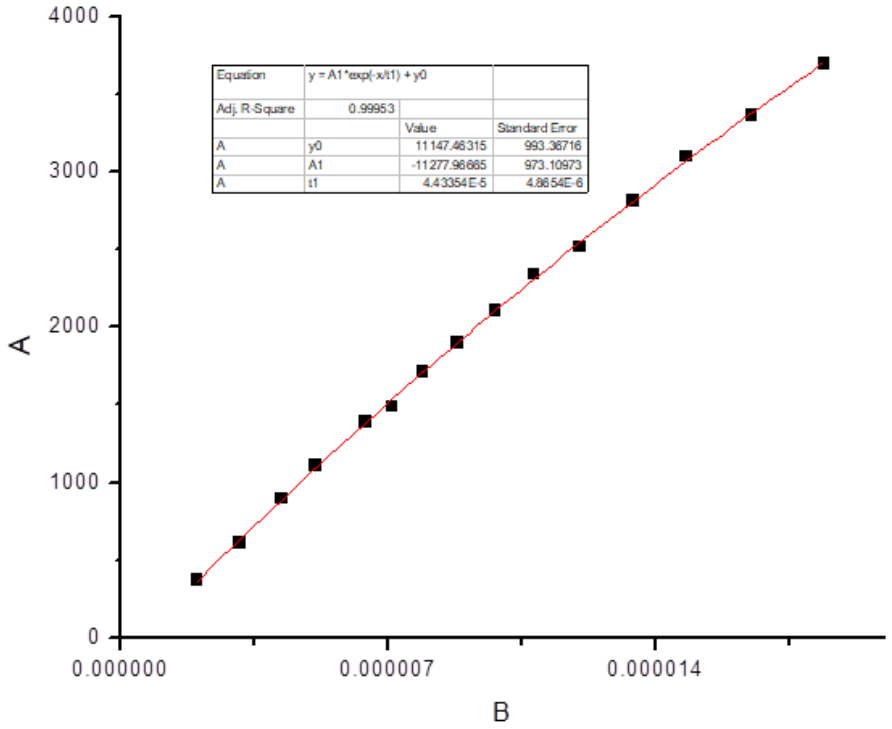

Fluoresence intensity as a function of concentration at 523 nm.

The aJQ-NH_2 appears to be a fairly fluorescent molecule

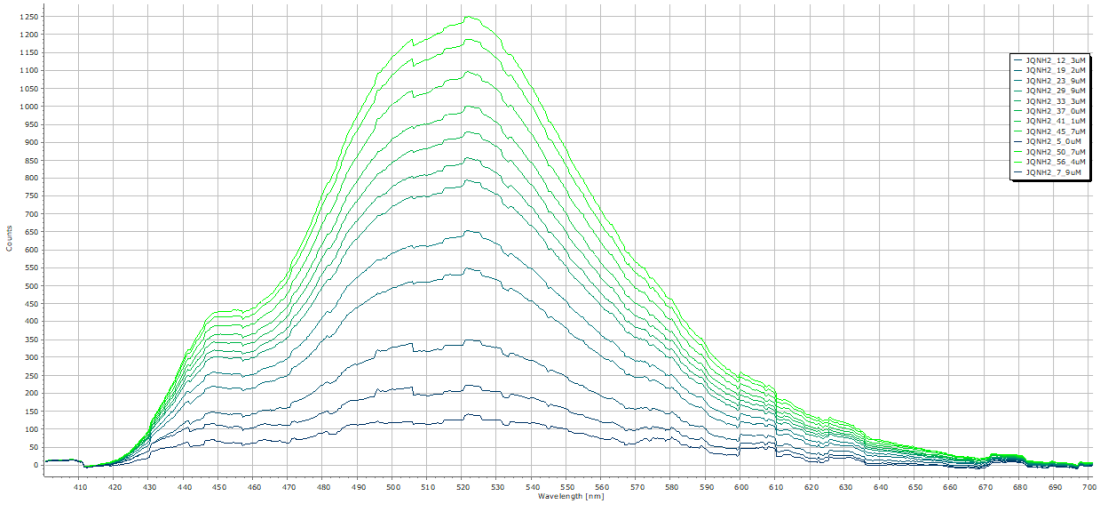

Shown, from 56.4 to 5.0 uM in MOPS, excitation 420

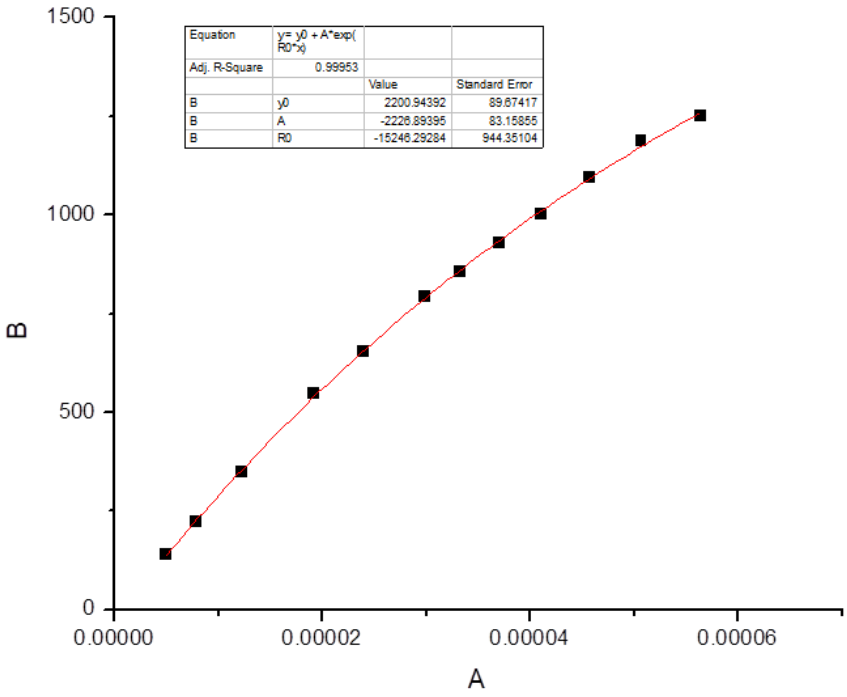

Shown, fluorescence as a function of concentration at 521 nm

The asymmetric Janus quinolone appears to deviate further from linearity than QMA, however this effect could be the result of self quenching via dimerization or some other unrelated process.

All Characterization Spectra can be found in the appendix

Synthesis of Biseneamine **37**
dimethyl 2,5-diaminocyclohexa-1,4-diene-1,4-dicarboxylate

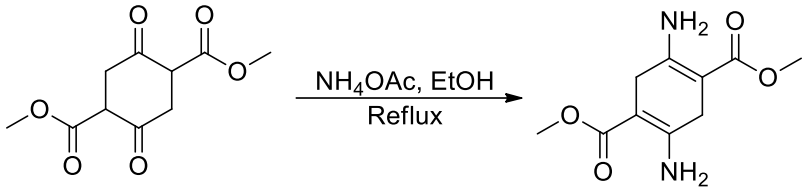

71.313g (0.925 mol) of ammonium acetate and 55.170g (0.241 mol) of DMSS was heated to reflux in 2 L of anhydrous ethanol for three hours. The reaction mixture was then allowed to cool to room temperature slowly before submerging in an ice bath for 2 hours to crystallize. The precipitate was collected via vacuum filtration and dried over multiple days under reduced pressure. Yield: 49.066g (90%), m.p. 208 – 210 °C.

1H NMR 300MHz ($CDCl_3$): δ 3.13 (m, 4H), 3.71 (s, 6H)

13C NMR 300MHz ($CDCl_3$): δ 169.3; 155.6; 86.8; 50.8; 30.4

Synthesis of dehydro-ASTP **38**
dimethyl 2-amino-5-((3-hydroxy-1-methoxy-1-oxopropan-2-yl)amino)cyclohexa-1,4-diene-1,4-dicarboxylate

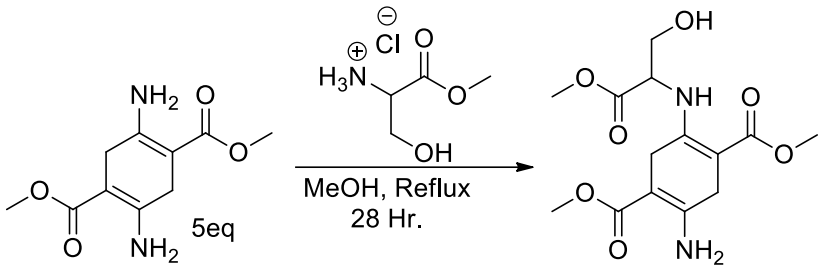

0.1585g (1.03 mmol) of serine methyl ester HCl and 0.4362g (1.93 mmol) of **37** was heated to reflux in 25 ml of anhydrous methanol for 21 hours. Once complete the reaction mixture was chilled on ice to precipitate **37**. The precipitate was separated via vacuum filtration and the filtrate was concentrated. The filtrate was then resuspended in 25 ml of CH_2Cl_2 and filtered. This was then concentrated via rotary evaporation and subjected to flash chromatography using 10% CH_3CN in CH_2Cl_2 as the eluent. Yield: 0.164g (50%), m.p. 181 – 182 ^oC

1H-NMR 500 MHz ($CDCl_3$): δ 2.25 (1H, t, J = 6.3 Hz), 3.16 (4H, m), 3.71 (3H, s), 3.71(3H, s), 3.78 (3H, s), 4.39 (1H, m), 9.37 (1H, d, J = 9.6 Hz)

13C-NMR 500 MHz ($CDCl_3$): δ 171.5, 169.5, 169.1, 155.9, 154.8, 87.3, 86.3, 63.9, 56.8, 52.7, 50.8, 50.7, 30.3, 26.7

Synthesis of bocASTP **39**
dimethyl 2-((tert-butoxycarbonyl)amino)-5-((3-hydroxy-1-methoxy-1-oxopropan-2-yl)amino)terephthalate

Mixed one pot method:

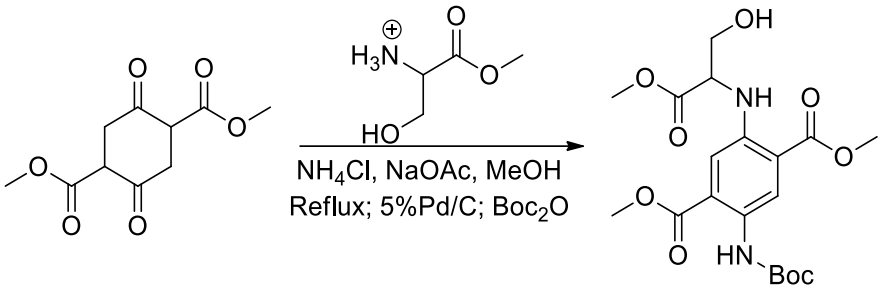

0.5071g (2.22 mmol) DMSS, 0.3437g (2.21 mmol) serine methyl ester HCl, 0.1203g (2.25 mmol) ammonium chloride and 0.3654g (4.45 mmol) sodium acetate was refluxed in 25 ml MeOH. After 5 hours at reflux, 0.0254g 5% (w/w) Pd/C was added and reflux continued for another 17 hours. At that point the mixture was filtered through a packed bed of celite which was washed with 100 ml of hot methanol. The filtrate was concentrated under reduced pressure and the product amine separated via flash chromatography to afford 0.112g (15.5%) of the amine. The amine was then refluxed in 10 ml of toluene with 0.132g (0.6 mmol) of Boc_2O overnight. The solvent was removed via rotary evaporator and the residual Boc_2O was remove via Hexanes crystallization. Yield: 0.151g (15.5%) of a bright orange solid. m.p. 175 - 176 ^oC, R_f 0.26 (10%CH_3CN in CH_2Cl_2)

Bis-eneamine transamination method:

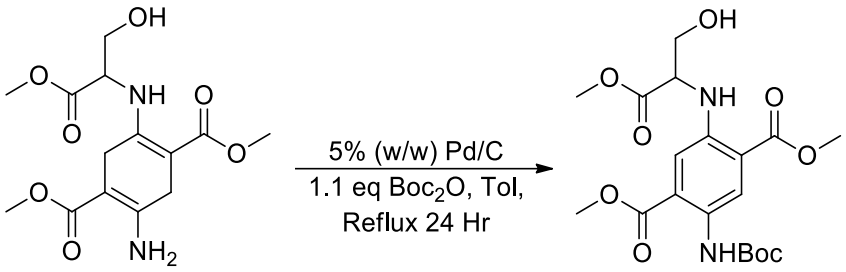

0.5005g (3.20 mmol) of serine methyl ester HCl and 2.854g (12.6 mmol) of **37** was heated to reflux in 150 ml of anhydrous methanol. Reflux was continued until TLC showed the disappearance of serine via acidic ninhydrin visualization, 28 hours. Once complete the reaction mixture was allowed to cool to room temperature slowly before chilling overnight at -20 ^{o}C. The precipitate was collected via vacuum filtration and the filtrate was concentrated via rotary evaporation. The crude residue from the filtrate was then suspended in 100 ml of CH_2Cl_2, filtered, dried over $MgSO_4$ and concentrated to afford 2.157g of a waxy solid determined by NMR to be a 2:1 mixture of **37** and **38**.

This solid was then resuspended in 100 ml of toluene with 4.052g (18.6 mmol) of Boc_2O and 0.125g of 5%(w/w) Pd/C. The mixture was heated to reflux and after 24 hours TLC showed the consumption of starting material(s). While still hot the reaction mixture was filtered through a 1 cm plug of vacuum packed celite and washed with 20 ml of CH_2Cl_2. The filtrate was concentrated, resuspended in 30 ml of CH_2Cl_2 and boiled down to 20 ml before cooling and chilling overnight. The solid was collected via vacuum filtration and the filtrate concentrated. The filtrate containing product was then crystallized from 20 ml of CH_2Cl_2 added to 150 ml of Boiling hexanes and then concentrated to 140 ml. The orange solid was collected via vacuum filtration to afford a yellow-orange solid. Yield: 1.1975g (97% based on **38** conversion), m.p. 168 – 170 ^{o}C.

1H-NMR 500 MHz ($CDCl_3$): δ 1.52 (9H, s), 2.15 (1H, t, J = 6.5 Hz) 3.81 (3H, s), 3.95 (6H, s), 4.05 (2H, dd, J = 2, 11 Hz), 4.36 (1H, dt, J = 2, 8 Hz), 7.31 (1H, s), 8.10 (1H ,d, J = 8 Hz), 8.96 (1H, s), 9.61 (1H, s)

13C-NMR 500 MHz ($CDCl_3$): δ 171.9, 168.1, 167.6, 143.5, 116.7, 113.5, 80.3, 63.0, 57.9, 52.7, 52.6, 52.3, 28.4

Synthesis of BSME **40**
dimethyl 2,5-bis((3-hydroxy-1-methoxy-1-oxopropan-2-yl)amino)terephthalate

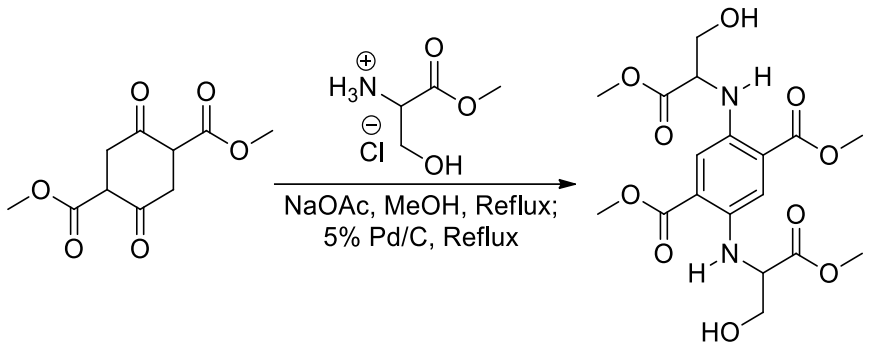

13.054g (84 mmol) of serine methyl ester HCl, 7.395g (32 mmol) of DMSS and 7.810g (95 mmol) of sodium acetate was suspended in 150 ml of methanol and set to reflux. After 3 hours the starting material was consumed and 0.2638g of 5% (w/w) palladium on carbon was added to the flask. Reflux was continued for 18 hours before TLC indicated total conversion. The mixture was then filtered hot through a 1cm pad of celite and concentrated. The crude residue was then dissolved in 300 ml of CH_2Cl_2 and the organics washed with 1000 ml of H_2O followed by 500 ml of sat. NaCl. The organics were collected and concentrated. The residue was then crystallized from CH_2Cl_2/Hexanes to afford 12.180g (90%) of a bright orange solid, M.P. 128 - 130 °C.

1H NMR 500 MHz ($CDCl_3$): δ 7.33 (s, 2H), 4.30 (t, *J* = 3 Hz, 2H), 4.00 (m, *J* = 3 Hz, 4H), 3.91 (s, 6H), 3.78 (s, 6H)

13C-NMR 500 MHz ($CDCl_3$): δ 172.3, 167.8, 140.3, 117.9, 115.2, 63.0, 58.5, 52.5, 52.2

Synthesis of BSEE **41**
dimethyl 2,5-bis((1-ethoxy-3-hydroxy-1-oxopropan-2-yl)amino)terephthalate

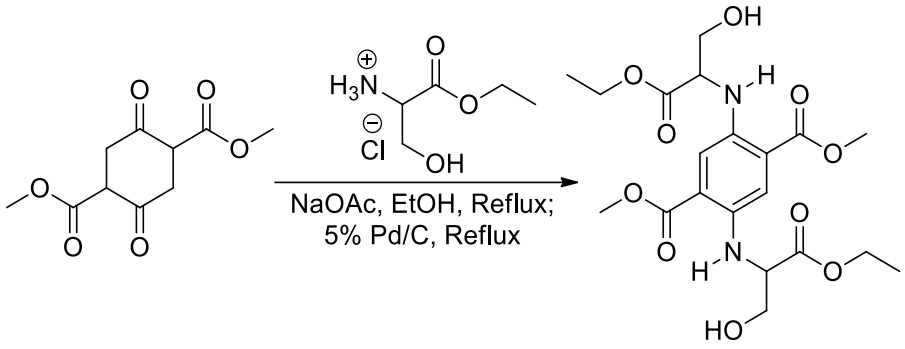

1.9961g (11.77 mmol) serine ethyl ester, 1.0412g (12.36 mmol) sodium acetate and 0.9337g (4.09 mmol) of DMSS was heated to reflux in 60 ml of anhydrous ethanol until DMSS's disappearance by TLC, 18 hours. Then 0.060g of 5%(w/w) Pd/C was added to the mixture and reflux was continued for 72 hours. Once aromatized, the mixture was filtered through a plug of celite while still hot and washed with hot EtOH. The filtrate was then concentrated and resuspended in CH_2Cl_2, washed with H_2O then sat. NaCl and dried over $MgSO_4$. The organic extracts were then concentrated and crystallized from CH_2Cl_2.

Yield: 0.8328g (45%)

1H NMR 500 MHz ($CDCl_3$): δ 1.29 (6H, m), 3.91 (6H, s), 3.99 (4H, m), 4.25 (6H, m), 7.32 (2H, s), 7.61 (2H, s)

Synthesis of BSME-Imid **42**
dimethyl 2,5-bis((3-((1H-imidazole-1-carbonyl)oxy)-1-methoxy-1-oxopropan-2-yl)amino)terephthalate

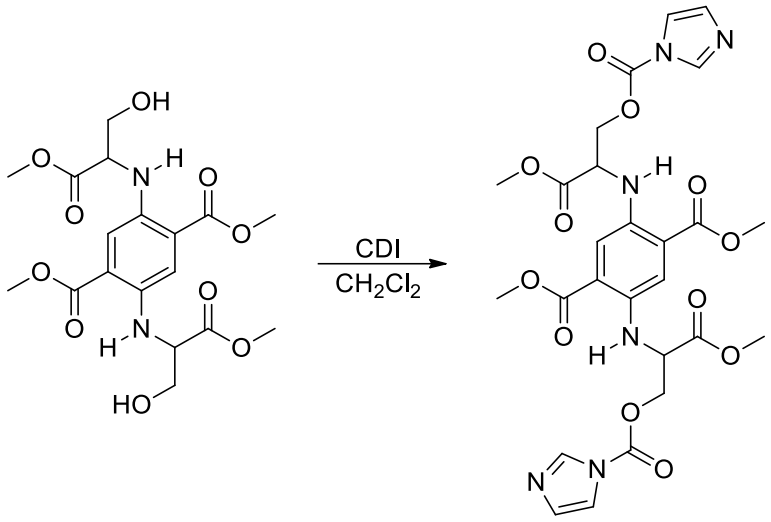

2.3610g (5.51 mmol) of **44** and 2.2356g (13.78 mmol) of CDI was combined in 50 ml of CH_2Cl_2 and stirred at room temperature. After 15 minutes TLC indicated the consumption of BSME and the reaction was stopped. The mixture was washed with 100 ml of H_2O then 100 ml of sat. NaCl. The organic extracts were dried over $MgSO_4$ then concentrated to afford a yellow solid. Yield: 3.397g (100%), m.p. 160 – 161 ^oC.

1H NMR 500 MHz ($CDCl_3$): δ 3.80 (6H, s), 3.90 (6H, s), 4.59 (2H, m), 4.73 (2H, dd, J = 4.5, 11 Hz), 4.84 (2H, dd, J = 4.5, 11 Hz), 7.07 (2H, m), 7.33 (2H, s), 7.43 (2H, t, J = 1.5 Hz), 7.86 (2H, d, J = 8.5 Hz), 8.16 (2H, s)

13C-NMR 500 MHz ($CDCl_3$): δ 170.4, 167.6, 148.2, 139.9, 137.2, 130.8, 118.0, 117.1, 115.0, 67.2, 55.4, 53.0, 52.3

Synthesis of BSME-Ms **43**
dimethyl 2,5-bis((1-methoxy-3-((methylsulfonyl)oxy)-1-oxopropan-2-yl)amino)terephthalate

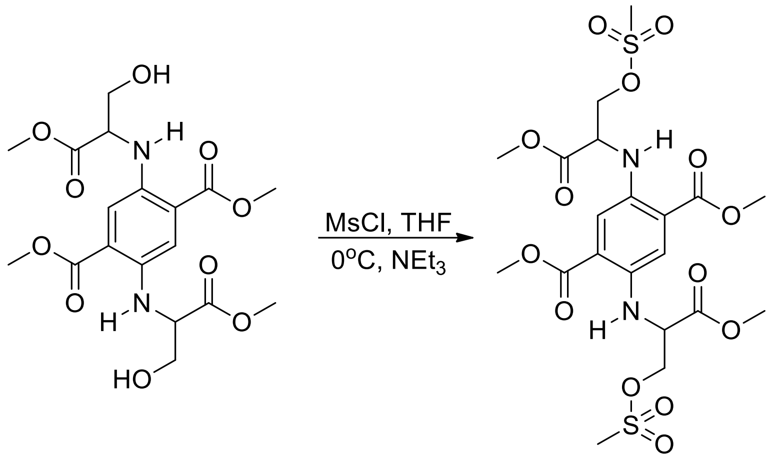

1.085g (2.53 mmol) of **44** was chilled to 0 °C in 50 ml of anhydrous THF. 0.40 ml (5.16 mmol) of MsCl was added and with rapid stirring, 1.105 g (10.93 mmol) of NEt_3 was added at a rate to maintain 0 °C. After 15 minutes the mixture was diluted into 200ml of CH_2Cl_2 and washed with 500 ml of sat. $NaHCO_3$ then 300 ml of sat. NaCl. The organics were combined, dried over $MgSO_4$ and concentrated. The product was recrystallized from CH_2Cl_2 and hexanes. Yield: 1.0753g (73%), m.p. 135 – 137 °C.

1H NMR 500 MHz ($CDCl_3$): δ 1.55 (2H, s_{broad}), 3.04 (6H, s), 3.81 (6H, s), 3.91 (6H, s), 4.50 (2H, s_{broad}), 4.62 (4H, m), 7.29 (2H, s), 7.73 (2H, s)

Synthesis of BAME-Ene **44**
dimethyl 2,5-bis((3-methoxy-3-oxoprop-1-en-2-yl)amino)terephthalate

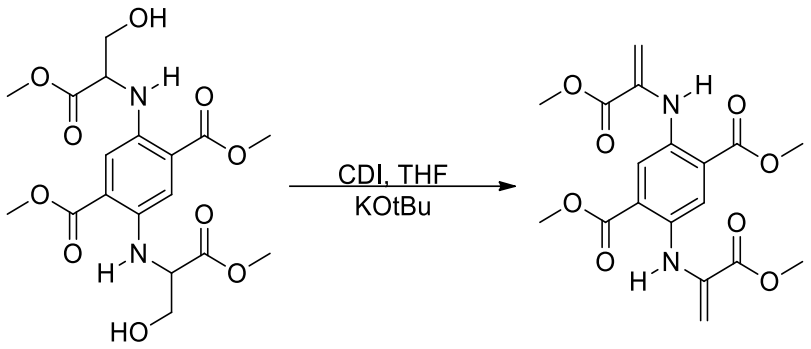

2.143g (5.00 mmol) of **44** and 1.9446g (12.00 mmol) of CDI was combined in 30 ml of THF and stirred at room temperature. After 10 minutes 11 ml of 1.0 M KOtBu in THF was added dropwise and slowly over 5 minutes with rapid stirring. After 15 minutes the solution was diluted into 300 ml of CH_2Cl_2 and washed with 500 ml of H_2O. The organics were then washed with 500 ml of Sat. NaCl, dried over $MgSO_4$ and concentrated. The Crude residue was then crystallized from 100 ml of CH_2Cl_2 and 100 ml of hexanes.

Yield: 0.9491g (48%), m.p. 172 – 173 °C.

1H NMR 500 MHz ($CDCl_3$): δ 3.88 (6H, s), 3.93 (6H, s), 5.28 (2H, d, J = 1.5 Hz), 5.50 (2H, t, J = 1.3 Hz), 8.09 (2H, s), 9.33 (2H, s)

13C-NMR 500 MHz ($CDCl_3$): δ 167.1, 165.4, 136.3, 135.0, 120.4, 120.1, 95.9, 52.8, 52.5

Synthesis of BSME-im **45**
dimethyl 2,5-bis((Z)-(1-methoxy-1-oxopropan-2-ylidene)amino)terephthalate

From MsCl:

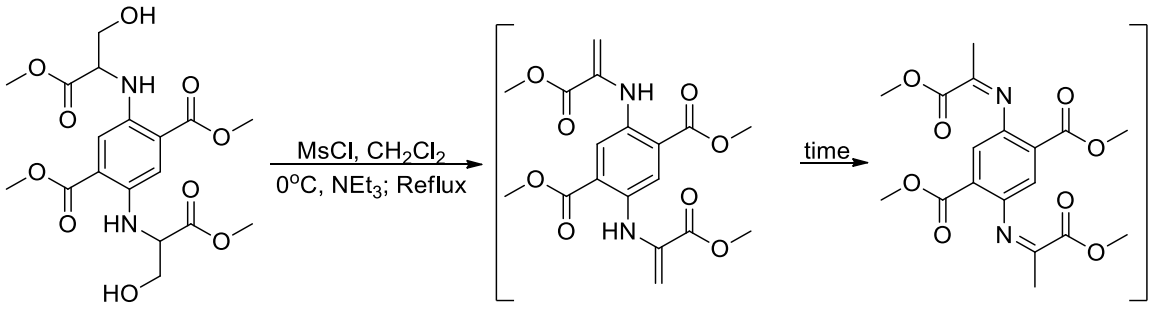

4.2863g (10.0 mmol) of **40** was dissolved into 75 ml of CH_2Cl_2 and chilled to 0 °C. 1.70 ml (22.0 mmol) of MsCl was added and while maintaining 0 °C, 5.1031g (50.5 mmol) of NEt_3 was added dropwise and slowly. After 15 minutes TLC indicated mesylation of starting material and the reaction mixture was heated to reflux. After 2 hours the reaction mixture was chilled and diluted to 500 ml of CH_2Cl_2. This was then washed with 1 L of sat. $NaHCO_3$ then 750 ml of sat. NaCl and the organics were dried over $MgSO_4$ before concentrating. The crude residue was crystallized from 125 ml of CH_2Cl_2 and 75 ml of hexanes.

Yield: 3.0884g (79%), m.p. 172 – 173 °C

Initial NMR

1H NMR 500 MHz ($CDCl_3$): δ 3.88 (6H, s), 3.93 (6H, s), 5.28 (2H, d, J = 1.5 Hz), 5.50 (2H, t, J = 1.3 Hz), 8.09 (2H, s), 9.33 (2H, s)

13C-NMR 500 MHz ($CDCl_3$): δ 167.1, 165.4, 136.3, 135.0, 120.4, 120.1, 95.9, 52.8, 52.5

Synthesis of QMA **46**
dimethyl 6-amino-4-oxo-1,4-dihydroquinoline-2,7-dicarboxylate

From BAME:

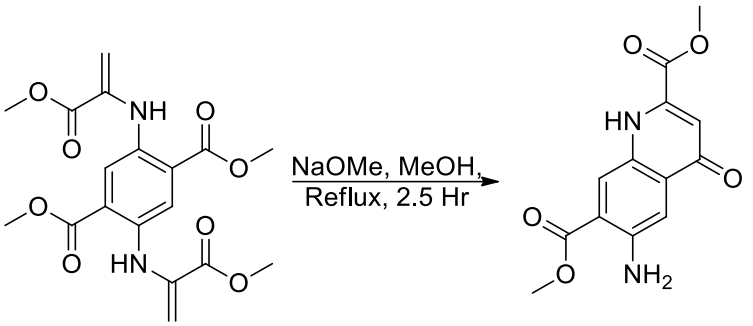

1.395g (60.7 mmol) of Na^{o} was dissolved into 40 ml of anhydrous methanol, then 2.457g (6.26 mmol) of **44** was added with rapid stirring. The solution was then brought to reflux for 2.5 hours after which 4.658g (77.6 mmol) of acetic acid in 20 ml of H_2O was added to the reaction mixture and 40 ml of solution was distilled off. This solution was then filtered and washed with 50ml of H_2O before drying under reduced pressure. The filtrate was then extracted with 500 ml of EtOAc, washed with 100 ml of Sat NaCl, dried over $MgSO_4$ and concentrated under reduced pressure. The precipitate and extract was then Triturated with 20ml of anhydrous methanol, filtered and dried under reduced pressure to afford a dark red-green solid. Yield: 0.752g (44%), M.P.: 276 – 277 ^{o}C (decomposition).

1H-NMR 500 MHz (DMSO-d6 + TFA): δ 3.91 (3H, s), 4.00 (3H, s), 7.27 (1H, s), 7.47 (1H, s), 8.87 (1H, s)

13C-NMR 500 MHz (DMSO-d6 + TFA): δ 52.9, 54.2, 105.0, 105.9, 120.3, 126.2, 126.8, 131.1, 139.1, 148.3, 161.0, 166.4, 169.7

From BSME:

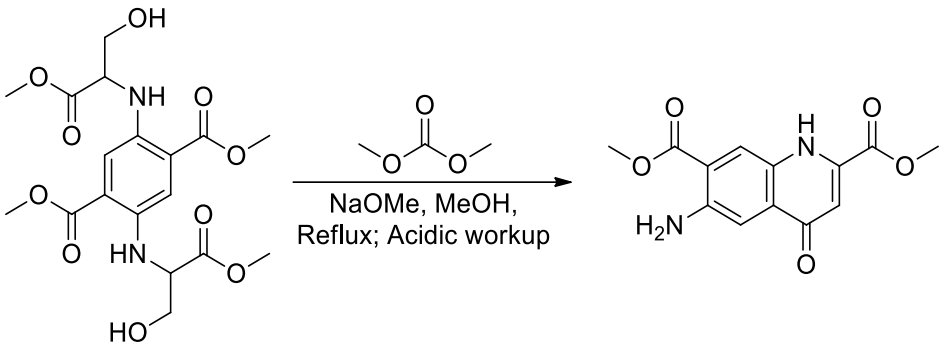

General Procedure:

1.0 mmol of **40** is suspended in DMC before addition of NaOMe in MeOH, the reaction is then heated to reflux for multiple hours. Once TLC shows no DATP upon mini workup (rxn mixture diluted into $AcOH_{aq}$ and then EtOAc floated on top to spot), the reaction is allowed to cool to room temperature. The methanol is then distilled off (rotovap) and the crude solid is treated with 50ml of a 50:50 mixture of AcOH: H_2O and stirred for 30 minutes. 50 ml of EtOAc is added to the solution, filtered and washed with 50 ml EtOAc and 50 ml H_2O. The filtrate is extracted with x2 50 ml EtOAc until no color remains in the organic layer. The organic extracts are then dried over $MgSO_4$ and concentrated, using large volumes of toluene to azeotropically dry the mixture and remove AcOH. The crude residue obtained is then triturated in 20 ml of anhydrous methanol and the precipitate/product filtered and dried under reduced pressure.

Note: The best yield and purity came from, 0.025M **40**, 0.5M NaOMe, 20 ml DMC, 20 ml MeOH at reflux for 5 hours.

1H-NMR 500 MHz (DMSO-d6): δ 3.89 (3H, s), 3.94 (3H, s), 6.44 (1H, s), 6.60 (2H, s_{broad}), 7.40 (1H, s), 8.53 (1H, s), 11.96 (1H, s)

Synthesis of ASTP-Imid **47**
dimethyl 2-((3-((1H-imidazole-1-carbonyl)oxy)-1-methoxy-1-oxopropan-2-yl)amino)-5-((tert-butoxycarbonyl)amino)terephthalate

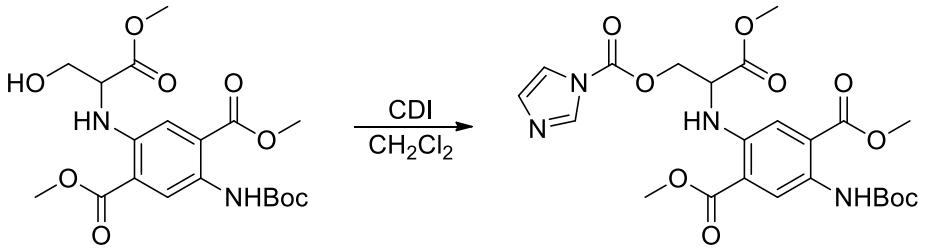

0.330g (0.774mmol) of **39** and 0.391g (2.40 mmol) of CDI was stirred in 15 ml of CH_2Cl_2 for 30 minutes. Once TLC showed consumption of the starting material the solution was diluted to 75ml of CH_2Cl_2 then washed with 100 ml of H_2O followed by 100 ml of sat. NaCl. The organic extracts were dried over $MgSO_4$ and concentrated. Yield:0.402g (100%), m.p: 91 – 92 ^oC

1H-NMR 500 MHz ($CDCl_3$): δ 1.53 (9H, s), 3.80 (3H, s), 3.91 (3H, s), 3.93 (3H, s), 4.65 (1H, dt, J = 4.5, 8.5 Hz), 4.75 (1H, dd, J = 4.5, 11 Hz), 4.86 (1H, dd, J = 4.5, 11 Hz), 7.07 (1H, m, J=1.0 Hz), 7.29 (1H, s), 7.43 (1H, t, J = 1.5 Hz), 8.16 (1H, t, J = 1.0 Hz), 8.25 (1H ,d, J = 8.5 Hz), 8.96 (1H, s), 9.61 (1H, s)

13C-NMR 500 MHz ($CDCl_3$): δ 170.1, 168.0, 167.4, 153.0, 148.2, 142.7, 137.2, 131.6, 130.9, 122.9, 120.3, 117.2, 117.0, 113.1, 80.4, 67.0, 54.9, 53.0, 52.7, 52.4, 28.3

Synthesis of AdATP **48**
dimethyl 2-((tert-butoxycarbonyl)amino)-5-((3-methoxy-3-oxoprop-1-en-2-yl)amino)terephthalate

From ASTP-Imid:

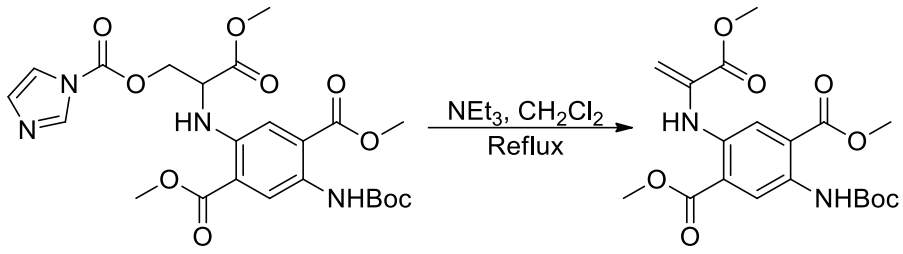

0.361g (0.696 mmol) of **47** and 0.941g (9.10 mmol) of NEt_3 was refluxed in 25ml of CH_2Cl_2 for 4 hours. Once complete the reaction mixture was diluted to 75 ml CH_2Cl_2 then washed x3 with 100 ml of H_2O then 100 ml of Sat. NaCl. The organic extracts were dried over $MgSO_4$ then concentrated. Yield: 0.283g (100%), m.p: 113 – 114 ^oC

1H-NMR 500 MHz ($CDCl_3$): δ 1.53 (9H, s), 3.88 (3H, s), 3.93 (3H, s), 3.95 (3H, s), 5.30 (1H, d, J = 1.4 Hz), 5.54 (1H, t, J = 1.2 Hz), 8.07 (1H, s), 9.00 (1H, s), 9.52 (1H, s), 9.79 (1H, s)

13C-NMR 500 MHz ($CDCl_3$): δ 167.6, 167.5, 165.3, 138.2, 134.9, 133.3, 122.2, 120.1, 119.1, 118.9, 96.8, 80.5, 52.8, 52.7, 52.6, 28.3

Synthesis of bocQMA **49**
dimethyl 6-((tert-butoxycarbonyl)amino)-4-oxo-1,4-dihydroquinoline-2,7-dicarboxylate

From ASTP:

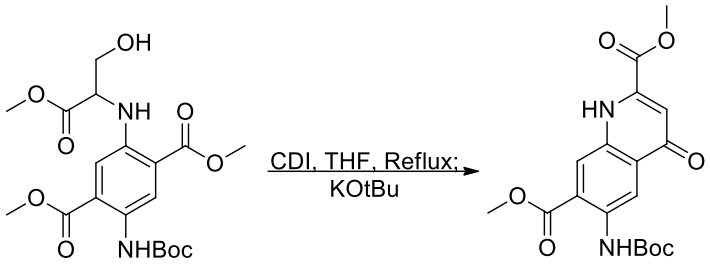

1.791g (4.20 mmol) of **39** was dissolved in 10 ml of THF with 1.091g (6.73 mmol) of CDI. Once imidazolide was formed, 16 ml of 1.0M KOtBu in THF was added to the reaction mixture dropwise and slowly. Once added reflux was continued for 1 hour after which, 2.379g (39.65 mmol) of acetic acid was added to the reaction mixture. The solution was allowed to cool to room temp before concentration under reduced pressure. The product was then obtained via multiple trituration in CH_2Cl_2. Yield: 1.271g (80%)

From AdATP:

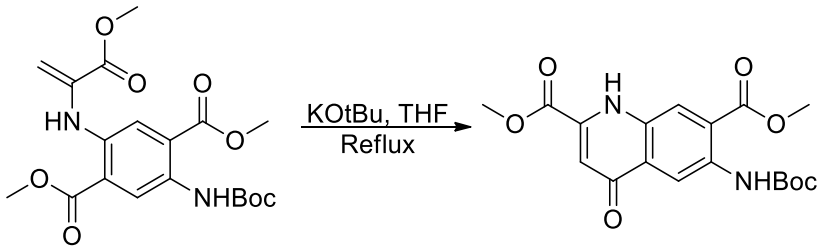

0.1783g (0.436 mmol) of **48** was heated in 25 ml of THF and with rapid stirring, 0.90 ml of 1.0 M KOtBu in THF was added dropwise and slowly. The solution was then brought to reflux for 1 hour then cooled to room temp before addition of 0.106g (1.76 mmol) of AcOH in 2 ml of H_2O. The reaction mixture was

then concentrated under reduced pressure and crystallized directly from CH_2Cl_2. Yield: 0.160g (98%), m.p: 247 ^oC turns red, 285 – 286 ^oC decomp.

1H-NMR 500 MHz (DMSO-d6): δ 1.48 (9H, s), 3.90 (3H, s), 3.95 (3H, s), 6.68 (1H, s_{broad}), 8.60 (1H, s), 8.64 (1H, s), 9.89 (1H, s), 12.22 (1H, s_{broad})

Synthesis of bocQAA **50**
6-((tert-butoxycarbonyl)amino)-4-oxo-1,4-dihydroquinoline-2,7-dicarboxylic acid

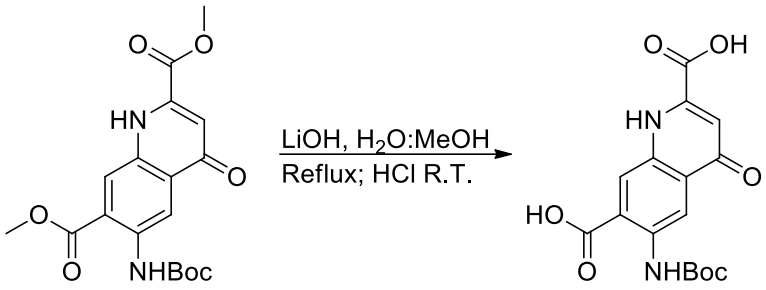

0.053g (140 µmol) of **49** was dissolved in 1ml of 1.001 M LiOH with 8 ml of 50:50 H_2O:MeOH and refluxed for 30 minutes. The reaction mixture was then cooled to room temp before addition of 1.0 ml of 1.001 M HCl. The solution was then filtered and the precipitate dried under reduced pressure. Yield: 0.0374g (78%) of a grey solid, M.P: +310^oC.

1H-NMR 500 MHz (DMSO-d6): δ 1.50 (9H, s), 6.60 (1H, s), 8.69 (1H, s), 8.84 (1H, s), 10.68 (1H, s_b), 12.00 (1H, s_b)

13C-NMR 500 MHz (DMSO-d6): δ 177.0, 169.3, 164.0, 152.5, 141.5, 136.3, 134.8, 129.0, 124.6, 122.6, 113.0, 109.1, 80.3, 28.4

Synthesis of QAA **51**
6-amino-4-oxo-1,4-dihydroquinoline-2,7-dicarboxylic acid

From QMA:

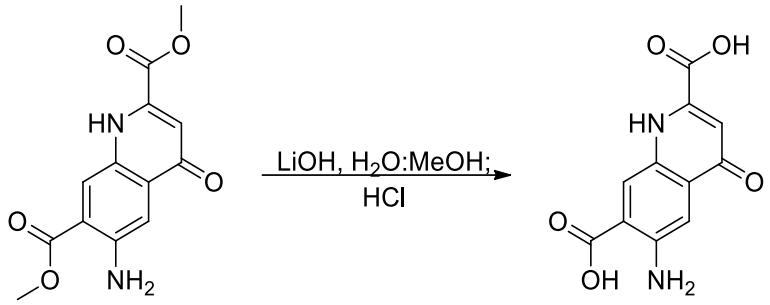

23mg (83.3µmol) of **46** was dissolved in 1.0ml of 1.001M LiOH and 8 ml 50:50 MeOH:H_2O and refluxed for 30 minutes to remove the methanol. Then 1.0 ml of 1.001M HCl was added to the still hot solution prior to cooling and filtering the bright red precipitate. Yield: 18mg M.P: +300^oC

1H-NMR 500 MHz (DMSO-d6): δ 6.46 (1H, s), 7.36 (1H, s), 8.51 (1H, s)

13C-NMR 500 MHz (TFA-H): δ 173.0, 168.4, 161.5, 144.1, 138.3, 132.3, 128.3, 127.4, 124.4, 121.1, 109.0

From bocQMA:

Synthesis of QAAM **52**
6-((2-nitrovinyl)amino)-4-oxo-1,4-dihydroquinoline-2,7-dicarboxylic acid

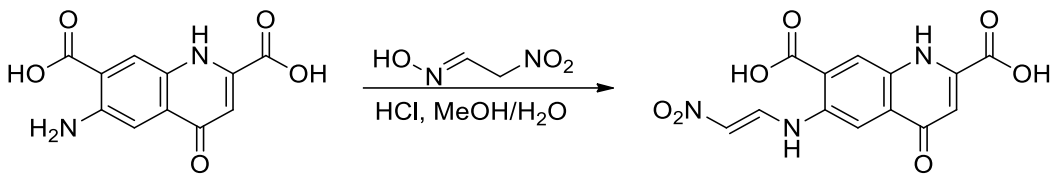

0.1853g (0.747 mmol) of **51** was dissolved in 40 ml of 50:50 MeOH:H_2O with 1 ml of 12 M HCl. This was stirred while methazoic acid was prepared.

Methazoic acid: 0.9422g (16.8 mmol) KOH was dissolved in 1.5 ml of H_2O and chilled to 30 ^oC. With rapid stirring, 0.6 ml (11.2 mmol) of nitromethane was added and the solution was warmed to 40 ^oC then chilled to 30 ^oC. Then another 0.6 ml (11.2 mmol) of nitromethane was added and the solution warmed to 55 ^oC for 5 minutes. The solution was then chilled to 30 ^oC, poured over 20g ice and acidified with 3 ml of 12 M HCl.

The methazoic acid solution was then immediately poured into the QAA solution. The mixture was allowed to stand for 24 hours before chilling and filtering. The red solid was dried under reduced pressure for multiple days. Yield: 0.1733g (73%). M.p. +320 ^oC.

1H-NMR 500 MHz (DMSO-d6): δ 6.67 (1H, s), 6.70 (1H, d, J = 6.5 Hz), 8.16 (1H, t, J = 6.5 Hz), 8.19 (1H, s), 8.76 (1H, s), 10.20 (1H, s), 12.92 (1H, d, J = 13.5 Hz), 16.2 (1H, s_{broad})

Synthesis of aJQ-NO_2 **53**
8-nitro-4,9-dioxo-1,4,6,9-tetrahydropyrido[2,3-g]quinoline-2-carboxylic acid

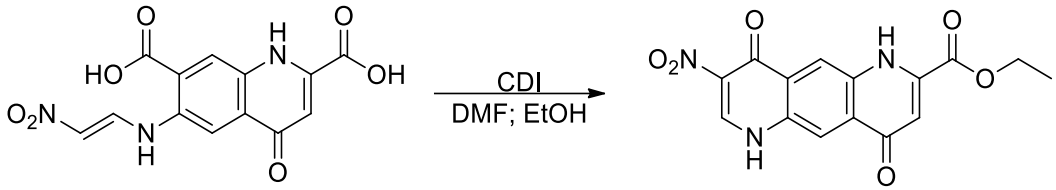

0.1365g (0.427 mmol) of **52** was dissolved in 0.5 ml of DMF and with stirring 0.2318g (1.429 mmol) of CDI was added in portions. Once added the reaction mixture was stirred for 18 hours. The solution was then diluted with 12 ml of EtOH, heated then chilled. The solid was then collected via centrifugation and dried under reduced pressure. Yield: 0.1272g (90%), m.p. +310 ^{o}C

1H-NMR 500 MHz (D_2O pH 12): δ 6.88 (1H, s), 8.48 (1H, s), 8.76 (1H, s), 9.10 (1H, s)

13C-NMR 500 MHz (D_2O pH 12): δ 175.6, 174.6, 172.2, 158.7, 150.6, 146.1, 143.7, 143.0, 130.2, 127.9, 125.3, 121.6, 106.2

Synthesis of aJQ-NH_2 **54**
8-amino-4,9-dioxo-1,4,6,9-tetrahydropyrido[2,3-g]quinoline-2-carboxylic acid

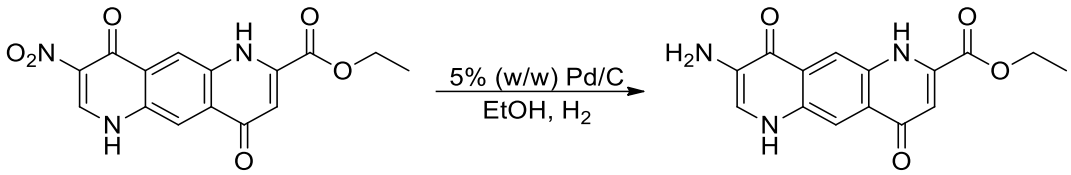

3.8 mg (11.5 µmol) **53** and 4 mg of 5% (w/w) Pd/C was stirred in 0.5 ml of EtOH while 4 L of H_2 was flushed through the system. H_2 was maintained at 1 atm throughout the reaction and after multiple days the reaction was worked up. The mixture was filtered through a plug of celite and washed with 20 ml of hot EtOH. The filtrate was then concentrated and dried under vacuum. Yield 1.9 mg (53%)

Synthesis of sJQ **55**
dimethyl 4,9-dioxo-1,4,6,9-tetrahydropyrido[2,3-g]quinoline-2,7-dicarboxylate

From BAME-Ene:

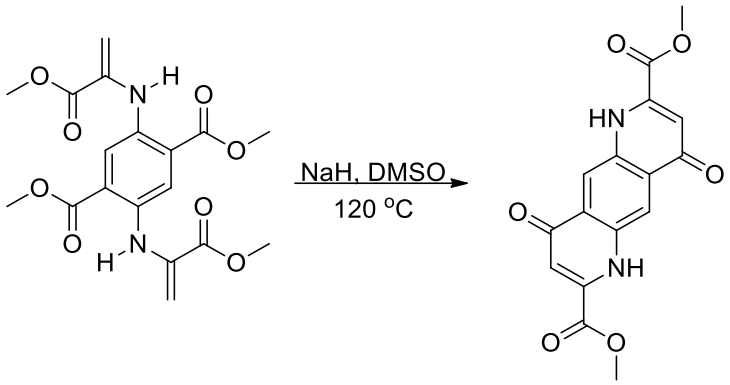

0.8346g (2.13 mmol) of **44** was suspended into 20 ml of warm DMSO (60 °C) and stirred to dissolve. To this was added 0.3573g (8.93mmol) of NaH (60% disp in oil), which was washed with 4 ml of THF to remove oil then suspended in 2 ml of THF to transfer to the warm DMSO solution. Once effervescence had stopped the reaction mixture was warmed to 120 °C for 24 hours. The reaction mixture was cooled to room temperature before dilution into 200 ml MeOH: 10 ml AcOH. This solution was then stirred for 30 minutes before filtering and drying under reduced pressure. Yield: 0.6031g (94%), m.p. 348°C

From BAME-Im:

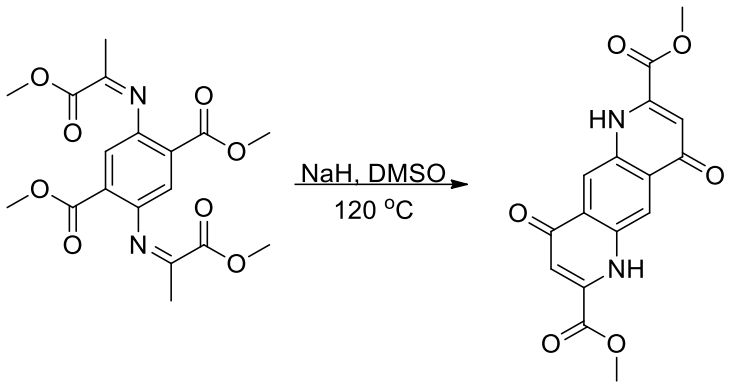

2.03g (5.17 mmol) of **45** was dissolved into 50 ml of warm DMSO (60 °C) and stirred to dissolve. To this was added 0.870g (21.7mmol) of NaH (60% disp in oil), which was washed with 8 ml of THF to remove oil then suspended in 5 ml of THF to transfer to the warm DMSO solution. Once effervescence had ceased the reaction mixture was warmed to 120 °C for 24 hours. The reaction mixture was cooled to room temperature before dilution into 400 ml MeOH: 10 ml AcOH. This solution was then stirred for 30 minutes before filtering and drying under reduced pressure. Yield: 1.645g (97%), m.p. 348°C

1H NMR 500 MHz (D_2O pH 12): δ 8.69 (s, 2H), 6.82 (s, 2H)

13C NMR 500 MHz (D_2O pH 12): δ 174.78, 174.49, 157.08, 143.59, 128.69, 120.34, 103.87

Synthesis of BE **56**
tetraethyl 2,2'-(1,4-phenylenebis(azanediyl))difumarate

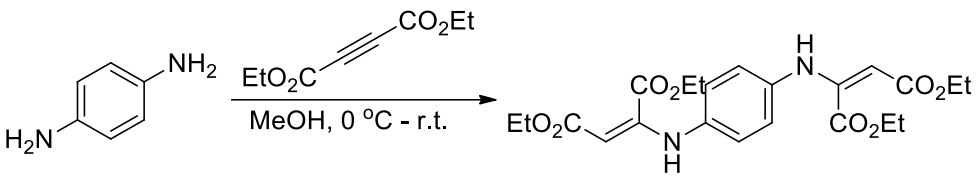

0.491g (4.54 mmol) of p-diaminobenzene was chilled to 0 °C in 4 ml of anhydrous methanol. 1.75 ml (10.4 mmol) of diethyl acethylene dicarboxylate was added slowly and with 1 ml of methanol for transfer. The solution was stirred for 2 hours before filtering the precipitate. The solid was washed with 20 ml of MTBE and 10 ml of hexanes before drying under reduced pressure overnight. Yield: 0.8503g (42%), m.p. 84 – 85 °C

1H-NMR 500 MHz ($CDCl_3$): δ 1.13 (6H, t, J = 7.2 Hz), 1.29 (6H, t, J = 7.2 Hz), 4.14 (4H, q, J = 7.2 Hz), 4.19 (4H, q, J = 7.2 Hz), 5.36 (2H, s), 6.83 (4H, s), 9.62 (2H, s)

13C-NMR 500 MHz ($CDCl_3$): δ 169.6, 164.2, 148.3, 136.9, 121.8, 121.6, 93.6, 93.3, 62.0, 59.9, 14.3, 13.7

Synthesis of sJQ-K **57**
diethyl 1,10-dioxo-1,4,7,10-tetrahydro-4,7-phenanthroline-3,8-dicarboxylate

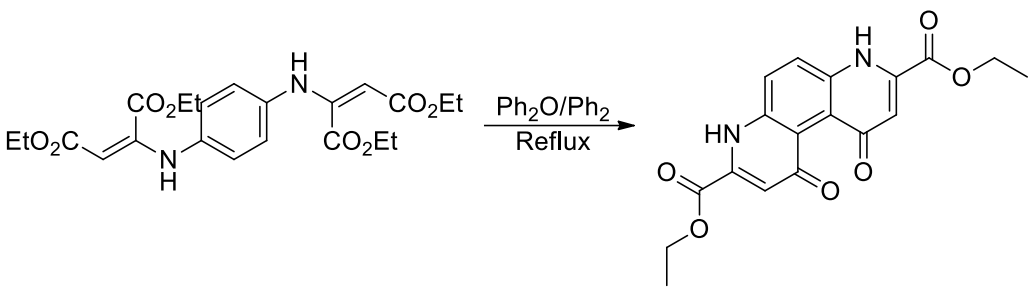

0.1956g (0.436 mmol) of **56** was suspended in 10 ml of dowtherm and heated to reflux for 30 minutes. The solution was then brought back to room temperature and diluted into 100 ml of hexanes, chilled and filtered. The solid was dried under reduced pressure. Yield: 0.0896g (58%), m.p. +300 ^{o}C.

1H NMR 500 MHz (D_2O pH 12): δ 7.22 (2H, s), 7.94 (2H, s)

13C NMR 500 MHz (D_2O pH 12): δ 173.6, 168.3, 154.2, 149.3, 131.9, 119.0, 110.4

Synthesis of (E)-2-((2-nitrovinyl)amino)benzoic acid **58a**

Aqueous method:

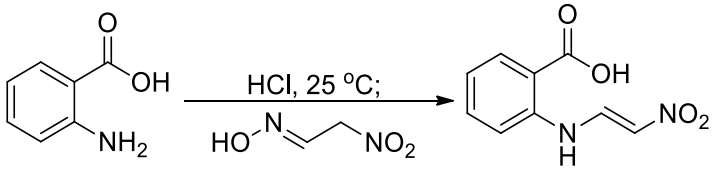

6.999g (0.051 mol) of anthranilic acid was dissolved into 100 ml of H_2O with 4.6 ml of 12M HCl with stirring. Once homogenous, the methazoic acid solution (described above) was added to the anthranilic acid solution and allowed to stand at room temperature for 3 hours. The product was collected via filtration

and the solid washed with cold H_2O before drhying under reduced pressure. Yield: 8.988g (85%), M.p. 193 – 194 °C

1H-NMR 500 MHz (DMSO): δ 6.75 (1H, d, J = 6 Hz), 7.22 (1H, t, J = 8, 14 Hz), 7.67 (1H, td, J = 1.5, 7 Hz), 7.73 (1H, d, J = 8.5 Hz), 8.03 (2H, m, J = 6.3 Hz), 13.05 (1H, d, J = 13.5 Hz).

13C- NMR 500 MHz (DMSO): δ 173.7, 146.1, 142.9, 139.8, 136.9, 128.7, 121.8, 120.6, 118.8

Non Aqueous Method:

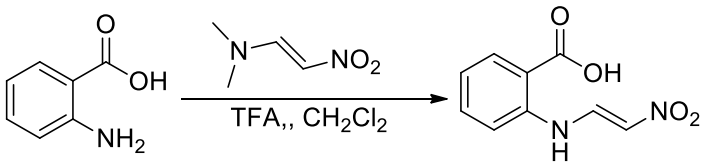

58a

0.1888g (1.38 mmol) of anthranilic acid and 0.1714g (1.48 mmol) of dimethylamino nitroethylene was stirred with 0.251g (2.20 mmol) of TFA at room temperature in 10 ml of CH_2Cl_2. After two days the reaction mixture was filtered and dried under vacuum. Yield: 0.2509g (88%), M.p. 193 – 194 °C.

1H-NMR 500 MHz (DMSO): δ 6.75 (1H, d, J = 6 Hz), 7.22 (1H, t, J = 8, 14 Hz), 7.67 (1H, td, J = 1.5, 7 Hz), 7.73 (1H, d, J = 8.5 Hz), 8.03 (2H, m, J = 6.3 Hz), 13.05 (1H, d, J = 13.5 Hz).

13C- NMR 500 MHz (DMSO): δ 173.7, 146.1, 142.9, 139.8, 136.9, 128.7, 121.8, 120.6, 118.8

Synthesis of methyl 2-((2-nitrovinyl)amino)benzoate **58b**

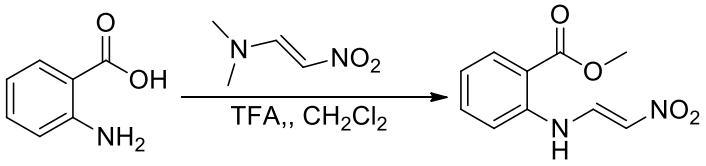

58b

0.1562g (1.03 mmol) of methyl anthranilate and 0.1253g (1.08 mmol) of dimethylamino nitroethylene was stirred with 0.1411g (1.24 mmol) of TFA in 10 ml of CH_2Cl_2. After two days the reaction was complete by TLC and 2 ml of hexanes was added to the reaction mixture to crystallize the product. The

crystals are collected via vacuum filtration and dried under vacuum. Yield: 0.133g (58%), m.p. 130 – 131°C

1H-NMR 500 MHz (DMSO): δ 3.92 (3H, s), 6.80 (1H, d, J = 6.2 Hz), 7.26 (1H, t, J = 7.1 Hz), 7.71 (1H, t, J = 8.5 Hz), 7.79 (1H, d, J = 8.5 Hz), 8.05 (1H, dd, J = 1.6, 8.0 Hz), 8.10 (1H, dd, J = 6.3, 13.5 Hz), 12.83 (1H, d, J = 12.4 Hz).

13C- NMR 500 MHz (DMSO): δ 167.2, 142.8, 141.1, 138.3, 135.4, 131.9, 124.2, 116.2, 114.3, 53.1

Synthesis of 3-nitro-4-quinolone **59**

With acetic anhydride:

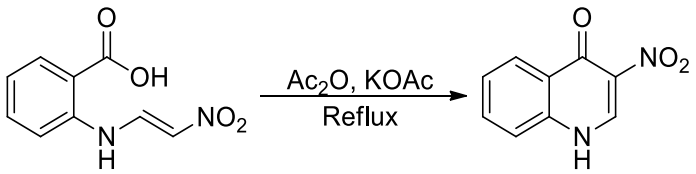

1.000g (4.8 mmol) of 2-(2-nitrovinylamino)benzoic acid was refluxed in 15ml of Ac_2O until the solution became clear and homogenous, about 15 minutes. Then 0.8970g (10.9 mmol) of sodium acetate was added and the reaction mixture brought back to reflux for 30 minutes. The solution was then allowed to cool to room temperature slowly and the precipitate collected via vacuum filtration. The solid was washed with glacial acetic acid until the filtrate ran clear then washed with 80 ml of H_2O. The precipitate was dried under reduced pressure to afford a beige solid. Yield: 0.3387g (37%), M.p. + 310 °C.

With CDI in DMF:

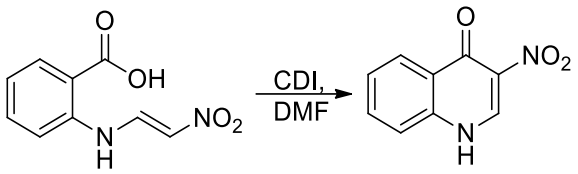

0.1378g (0.66 mmol) of 2-((2-nitrovinyl)amino)benzoic acid was stirred in 1.0 ml of DMF to dissolve before addition of 0.1544g (0.95 mmol) of carbonyl diimidazole. The reaction was then stirred at room temperature overnight. Once complete the reaction mixture was diluted into 5 ml of acetonitrile and chilled. The precipitate was collected via vacuum filtration and washed with ether. Yield 0.106g (85%) of 3-nitro-4-quinolone as a pale yellow solid.

1H-NMR 500 MHz (DMSO): δ 7.52 (1H, td, J = 7.0, 16.1 Hz), 7.72 (1H, d, J = 8.0 Hz), 7.81 (1H, td, J = 1.5, 7 Hz), 8.26 (1H, dd, J = 1.4, 8.1 Hz), 9.18 (1H, s)

13C- NMR 500 MHz (DMSO): δ 168.1, 142.8, 138.7, 133.6, 131.4, 128.5, 126.4, 126.2, 120.0

Synthesis of N,N'-dimethylaminonitroethylene **60**

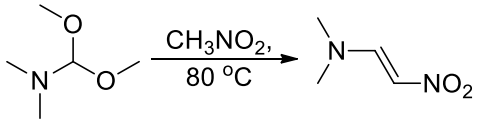

31%

1H-NMR 500 MHz ($CDCl_3$): δ 2.86 (3H, s), 3.19 (3H, s), 6.61 (1H, d, J = 10.7 Hz), 8.11 (1H, d, J = 10.7 Hz).

13C- NMR 500 MHz ($CDCl_3$): δ 151.2, 112.3, 45.6, 38.1

References

(1) Kyba, E. P.; Helgeson, R. C.; Madan, K.; Gokel, G. W.; Tarnowski, T. L.; Stephen Moore, lb S.; Cram, D. J. *Host-Guest Complexation. 1. Concept and Illustration13*; UTC, 2021; Vol. 20.

(2) Zhang, X.; Whitten, D. G. Preface to the Supramolecular Chemistry at Interfaces Special Issue. *Langmuir*. February 15, 2011, p 1245. https://doi.org/10.1021/la104879j.

(3) Pedersen, C. J. Cyclic Polyethers and Their Complexes with Metal Salts. *Journal of the American Chemical Society* **1967**, *89* (10). https://doi.org/10.1021/ja00986a052.

(4) Izatt, R. M. Charles J. Pedersen's Legacy to Chemistry. *Chemical Society Reviews* **2017**, *46* (9). https://doi.org/10.1039/C7CS00128B.

(5) Smulders, M. M. J.; Zarra, S.; Nitschke, J. R. Quantitative Understanding of Guest Binding Enables the Design of Complex Host-Guest Behavior. *Journal of the American Chemical Society* **2013**, *135* (18), 7039–7046. https://doi.org/10.1021/ja402084x.

(6) Sears, M. E. Chelation: Harnessing and Enhancing Heavy Metal Detoxification—A Review. *The Scientific World Journal* **2013**, *2013*. https://doi.org/10.1155/2013/219840.

(7) Lilis, R. Chelation Therapy in Workers Exposed to Lead. *JAMA* **1976**, *235* (26). https://doi.org/10.1001/jama.1976.03260520017014.

(8) Hart, J. R.; Xhscoo-^nchjchin^ -Oocch, -Oocch. *Household and Personal Products Industry*; American Chemical Society, 1982; Vol. 6.

(9) Zaitoun, M. A.; Lin, C. T. *Chelating Behavior between Metal Ions and EDTA in Sol-Gel Matrix*; 1997.

(10) Spedding, F. H.; Porter, P. E.; Wright, J. M. *The Acid Dissociation Constants of Diethylenetriaminepentaacetic Acid and the Stability Constants of Some of Its Metal Chelates1*; 1952; Vol. 74.

(11) Olson, D. C.; Margerum Vol, D. W.; C Olson, B. D.; Margerum, D. W.; Theor, E.; HeYClg Exptl, assuming. *Downloaded via UNIV OF WISCONSIN-MILWAUKEE On*; UTC, 1952; Vol. 74.

(12) Rodell, C. B.; Mealy, J. E.; Burdick, J. A. Supramolecular Guest-Host Interactions for the Preparation of Biomedical Materials. *Bioconjugate Chemistry*. American Chemical Society December 16, 2015, pp 2279–2289. https://doi.org/10.1021/acs.bioconjchem.5b00483.

(13) Radford, R. J.; Lippard, S. J. Chelators for Investigating Zinc Metalloneurochemistry. *Current Opinion in Chemical Biology* **2013**, *17* (2), 129–136. https://doi.org/10.1016/j.cbpa.2013.01.009.

(14) Zhang, D. Y.; Azrad, M.; Demark-Wahnefried, W.; Frederickson, C. J.; Lippard, S. J.; Radford, R. J. Peptide-Based, Two-Fluorophore, Ratiometric Probe for Quantifying Mobile Zinc in Biological Solutions. *ACS Chemical Biology* **2015**, *10* (2), 385–389. https://doi.org/10.1021/cb500617c.

(15) Nolan, E. M.; Lippard, S. J. Small-Molecule Fluorescent Sensors for Investigating Zinc Metalloneurochemistry. *Accounts of Chemical Research* **2009**, *42* (1), 193–203. https://doi.org/10.1021/ar8001409.

(16) Jaishankar, M.; Tseten, T.; Anbalagan, N.; Mathew, B. B.; Beeregowda, K. N. Toxicity, Mechanism and Health Effects of Some Heavy Metals. *Interdisciplinary Toxicology* **2014**, *7* (2). https://doi.org/10.2478/intox-2014-0009.

(17) Rabin, R. The Lead Industry and Lead Water Pipes "A MODEST CAMPAIGN." *American Journal of Public Health* **2008**, *98* (9). https://doi.org/10.2105/AJPH.2007.113555.

(18) Reddy, A.; Braun, C. L. Lead and the Romans. *Journal of Chemical Education* **2010**, *87* (10). https://doi.org/10.1021/ed100631y.

(19) Payne, M. Lead in Drinking Water. *Canadian Medical Association Journal* **2008**, *179* (3). https://doi.org/10.1503/cmaj.071483.

(20) Wani, A. L.; Ara, A.; Usmani, J. A. Lead Toxicity: A Review. *Interdisciplinary Toxicology* **2015**, *8* (2). https://doi.org/10.1515/intox-2015-0009.

(21) Azeh Engwa, G.; Udoka Ferdinand, P.; Nweke Nwalo, F.; N. Unachukwu, M. Mechanism and Health Effects of Heavy Metal Toxicity in Humans. In *Poisoning in the Modern World - New Tricks for an Old Dog?*; IntechOpen, 2019. https://doi.org/10.5772/intechopen.82511.

(22) Hauptman, M.; Bruccoleri, R.; Woolf, A. D. An Update on Childhood Lead Poisoning. *Clinical Pediatric Emergency Medicine* **2017**, *18* (3). https://doi.org/10.1016/j.cpem.2017.07.010.

(23) Renner, R. Exposure on Tap: Drinking Water as an Overlooked Source of Lead. *Environmental Health Perspectives* **2010**, *118* (2). https://doi.org/10.1289/ehp.118-a68.

(24) Tchounwou, P. B.; Yedjou, C. G.; Patlolla, A. K.; Sutton, D. J. Heavy Metal Toxicity and the Environment; 2012. https://doi.org/10.1007/978-3-7643-8340-4_6.

(25) Renu; Agarwal, M.; Singh, K. Heavy Metal Removal from Wastewater Using Various Adsorbents: A Review. *Journal of Water Reuse and Desalination* **2017**, *7* (4). https://doi.org/10.2166/wrd.2016.104.

(26) Fu, F.; Wang, Q. Removal of Heavy Metal Ions from Wastewaters: A Review. *Journal of Environmental Management* **2011**, *92* (3). https://doi.org/10.1016/j.jenvman.2010.11.011.

(27) Baysal, A.; Ozbek, N.; Akm, S. Determination of Trace Metals in Waste Water and Their Removal Processes. In *Waste Water - Treatment Technologies and Recent Analytical Developments*; InTech, 2013. https://doi.org/10.5772/52025.

(28) BEEK, H. C. A. van; HEERTJES, P. M. Fading by Light of Organic Dyes on Textiles and Other Materials. *Studies in Conservation* **1966**, *11* (3). https://doi.org/10.1179/sic.1966.016.

(29) The Staffs of the Textile Research Institute and The Textile. Review of Research and Development in the Field of Textiles During 1949. *Textile Research Journal* **1950**, *20* (5). https://doi.org/10.1177/004051755002000507.

(30) Liss, T. A.; Baer, D. R. Metal Complexes of Azo Dyes. I. Quadridentate Complexes from Bidentate Azo Compounds and Alkanediamines or Ethanolamine. *Inorganic Chemistry* **1969**, *8* (6). https://doi.org/10.1021/ic50076a026.

(31) Jezorek, J. R.; Freiser, Henry. 4-(Pyridylazo)Resorcinol-Based Continuous Detection System for Trace Levels of Metal Ions. *Analytical Chemistry* **1979**, *51* (3). https://doi.org/10.1021/ac50039a012.

(32) Sharma, V.; McKone, H. T.; Markow, P. G. A Global Perspective on the History, Use, and Identification of Synthetic Food Dyes. *Journal of Chemical Education* **2011**, *88* (1). https://doi.org/10.1021/ed100545v.

(33) Potera, C. DIET AND NUTRITION: The Artificial Food Dye Blues. *Environmental Health Perspectives* **2010**, *118* (10). https://doi.org/10.1289/ehp.118-a428.

(34) Reconsideration of the Temporary ADI and Refined Exposure Assessment for Sunset Yellow FCF (E 110). *EFSA Journal* **2014**, *12* (7). https://doi.org/10.2903/j.efsa.2014.3765.

(35) Grudpan, K.; Taylor, C. G. Some Azo-Dye Reagents for the Spectrophotometric Determination of Cadmium. *Talanta* **1989**, *36* (10). https://doi.org/10.1016/0039-9140(89)80183-3.

(36) Wang, M.; Funabiki, K.; Matsui, M. Synthesis and Properties of Bis(Hetaryl)Azo Dyes. *Dyes and Pigments* **2003**, *57* (1). https://doi.org/10.1016/S0143-7208(03)00011-1.

(37) Benkhaya, S.; M'rabet, S.; el Harfi, A. Classifications, Properties, Recent Synthesis and Applications of Azo Dyes. *Heliyon* **2020**, *6* (1). https://doi.org/10.1016/j.heliyon.2020.e03271.

(38) Hubbard, A.; Okazaki, T.; Laali, K. K. Halo- and Azidodediazoniation of Arenediazonium Tetrafluoroborates with Trimethylsilyl Halides and Trimethylsilyl Azide and Sandmeyer-Type Bromodediazoniation with Cu(I)Br in [BMIM][PF_6] Ionic Liquid. *The Journal of Organic Chemistry* **2008**, *73* (1). https://doi.org/10.1021/jo701937e.

(39) Beletskaya, I.; Sigeev, A.; Peregudov, A.; Petrovskii, P. Catalytic Sandmeyer Bromination. *Synthesis* **2007**, *2007* (16). https://doi.org/10.1055/s-2007-983784.

(40) Bonin, H.; Fouquet, E.; Felpin, F.-X. Aryl Diazonium versus Iodonium Salts: Preparation, Applications and Mechanisms for the Suzuki-Miyaura Cross-Coupling Reaction. *Advanced Synthesis & Catalysis* **2011**, *353* (17). https://doi.org/10.1002/adsc.201100531.

(41) Filimonov, V. D.; Trusova, M.; Postnikov, P.; Krasnokutskaya, E. A.; Lee, Y. M.; Hwang, H. Y.; Kim, H.; Chi, K.-W. Unusually Stable, Versatile, and Pure Arenediazonium Tosylates: Their Preparation, Structures, and Synthetic Applicability. *Organic Letters* **2008**, *10* (18). https://doi.org/10.1021/ol8013528.

(42) Lynch, J. K. Preparation of Heterocyclic Ethers as Neuronal Nicotinic Receptor Ligands. WO 9932480, July 1, 1991.

(43) Hansen, M. J.; Lerch, M. M.; Szymanski, W.; Feringa, B. L. Direct and Versatile Synthesis of Red-Shifted Azobenzenes. *Angewandte Chemie - International Edition* **2016**, *55* (43), 13514–13518. https://doi.org/10.1002/anie.201607529.

(44) Smith, B. A.; Akers, W. J.; Leevy, W. M.; Lampkins, A. J.; Xiao, S.; Wolter, W.; Suckow, M. A.; Achilefu, S.; Smith, B. D. Optical Imaging of Mammary and Prostate Tumors in Living Animals Using a Synthetic Near Infrared Zinc(II)-Dipicolylamine Probe for Anionic Cell Surfaces. *Journal of the American Chemical Society* **2010**, *132* (1). https://doi.org/10.1021/ja908467y.

(45) Prandina, A.; Radix, S.; le Borgne, M.; Jordheim, L. P.; Bousfiha, Z.; Fröhlich, C.; Leiros, H.-K. S.; Samuelsen, Ø.; Frøvold, E.; Rongved, P.; Åstrand, O. A. H. Synthesis and Biological Evaluation of New Dipicolylamine Zinc Chelators as Metallo-β-Lactamase Inhibitors. *Tetrahedron* **2019**, *75* (11). https://doi.org/10.1016/j.tet.2019.02.004.

(46) Lee, H. G.; Lee, J. H.; Jang, S. P.; Hwang, I. H.; Kim, S.-J.; Kim, Y.; Kim, C.; Harrison, R. G. Zinc Selective Chemosensors Based on the Flexible Dipicolylamine and Quinoline. *Inorganica Chimica Acta* **2013**, *394*. https://doi.org/10.1016/j.ica.2012.09.009.

(47) Matias, C. M.; Sousa, J. M.; Quinta-Ferreira, M. E.; Arif, M.; Burrows, H. D. Validation of TPEN as a Zinc Chelator in Fluorescence Probing of Calcium in Cells with the Indicator Fura-2. *Journal of Fluorescence* **2010**, *20* (1). https://doi.org/10.1007/s10895-009-0539-y.

(48) Zhou, R.; Fang, S.; Zhang, M.; Zhang, Q.; Hu, J.; Wang, M.; Wang, C.; Zhu, J.; Shen, A.; Chen, X.; Zheng, C. Design, Synthesis, and Bioactivity Evaluation of Novel Bcl-2/HDAC Dual-Target Inhibitors for the Treatment of Multiple Myeloma. *Bioorganic & Medicinal Chemistry Letters* **2019**, *29* (3). https://doi.org/10.1016/j.bmcl.2018.12.052.

(49) Yang, H.; Chen, K. H.; Nowick, J. S. Elucidation of the Teixobactin Pharmacophore. *ACS Chemical Biology* **2016**. https://doi.org/10.1021/acschembio.6b00295.

(50) Jad, Y. E.; Acosta, G. A.; Naicker, T.; Ramtahal, M.; El-Faham, A.; Govender, T.; Kruger, H. G.; de La Torre, B. G.; Albericio, F. Synthesis and Biological Evaluation of a Teixobactin Analogue. *Organic Letters* **2015**, *17* (24), 6182–6185. https://doi.org/10.1021/acs.orglett.5b03176.

(51) von Nussbaum, F.; Süssmuth, R. D. Multiple Attack on Bacteria by the New Antibiotic Teixobactin. *Angewandte Chemie - International Edition* **2015**. https://doi.org/10.1002/anie.201501440.

(52) Tsuchiya, K.; Takeuchi, Y. Enduracidin, an Inhibitor of Cell Wall Synthesis. *Journal of Antibiotics* **1968**, *21* (6), 426–428. https://doi.org/10.7164/antibiotics.21.426.

(53) Jin, K.; Po, K. H. L.; Kong, W. Y.; Lo, C. H.; Lo, C. W.; Lam, H. Y.; Sirinimal, A.; Reuven, J. A.; Chen, S.; Li, X. Synthesis and Antibacterial Studies of Teixobactin Analogues with Non-Isostere Substitution of Enduracididine. *Bioorganic and Medicinal Chemistry* **2018**. https://doi.org/10.1016/j.bmc.2018.01.016.

(54) Burroughs, A. M.; Hoppe, R. W.; Goebel, N. C.; Sayyed, B. H.; Voegtline, T. J.; Schwabacher, A. W.; Zabriskie, T. M.; Silvaggi, N. R. Structural and Functional Characterization of MppR, an Enduracididine Biosynthetic Enzyme from Streptomyces Hygroscopicus: Functional Diversity in the Acetoacetate Decarboxylase-like Superfamily. *Biochemistry* **2013**, *52* (26), 4492–4506. https://doi.org/10.1021/bi400397k.

(55) Burroughs, A. M.; Hoppe, R. W.; Goebel, N. C.; Sayyed, B. H.; Voegtline, T. J.; Schwabacher, A. W.; Zabriskie, T. M.; Silvaggi, N. R. Structural and Functional Characterization of MppR, an Enduracididine Biosynthetic Enzyme from Streptomyces Hygroscopicus: Functional Diversity in the Acetoacetate Decarboxylase-like Superfamily. *Biochemistry* **2013**, *52* (26), 4492–4506. https://doi.org/10.1021/bi400397k.

(56) Han, L.; Schwabacher, A. W.; Moran, G. R.; Silvaggi, N. R. Streptomyces Wadayamensis MppP Is a Pyridoxal 5'-Phosphate-Dependent l -Arginine α-Deaminase, γ-Hydroxylase in the Enduracididine Biosynthetic Pathway. *Biochemistry* **2015**. https://doi.org/10.1021/acs.biochem.5b01016.

(57) Han, L.; Schwabacher, A. W.; Moran, G. R.; Silvaggi, N. R. Streptomyces Wadayamensis MppP Is a Pyridoxal 5 ' -Phosphate- Dependent. **2015**. https://doi.org/10.1021/acs.biochem.5b01016.

(58) Han, L.; Vuksanovic, N.; Oehm, S. A.; Fenske, T. G.; Schwabacher, A. W.; Silvaggi, N. R. Streptomyces Wadayamensis MppP Is a PLP-Dependent Oxidase, Not an Oxygenase. *Biochemistry* **2018**. https://doi.org/10.1021/acs.biochem.8b00130.

(59) Craig, W.; Chen, J.; Richardson, D.; Thorpe, R.; Yuan, Y. A Highly Stereoselective and Scalable Synthesis of l -Allo-Enduracididine. *Organic Letters* **2015**, *17* (18), 4620–4623. https://doi.org/10.1021/acs.orglett.5b02362.

(60) Mower, M. P.; Blackmond, D. G. Mechanistic Rationalization of Unusual Sigmoidal Kinetic Profiles in the Machetti-de Sarlo Cycloaddition Reaction. *Journal of the American Chemical Society* **2015**, *137* (6), 2386–2391. https://doi.org/10.1021/ja512753v.

(61) Mower, M. P.; Blackmond, D. G. Mechanistic Rationalization of Unusual Autoinductive Kinetics in an Aqueous 1 , 3-Dipolar Cycloaddition. No. 2, 1–43.

(62) Curran, D. P. A2-Isoxazolines. 3. * Raney-Nickel Catalyzed Formation of ,&Hydroxy Ketones. *Journal of the American Chemical Society* **1983**, *105*, 5826–5833. https://doi.org/10.1021/ja00356a021.

(63) Kozikowski, A. P. The Isoxazoline Route to the Molecules of Nature. **1984**, *2784* (1971), 410–416. https://doi.org/10.1021/ar00108a001.

(64) Boyd, E. C. Synthetic Applications of Nitrile Oxide / Isoxazoline Chemistry. **1992**.

(65) Tranmer, G. K.; Tam, W. Molybdenum-Mediated Cleavage Reactions of Isoxazoline Rings Fused in Bicyclic Frameworks. **2002**, No. 4. https://doi.org/10.1021/ol026846k.

(66) Nagireddy, J. R.; Tranmer, G. K.; Carlson, E.; Tam, W. N-o Cleavage Reactions of Heterobicycloalkene-Fused 2-Isoxazolines. *Beilstein Journal of Organic Chemistry* **2014**, *10* (Table 1), 2200–2205. https://doi.org/10.3762/bjoc.10.227.

(67) Jiang, D.; Chen, Y. Reduction of Δ 2 -Isoxazolines to -Hydroxy Ketones with Iron and Ammonium Chloride As. **2008**, No. 8, 9181–9183.

(68) Bode, J. W.; Carreira, E. M. LETTERS A Mild and Chemoselective Method for the Reduction of Conjugated Isoxazolines to -Hydroxy Ketones. **2001**, No. 6, 5704–5705. https://doi.org/10.1021/ol015885d.

(69) Yoon, G.; Zabriskie, T. M.; Seung, H. C. Synthesis of [Guanido-13C]-γ-Hydroxyarginine. *Journal of Labelled Compounds and Radiopharmaceuticals* **2009**, *52* (2), 53–55. https://doi.org/10.1002/jlcr.1570.

(70) Schaefer, F. C. Synthesis of the S-Triazine System. VI. [1] Preparation of Unsymmetrically Substituted s-Triazines by Reaction of Amidine Salts with Imidates. *The Journal of Organic Chemistry* **1962**, *27* (10). https://doi.org/10.1021/jo01057a052.

(71) Schroif-Grégoire, C.; Barale, K.; Zaparucha, A.; Al-Mourabit, A. Preparation of N-Alkyl-N'-Carboalkoxy Guanidines: Unexpected Effective Trans-Alkoxylation Transforming the 2,2,2-Trichloroethoxycarbonyl into Various Carbamates. *Tetrahedron Letters* **2007**, *48* (13). https://doi.org/10.1016/j.tetlet.2007.01.126.

(72) Dolbois, A.; Batiste, L.; Wiedmer, L.; Dong, J.; Brütsch, M.; Huang, D.; Deerain, N. M.; Spiliotopoulos, D.; Cheng-Sánchez, I.; Laul, E.; Nevado, C.; Śledź, P.; Caflisch, A. Hitting a Moving Target: Simulation and Crystallography Study of ATAD2 Bromodomain Blockers. *ACS Medicinal Chemistry Letters* **2020**, *11* (8). https://doi.org/10.1021/acsmedchemlett.0c00080.

(73) Hu, B.; Vāvere, A. L.; Neumann, K. D.; Shulkin, B. L.; DiMagno, S. G.; Snyder, S. E. A Practical, Automated Synthesis of *Meta* -[^{18} F]Fluorobenzylguanidine for Clinical Use. *ACS Chemical Neuroscience* **2015**, *6* (11). https://doi.org/10.1021/acschemneuro.5b00202.

(74) Tomasek, D.; Rawson, S.; Lee, J.; Wzorek, J. S.; Harrison, S. C.; Li, Z.; Kahne, D. Structure of a Nascent Membrane Protein as It Folds on the BAM Complex. *Nature* **2020**, *583* (7816). https://doi.org/10.1038/s41586-020-2370-1.

(75) Plummer, A. M.; Fleming, K. G. BamA Alone Accelerates Outer Membrane Protein Folding In Vitro through a Catalytic Mechanism. *Biochemistry* **2015**, *54* (39). https://doi.org/10.1021/acs.biochem.5b00950.

(76) Heuck, A.; Schleiffer, A.; Clausen, T. Augmenting β-Augmentation: Structural Basis of How BamB Binds BamA and May Support Folding of Outer Membrane Proteins. *Journal of Molecular Biology* **2011**, *406* (5). https://doi.org/10.1016/j.jmb.2011.01.002.

(77) Patel, G. J.; Kleinschmidt, J. H. The Lipid Bilayer-Inserted Membrane Protein BamA of *Escherichia Coli* Facilitates Insertion and Folding of Outer Membrane Protein A from Its Complex with Skp. *Biochemistry* **2013**, *52* (23). https://doi.org/10.1021/bi400103t.

(78) Hagan, C. L.; Westwood, D. B.; Kahne, D. Bam Lipoproteins Assemble BamA in Vitro. *Biochemistry* **2013**, *52* (35), 6108–6113. https://doi.org/10.1021/bi400865z.

(79) Freinkman, E.; Okuda, S.; Ruiz, N.; Kahne, D. Regulated Assembly of the Transenvelope Protein Complex Required for Lipopolysaccharide Export. *Biochemistry* **2012**, *51* (24), 4800–4806. https://doi.org/10.1021/bi300592.

(80) May, K. L.; Grabowicz, M. The Bacterial Outer Membrane Is an Evolving Antibiotic Barrier. *Proceedings of the National Academy of Sciences* **2018**, *115* (36). https://doi.org/10.1073/pnas.1812779115.

(81) Doerner, P. A.; Sousa, M. C. Extreme Dynamics in the BamA β-Barrel Seam. *Biochemistry* **2017**, *56* (24). https://doi.org/10.1021/acs.biochem.7b00281.

(82) McLaughlin, M. I.; van der Donk, W. A. The Fellowship of the Rings: Macrocyclic Antibiotic Peptides Reveal an Anti-Gram-Negative Target. *Biochemistry* **2020**, *59* (4). https://doi.org/10.1021/acs.biochem.9b01086.

(83) Hart, E. M.; Mitchell, A. M.; Konovalova, A.; Grabowicz, M.; Sheng, J.; Han, X.; Rodriguez-Rivera, F. P.; Schwaid, A. G.; Malinverni, J. C.; Balibar, C. J.; Bodea, S.; Si, Q.; Wang, H.; Homsher, M. F.; Painter, R. E.; Ogawa, A. K.; Sutterlin, H.; Roemer, T.; Black, T. A.; Rothman, D. M.; Walker, S. S.; Silhavy, T. J. A Small-Molecule Inhibitor of BamA Impervious to Efflux and the Outer Membrane Permeability Barrier. *Proceedings of the National Academy of Sciences* **2019**, *116* (43). https://doi.org/10.1073/pnas.1912345116.

(84) Kaur, H.; Jakob, R. P.; Marzinek, J. K.; Green, R.; Imai, Y.; Bolla, J. R.; Agustoni, E.; Robinson, C. v.; Bond, P. J.; Lewis, K.; Maier, T.; Hiller, S. The Antibiotic Darobactin Mimics a β-Strand to Inhibit Outer Membrane Insertase. *Nature* **2021**, *593* (7857), 125–129. https://doi.org/10.1038/s41586-021-03455-w.

(85) Noinaj, N.; Kuszak, A. J.; Balusek, C.; Gumbart, J. C.; Buchanan, S. K. Lateral Opening and Exit Pore Formation Are Required for BamA Function. *Structure* **2014**, *22* (7). https://doi.org/10.1016/j.str.2014.05.008.

(86) Nowick, J. S. Exploring β-Sheet Structure and Interactions with Chemical Model Systems. *Accounts of Chemical Research* **2008**, *41* (10), 1319–1330. https://doi.org/10.1021/ar800064f.

(87) Nowick, J. S.; Chung, D. M.; Maitra, K.; Maitra, S.; Stigers, K. D.; Sun, Y. An Unnatural Amino Acid That Mimics a Tripeptide ??-Strand and Forms ??-Sheetlike Hydrogen-Bonded Dimers. *Journal of the American Chemical Society* **2000**, *122* (32), 7654–7661. https://doi.org/10.1021/ja001142w.

(88) Kemp, D. S.; Bowen, B. R.; Muendel, C. C. Synthesis and Conformational Analysis of Epindolidione-Derived Peptide Models for .Beta.-Sheet Formation. *The Journal of Organic Chemistry* **1990**, *55* (15). https://doi.org/10.1021/jo00302a033.

(89) Nowick, J. S. Exploring β-Sheet Structure and Interactions with Chemical Model Systems. *Accounts of Chemical Research* **2008**, *41* (10), 1319–1330. https://doi.org/10.1021/ar800064f.

(90) Pham, J. D.; Demeler, B.; Nowick, J. S. Polymorphism of Oligomers of a Peptide from Beta-Amyloid. *J Am Chem Soc* **2014**, *136* (14), 5432–5442. https://doi.org/10.1021/ja500996d [doi].

(91) Pham, J. D.; Chim, N.; Goulding, C. W.; Nowick, J. S. Structures of Oligomers of a Peptide from β-Amyloid. *Journal of the American Chemical Society* **2013**, *135* (33), 12460–12467. https://doi.org/10.1021/ja4068854.

(92) Pham, J. D.; Spencer, R. K.; Chen, K. H.; Nowick, J. S. A Fibril-like Assembly of Oligomers of a Peptide Derived from β-Amyloid. *Journal of the American Chemical Society* **2014**, *136* (36), 12682–12690. https://doi.org/10.1021/ja505713y.

(93) Pham, J. D.; Spencer, R. K.; Chen, K. H.; Nowick, J. S. A Fibril-like Assembly of Oligomers of a Peptide Derived from β-Amyloid. *Journal of the American Chemical Society* **2014**, *136* (36), 12682–12690. https://doi.org/10.1021/ja505713y.

(94) Kumari, M.; Bera, S. K.; Blickle, S.; Kaim, W.; Lahiri, G. K. The Indigo Isomer Epindolidione as a Redox-Active Bridging Ligand for Diruthenium Complexes. *Chemistry – A European Journal* **2021**, *27* (17). https://doi.org/10.1002/chem.202004747.

(95) Labana, S. S.; Labana, L. L. Quinacridones. *Chemical Reviews* **1967**, *67* (1). https://doi.org/10.1021/cr60245a001.

(96) Lomax, S. Q. Phthalocyanine and Quinacridone Pigments: Their History, Properties and Use. *Studies in Conservation* **2005**, *50* (sup1). https://doi.org/10.1179/sic.2005.50.Supplement-1.19.

(97) Bekhli, A. F. ; M. F. S. ; K. A. I. ; R. S. A. ; G. V. F. Pyrido[2,3-g]Quinolines. IiI. Synthesis of 4,9-Diamino Derivatives of Pyrido[2,3-g]Quinoline. *Khimiko-Farmatsevticheskii Zhurnal* **1972**, *6* (3), 24–26.

(98) Liewald, C.; Strohmair, S.; Hecht, H.; Głowacki, E. D.; Nickel, B. Scanning Photocurrent Microscopy of Electrons and Holes in the Pigment Semiconductor Epindolidione. *Organic Electronics* **2018**, *60*. https://doi.org/10.1016/j.orgel.2018.05.032.

(99) Hall, C. M.; Wright, J. B.; Johnson, H. G.; Taylor, A. J. Quinoline Derivatives as Antiallergy Agents. 2. Fused-Ring Quinaldic Acids. *Journal of Medicinal Chemistry* **1977**, *20* (10). https://doi.org/10.1021/jm00220a022.

(100) Fahim, A. M.; Farag, A. M.; Nawwar, G. A. M.; Yakout, E. S. M. A.; Ragab, E. A. Chemistry of Terephthalate Derivatives: A Review. *International Journal of Environment and Waste Management* **2019**, *24* (3). https://doi.org/10.1504/IJEWM.2019.103104.

(101) Yang, Q.; Sheng, M.; Henkelis, J. J.; Tu, S.; Wiensch, E.; Zhang, H.; Zhang, Y.; Tucker, C.; Ejeh, D. E. Explosion Hazards of Sodium Hydride in Dimethyl Sulfoxide, *N* , *N* -Dimethylformamide, and *N* , *N* -Dimethylacetamide. *Organic Process Research & Development* **2019**, *23* (10). https://doi.org/10.1021/acs.oprd.9b00276.

(102) Bachman, G. B.; Welton, D. E.; Jenkins, G. L.; Christian, J. E. Quinoline Derivatives from 3-Nitro-4-Hydroxyquinoline [1]. *Journal of the American Chemical Society* **1947**, *69* (2). https://doi.org/10.1021/ja01194a060.

(103) Fuchss, T. S. K. Preparation of Imidazoquinolines and Use Thereof as ATM Kinase Inhibitors. WO 2016155884, October 6, 2016.

(104) Stauffer, F.; Maira, S.-M.; Furet, P.; García-Echeverría, C. Imidazo[4,5-c]Quinolines as Inhibitors of the PI3K/PKB-Pathway. *Bioorganic & Medicinal Chemistry Letters* **2008**, *18* (3). https://doi.org/10.1016/j.bmcl.2007.12.018.

(105) Hadida, S.; van Goor, F.; Zhou, J.; Arumugam, V.; McCartney, J.; Hazlewood, A.; Decker, C.; Negulescu, P.; Grootenhuis, P. D. J. Discovery of *N* -(2,4-Di- *Tert* -Butyl-5-Hydroxyphenyl)-4-Oxo-1,4-Dihydroquinoline-3-Carboxamide (VX-770, Ivacaftor), a Potent and Orally Bioavailable CFTR Potentiator. *Journal of Medicinal Chemistry* **2014**, *57* (23). https://doi.org/10.1021/jm5012808.

(106) Rusinov, V. L.; Petrov, A. Yu.; Chupakhin, O. N. Nitroazines. 20. Simple Syntheses of Nitropyrazolopyridines from Aliphatic Nitrosynthons and Aminopyrazoles. *Chemistry of Heterocyclic Compounds* **1992**, *28* (11). https://doi.org/10.1007/BF00532089.

(107) Son, J.-H.; Phuan, P.-W.; Zhu, J. S.; Lipman, E.; Cheung, A.; Tsui, K. Y.; Tantillo, D. J.; Verkman, A. S.; Haggie, P. M.; Kurth, M. J. 1-BENZYLSPIRO[PIPERIDINE-4,1'-PYRIDO[3,4-b]Indole] 'Co-Potentiators' for Minimal Function CFTR Mutants. *European Journal of Medicinal Chemistry* **2021**, *209*. https://doi.org/10.1016/j.ejmech.2020.112888.

Appendix: Compound Characterization Spectra

Appendix: Compound Characterization Spectra

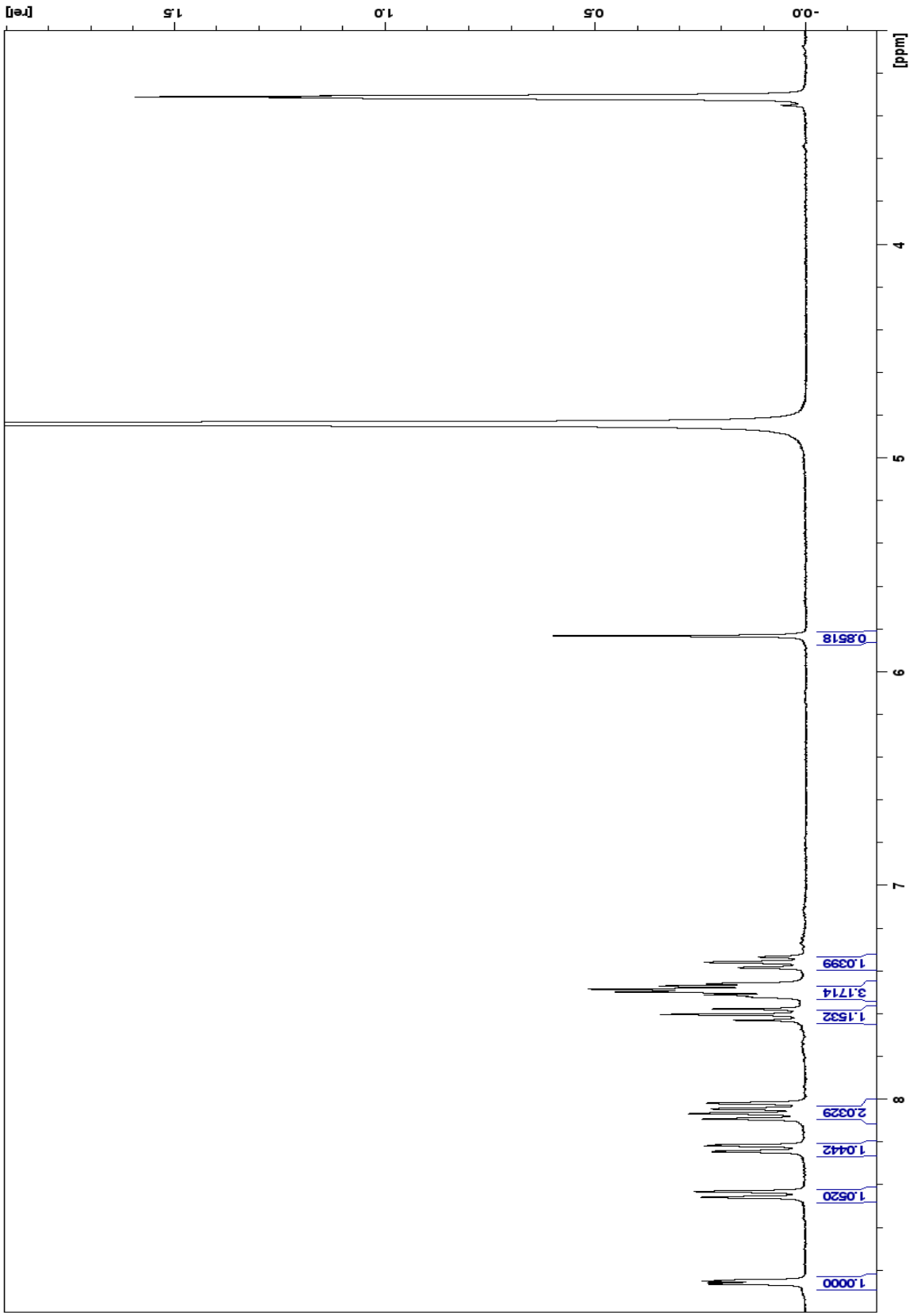

Spectrum 1*: 1b* ***¹H NMR (300 MHz, MeOD)***

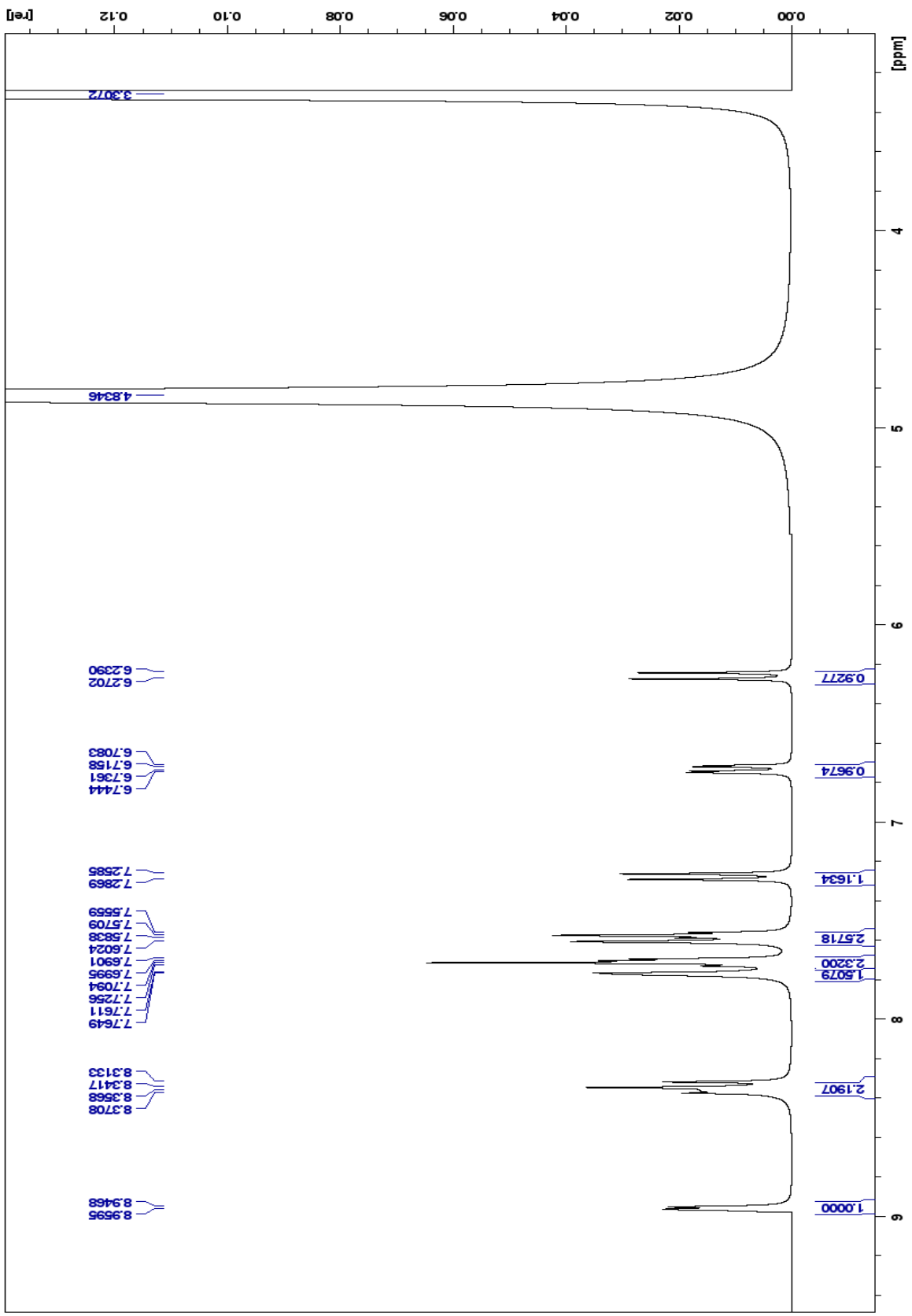

Spectrum 2: *1c* ^{1}*H NMR (300 MHz, MeOD)*

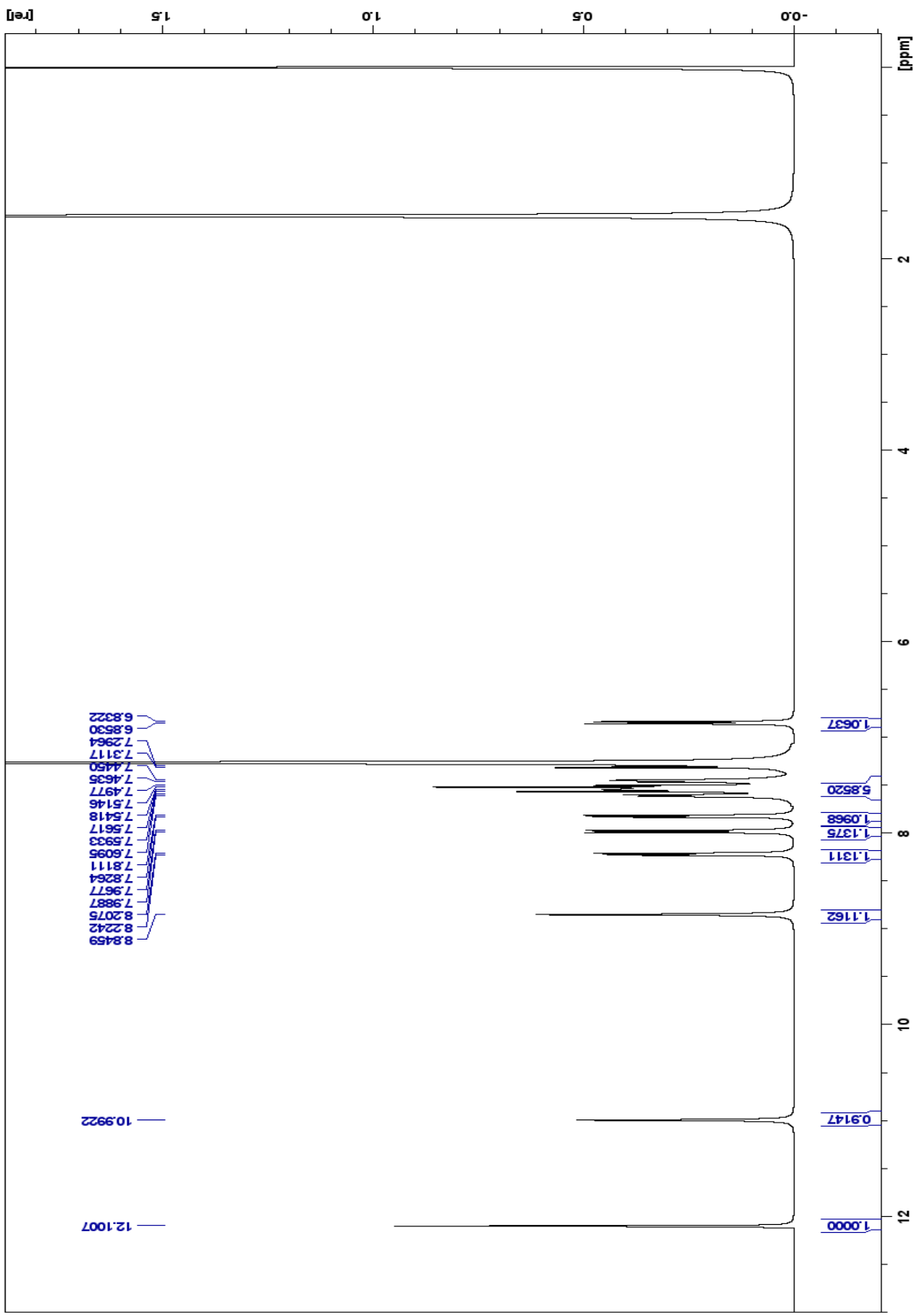

Spectrum 3*: 1d* ^{1}***H NMR (500 MHz,*** $CDCl_3$***)***

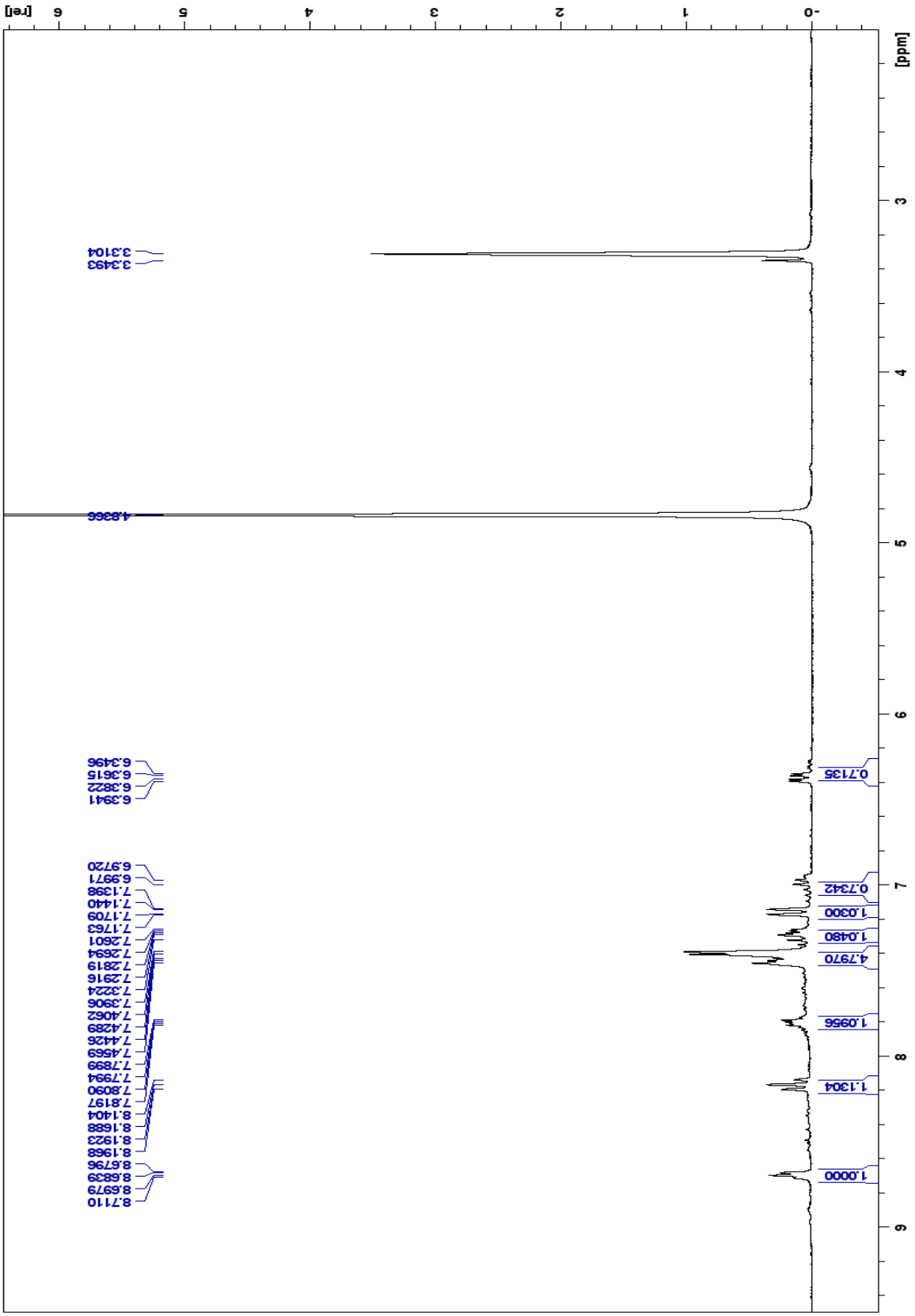

Spectrum 4*: 1e* ***^{1}H NMR (300 MHz, MeOD)***

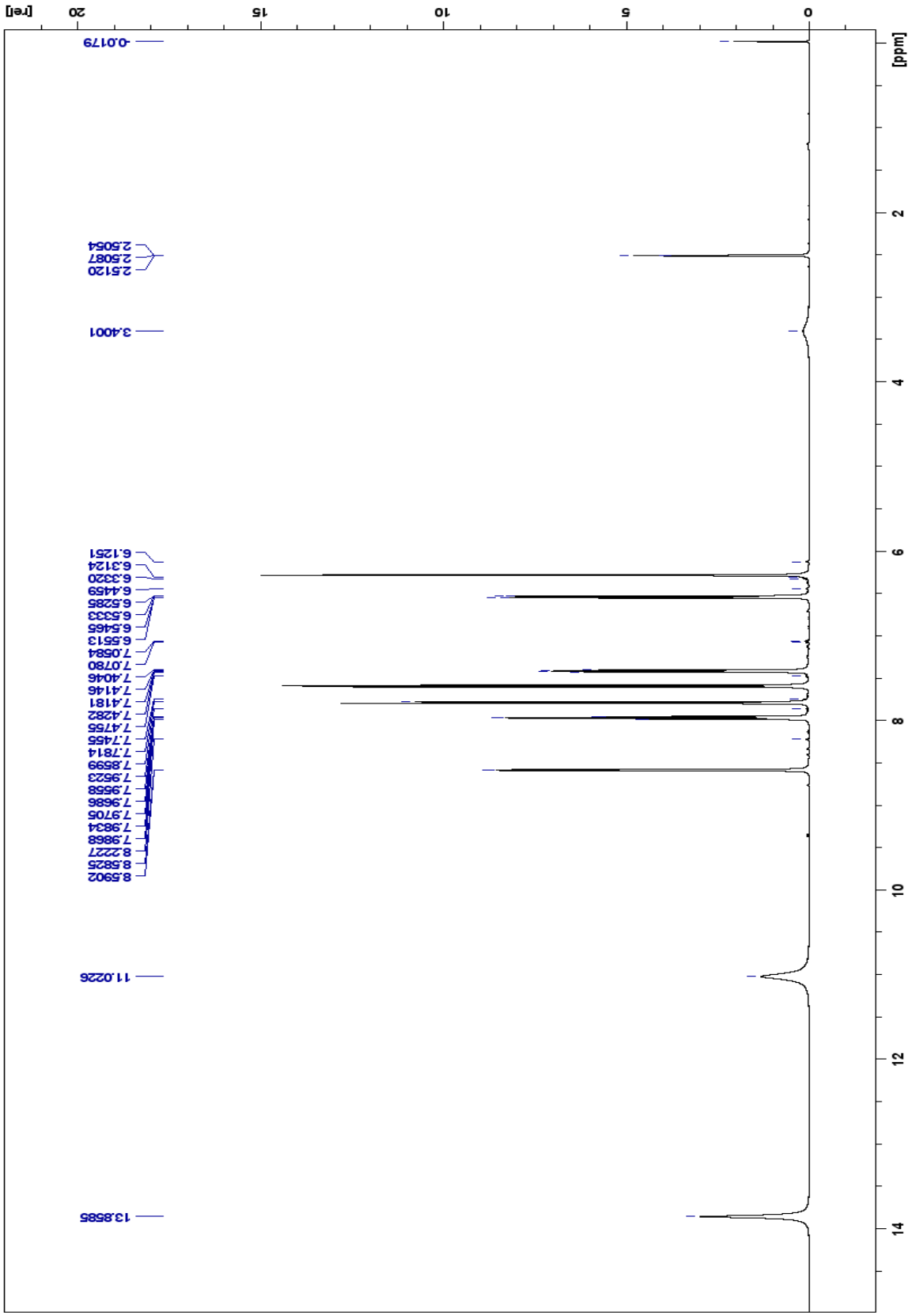

Spectrum 5*: 2a* ***^{1}H NMR (500 MHz, DMSO-d6)***

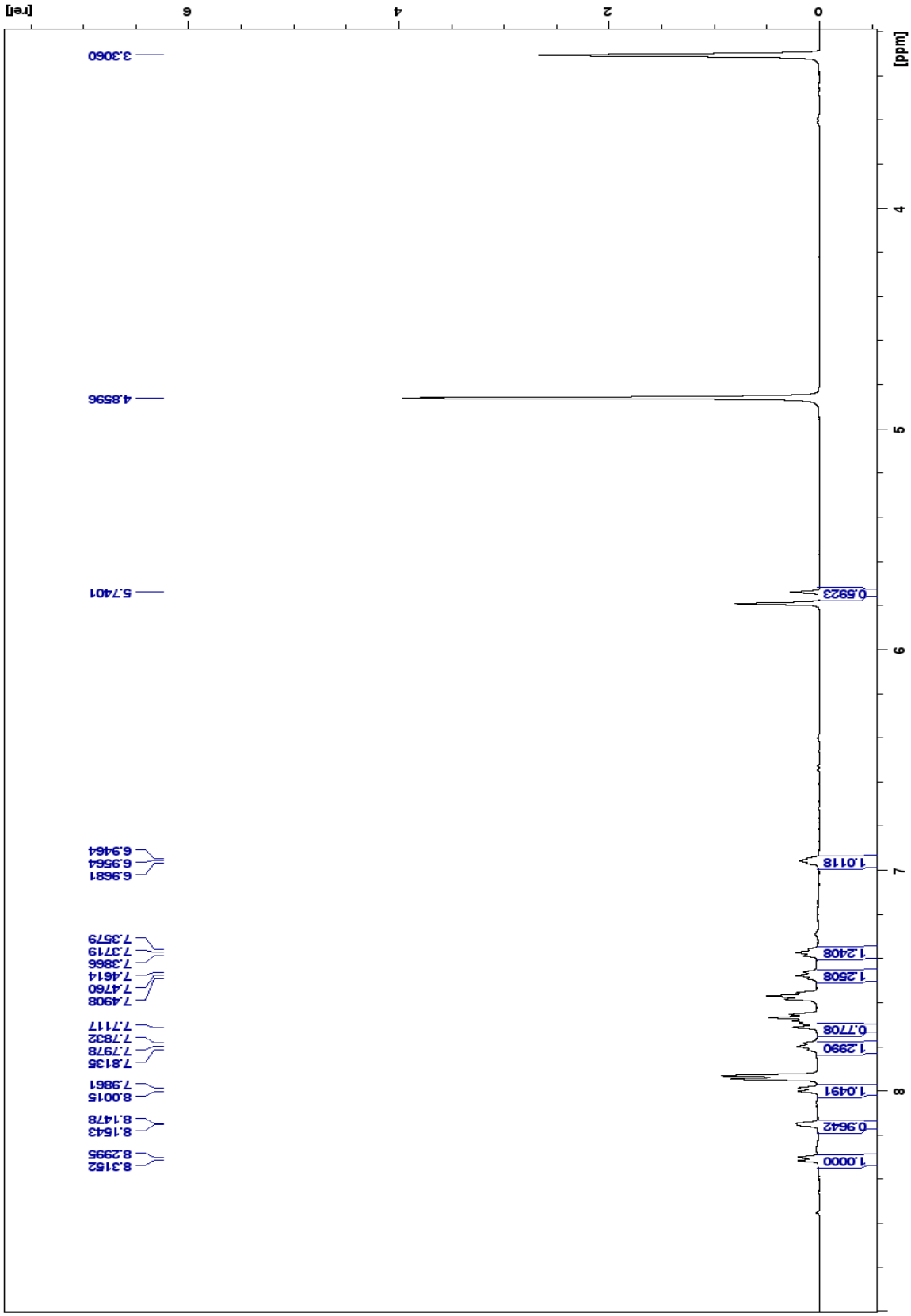

Spectrum 6*: 2b* ***^{1}H NMR (500 MHz, DMSO-d6)***

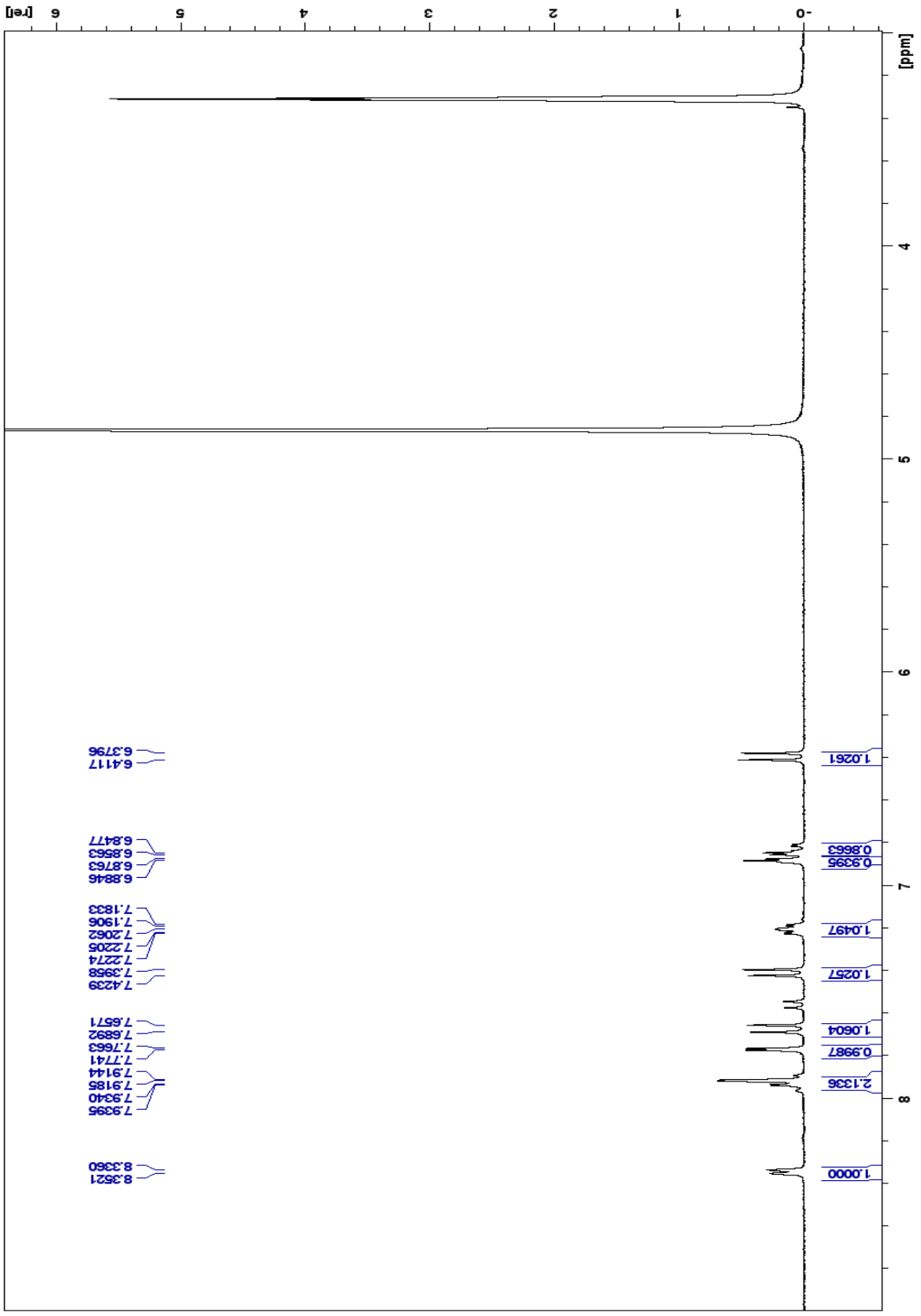

Spectrum 7*: 2c* ***¹H NMR (300 MHz, MeOD)***

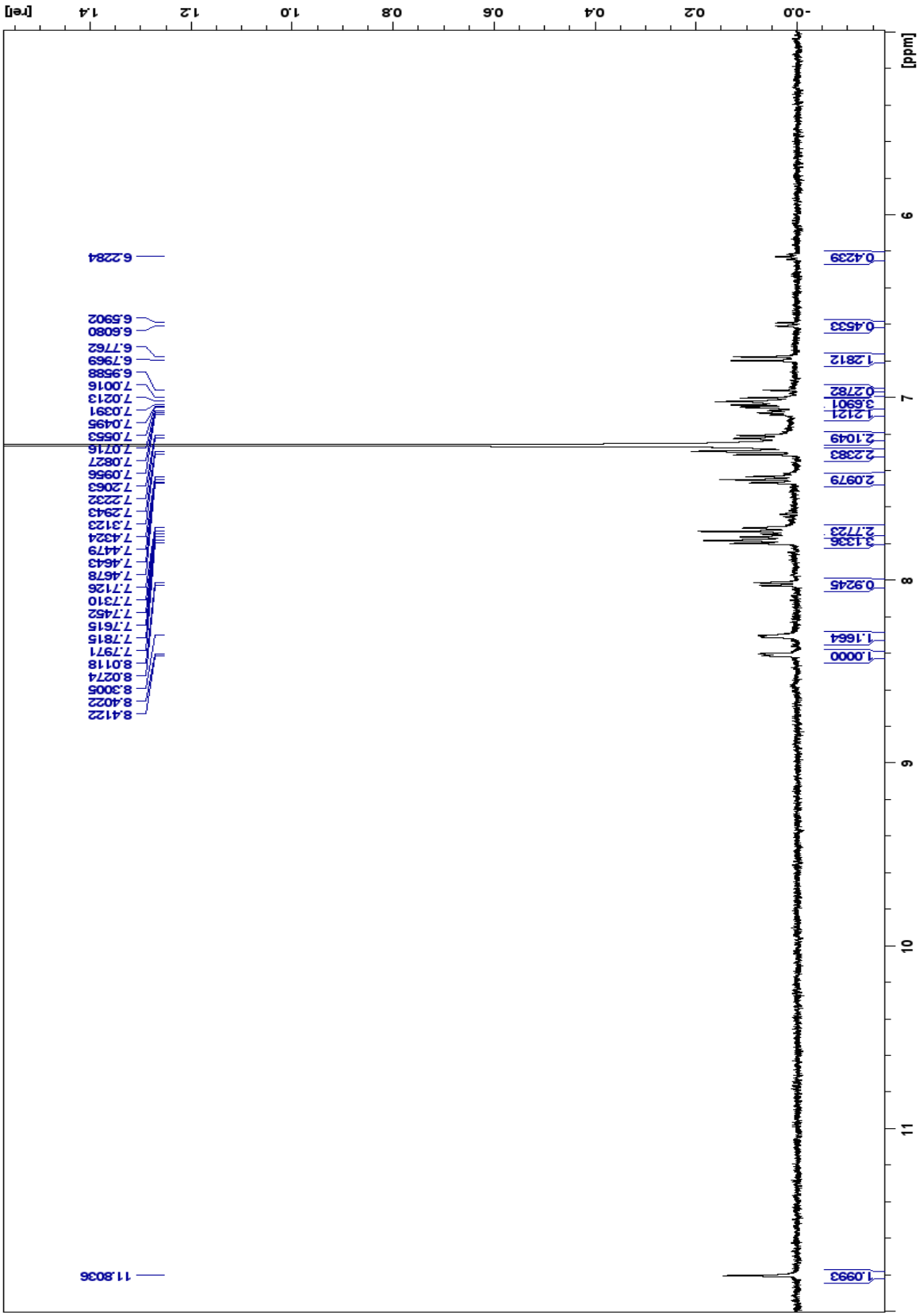

Spectrum 8*: 2d ^{1}H NMR (500 MHz, $CDCl_3$) -Mixture of tautomers*

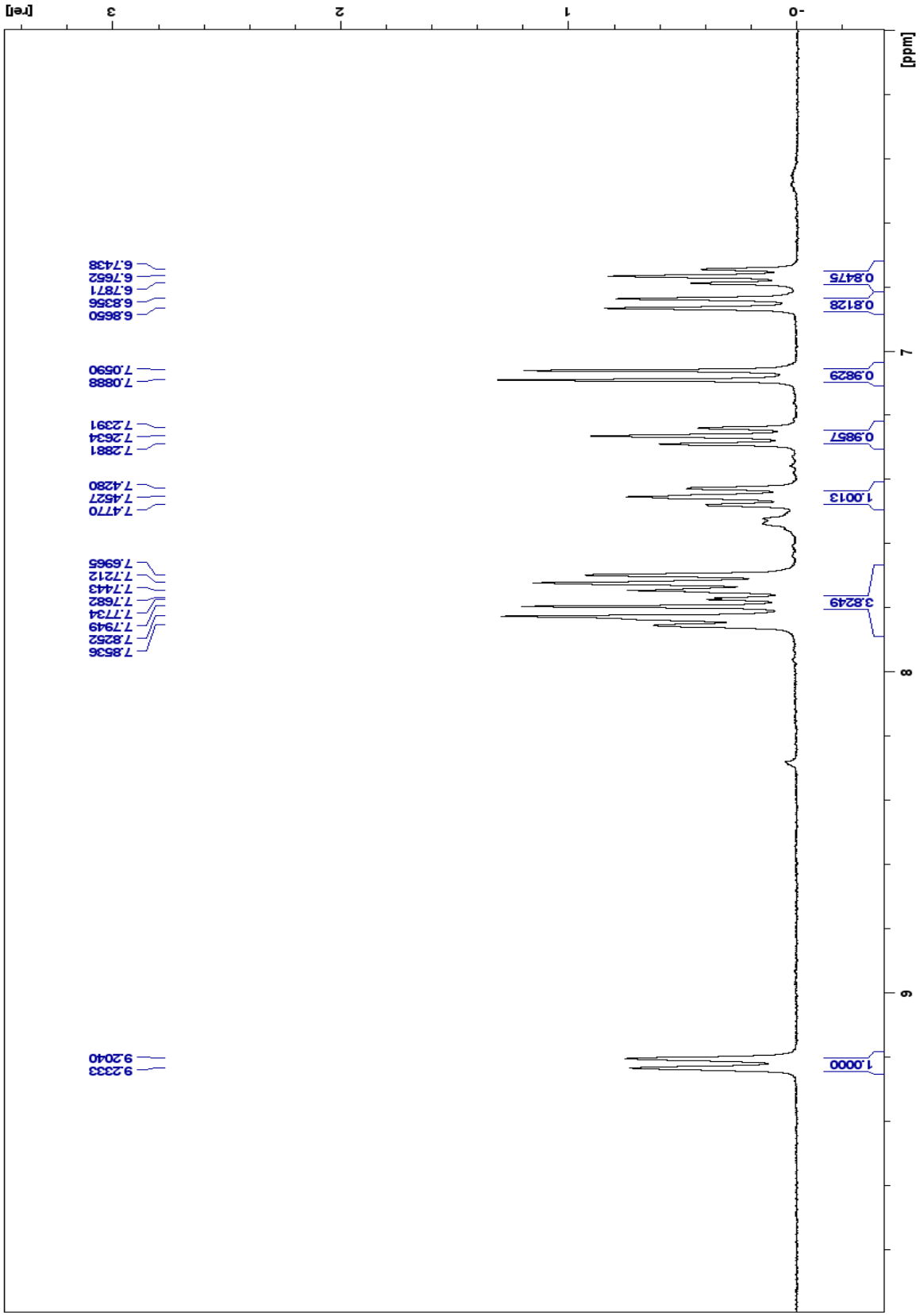

Spectrum 9*: 2e* ***^{1}H NMR (300 MHz, MeOD)***

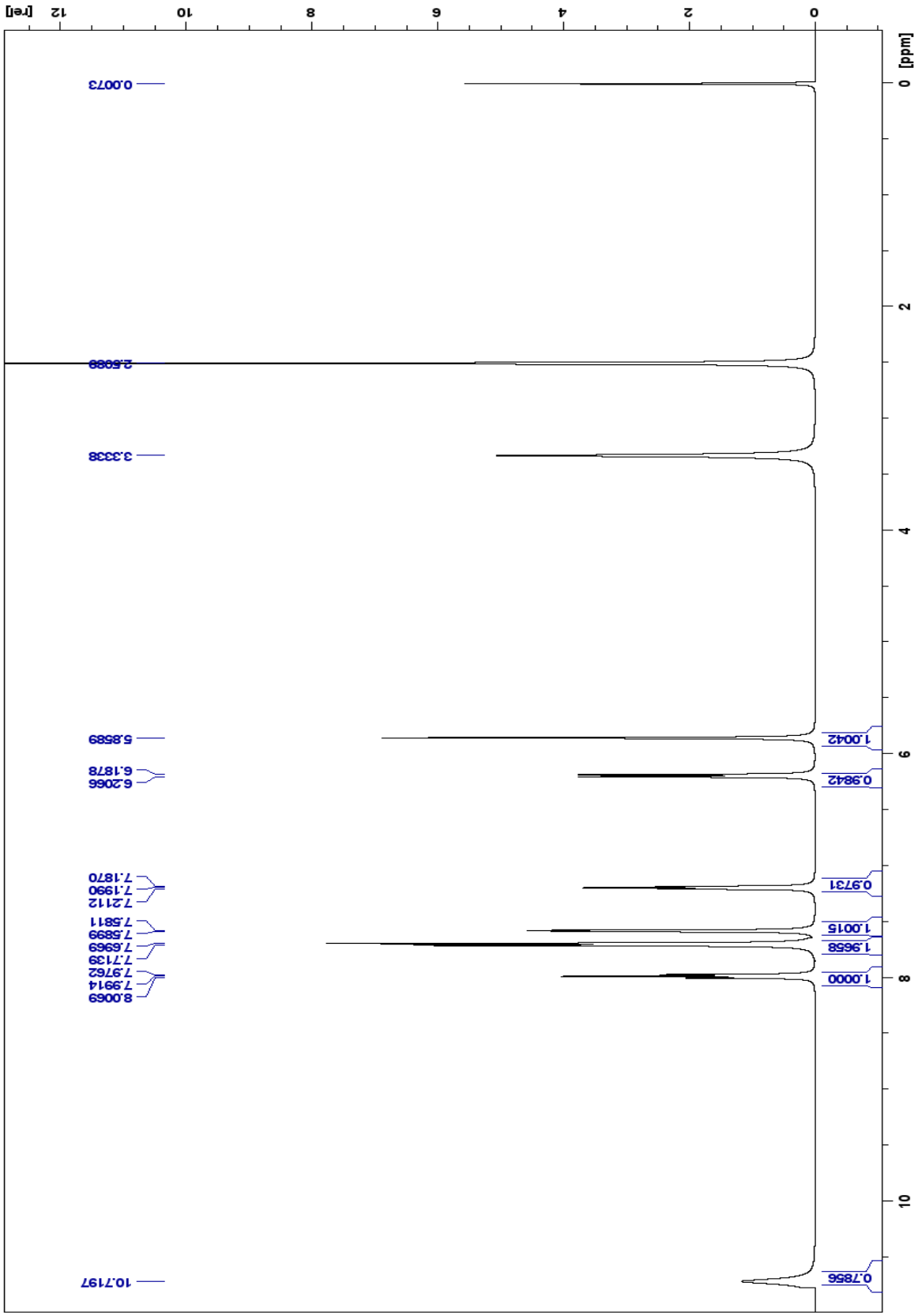

Spectrum 10*: 3a* ***^{1}H NMR (500 MHz, DMSO-d6)***

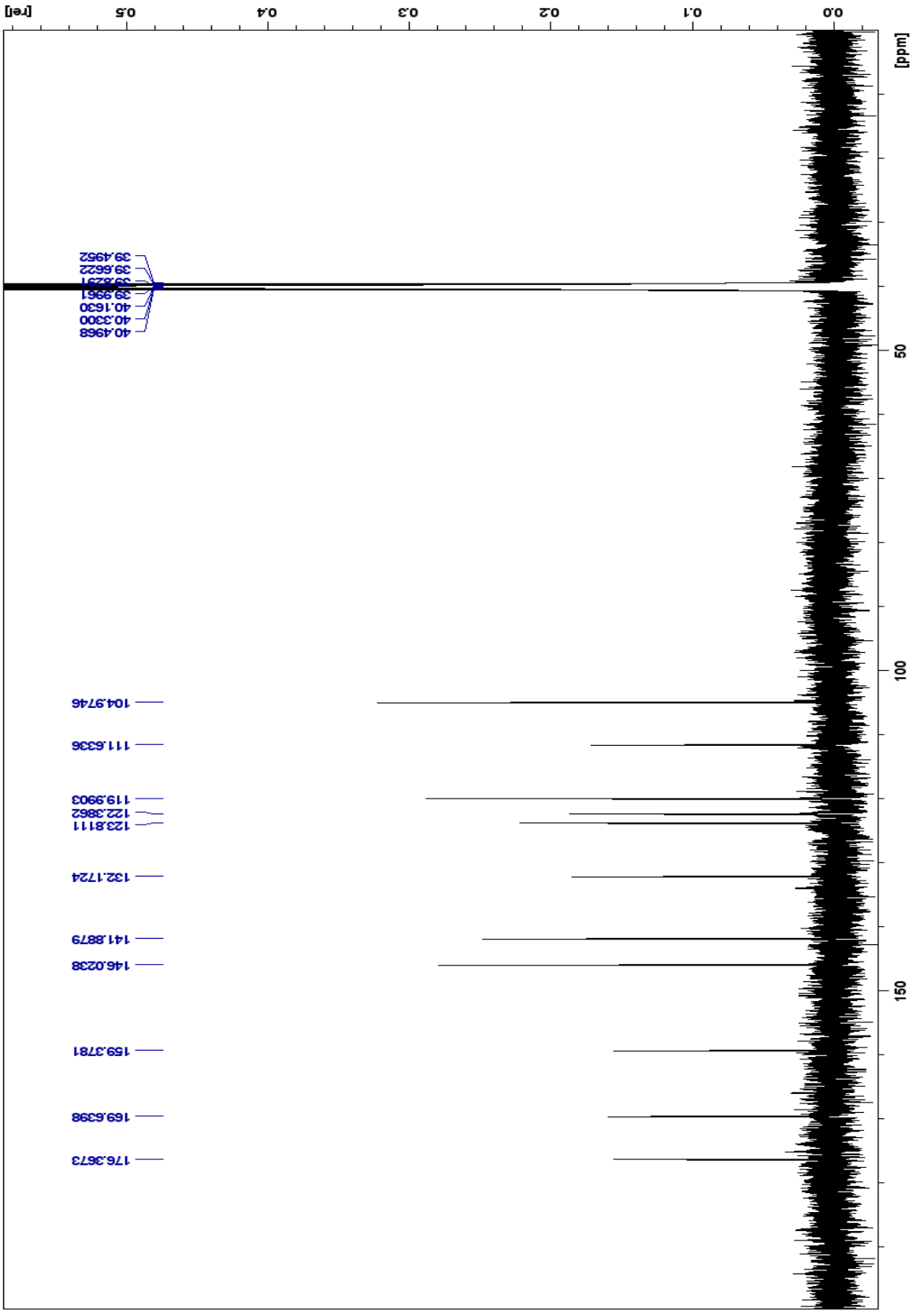

Spectrum 11*: 3a* ***^{13}C NMR (500 MHz, DMSO-d6)***

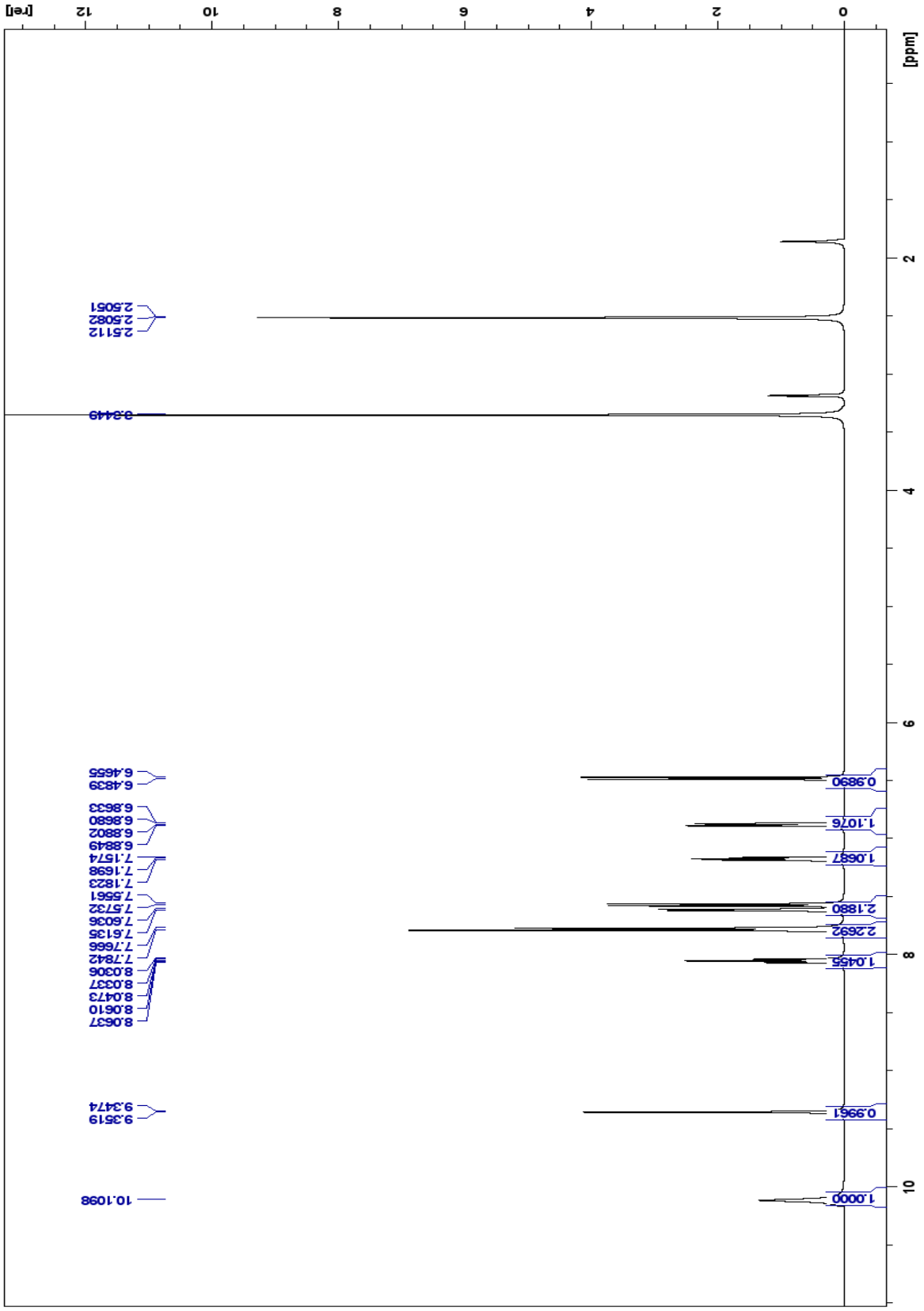

Spectrum 12*: 3b* ^{1}***H NMR (500 MHz, DMSO-d6)***

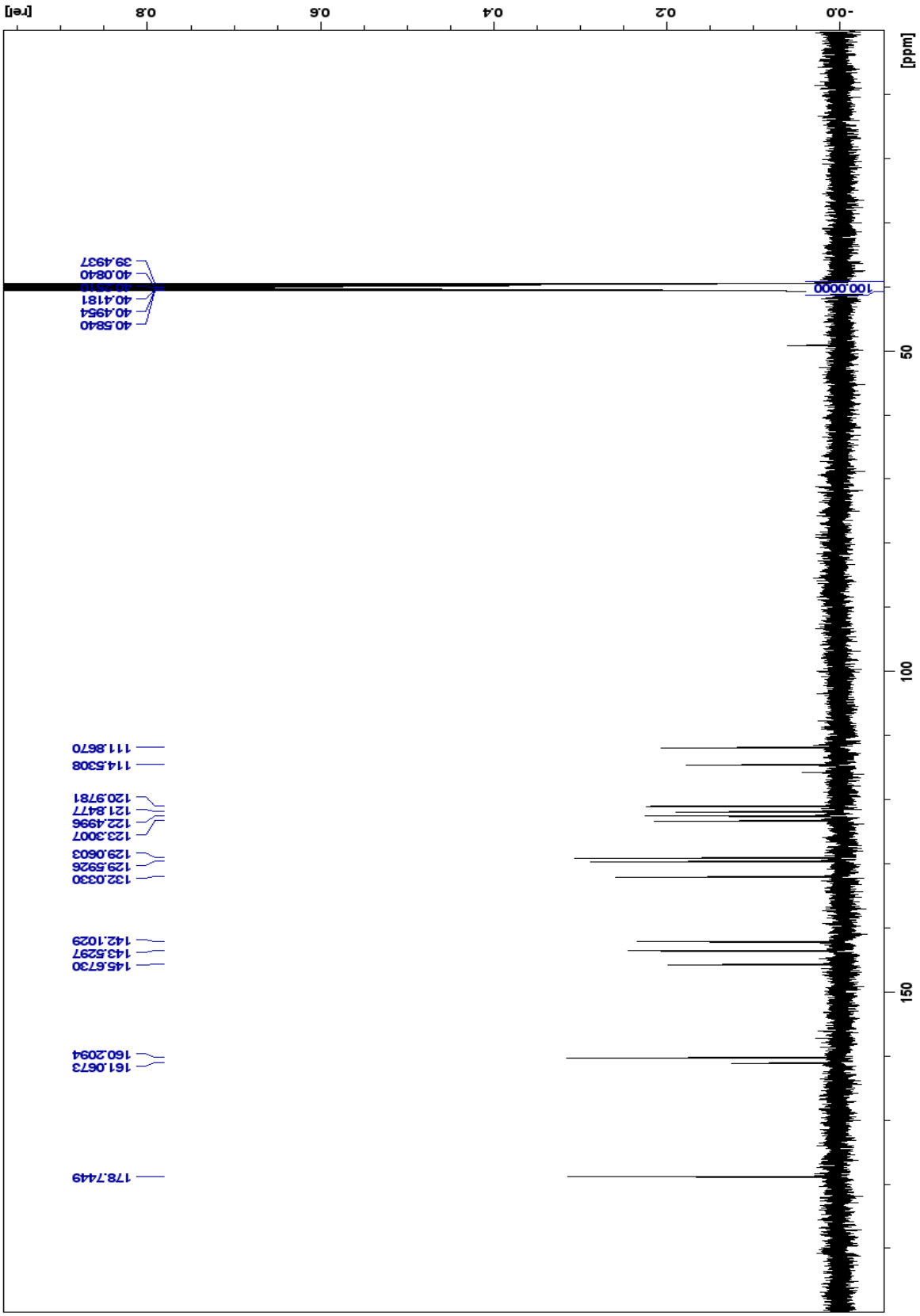

Spectrum 13*: 3b* ***^{13}C NMR (500 MHz, DMSO-d6)***

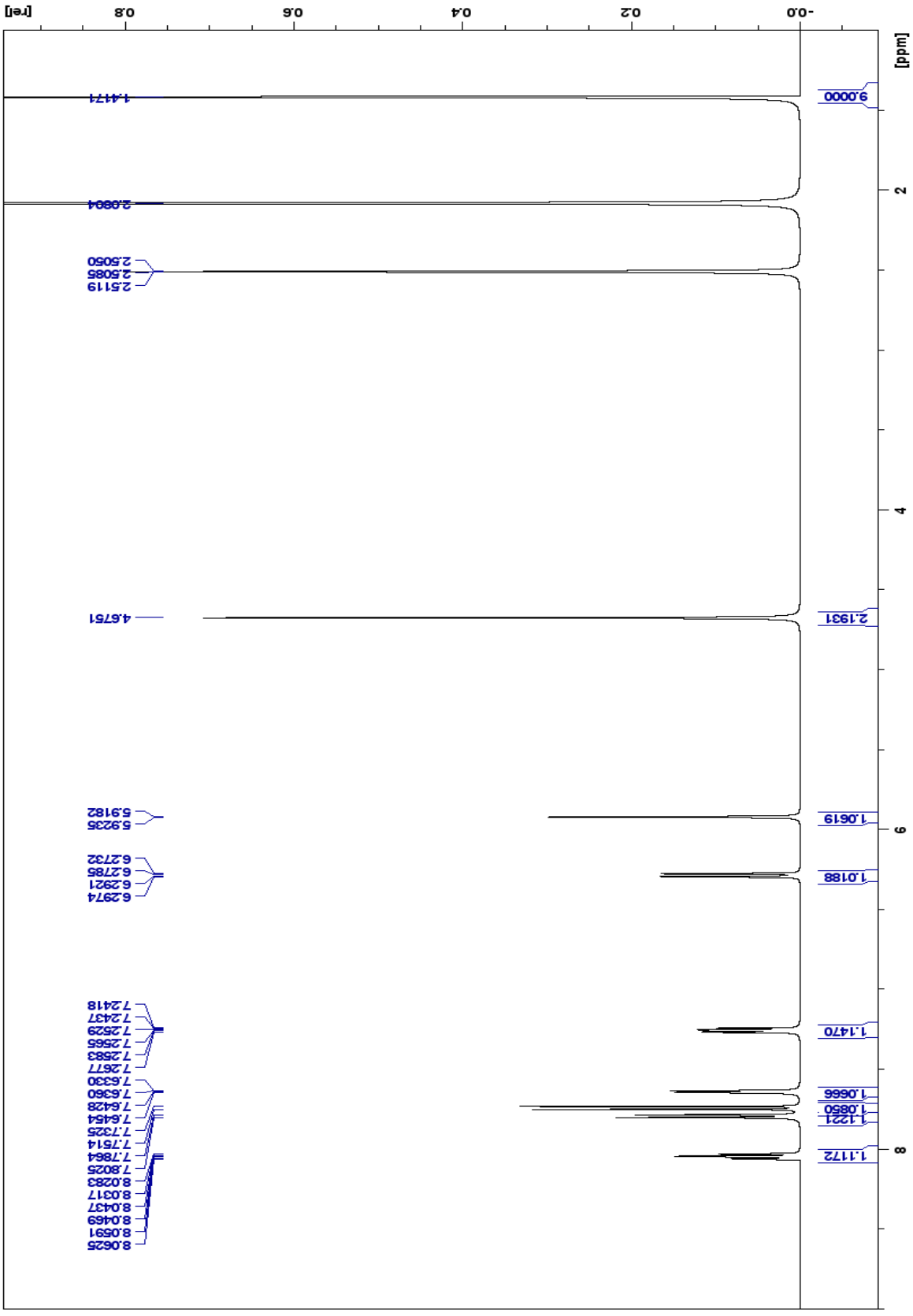

Spectrum 14*: 4a* ^{1}***H NMR (500 Mhz, DMSO-d6)***

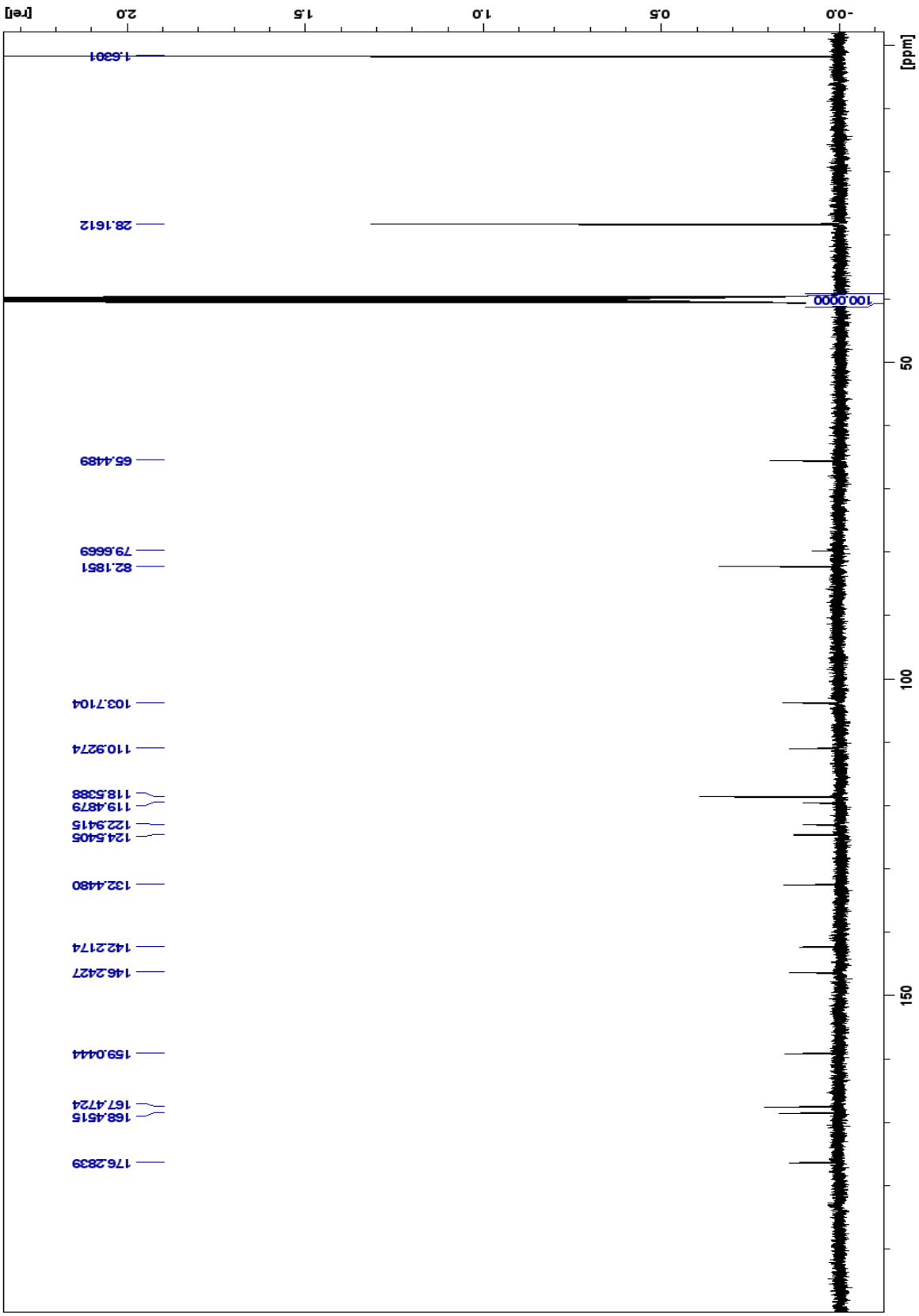

Spectrum 15*: 4a* ***^{13}C NMR (500 Mhz, DMSO-d6)***

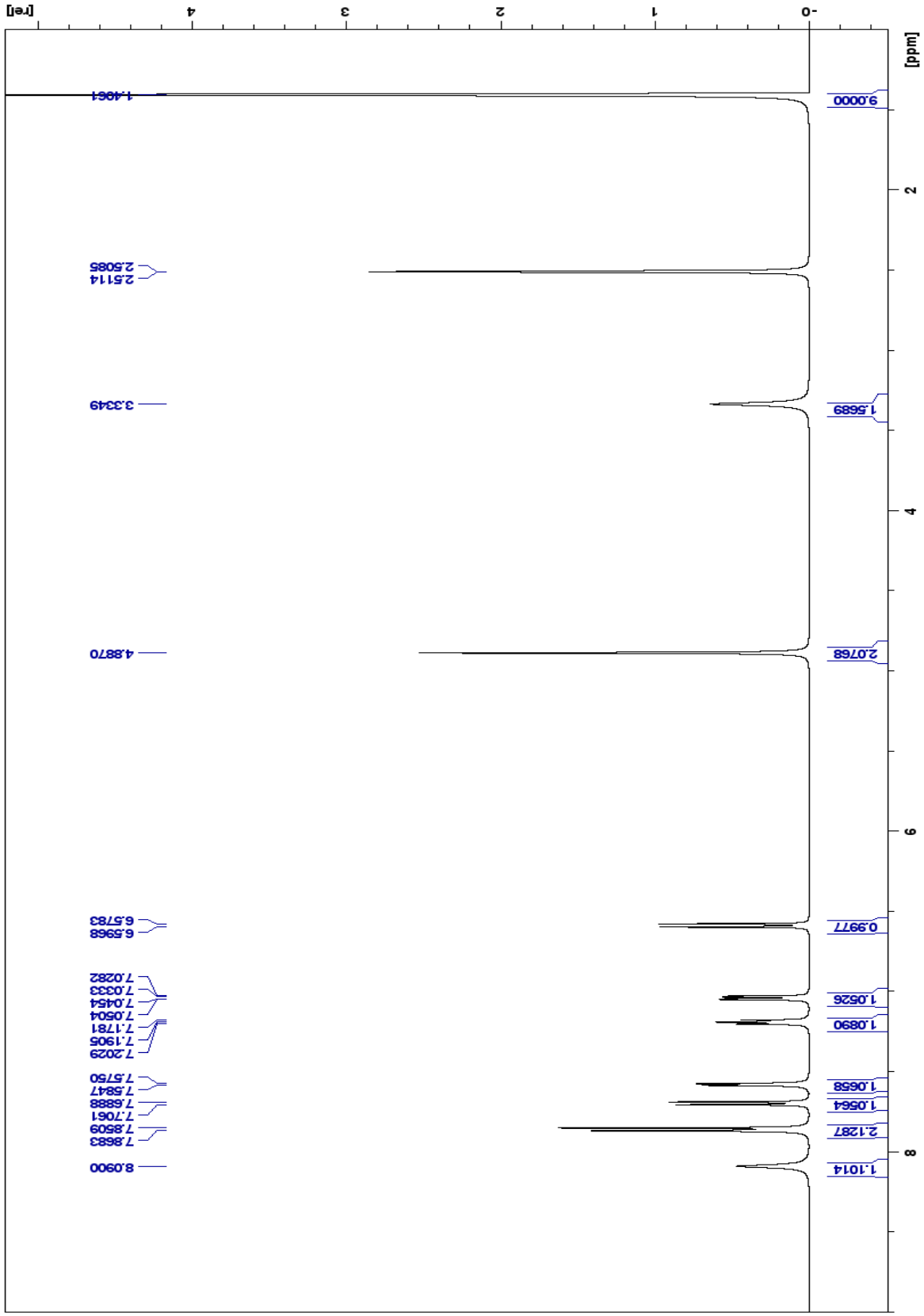

Spectrum 16*: 4b* ***[1]H NMR (500 MHz, DMSO-d6)***

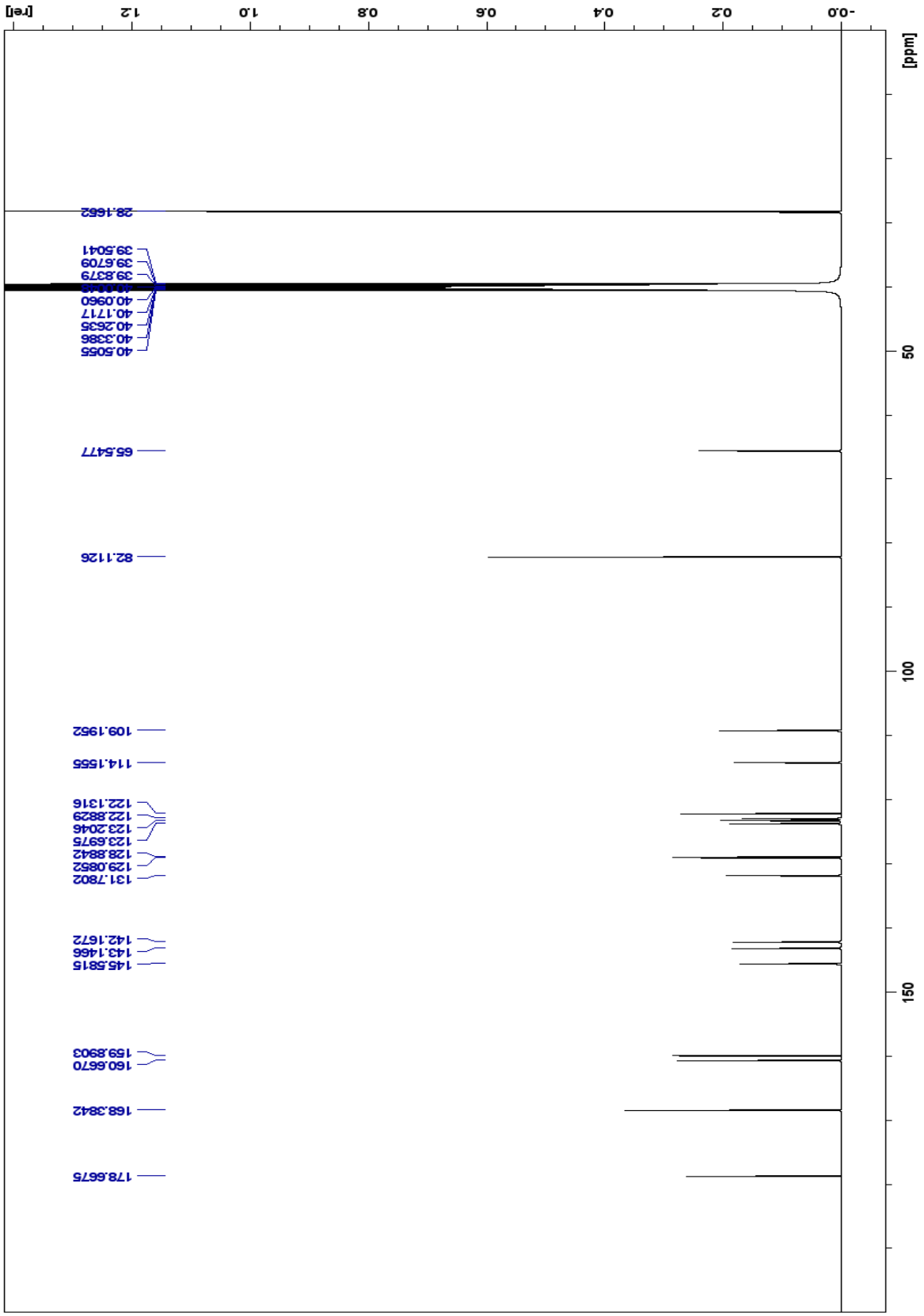

Spectrum 17*: 4b* ***^{13}NMR (500 MHz, DMSO-d6)***

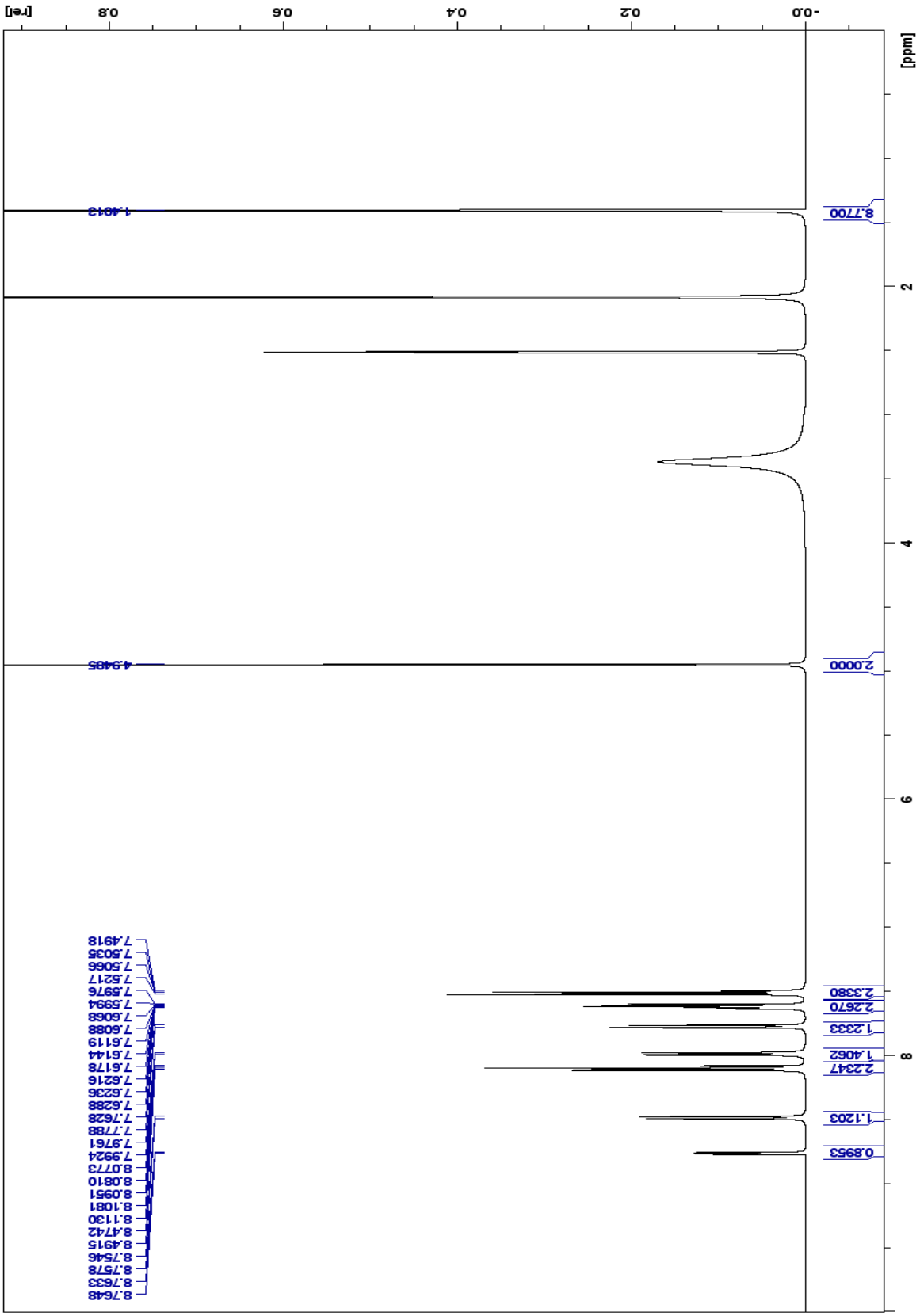

Spectrum 18*: 4c* ***^{1}H NMR (500 Mhz, DMSO-d6)***

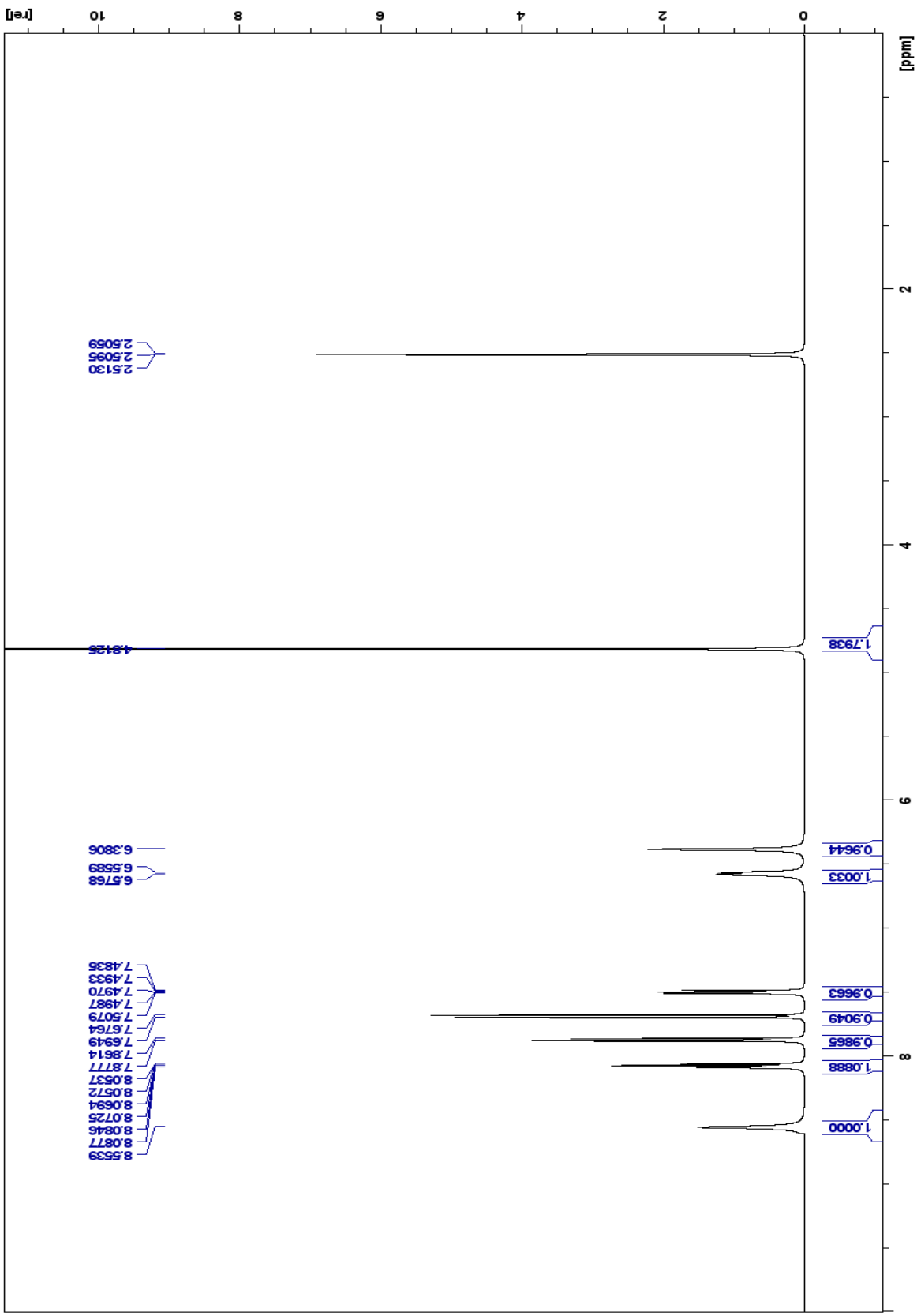

Spectrum 19*: 5a* ^{1}***H NMR (500 MHz, DMSO-d6)***

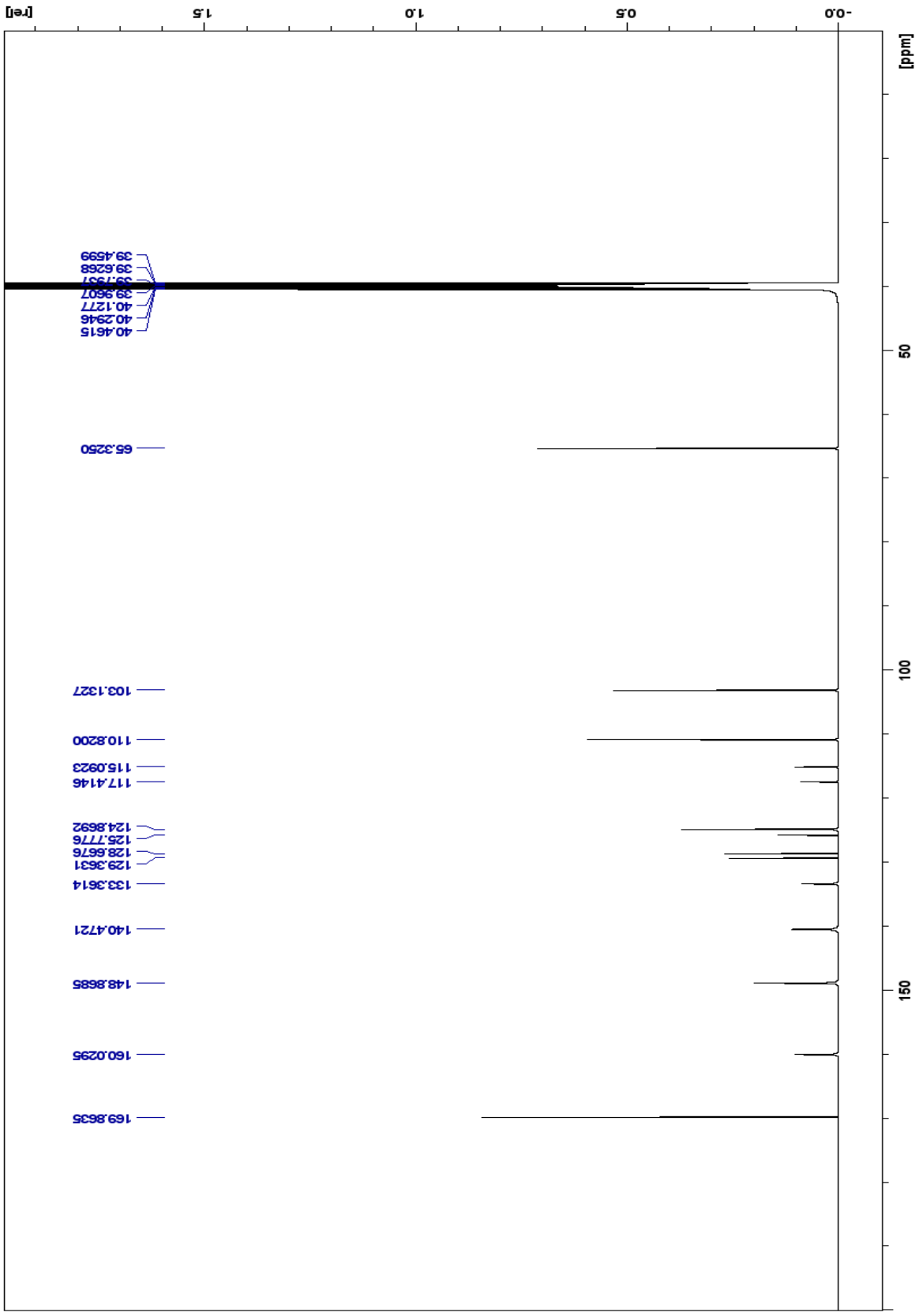

Spectrum 20*: 5a* ***^{13}C NMR (500 MHz, DMSO-d6)***

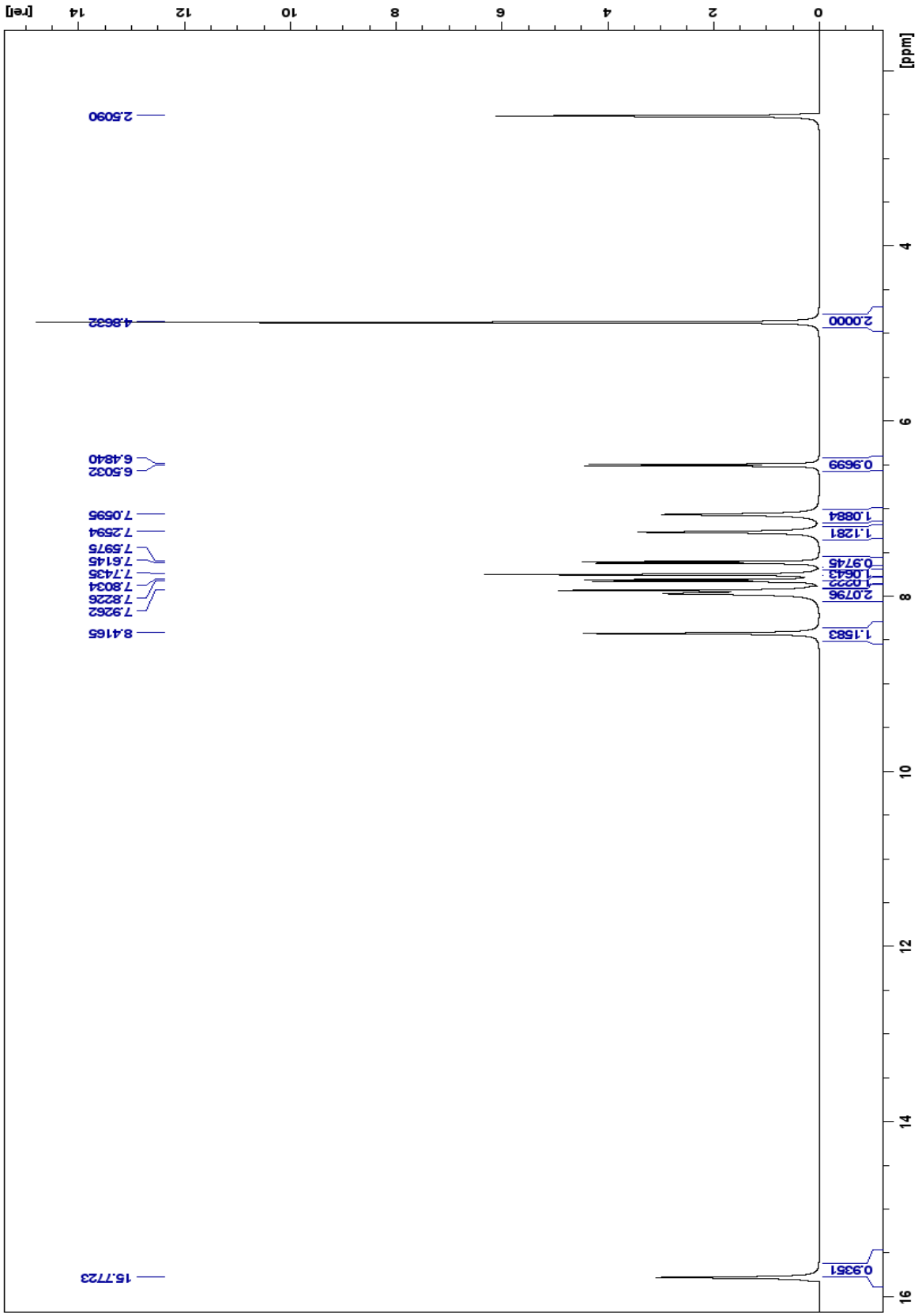

Spectrum 21*: 5b* ***^{1}H NMR (500 MHz, DMSO-d6)***

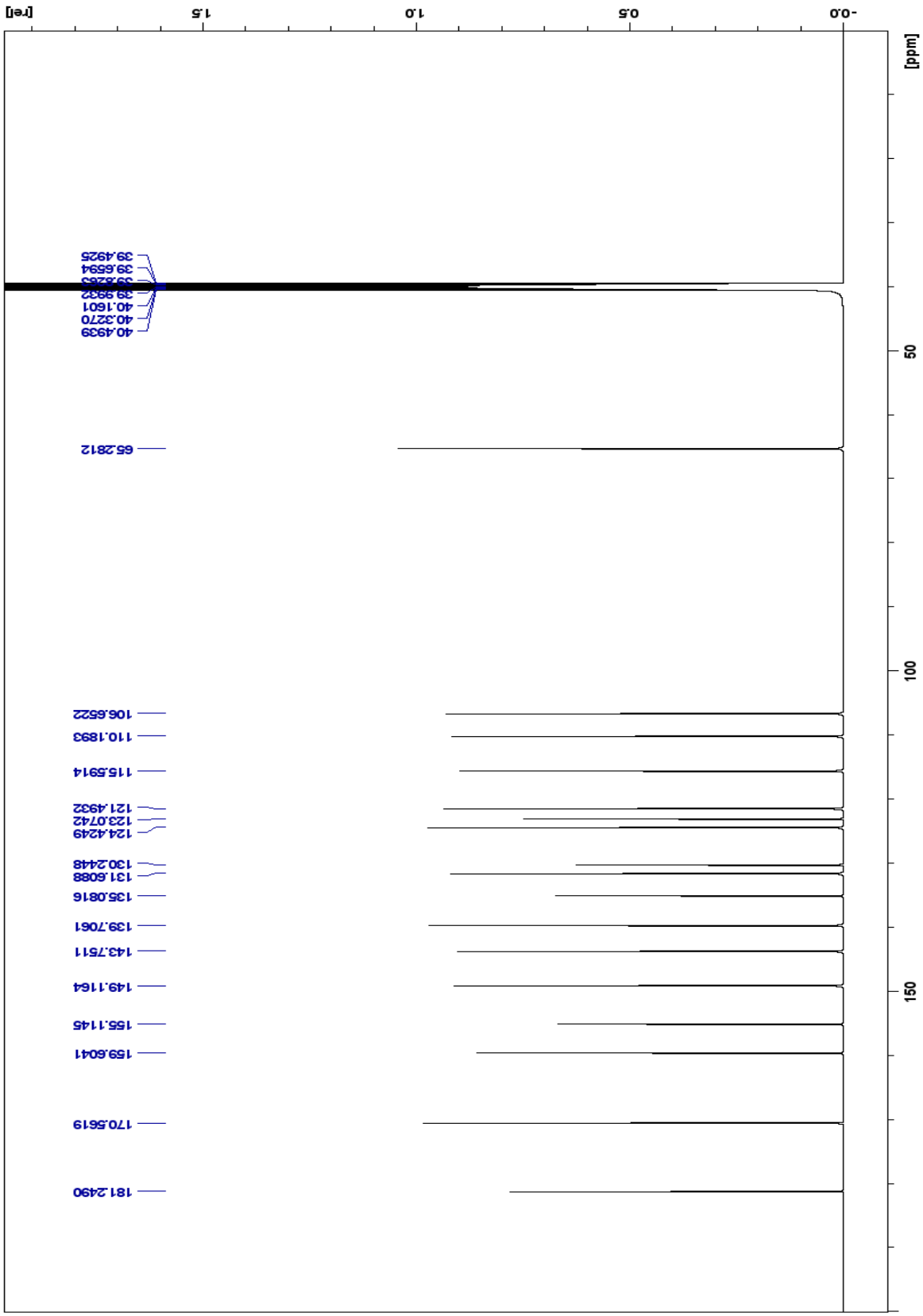

Spectrum 22*: 5b* ***^{1}H NMR (500 MHz, DMSO-d6)***

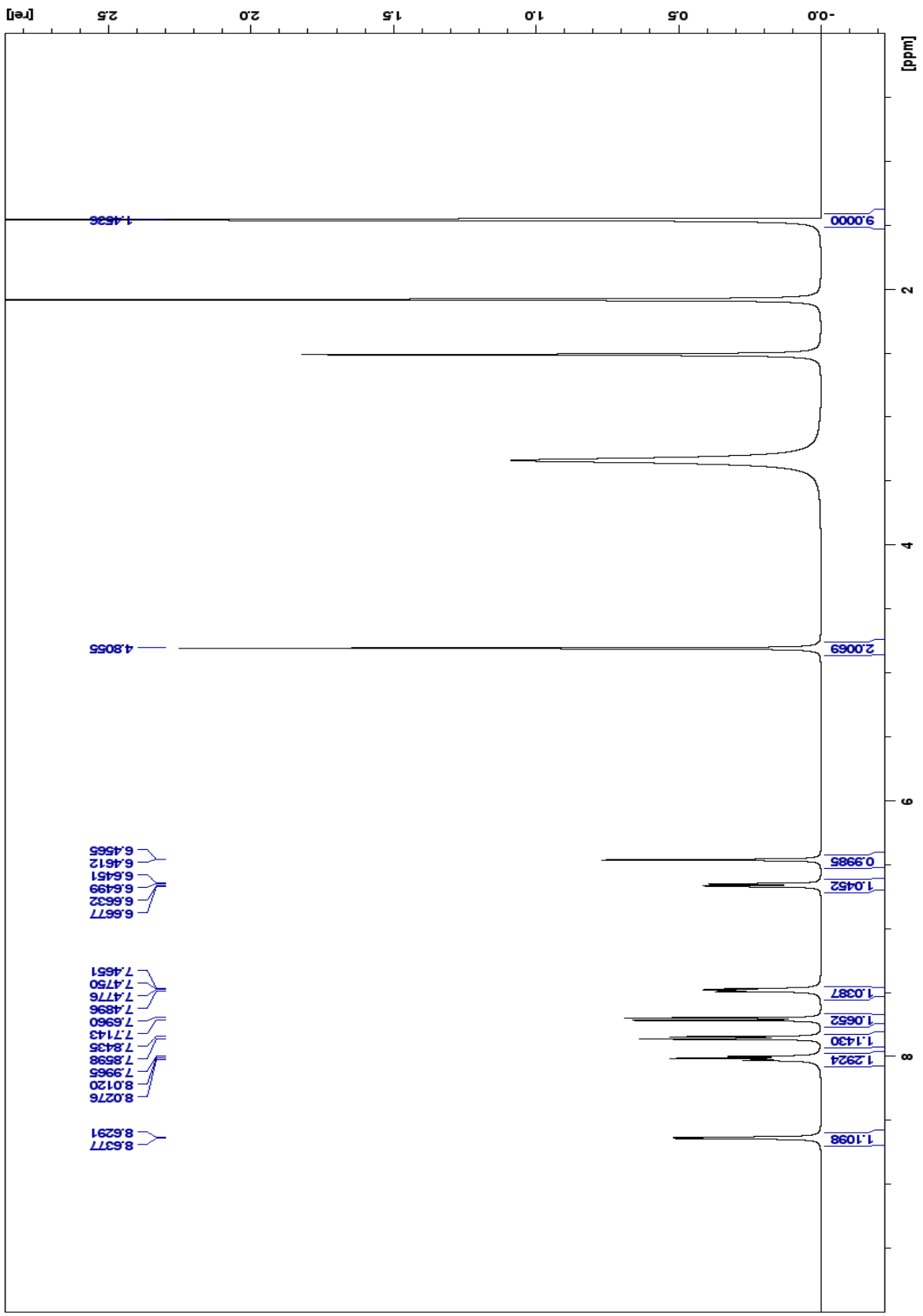

Spectrum 23*: 6* ^{1}***H NMR (500 MHz, DMSO-d6)***

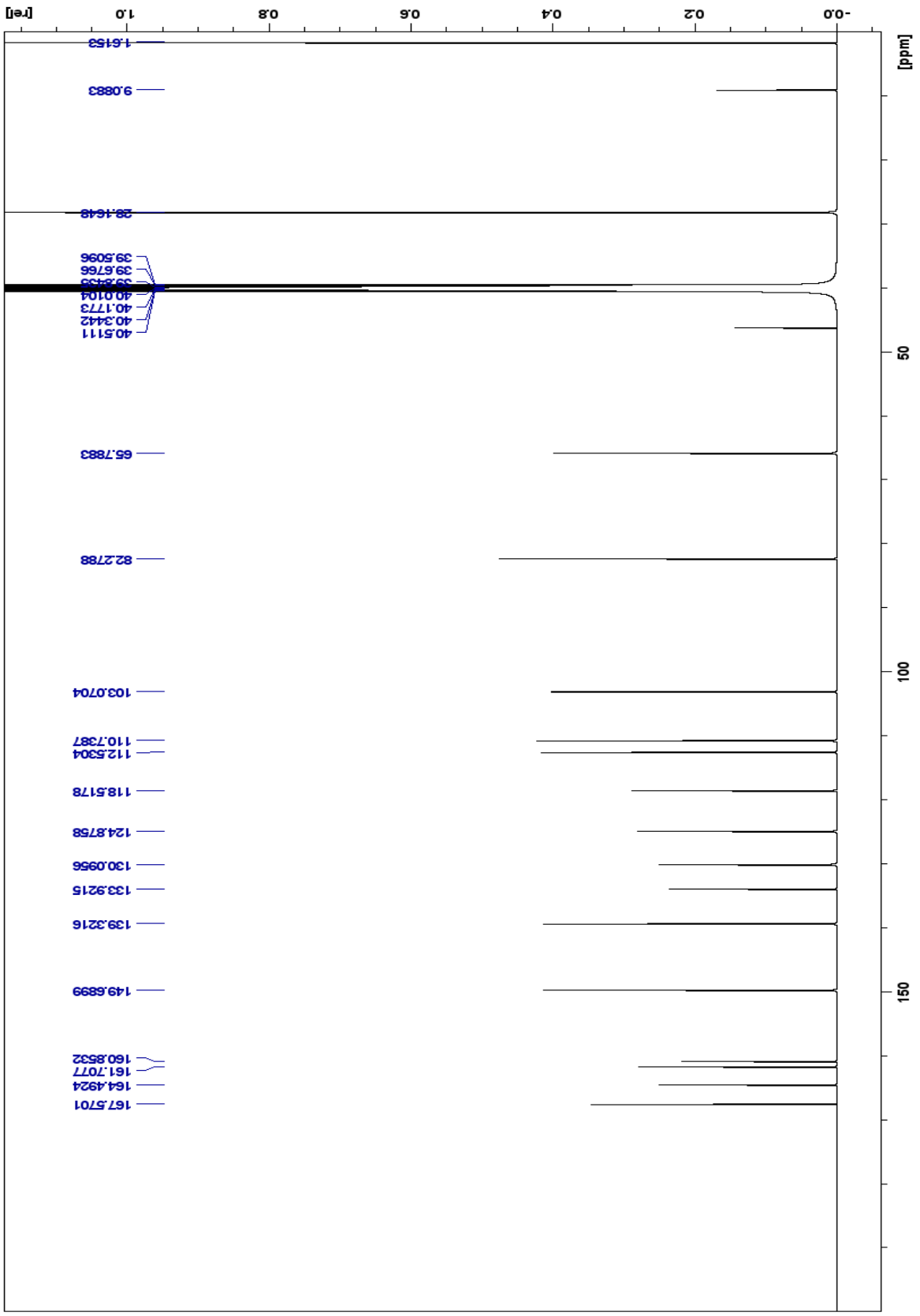

Spectrum 24*: 6 ^{13}C NMR (500 MHz, DMSO-d6)*

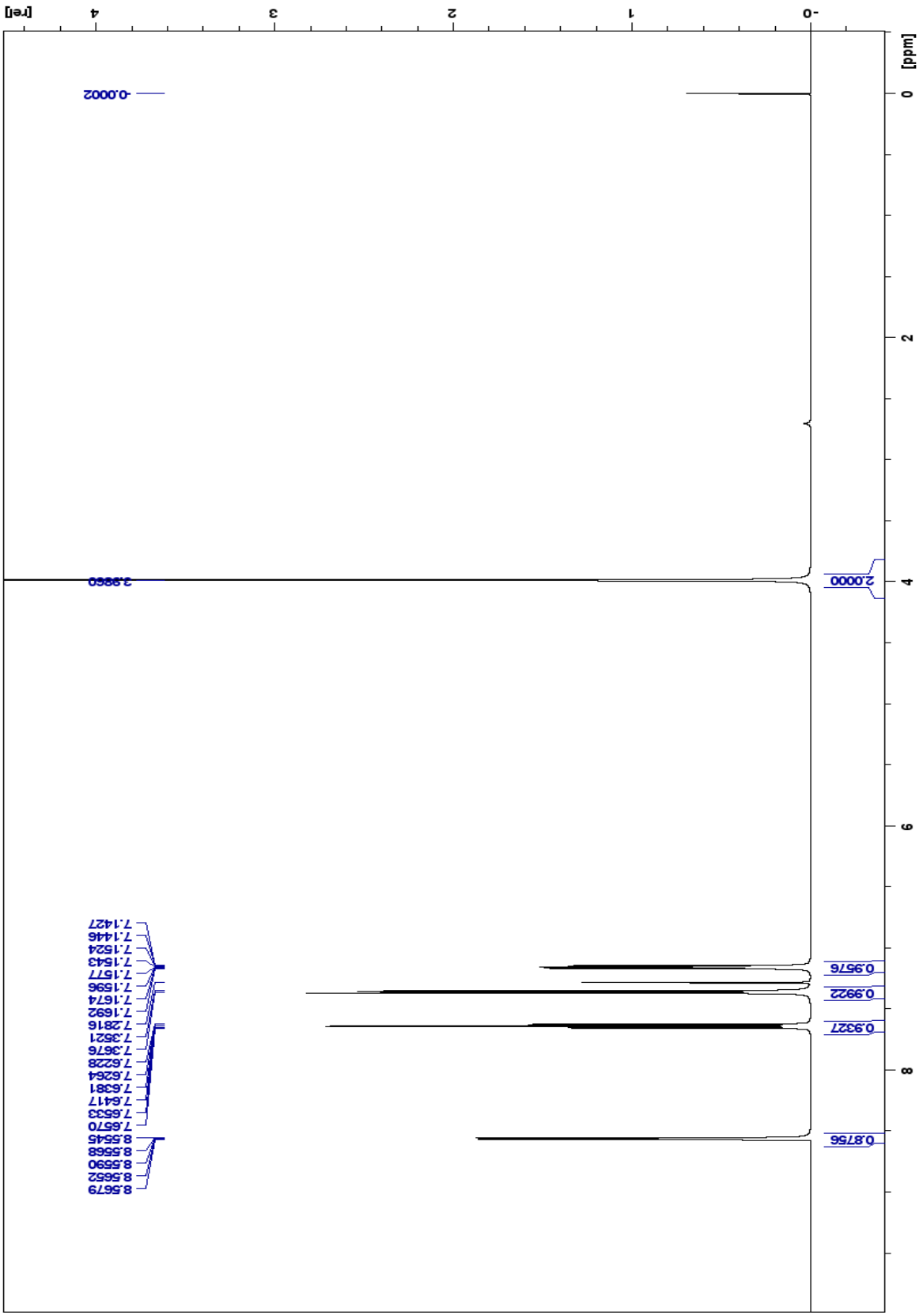

Spectrum 25*: 7a* ^{1}***H NMR (500 MHz,*** $CDCl_3$***)***

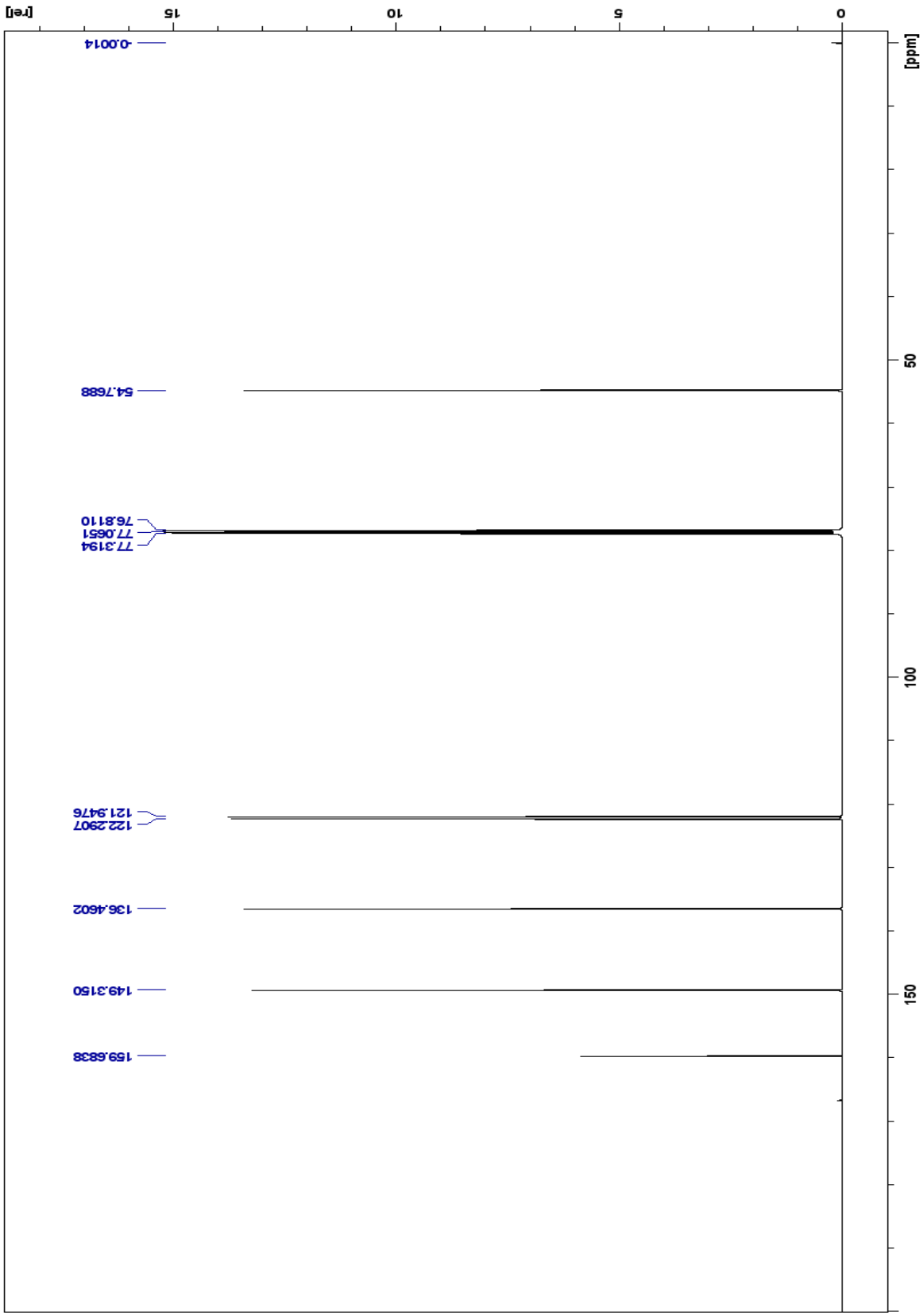

Spectrum 26*: 7a* ***^{13}C NMR (500 MHz, $CDCl_3$)***

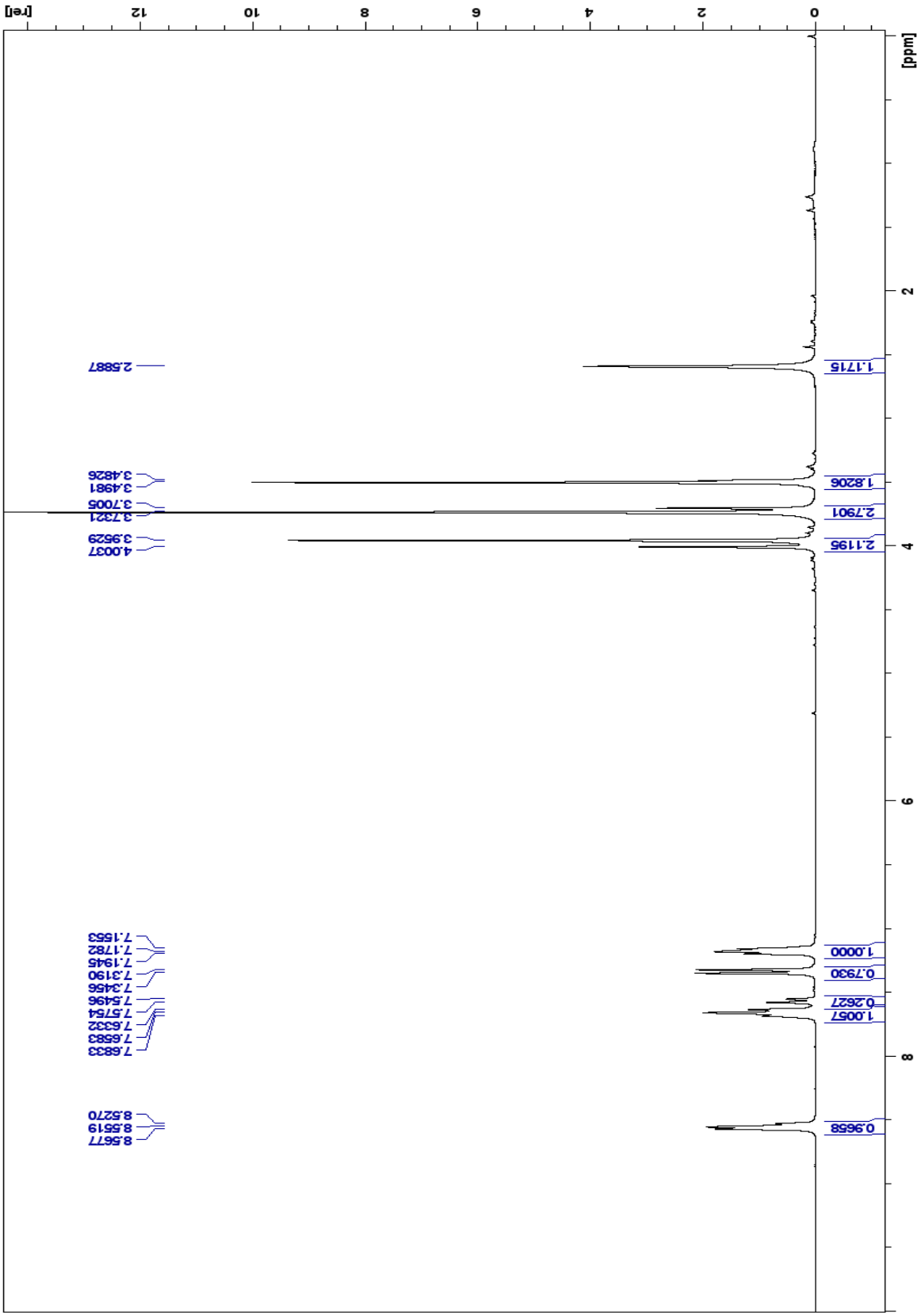

Spectrum 27*: 7b* ***[1]H NMR (300 Mhz, DMSO-d6)***

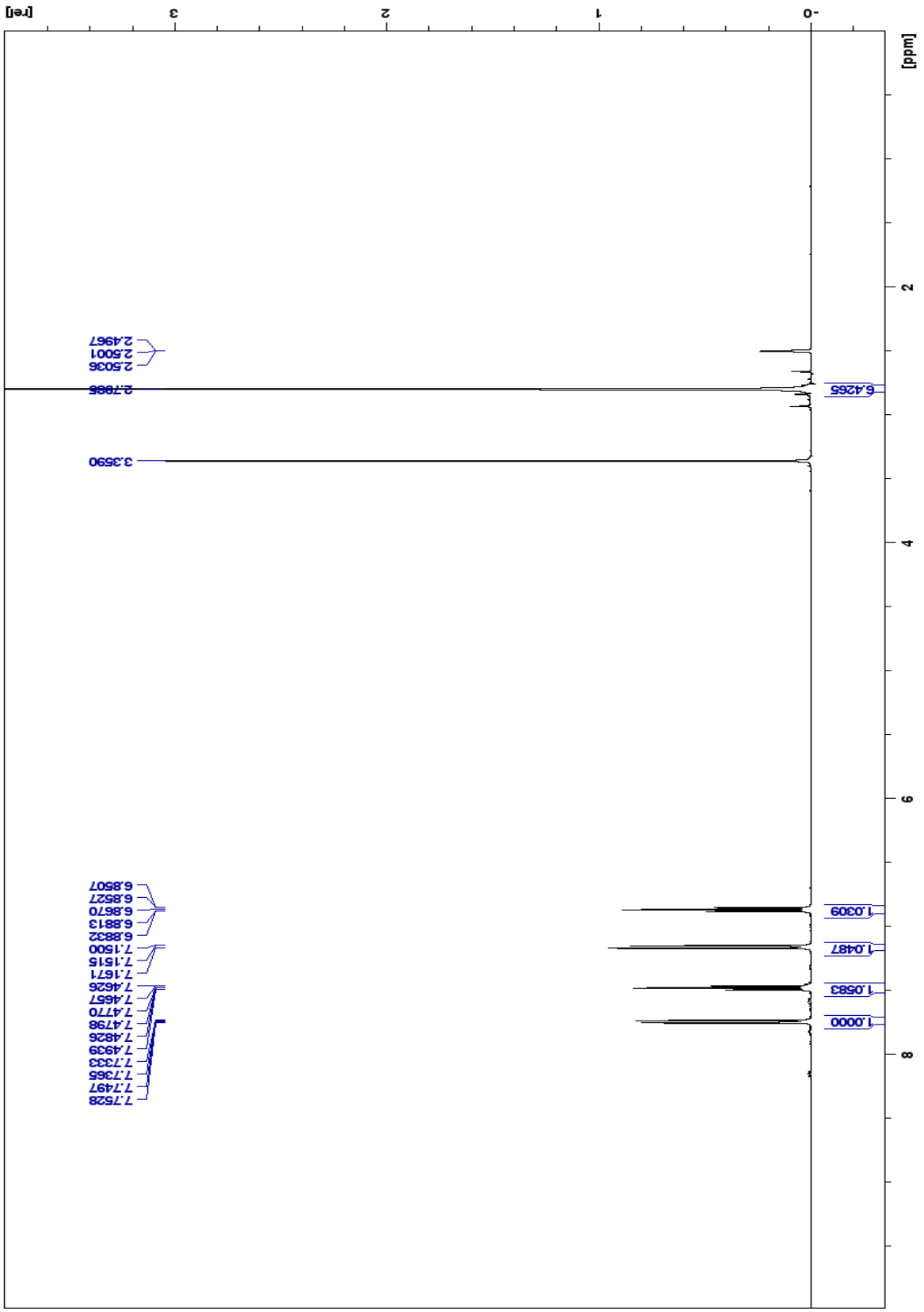

Spectrum 28*: 8a* ***¹H NMR (500 Mhz, DMSO-d6)***

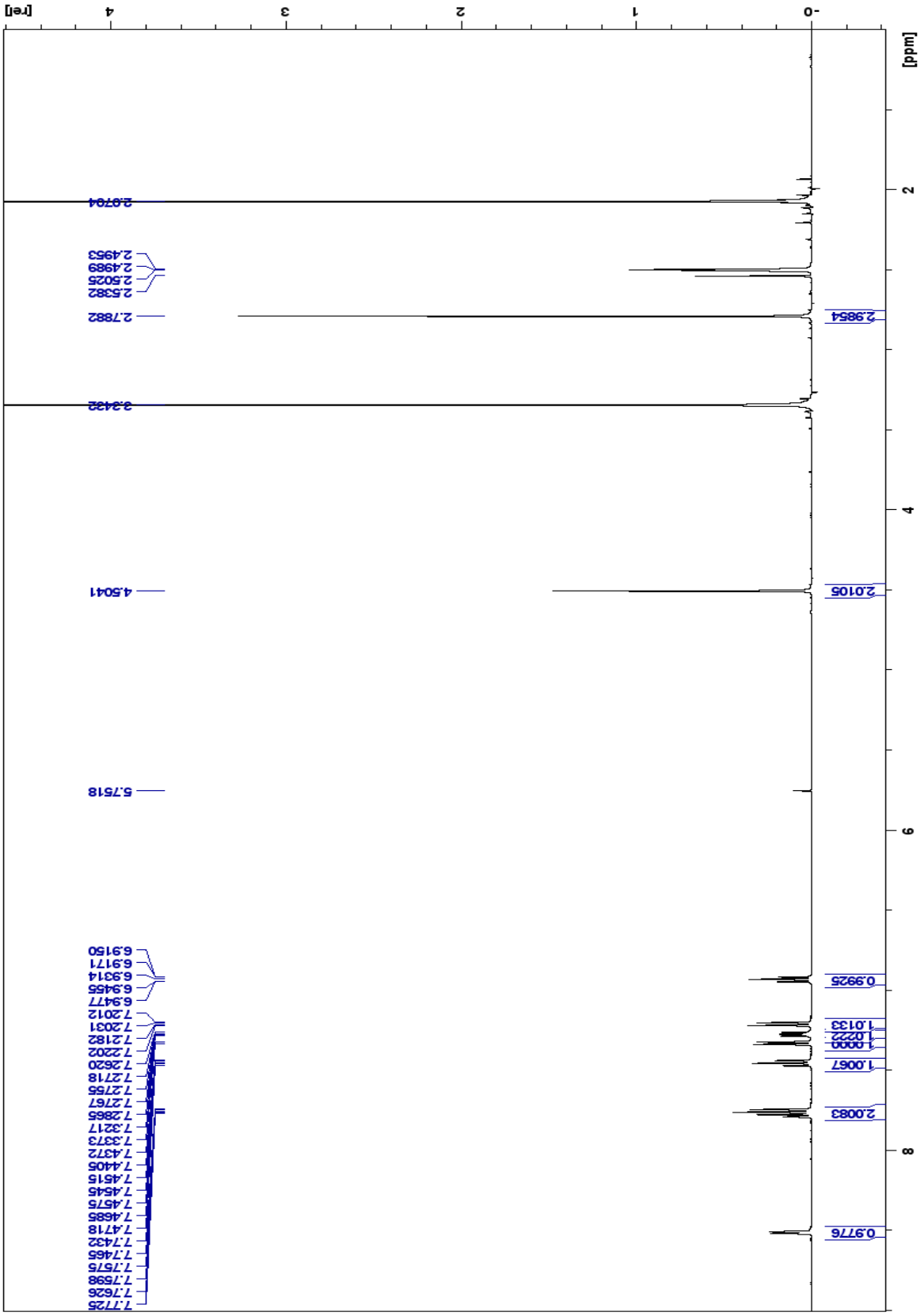

Spectrum 29*: 8b* ***[1]H NMR (500 MHz, DMSO-d6)***

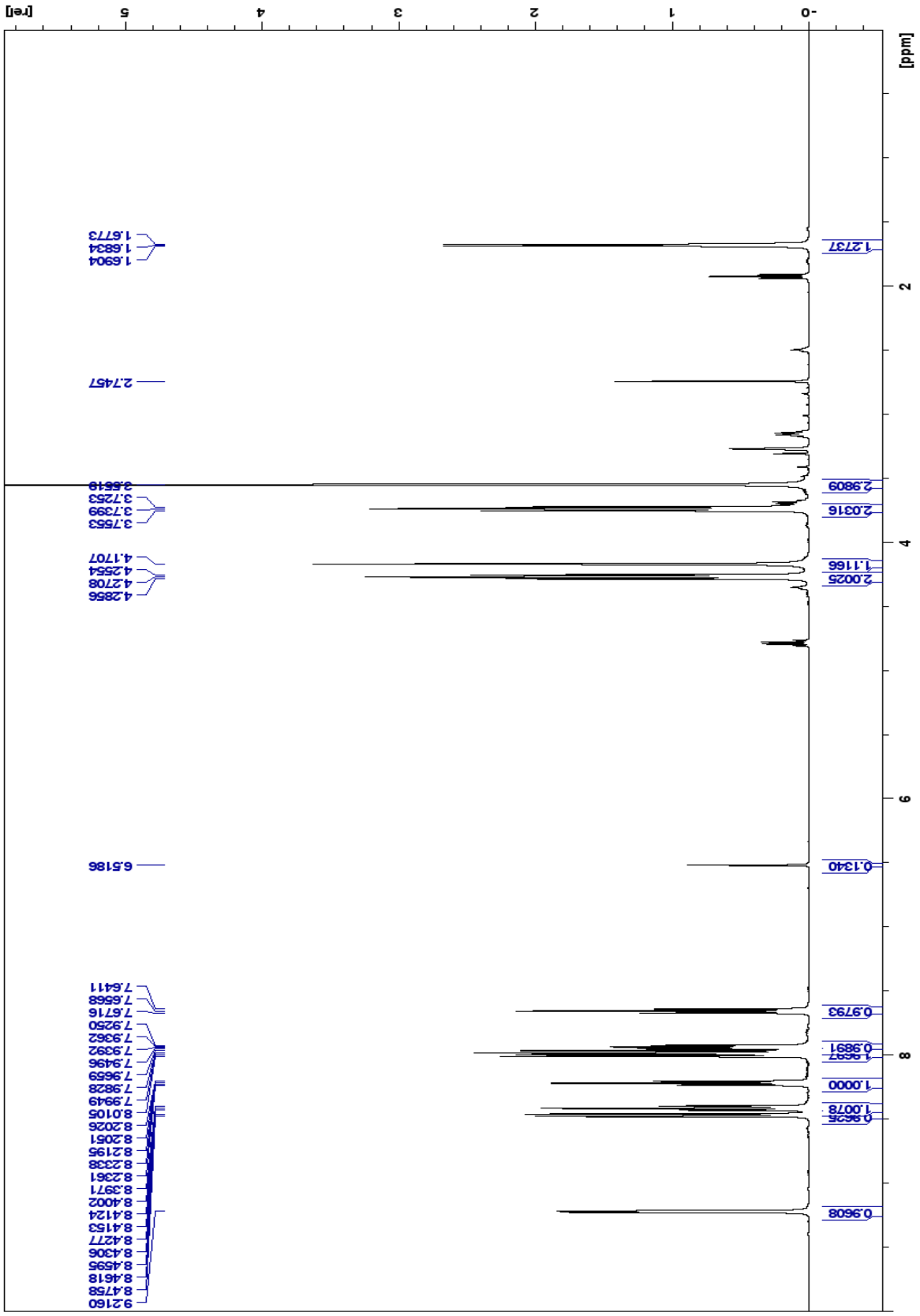

Spectrum 30*: 8c* ***¹H NMR (500 MHz, DMSO-d6)***

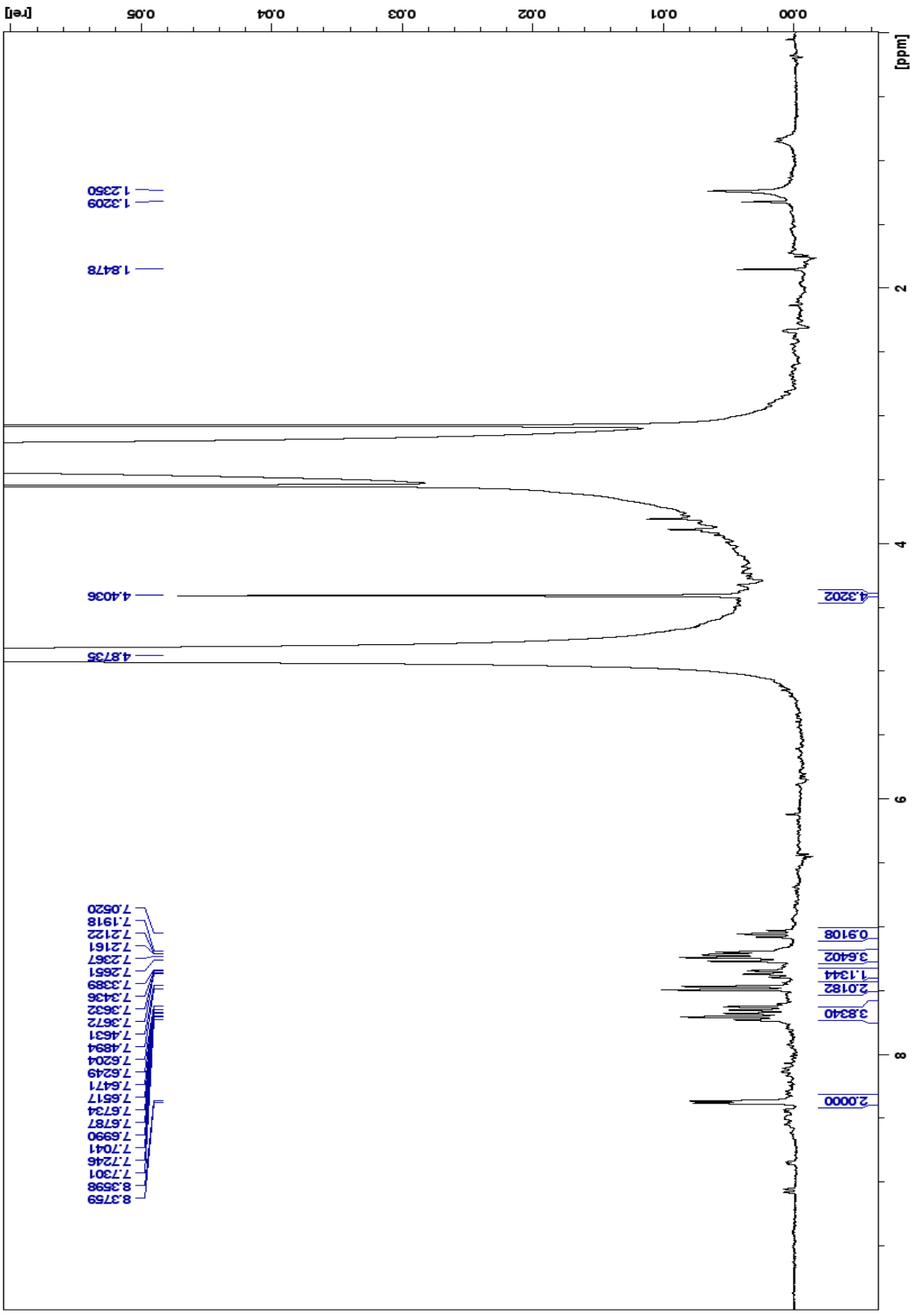

Spectrum 31*: 8d* ^{1}***H NMR (500 MHz, MeOH No-D)***

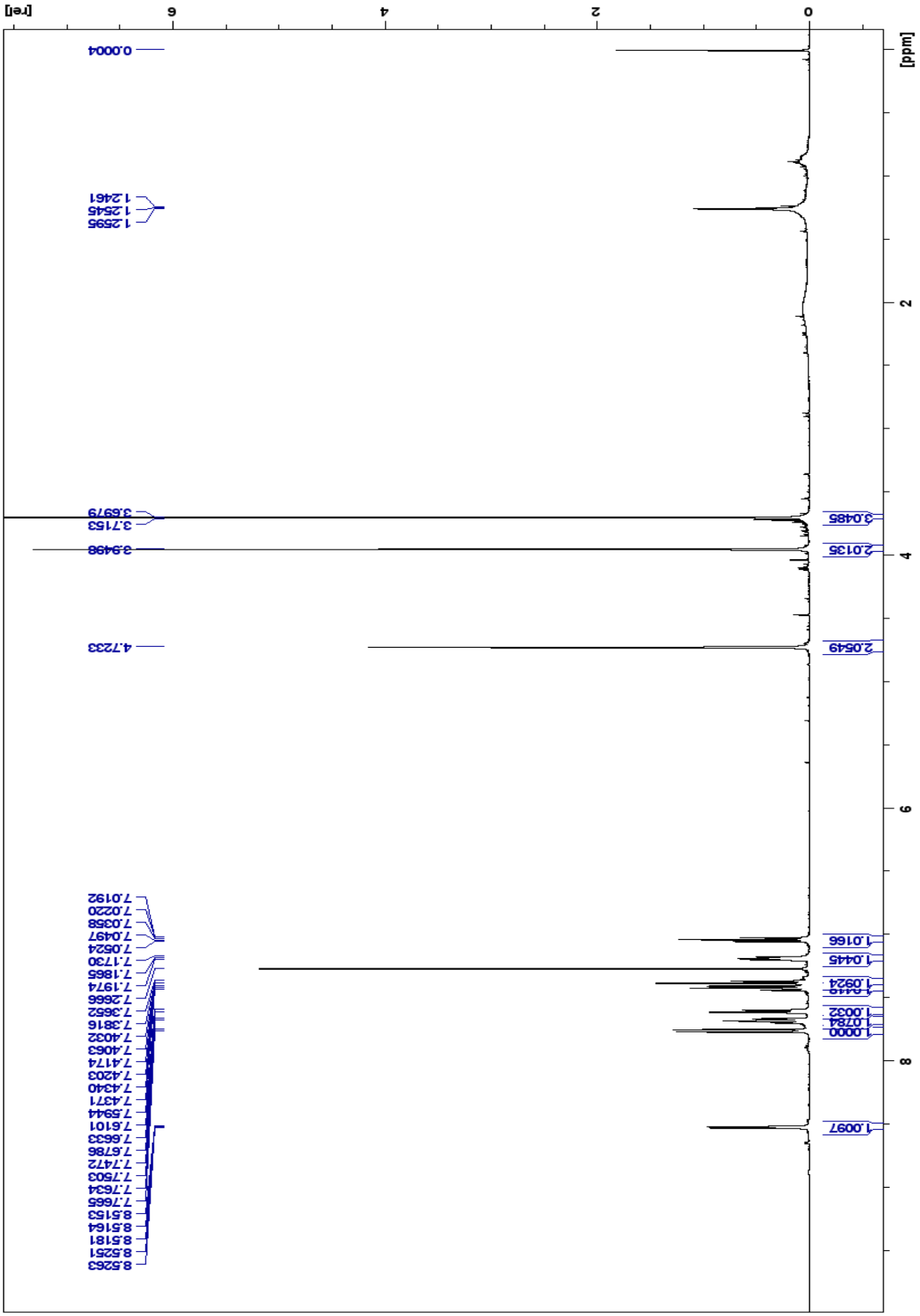

Spectrum 32*: 8e* ^{1}***H NMR (500 MHz,*** $CDCl_3$***)***

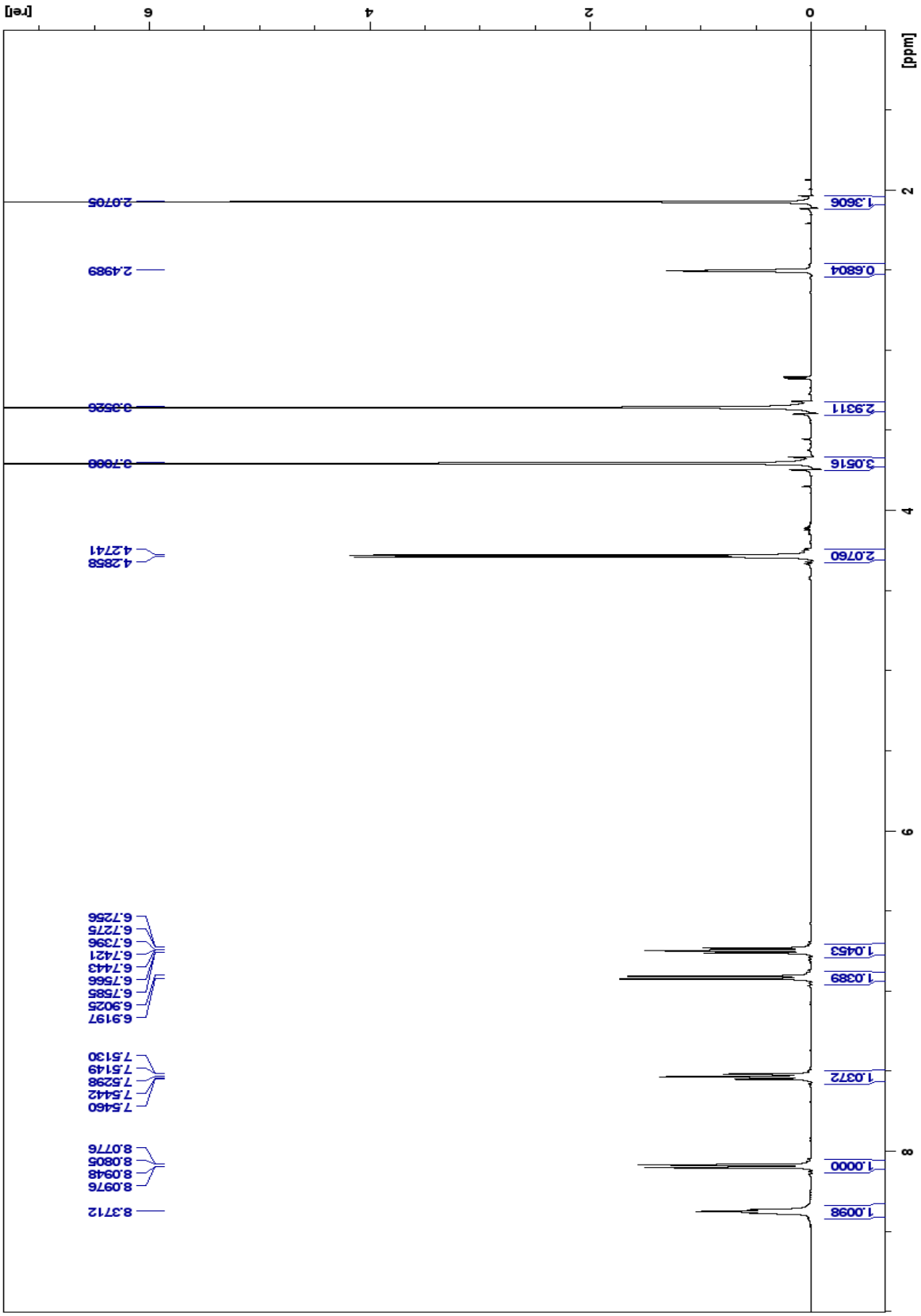

Spectrum 33*: 8f* ^{1}***H NMR (500 MHz, DMSO-d6)***

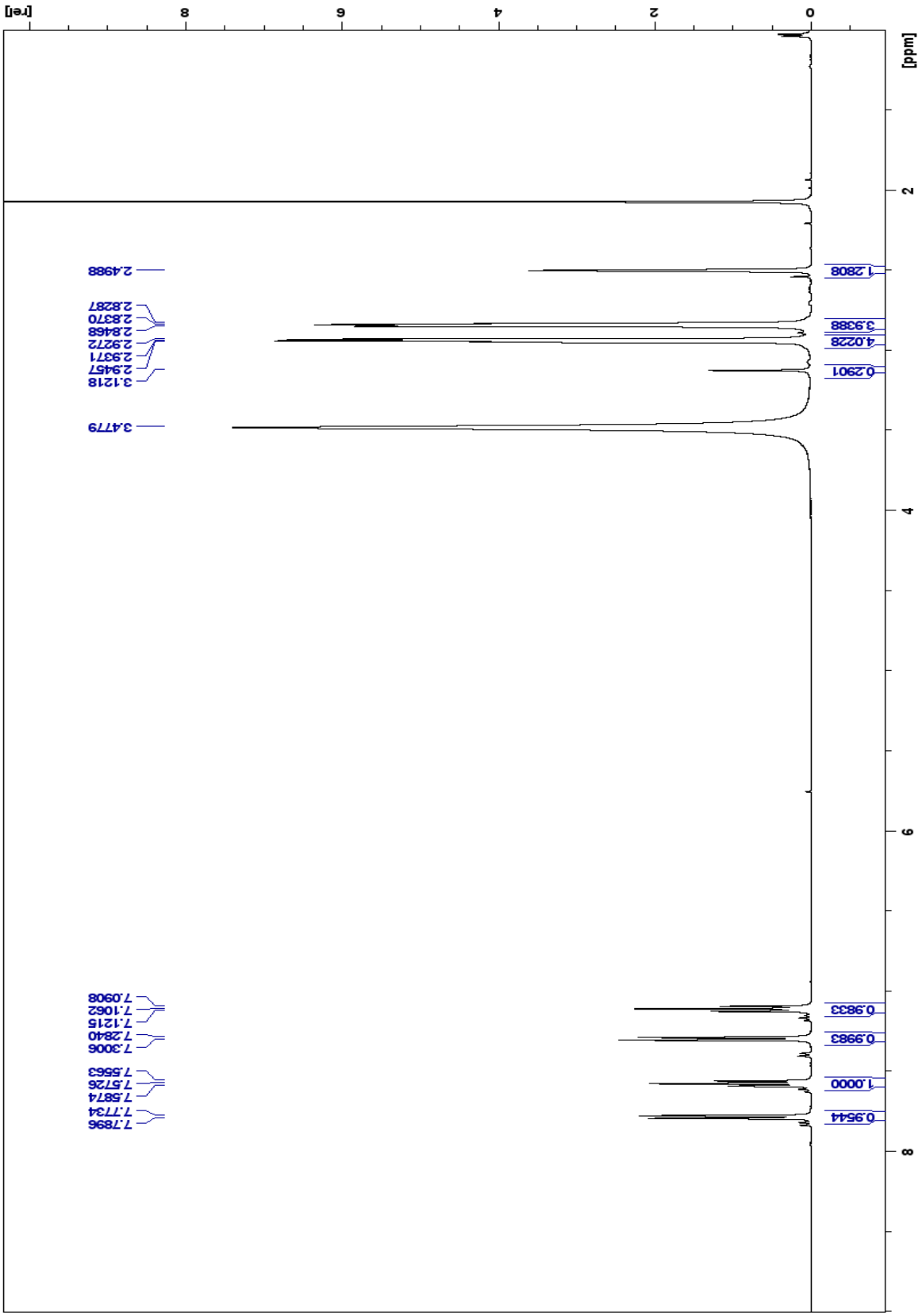

Spectrum 34*: 8g* ***^{1}H NMR (500 MHz, DMSO-d6)***

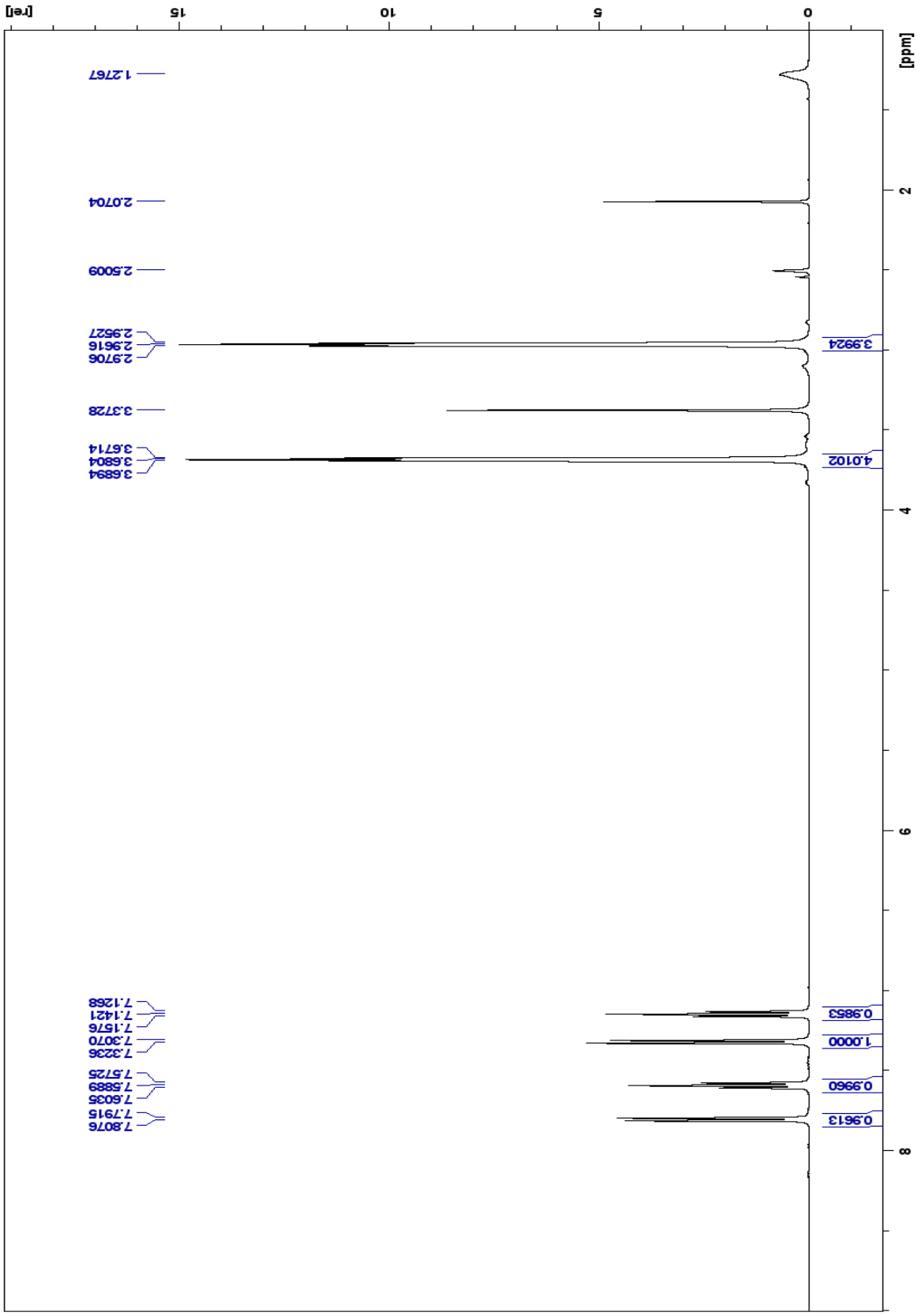

Spectrum 35*: 8h* ***^{1}H NMR (500 MHz, DMSO-d6)***

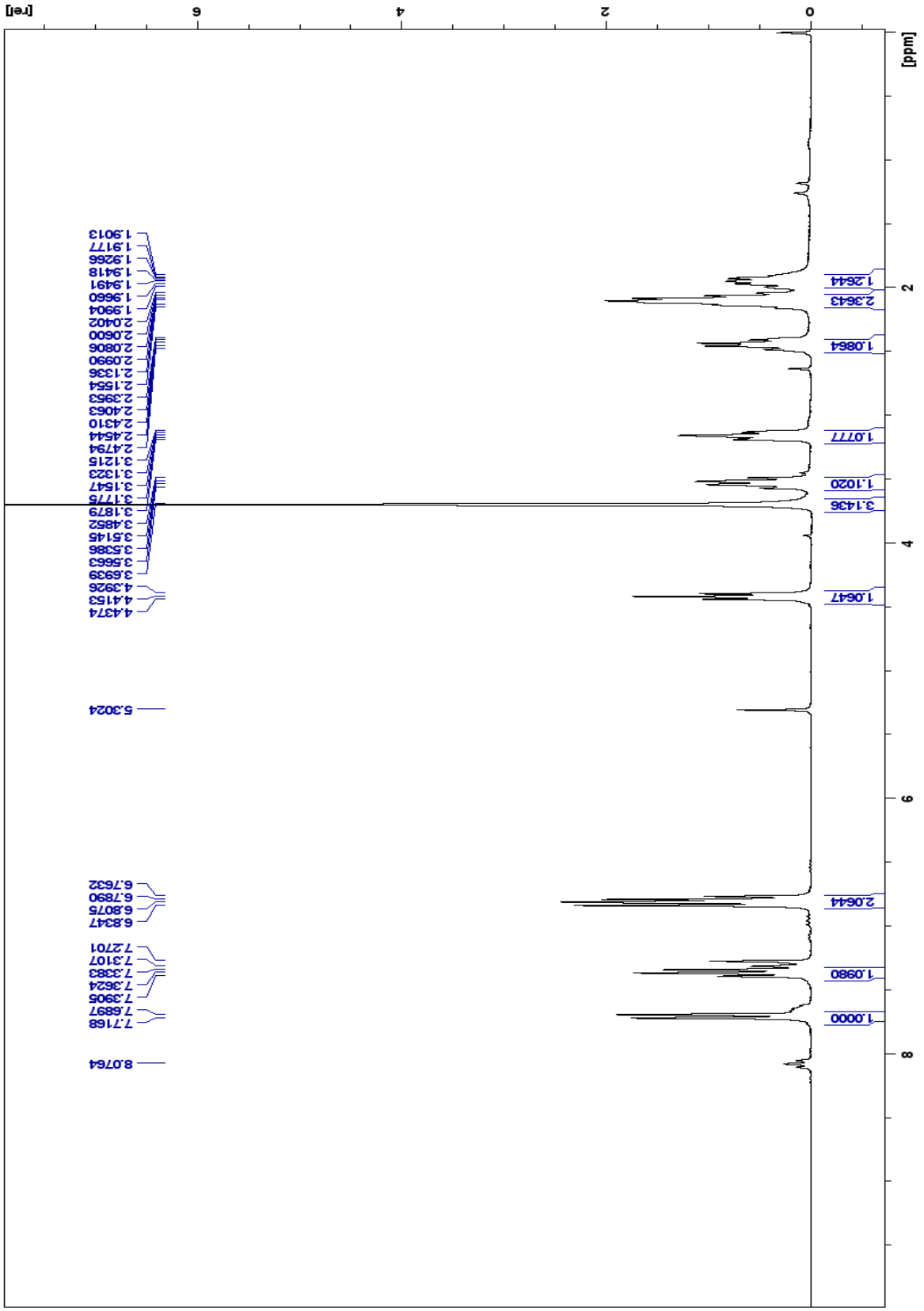

Spectrum 36*: 8i* ^{1}***H NMR (300 MHz, DMSO-d6)***

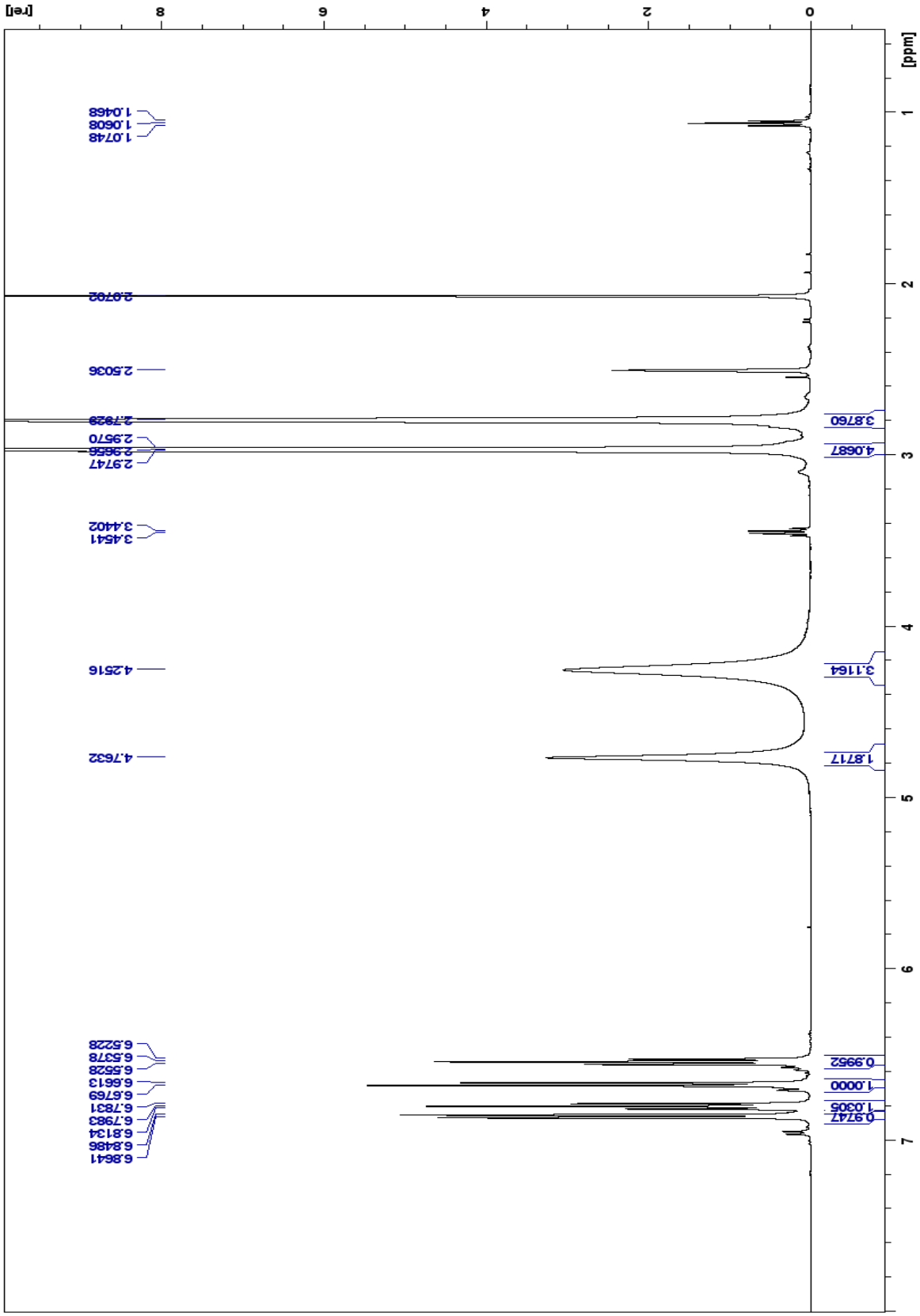

Spectrum 37*: 9a* ^{1}***H NMR (500 MHz, DMSO-d6)***

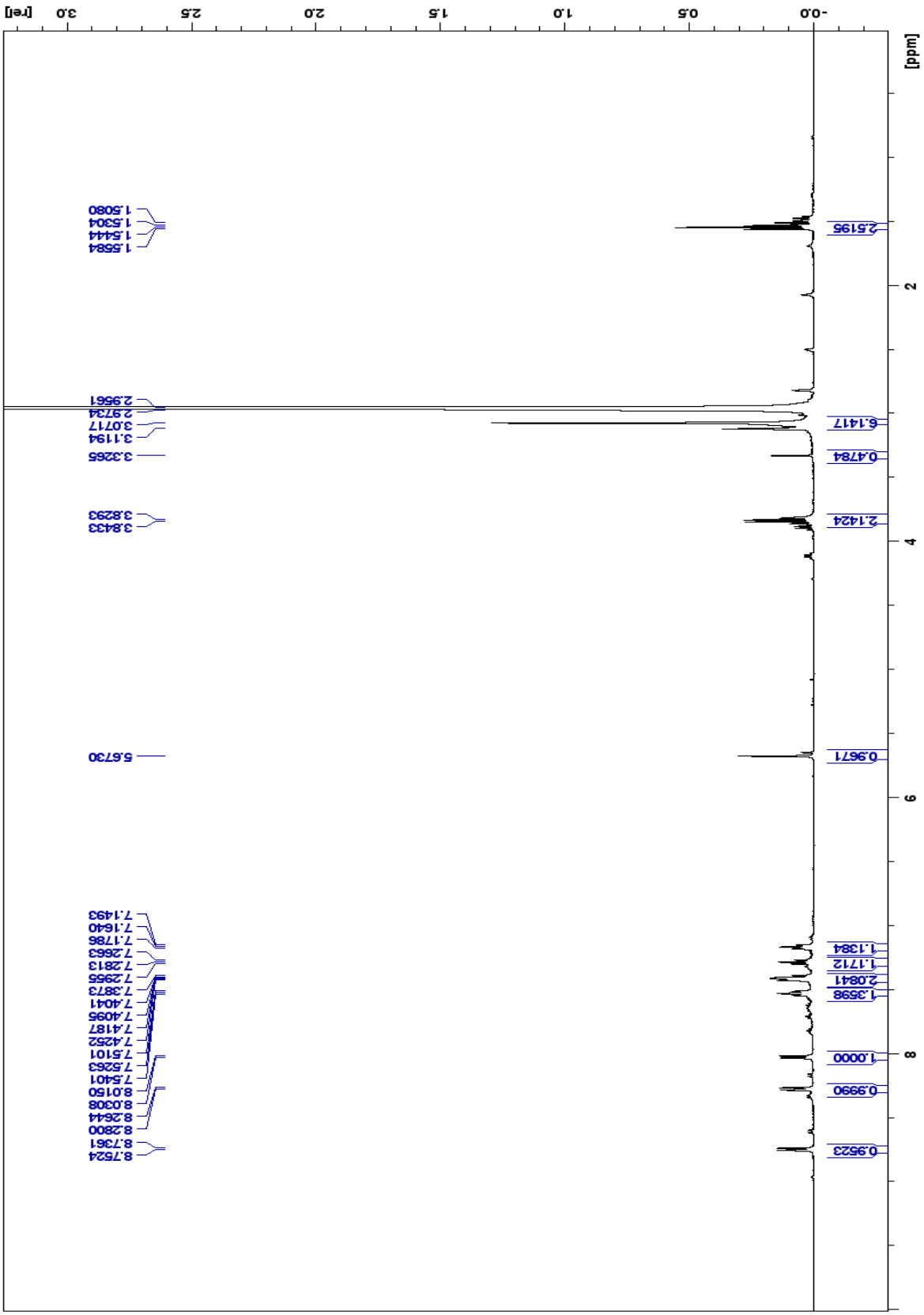

Spectrum 38*: 10a* ***^{1}H NMR (500 MHz, DMSO-d6)***

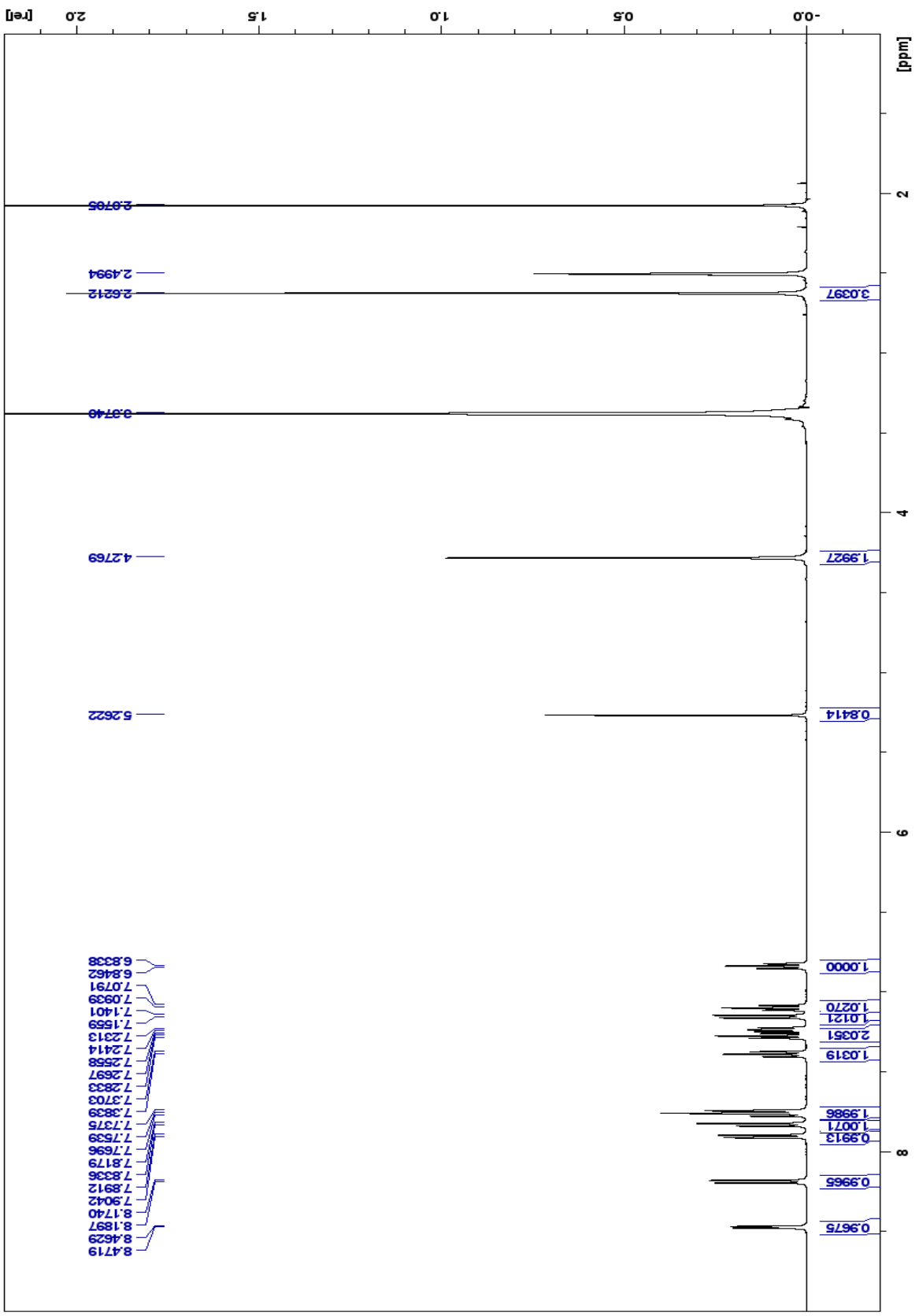

Spectrum 39*: 10b* ***¹H NMR (500 MHz, DMSO-d6)***

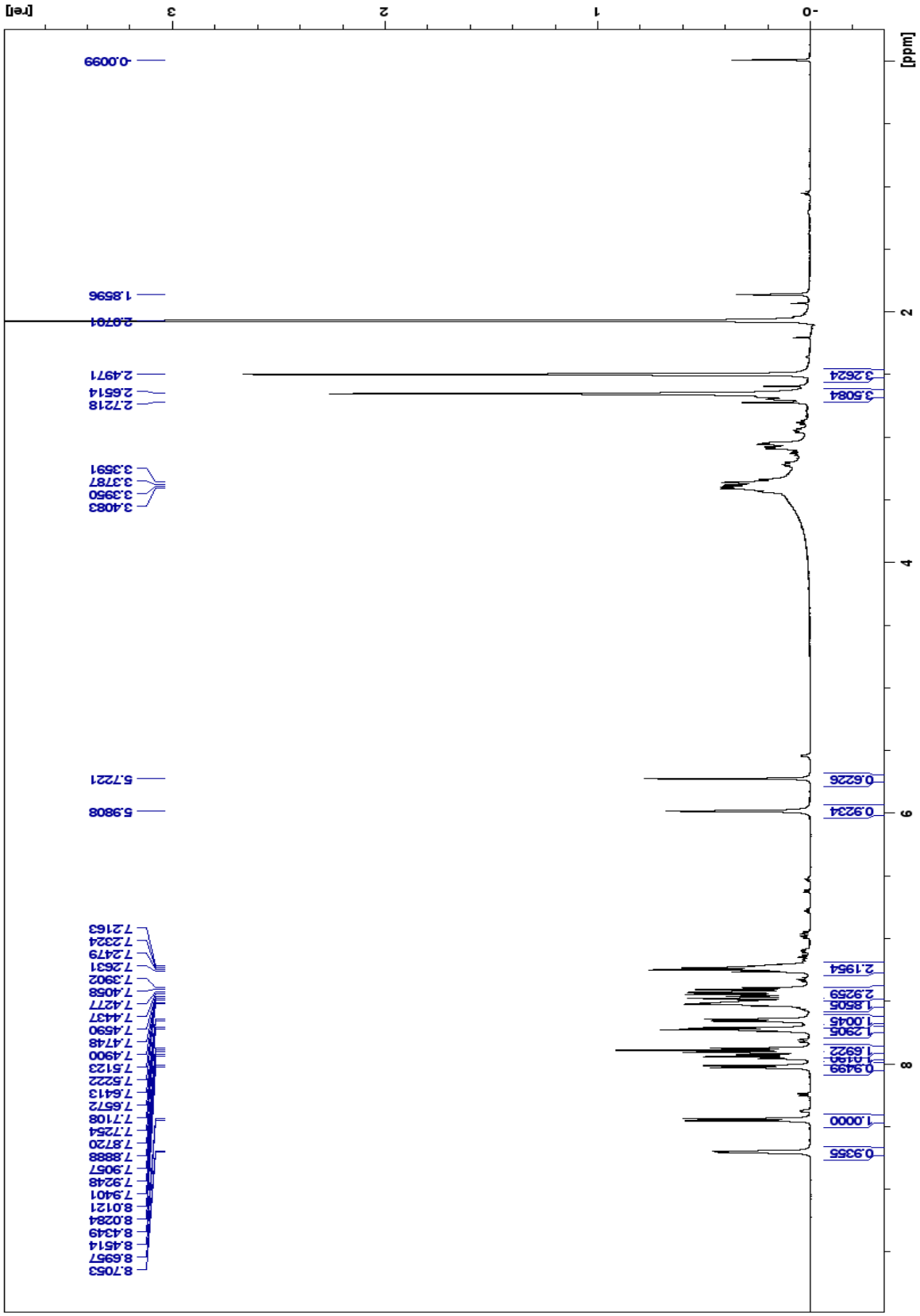

Spectrum 40*: 10b-Zn* ***^{1}H NMR (500 MHz, DMSO-d6)***

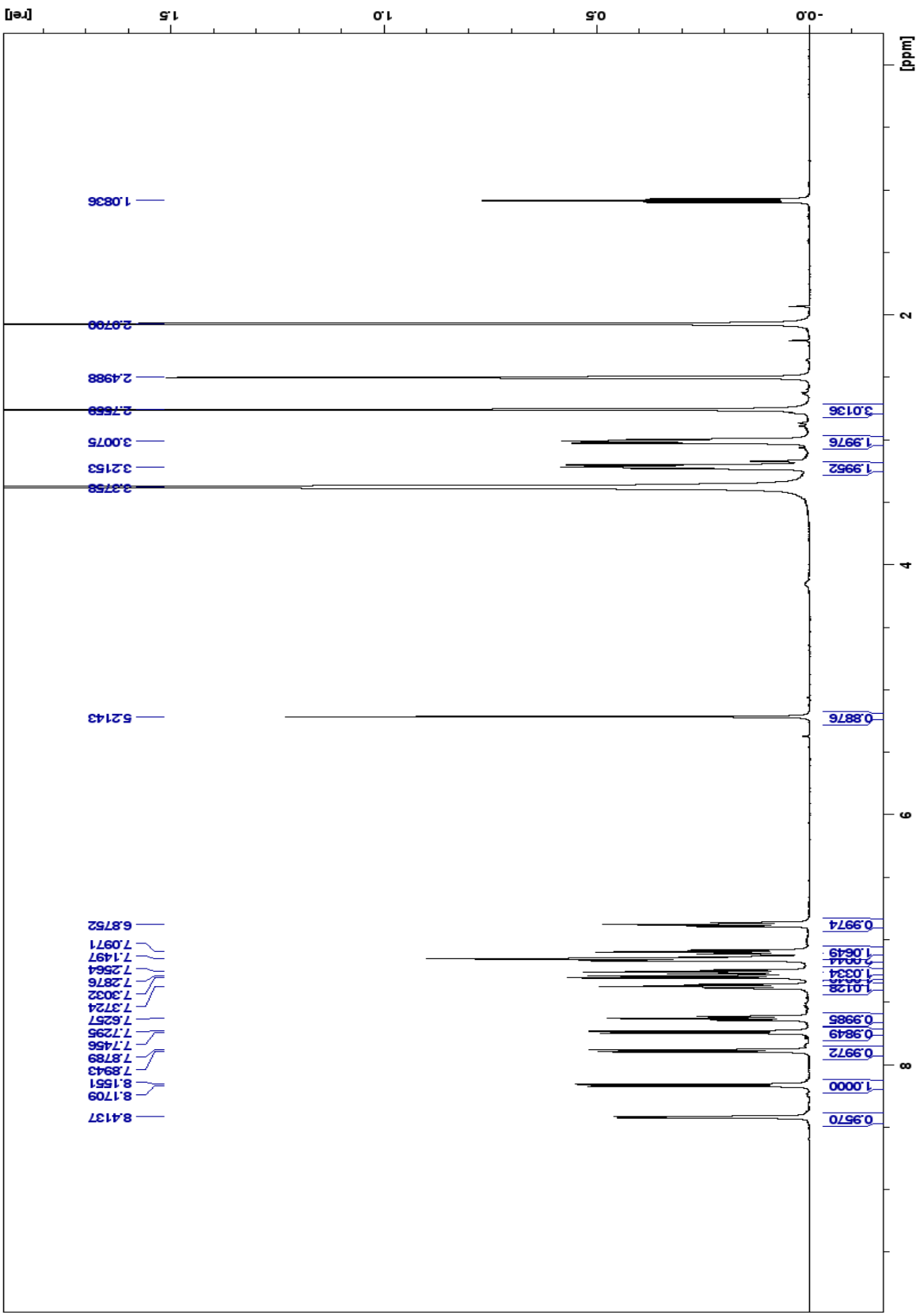

Spectrum 41*: 10c* ***¹H NMR (500 MHz, DMSO-d6)***

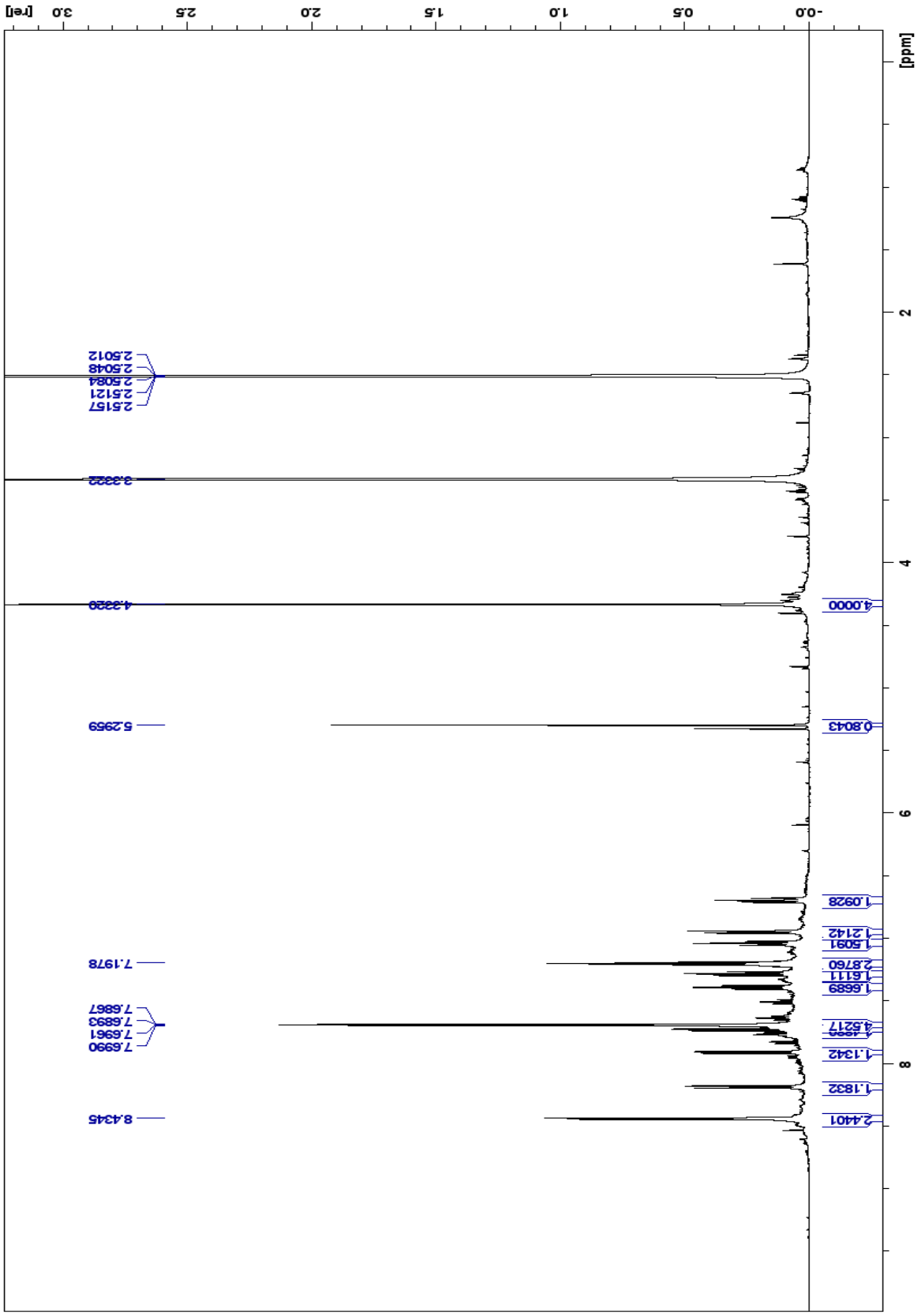

Spectrum 42*: 10d* ***^{1}H NMR (500 MHz, DMSO-d6)***

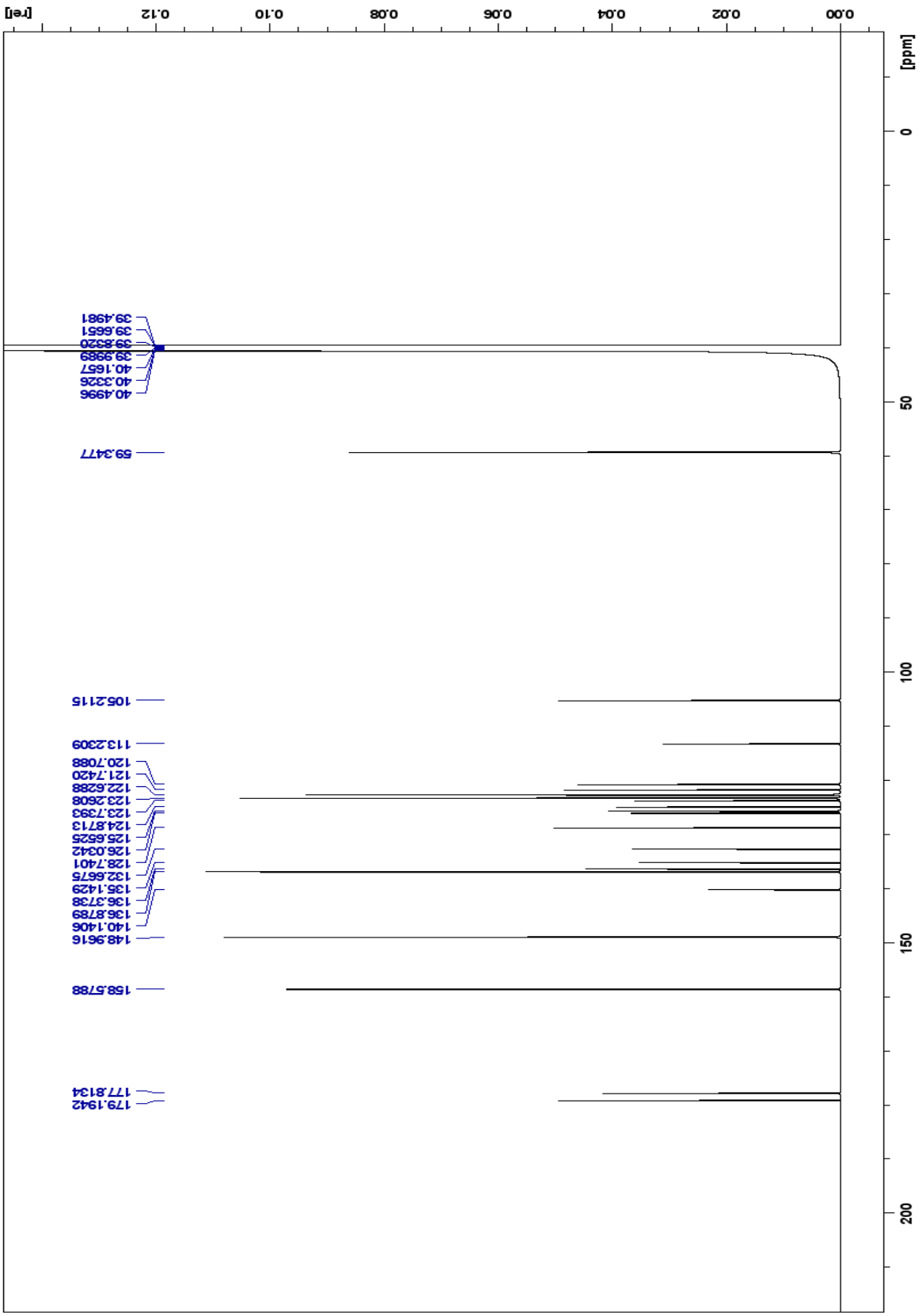

Spectrum 43*: 10d* ***^{13}C NMR (500 MHz, DMSO-d6)***

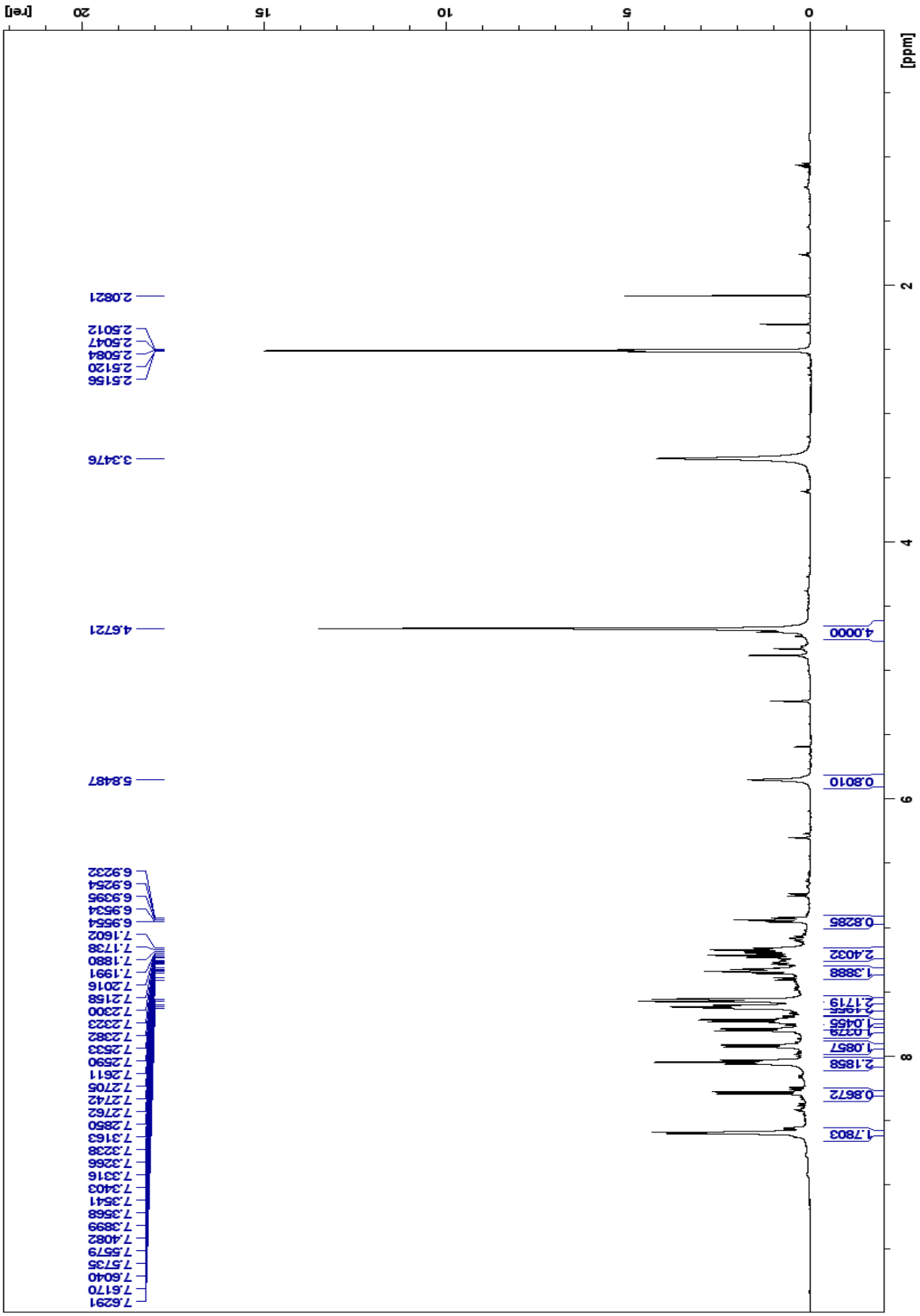

Spectrum 44*: 10d-zn* ***¹H NMR (500 MHz, DMSO-d6)***

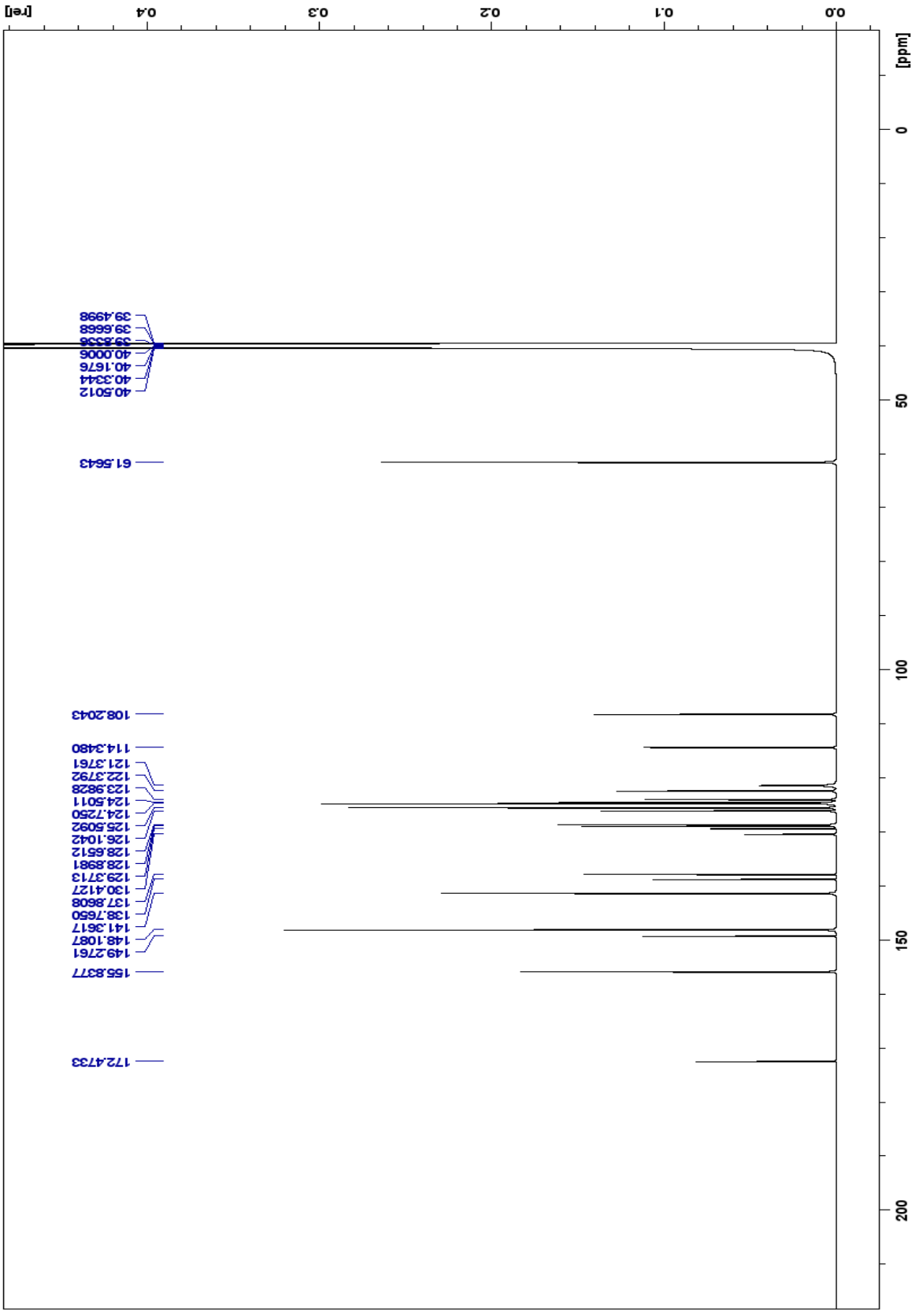

Spectrum 45*: 10d-Zn* ***^{13}C NMR (500 MHz, DMSO-d6)***

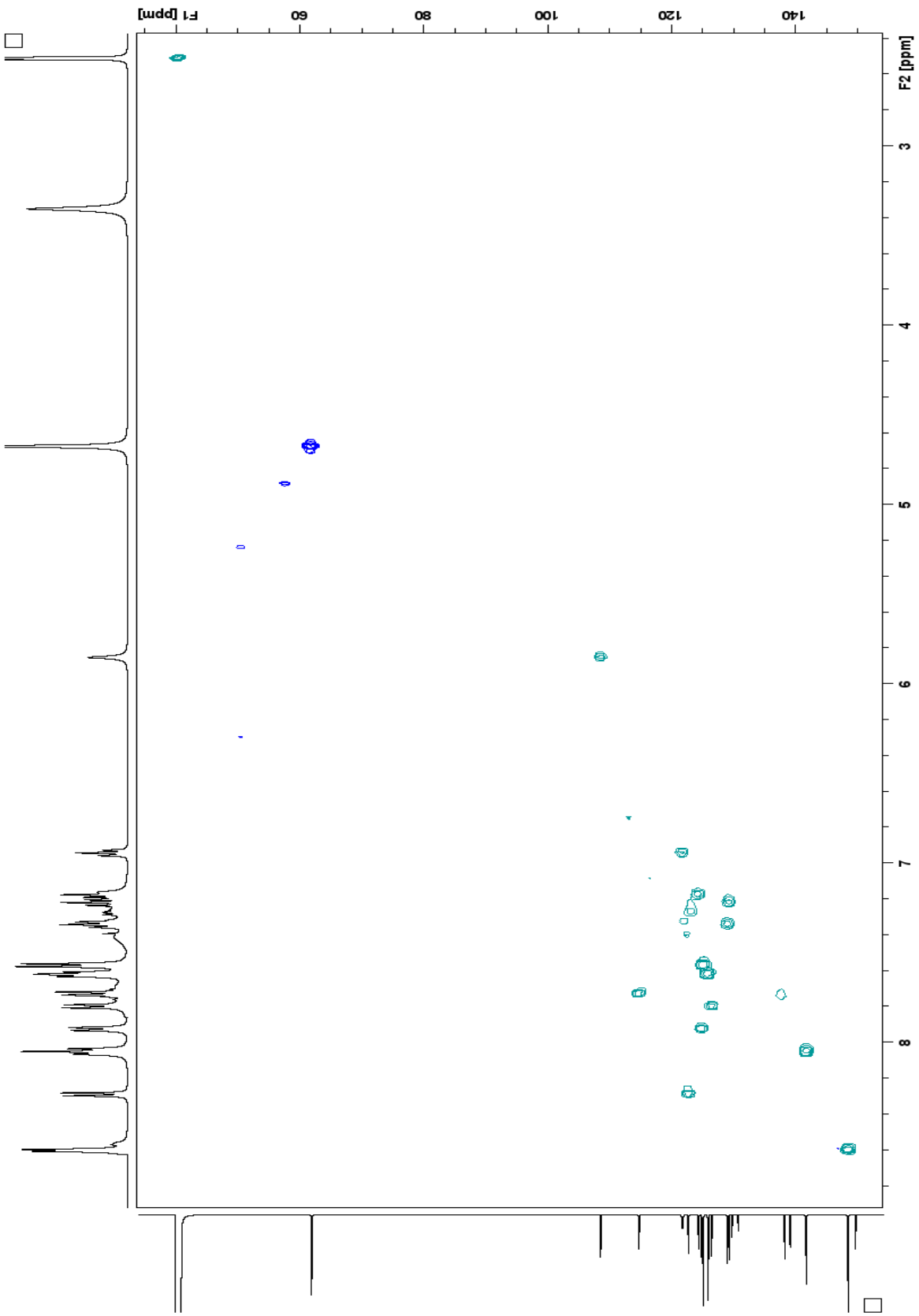

Spectrum 46*: 10d-Zn* ***HSQC (500 MHz, DMSO-d6)***

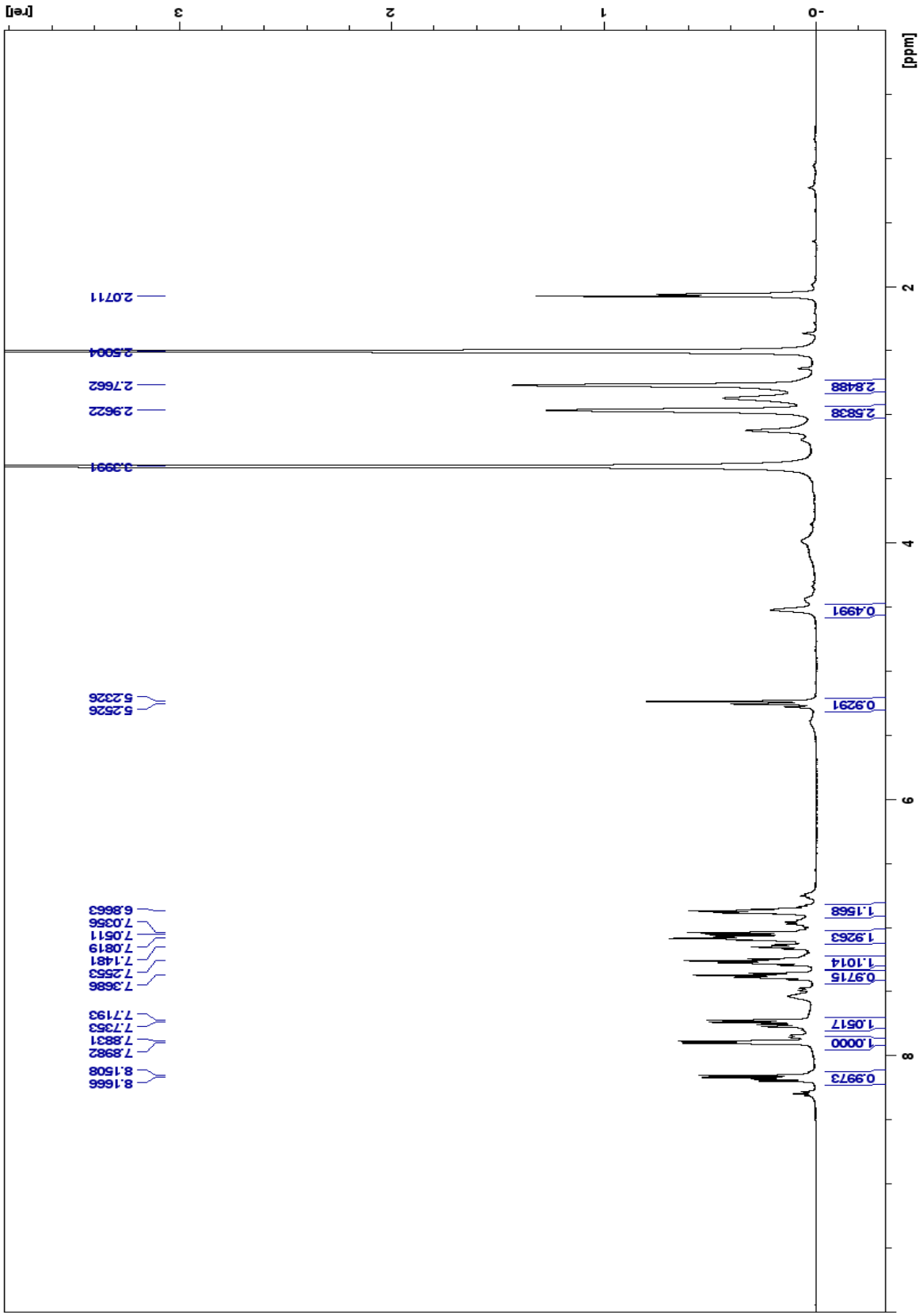

Spectrum 47*: 10e* ***^{1}H NMR (500 MHz, DMSO-d6)***

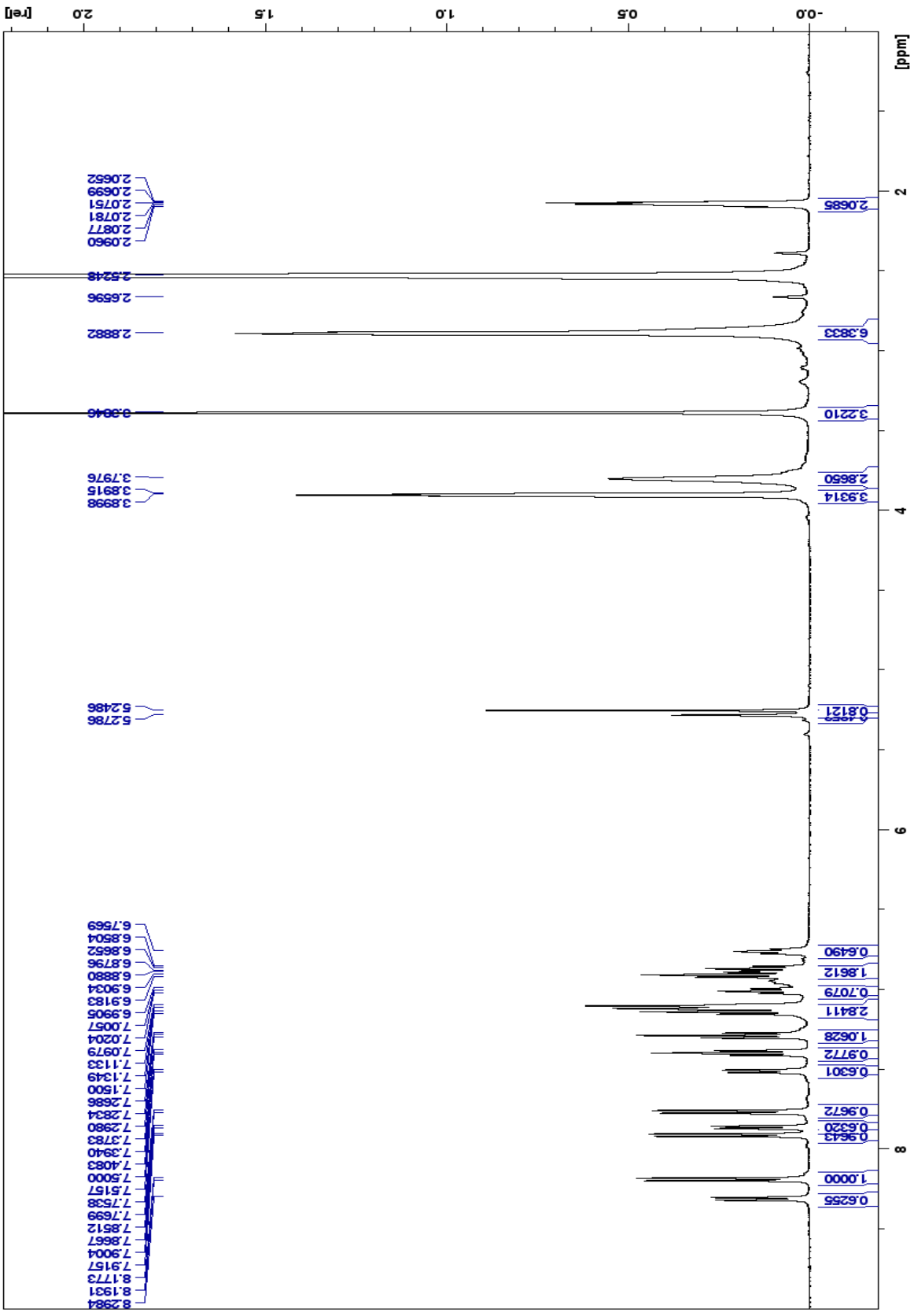

Spectrum 48*: 10f* ^{1}***H NMR (500 MHz, DMSO-d6)***

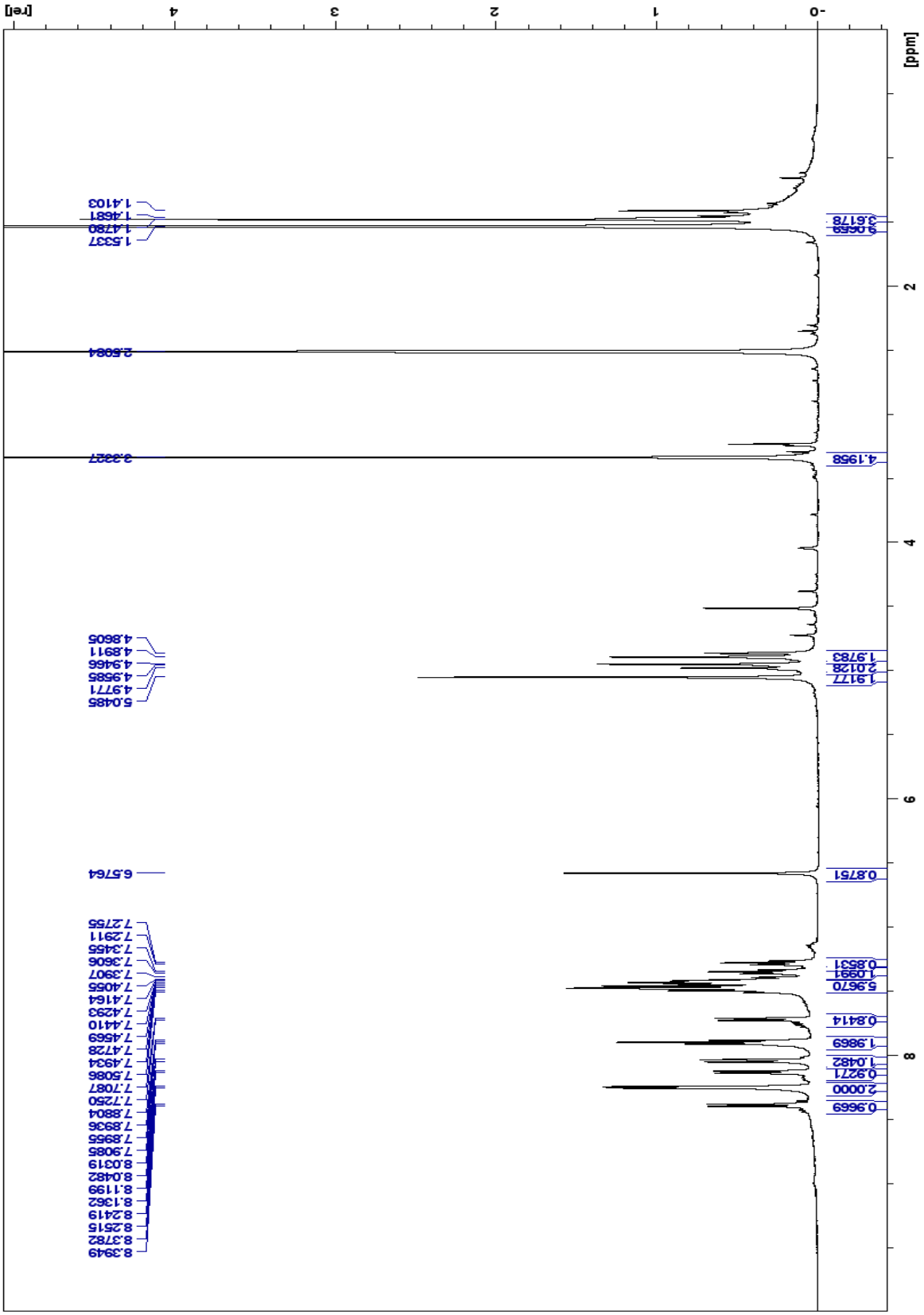

Spectrum 49*: 11* ^{1}***H NMR (500 MHz, DMSO-d6)***

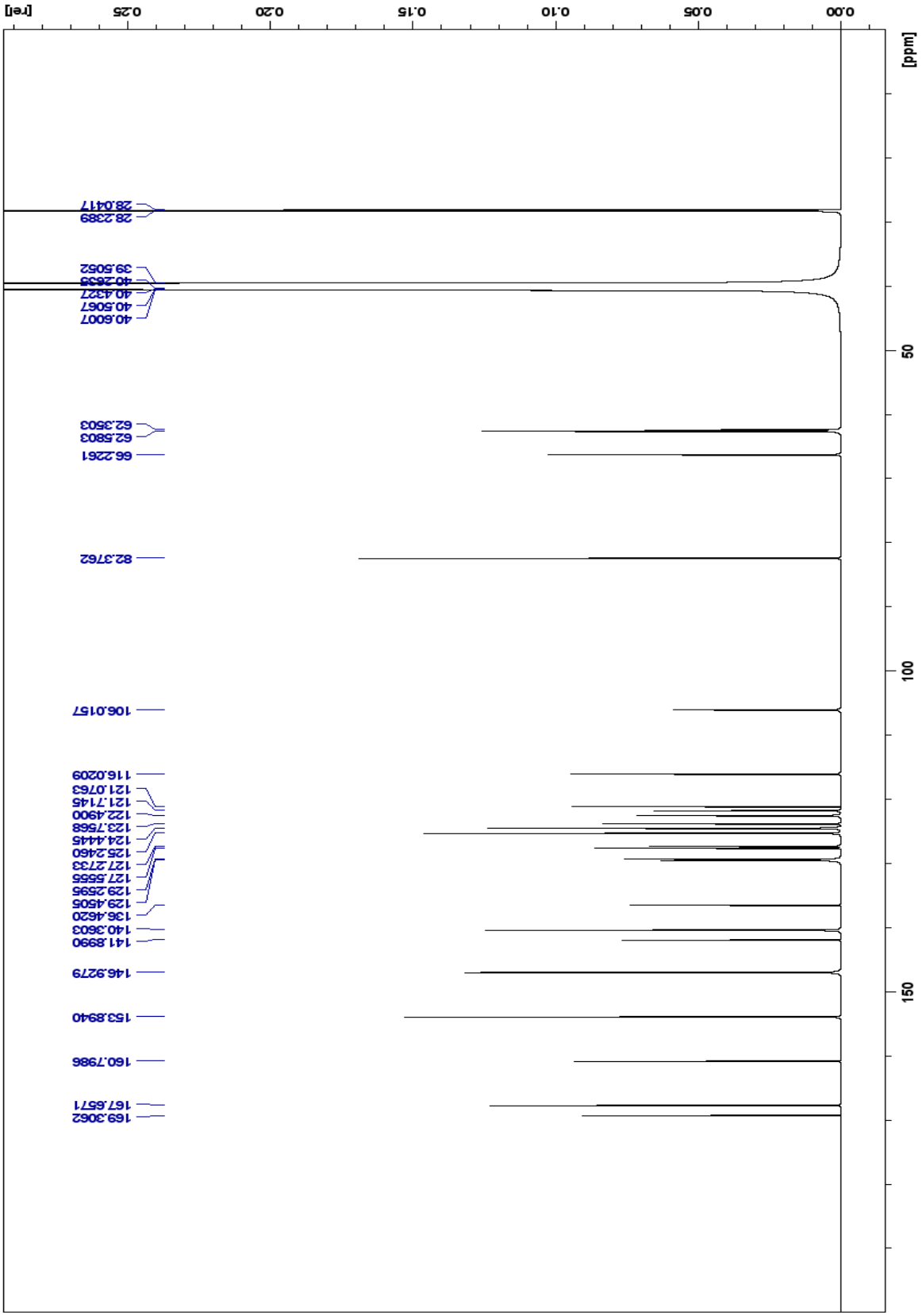

Spectrum 50*: 11 ^{13}C NMR (500 MHz, DMSO-d6)*

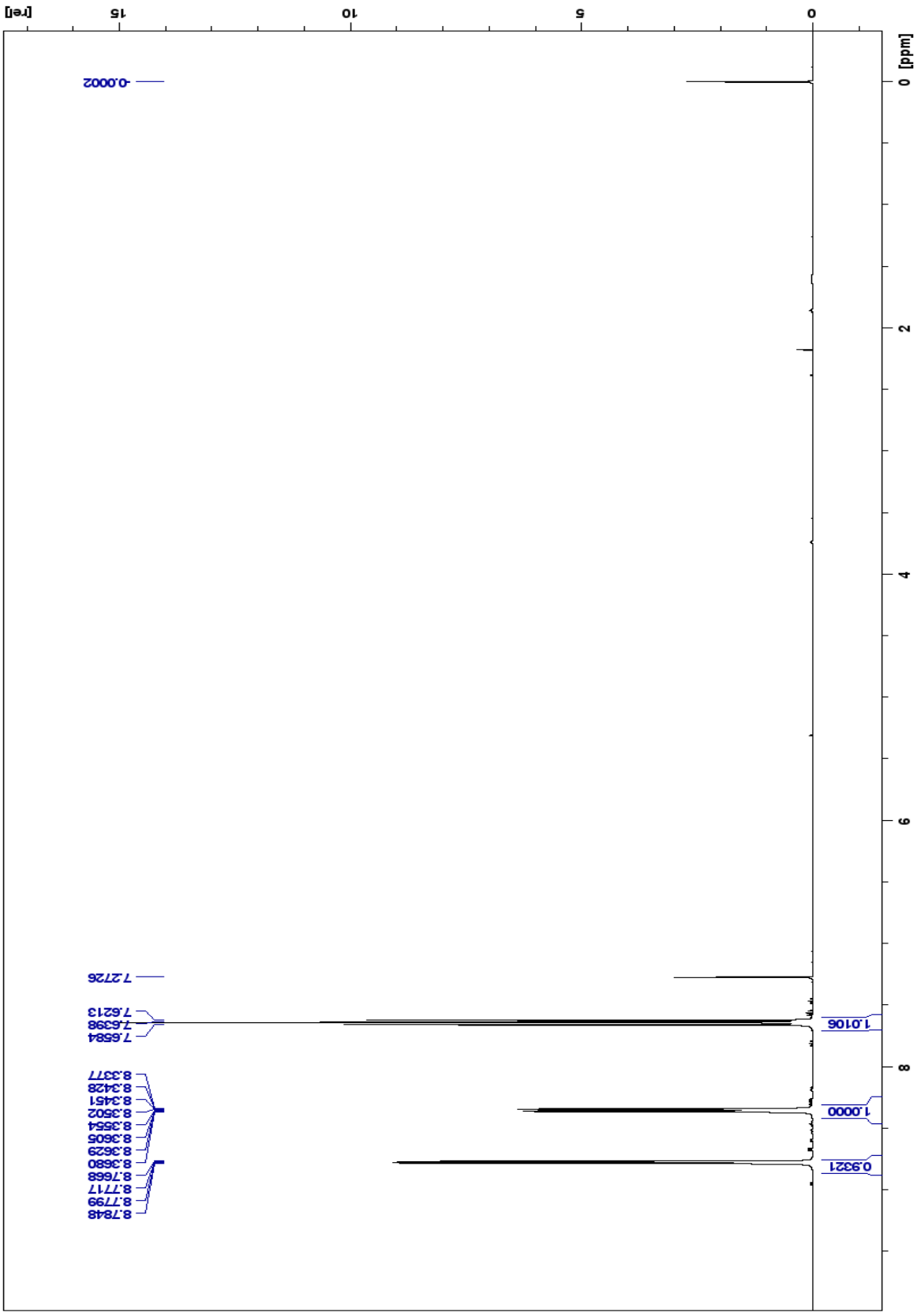

Spectrum 51*: 12* ***^{1}H NMR (500 MHz, $CDCl_3$)***

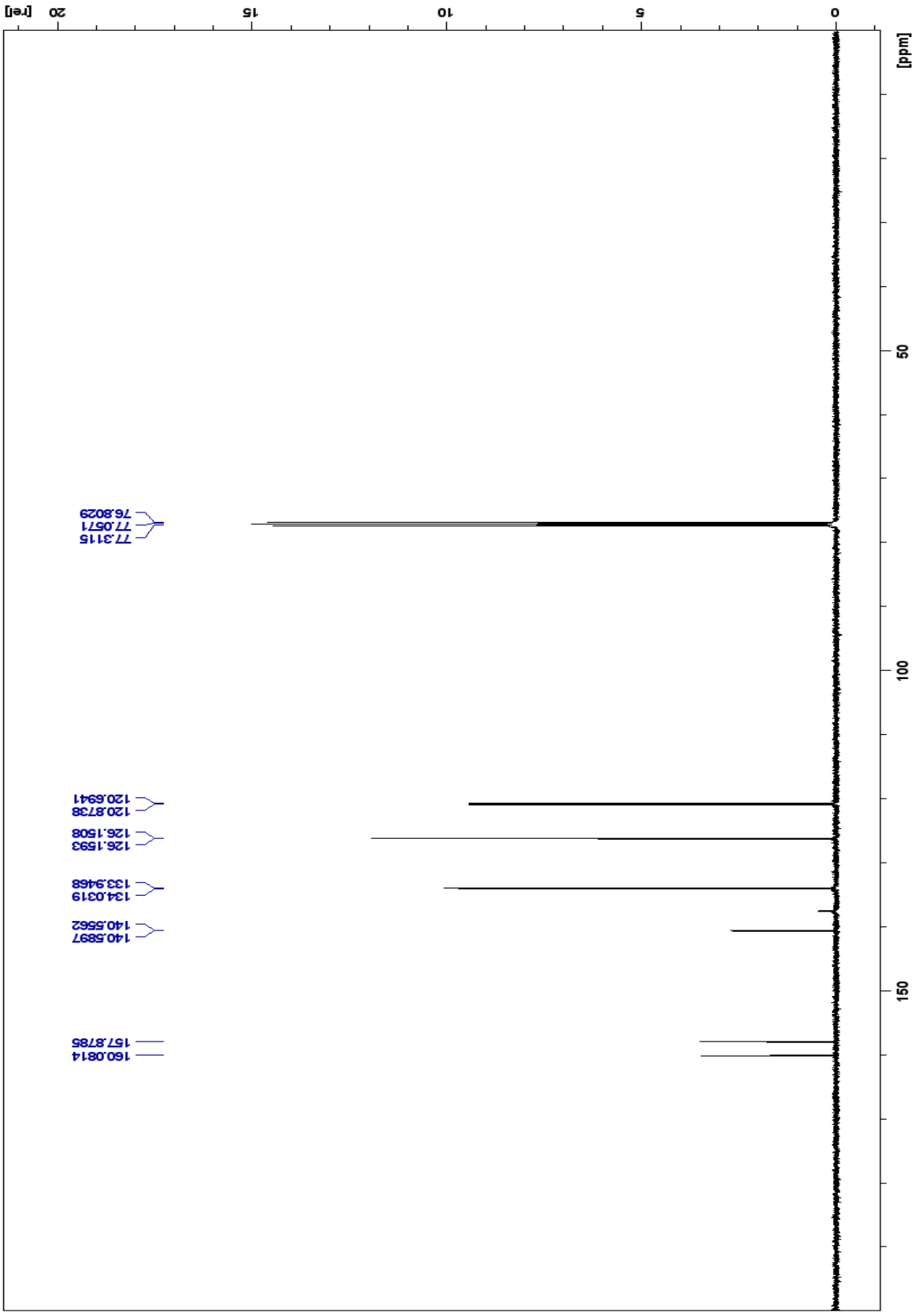

Spectrum 52*: 12* ^{13}*C NMR (500 MHz,* $CDCl_3$*)*

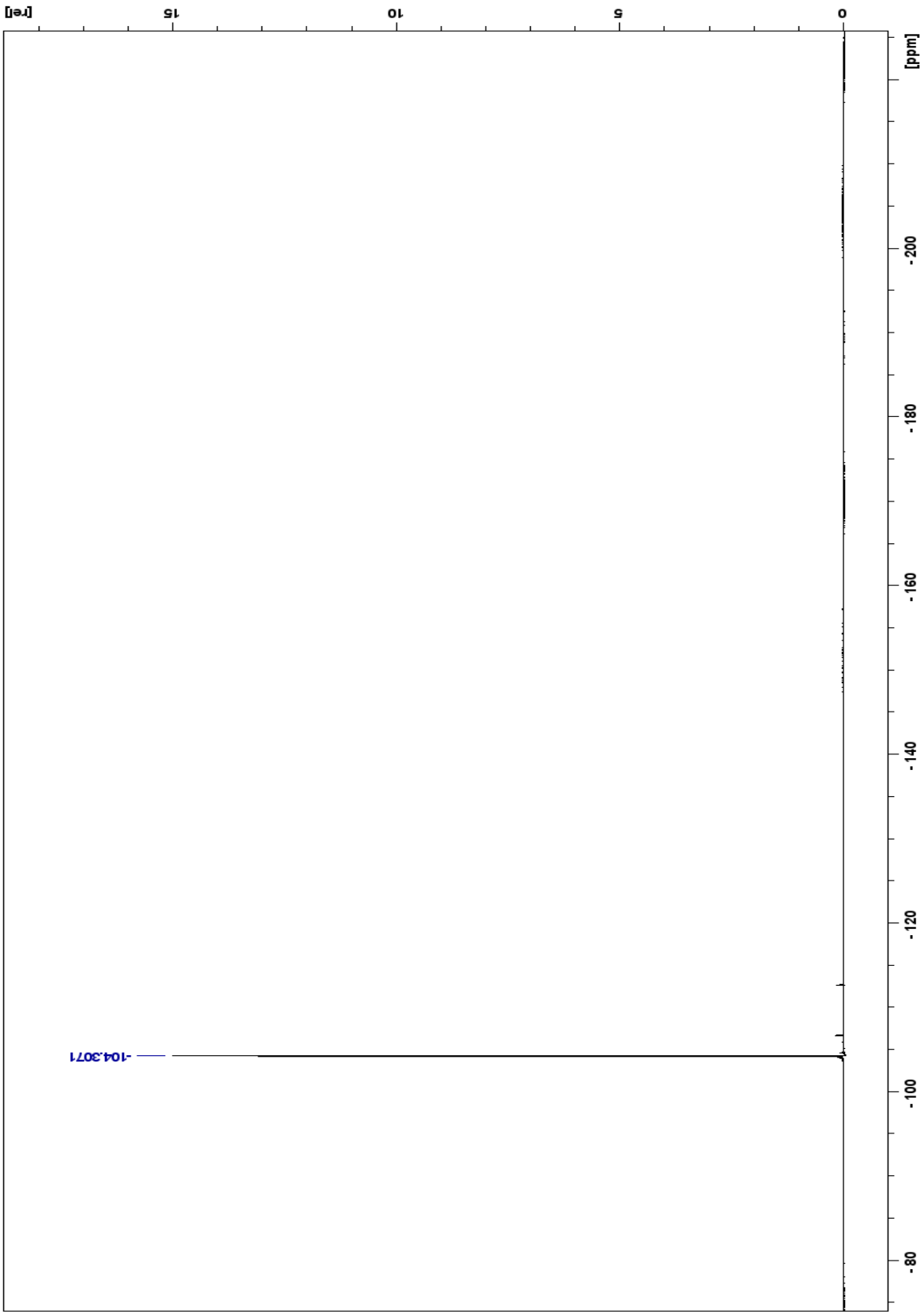

Spectrum 53*: 12 ^{19}F NMR (500 MHz, $CDCl_3$)*

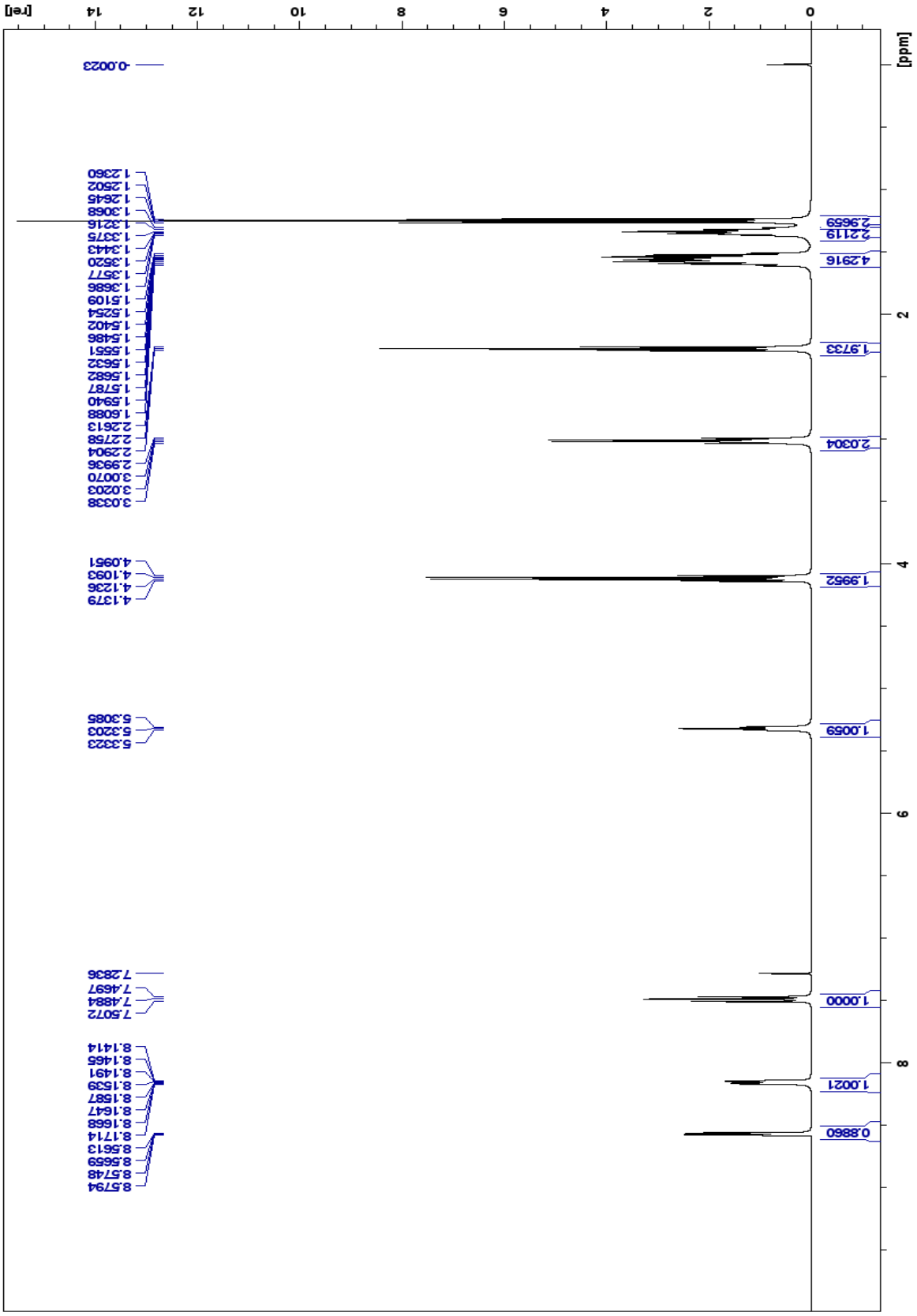

Spectrum 54*: 13* ^{1}***H NMR (500 MHz,*** $CDCl_3$***)***

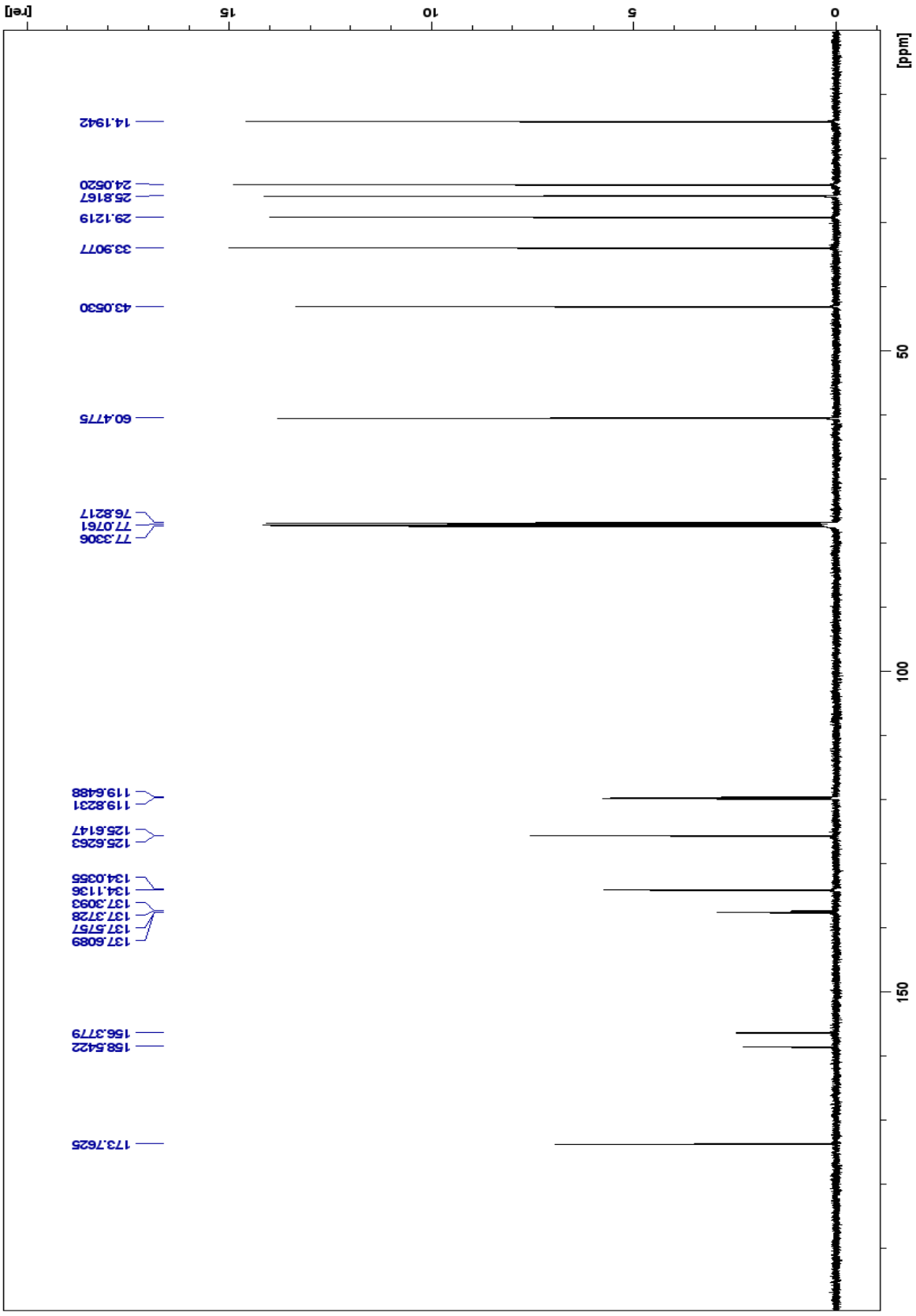

Spectrum 55*: 13* ^{13}*C NMR (500 MHz, CDCl*$_3$*)*

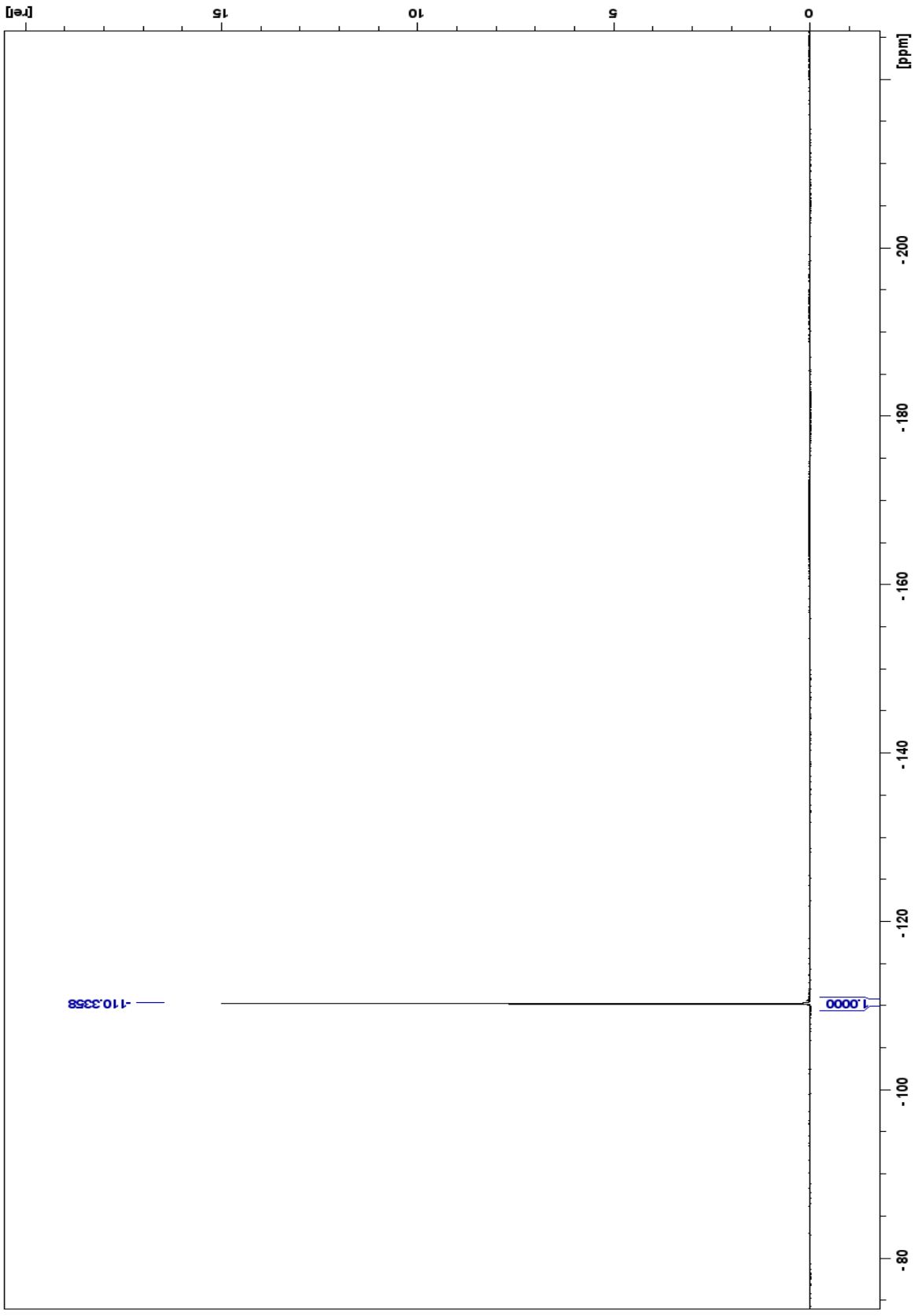

Spectrum 56*: 13* ***^{19}F NMR (500 MHz, $CDCl_3$)***

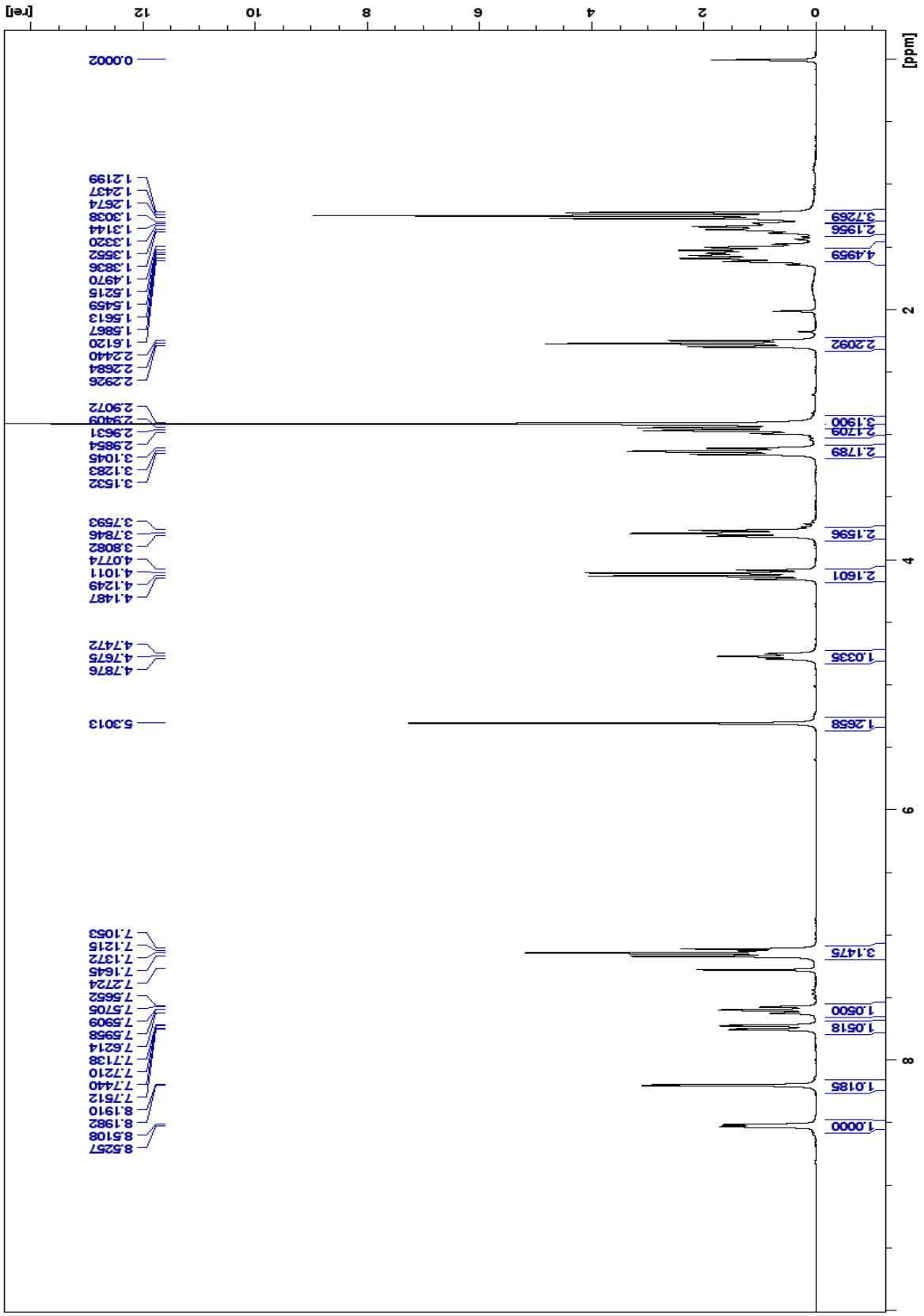

Spectrum 57*: 14a* ^{1}***H NMR (300 MHz,*** $CDCl_3$***)***

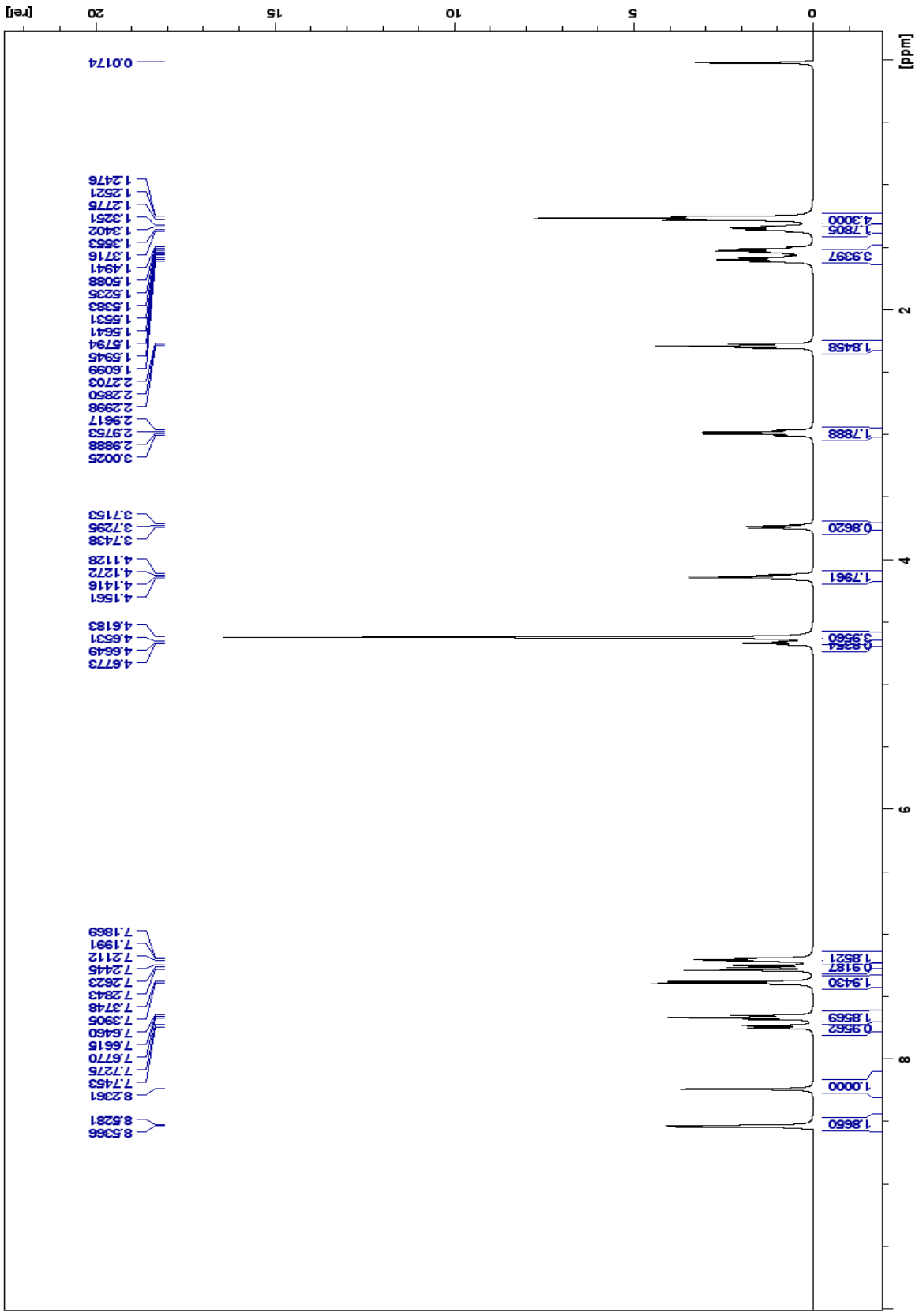

Spectrum 58*: 14b* ***^{1}H NMR (500 MHz, $CDCl_3$)***

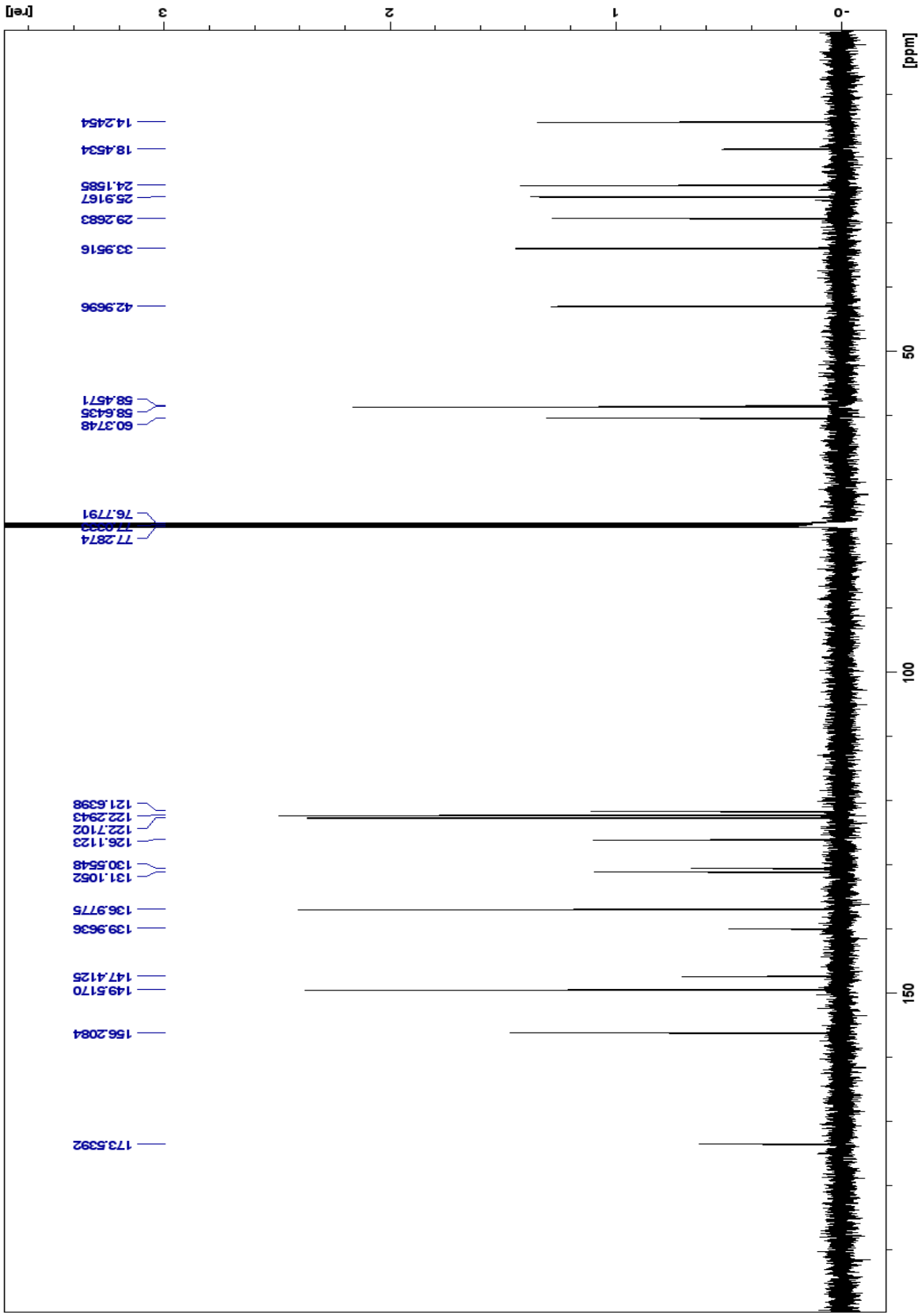

Spectrum 59*: 14b* ***^{13}C NMR (500 MHz, $CDCl_3$)***

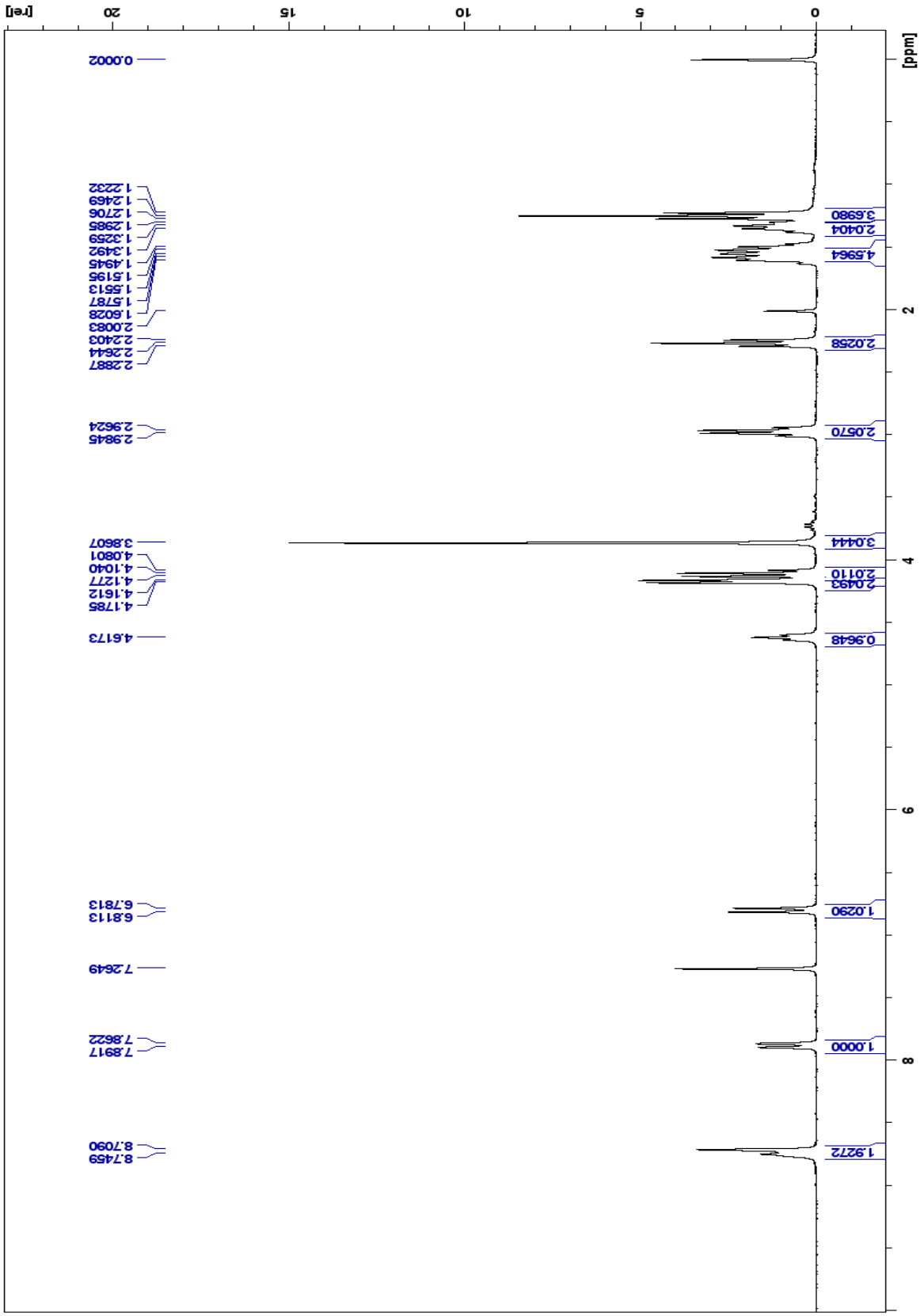

Spectrum 60*: 14c* ***^{1}H NMR (300 MHz, $CDCl_3$)***

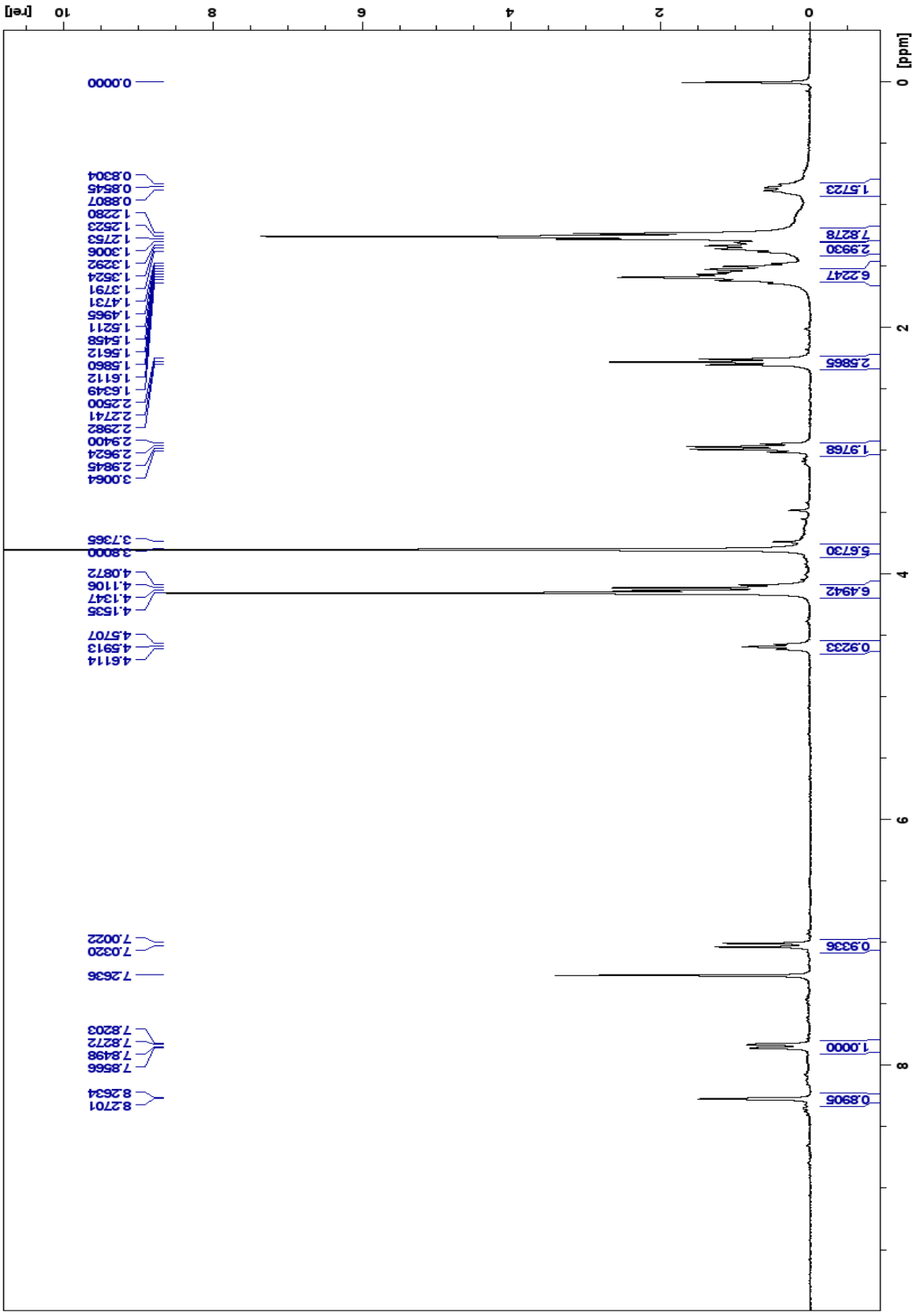

Spectrum 61*: 14d* ^{1}***H NMR (300 MHz,*** $CDCl_3$***)***

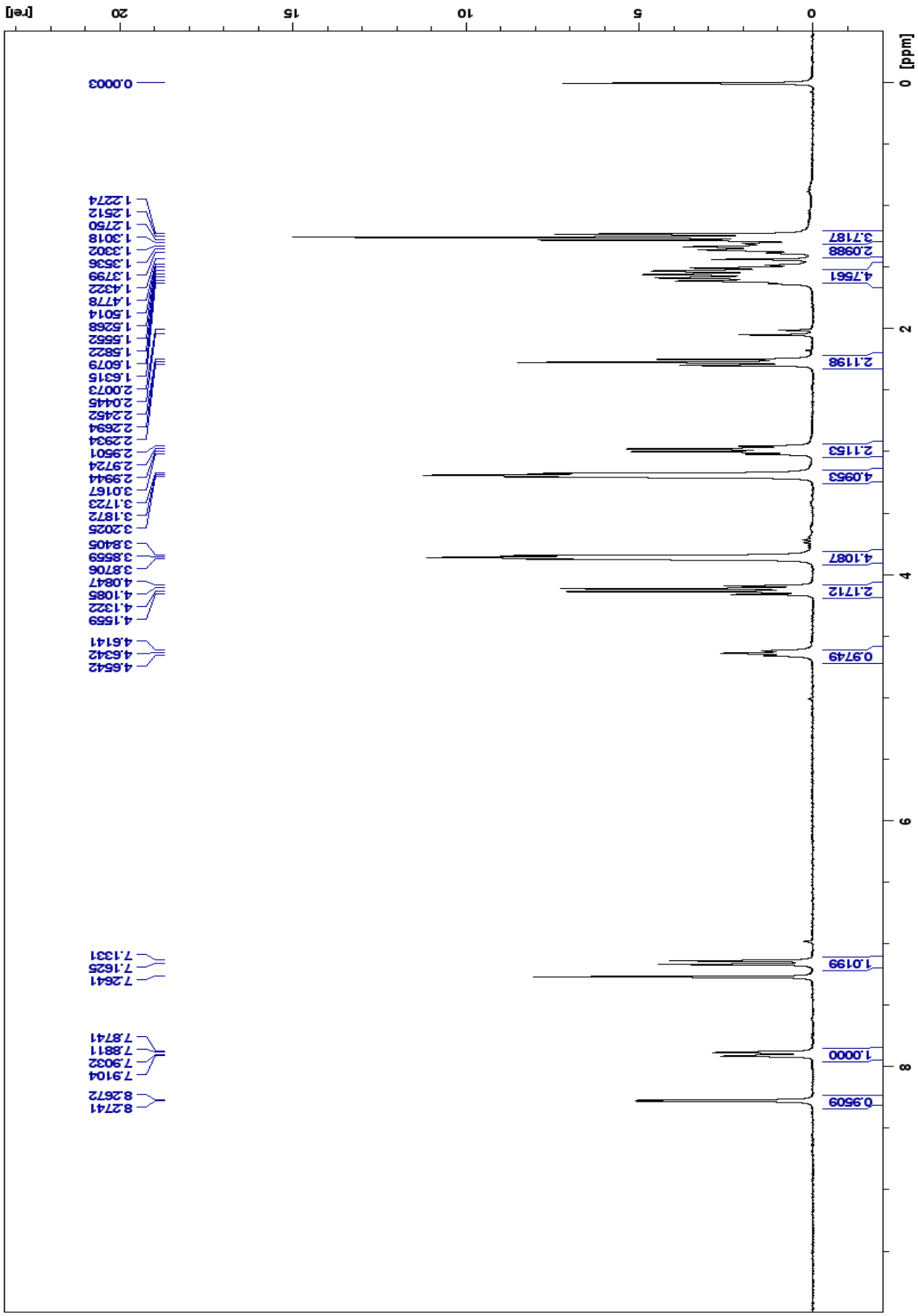

Spectrum 62*: 14e* ***^{1}H NMR (300 MHz, $CDCl_3$)***

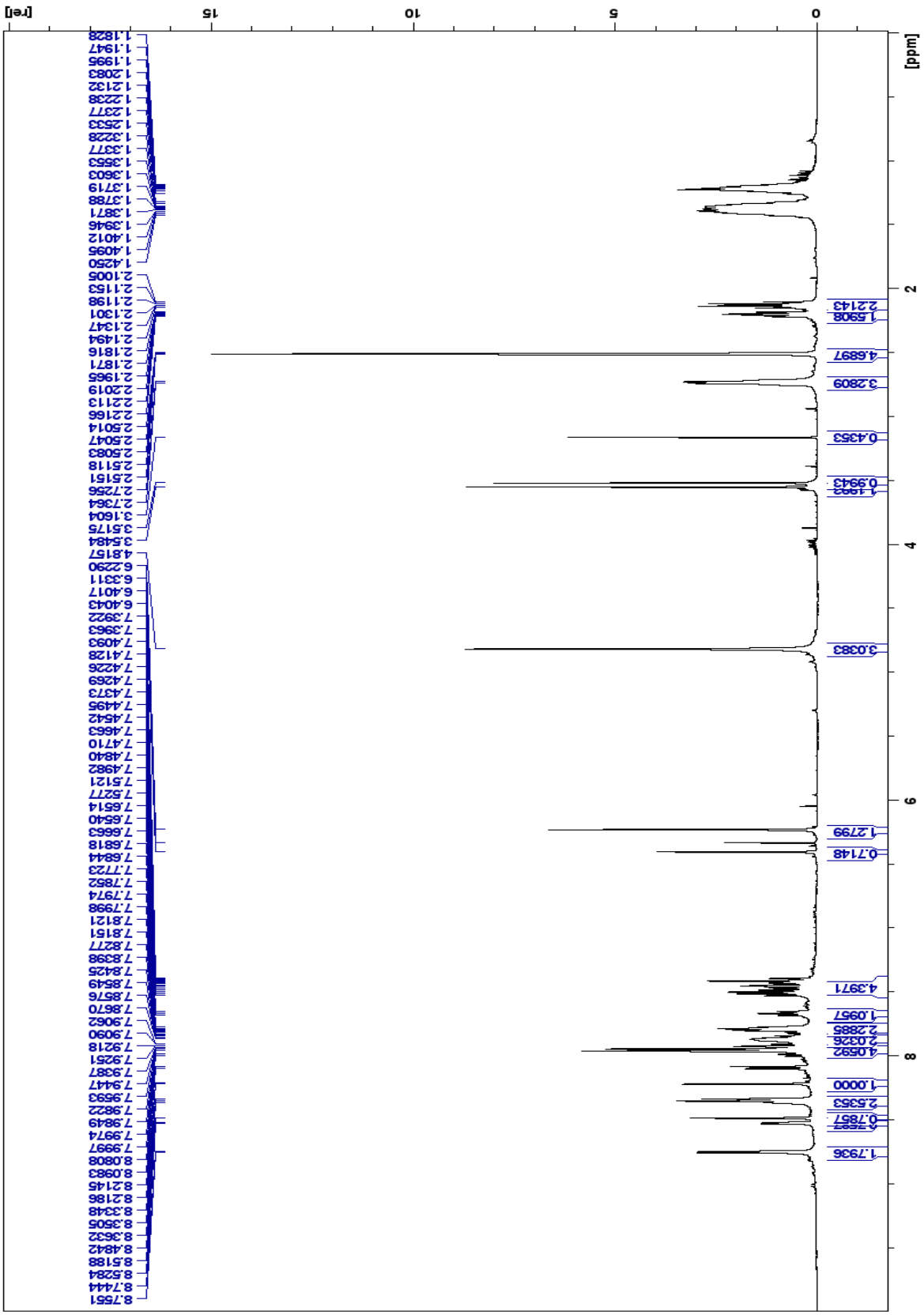

Spectrum 63*: 16a* ***[1]H NMR (500 MHz, DMSO-d6)***

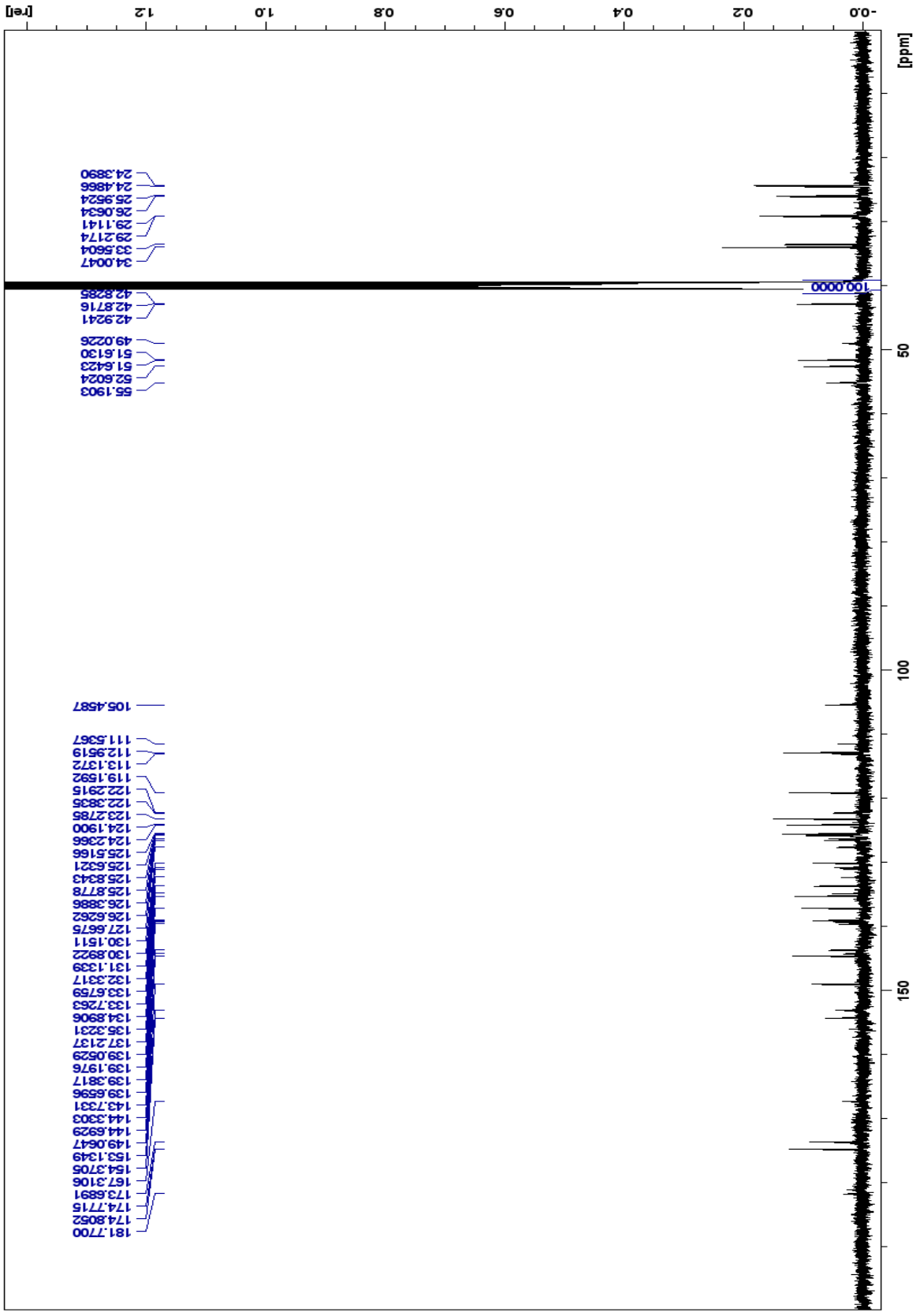

Spectrum 64*: 16a* ***^{13}C NMR (500 MHz, DMSO-d6)***

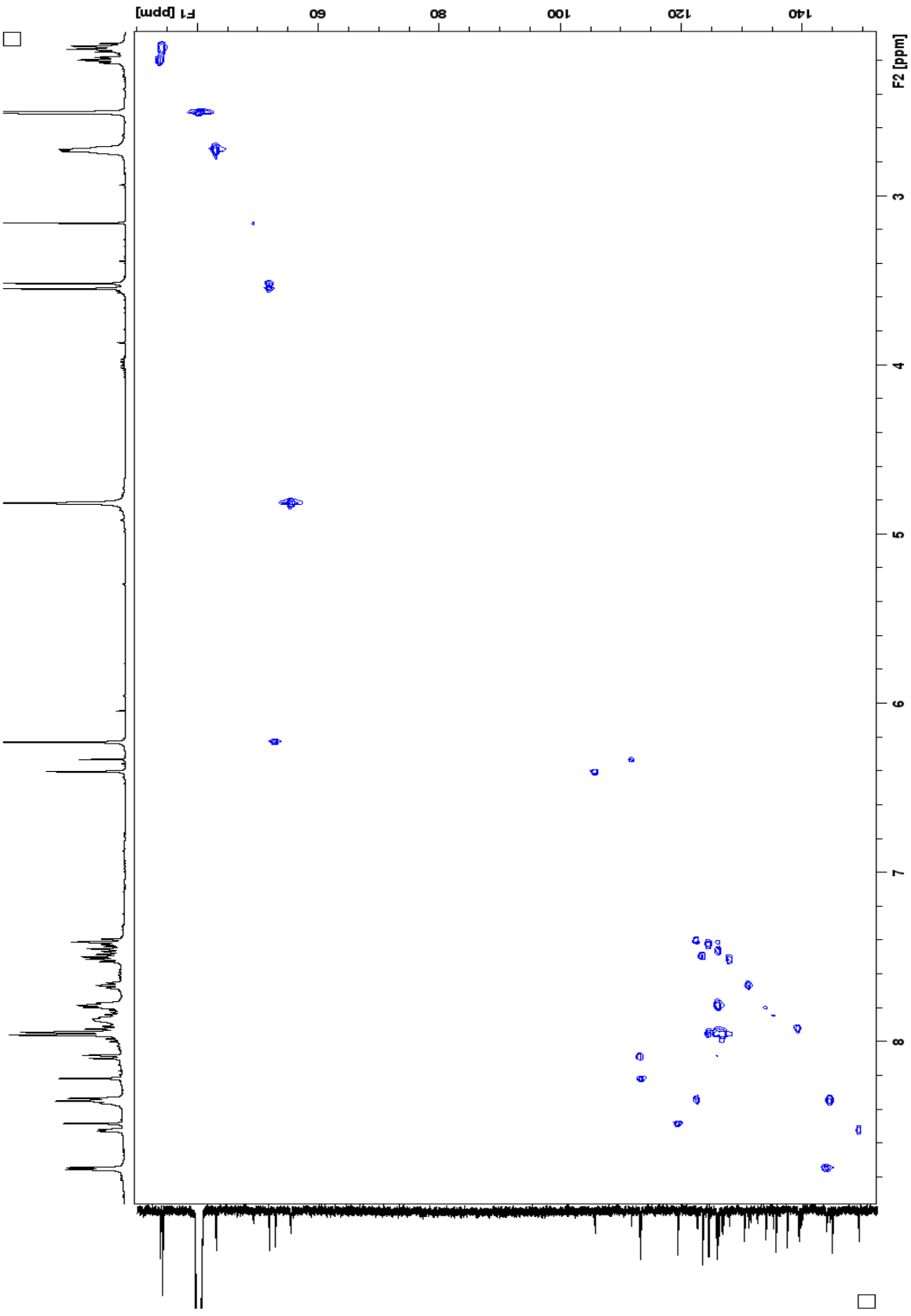

Spectrum 65*: 16a* ***HSQC (500MHz, DMSO-d6)***

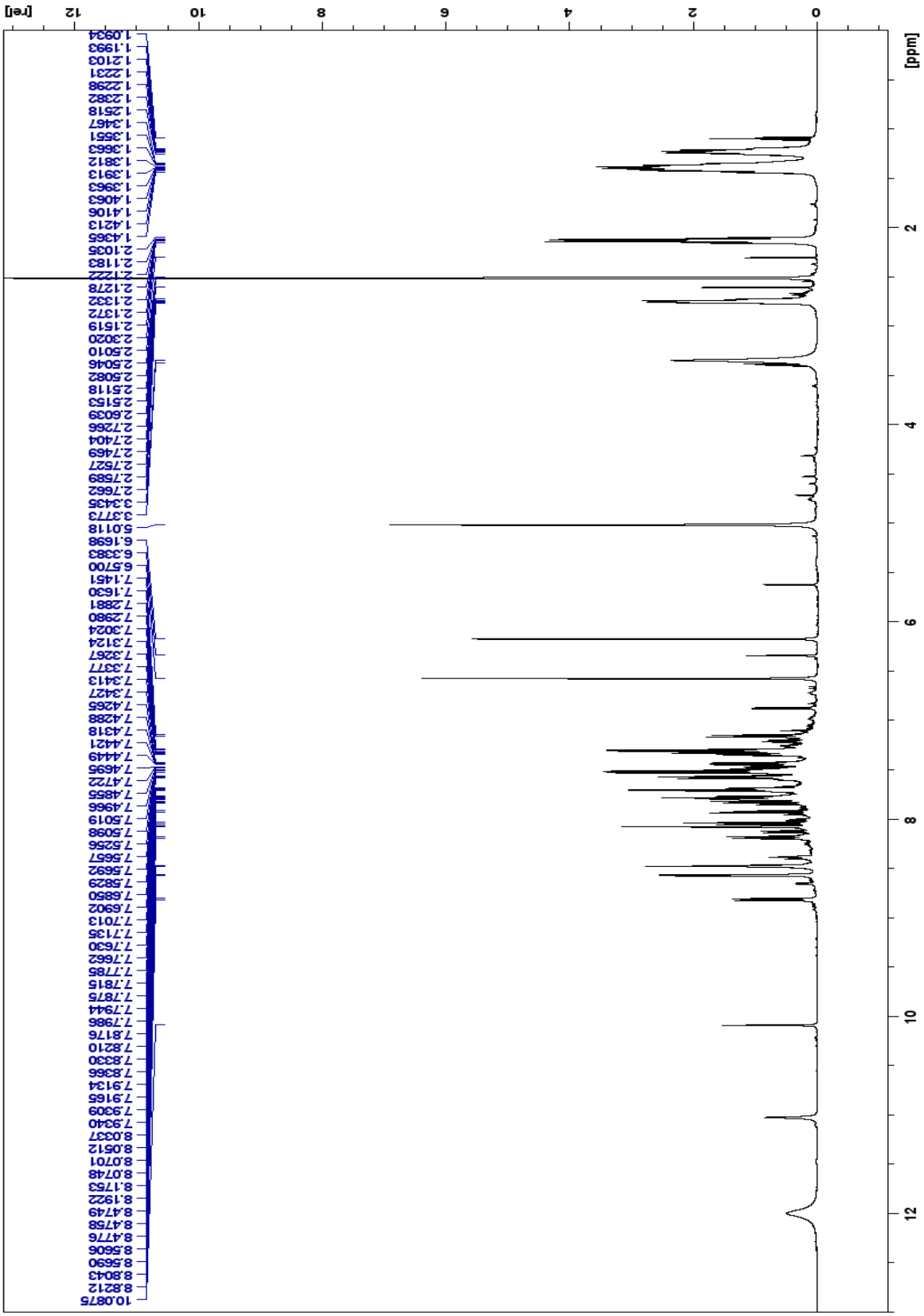

Spectrum 66*: 16b* ***^{1}H NMR (500 MHz, DMSO-d6)***

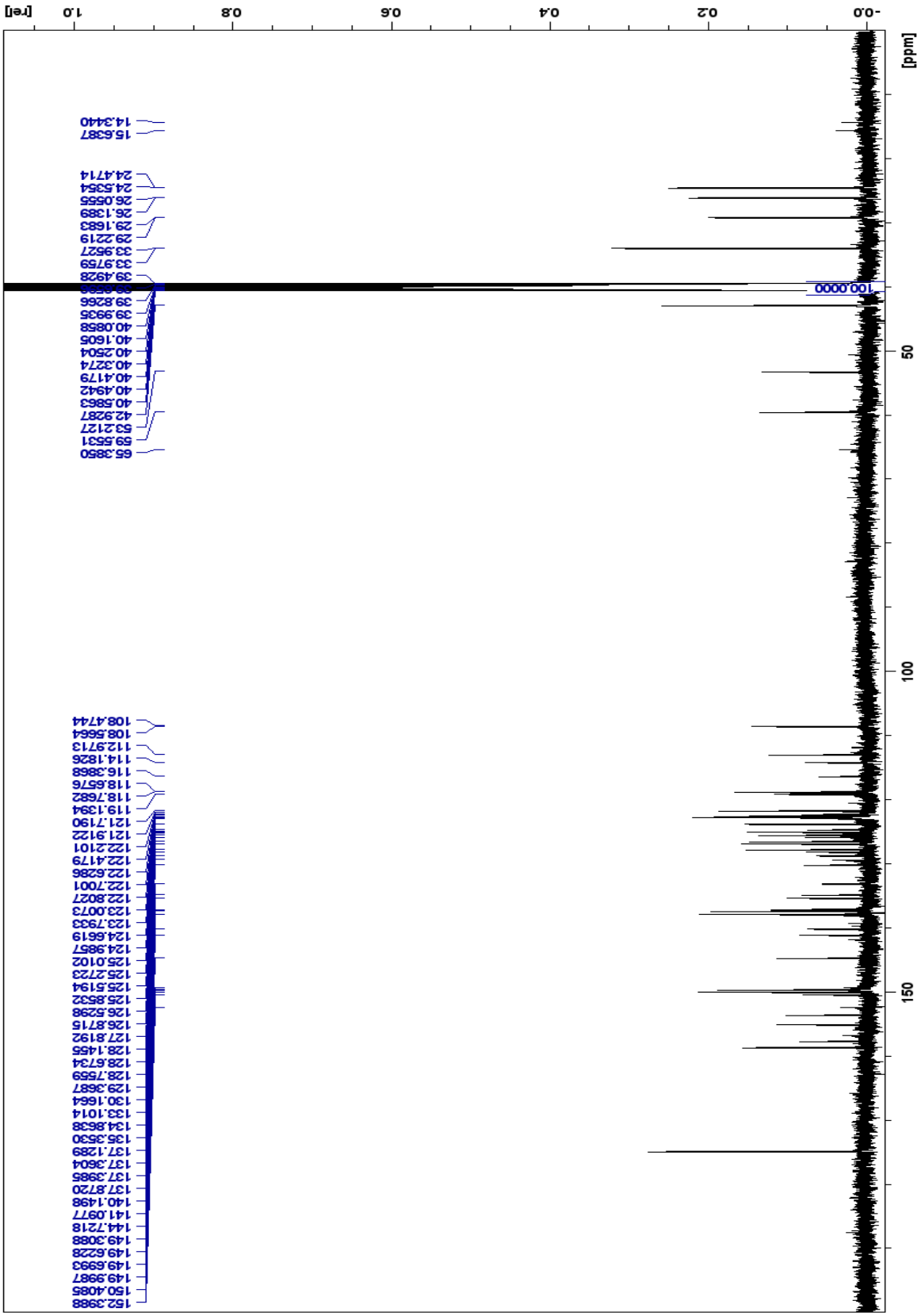

Spectrum 67*: 16b* ***^{13}C NMR (500 MHz, DMSO-d6)***

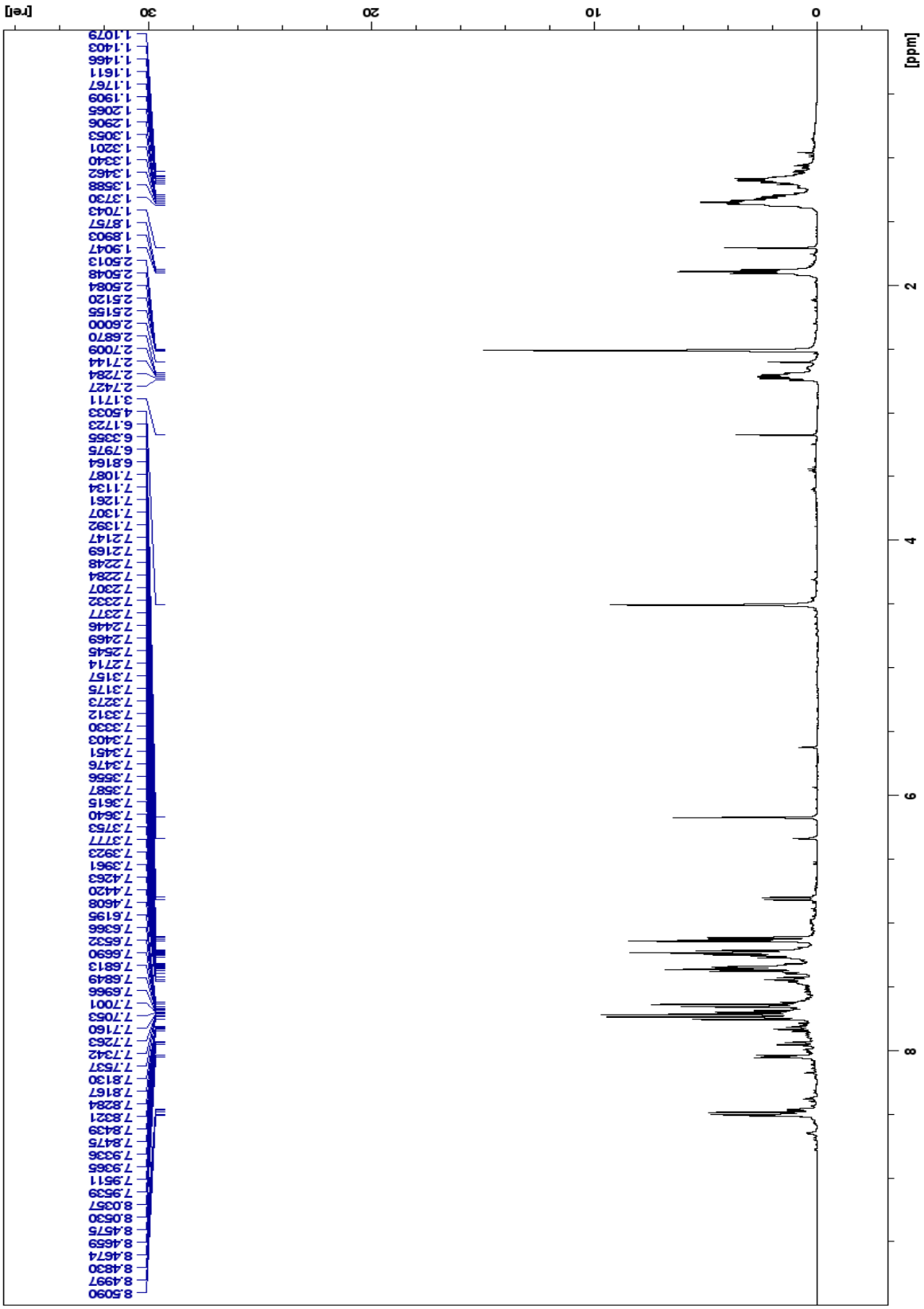

Spectrum 68*: 16c* ***^{1}H NMR (500 MHz, DMSO-d6)***

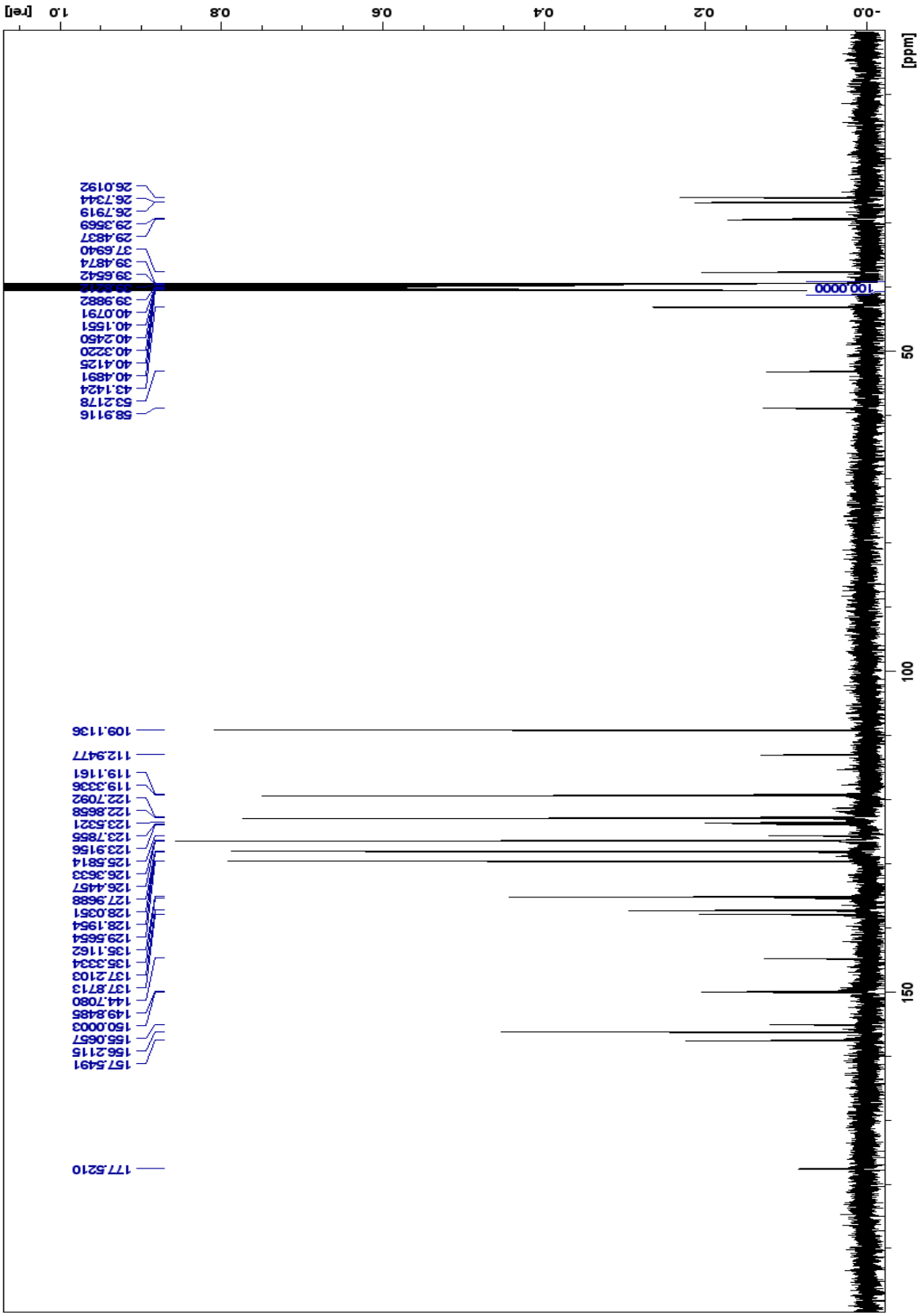

Spectrum 69*: 16c* ***^{13}C NMR (500 MHz, DMSO-d6)***

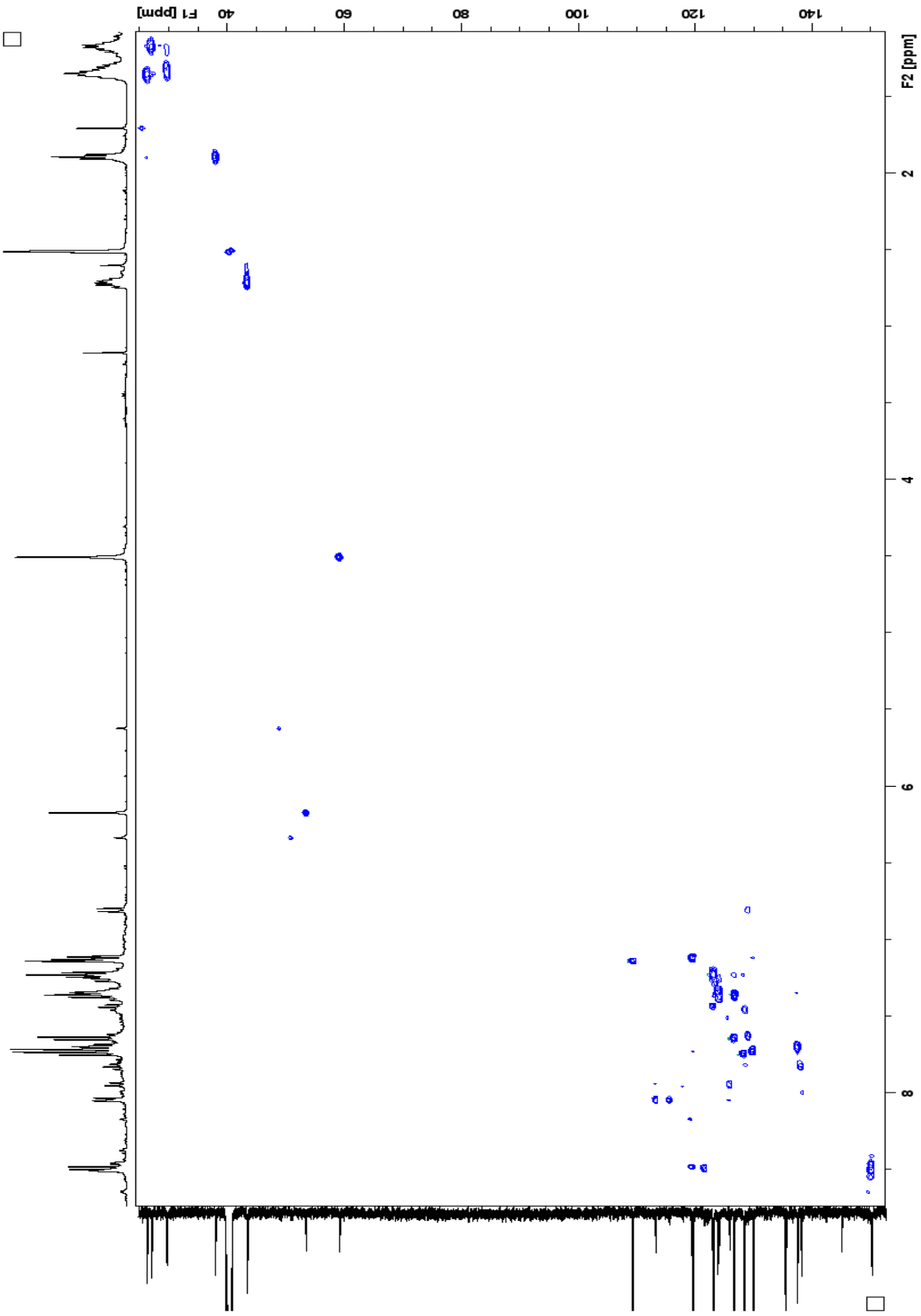

Spectrum 70*: 16c* ***HSQC (500 MHz, DMSO-d6)***

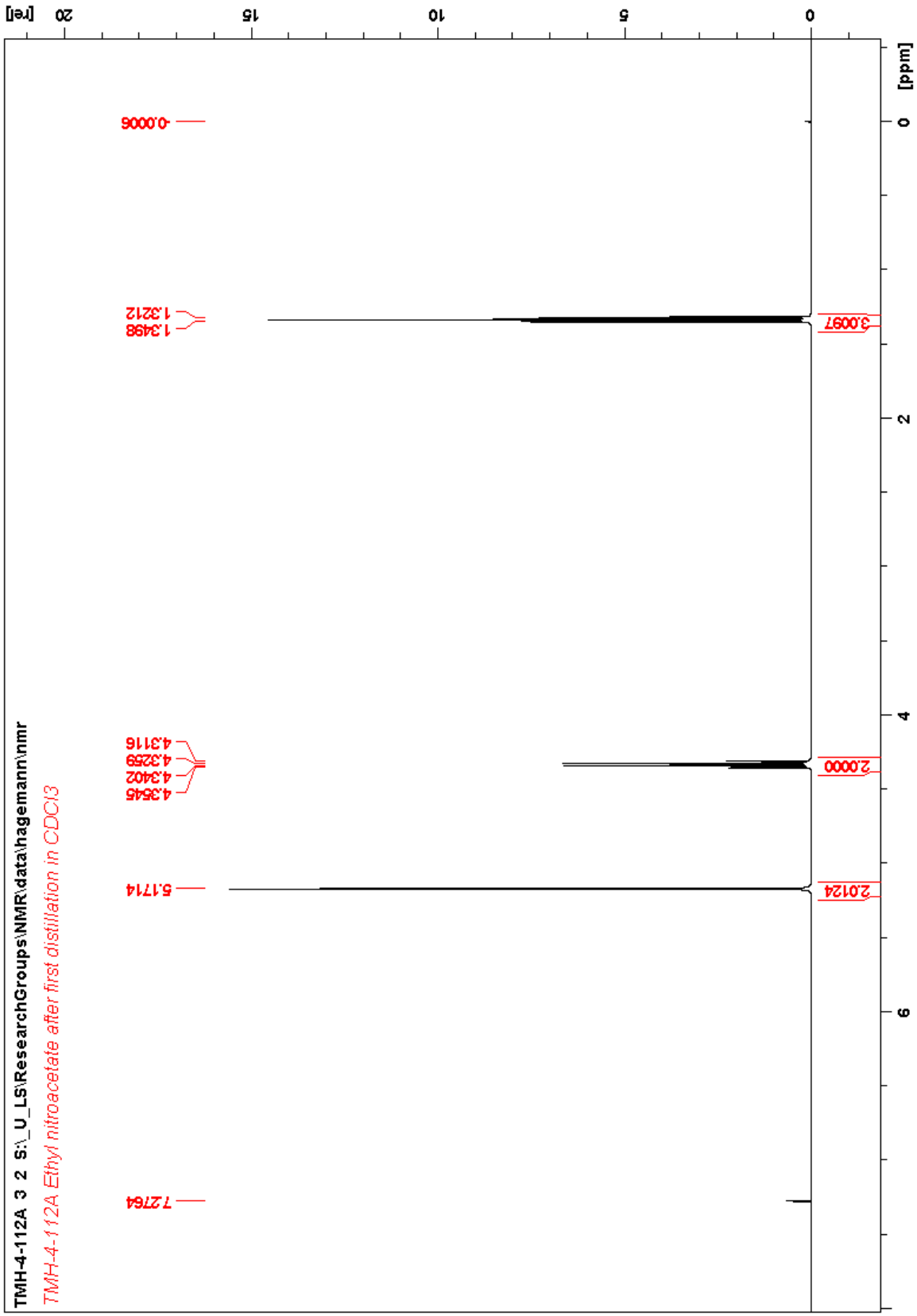

Spectrum 71*: 18* **^{1}H NMR (500 MHz, $CDCl_3$)**

Shimadzu LCMS-2020 Data Report

Mass Spectrum for Sample
10-12-2018_10122018_011.lcd

Operator:Trevor Hagemann

Data Filename: []\DB\7\b593aa30be114a6590895c2dbfc76318\125bbb3df63a46239a3da378c3f7483a\hagemann 2020\LCMS-2020\08D6306460
Spetrum Mode: Averaged
Retention Time: ----
Interface Type (ESI, APCI, DUIS): DUIS
Aquisition Mode: (Scan, SIM, Profife): Scan
Polarity: +
H2O/0.1% HCOOH, MeOH/0.1% HCOOH

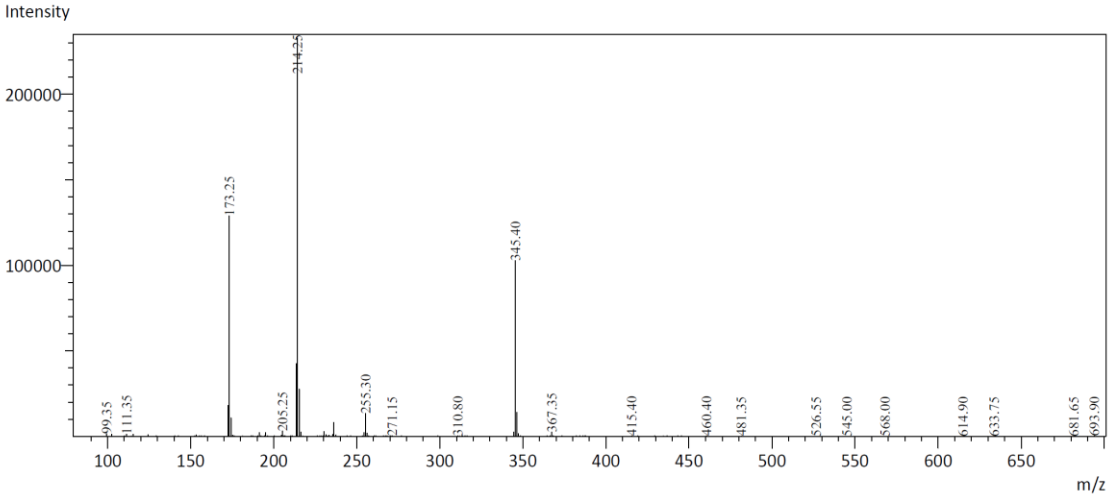

Operator:Trevor Hagemann

Data Filename: []\DB\7\b593aa30be114a6590895c2dbfc76318\125bbb3df63a46239a3da378c3f7483a\hagemann 2020\LCMS-2020\08D6306460
Spetrum Mode: Averaged
Retention Time: ----
Interface Type (ESI, APCI, DUIS): DUIS
Aquisition Mode: (Scan, SIM, Profife): Scan
Polarity: -
H2O/0.1% HCOOH, MeOH/0.1% HCOOH

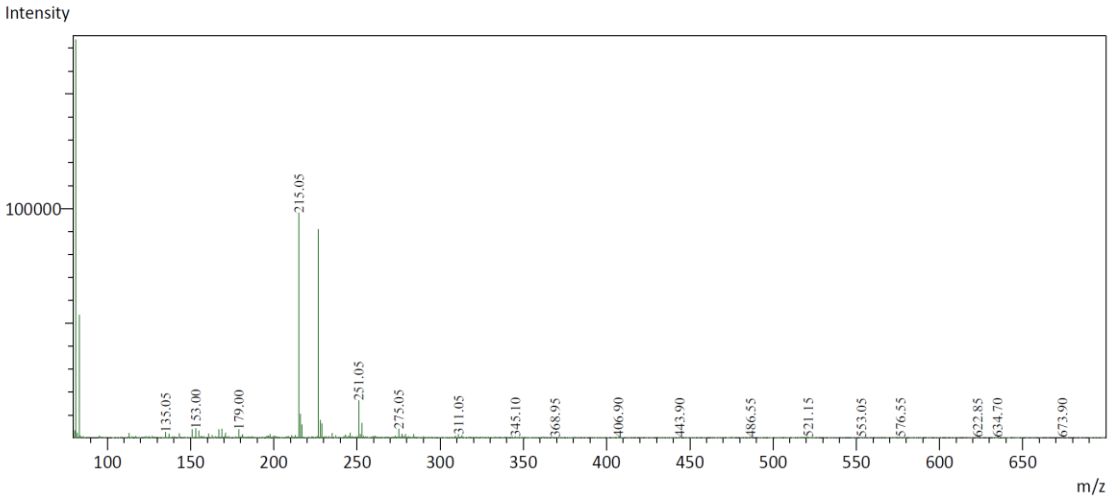

Spectrum 72*: 18* ***ESI-LCMS Spectra***

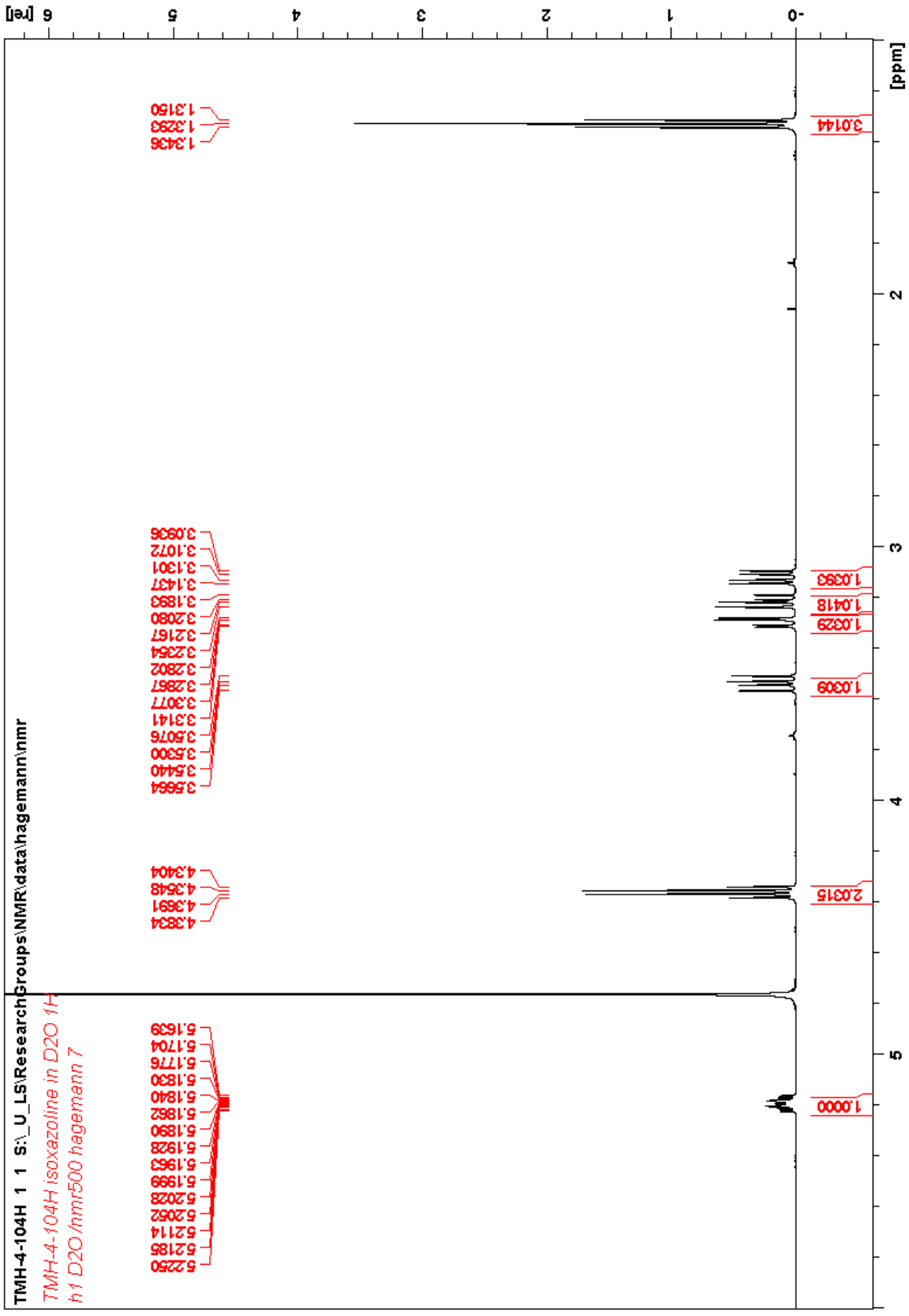

Spectrum 73*: 19* ^{1}***H NMR (500 MHz,*** D_2O***)***

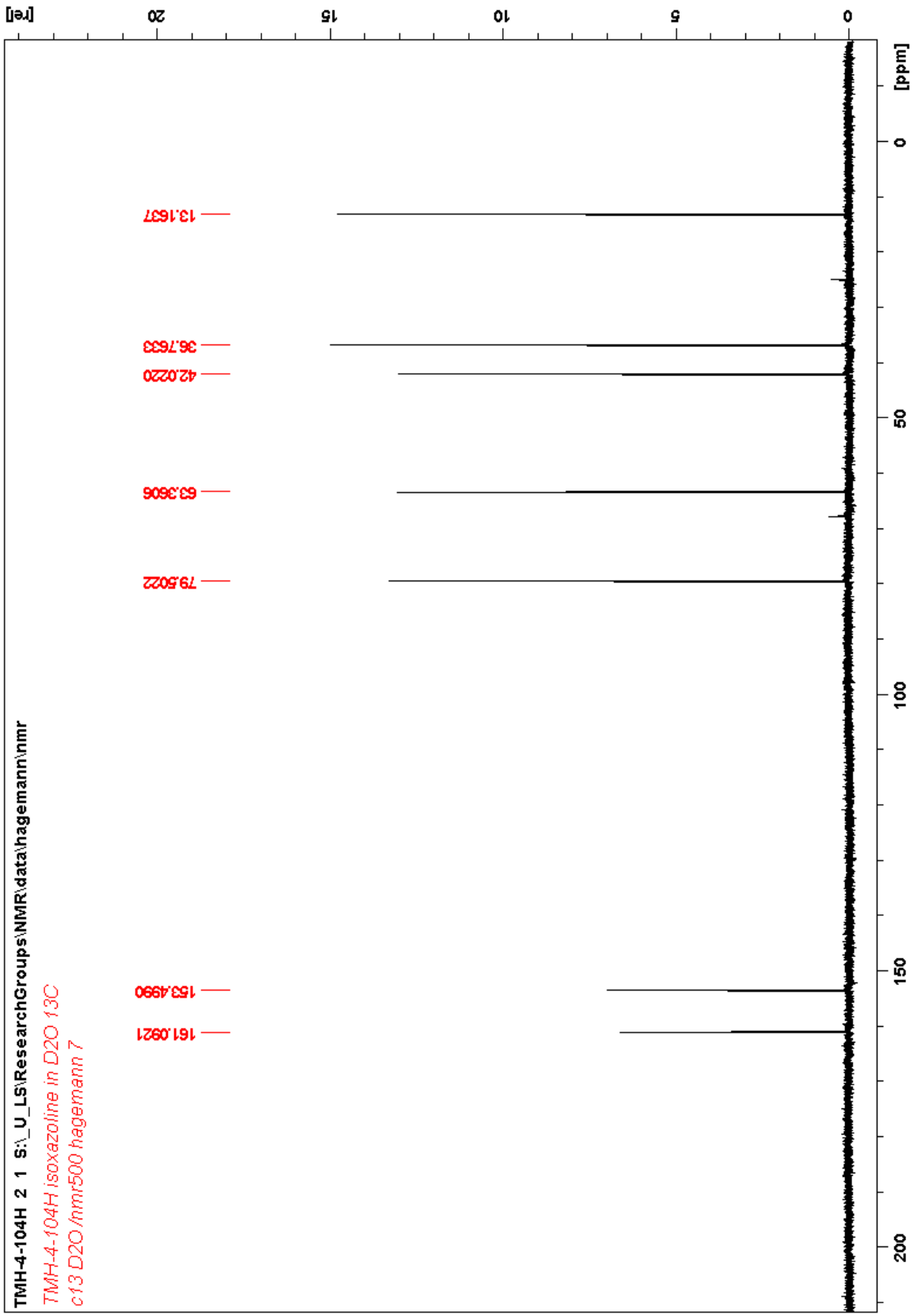

Spectrum 74: *19* ***^{13}C NMR (500 MHz, D_2O)***

Shimadzu LCMS-2020 Data Report

Mass Spectrum for Sample
10-12-2018_10122018_012.lcd

Operator:Trevor Hagemann

Data Filename: []\DB\7\7fc59c55589c4d0c87e525af09854fb0\ffa6b366b8954b10be4fdd897f8cc528\hagemann 2020\LCMS-2020\08D63064B9B4CA80\1\
Spetrum Mode: Averaged
Retention Time: ----
Interface Type (ESI, APCI, DUIS): DUIS
Aquisition Mode: (Scan, SIM, Profife): Scan
Polarity: +
H2O/0.1% HCOOH, MeOH/0.1% HCOOH

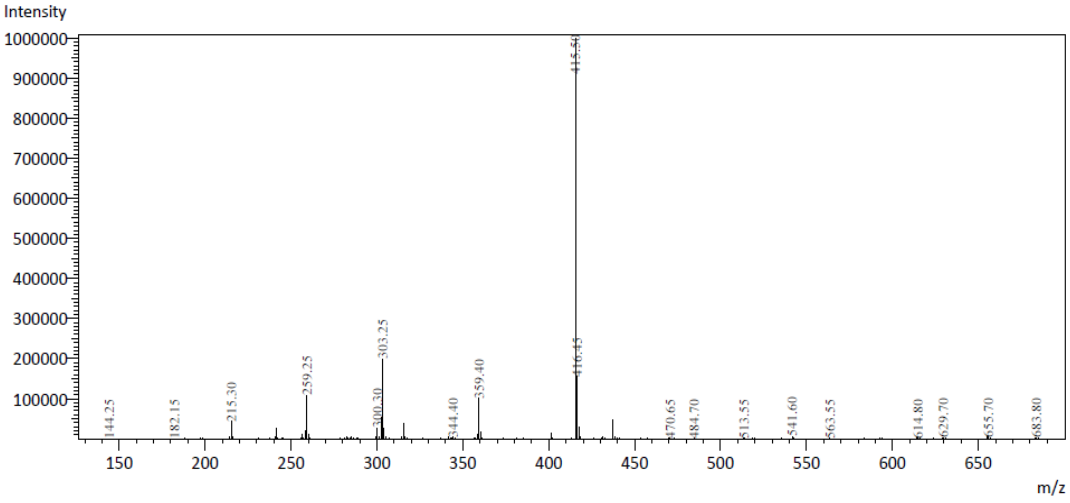

Operator:Trevor Hagemann

Data Filename: []\DB\7\7fc59c55589c4d0c87e525af09854fb0\ffa6b366b8954b10be4fdd897f8cc528\hagemann 2020\LCMS-2020\08D63064B9B4CA80\1\
Spetrum Mode: Averaged
Retention Time: ----
Interface Type (ESI, APCI, DUIS): DUIS
Aquisition Mode: (Scan, SIM, Profife): Scan
Polarity: -
H2O/0.1% HCOOH, MeOH/0.1% HCOOH

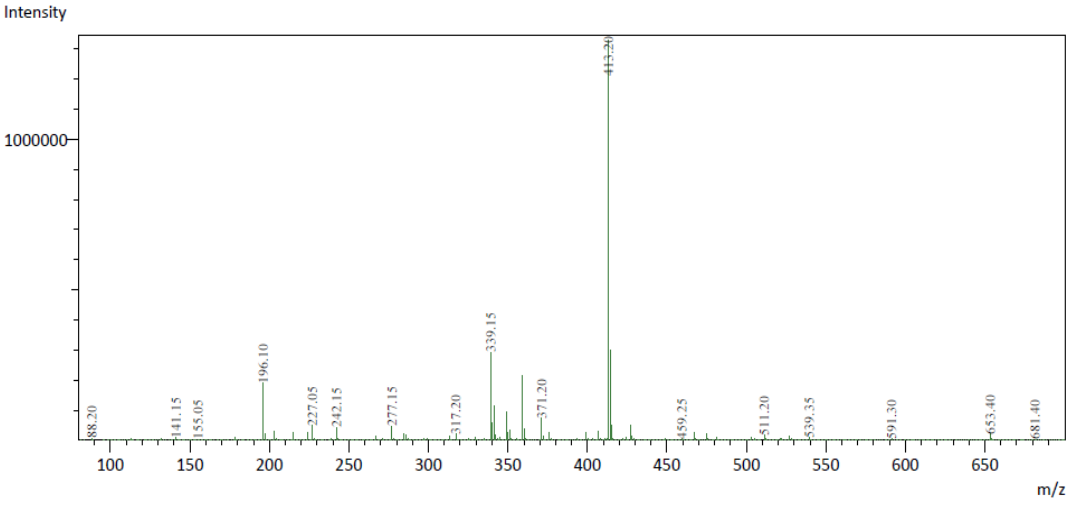

Spectrum 75*: 19 ESI-LCMS Spectra*

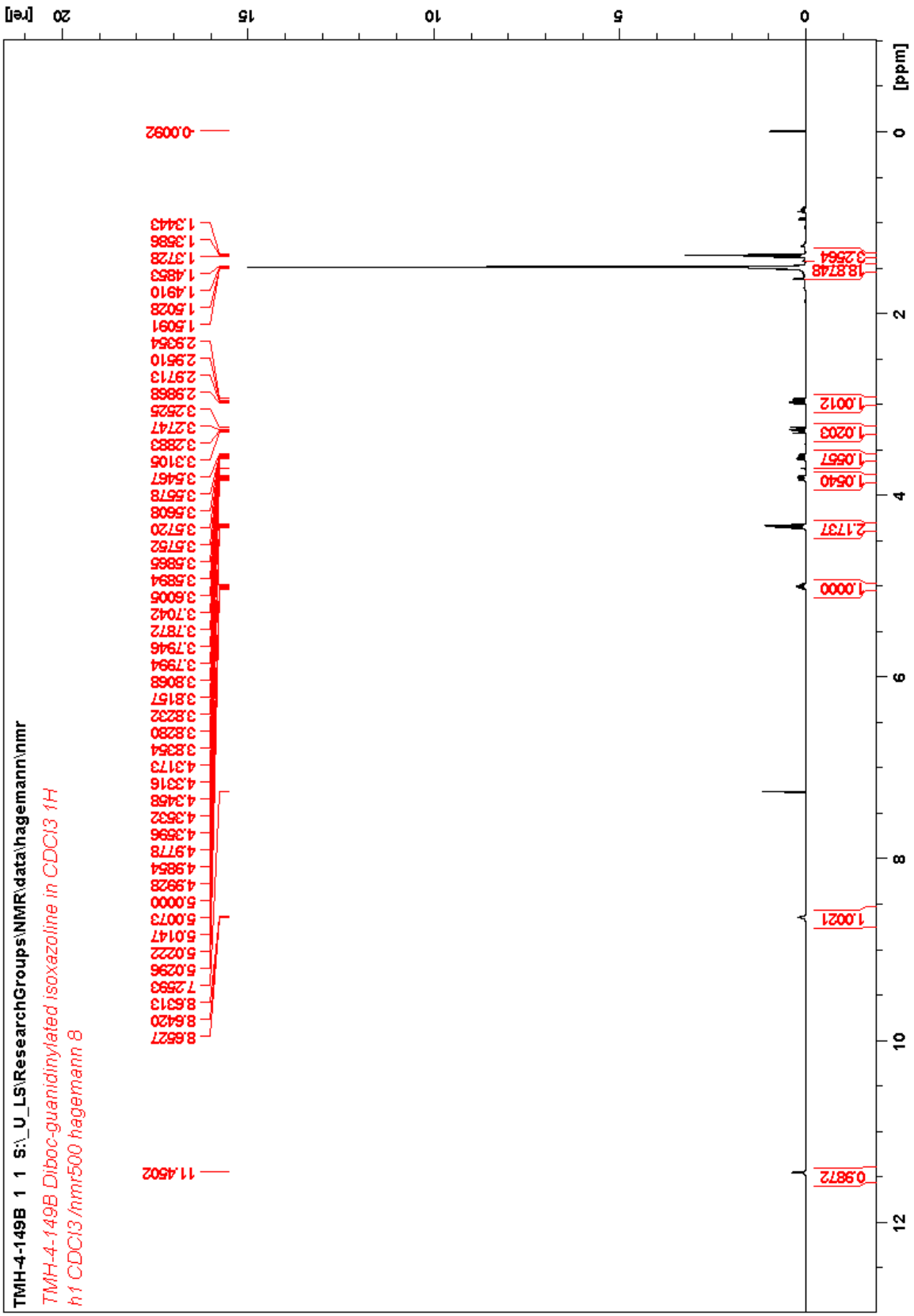

Spectrum 76*: 20* ^{1}***H NMR (500 MHz,*** $CDCl_3$***)***

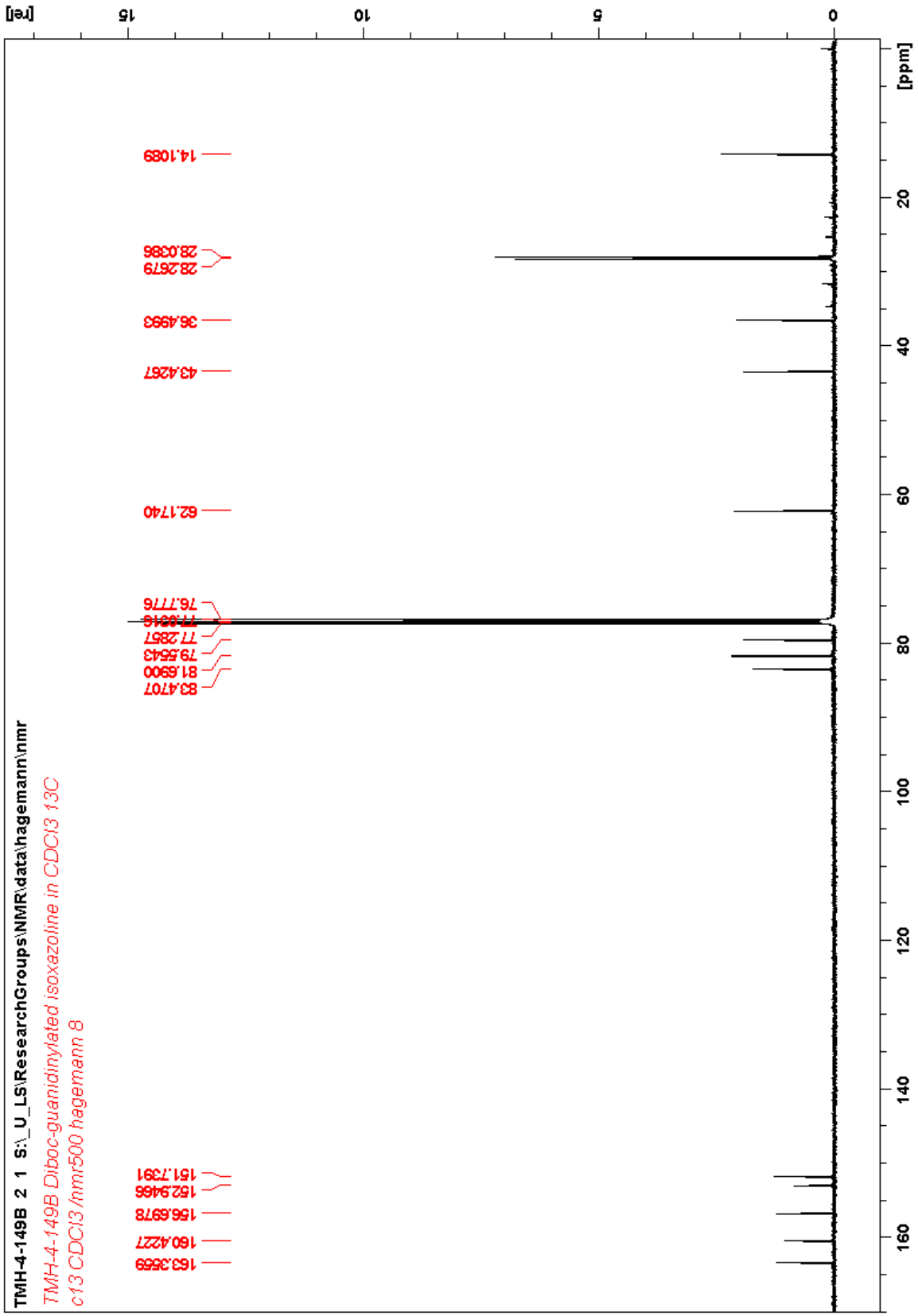

Spectrum 77*: 20* ^{13}***C NMR (500 MHz, CDCl*$_3$*)***

Shimadzu LCMS-2020 Data Report

Mass Spectrum for Sample
10-12-2018_10122018_013.lcd

Operator:Trevor Hagemann

Data Filename: []\DB\7\dcba5c039d8b493e9c53f33eaeead336\43151eb8ccbb4969b536e311c9a299c5\hagemann 2020\LCMS-2020\08D6306516
Spetrum Mode: Averaged
Retention Time: ----
Interface Type (ESI, APCI, DUIS): DUIS
Aquisition Mode: (Scan, SIM, Profife): Scan
Polarity: +
H2O/0.1% HCOOH, MeOH/0.1% HCOOH

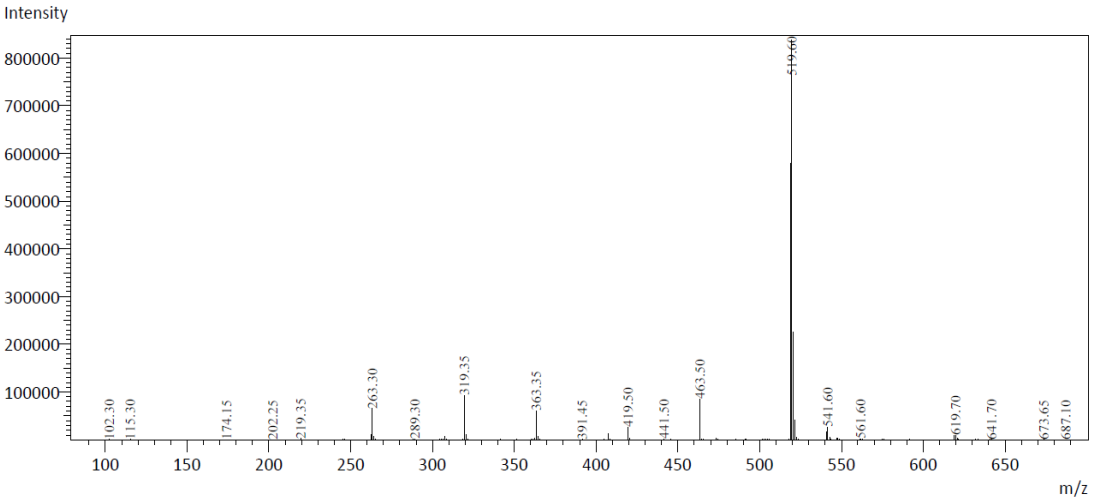

Operator:Trevor Hagemann

Data Filename: []\DB\7\dcba5c039d8b493e9c53f33eaeead336\43151eb8ccbb4969b536e311c9a299c5\hagemann 2020\LCMS-2020\08D6306516
Spetrum Mode: Averaged
Retention Time: ----
Interface Type (ESI, APCI, DUIS): DUIS
Aquisition Mode: (Scan, SIM, Profife): Scan
Polarity: -
H2O/0.1% HCOOH, MeOH/0.1% HCOOH

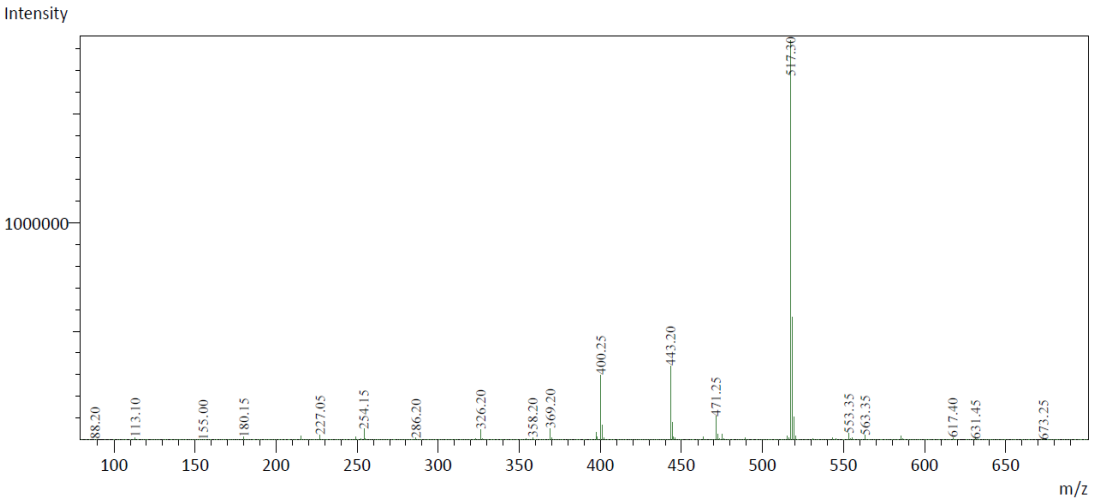

Spectrum 78*: 20* ***ESI-LCMS Spectra***

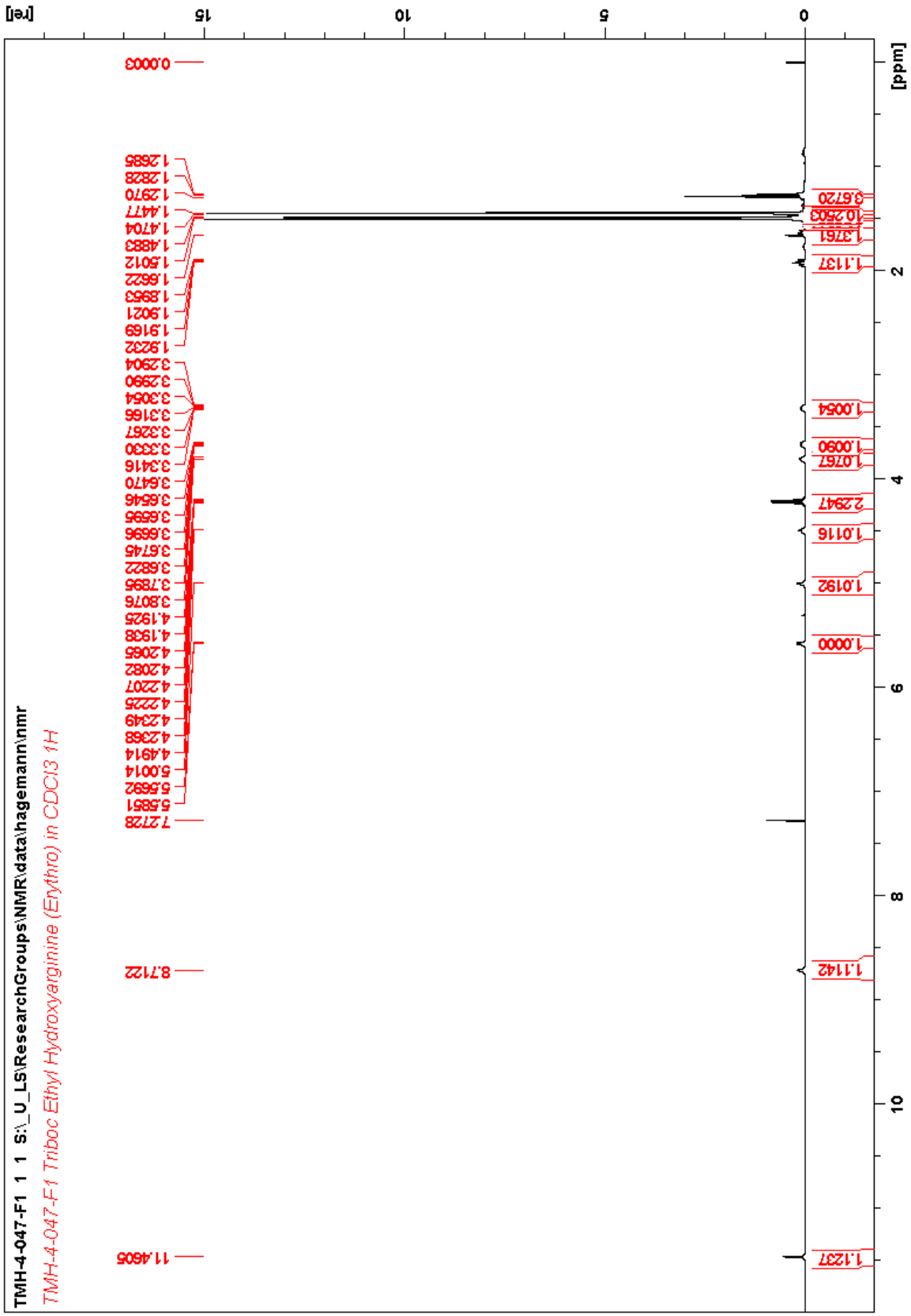

Spectrum 79: *21e ^{1}H NMR (500 MHz, $CDCl_3$)*

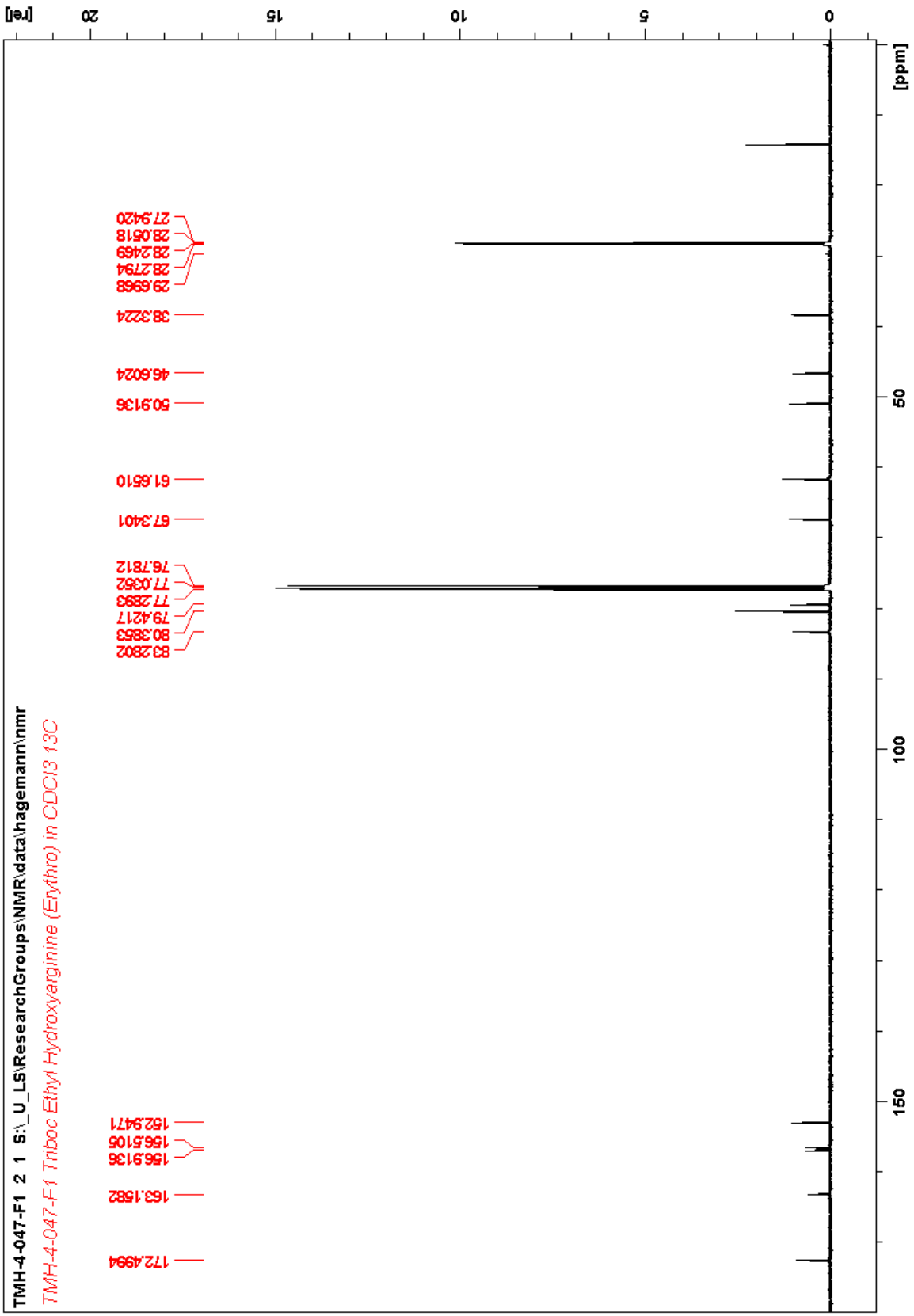

Spectrum 80*: 21e* ***^{1}H NMR (500 MHz, $CDCl_3$)***

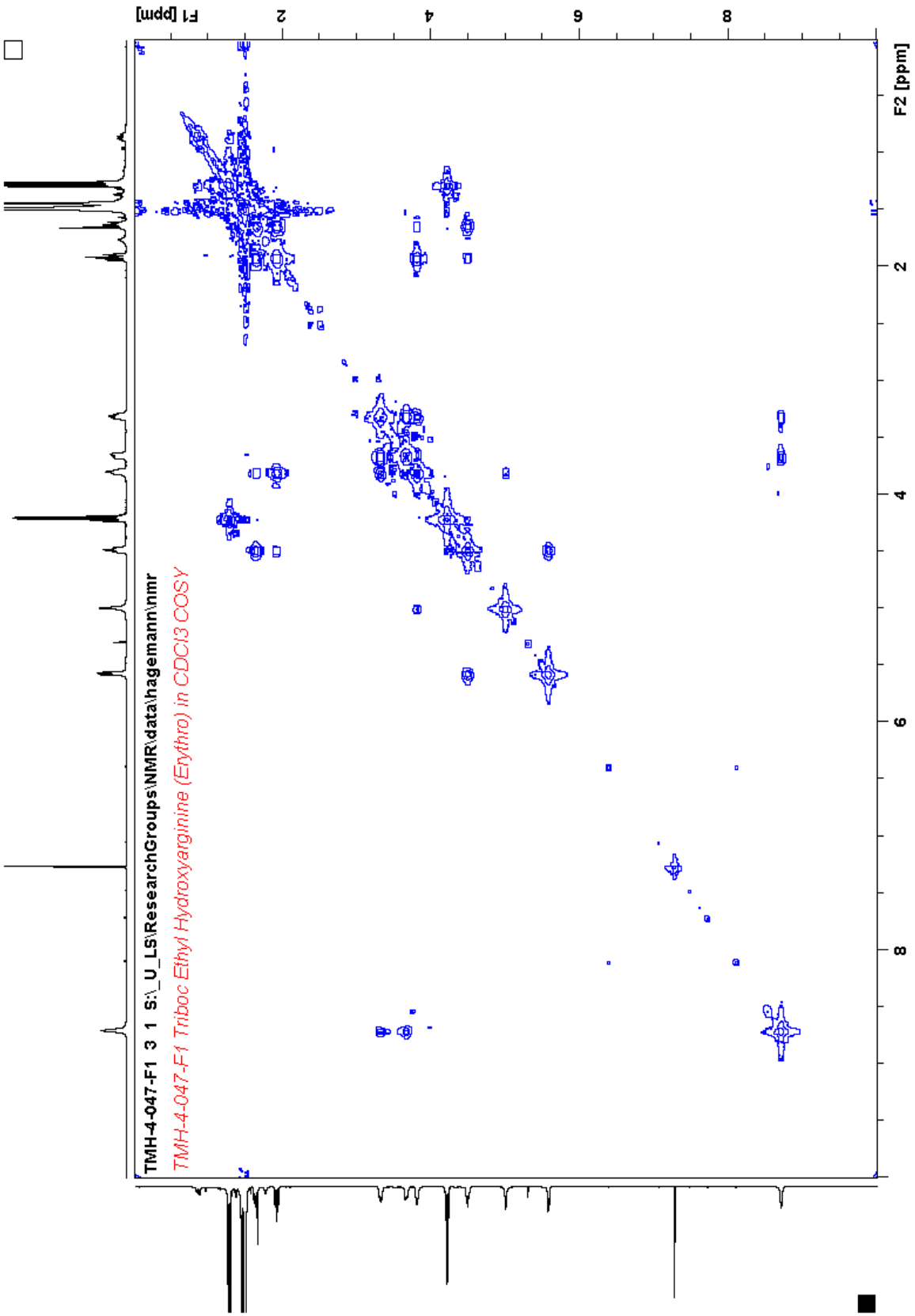

Spectrum 81*: 21e* ***COESY NMR (500 MHz, $CDCl_3$)***

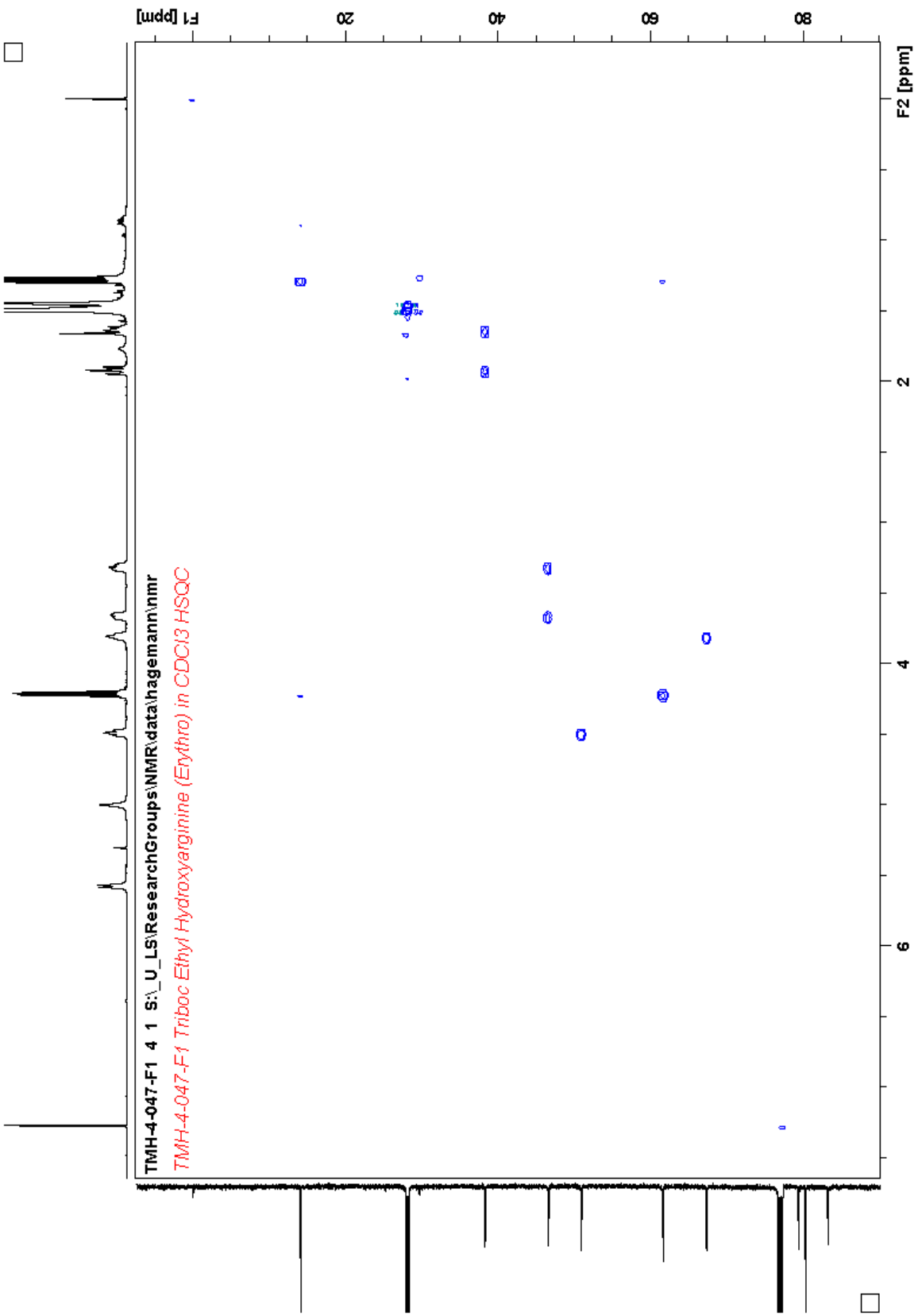

Spectrum 82*: 21e* ***HSQC NMR (500 MHz, $CDCl_3$)***

Shimadzu LCMS-2020 Data Report

Mass Spectrum for Sample
10-12-2018_10122018_014.lcd

Operator:Trevor Hagemann

Data Filename: []\DB\7\75ee246ba213429ca0bf0b3afb677ea8\88022f3790e24390a3346ad6829a9d85\hagemann 2020\LCMS-2020\08D6306570B146
Spetrum Mode: Averaged
Retention Time: ----
Interface Type (ESI, APCI, DUIS): DUIS
Aquisition Mode: (Scan, SIM, Profife): Scan
Polarity: +
H2O/0.1% HCOOH, MeOH/0.1% HCOOH

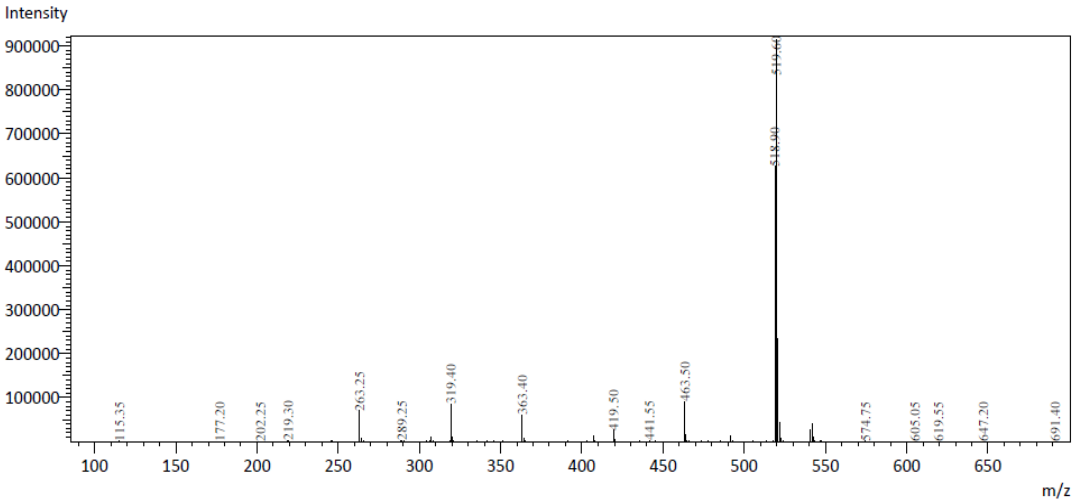

Operator:Trevor Hagemann

Data Filename: []\DB\7\75ee246ba213429ca0bf0b3afb677ea8\88022f3790e24390a3346ad6829a9d85\hagemann 2020\LCMS-2020\08D6306570B146
Spetrum Mode: Averaged
Retention Time: ----
Interface Type (ESI, APCI, DUIS): DUIS
Aquisition Mode: (Scan, SIM, Profife): Scan
Polarity: -
H2O/0.1% HCOOH, MeOH/0.1% HCOOH

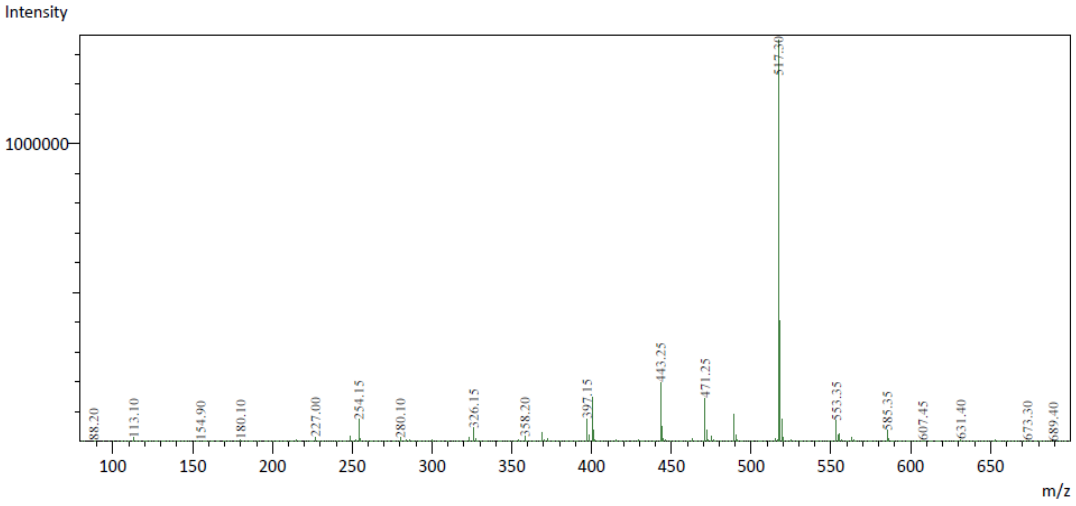

Spectrum 83*: 21e* ***ESI-LCMS Spectra***

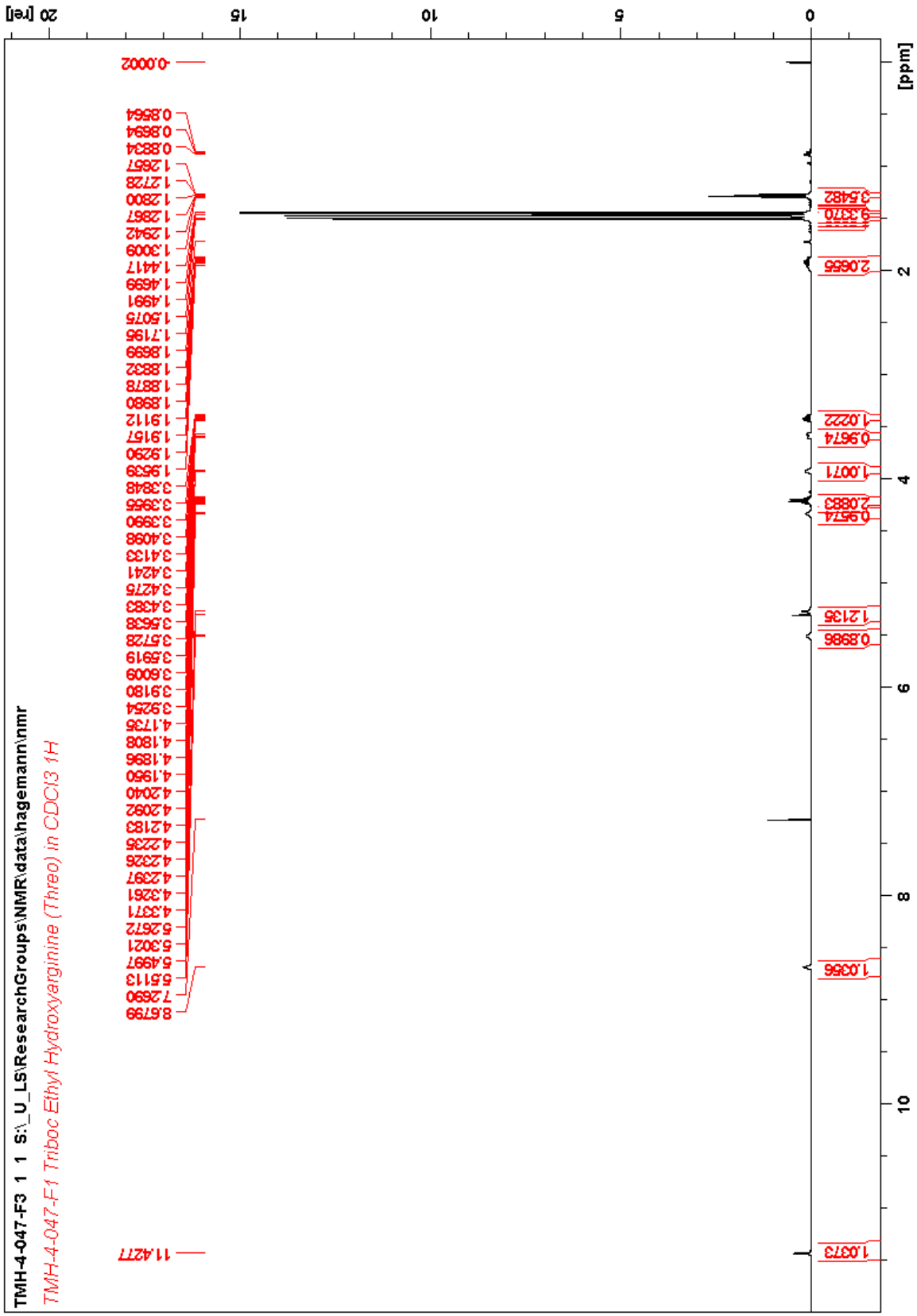

Spectrum 84*: 21t* ***^{1}H NMR (500 MHz, $CDCl_3$)***

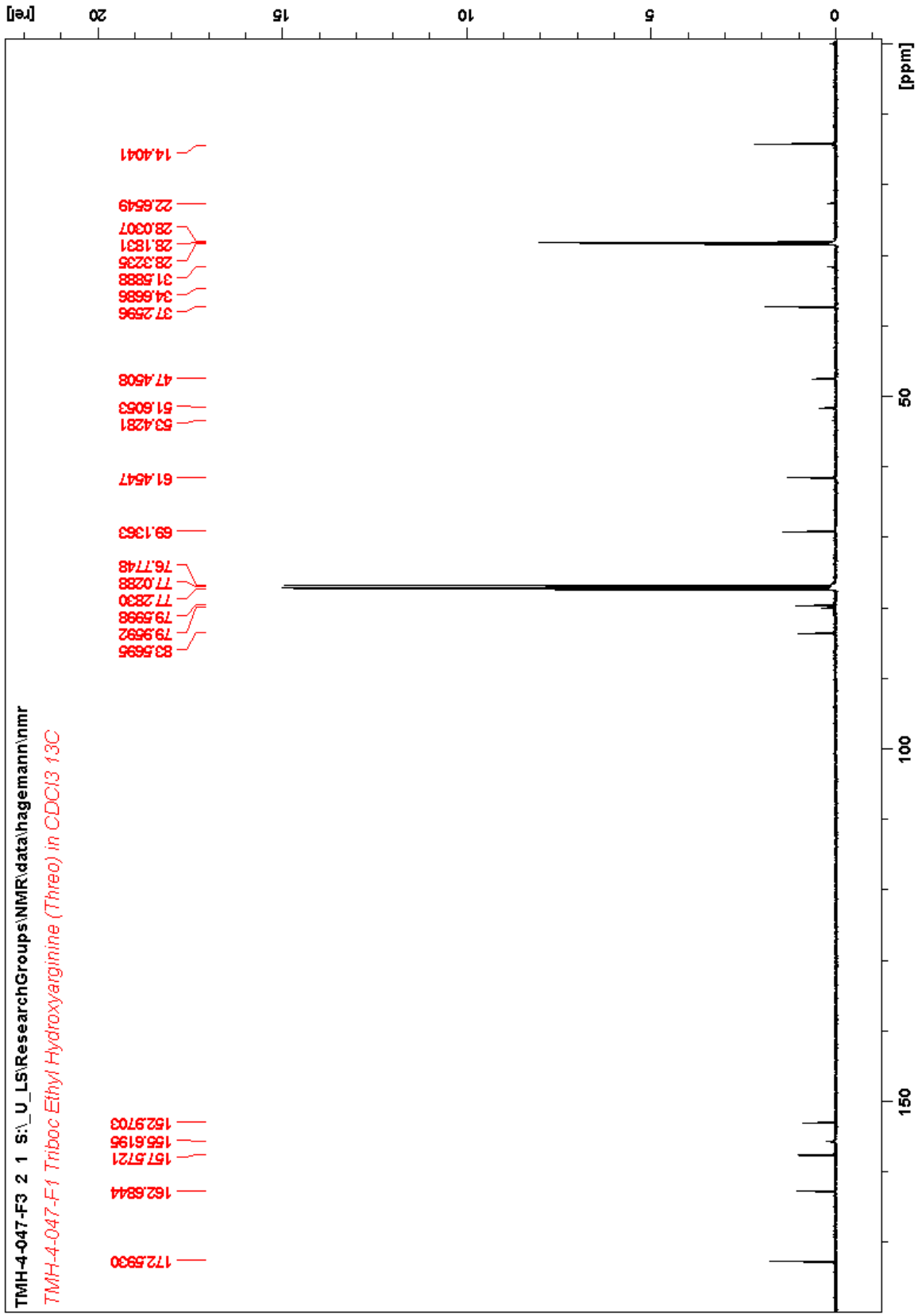

Spectrum 85*: 21t* ^{13}***C NMR (500 MHz, CDCl*$_3$*)***

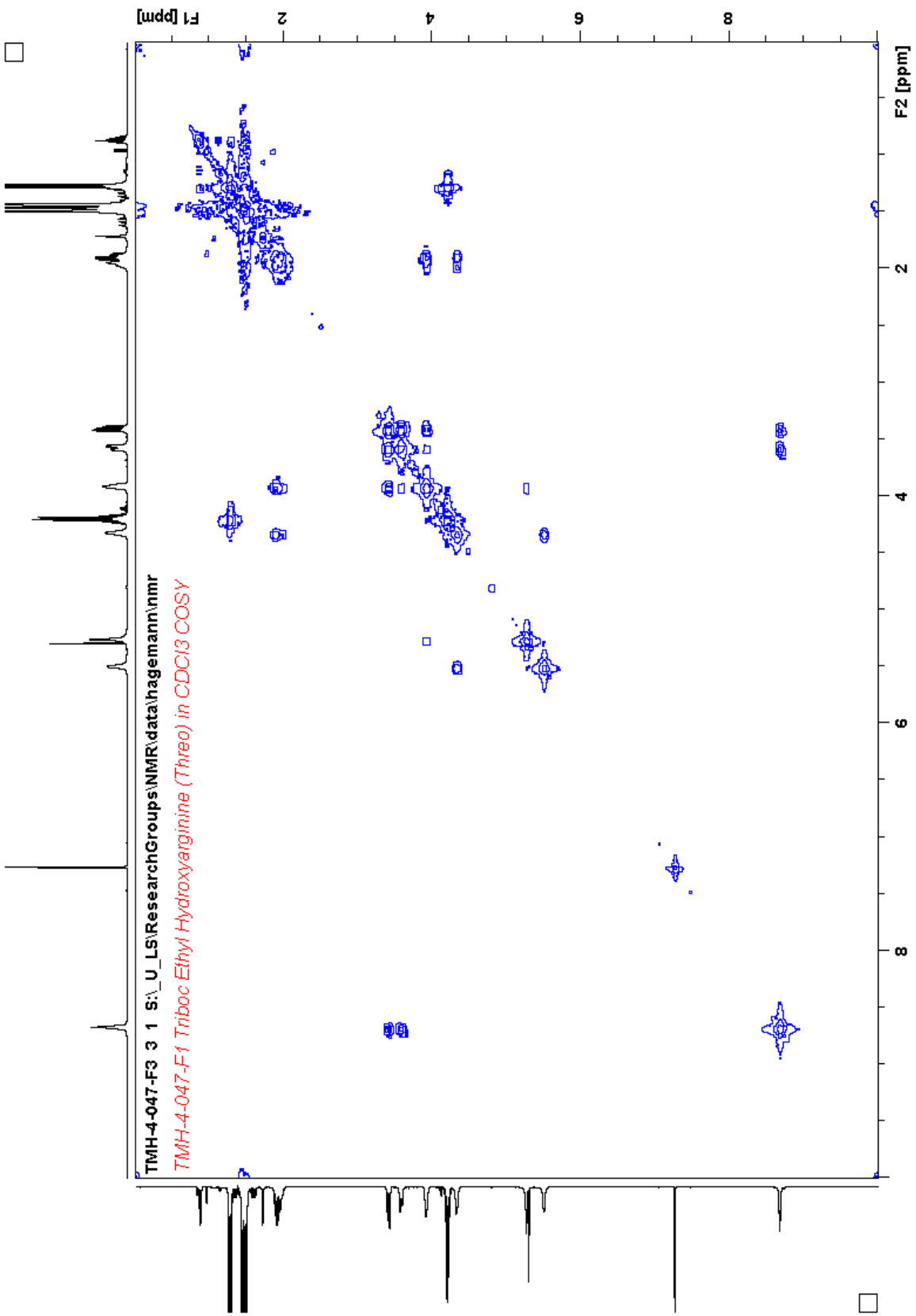

Spectrum 86*: 21t* ***COESY NMR (500 MHz, $CDCl_3$)***

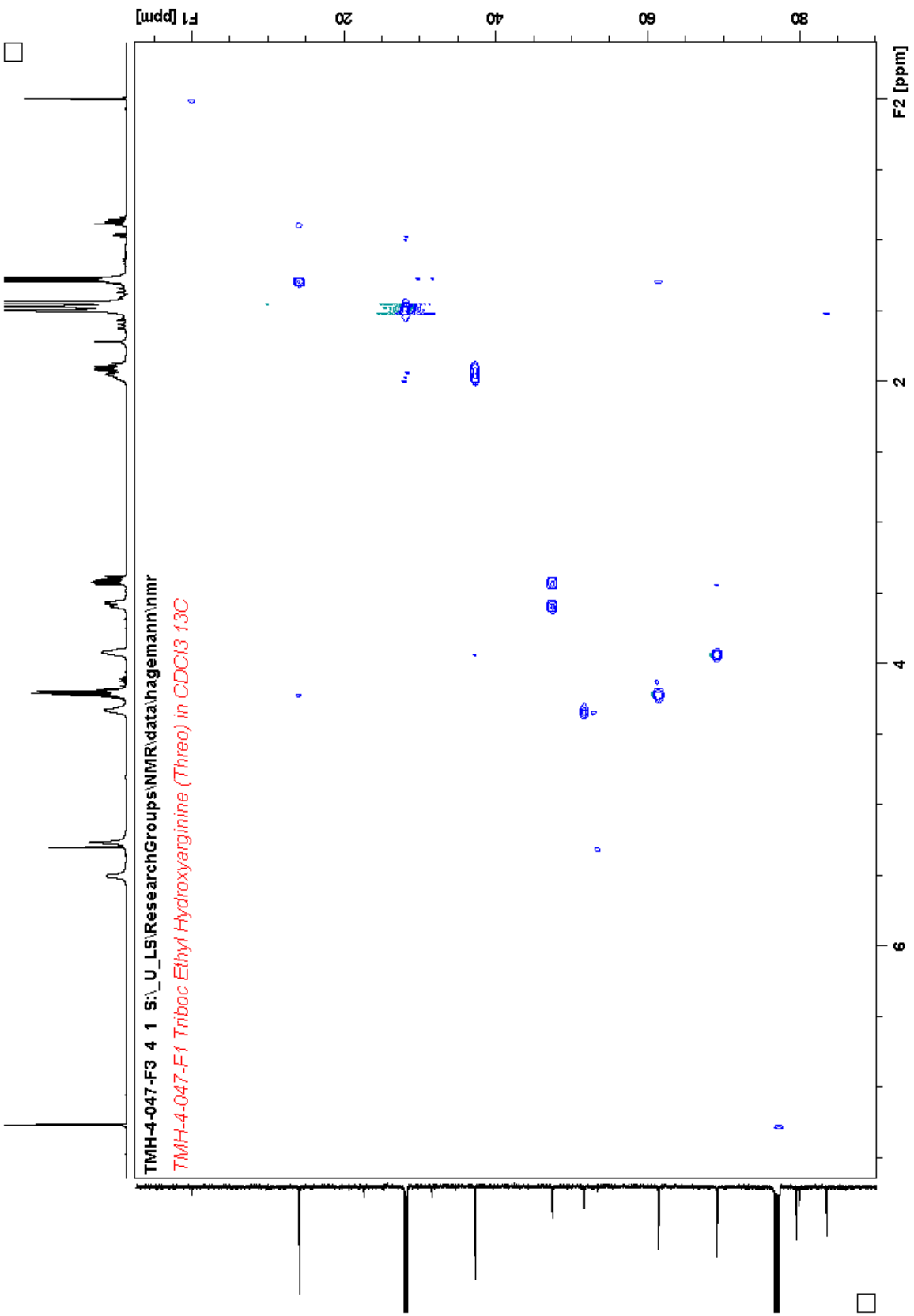

Spectrum 87*: 21t* ***HSQC NMR (500 MHz, $CDCl_3$)***

Shimadzu LCMS-2020 Data Report

Mass Spectrum for Sample
10-12-2018_10122018_013.lcd

Operator:Trevor Hagemann

Data Filename: []\DB\7\dcba5c039d8b493e9c53f33eaeead336\43151eb8ccbb4969b536e311c9a299c5\hagemann 2020\LCMS-2020\08D6306516
Spetrum Mode: Averaged
Retention Time: ----
Interface Type (ESI, APCI, DUIS): DUIS
Aquisition Mode: (Scan, SIM, Profife): Scan
Polarity: +
H2O/0.1% HCOOH, MeOH/0.1% HCOOH

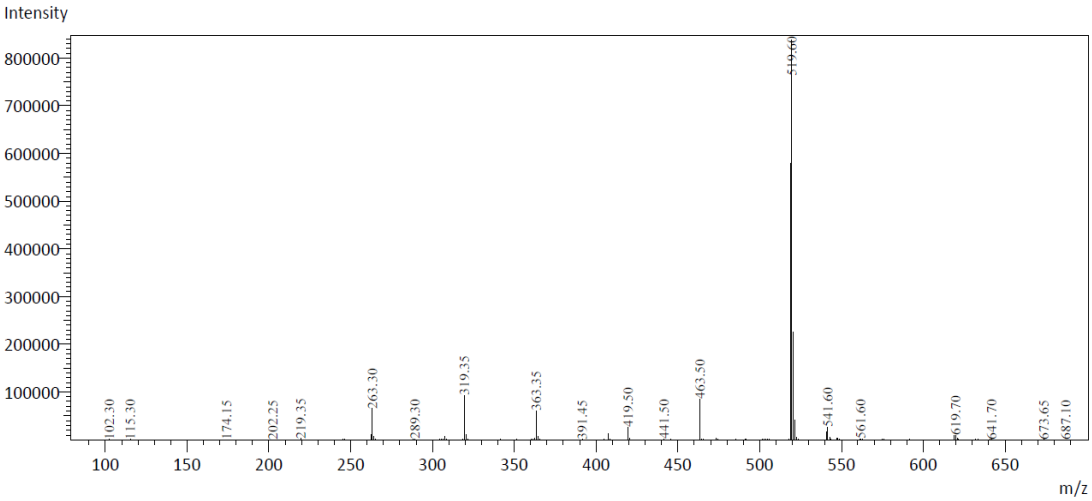

Operator:Trevor Hagemann

Data Filename: []\DB\7\dcba5c039d8b493e9c53f33eaeead336\43151eb8ccbb4969b536e311c9a299c5\hagemann 2020\LCMS-2020\08D6306516
Spetrum Mode: Averaged
Retention Time: ----
Interface Type (ESI, APCI, DUIS): DUIS
Aquisition Mode: (Scan, SIM, Profife): Scan
Polarity: -
H2O/0.1% HCOOH, MeOH/0.1% HCOOH

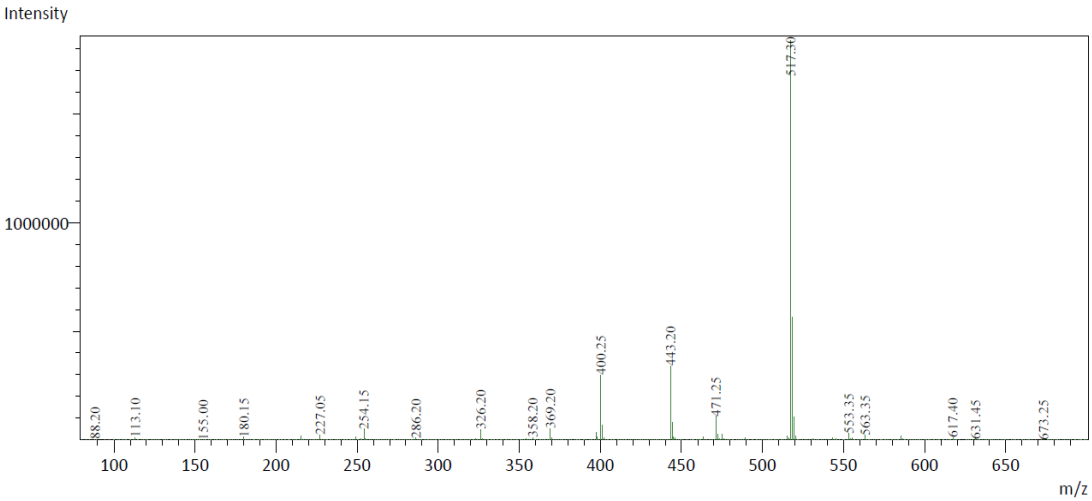

Spectrum 88*: 21t* ***ESI-LCMS Spectra***

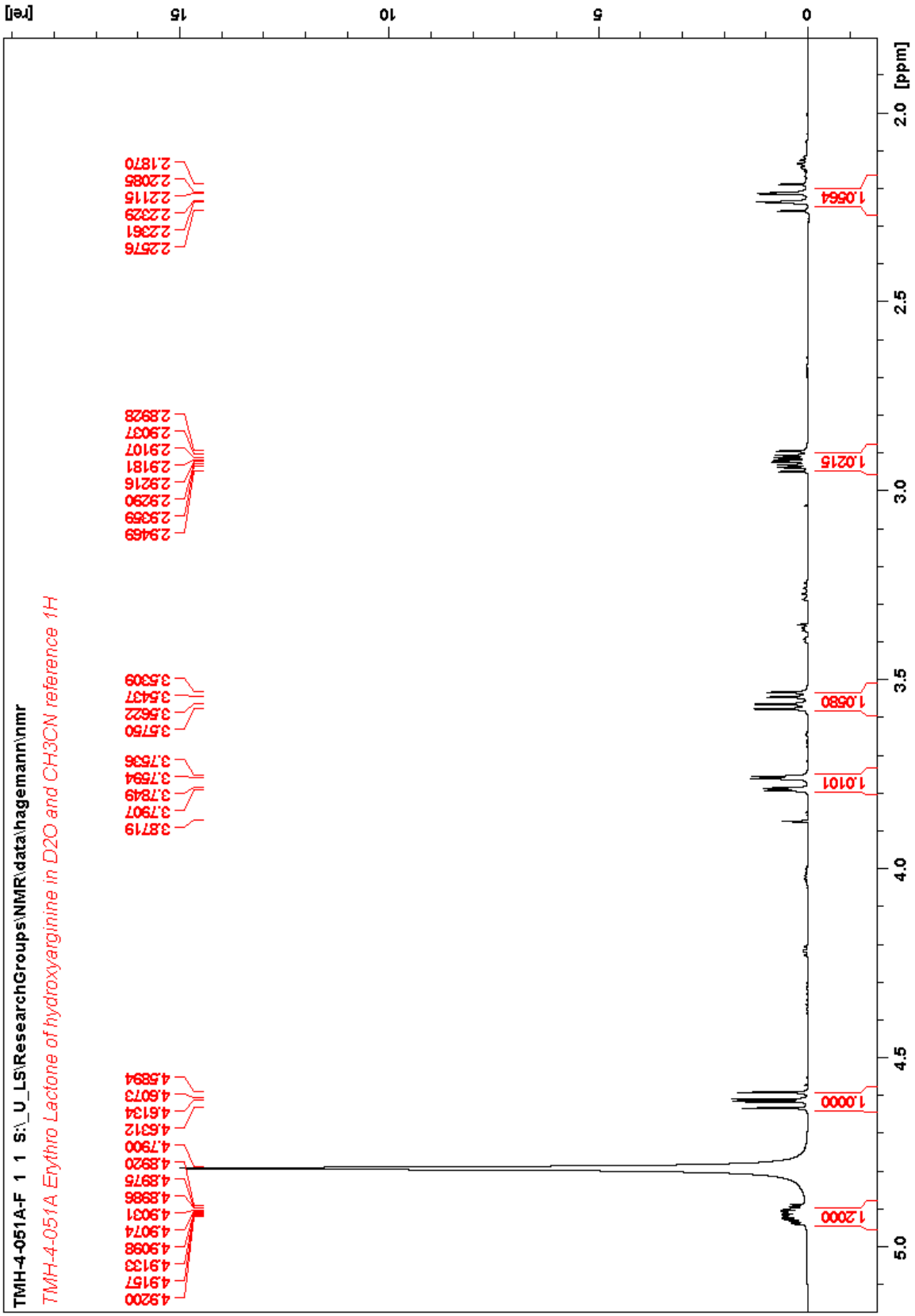

Spectrum 89*: 22e* ***^{1}H NMR (500 MHz, D_2O)***

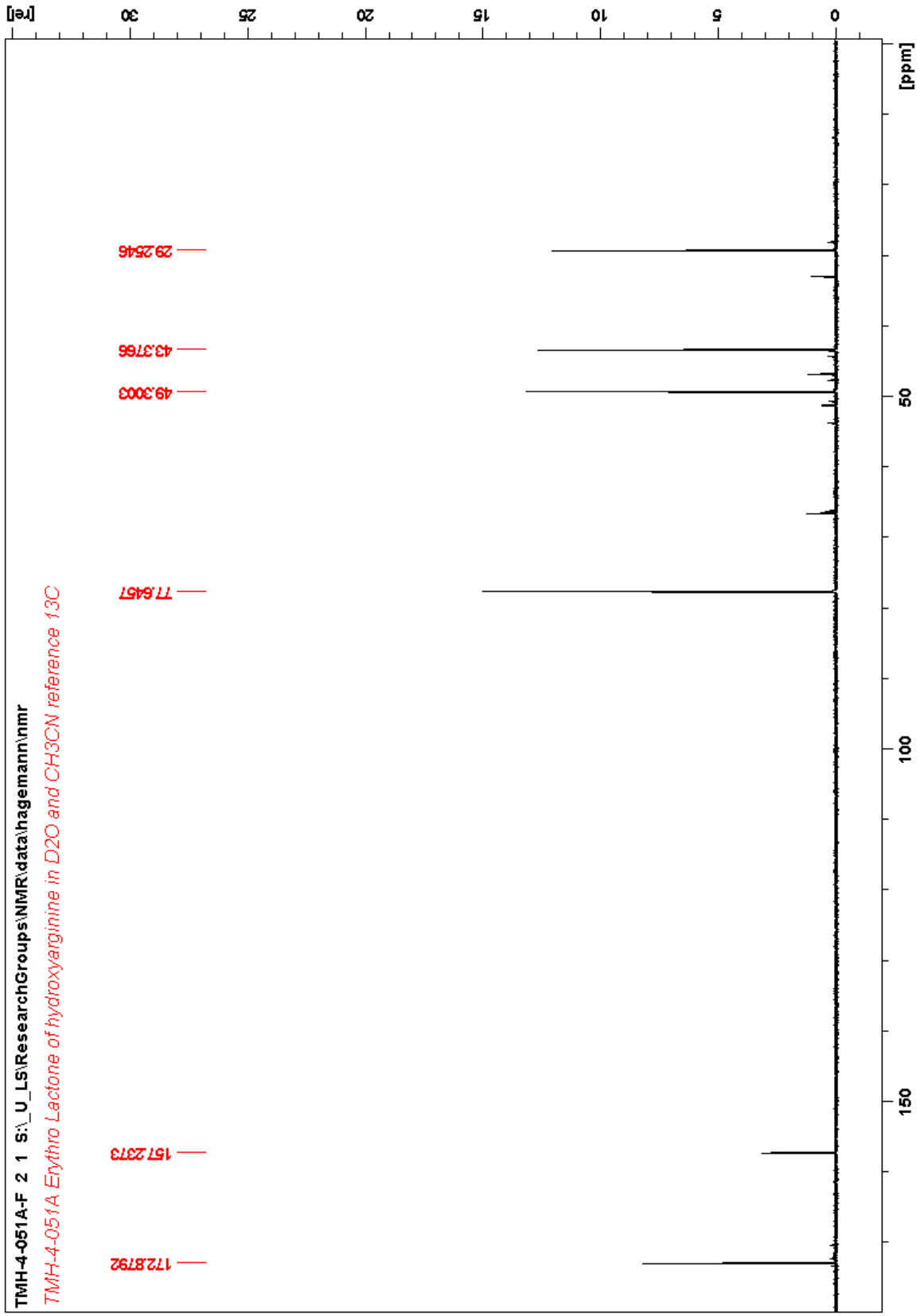

Spectrum 90*: 22e* ***^{13}C NMR (500 MHz, D_2O)***

Shimadzu LCMS-2020 Data Report

Mass Spectrum for Sample
10-12-2018_10122018_015.lcd

Operator:Trevor Hagemann

Data Filename: []\DB\7\ba6cbeae87af466eb8897adb53a205c8\8d454ad1172a48bebd00d7d351518e62\hagemann 2020\LCMS-2020\08D63065C
Spetrum Mode: Averaged
Retention Time: ----
Interface Type (ESI, APCI, DUIS): DUIS
Aquisition Mode: (Scan, SIM, Profife): Scan
Polarity: +
H2O/0.1% HCOOH, MeOH/0.1% HCOOH

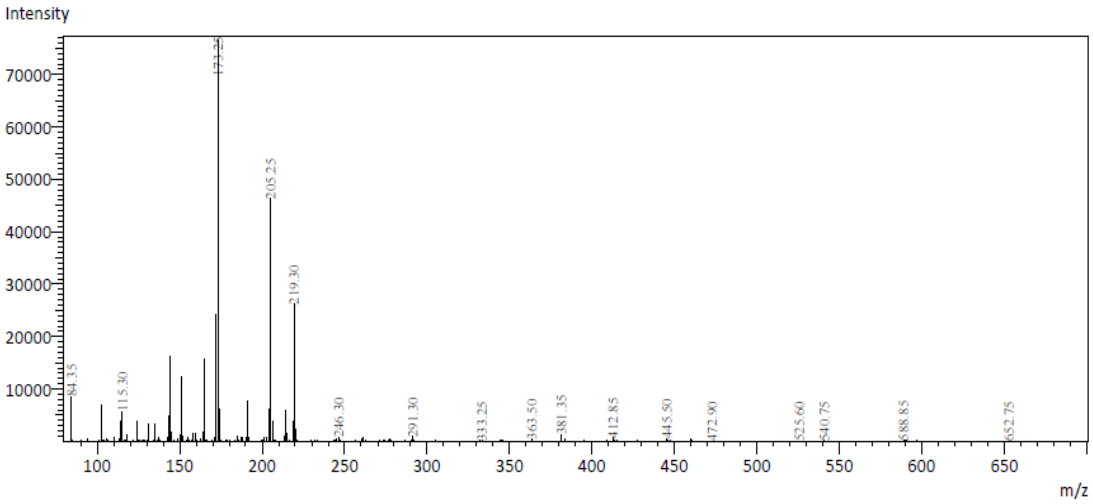

Operator:Trevor Hagemann

Data Filename: []\DB\7\ba6cbeae87af466eb8897adb53a205c8\8d454ad1172a48bebd00d7d351518e62\hagemann 2020\LCMS-2020\08D63065C
Spetrum Mode: Averaged
Retention Time: ----
Interface Type (ESI, APCI, DUIS): DUIS
Aquisition Mode: (Scan, SIM, Profife): Scan
Polarity: -
H2O/0.1% HCOOH, MeOH/0.1% HCOOH

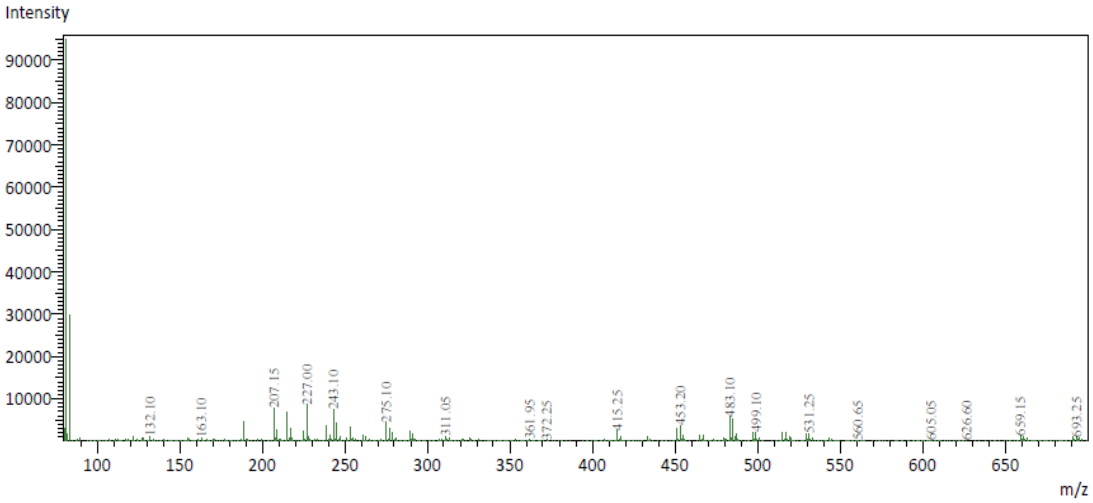

Spectrum 91*: 22e* ***ESI-LCMS Spectra***

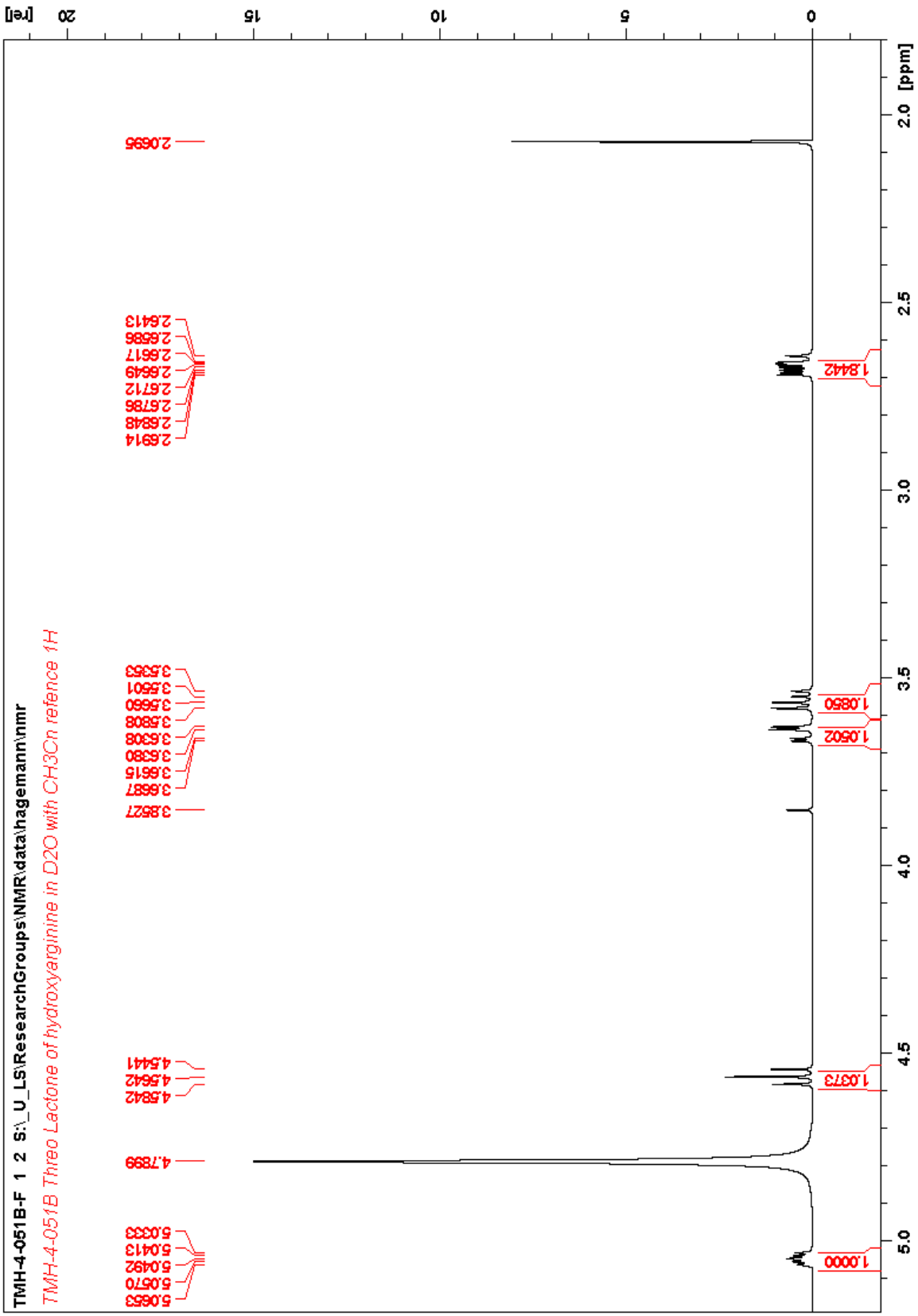

Spectrum 92*: 22t* ***^{1}H NMR (500 MHz, D_2O)***

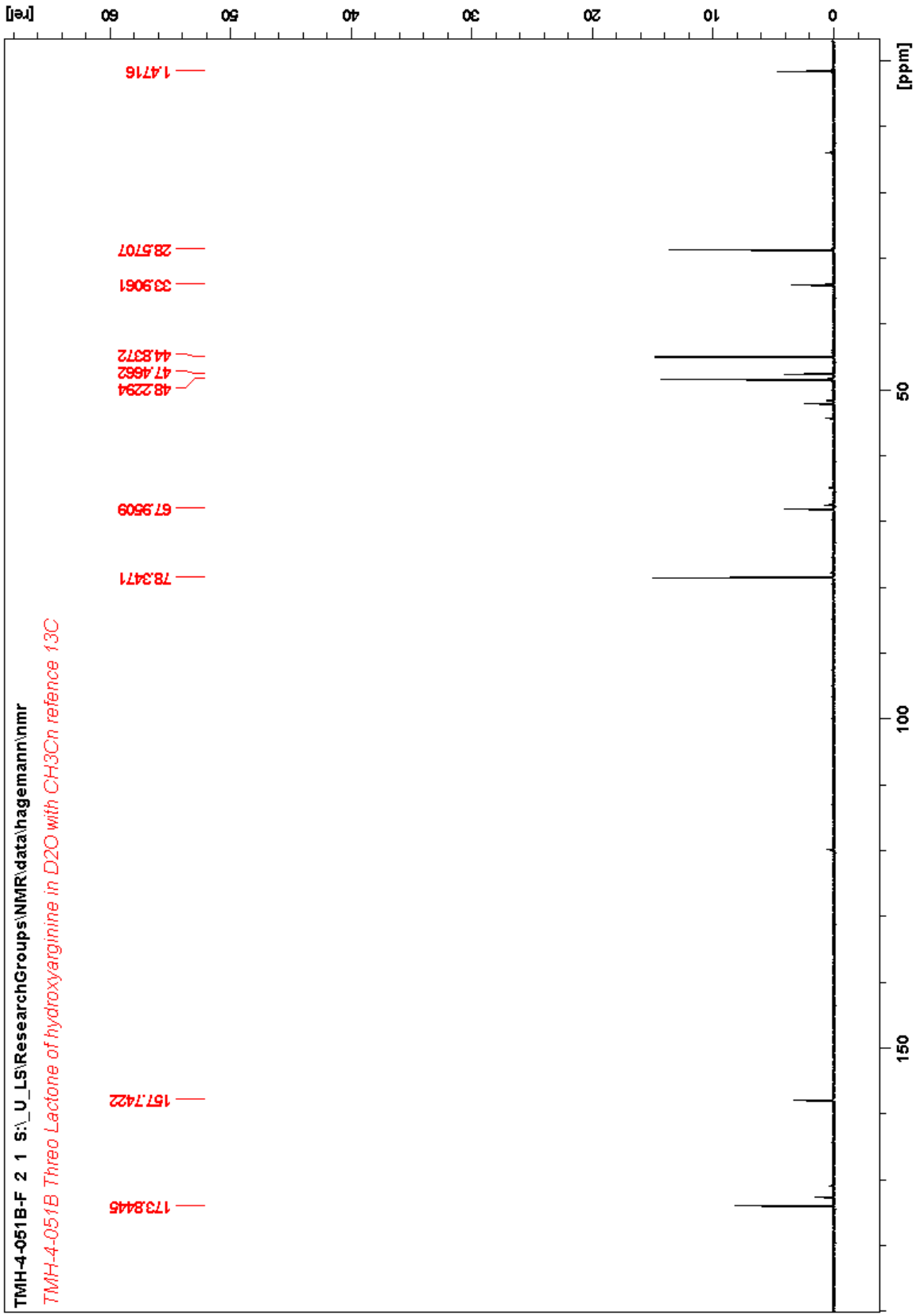

Spectrum 93*: 22t* ***^{13}C NMR (500 MHz, D_2O)***

Shimadzu LCMS-2020 Data Report

Mass Spectrum for Sample
10-12-2018_10122018_016.lcd

Operator:Trevor Hagemann

Data Filename: []\DB\7\bcd96fce4b7e48f4b4686b45a2c8daca\9a7c42e5867d43d0b30a911922846280\hagemann 2020\LCMS-2020\08D6306629
Spetrum Mode: Averaged
Retention Time: ----
Interface Type (ESI, APCI, DUIS): DUIS
Aquisition Mode: (Scan, SIM, Profife): Scan
Polarity: +
H2O/0.1% HCOOH, MeOH/0.1% HCOOH

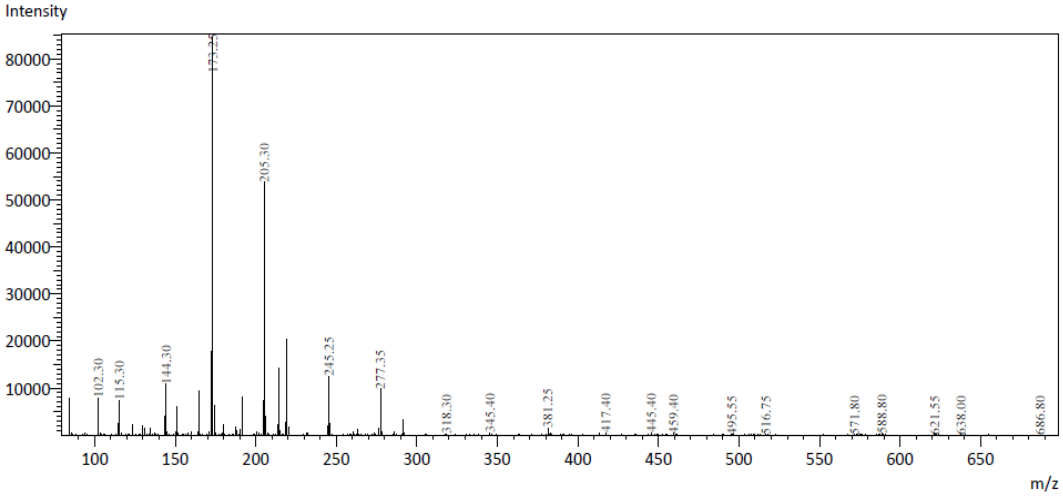

Operator:Trevor Hagemann

Data Filename: []\DB\7\bcd96fce4b7e48f4b4686b45a2c8daca\9a7c42e5867d43d0b30a911922846280\hagemann 2020\LCMS-2020\08D6306629
Spetrum Mode: Averaged
Retention Time: ----
Interface Type (ESI, APCI, DUIS): DUIS
Aquisition Mode: (Scan, SIM, Profife): Scan
Polarity: -
H2O/0.1% HCOOH, MeOH/0.1% HCOOH

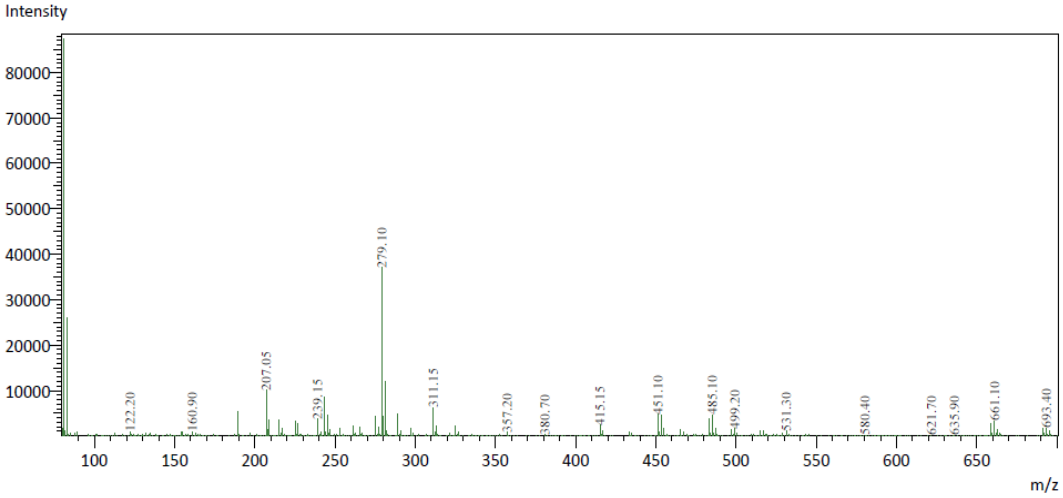

Spectrum 94*: 22t* ***ESI-LCMS Spectra***

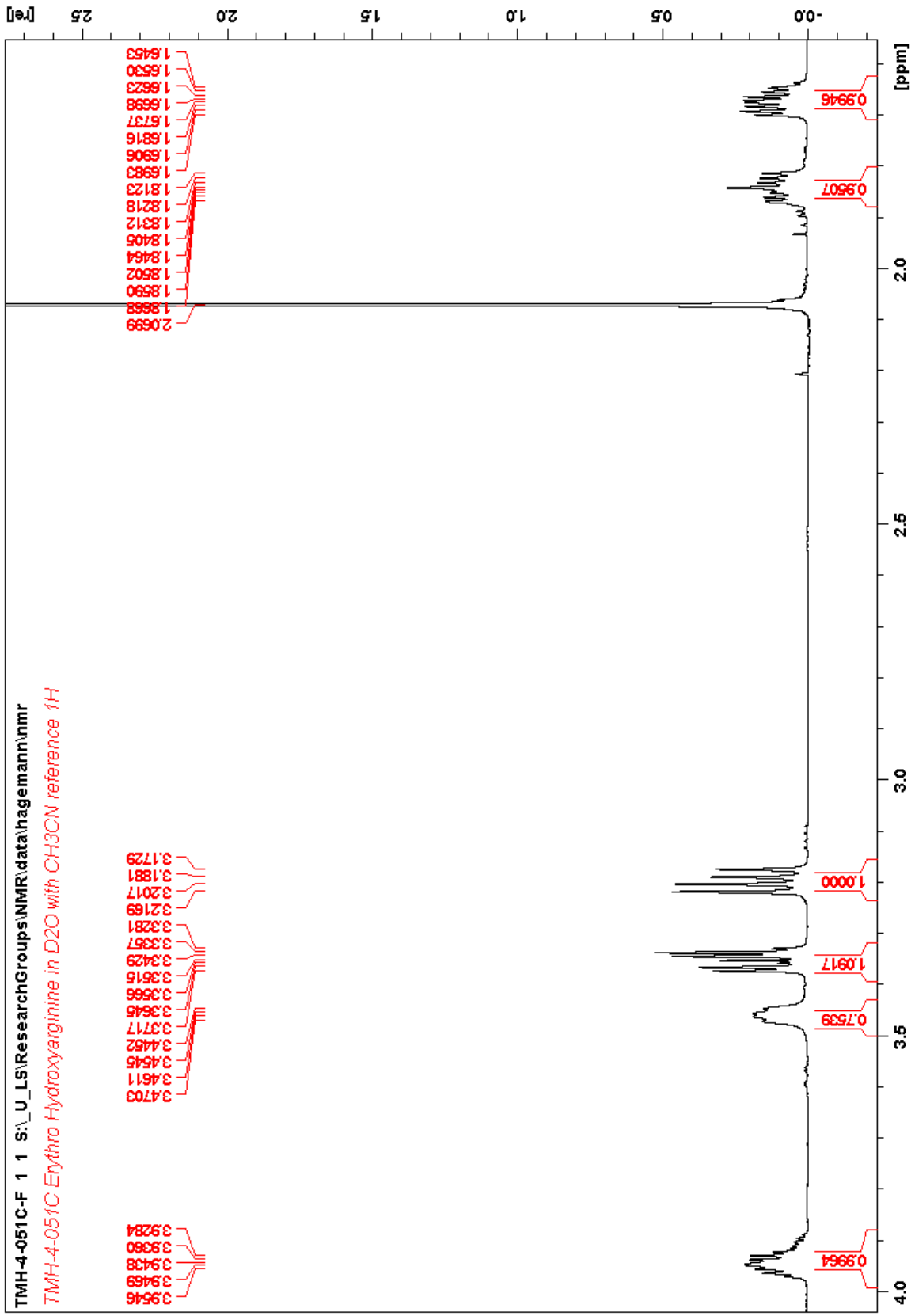

Spectrum 95*: 23e* ***^{1}H NMR (500 MHz, D_2O)***

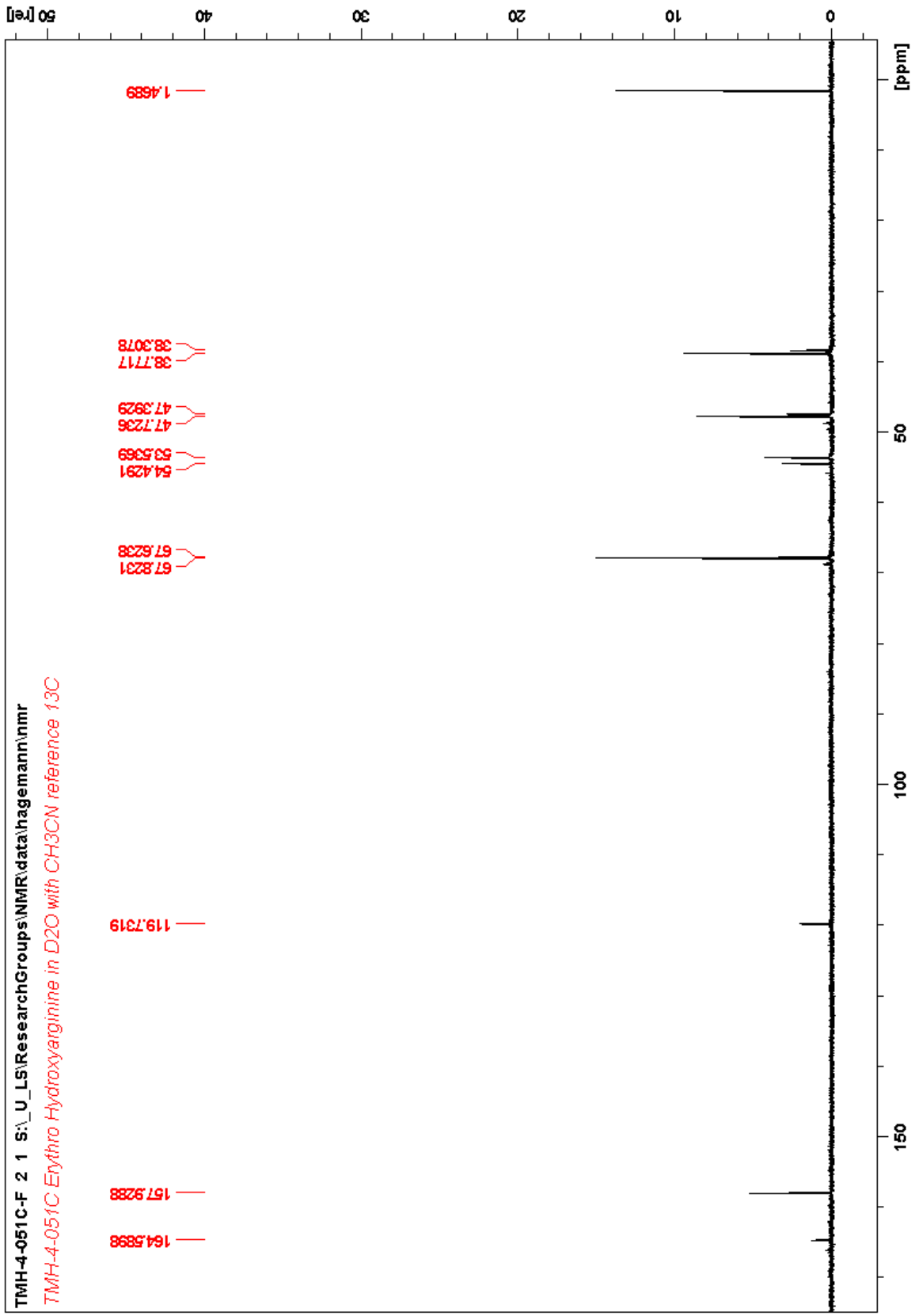

Spectrum 96*: 23e* **^{13}C NMR (500 MHz, D_2O)**

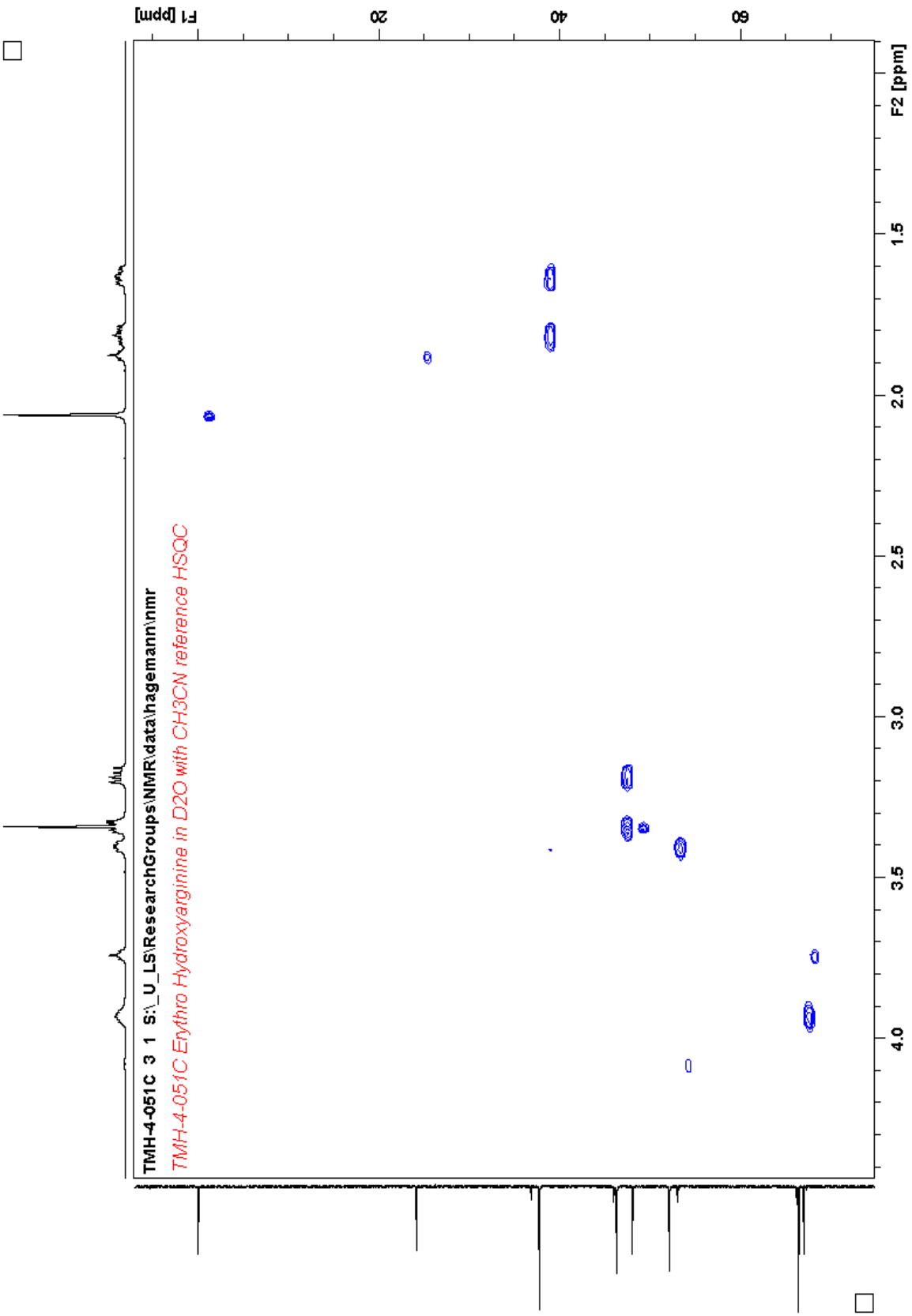

Spectrum 97*: 23e* ***HSQC NMR (500 MHz, D_2O)***

<Spectrum>

R.Time:----(Scan#:----)
MassPeaks:601 BasePeak:191(98507)
Spectrum Mode:Averaged 0.140-0.303(85-183)
BG Mode:None Polarity:Positive Segment 1 - Event 1

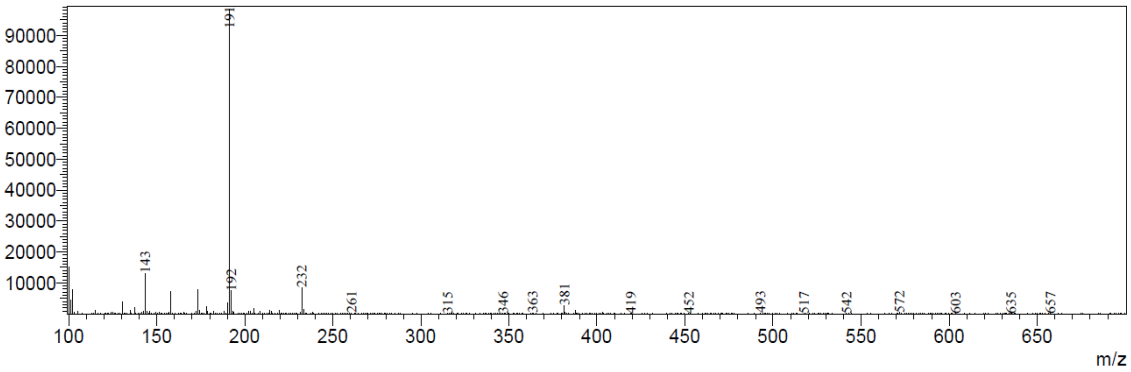

R.Time:----(Scan#:----)
MassPeaks:601 BasePeak:415(72910)
Spectrum Mode:Averaged 0.142-0.305(86-184)
BG Mode:None Polarity:Negative Segment 1 - Event 2

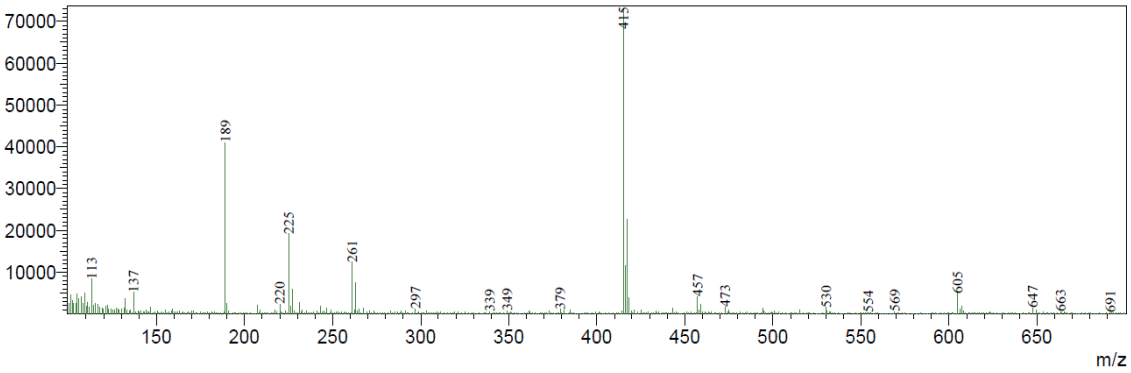

Spectrum 98*: 23e* ***ESI-LCMS Spectra***

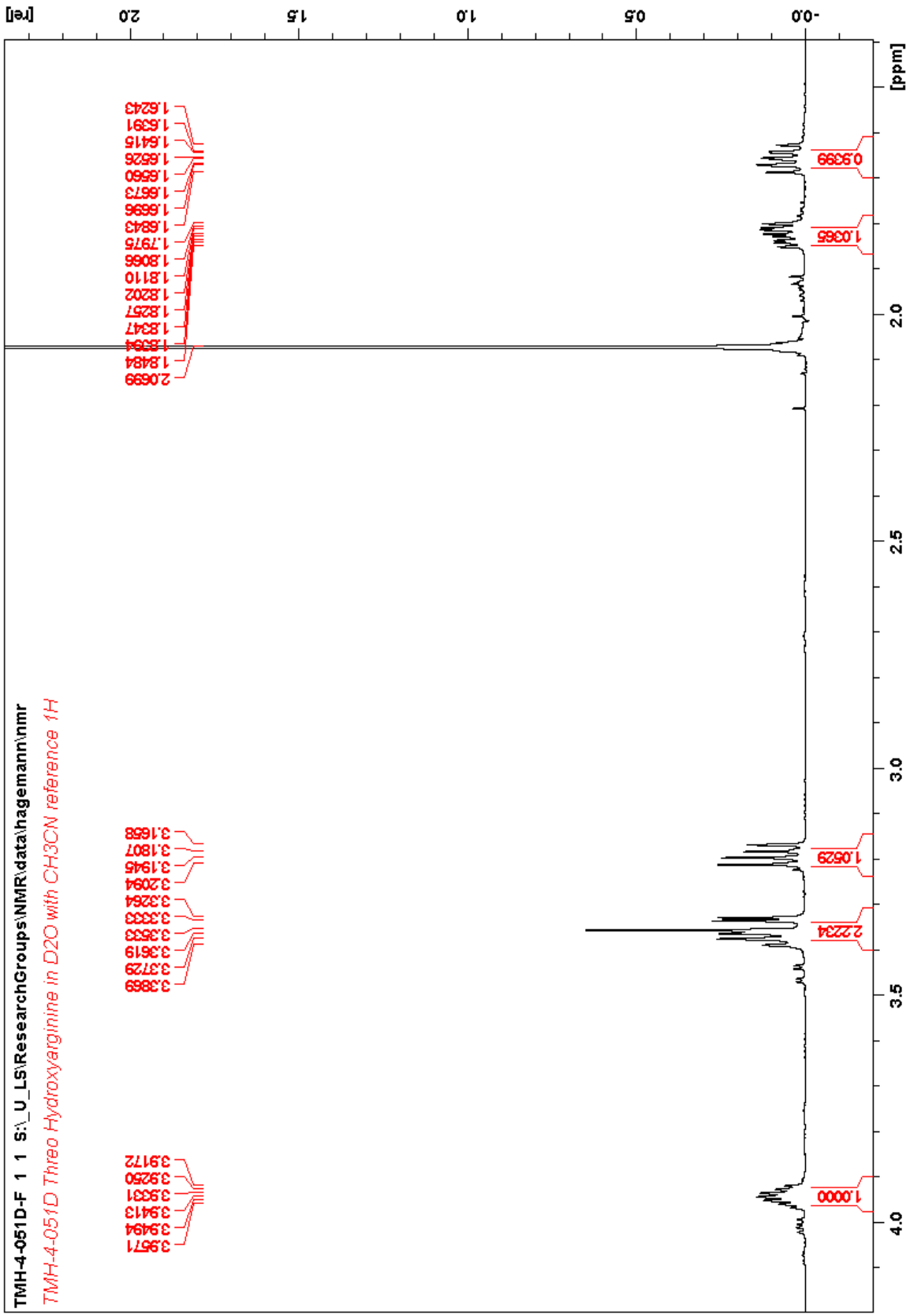

Spectrum 99*: 23t* ^{1}***H NMR (500 MHz,*** D_2O***)***

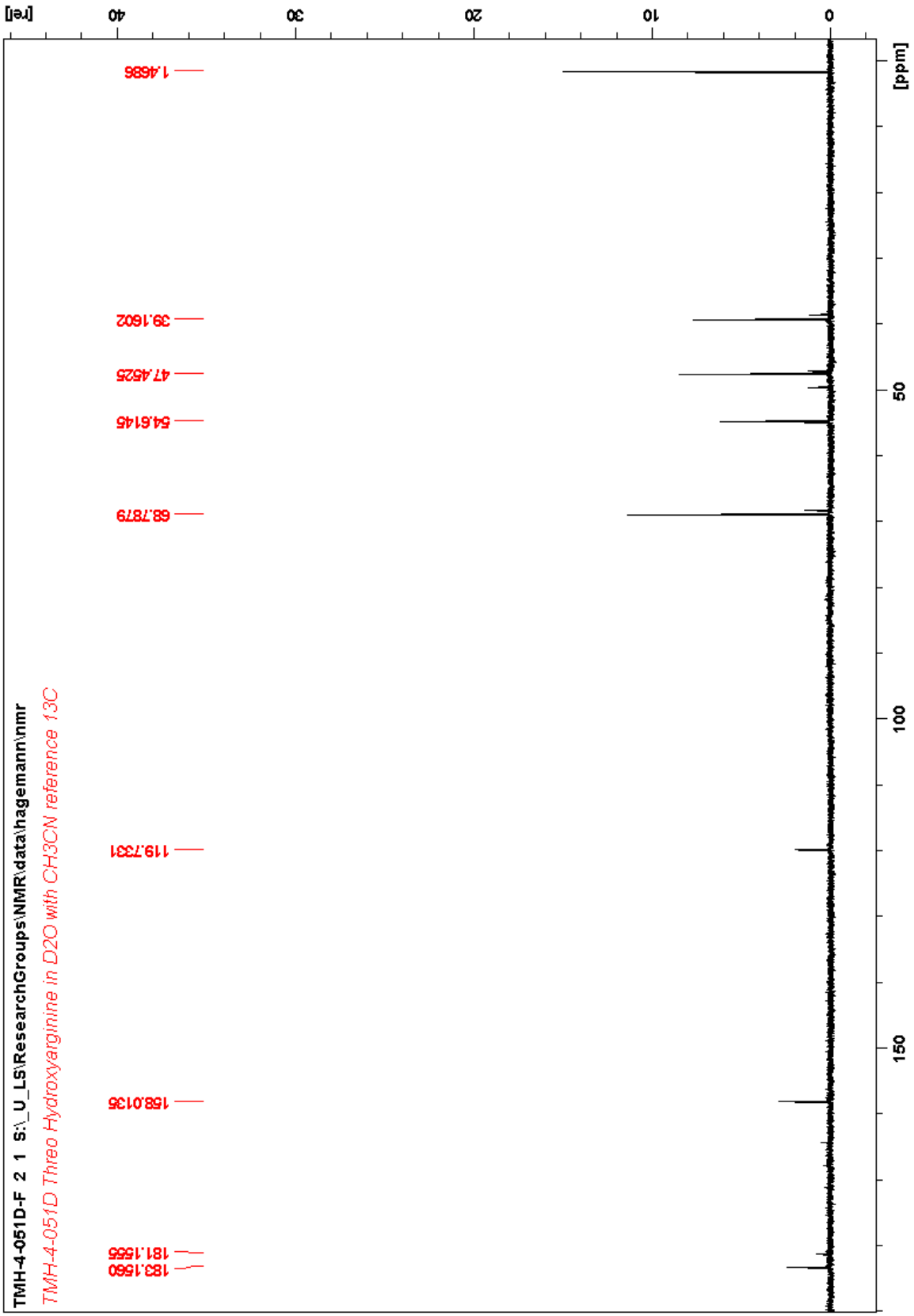

Spectrum 100*: 23t* ***^{13}C NMR (500 MHz, D_2O)***

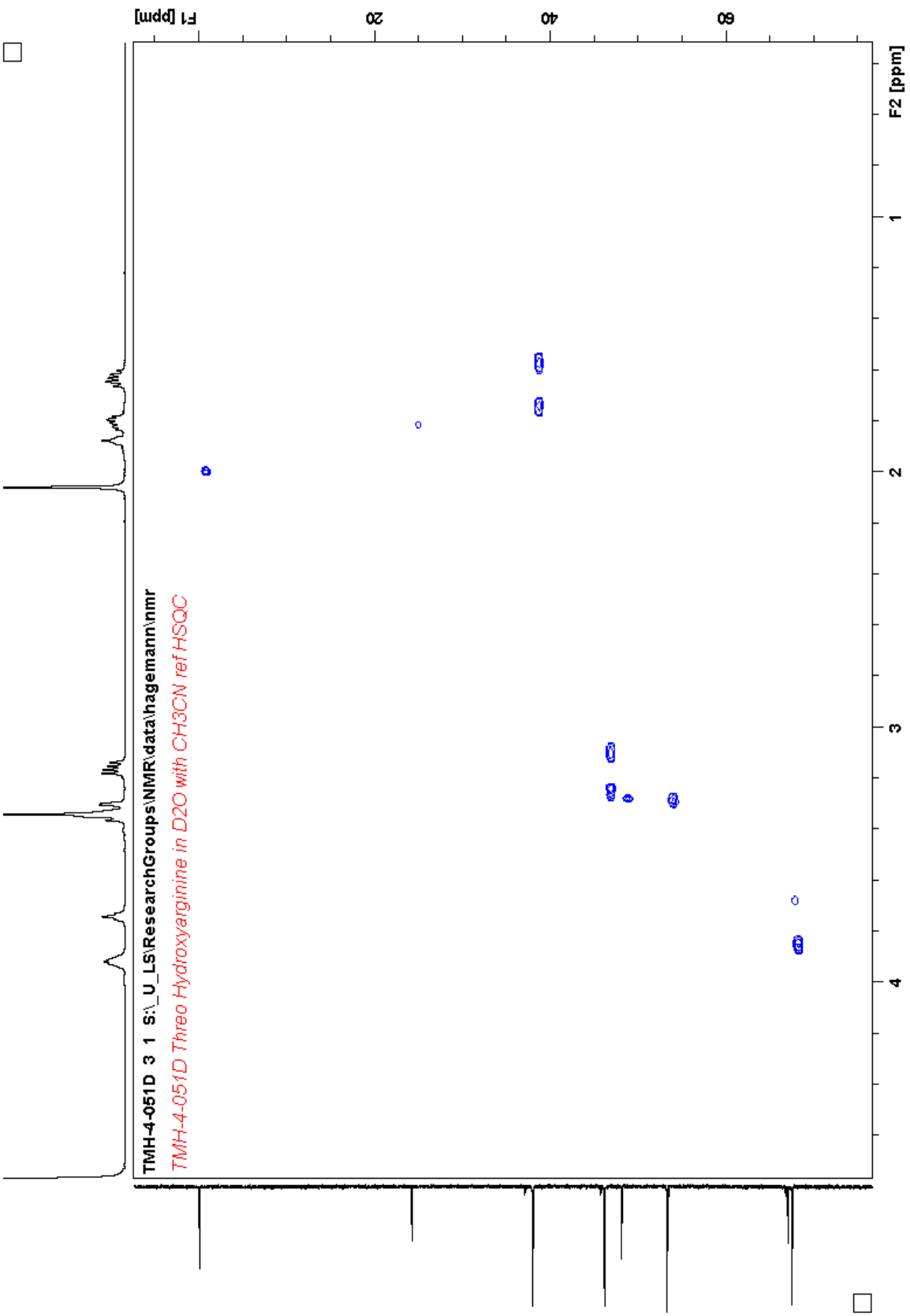

Spectrum 101*: 23t* ***HSQC NMR (500 MHz, D_2O)***

<Spectrum>

R.Time:----(Scan#:----)
MassPeaks:421 BasePeak:191(40814)
Spectrum Mode:Averaged 0.147-0.310(89-187)
BG Mode:Averaged 0.030-0.093(19-57) Polarity:Positive Segment 1 - Event 1

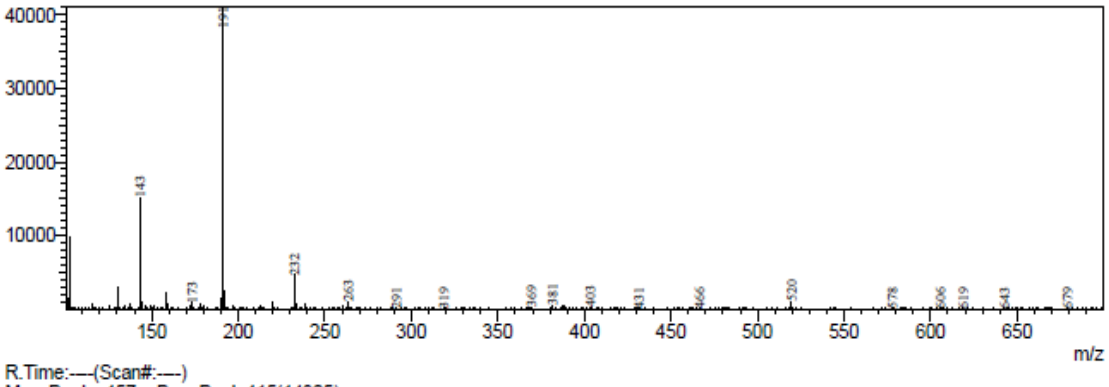

R.Time:----(Scan#:----)
MassPeaks:457 BasePeak:415(14325)
Spectrum Mode:Averaged 0.148-0.312(90-188)
BG Mode:Averaged 0.032-0.095(20-58) Polarity:Negative Segment 1 - Event 2

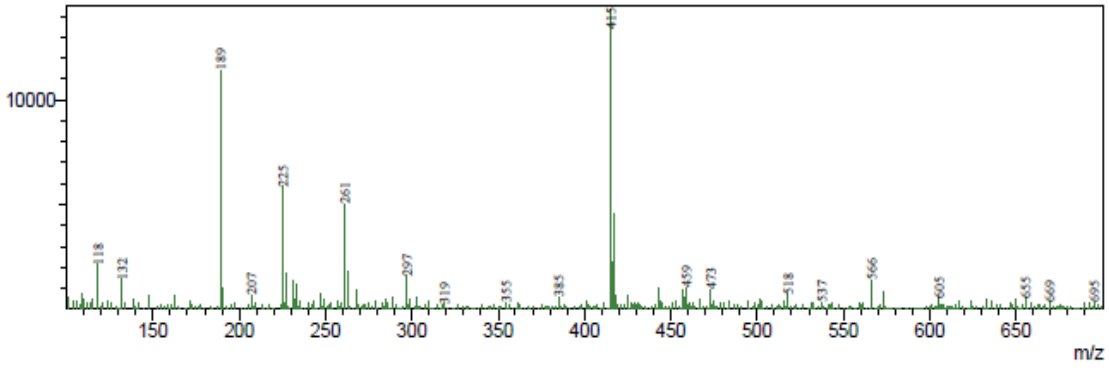

Spectrum 102*: 23t* ***ESI-LCMS Spectra***

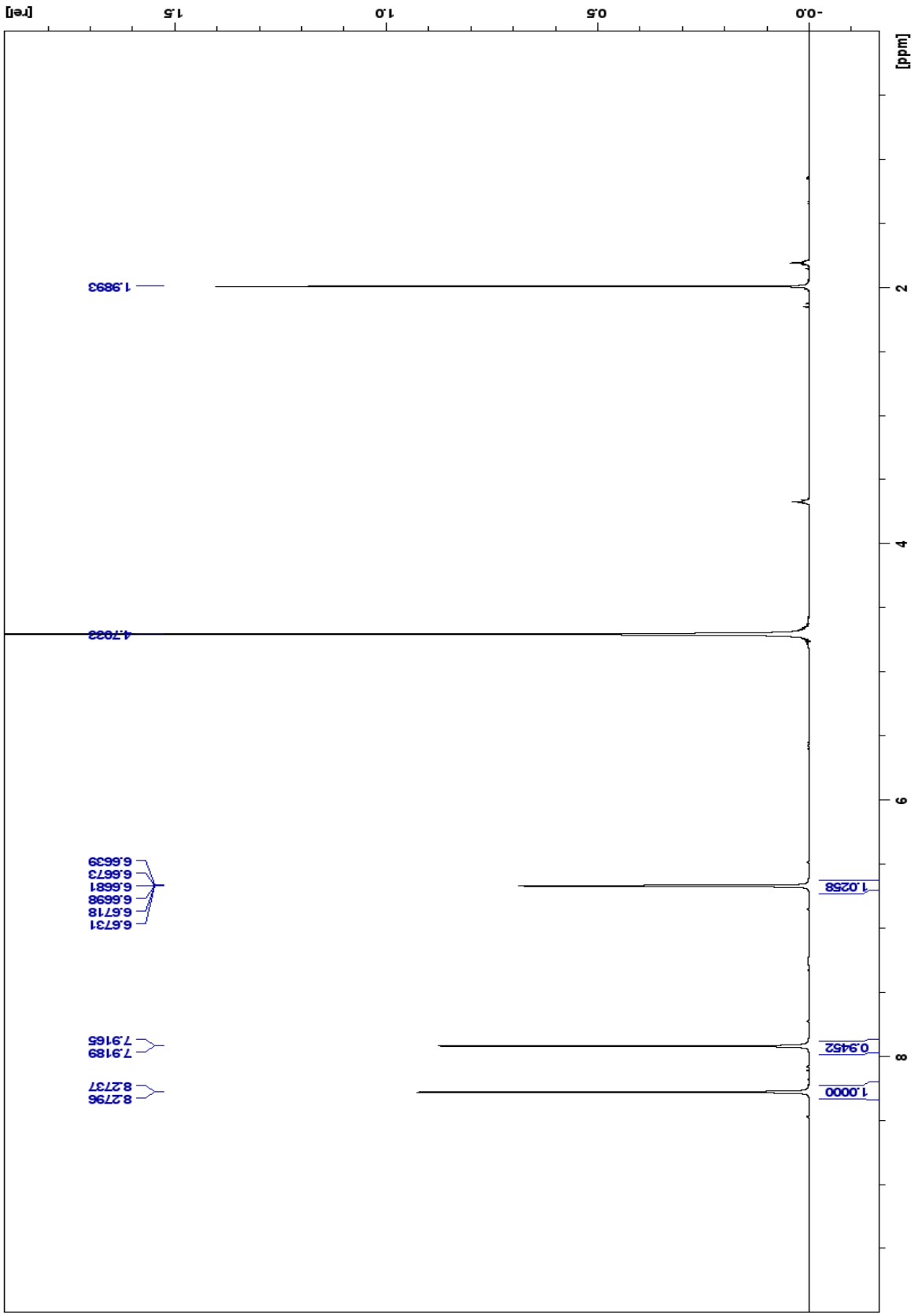

Spectrum 103*: 24 ^{1}H NMR (500 MHz, D_2O)*

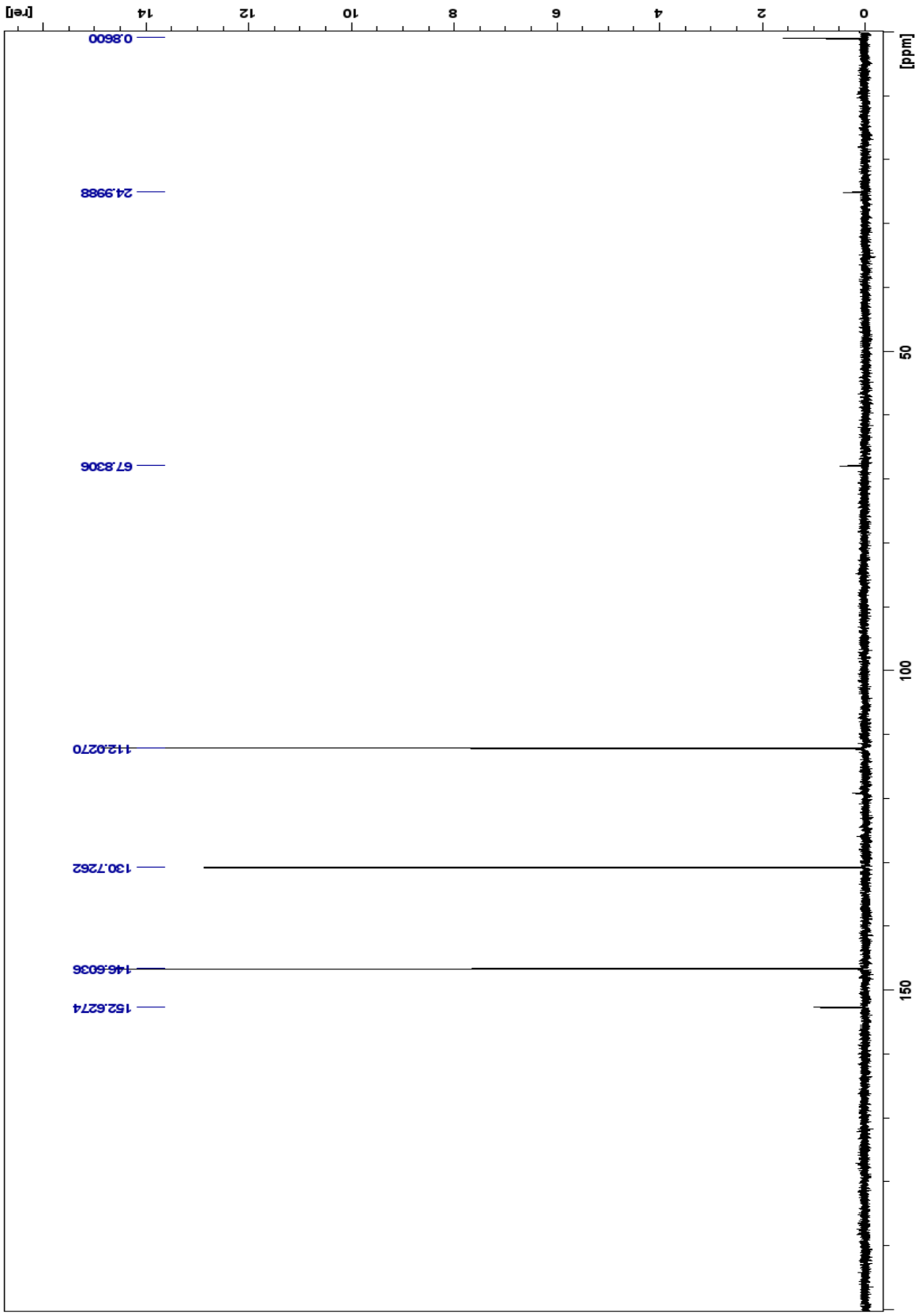

Spectrum 104*: 24 ^{13}C NMR (500 MHz, D_2O)*

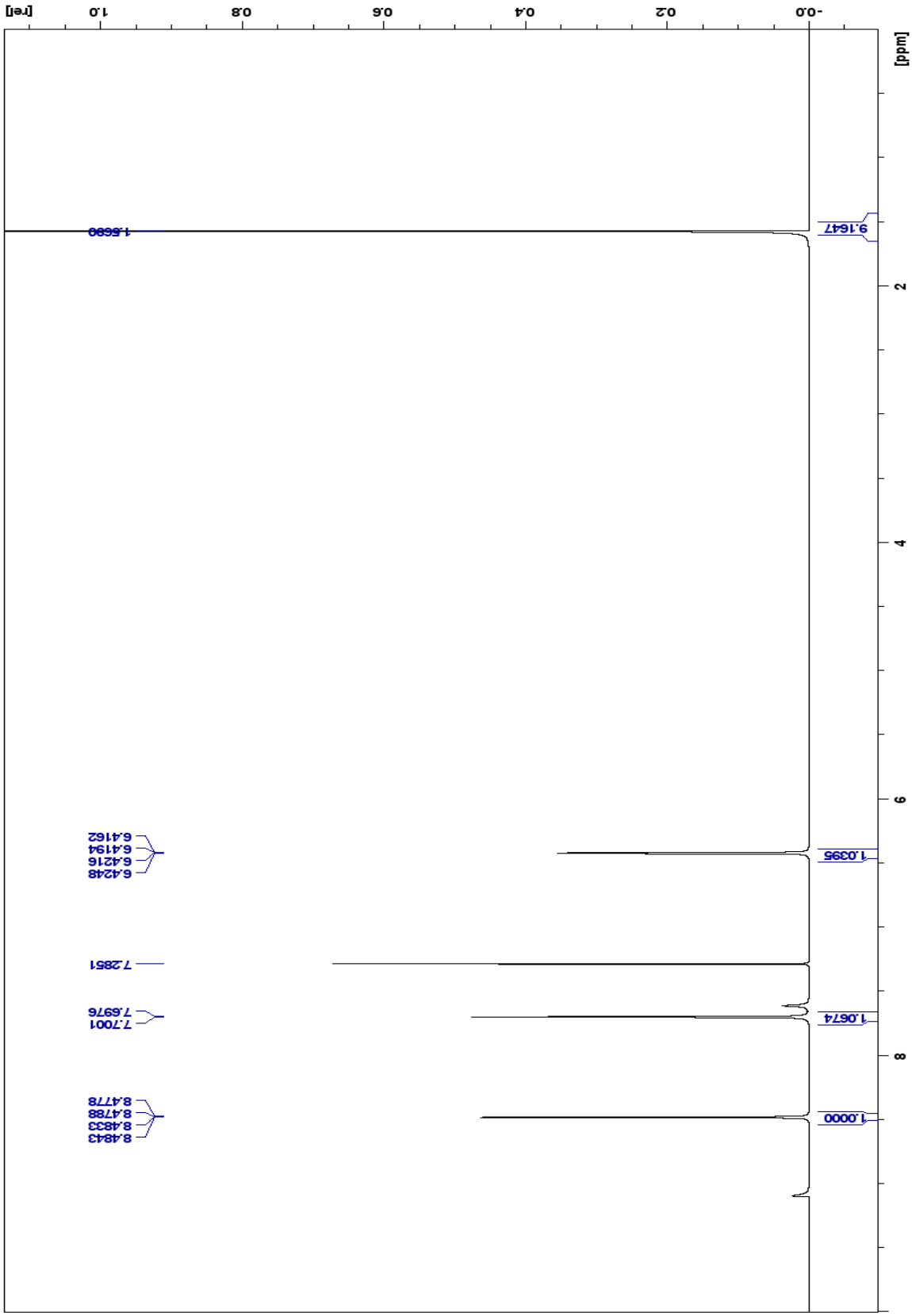

Spectrum 105*: 25 ^{1}H NMR (500 MHz, $CDCl_3$)*

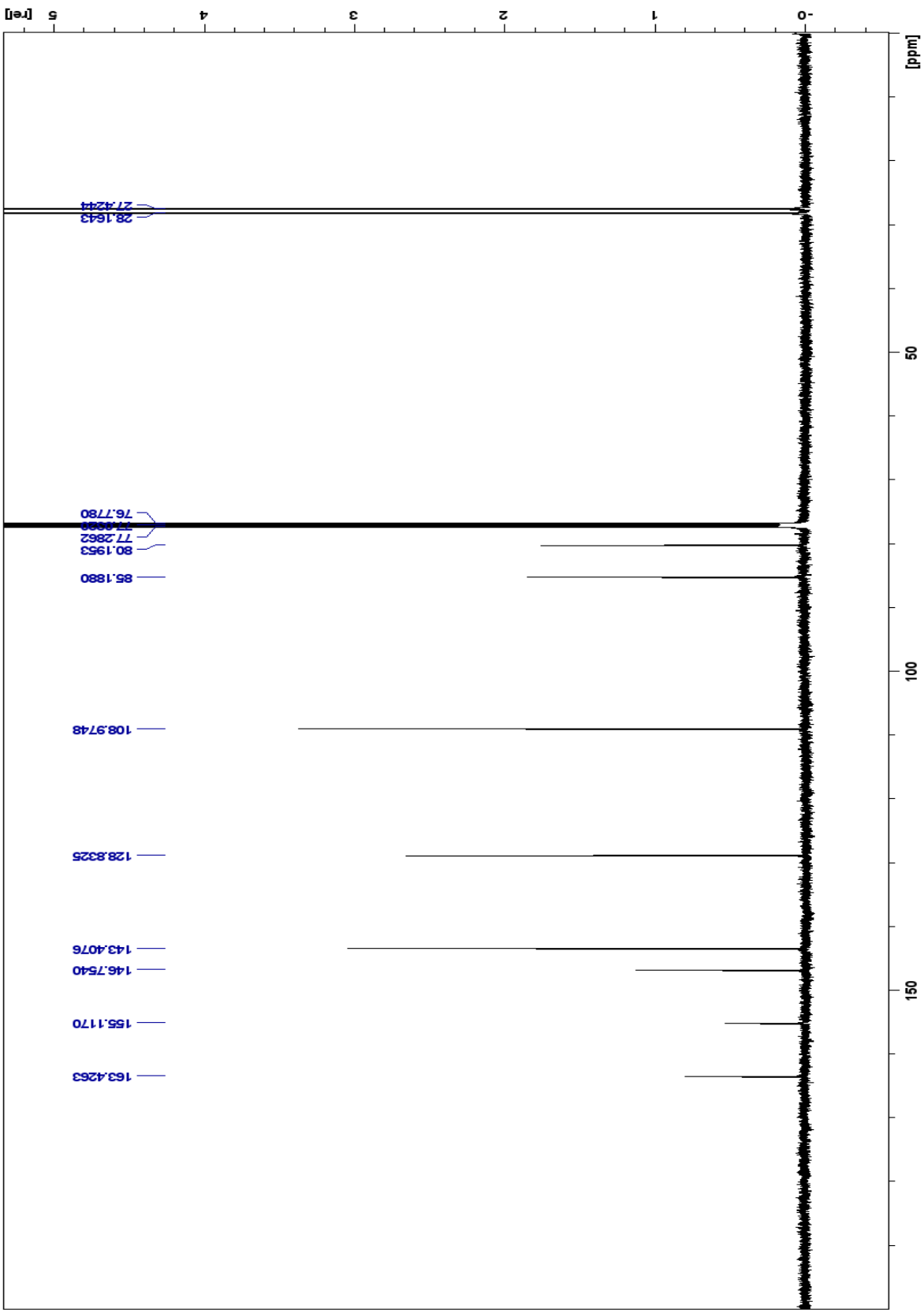

Spectrum 106*: 25* ***^{13}C NMR (500 MHz, $CDCl_3$)***

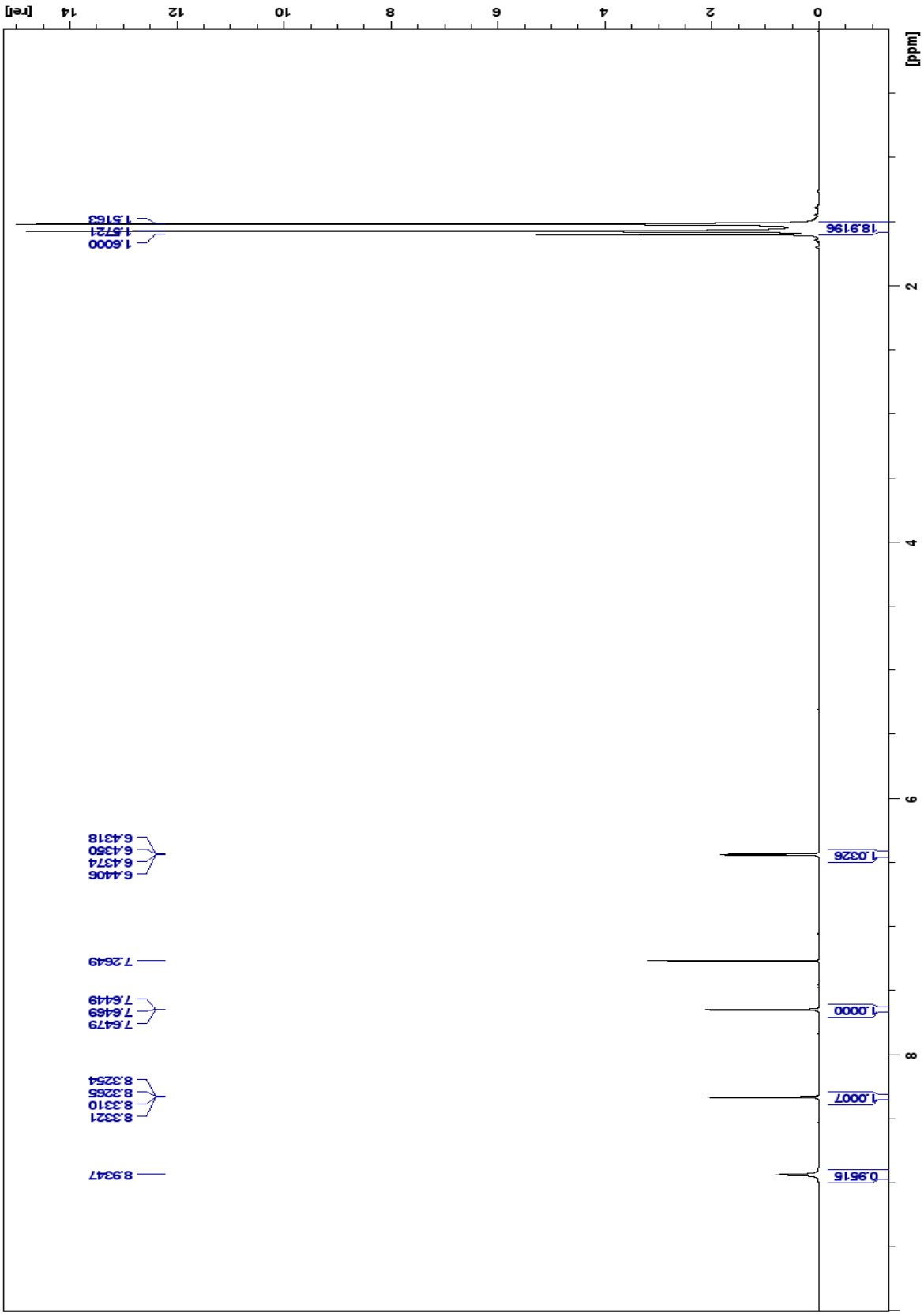

Spectrum 107*: 26 ^{1}H NMR (500 MHz, $CDCl_3$)*

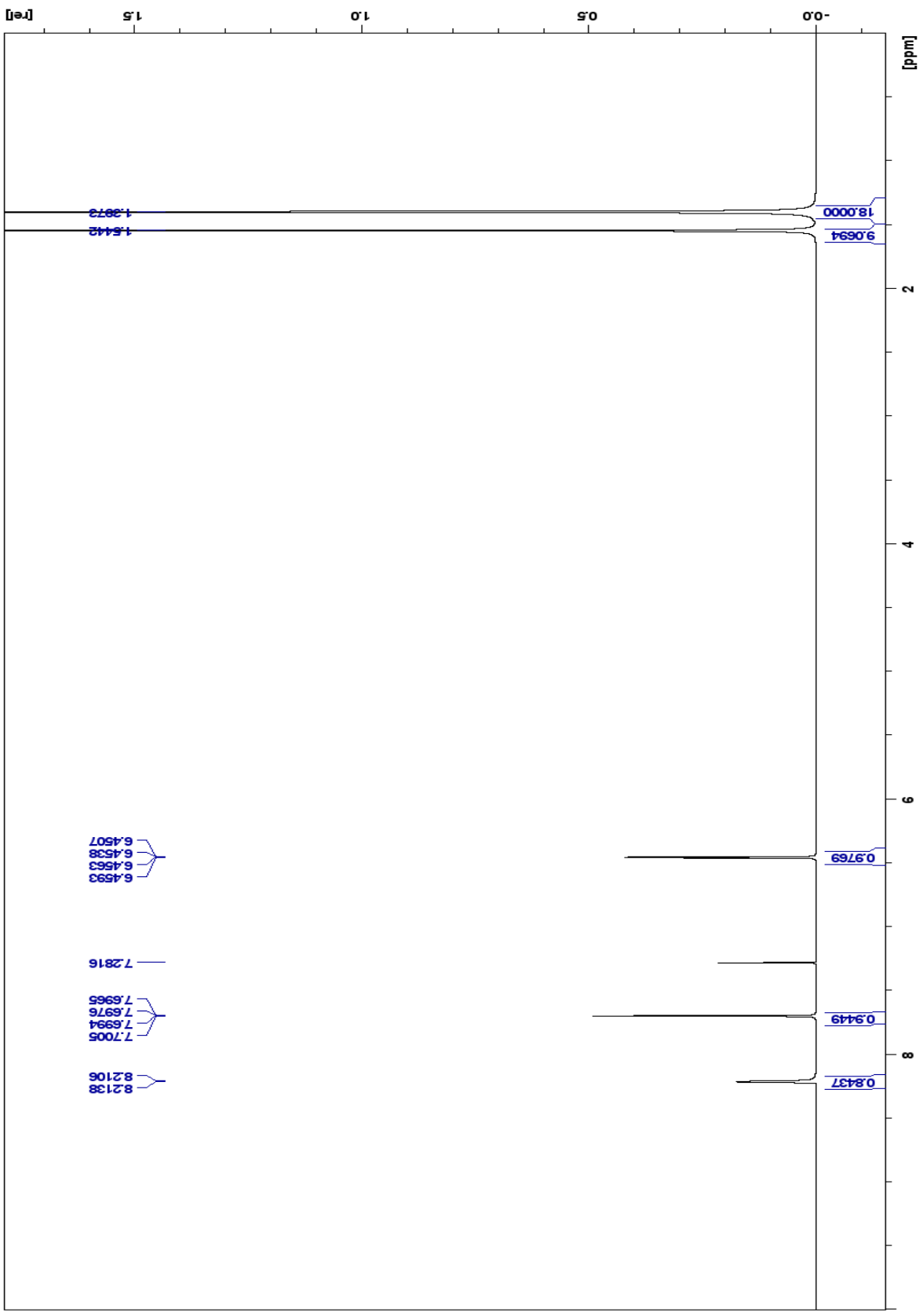

Spectrum 108*: 27* ^{1}***H NMR (500 MHz,*** $CDCl_3$***)***

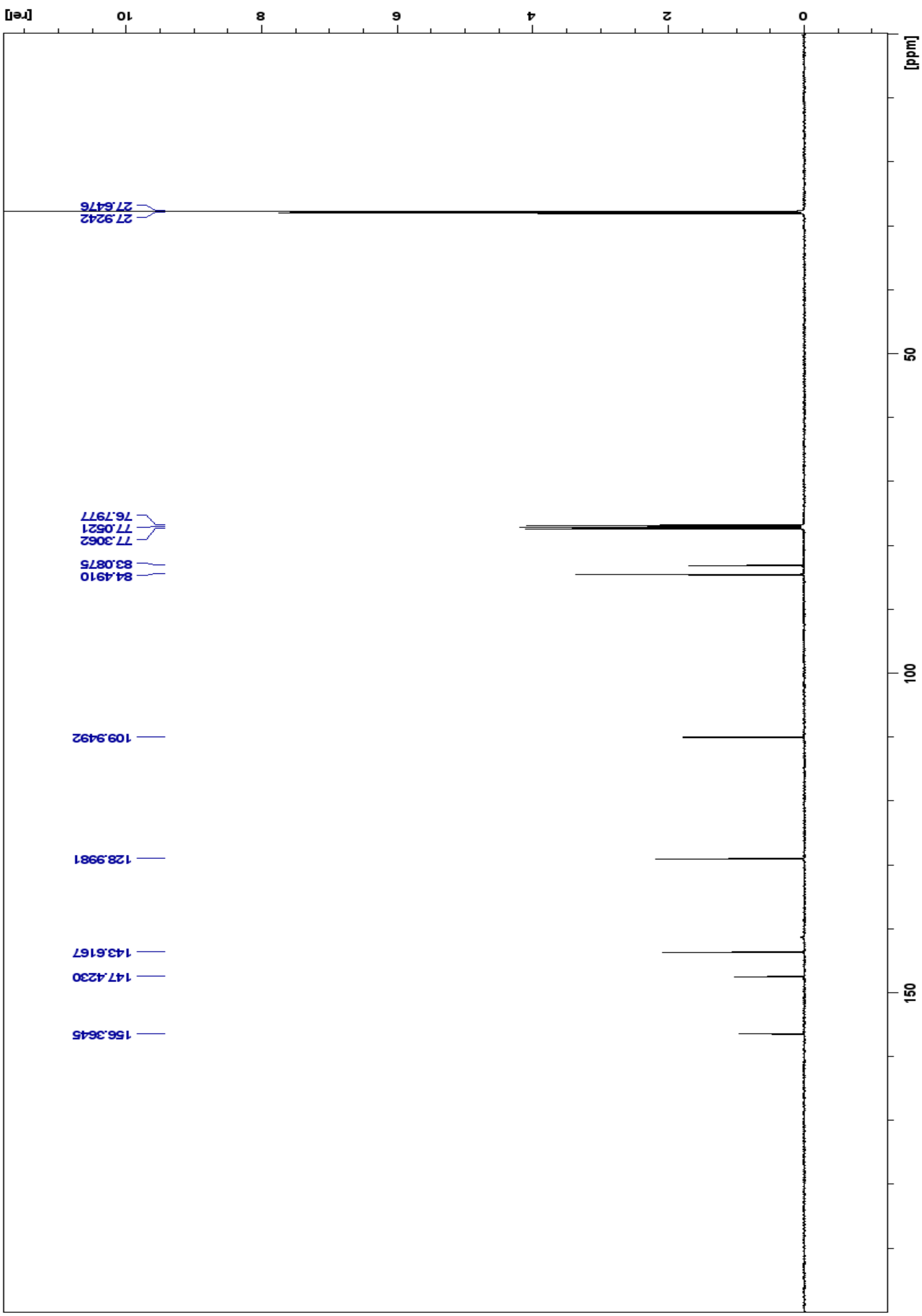

Spectrum 109*: 27 ^{13}C NMR (500 MHz, CDCl$_3$)*

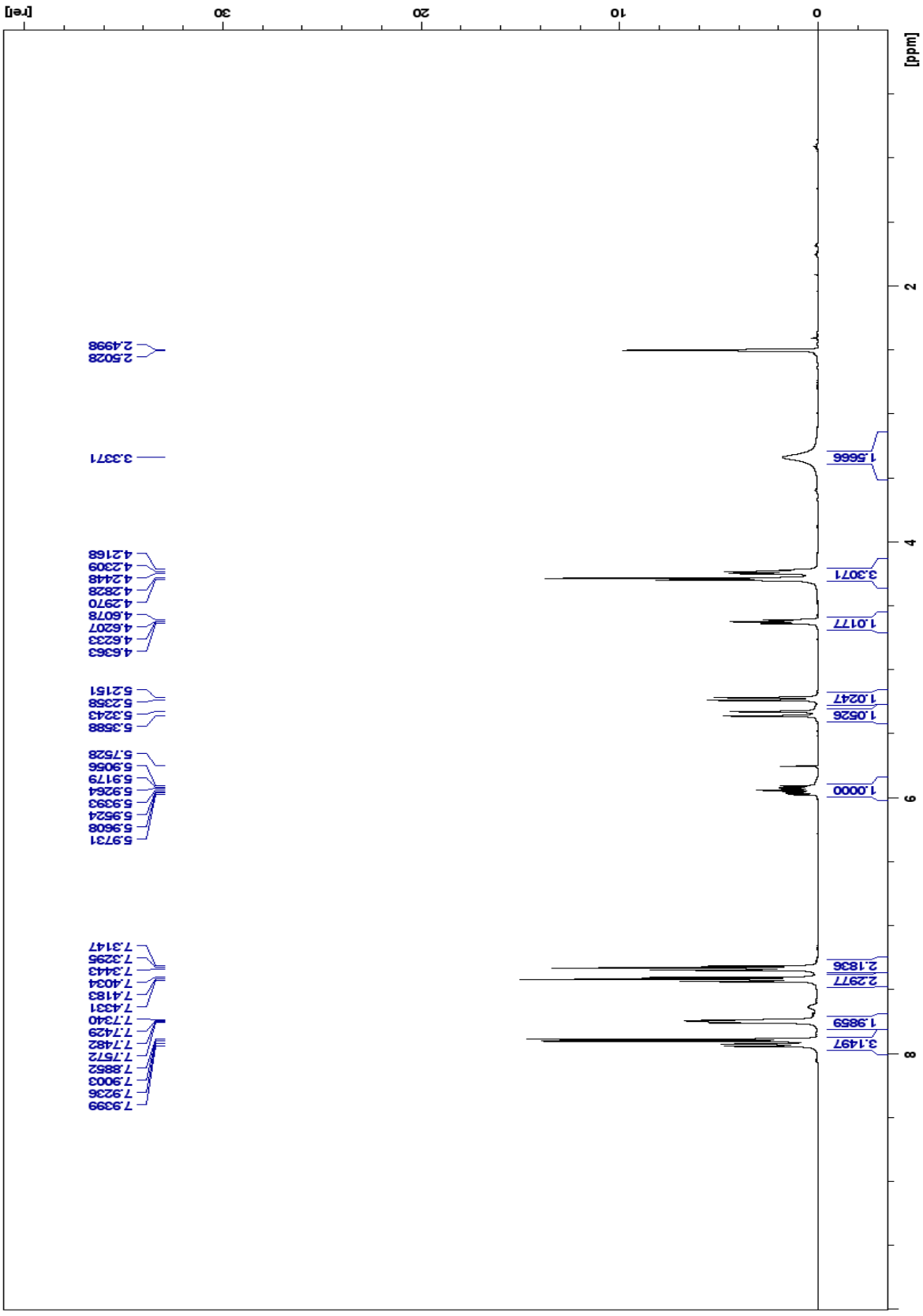

Spectrum 110*: 30* ^{1}***H NMR (500 MHz, DMSO-d6)***

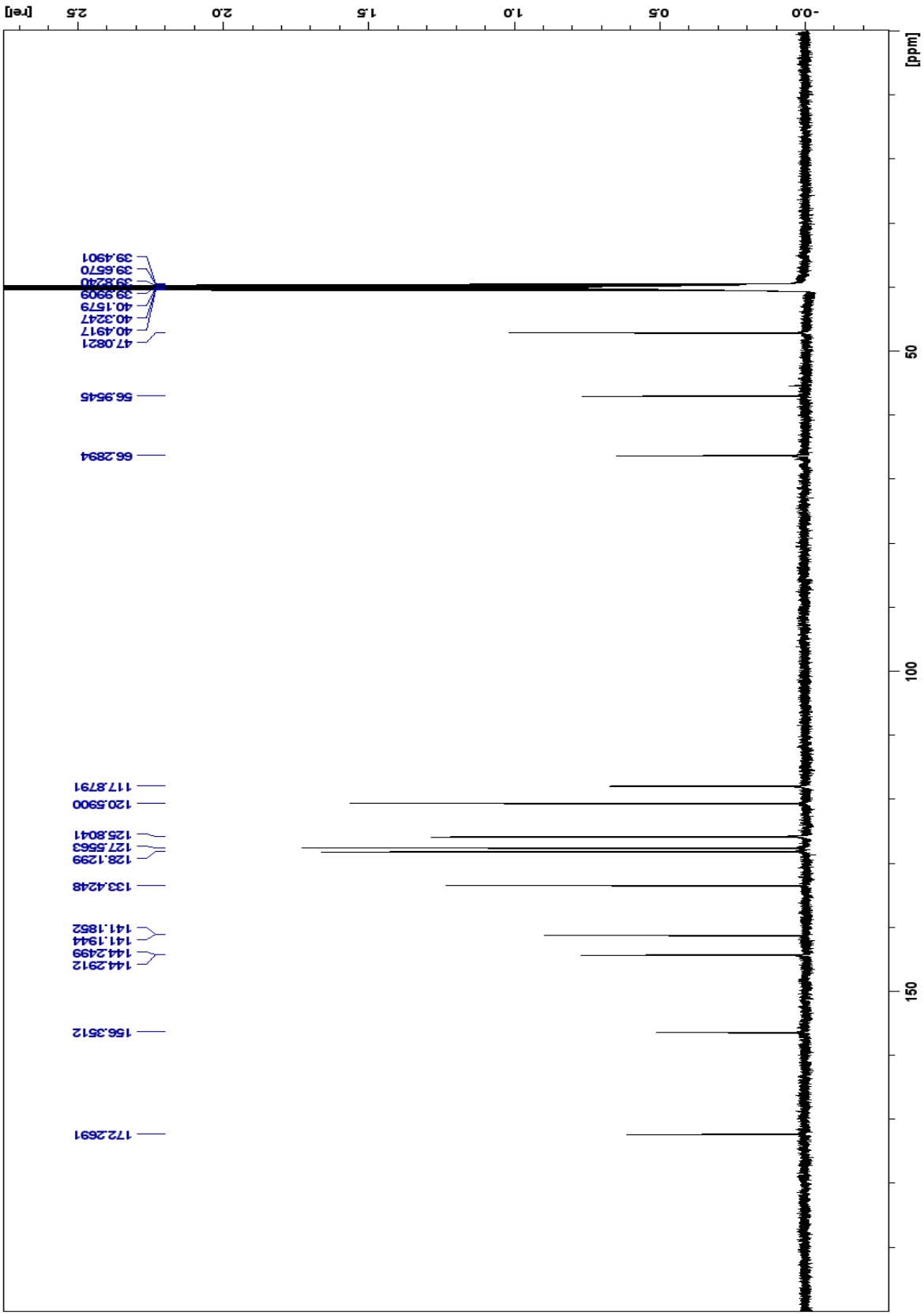

Spectrum 111*: 30 ^{13}C NMR (500 MHz, DMSO-d6)*

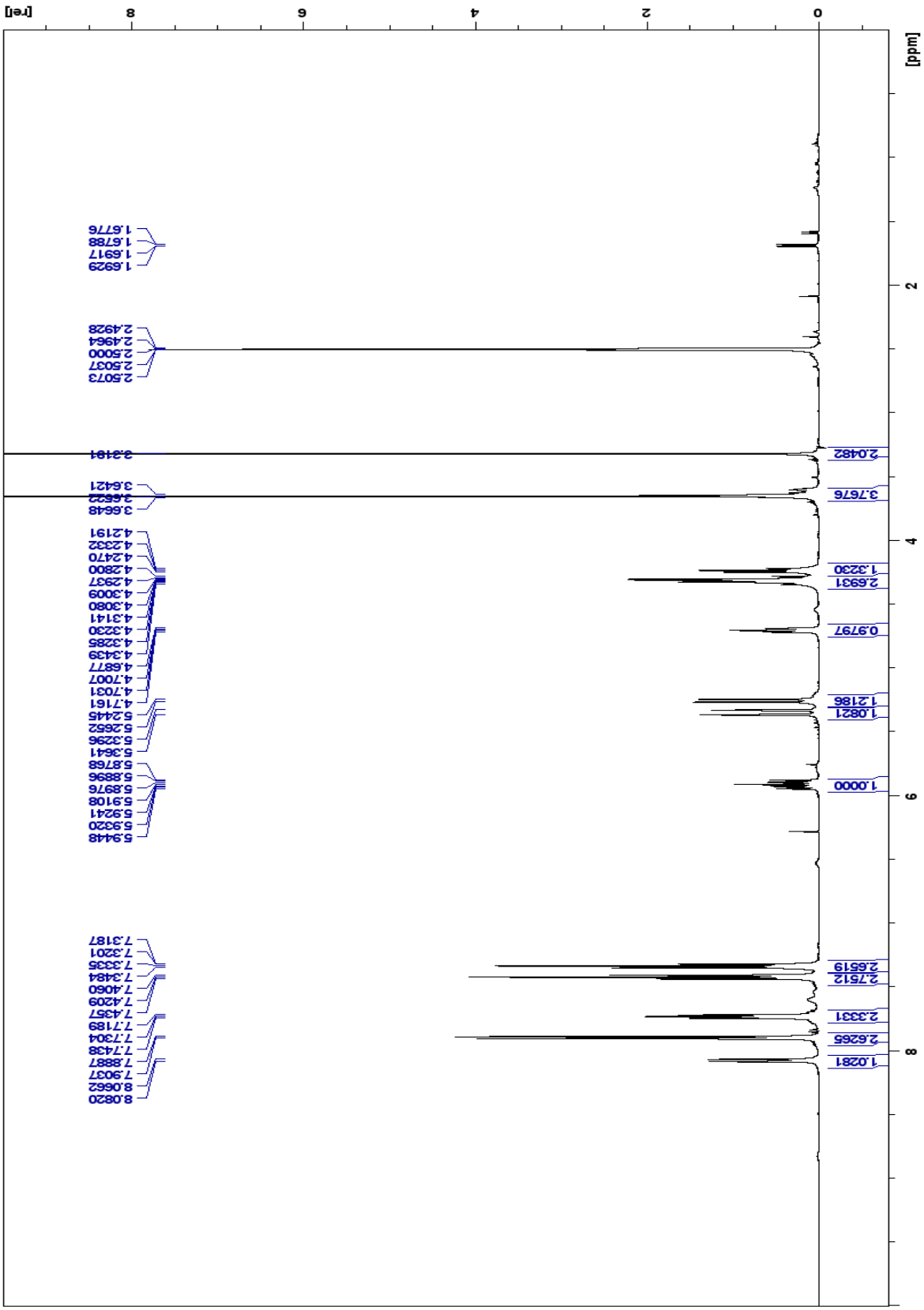

Spectrum 112*: 31* ***^{1}H NMR (500 MHz, DMSO-d6)***

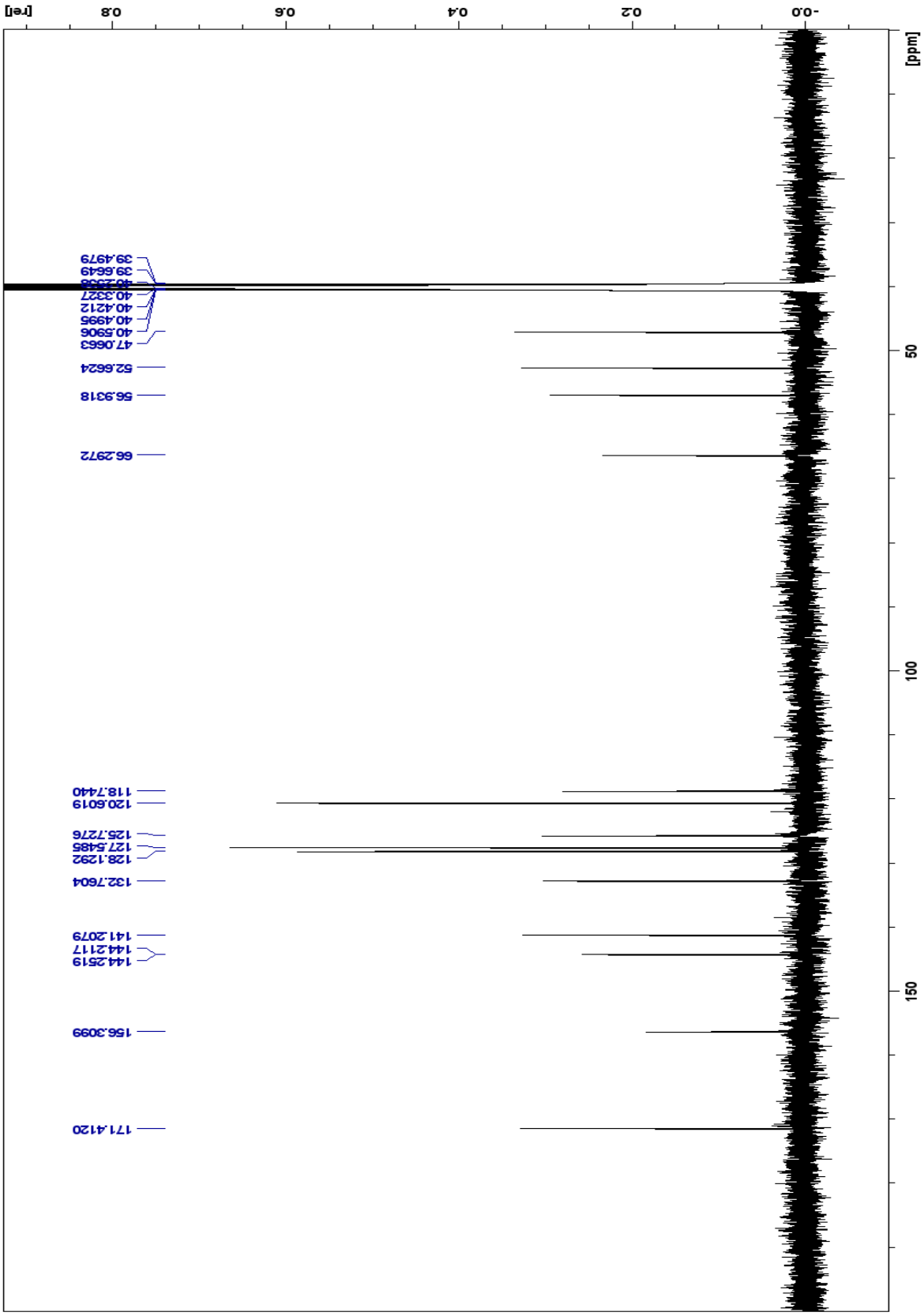

Spectrum 113*: 31 ^{13}C NMR*

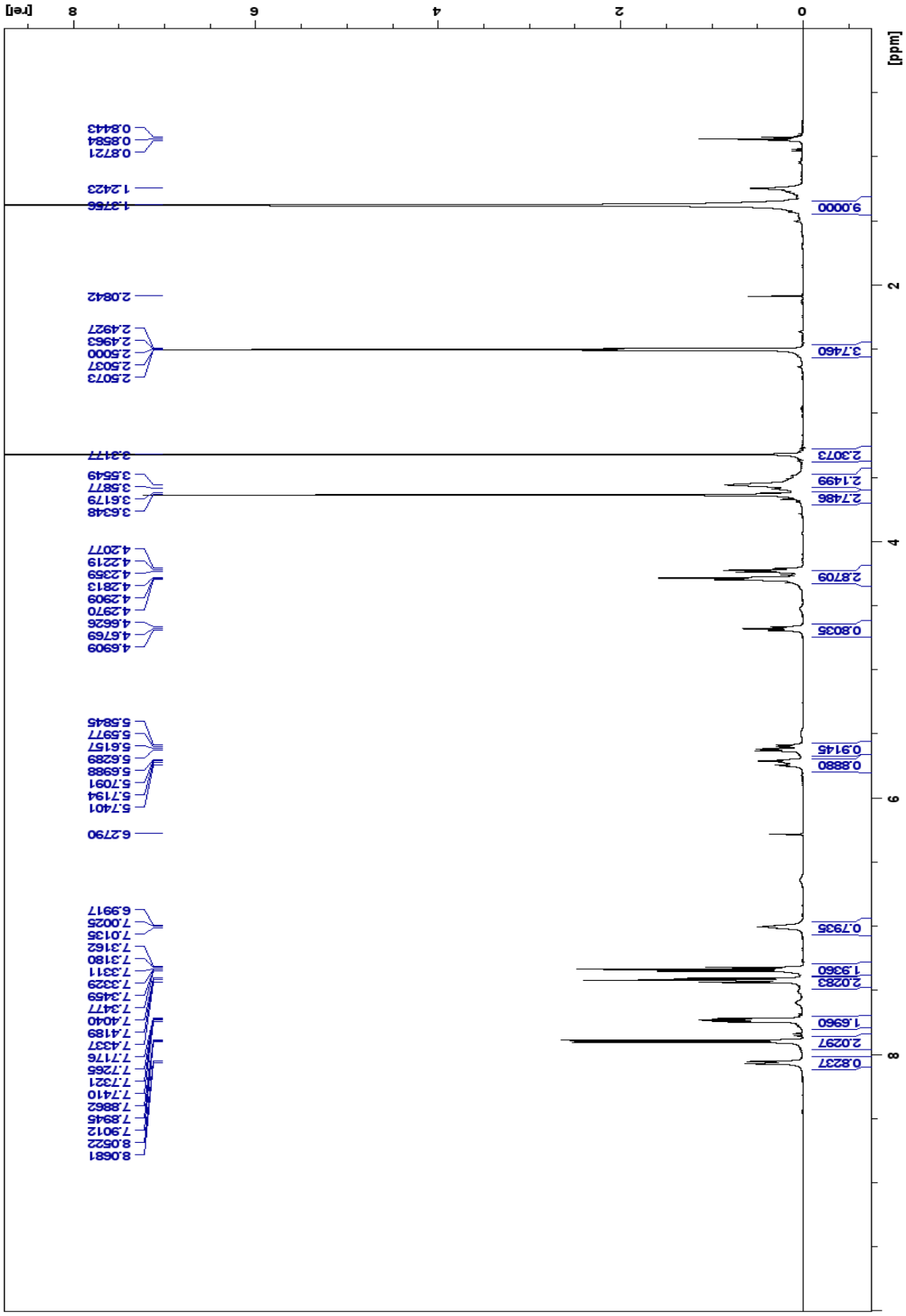

Spectrum 114*: 32 ^{1}H NMR (500 MHz, DMSO-d6)*

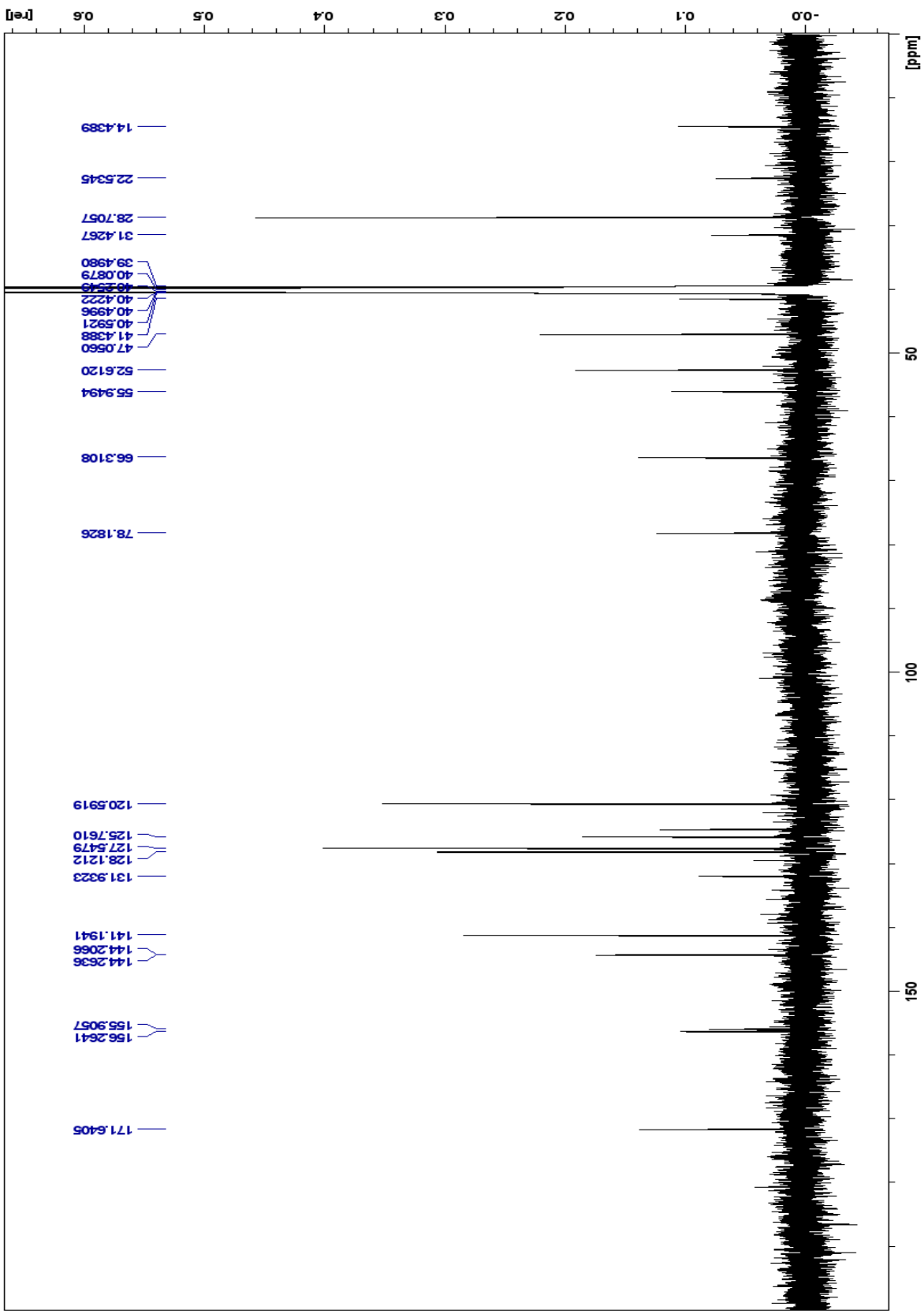

Spectrum 115*: 32 ^{13}C NMR (500 MHz, DMSO-d6)*

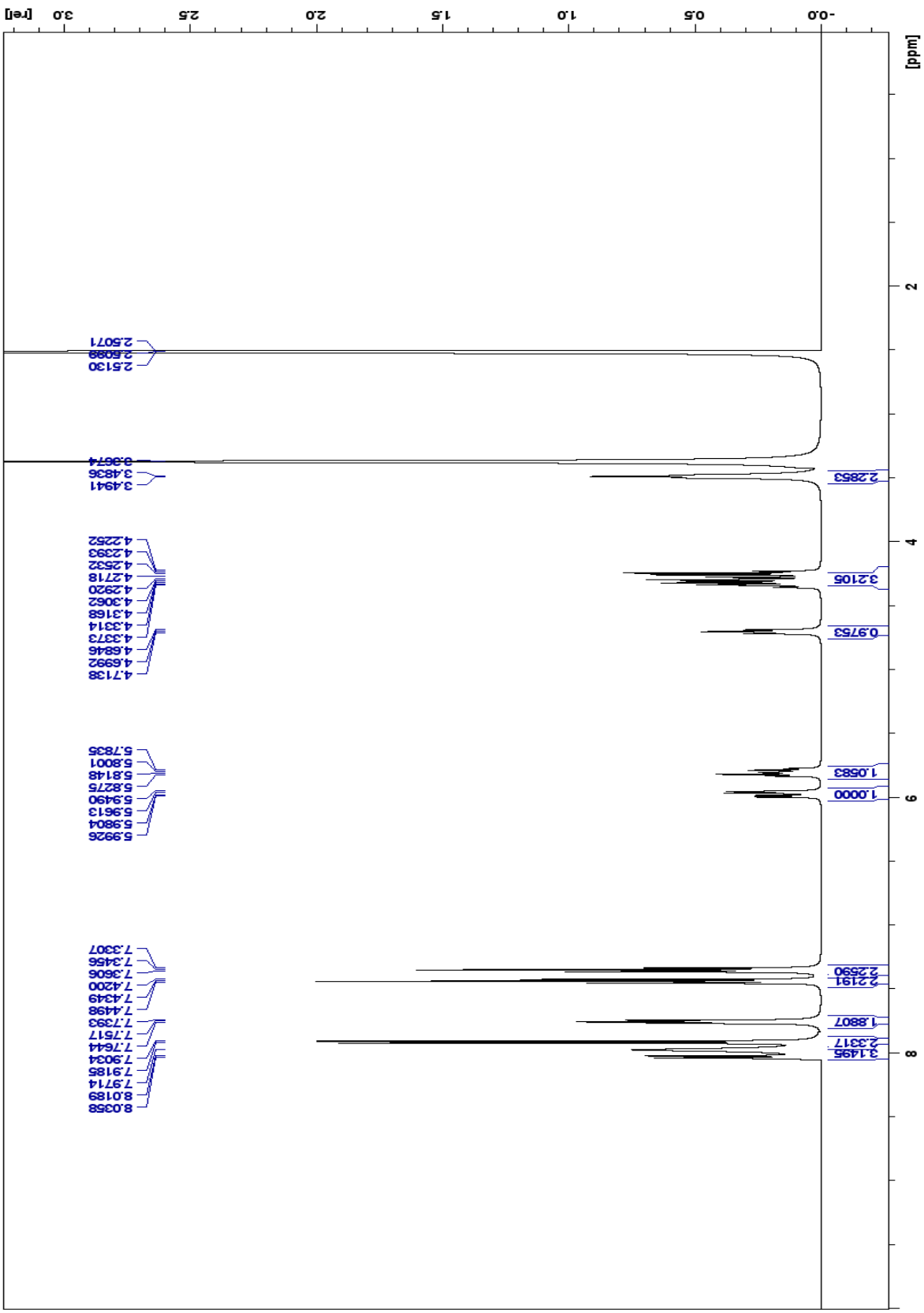

Spectrum 116*: 33* ***¹H NMR (500 MHz, DMSO-d6)***

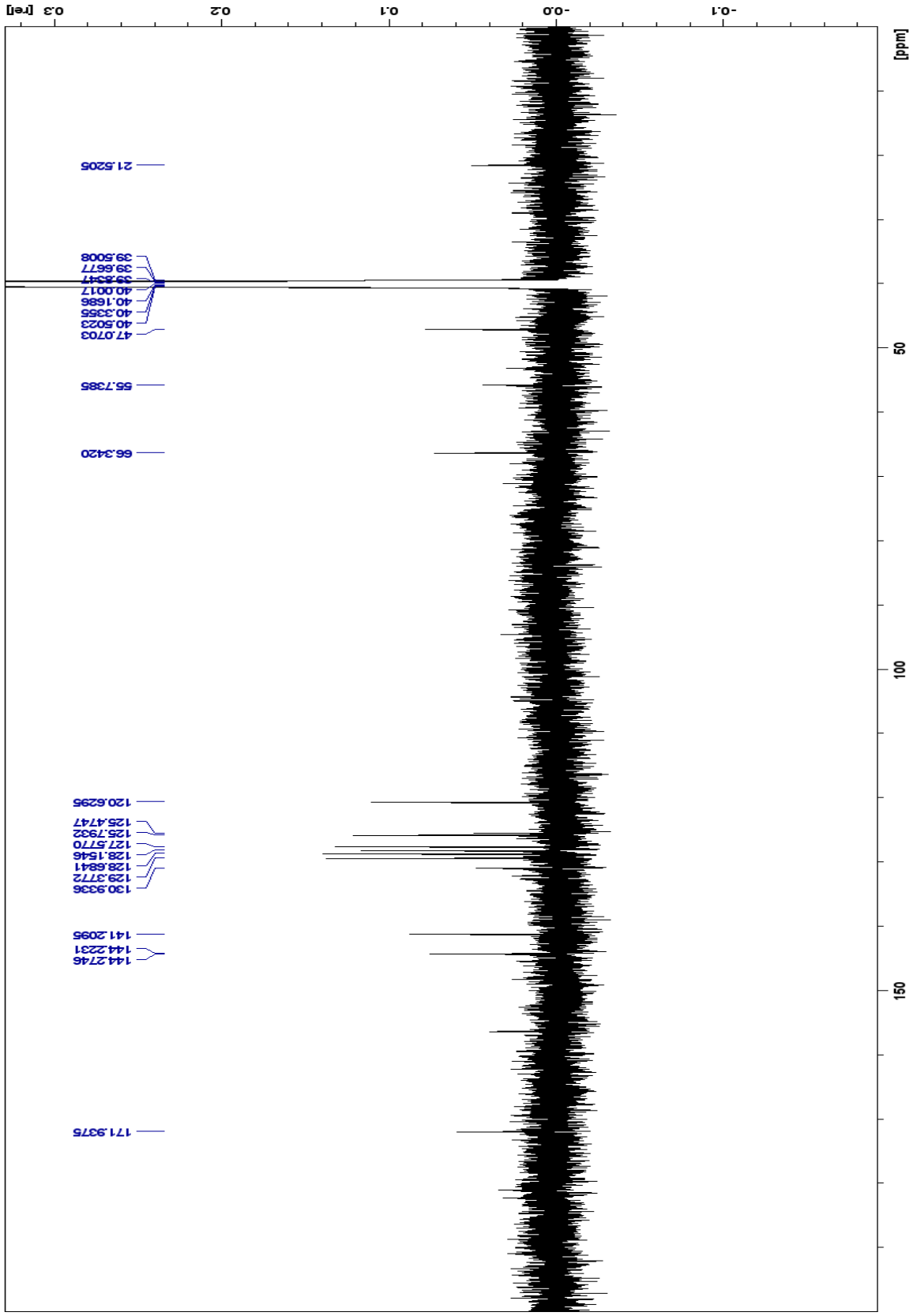

Spectrum 117*: 33 ^{13}C NMR (500 MHz, DMSO-d6)*

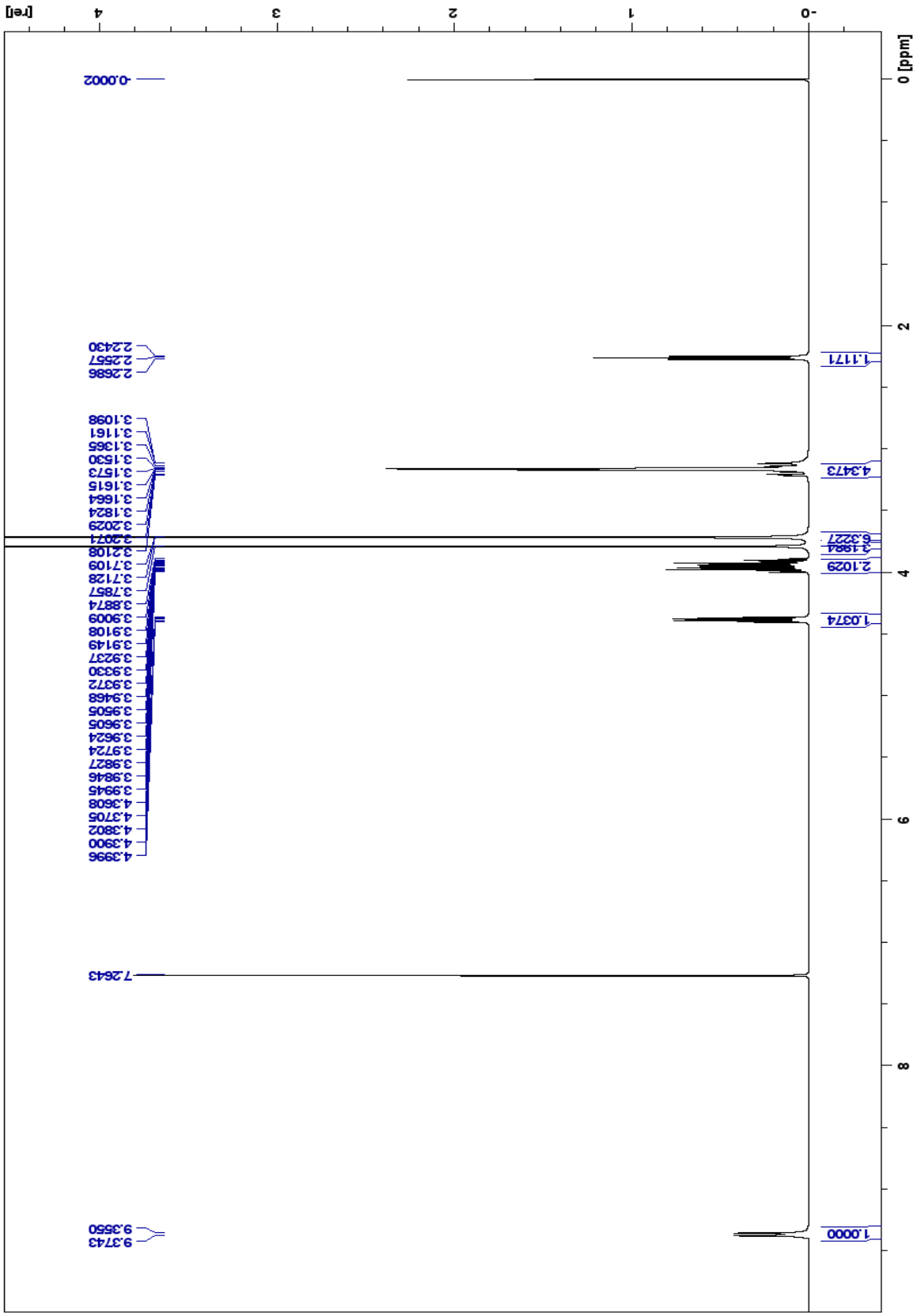

Spectrum 118*: 38 ^{1}H NMR (500 MHz, $CDCl_3$)*

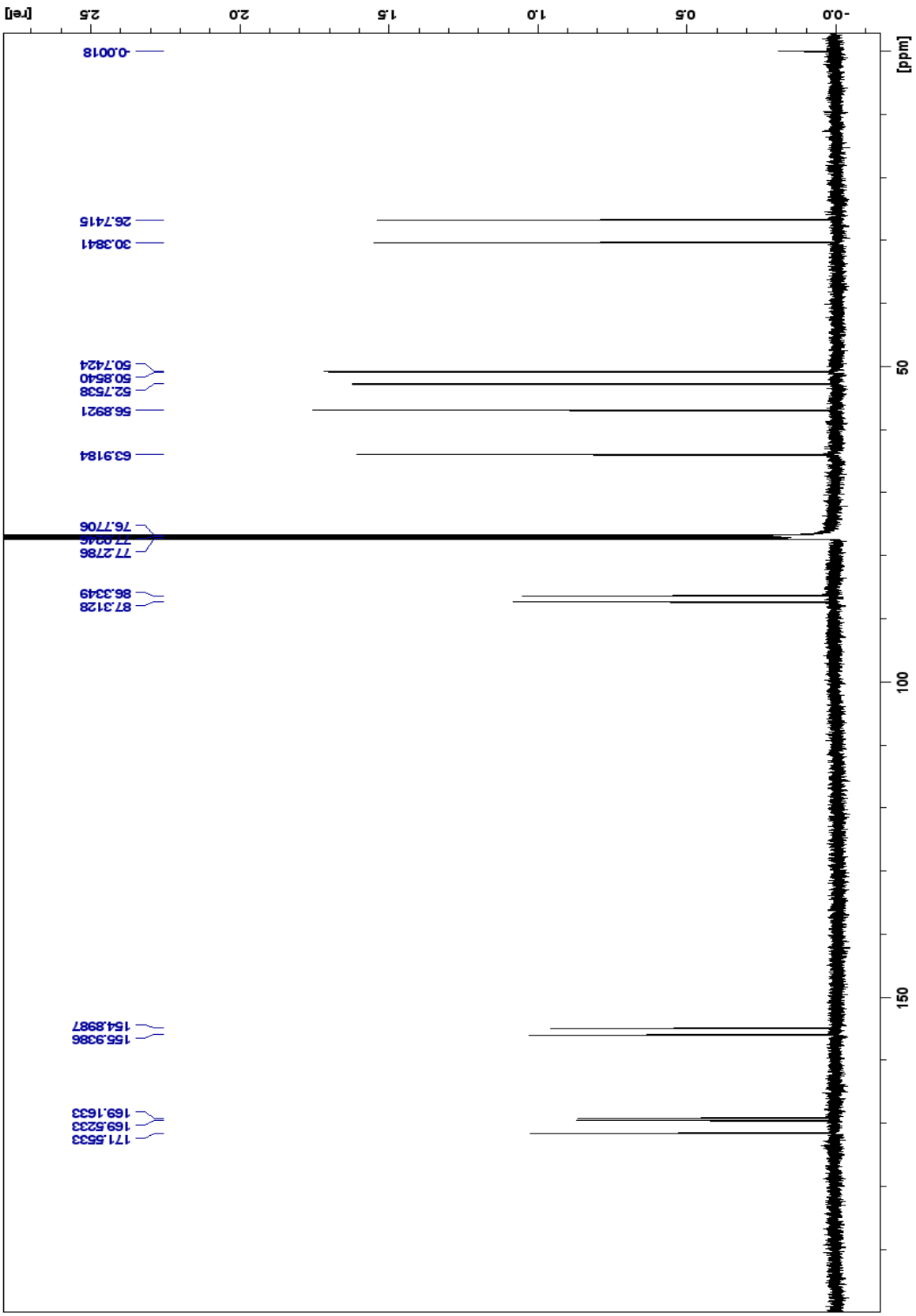

Spectrum 119*: 38 ^{13}C NMR (500 MHz, $CDCl_3$)*

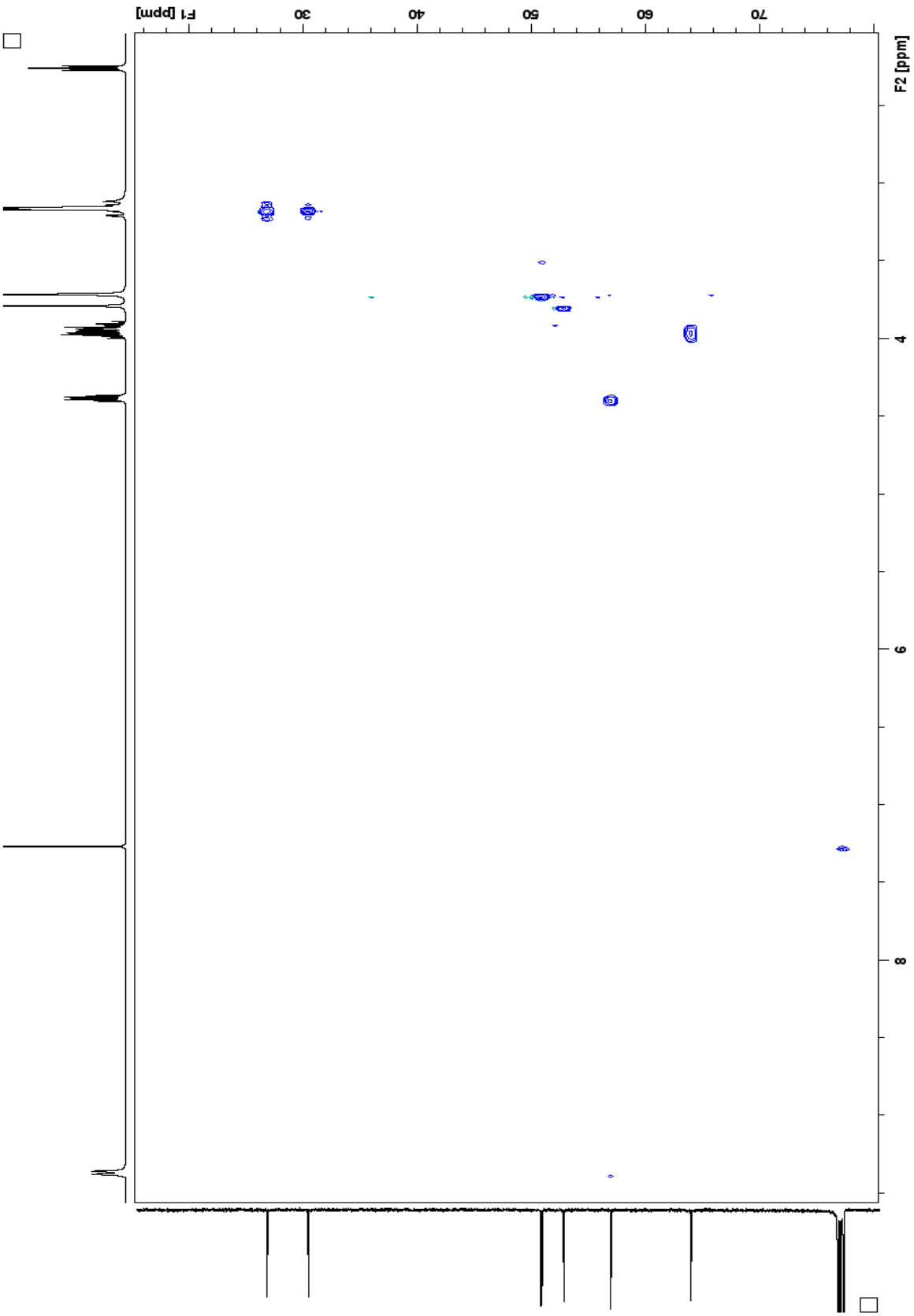

Spectrum 120*: 38* ***HSCQ NMR (500 MHz, $CDCl_3$)***

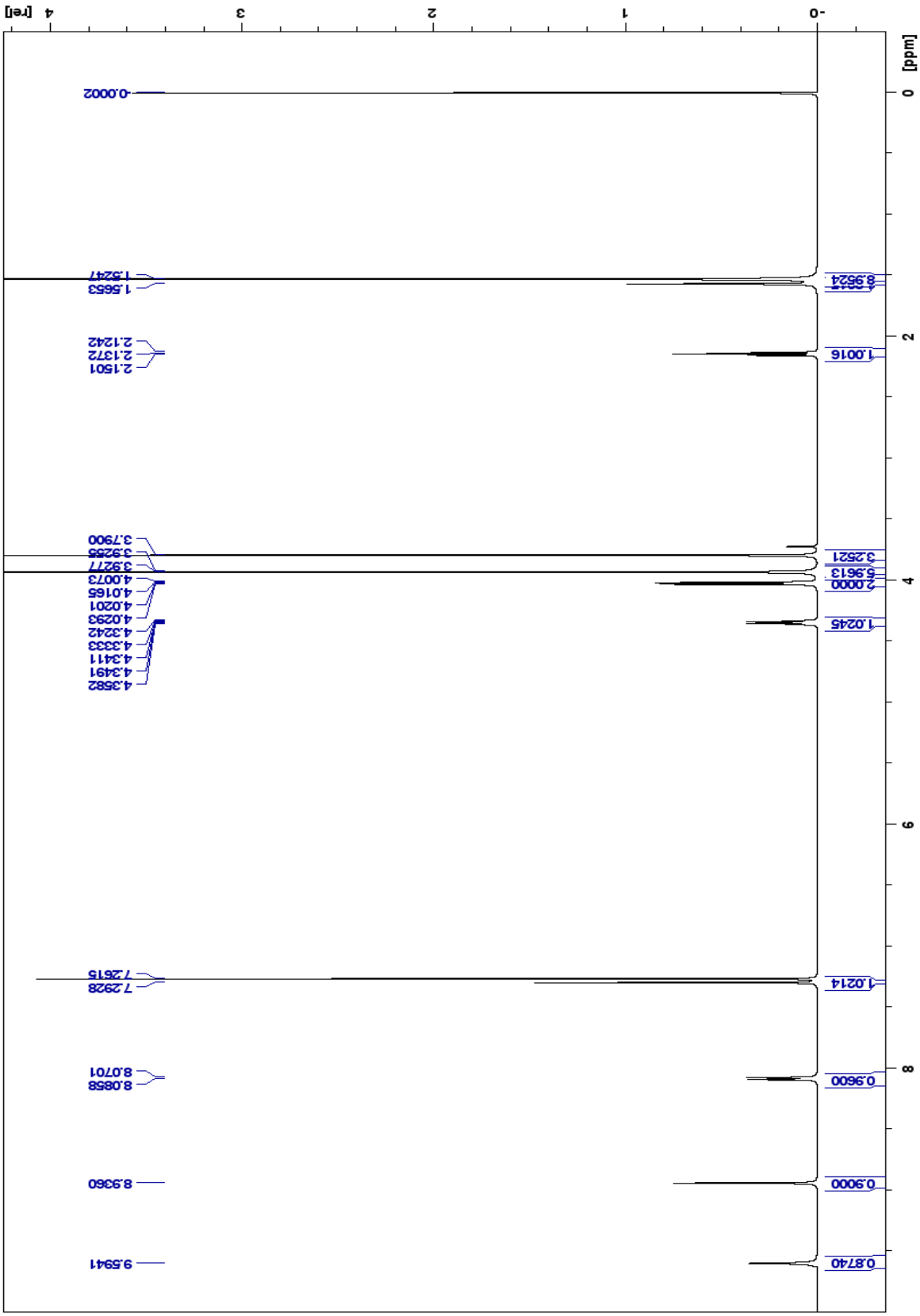

Spectrum 121*: 39* ***^{1}H NMR (500 MHz, $CDCl_3$)***

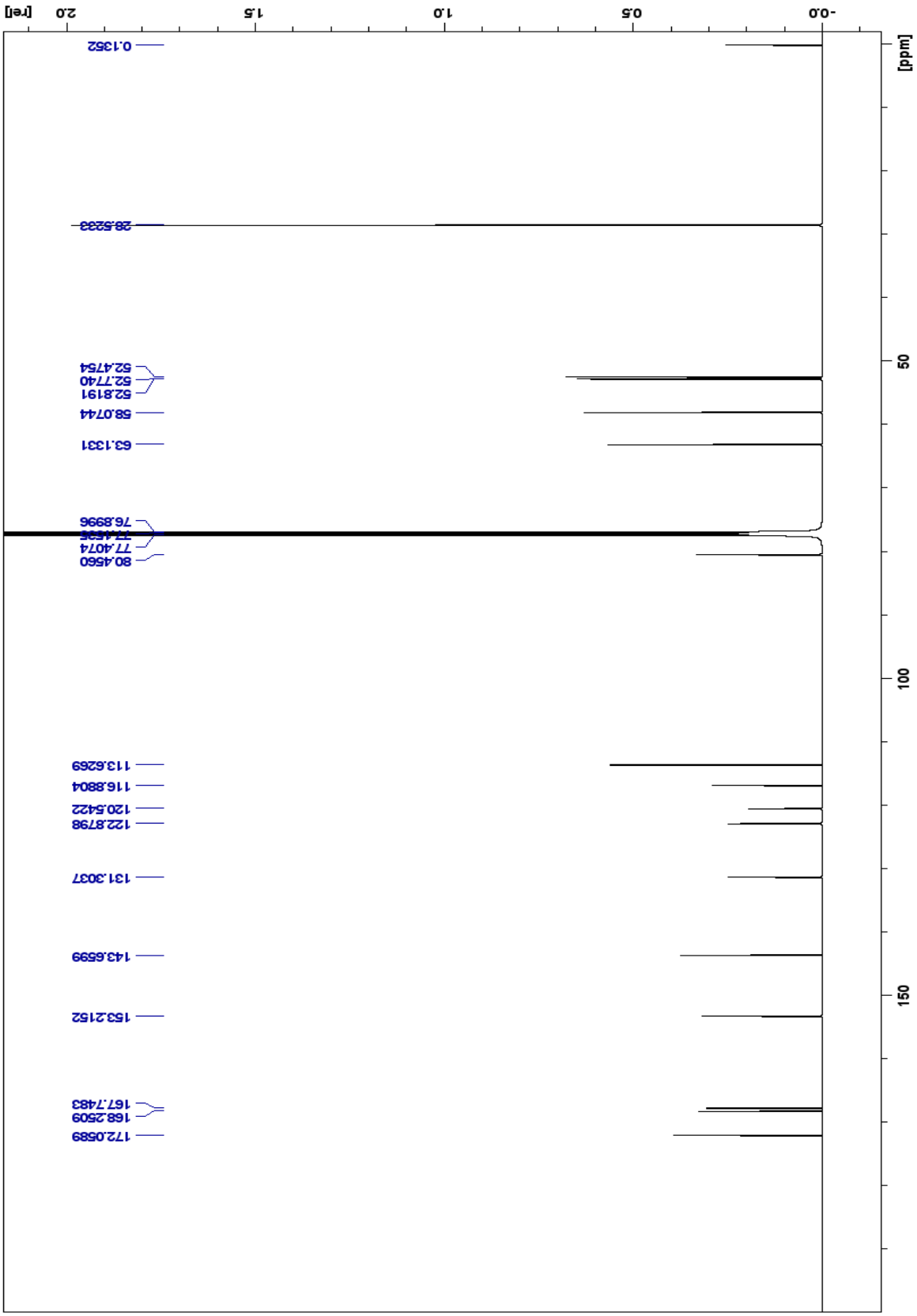

Spectrum 122*: 39* ***^{13}C NMR (500 MHz, $CDCl_3$)***

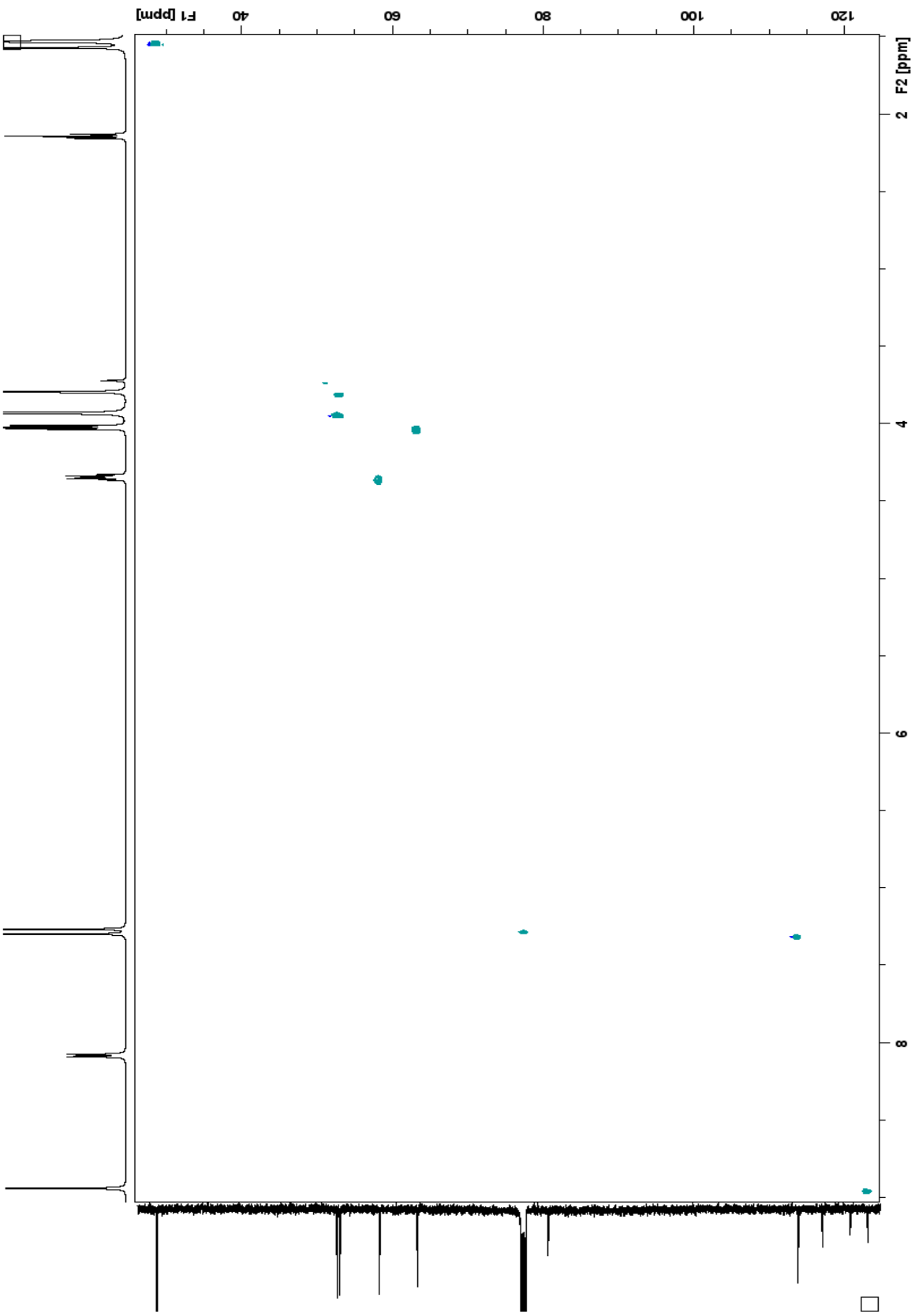

Spectrum 123*: 39* ***HSQC NMR (500 MHz, $CDCl_3$)***

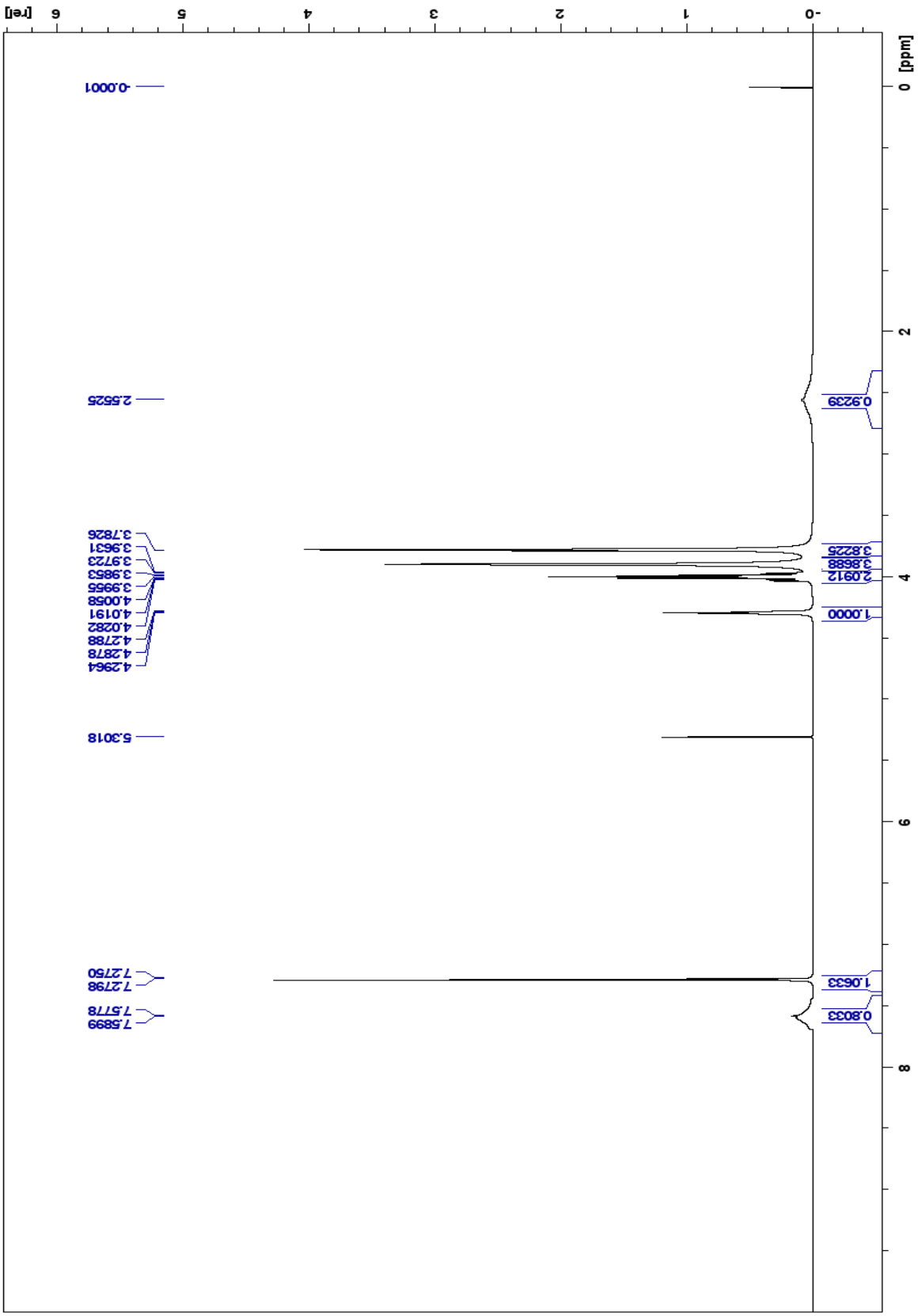

Spectrum 124*: 40* ^{1}***H NMR (500 MHz,*** $CDCl_3$***)***

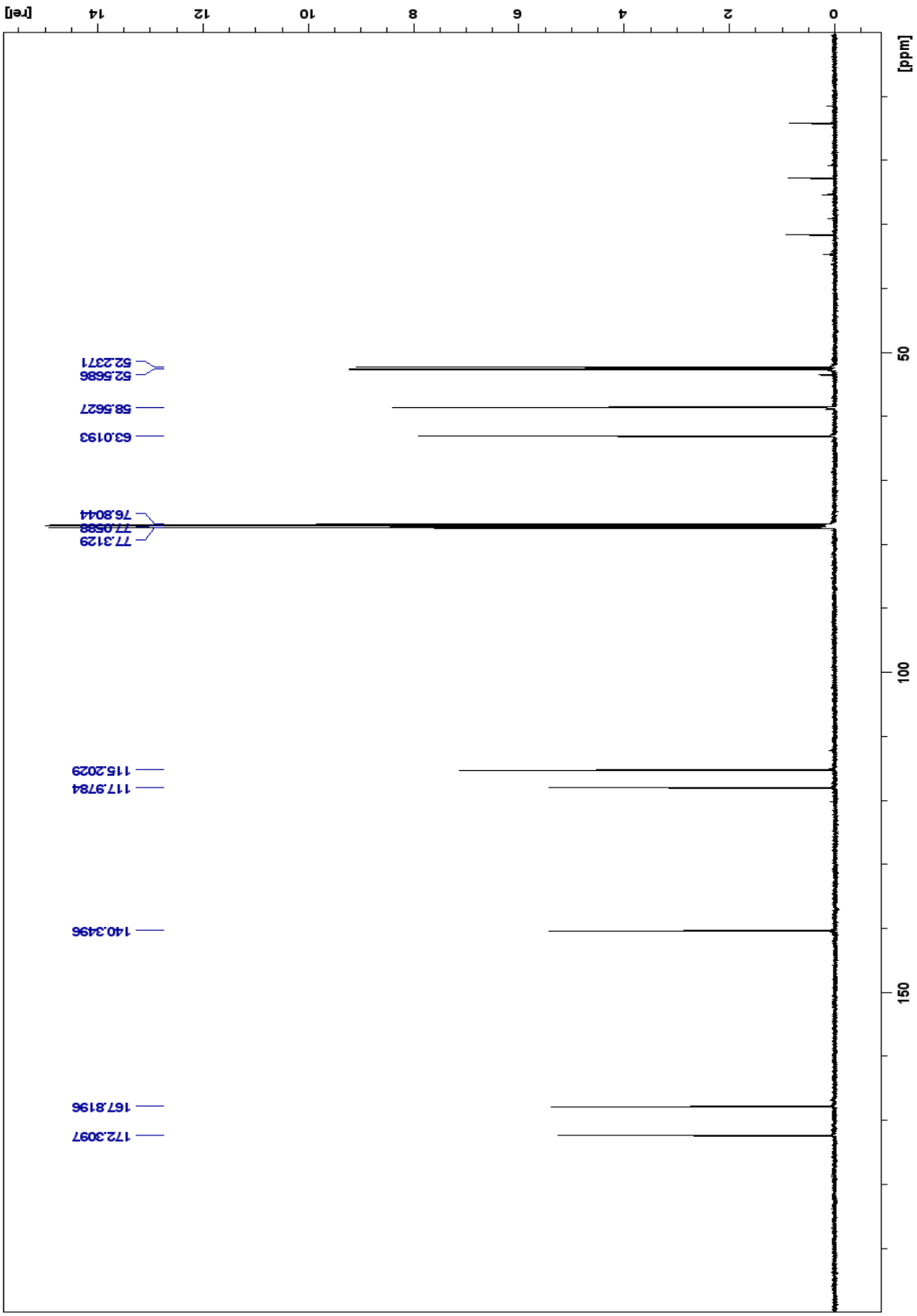

Spectrum 125*: 40 ^{13}C NMR (500 MHz, $CDCl_3$)*

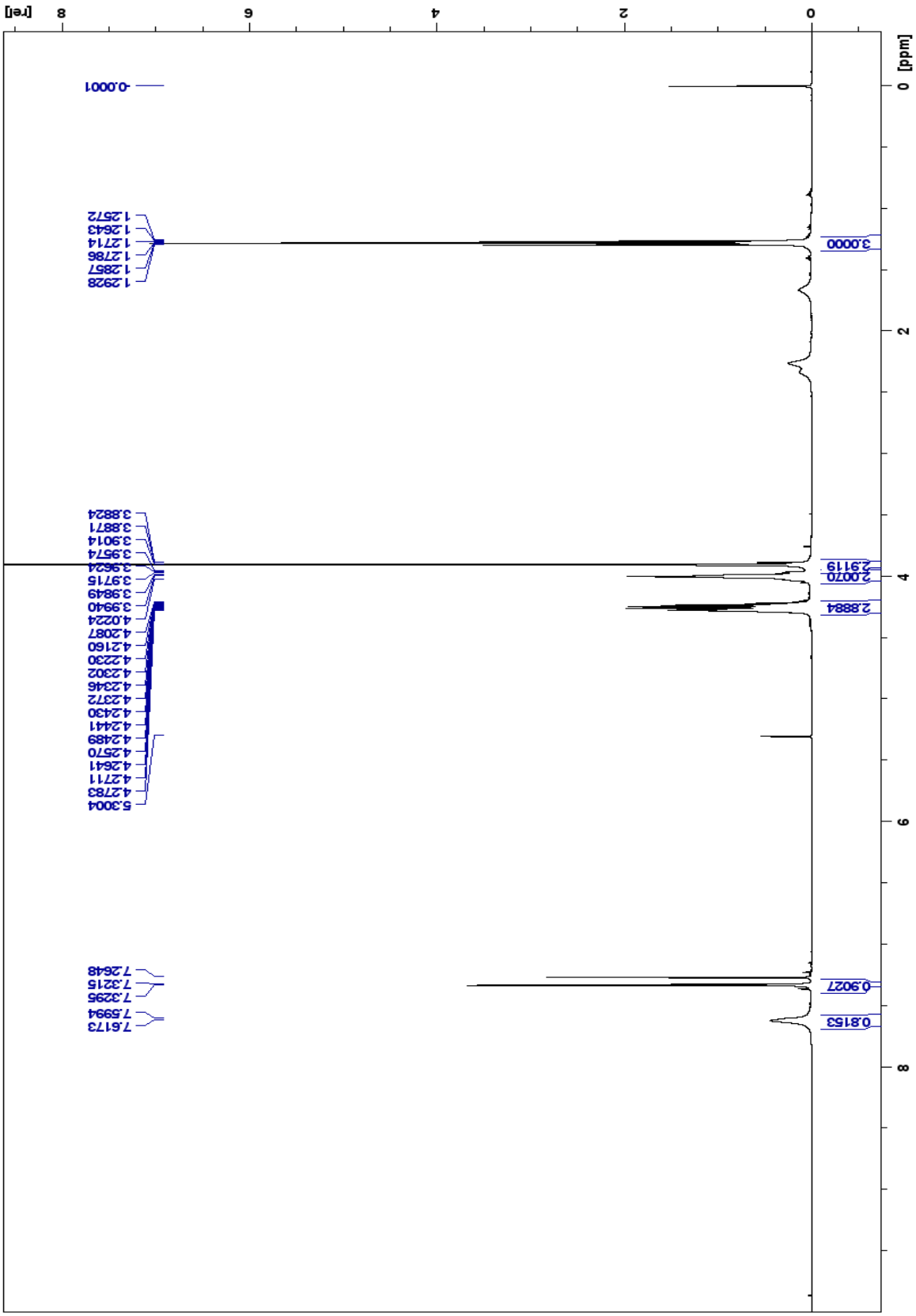

Spectrum 126*: 41* ^{1}***H NMR (500 MHz,*** $CDCl_3$***)***

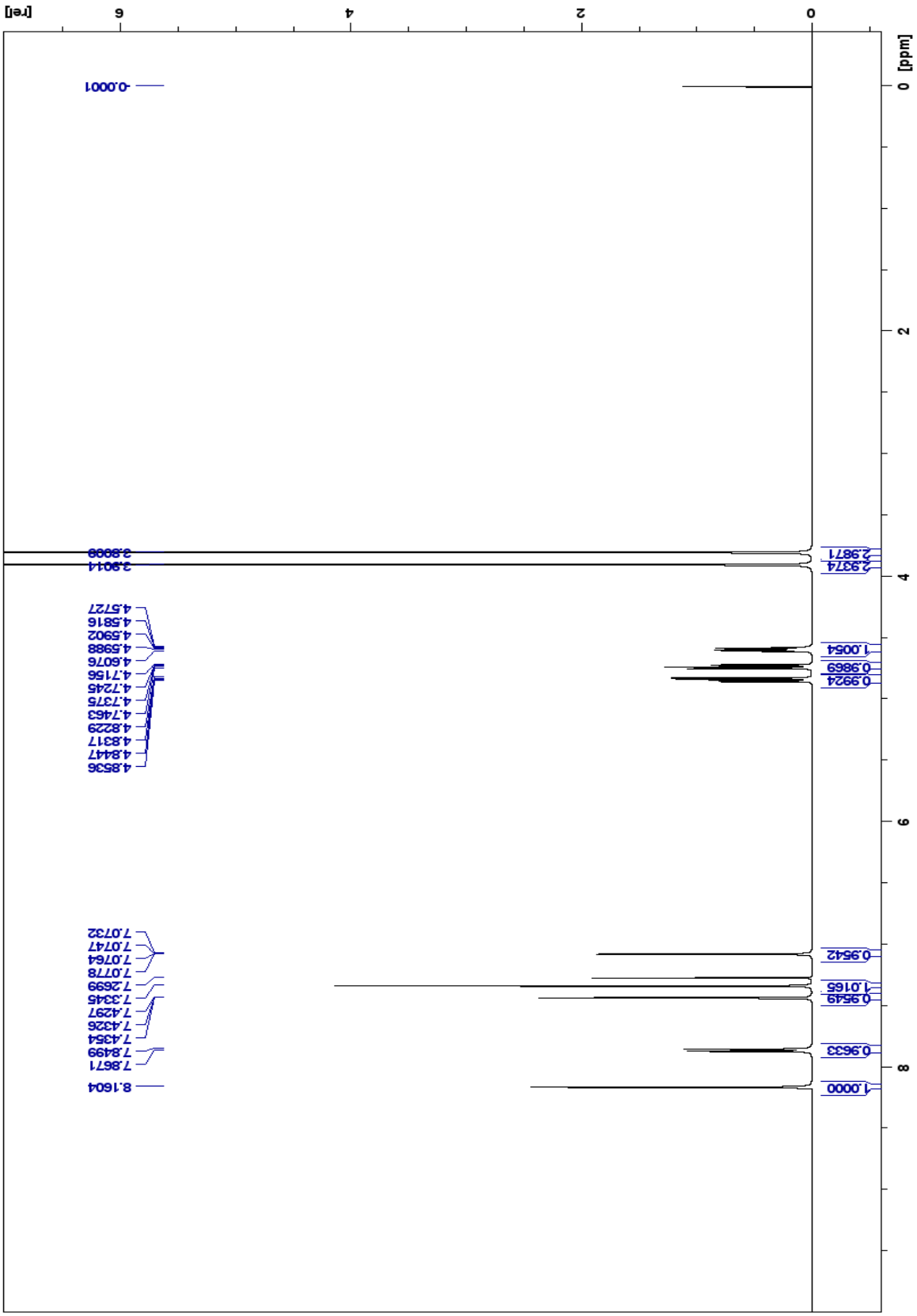

Spectrum 127*: 42* ^{1}***H NMR (500 MHz,*** $CDCl_3$***)***

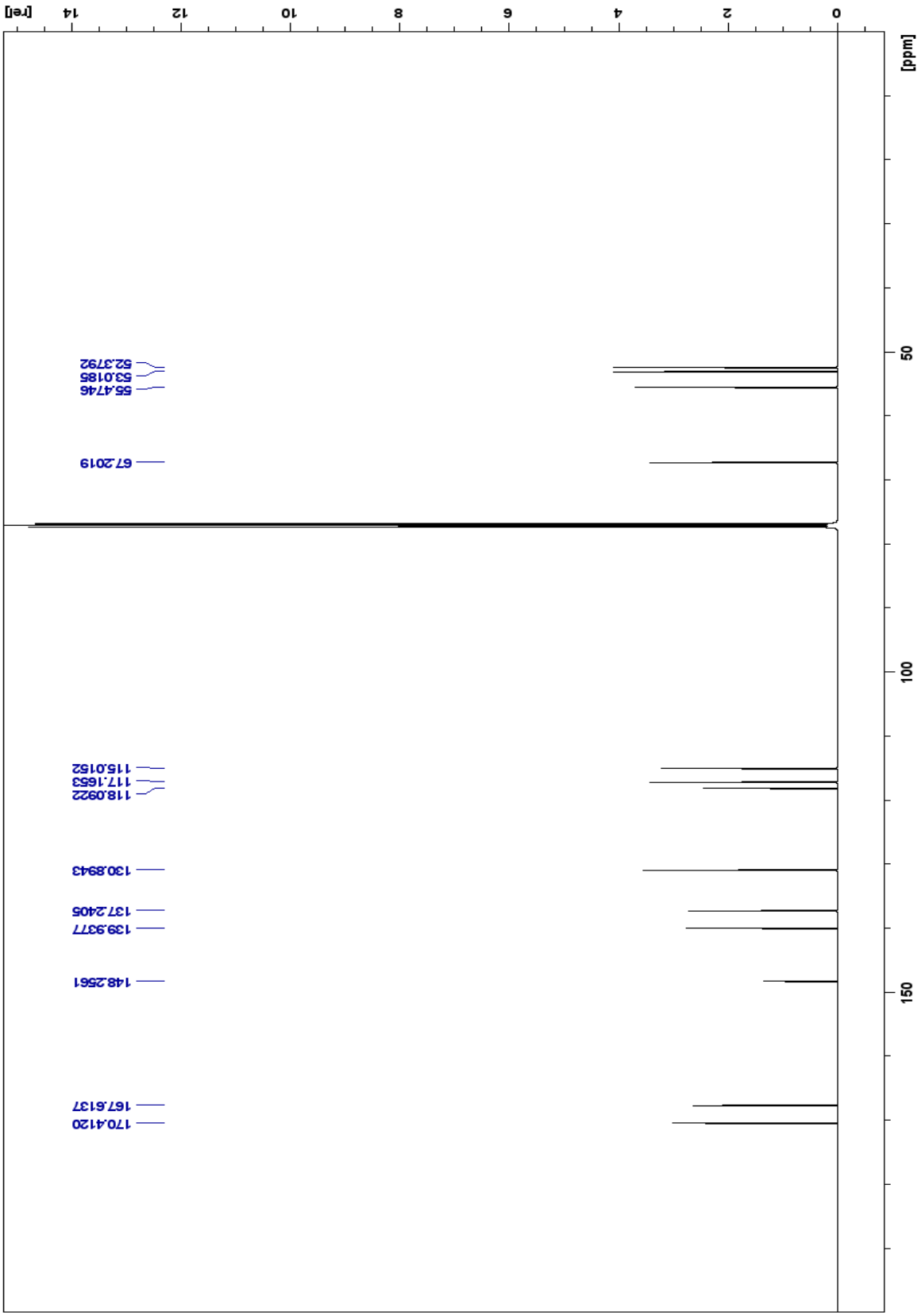

Spectrum 128*: 42* ***^{13}C NMR (500 MHz, $CDCl_3$)***

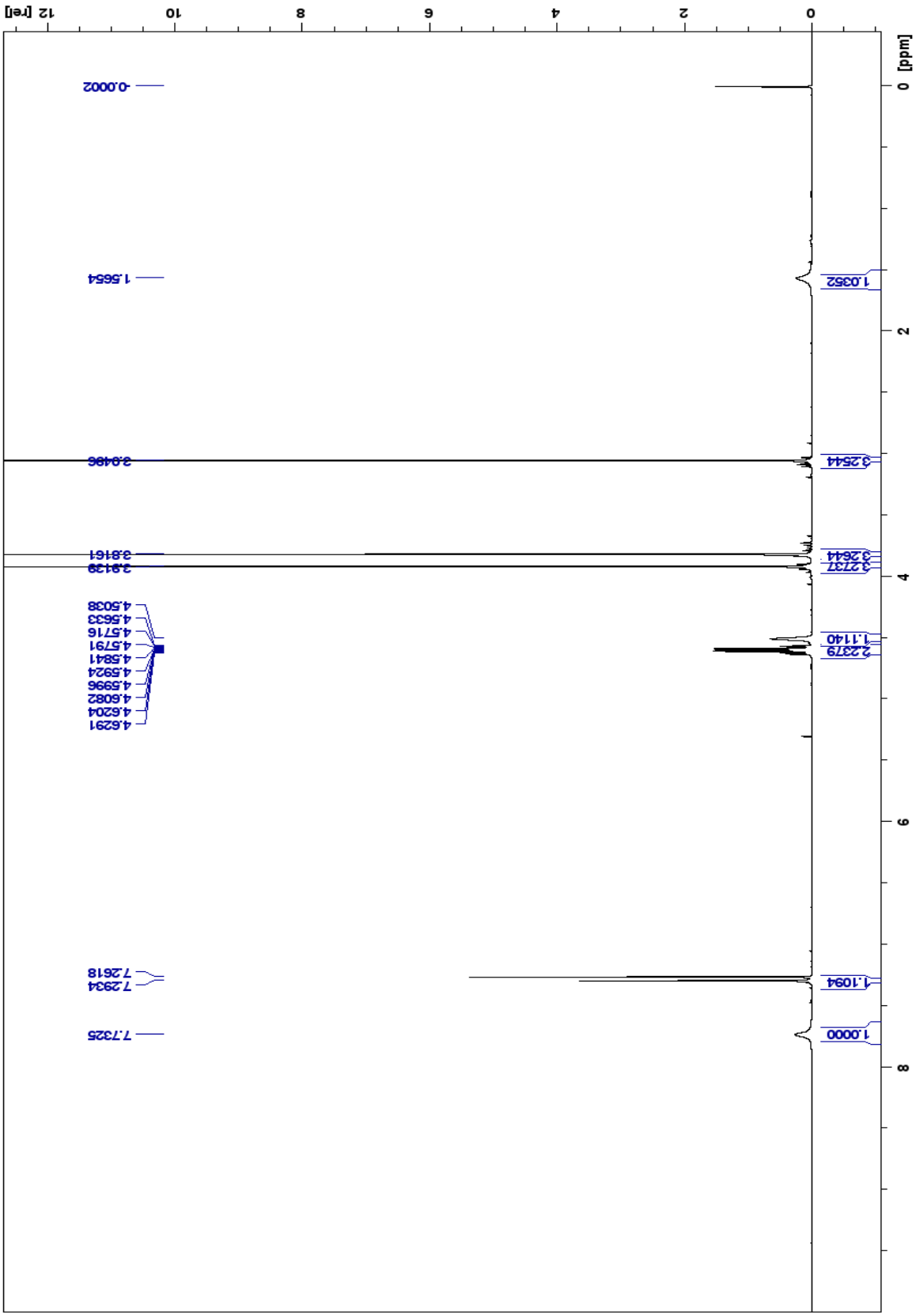

Spectrum 129*: 43 ^{1}H NMR (500 MHz, $CDCl_3$)*

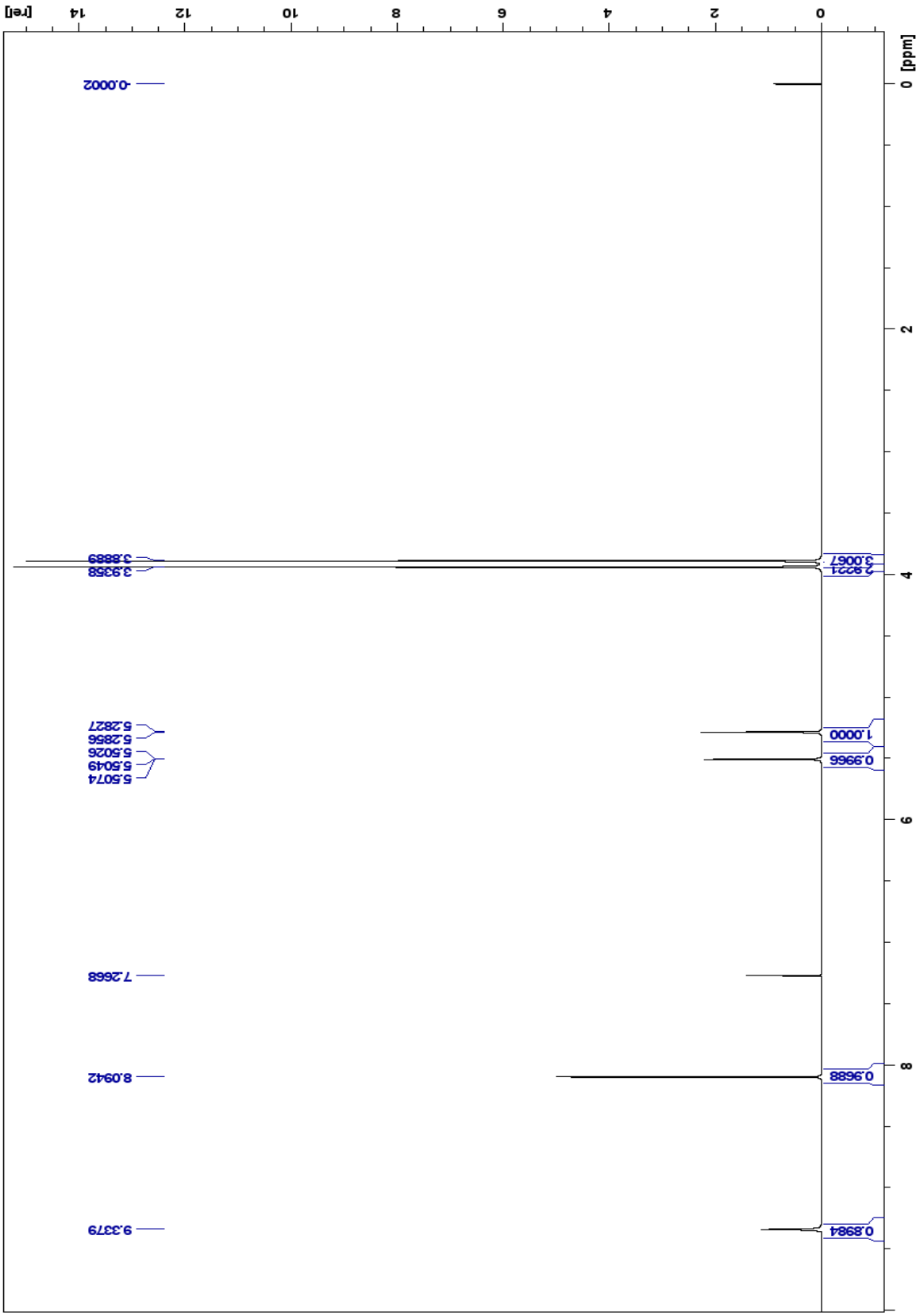

Spectrum 130*: 44 ^{1}H NMR (500 MHz, $CDCl_3$)*

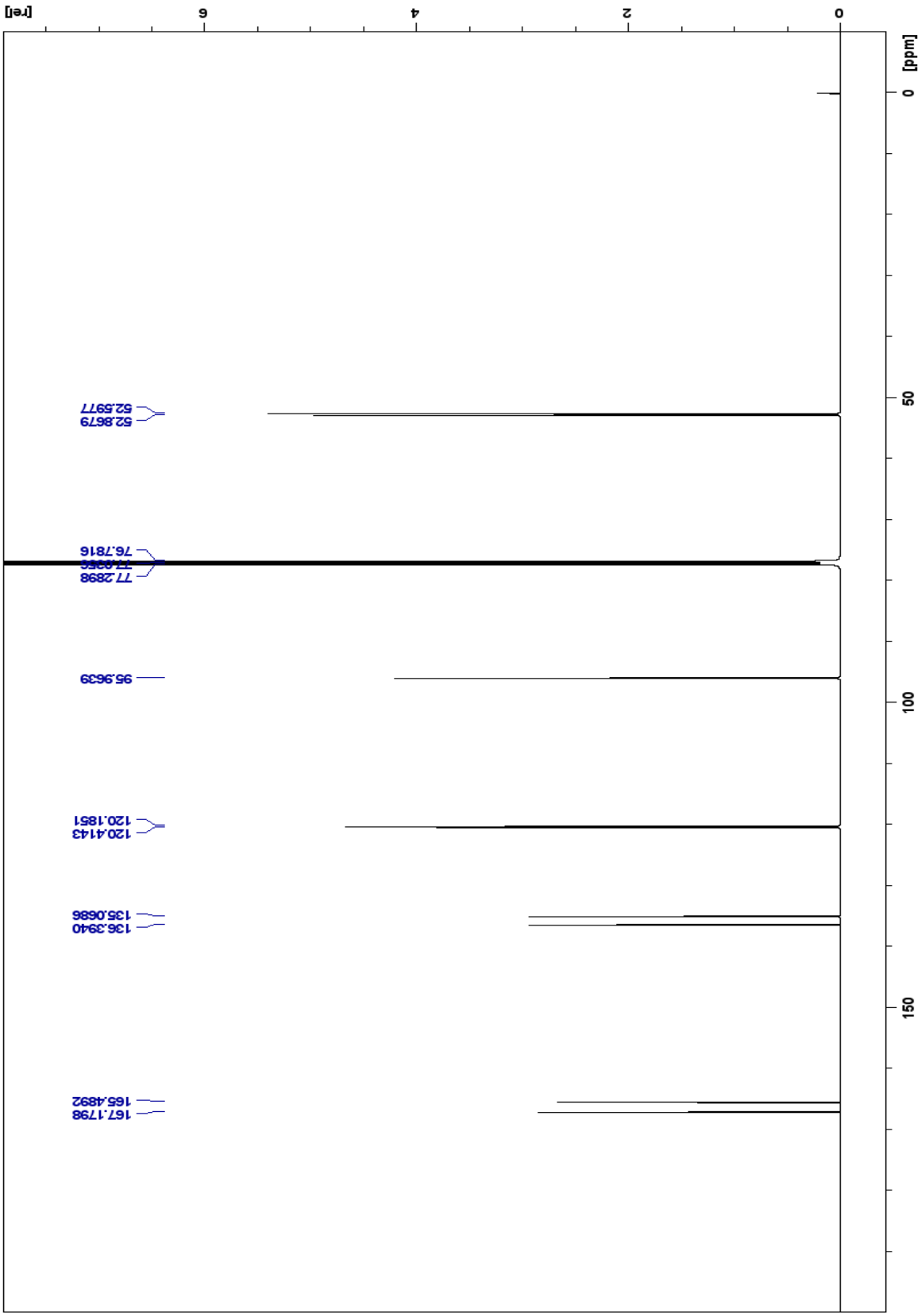

Spectrum 131*: 44 ^{13}C NMR (500 MHz, $CDCl_3$)*

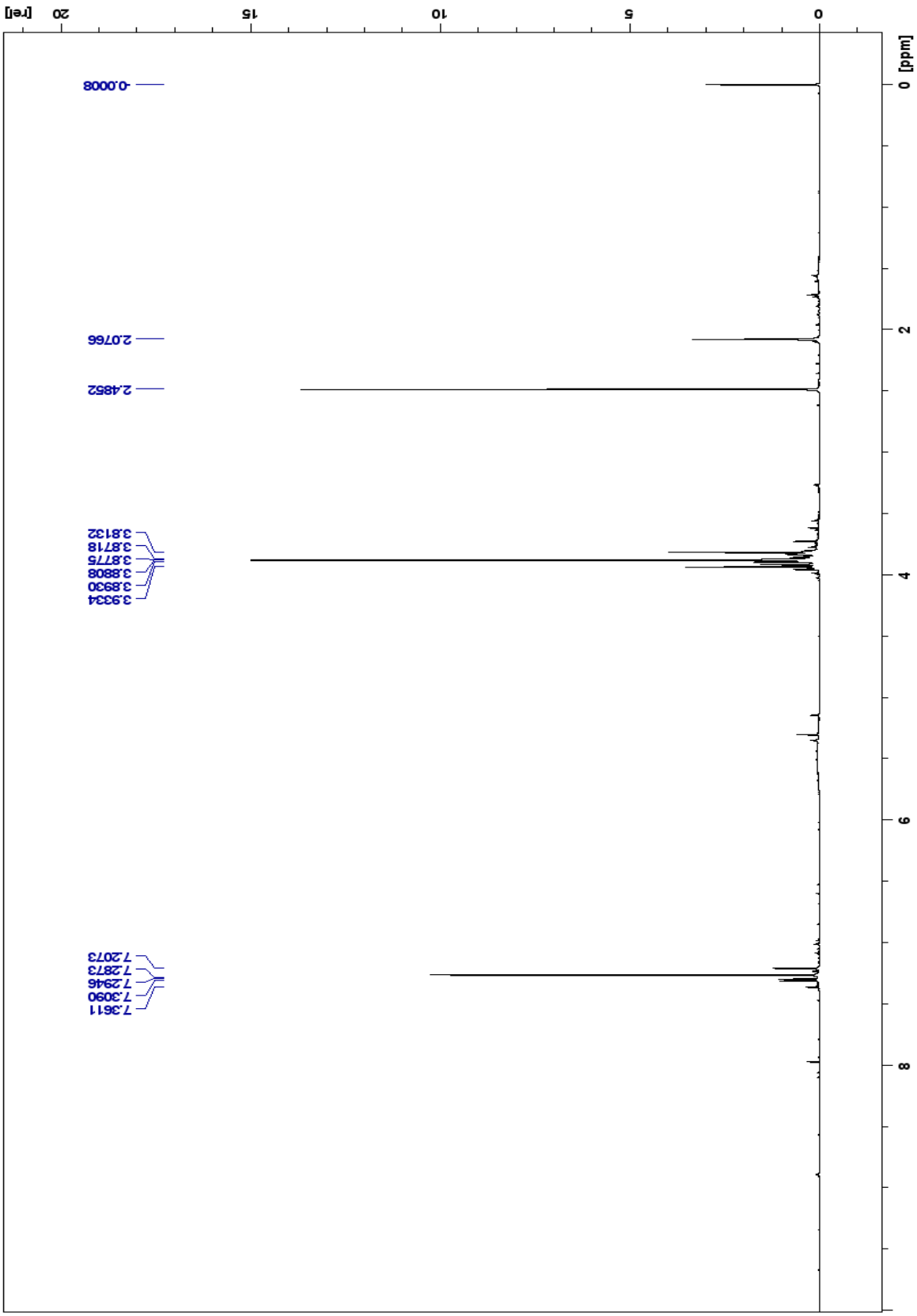

Spectrum 132*: 45 ^{1}H NMR (500 MHz, $CDCl_3$)*

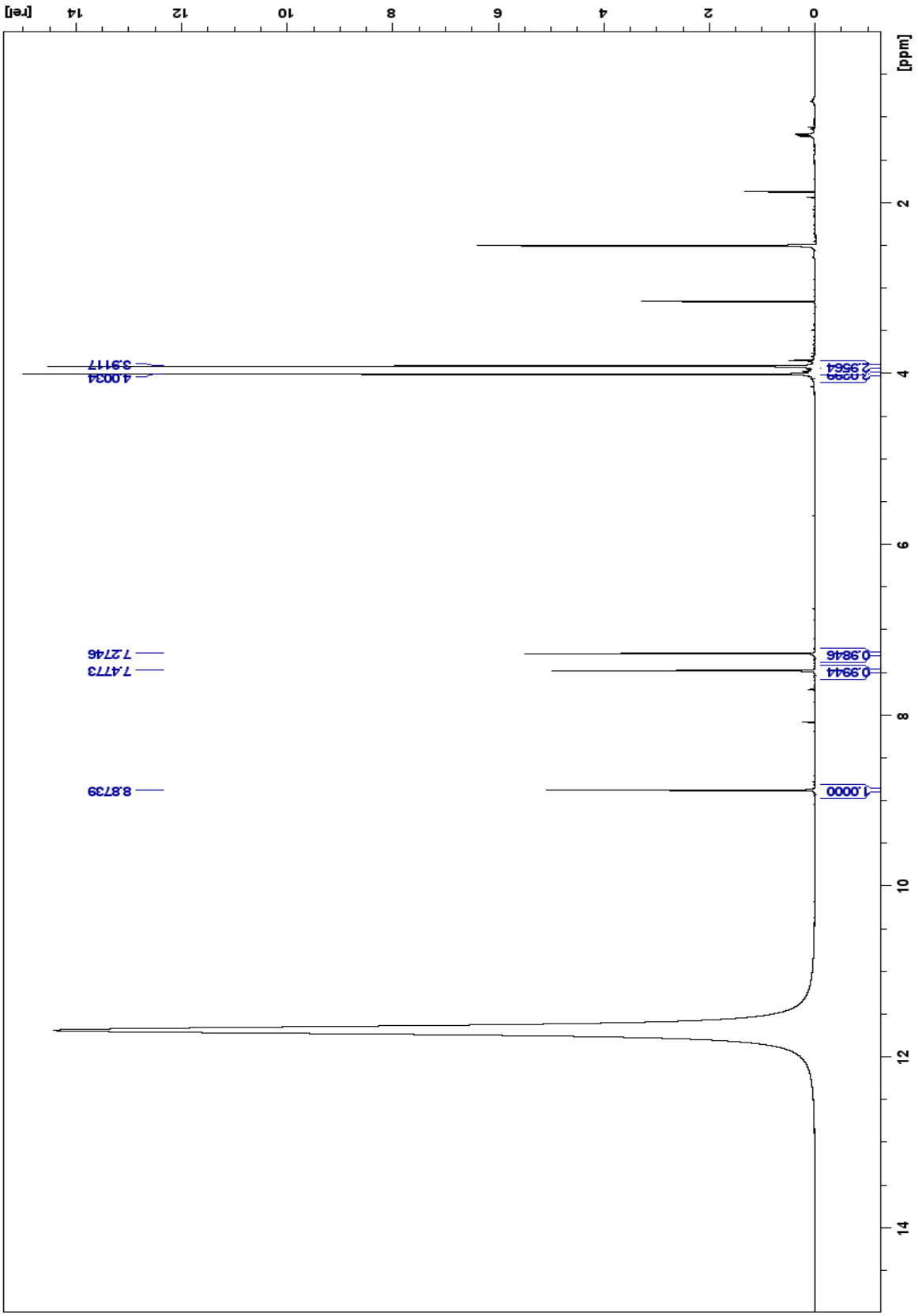

Spectrum 133*: 46* ^{1}***H NMR (500 MHz, TFA:DMSO-d6)***

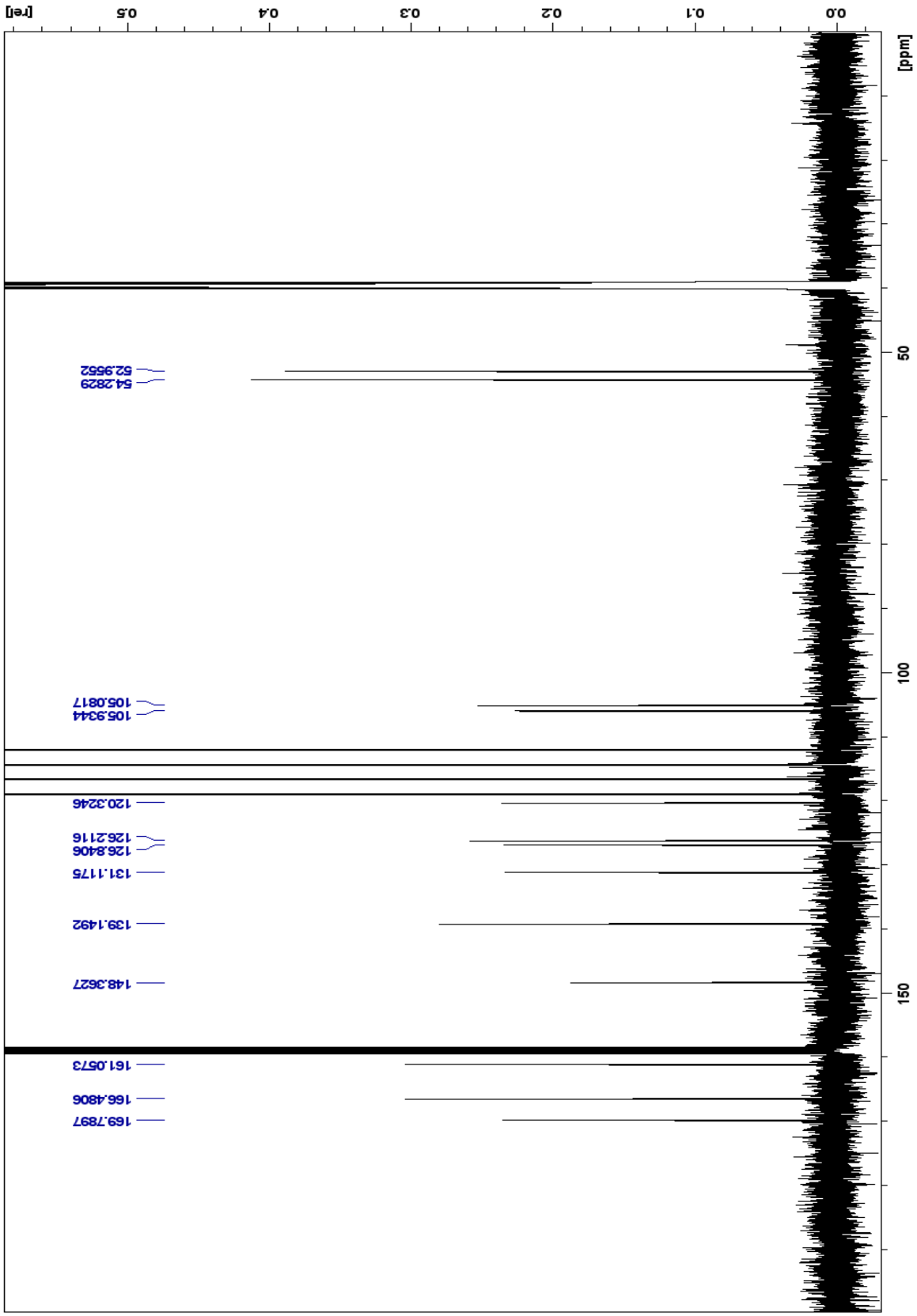

Spectrum 134*: 46 ^{13}C NMR (500 MHz, TFA:DMSO-d6)*

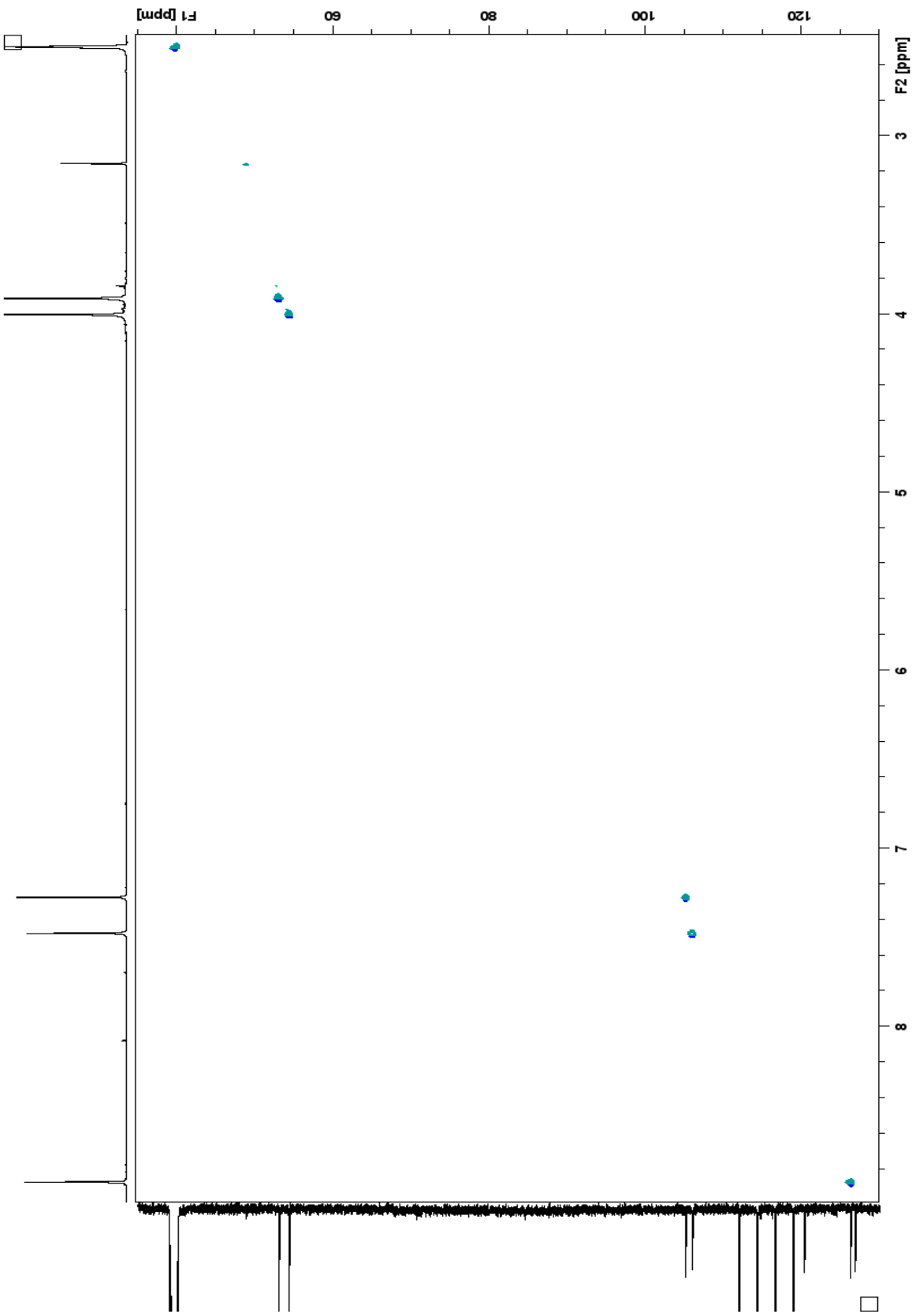

Spectrum 135*: 46* ***HSQC NMR (500 MHz, TFA:DMSO-d6)***

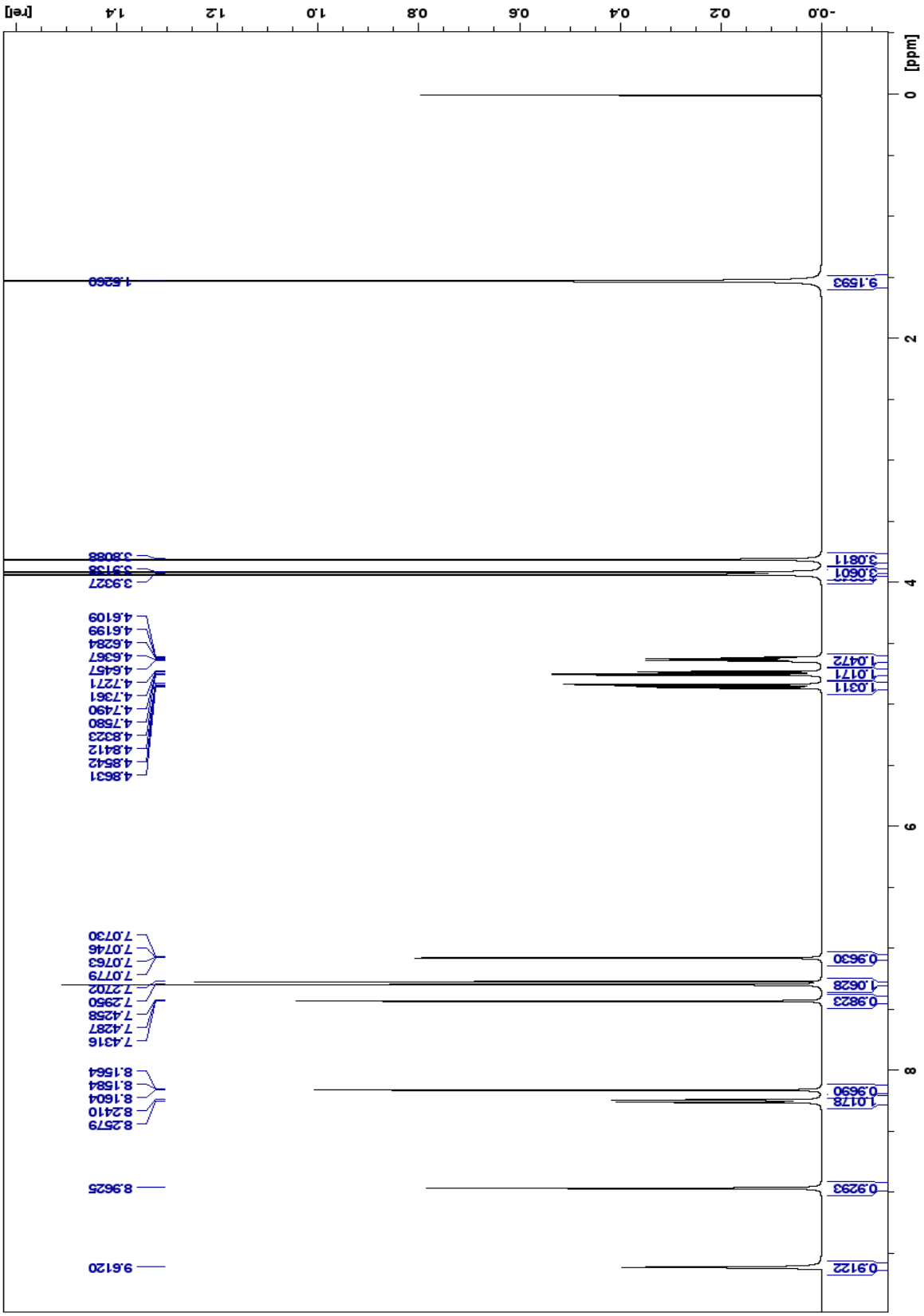

Spectrum 136*: 47* ^{1}***H NMR (500 MHz,*** $CDCl_3$***)***

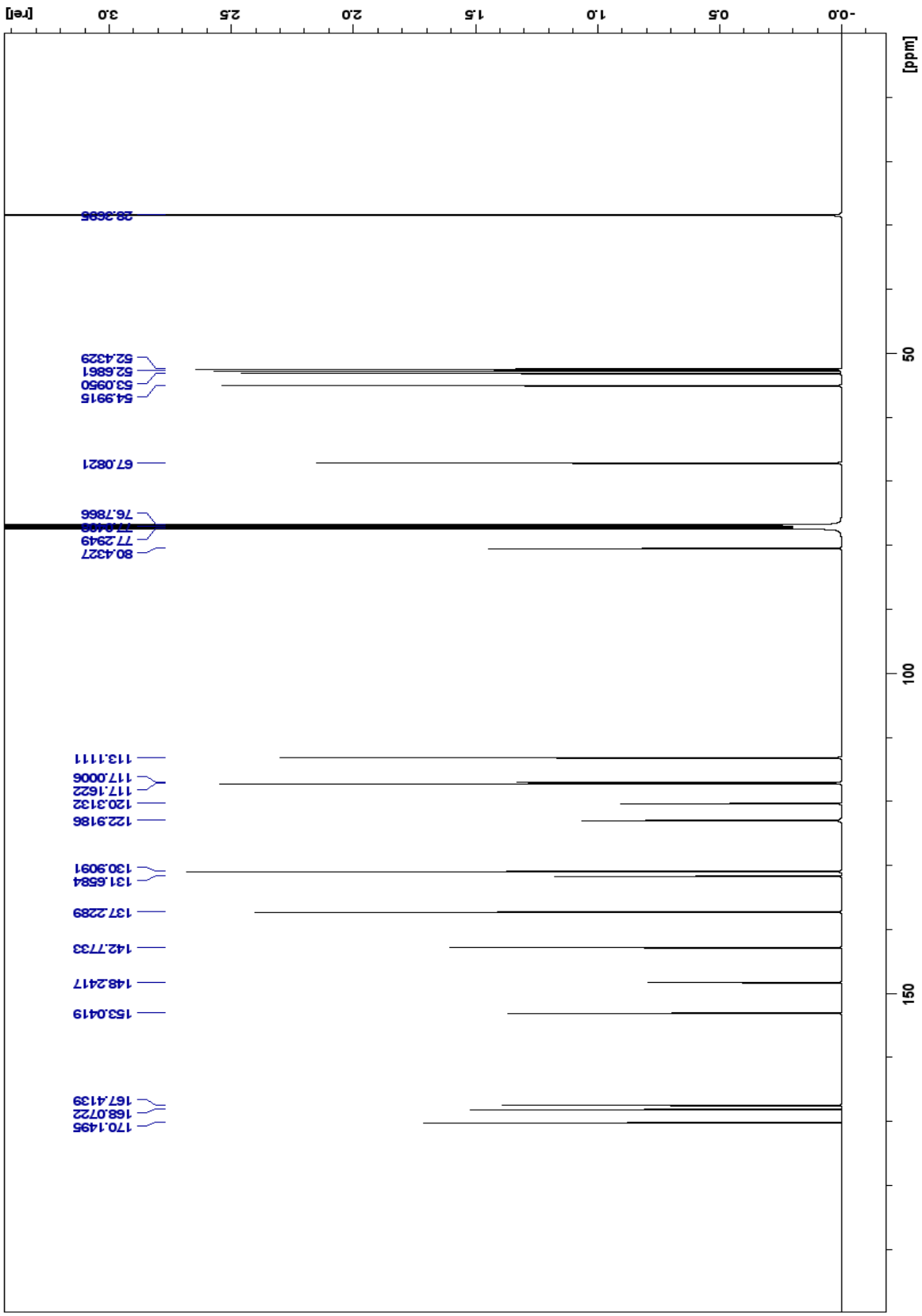

Spectrum 137*: 47* ^{13}***C NMR***

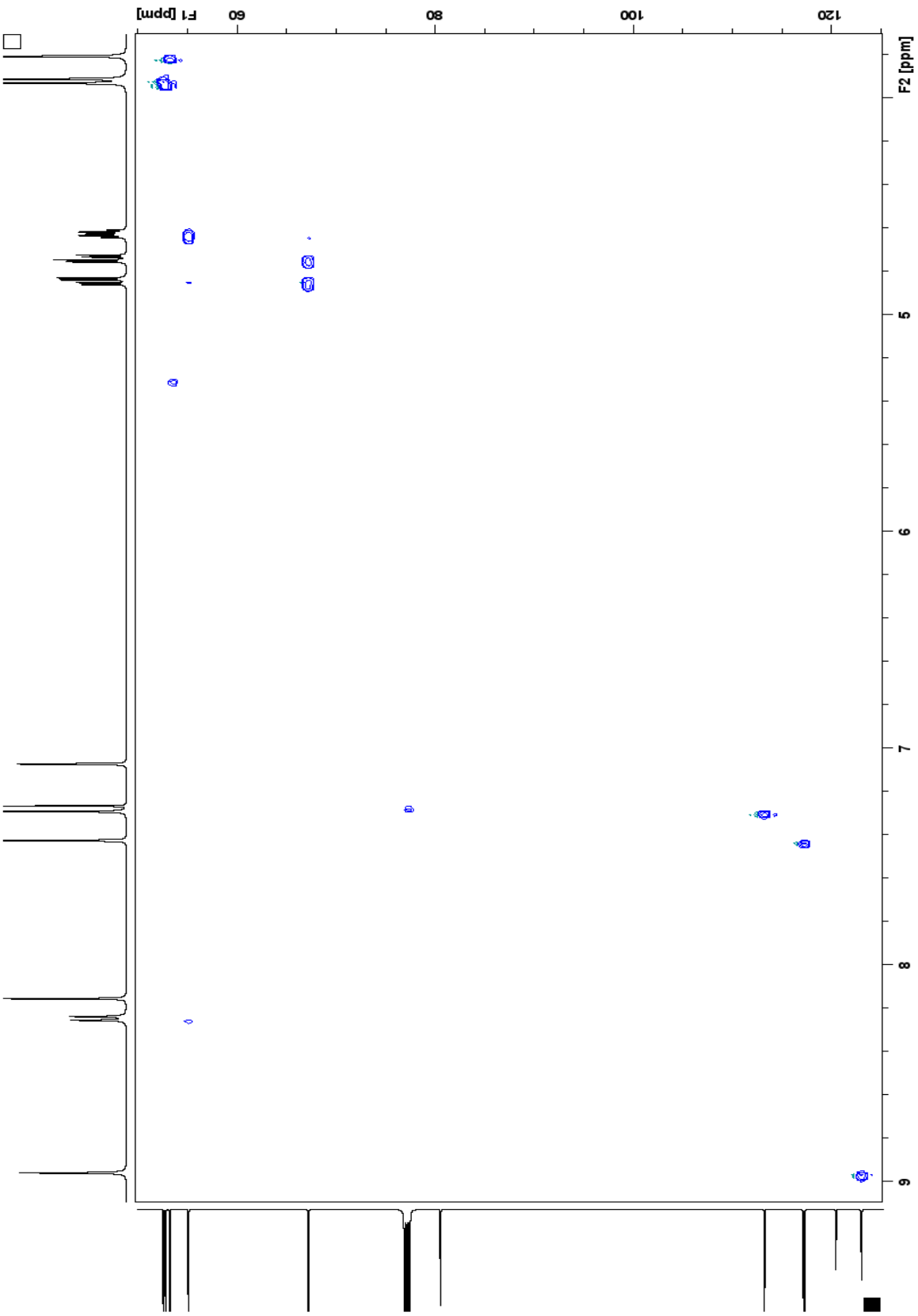

Spectrum 138*: 47* ***HSCQ NMR (500 MHz, $CDCl_3$)***

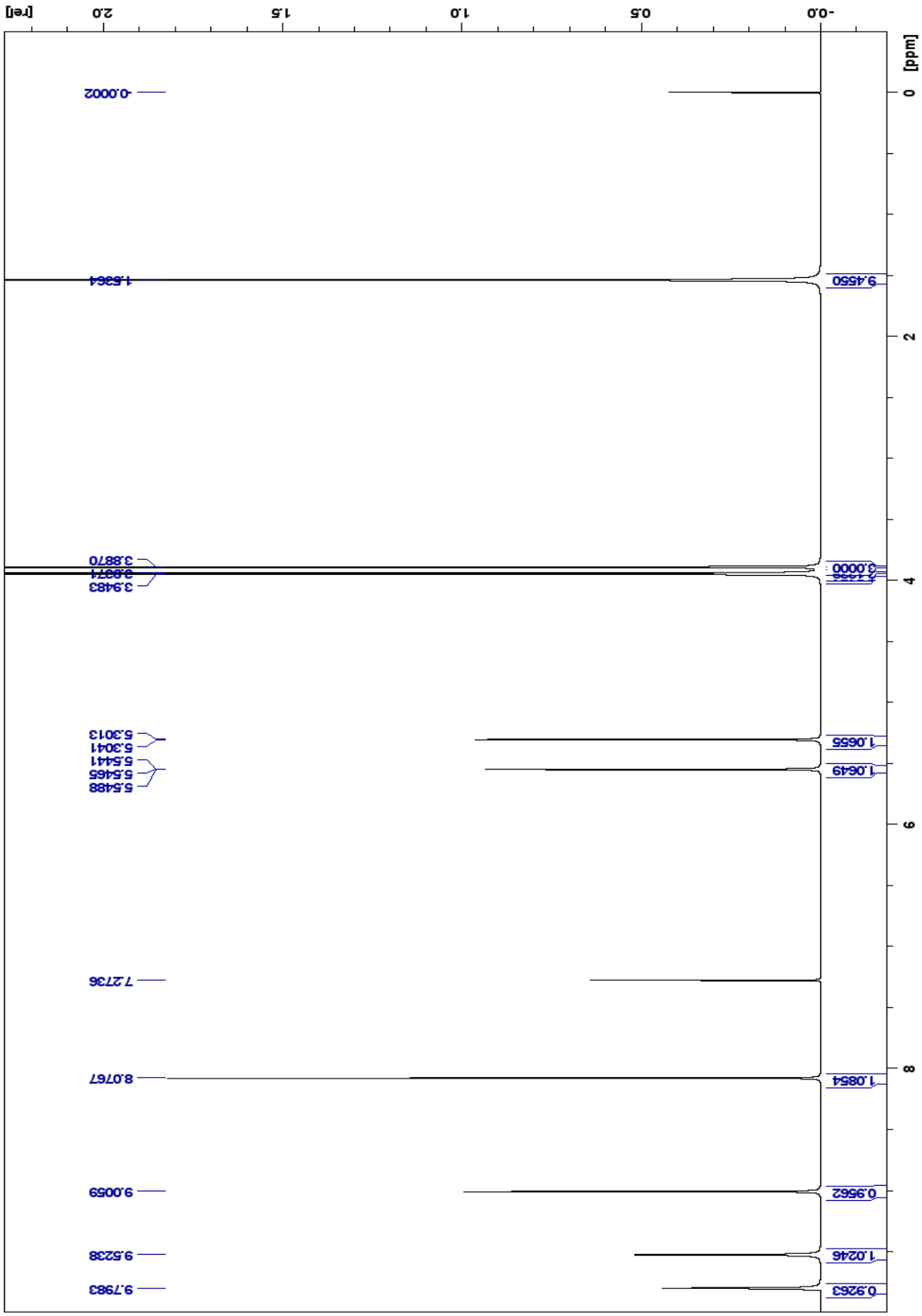

Spectrum 139*: 48 ^{1}H NMR (500 MHz, $CDCl_3$)*

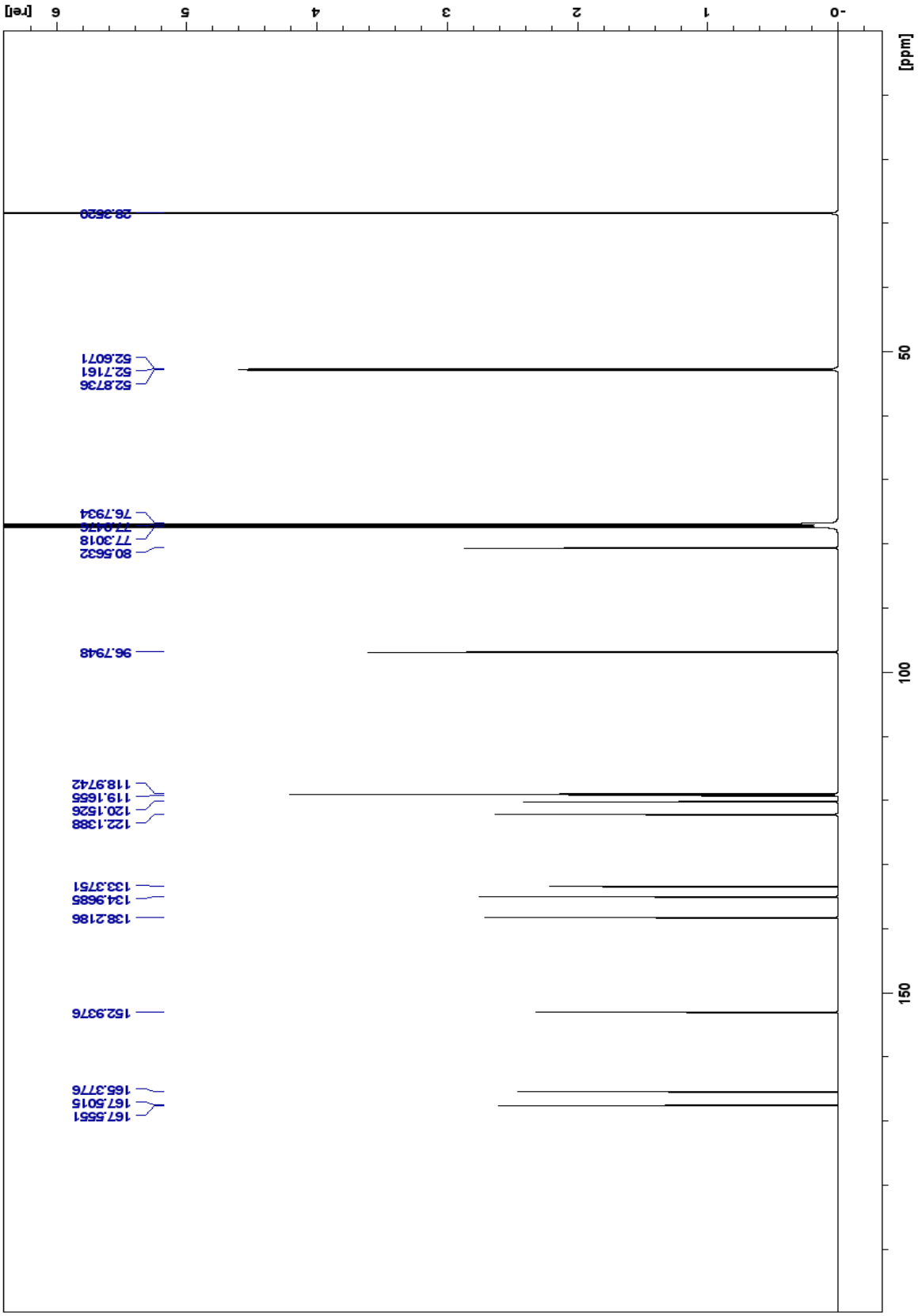

Spectrum 140*: 48 ^{13}C NMR (500 MHz, $CDCl_3$)*

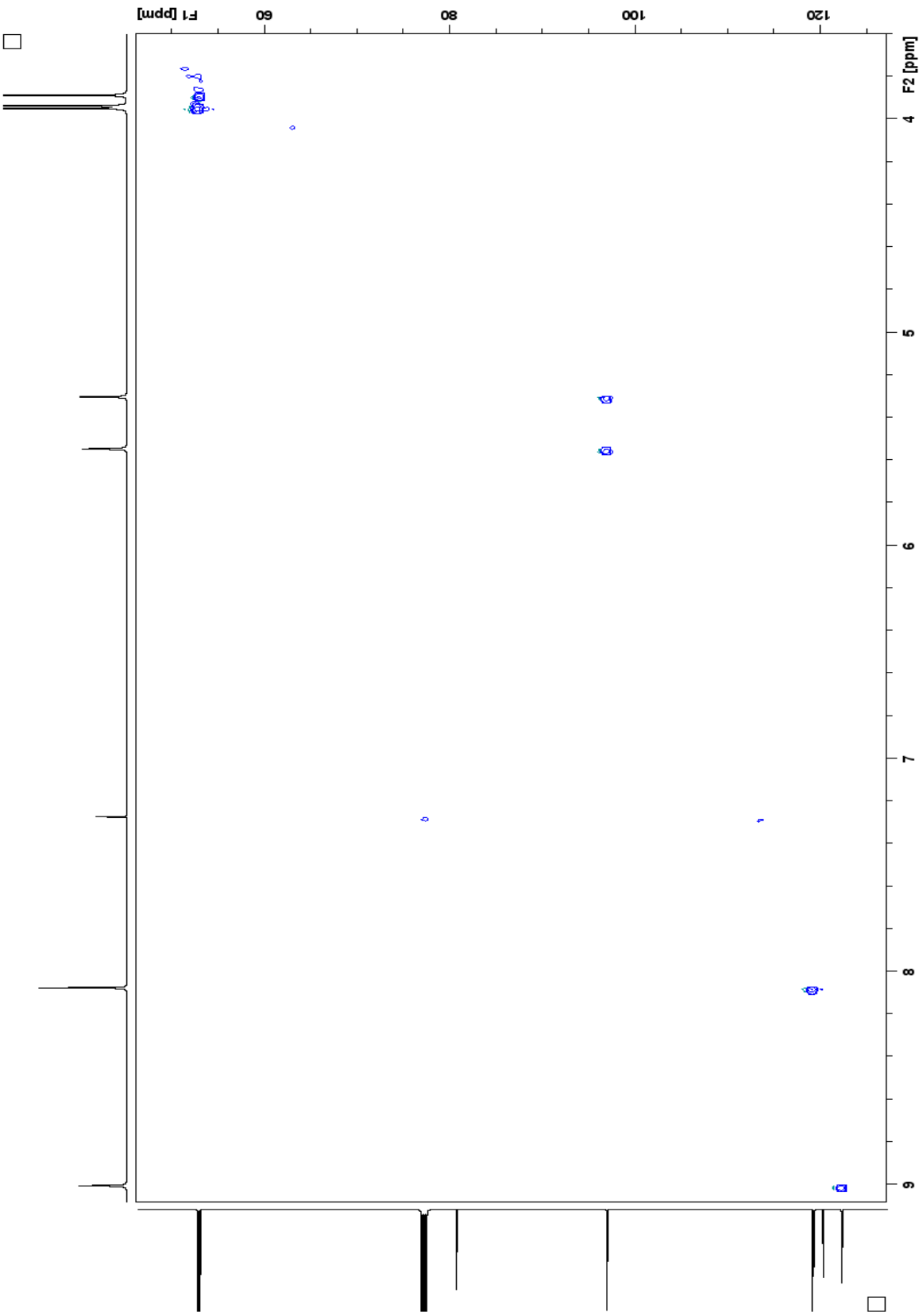

Spectrum 141*: 48* ***HSQC NMR (500 MHz, $CDCl_3$)***

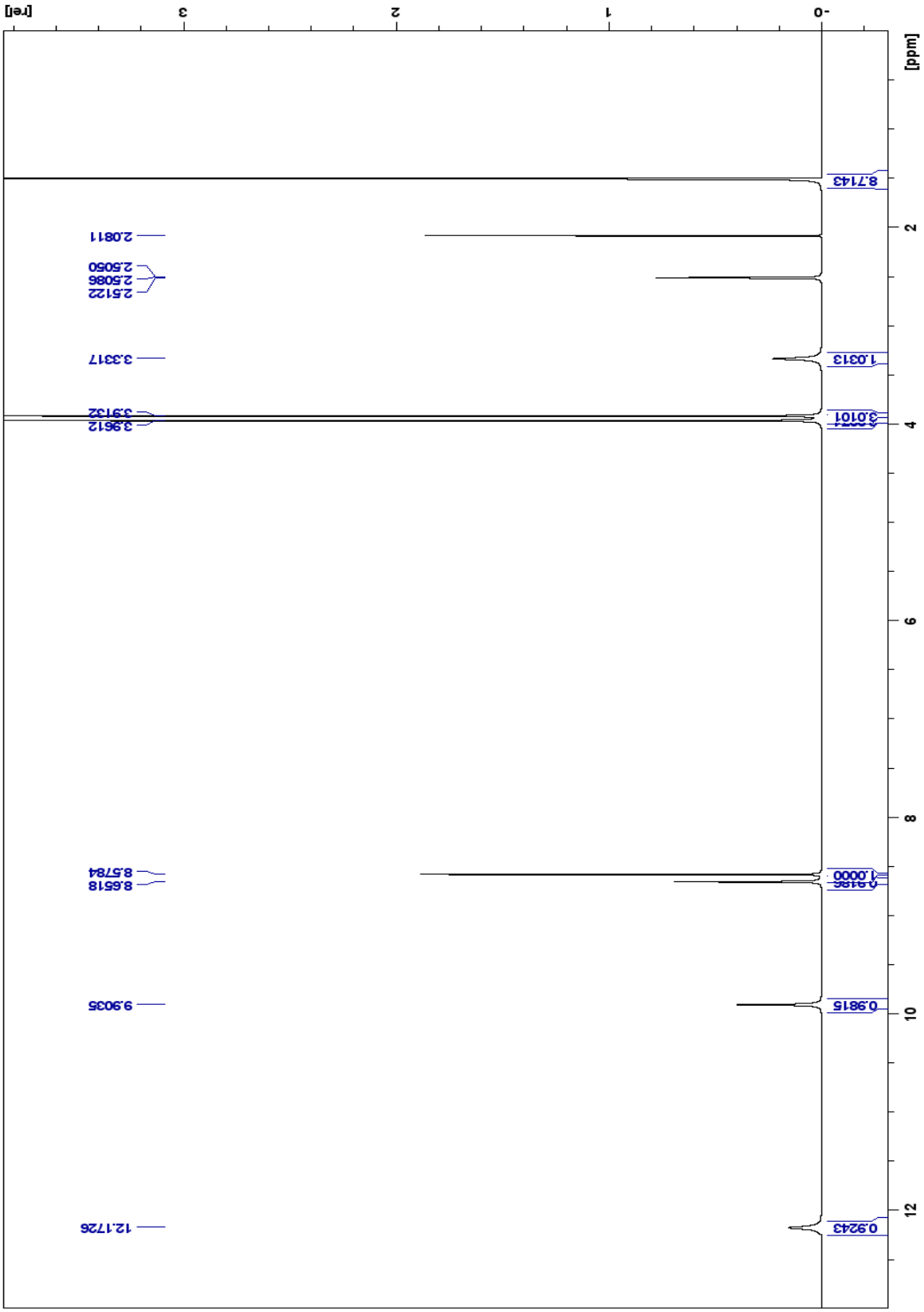

Spectrum 142*: 49 ^{1}H NMR (500 MHz, DMSO-d6)*

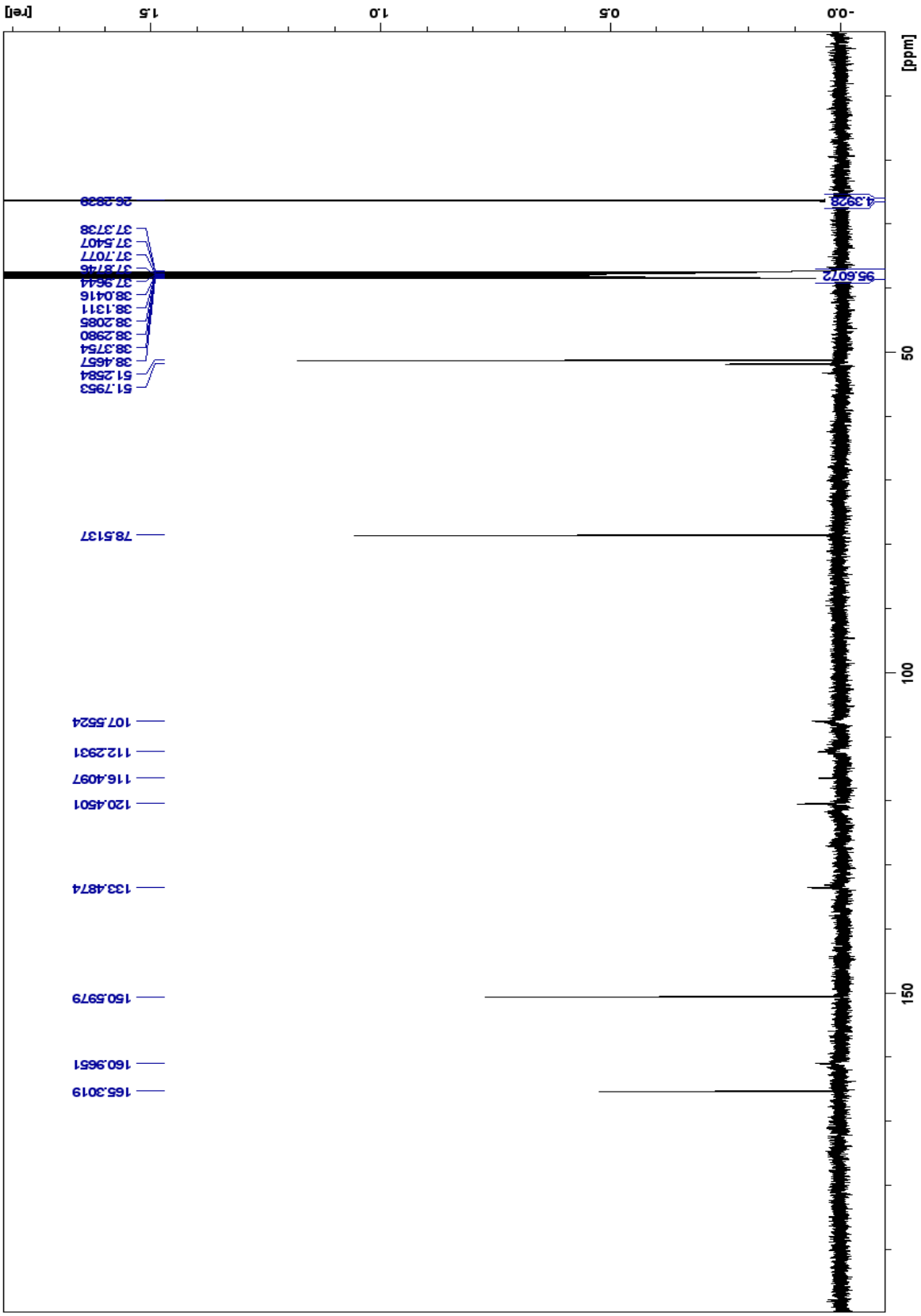

Spectrum 143*: 49* ***^{13}C NMR (500 MHz, DMSO-d6)***

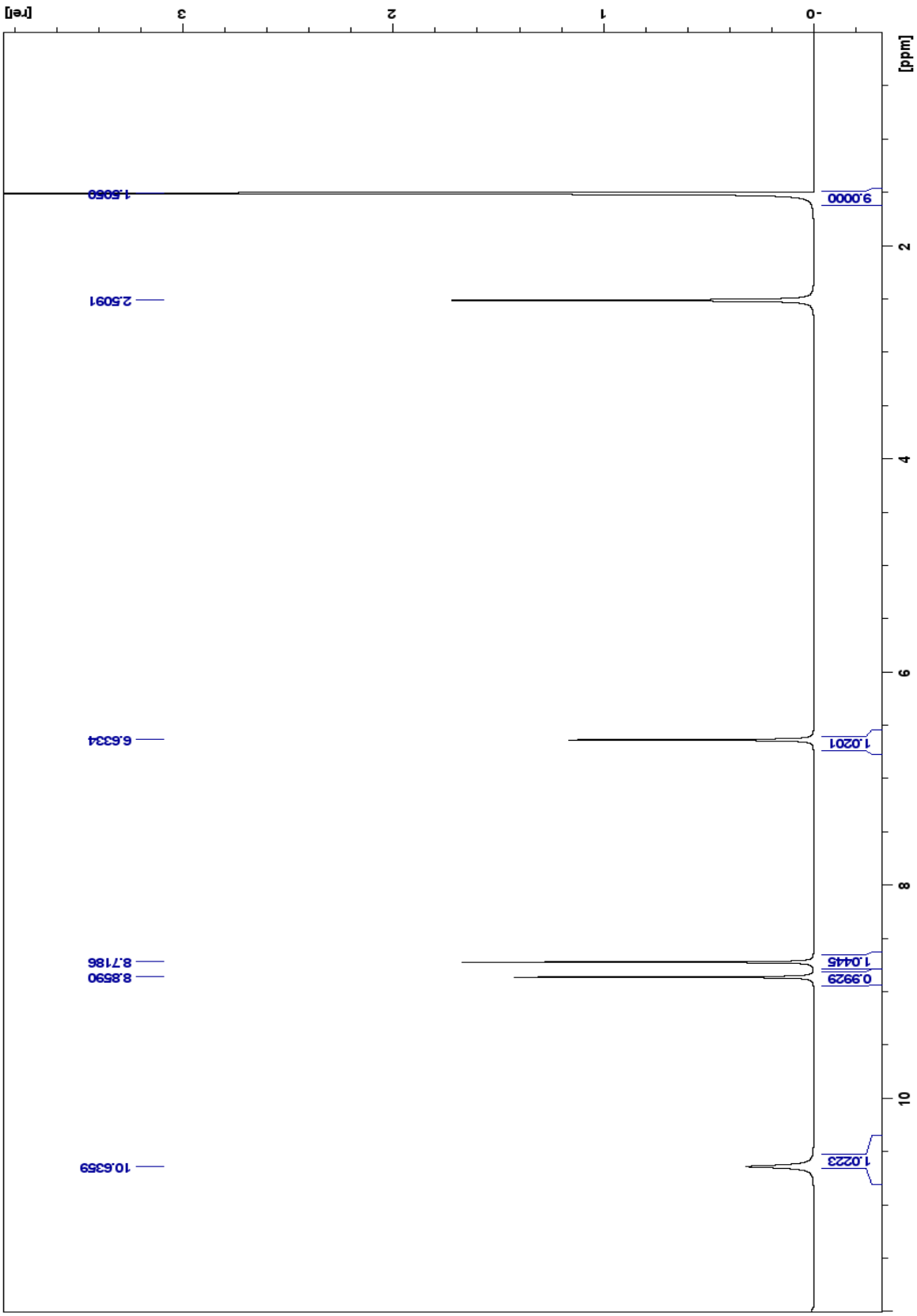

Spectrum 144*: 50* ***^{1}H NMR (500 MHz, DMSO-d6)***

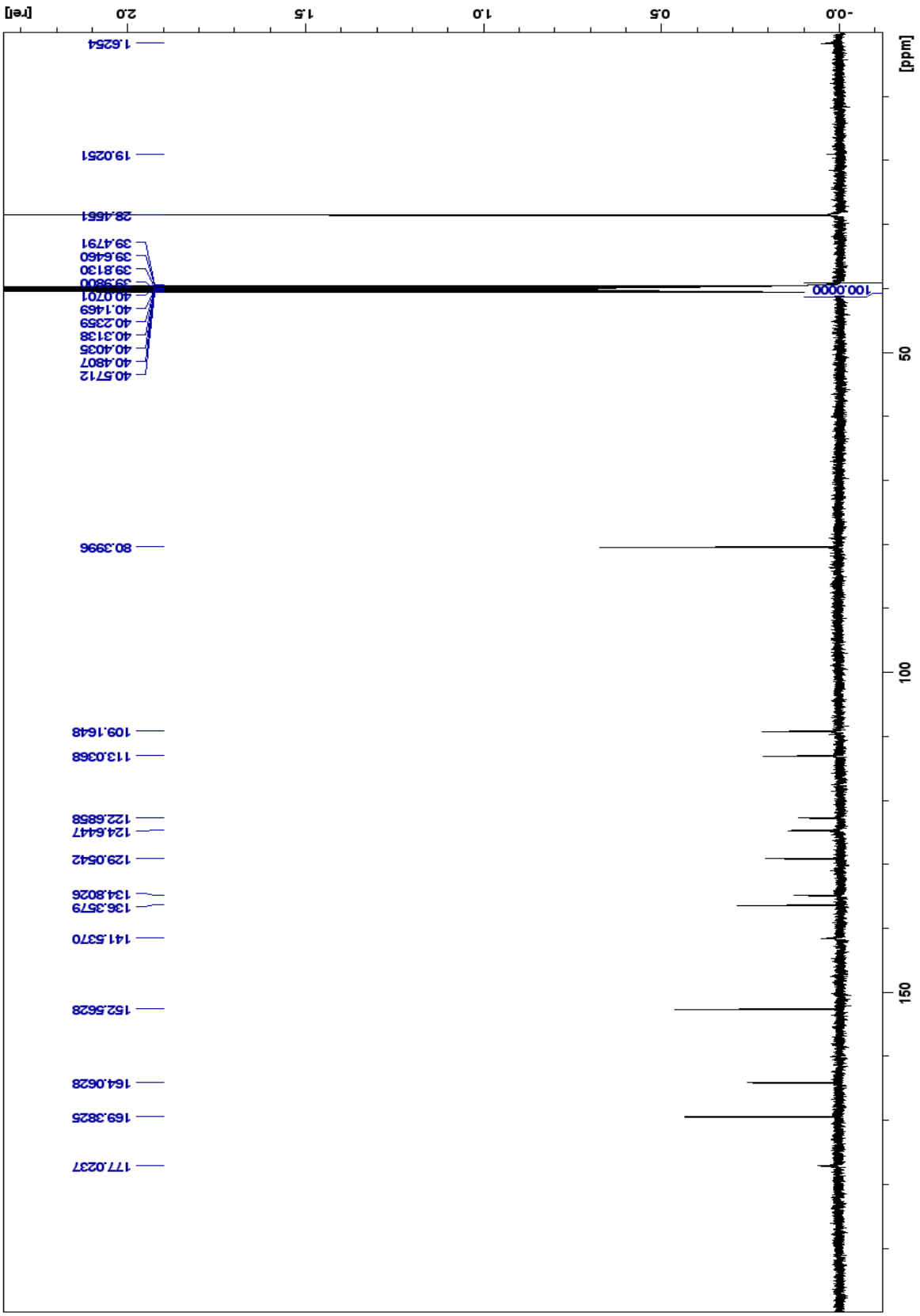

Spectrum 145*: 50 ^{13}C NMR (500 MHz, DMSO-d6)*

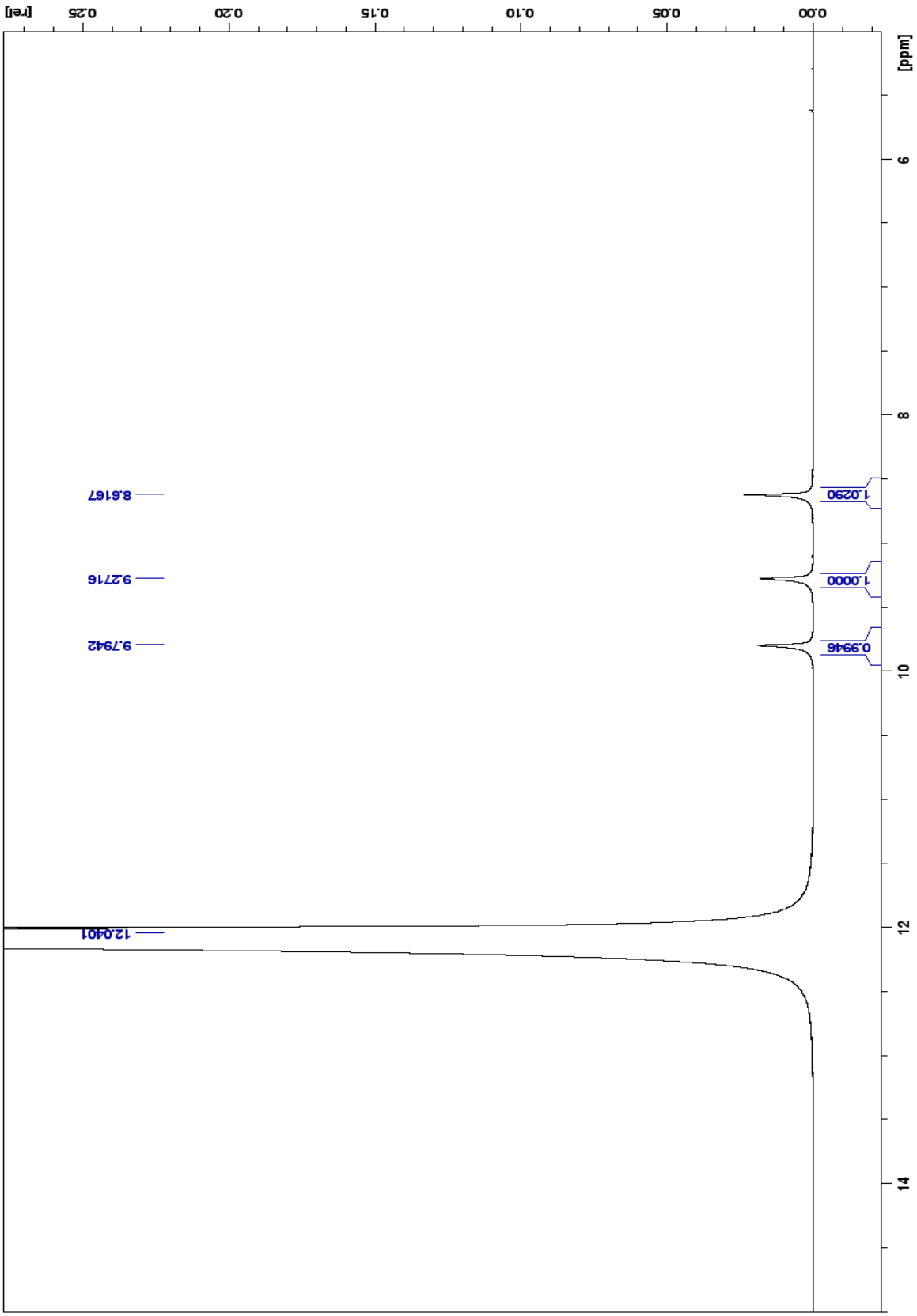

Spectrum 146*: 51* ***^{1}H NMR (500 MHz, TFA)***

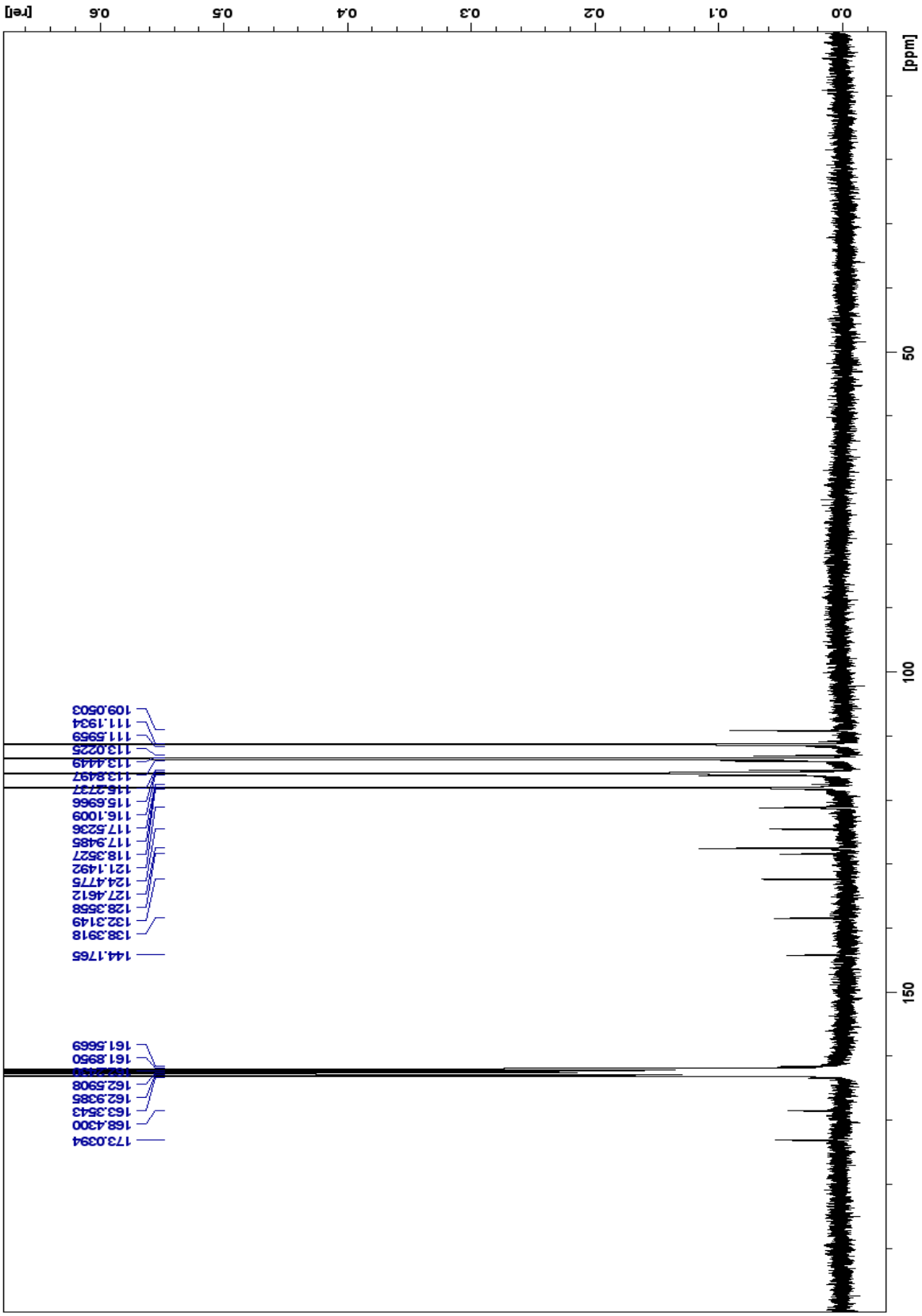

Spectrum 147*: 51* ***^{13}C NMR (500 MHz, TFA)***

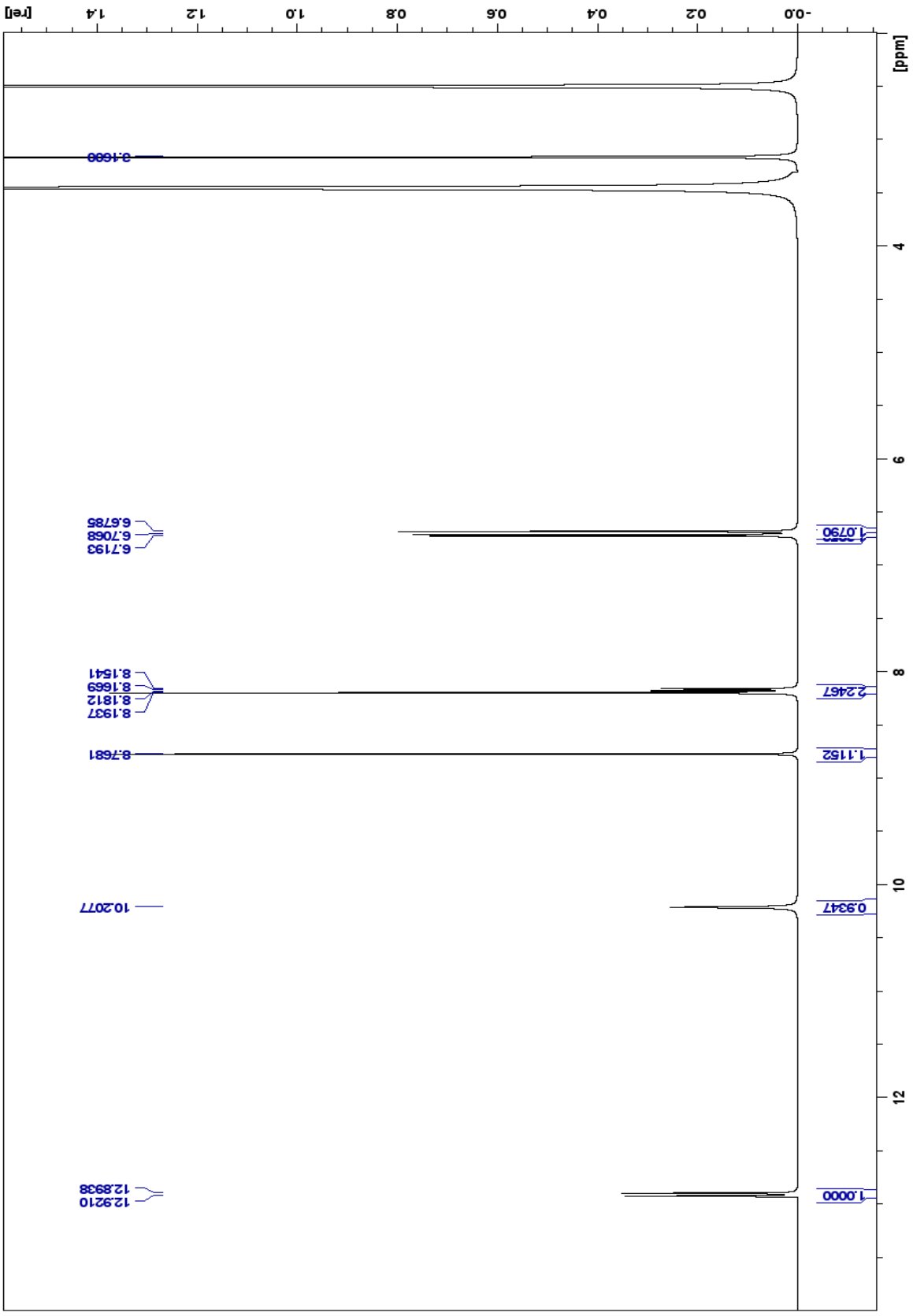
[rel]
14
12
10
0.8
0.6
0.4
0.2
-0.0
[ppm]
4
6
8
10
12
3.1688
6.7193
6.7068
6.6785
8.1541
8.1669
8.1812
8.1937
8.7681
10.2077
12.9210
12.8938
1.0790
2.2467
1.1152
0.9347
1.0000

Spectrum 148*: 52* ***^{1}H NMR (500 MHz, DMSO-d6)***

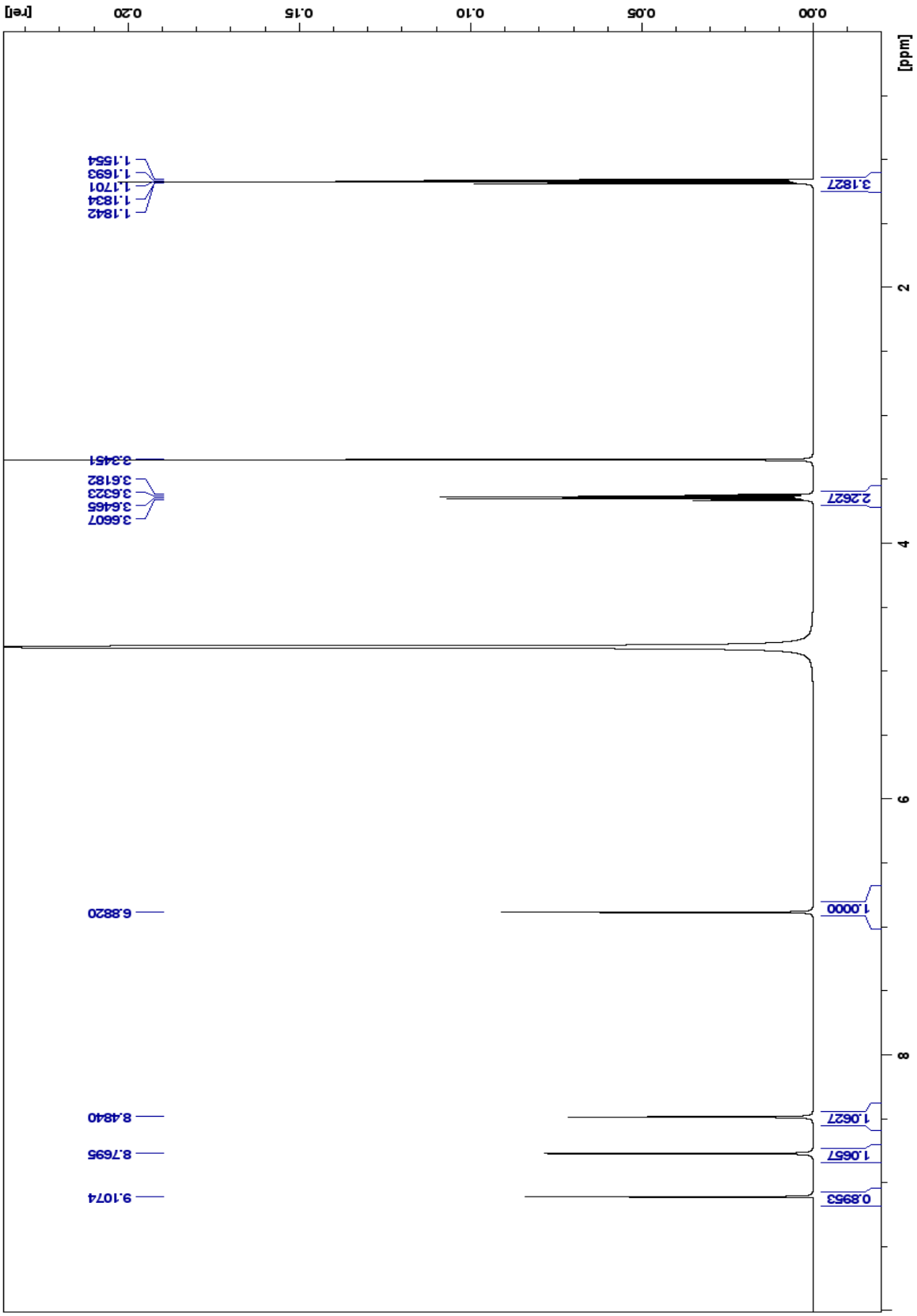

Spectrum 149*: 53* ^{1}***H NMR (500 MHz,*** D_2O ***+ KOH)***

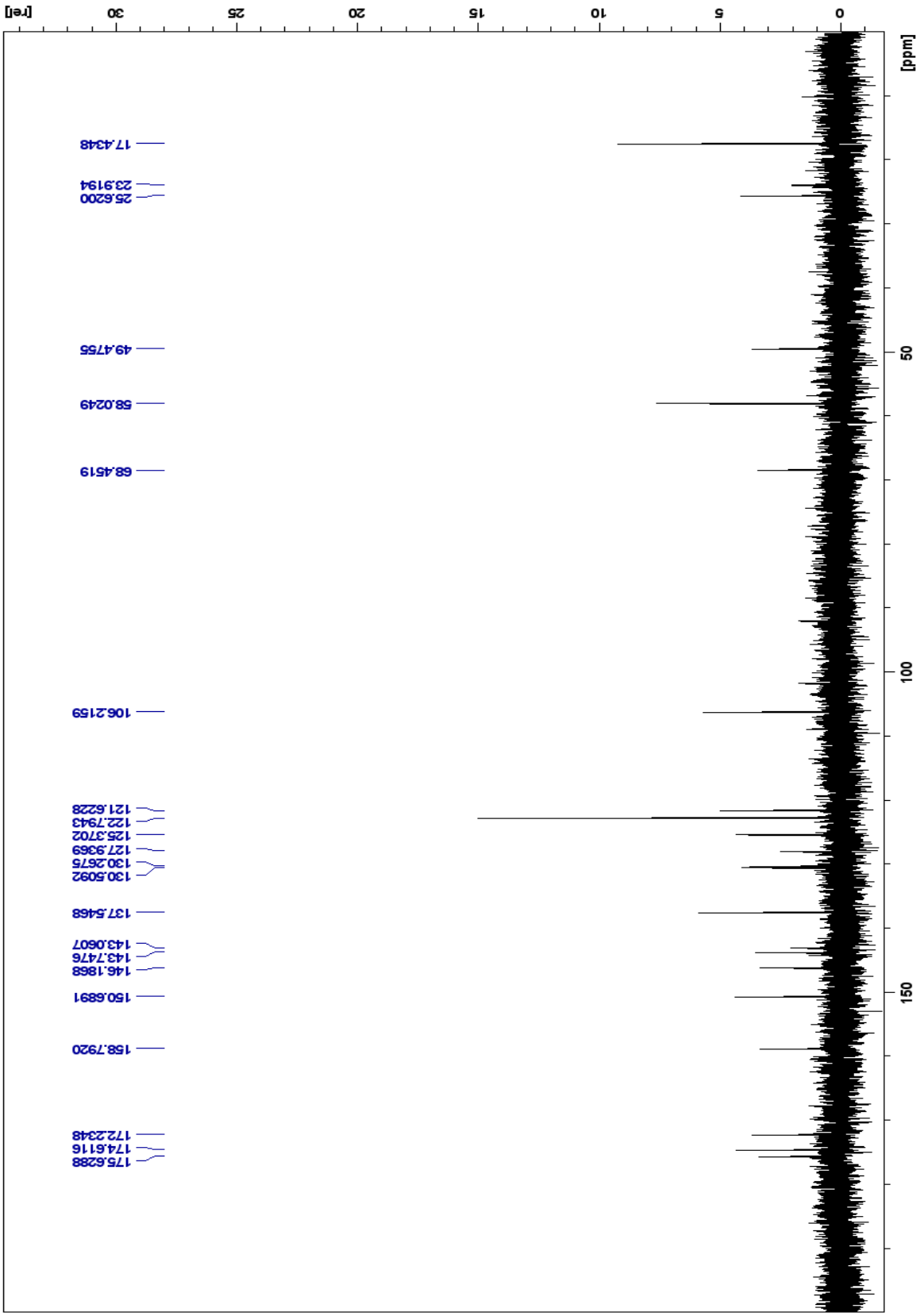

Spectrum 150*: 53 ^{13}C NMR (500 MHz, D_2O + KOH)*

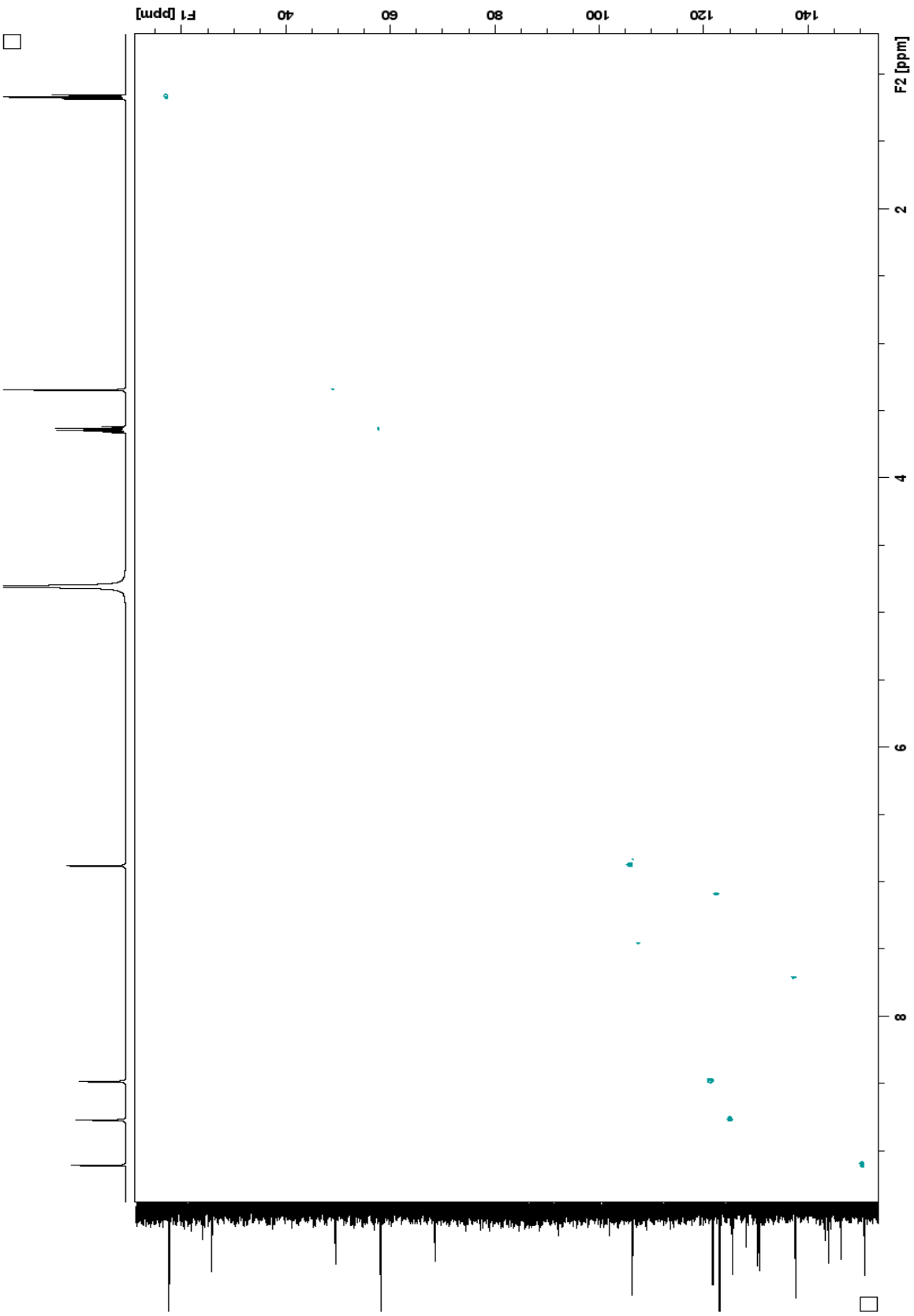

Spectrum 151*: 53* ***HSQC NMR (500 MHz, D_2O + KOH)***

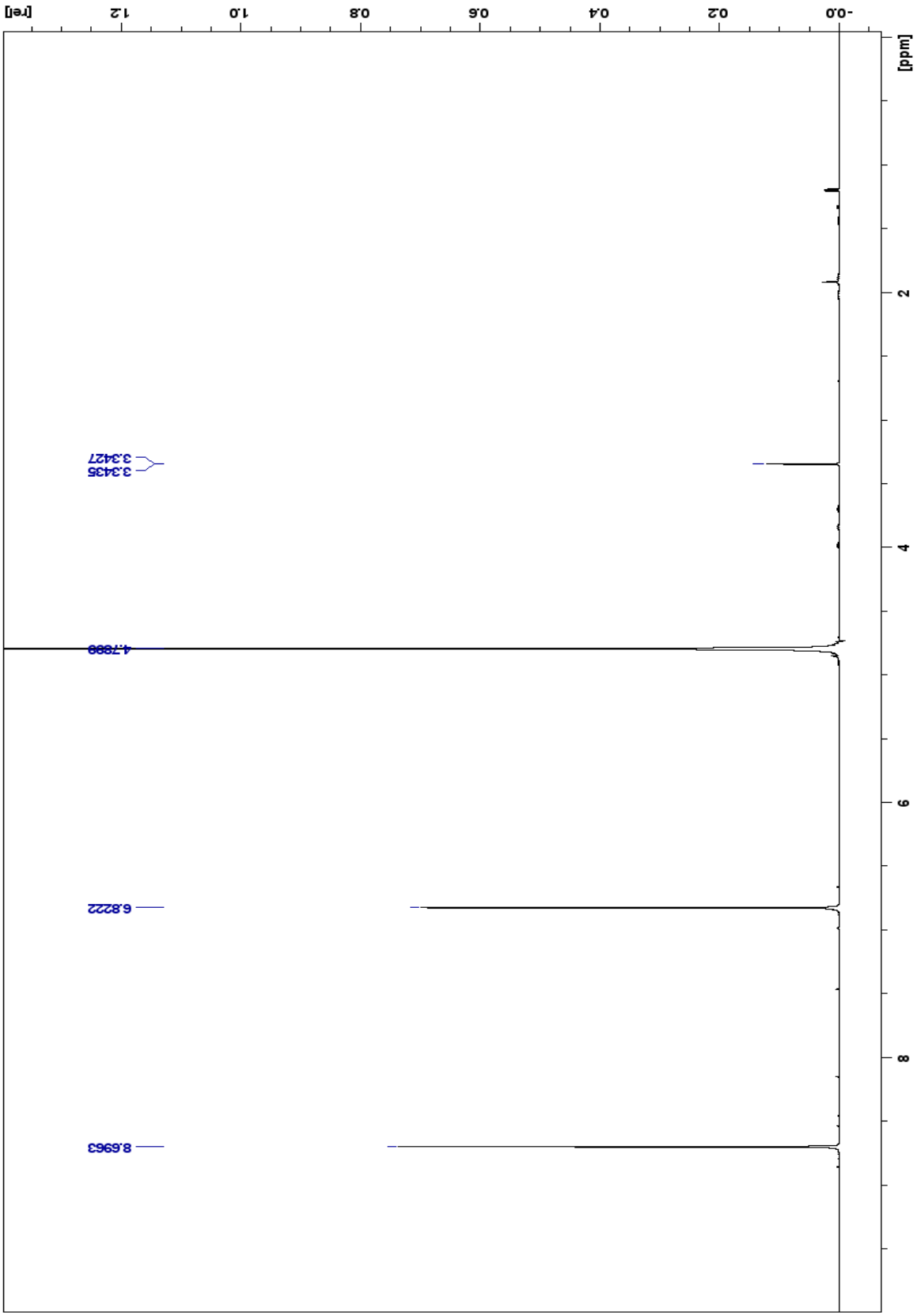

Spectrum 152*: 55* ^{1}***H NMR (500 MHz,*** D_2O ***+ KOH)***

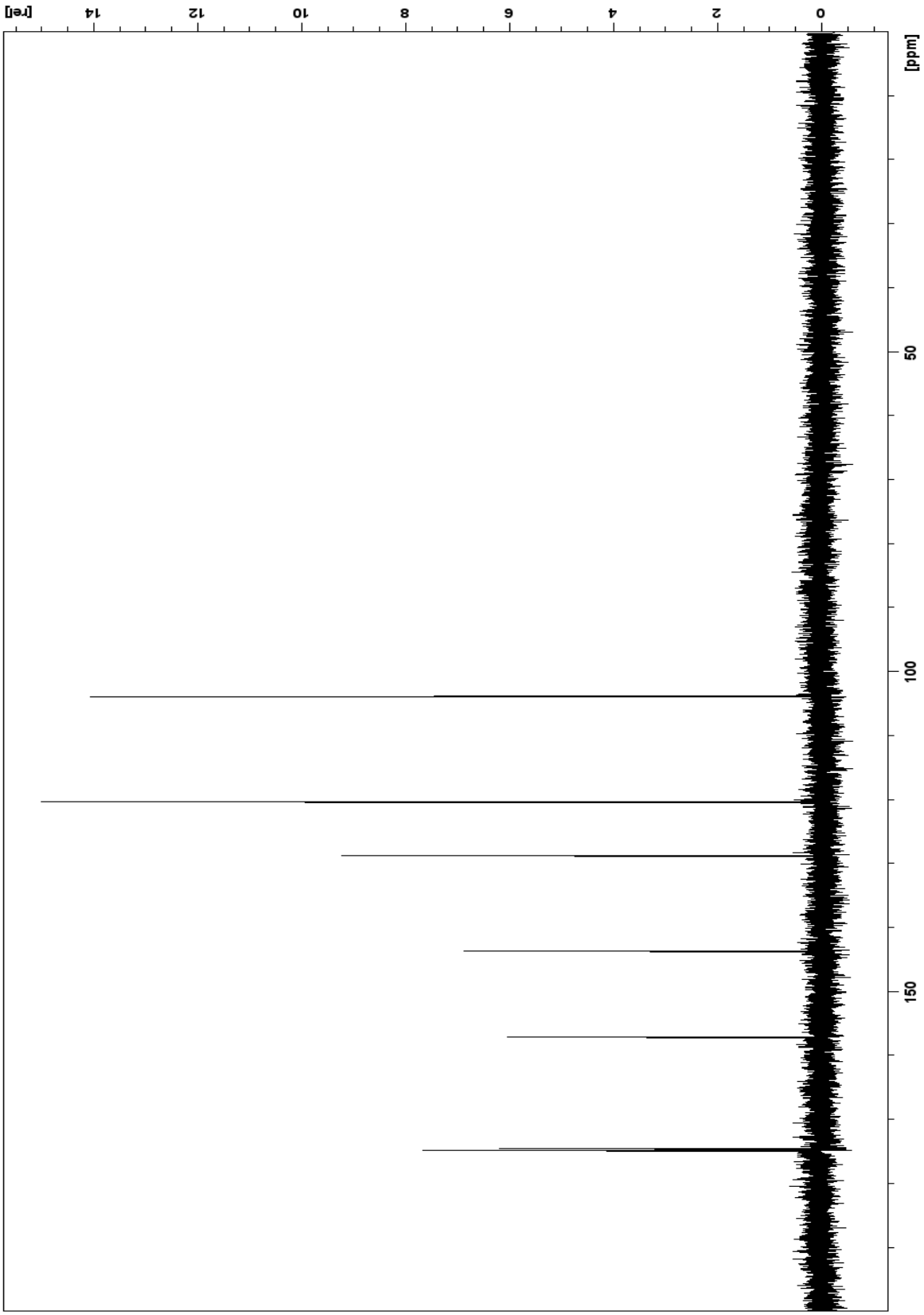

Spectrum 153*: 55* ***^{13}C NMR (500 MHz, D_2O + KOH)***

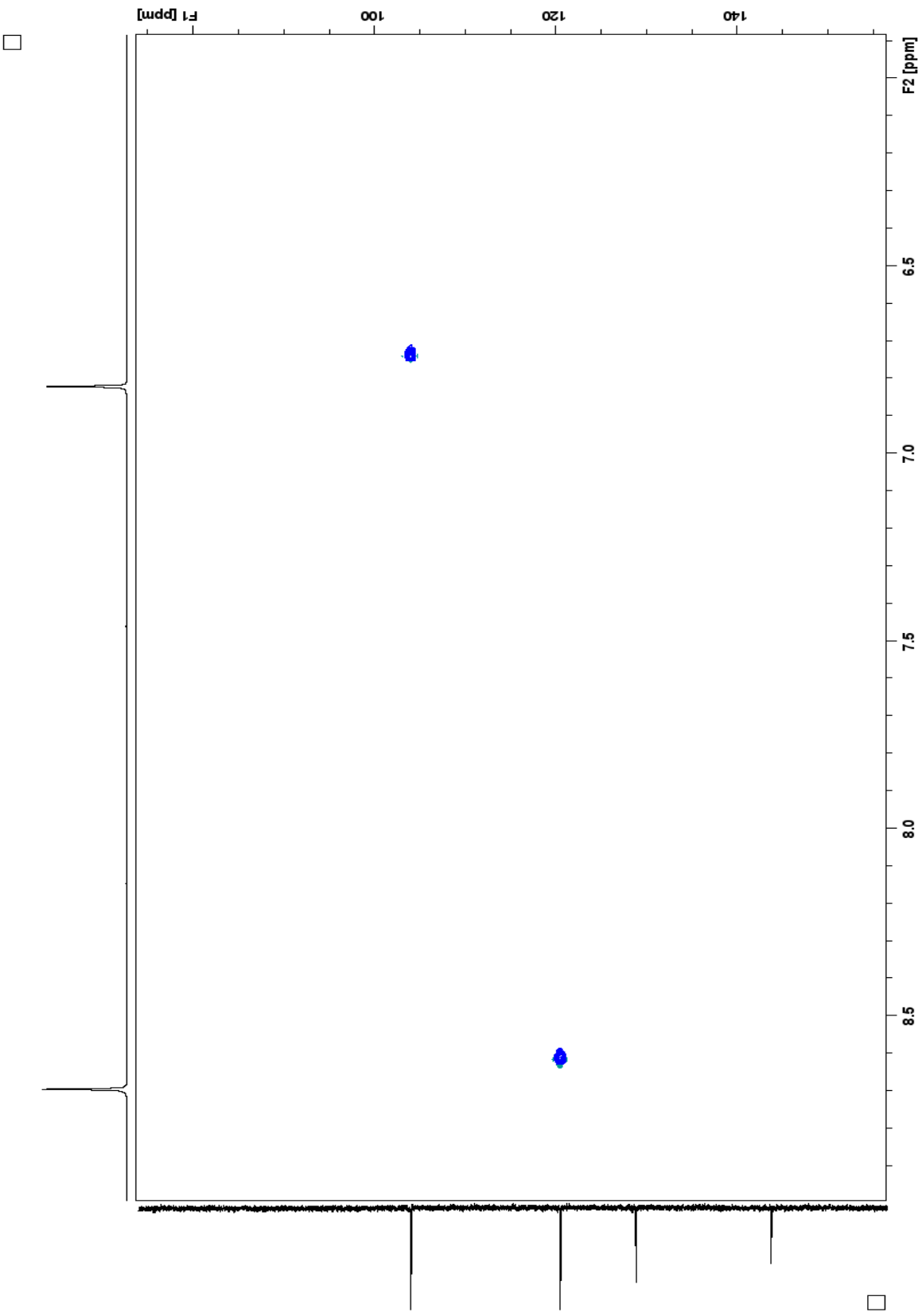

Spectrum 154*: 55* ***HSQC NMR (500 MHz, D_2O + KOH)***

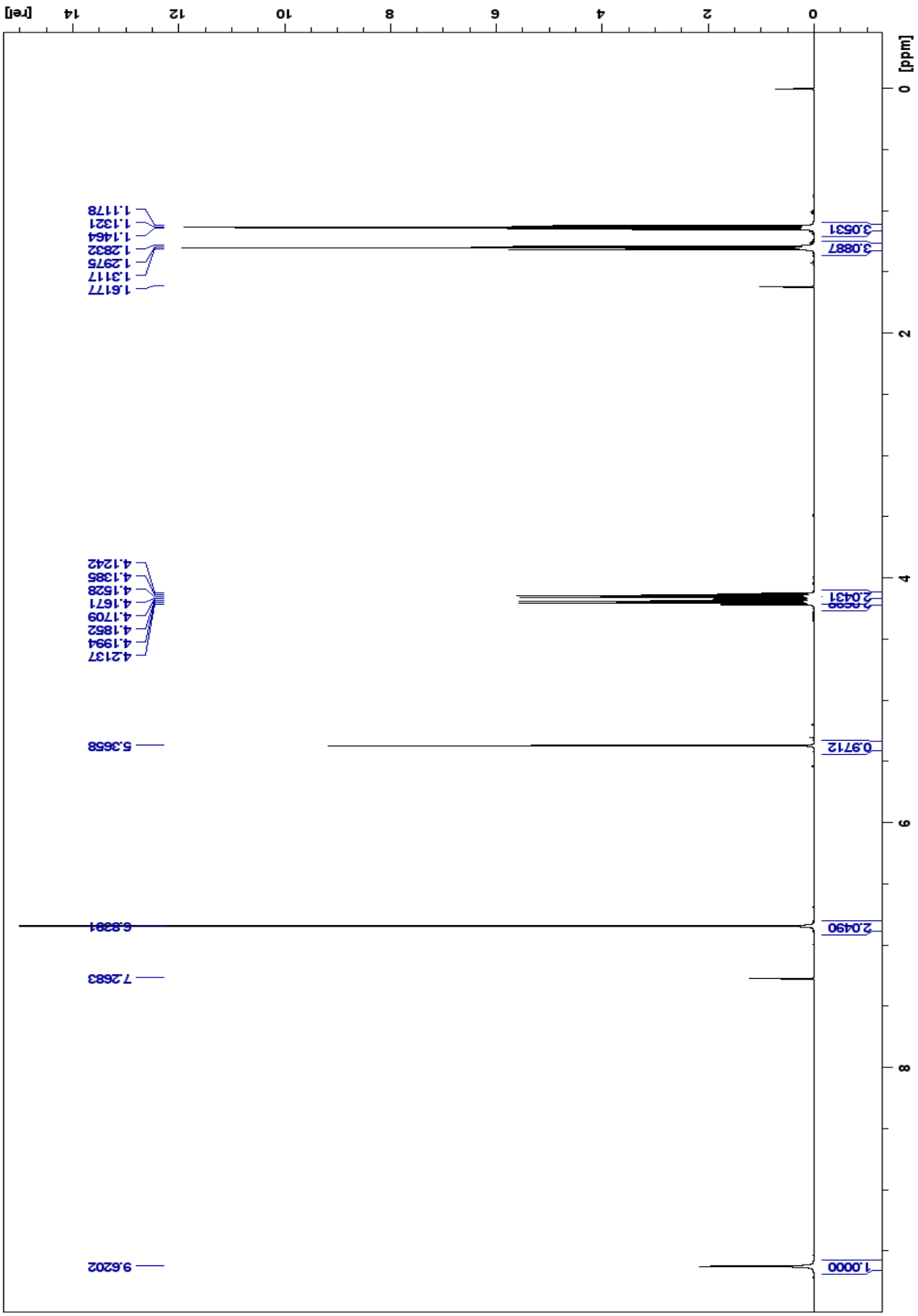

Spectrum 155*: 56 ^{1}H NMR (500 MHz, $CDCl_3$)*

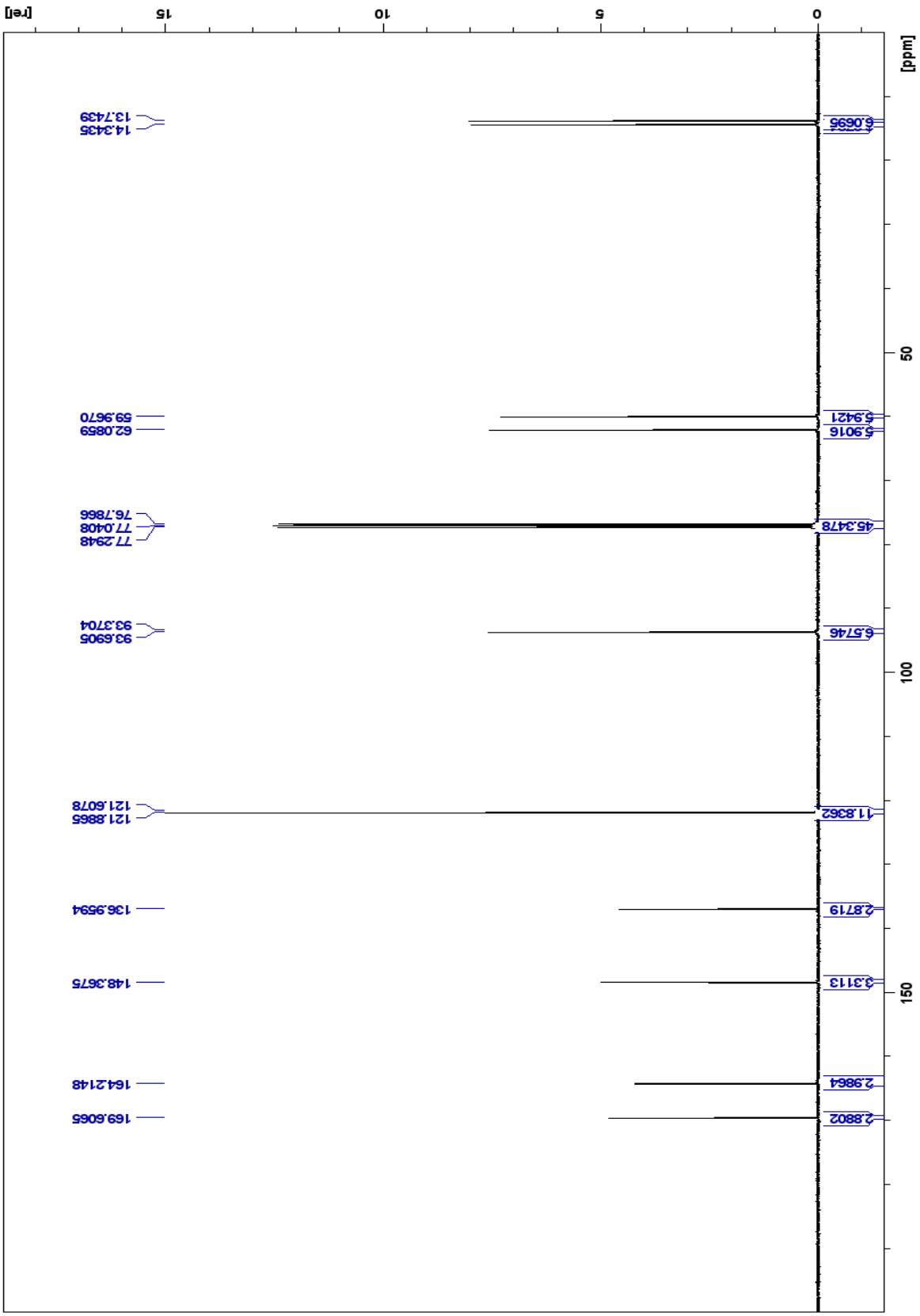

Spectrum 156*: 56* ***^{13}C NMR (500 MHz, $CDCl_3$)***

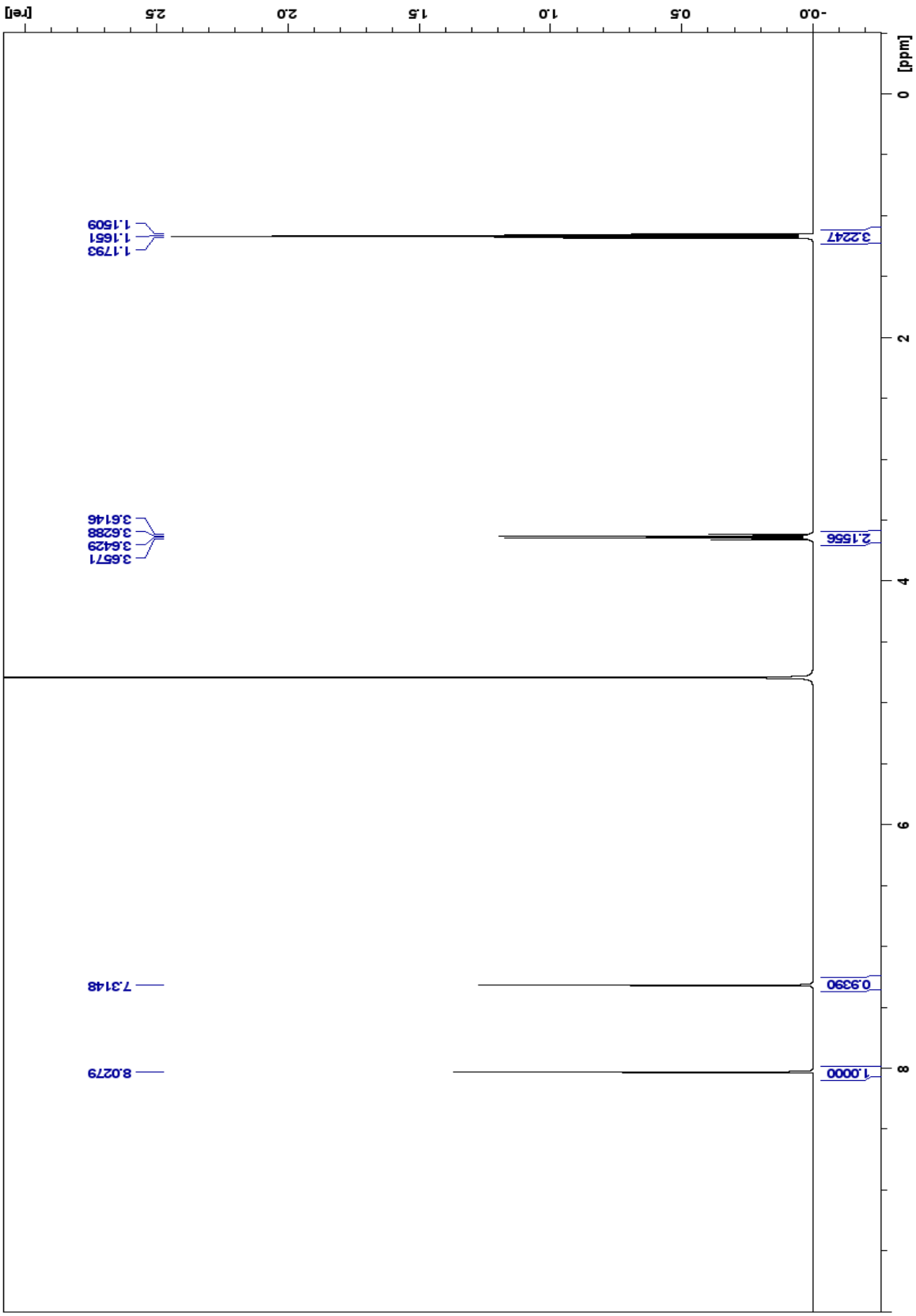

Spectrum 157*: 57* ^{1}***H NMR (500 MHz,*** D_2O ***+ KOH)***

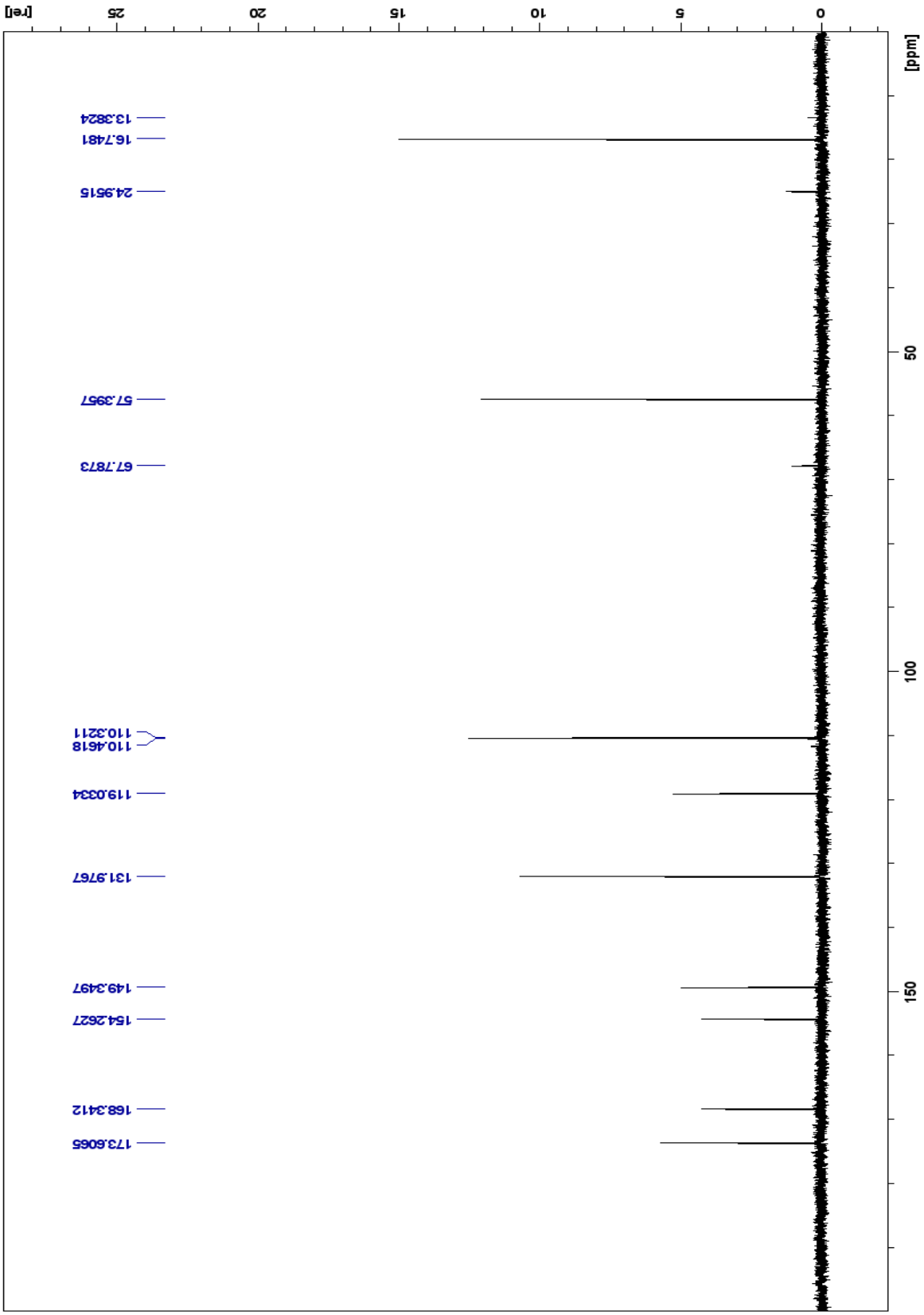

Spectrum 158*: 57* ***^{13}C NMR (500 MHz, D_2O + KOH)***

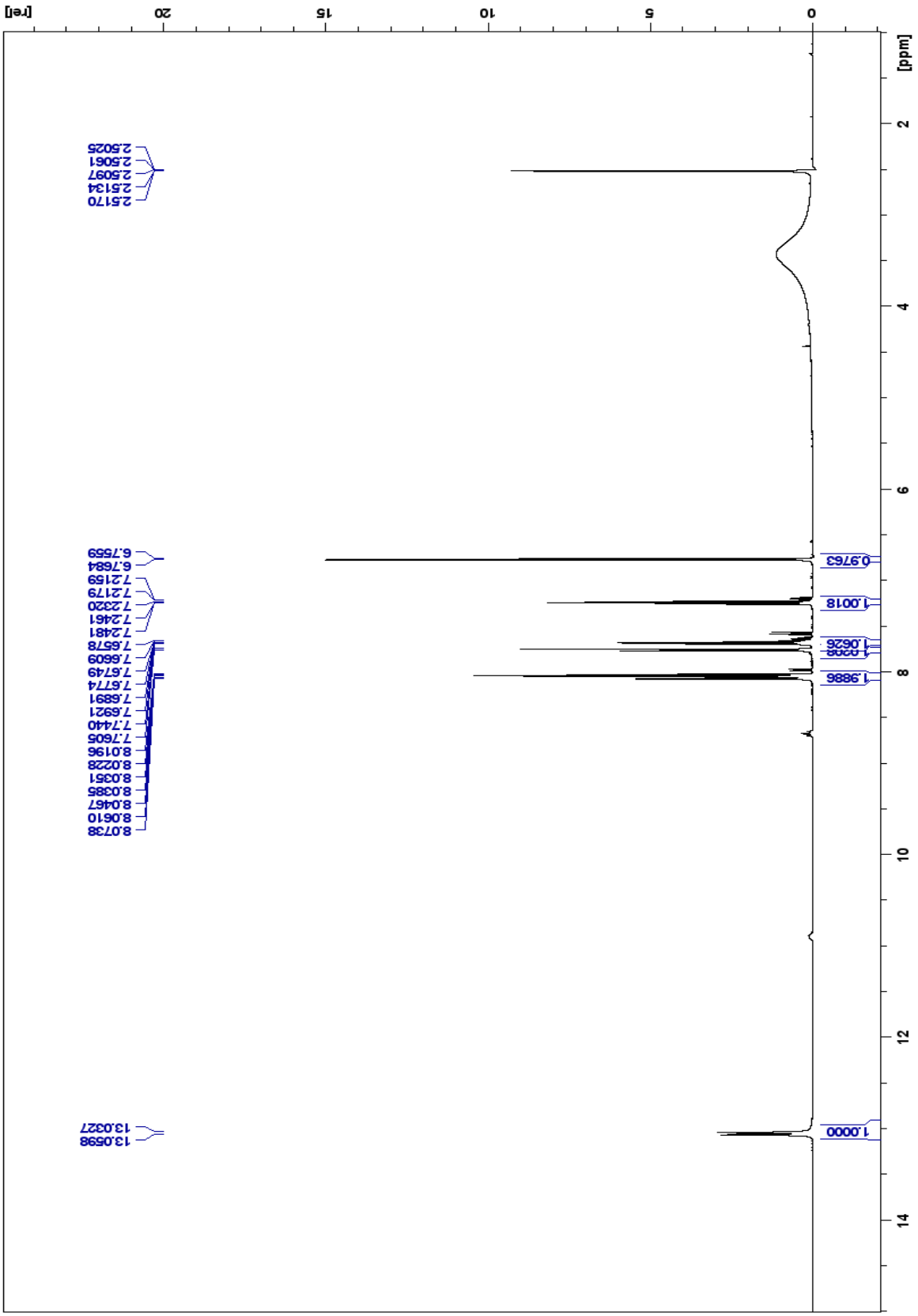

Spectrum 159*: 58a* ***^{1}H NMR (500 MHz, DMSO-d6)***

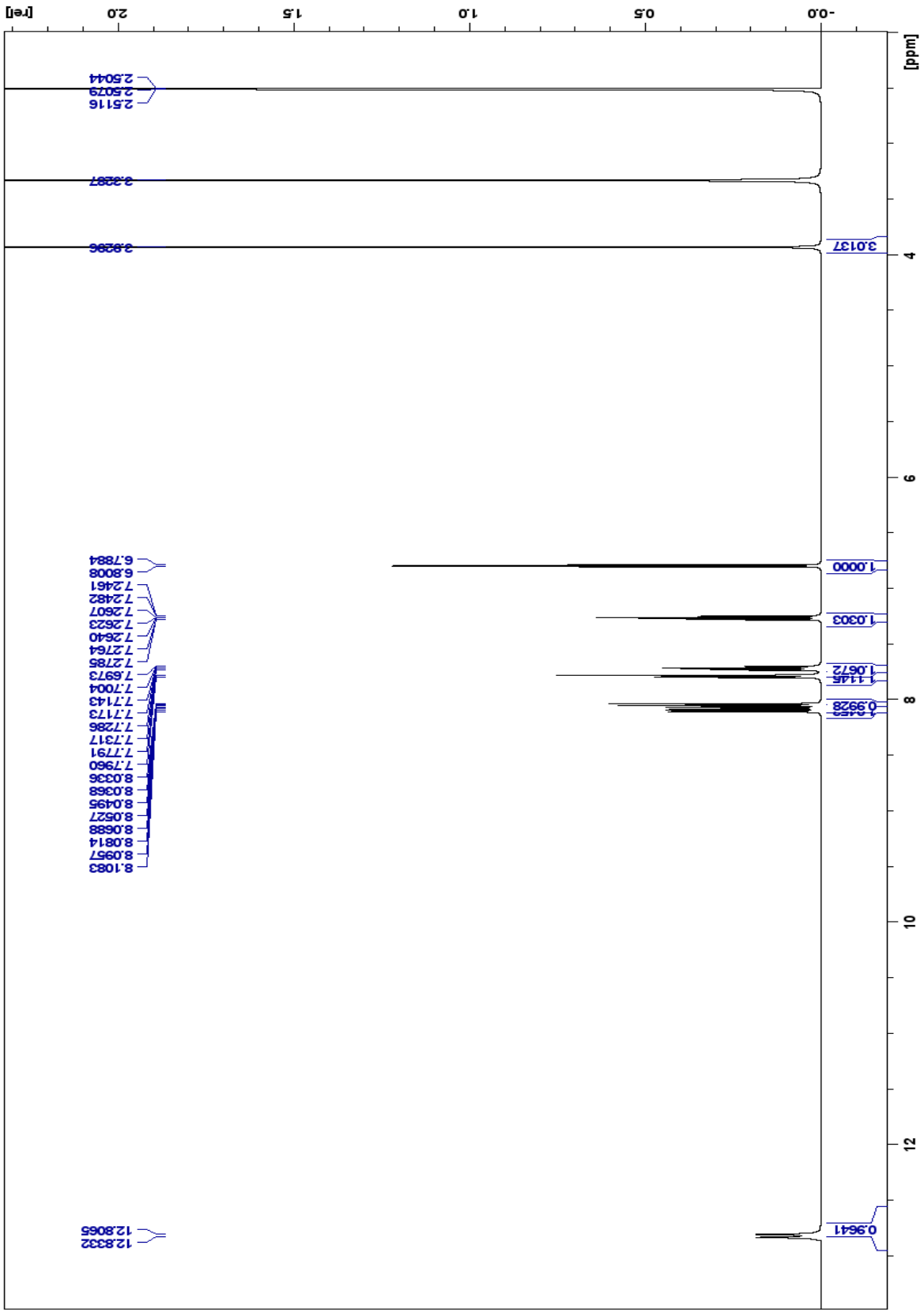

Spectrum 160: 58b **^{1}H NMR (500 MHz, DMSO-d6)**

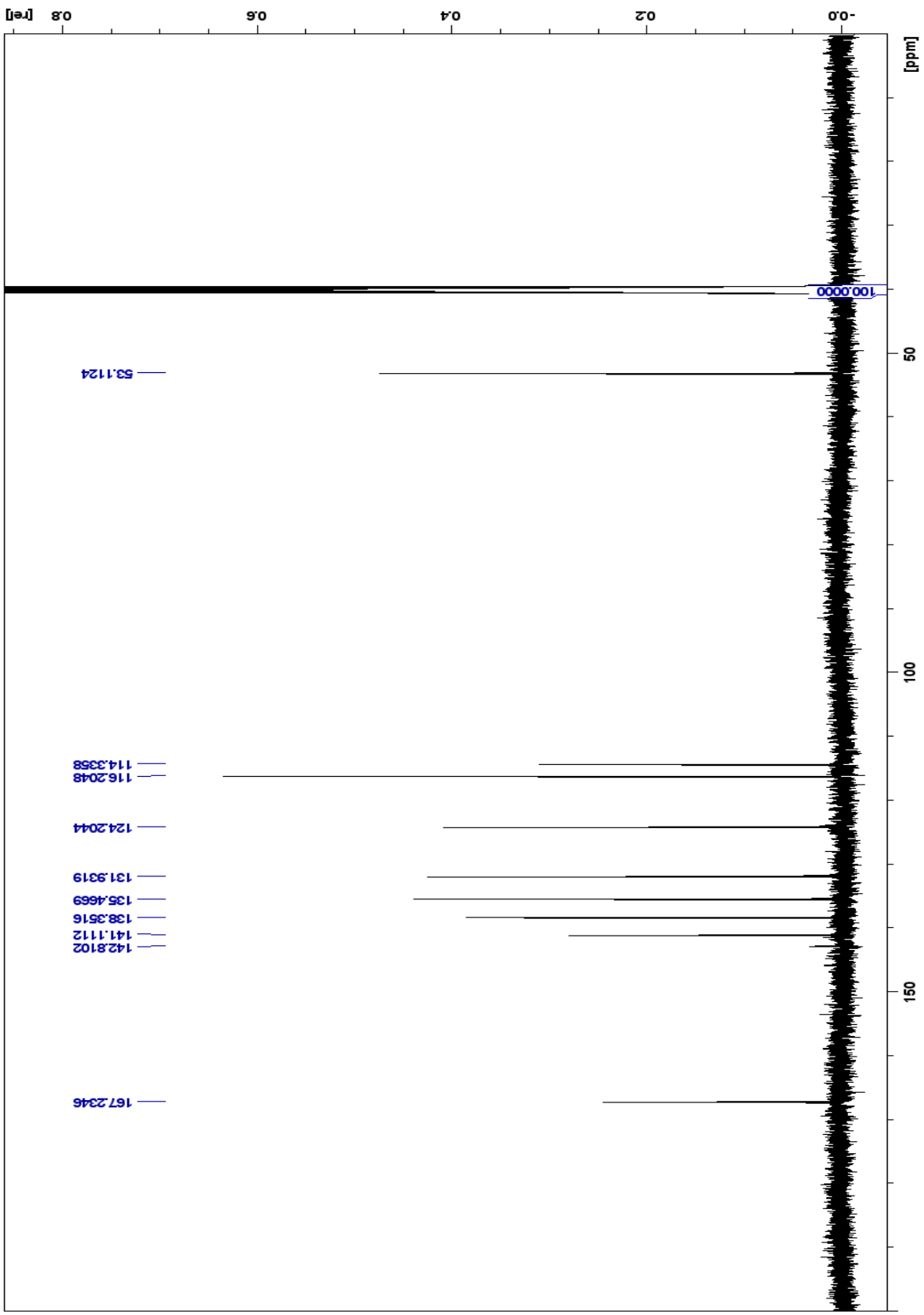

Spectrum 161: 58b **^{1}H NMR (500 MHz, DMSO-d6)**

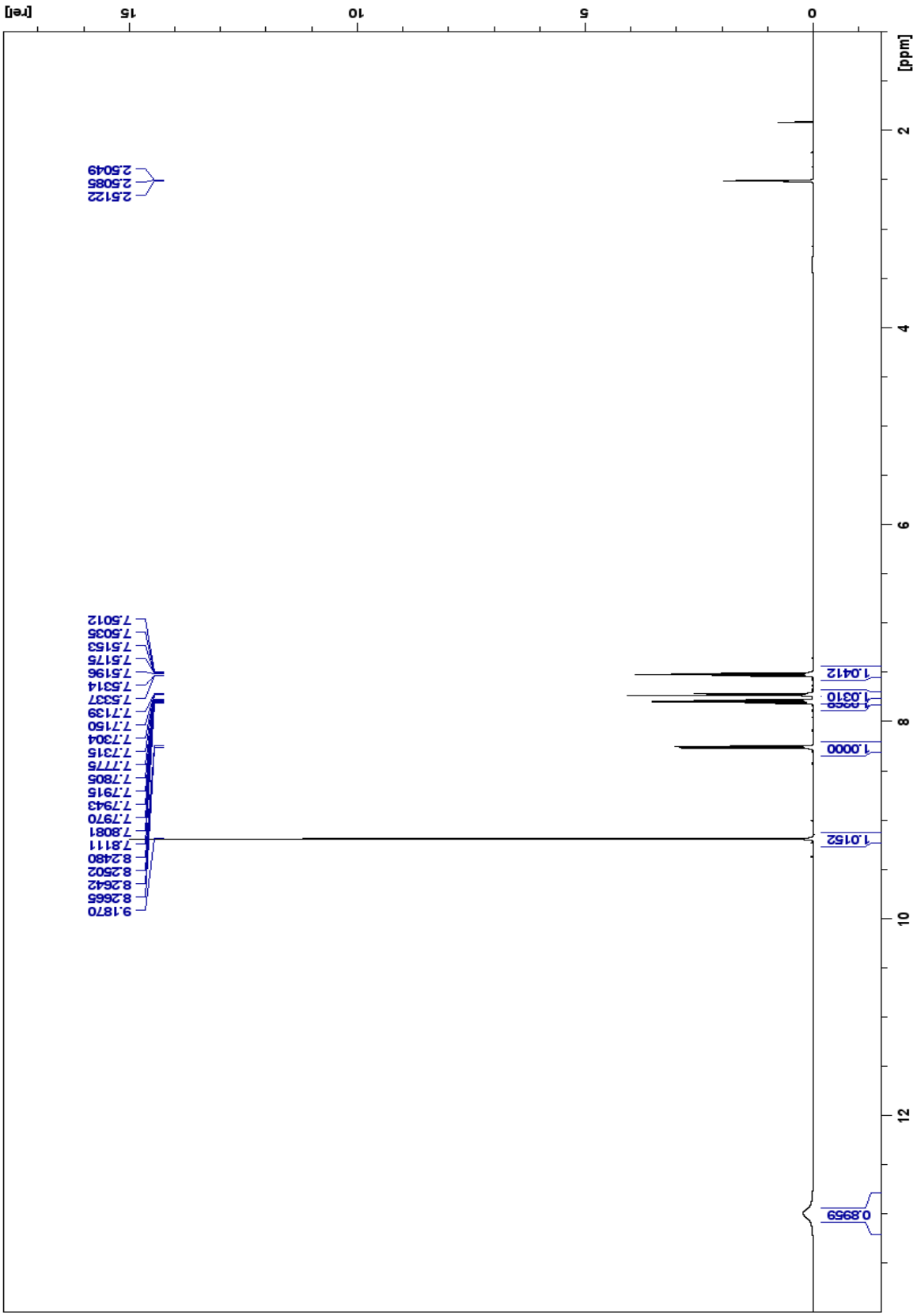

Spectrum 162*: 59* ***^{1}H NMR (500 MHz, DMSO-d6)***

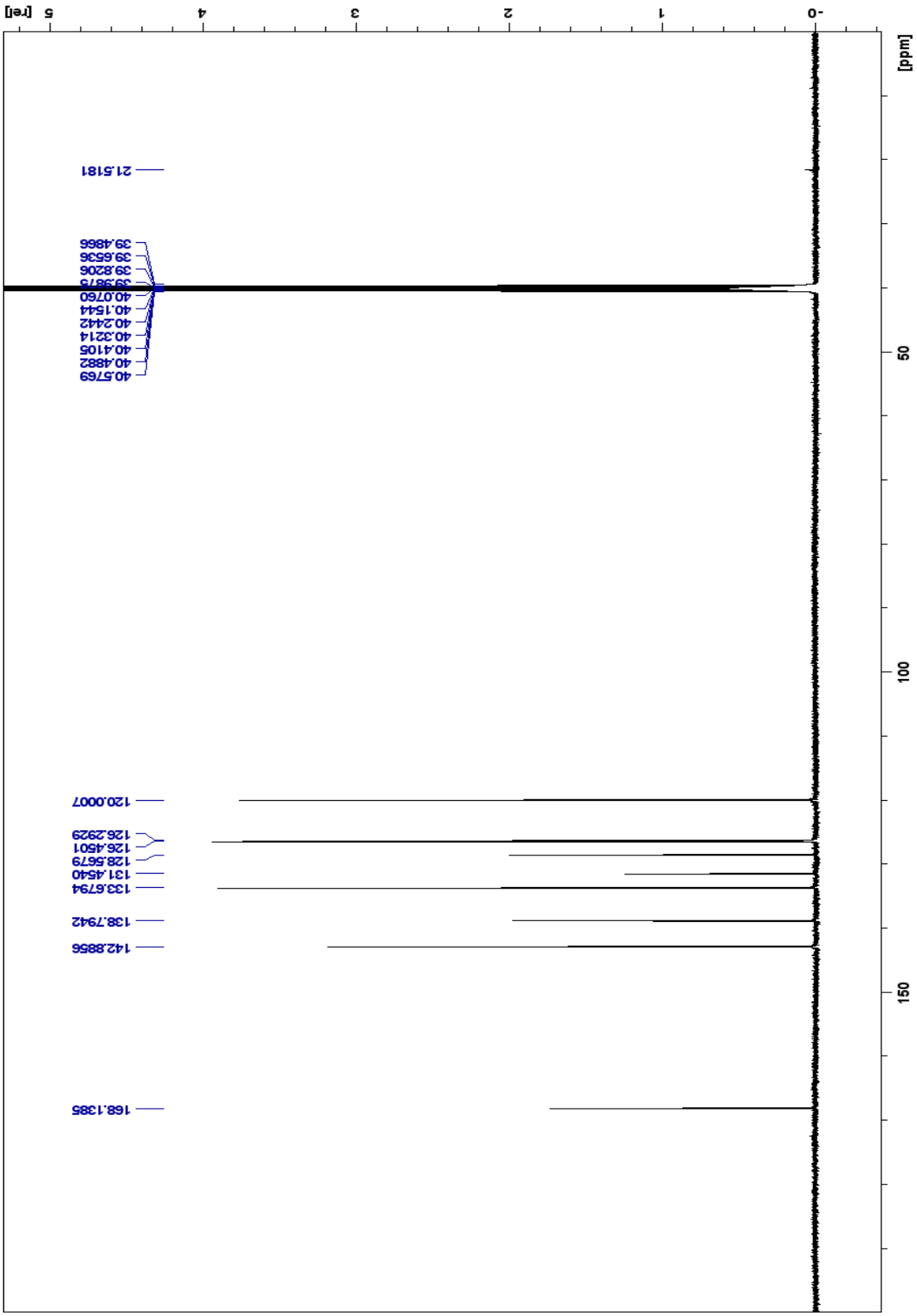

Spectrum 163*: 59 ^{13}C NMR (500 MHz, DMSO-d6)*

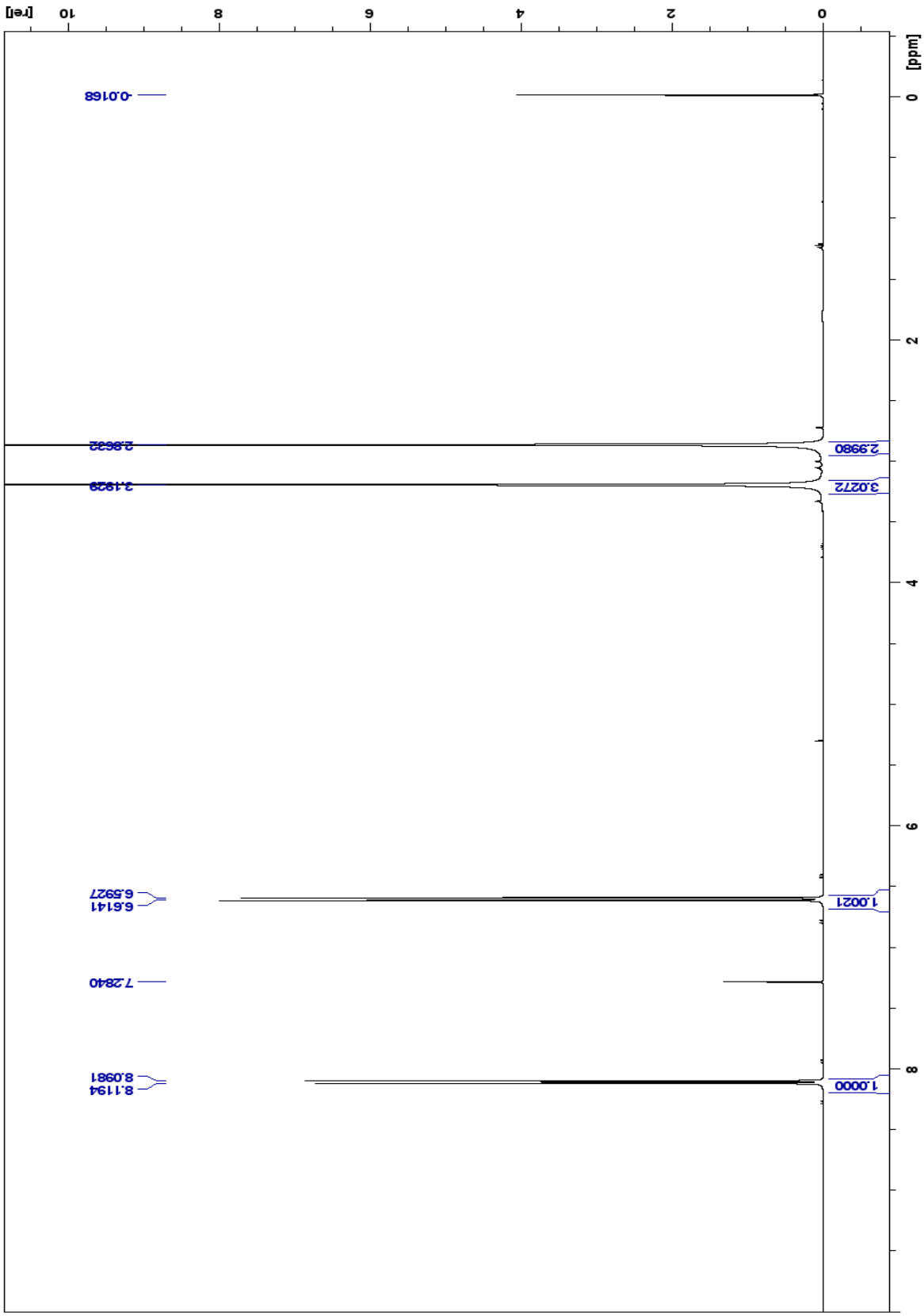

Spectrum 164: 60 ^{1}**H NMR (500 MHz, CDCl$_3$)**

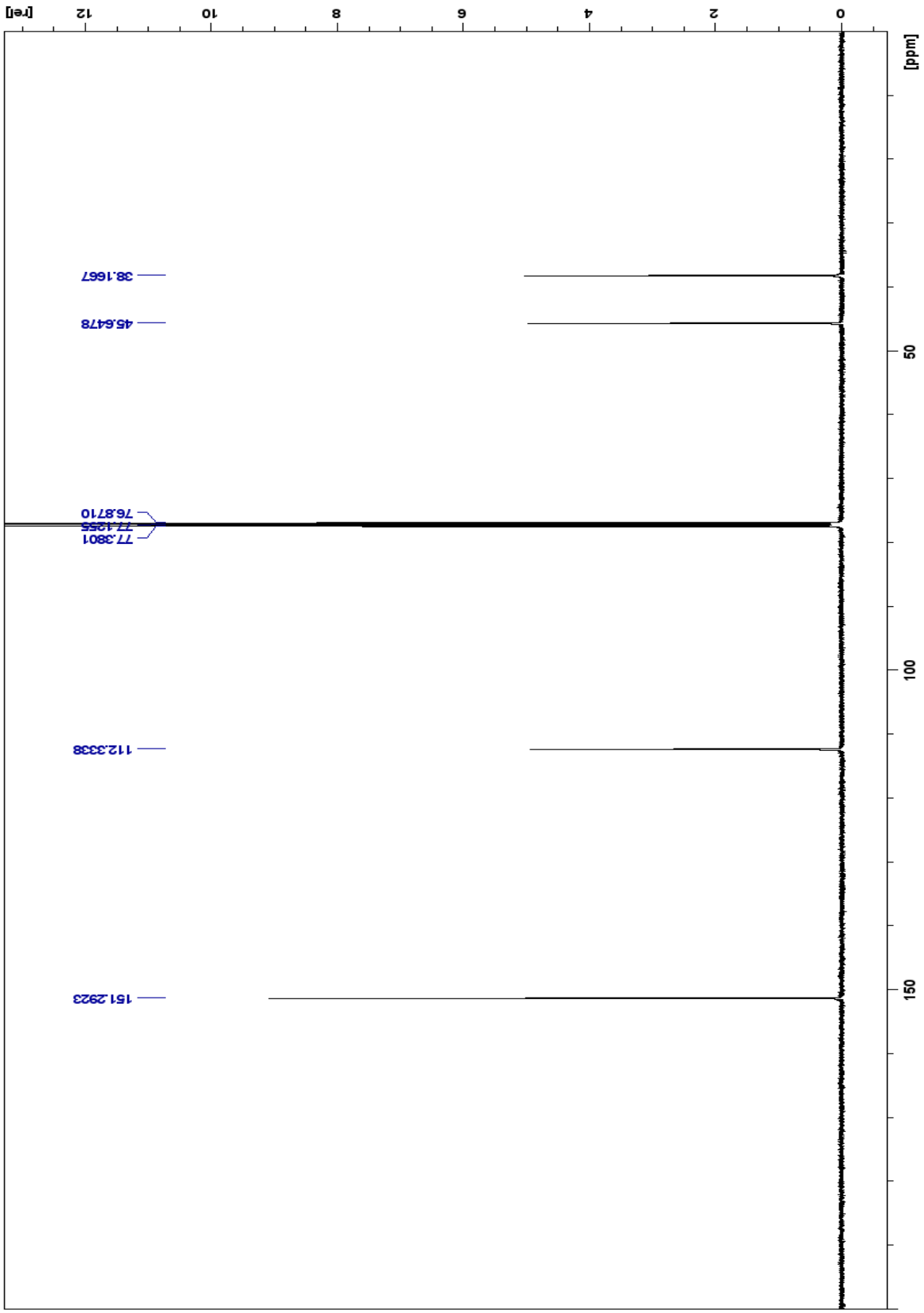

Spectrum 165: 60 ^{13}C NMR (500 MHz, $CDCl_3$)

Metal Ion Response Spectra

1b QAN-4OH

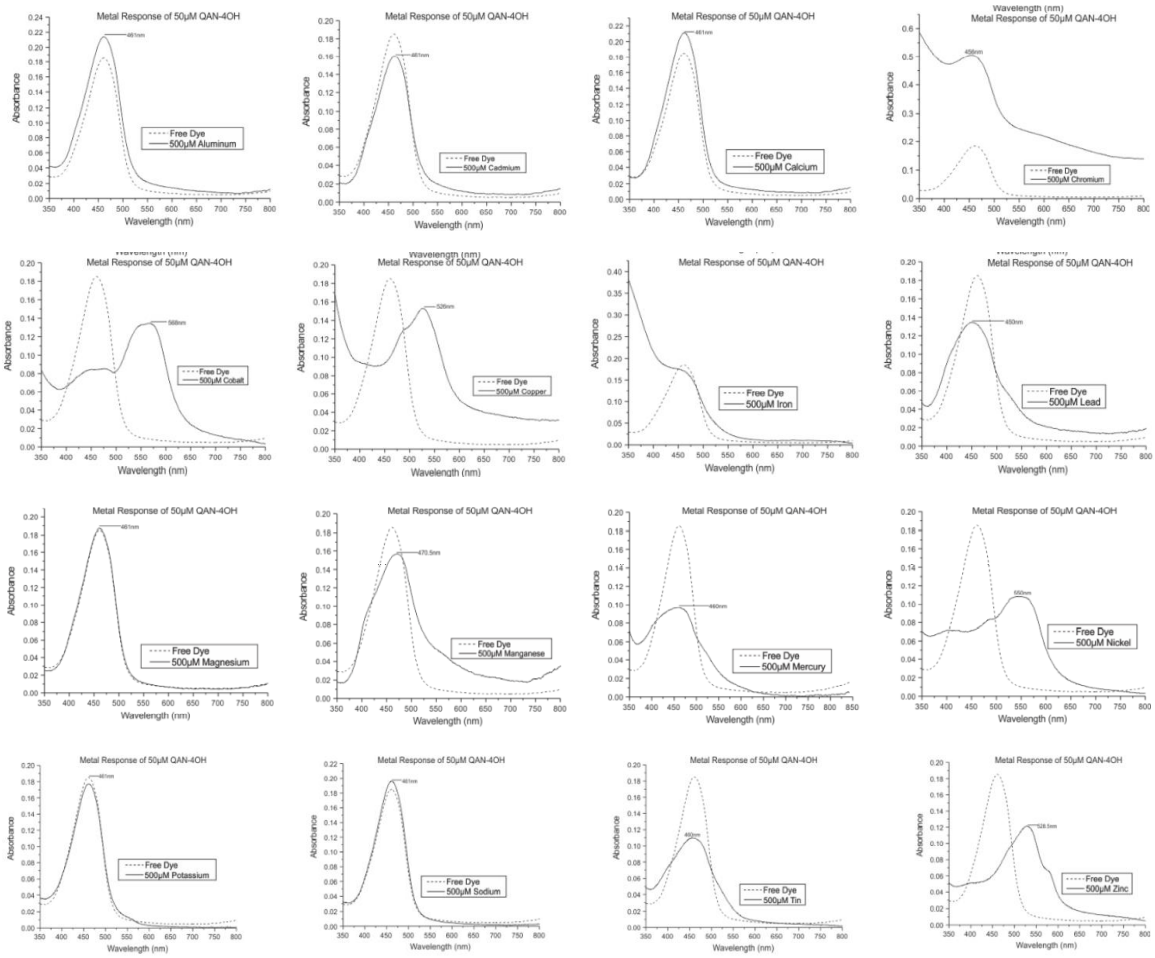

1c QAN-7OH

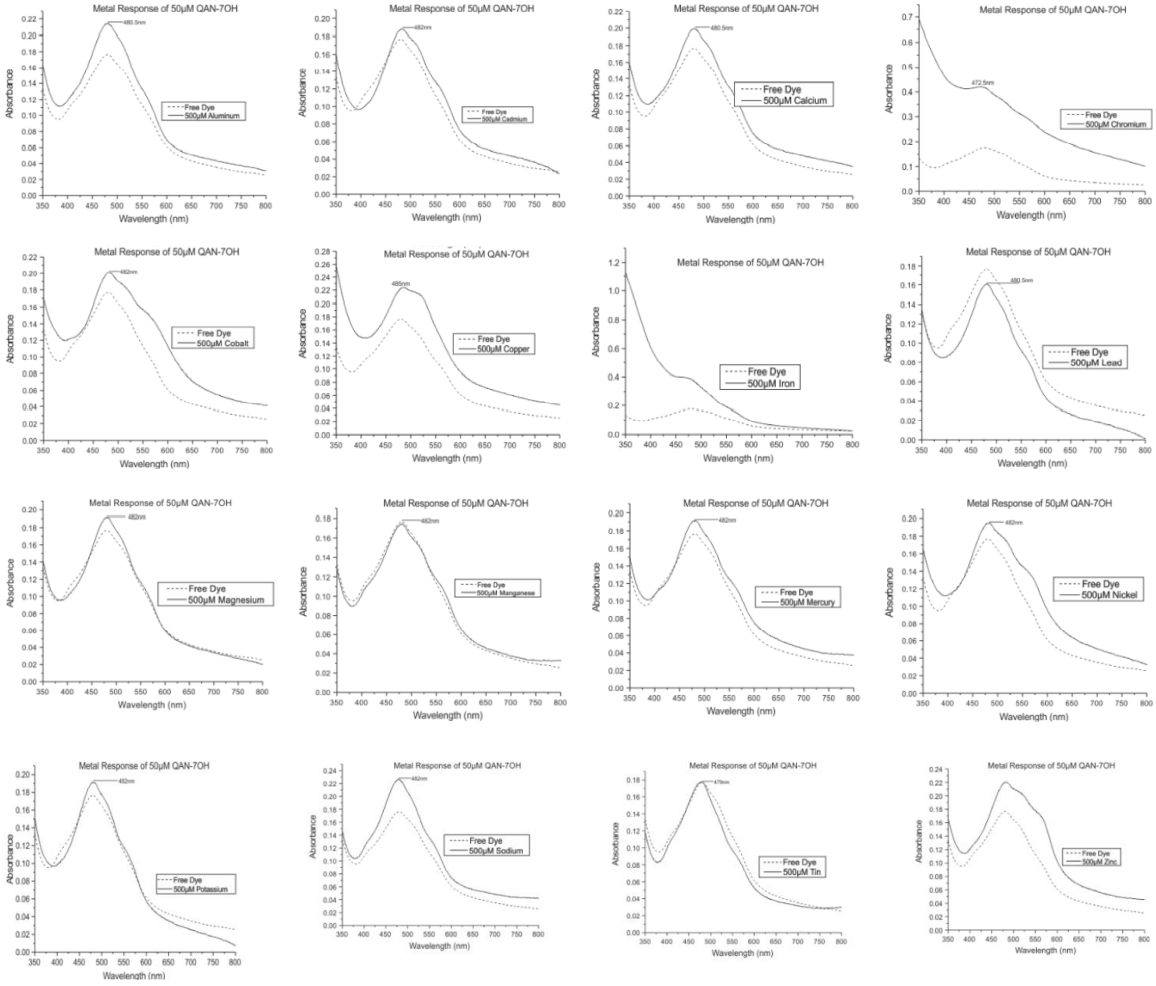
Metal Response of 50µM QAN-7OH
Absorbance
Wavelength (nm)
Free Dye
500µM Aluminum
500µM Cadmium
500µM Calcium
500µM Chromium
500µM Cobalt
500µM Copper
500µM Iron
500µM Lead
500µM Magnesium
500µM Manganese
500µM Mercury
500µM Nickel
500µM Potassium
500µM Sodium
500µM Tin
500µM Zinc

1d QAN-1,5OH

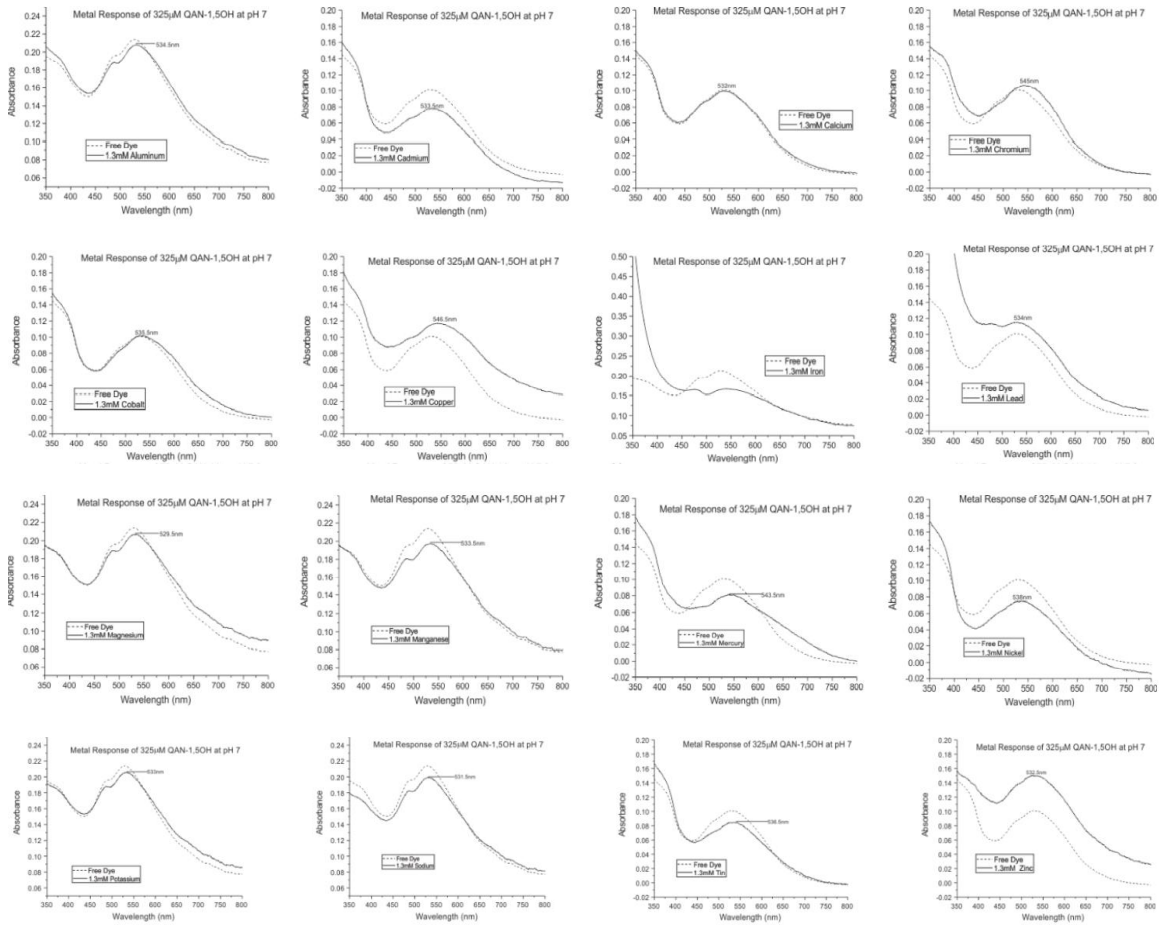
Metal Response of 325μM QAN-1,5OH at pH 7
Absorbance
Wavelength (nm)
Free Dye
1.3mM Aluminum
1.3mM Cadmium
1.3mM Calcium
1.3mM Chromium
1.3mM Cobalt
1.3mM Copper
1.3mM Iron
1.3mM Lead
1.3mM Magnesium
1.3mM Manganese
1.3mM Mercury
1.3mM Nickel
1.3mM Potassium
1.3mM Sodium
1.3mM Tin
1.3mM Zinc

2b

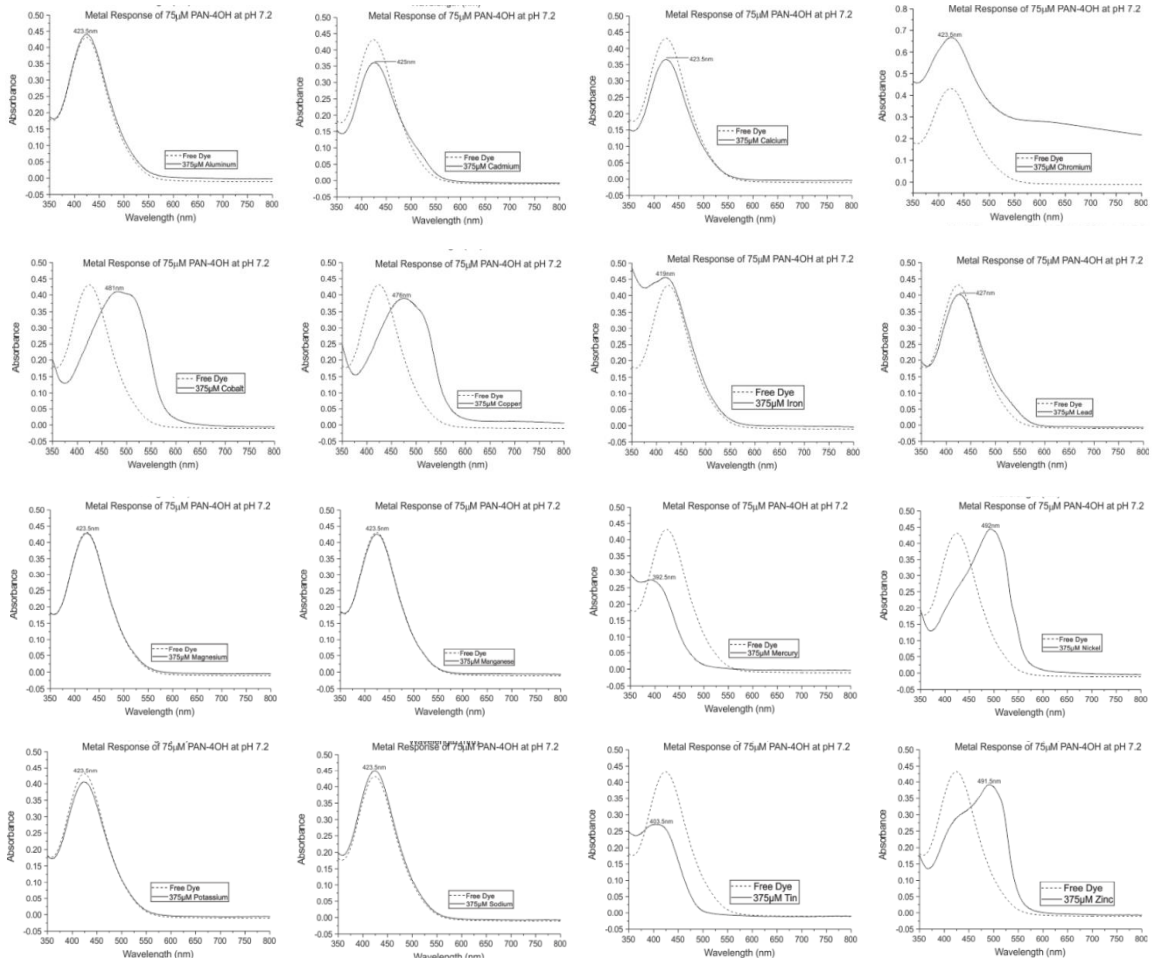
Metal Response of 75μM PAN-4OH at pH 7.2
Absorbance
Wavelength (nm)
Free Dye
375μM Aluminum
375μM Cadmium
375μM Calcium
375μM Chromium
375μM Cobalt
375μM Copper
375μM Iron
375μM Lead
375μM Magnesium
375μM Manganese
375μM Mercury
375μM Nickel
375μM Potassium
375μM Sodium
375μM Tin
375μM Zinc

2c

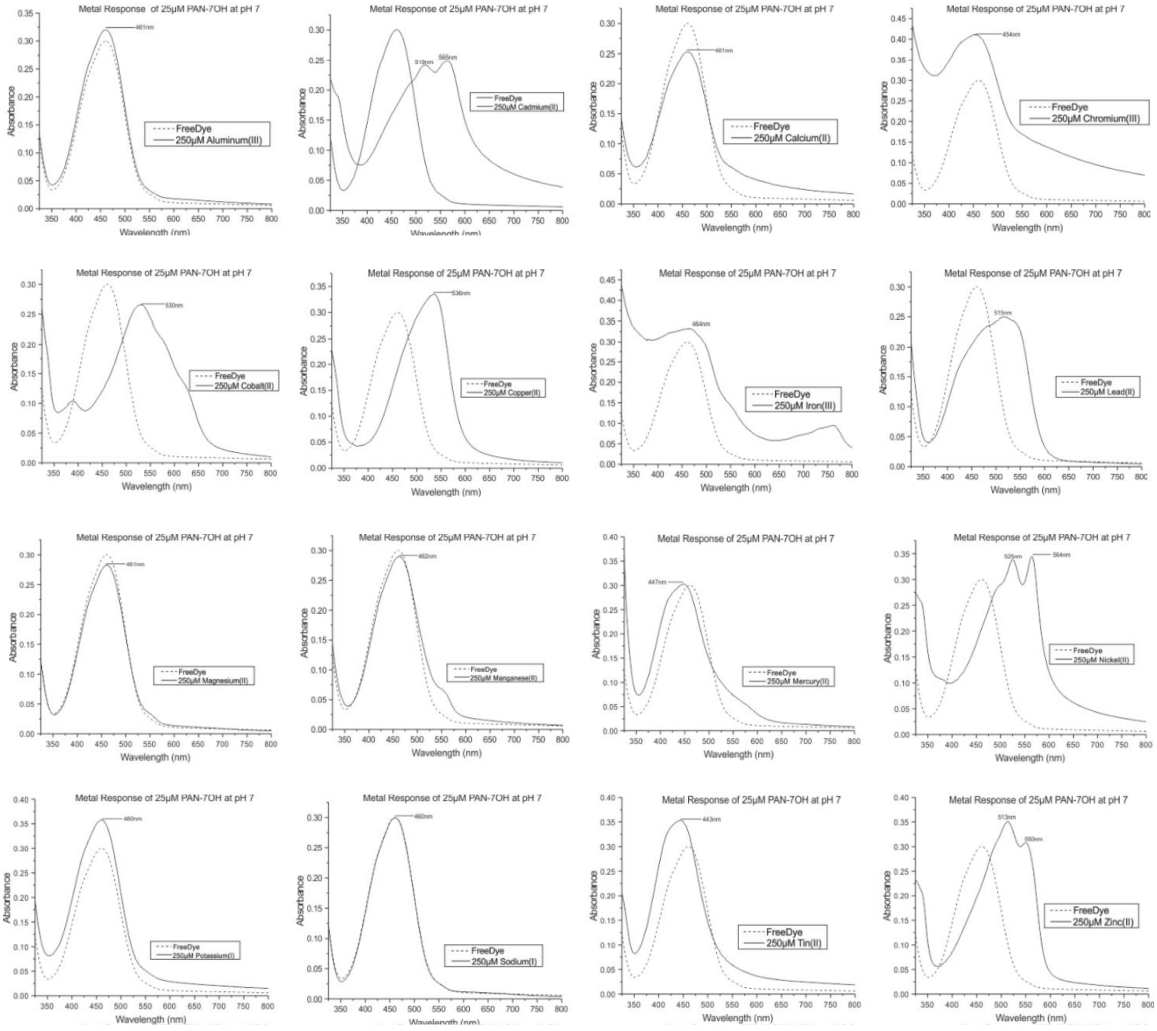
Metal Response of 25μM PAN-7OH at pH 7
Absorbance
Wavelength (nm)
461nm
FreeDye
250μM Aluminum(III)
Metal Response of 25μM PAN-7OH at pH 7
Absorbance
Wavelength (nm)
565nm
FreeDye
250μM Cadmium(II)
Metal Response of 25μM PAN-7OH at pH 7
Absorbance
Wavelength (nm)
461nm
FreeDye
250μM Calcium(II)
Metal Response of 25μM PAN-7OH at pH 7
Absorbance
Wavelength (nm)
454nm
FreeDye
250μM Chromium(III)
Metal Response of 25μM PAN-7OH at pH 7
Absorbance
Wavelength (nm)
530nm
FreeDye
250μM Cobalt(II)
Metal Response of 25μM PAN-7OH at pH 7
Absorbance
Wavelength (nm)
536nm
FreeDye
250μM Copper(II)
Metal Response of 25μM PAN-7OH at pH 7
Absorbance
Wavelength (nm)
464nm
FreeDye
250μM Iron(III)
Metal Response of 25μM PAN-7OH at pH 7
Absorbance
Wavelength (nm)
515nm
FreeDye
250μM Lead(II)
Metal Response of 25μM PAN-7OH at pH 7
Absorbance
Wavelength (nm)
461nm
FreeDye
250μM Magnesium(II)
Metal Response of 25μM PAN-7OH at pH 7
Absorbance
Wavelength (nm)
462nm
FreeDye
250μM Manganese(II)
Metal Response of 25μM PAN-7OH at pH 7
Absorbance
Wavelength (nm)
447nm
FreeDye
250μM Mercury(II)
Metal Response of 25μM PAN-7OH at pH 7
Absorbance
Wavelength (nm)
525nm
564nm
FreeDye
250μM Nickel(II)
Metal Response of 25μM PAN-7OH at pH 7
Absorbance
Wavelength (nm)
460nm
FreeDye
250μM Potassium(I)
Metal Response of 25μM PAN-7OH at pH 7
Absorbance
Wavelength (nm)
460nm
FreeDye
250μM Sodium(I)
Metal Response of 25μM PAN-7OH at pH 7
Absorbance
Wavelength (nm)
443nm
FreeDye
250μM Tin(II)
Metal Response of 25μM PAN-7OH at pH 7
Absorbance
Wavelength (nm)
513nm
550nm
FreeDye
250μM Zinc(II)

2d

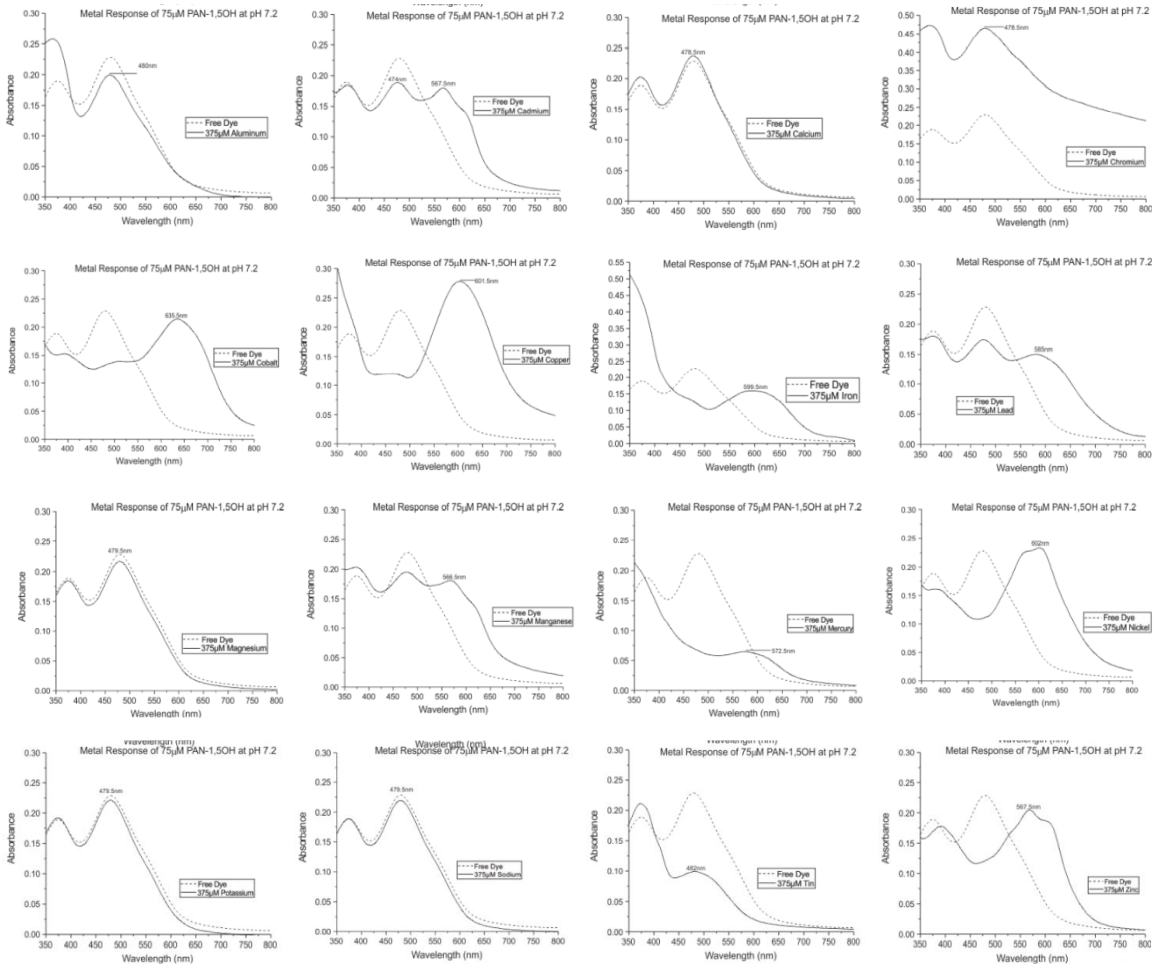
Metal Response of 75μM PAN-1,5OH at pH 7.2
Absorbance
Wavelength (nm)
480nm
Free Dye
375μM Aluminum
474nm
567.5nm
375μM Cadmium
478.5nm
375μM Calcium
375μM Chromium
635.5nm
375μM Cobalt
601.5nm
375μM Copper
599.5nm
375μM Iron
585nm
375μM Lead
479.5nm
375μM Magnesium
566.5nm
375μM Manganese
572.5nm
375μM Mercury
602nm
375μM Nickel
375μM Potassium
375μM Sodium
462nm
375μM Tin
375μM Zinc